UNIVERSIDAD AUTÓNOMA DE MADRID
FACULTAD DE CIENCIAS
DEPARTAMENTO DE BIOLOGÍA MOLECULAR

FUNCIÓN DE LA POLARIDAD APICOBASAL DE LAS CÉLULAS HEPÁTICAS EN LA ADHESIÓN LINFOCITARIA. IMPLICACIONES EN LA RESPUESTA INFLAMATORIA DEL HÍGADO.

NATALIA REGLERO REAL

MADRID 2013

MEMORIA PRESENTADA POR NATALIA REGLERO REAL, LICENCIADA EN FARMACIA,

PARA OPTAR AL TÍTULO DE DOCTOR EN BIOQUÍMICA, BIOLOGÍA MOLECULAR, BIOMEDICINA Y BIOTECNOLOGÍA

DIRECTORES DE LA TESIS:

Dr. JAIME MILLÁN MARTÍNEZ

Dr. MIGUEL ÁNGEL ALONSO LEBRERO

Este trabajo ha sido realizado en el
Departamento de Biología Molecular.
Centro de Biología Molecular 'Severo Ochoa'
(CSIC-UAM)

Este trabajo ha sido realizado en el Centro de Biología Molecular Severo Ochoa (CSIC-UAM) bajo la dirección de los doctores Jaime Millán Martínez, Científico Titular del CSIC, y Miguel Ángel Alonso Lebrero, Profesor de Investigación del CSIC.

La realización de esta Tesis ha sido posible gracias a una beca predoctoral JAE concedida a Natalia Reglero Real por el Consejo Superior de Investigaciones Científicas.

ÍNDICE

PÁGINA

Abreviaturas 17

I. RESUMEN/ SUMMARY 23

II. INTRODUCCIÓN 29

1. EL HÍGADO 29

1.1. Estructura y fisiología

1.2. Función de defensa y tolerancia inmune

2. INFILTRACIÓN LEUCOCITARIA EN LA RESPUESTA INFLAMATORIA HEPÁTICA 34

2.1. Aspectos generales de la infiltración leucocitaria

2.2. Infiltración leucocitaria del parénquima hepático

3. EL RECEPTOR DE ADHESIÓN ICAM-1 EN LA RESPUESTA INFLAMATORIA. 37

3.1. Estructura

3.2. Función

3.3. Conexión de ICAM-1 al citoesqueleto de actina: Las proteínas ERMs.

3.4. Regulación de ICAM-1 por la citoquina inflamatoria TNF-a. Relevancia en enfermedades inflamatorias hepáticas.

3.5. Función de ICAM-1 en el parénquima hepático.

4. POLARIDAD HEPATOCELULAR Y FUNCIÓN. 41

4.1. Aspectos generales de la polaridad celular epitelial.

4.2. Mecanismos implicados en el establecimiento de la polaridad apicobasal del hepatocito.

4.2.1.Transporte vesicular polarizado.

4.2.2. Uniones intercelulares

4.2.3. Proteínas reguladoras del citoesqueleto: Rho GTPasas

4.2.4. Proteínas reguladoras del citoesqueleto: ERMs

5. POLARIDAD HEPATOCELULAR Y DAÑO HEPÁTICO. 47

III. OBJETIVOS 51

IV. MATERIALES Y MÉTODOS 55

1. MATERIALES 55

1.1. Anticuerpos

1.1.1 Anticuerpos primarios

1.1.2. Anticuerpos secundarios

1.2. Reactivos

1.3. Plásmidos

1.4. Oligonucleótidos

1.5. Enzimas

1.5.1 De restricción

1.5.2. Polimerasas

2. IMÉTODOS 58

2.1. Líneas celulares, cultivos primarios y condiciones de cultivo.

2.2. Tejidos

2.3. Clonajes

2.4. Transfección de ADN y generación de clones estables.

2.5. Transfección de siRNA

2.6. Obtención de extractos proteicos

2.7. Electroforesis de proteínas (SDS-PAGE), electrotransferencia e inmunodetección (Western-Blot)

2.8. Modulación de la polaridad celular en HepG2

2.9. Ensayos de adhesión.

2.10. Inmunohistoquímica

2.11. Inmunofluorescencia y microscopía confocal

2.12. Ensayos de entrecruzamiento (*crosslinking)* y análisis de colocalización subcelular

2.13. Ensayos de biotinilación

2.14. Ensayos de asociación de proteínas por *pull-down*

2.15. Microscopía *time-lapse* o microscopía de células vivas

2.15.1. Ensayos de fotoactivación

2.15.2. Vídeo-microscopía de las interacciones entre linfocitos-T y HepG2

2.16. Microscopía electrónica de barrido

V. RESULTADOS 71

1. LA POLARIDAD HEPATOCELULAR REGULA LA ADHESIÓN LINFOCITARIA A TRAVÉS DEL RECEPTOR DE ADHESIÓN ICAM-1 71

1.1. La pérdida de polaridad apicobasal aumenta la adhesión de linfocitos a células HepG2

1.2. ICAM-1 se acumula en el dominio apical de células HepG2 y hepatocitos humanos *in vitro* e *in vivo*

1.3. La exposición de ICAM-1 apical a células inmunes aumenta en respuesta a la pérdida de polaridad hepatocelular

1.4. ICAM-1 media la adhesión de linfocitos T a células HepG2 despolarizadas.

2. BASES MOLECULARES QUE DETERMINAN LA POLARIDAD APICAL DE ICAM-1 EN CÉLULAS HEPÁTICAS. 82

2.1. ICAM-1 basolateral se redirige y confina en el canalículo biliar.

2.2. El dominio citoplásmico de ICAM-1 es necesario para su completa polarización.

2.3. ICAM-1 se asocia a las proteínas ERM en la membrana plasmática células HepG2

2.3.1. CAM-1 colocaliza con ezrina y radixina en células HepG2

2.3.2. La asociación de pERM con ICAM-1 depende de su segmento citoplásmico

1.6.3. La asociación de Ezrina y Radixina con ICAM-1 depen-

de de tres residuos de lisina en el dominio C-terminal del receptor

3. EFECTO DE LA INFLAMACIÓN SOBRE LA POLARIDAD HEPATOCELULAR DE ICAM-1 91

3.1. La estimulación a largo plazo con TNF-α aumenta la exposición basolateral de ICAM-1

3.2. La activación de ERM y su localización basolateral en hepatocitos polarizados aumentan en respuesta a la estimulación con TNF-α a largo plazo

3.2.1 La expresión del mutante constitutivamente activo de ezrina es suficiente para desplazar ICAM-1 hacia la membrana basolateral

3.2.3. La inhibición simultánea de PKC y ROCK reduce la fosforilación de las proteínas ERM y la exposición de ICAM-1 en la superficie basolateral en respuesta a TNF-α

4. DISTRIBUCIÓN DE ICAM-1 *IN VIVO* EN PATOLOGÍAS HEPÁTICAS CON DISTINTO COMPONENTE INFLAMATORIO 98

4.1. El receptor ICAM-1 hepatocítico pierde polaridad durante daño hepático agudo en modelos murinos

4.2. ICAM-1 se encuentra confinado en el dominio apical en hepatocitos y células epiteliales de los ductos biliares en muestras humanas de rechazo hepático

4.3. ICAM-1 presenta una distribución heterogénea en el parénquima hepático en muestras humanas de hígados infectados de forma crónica por los virus de la hepatitis B y C

VI DISCUSIÓN 109

1. LA PÉRDIDA DE POLARIDAD HEPATOCELULAR AUMENTA LA ADHESIÓN LEUCOCITARIA A TRAVÉS DE UN MECANISMO DEPENDIENTE DE ICAM-1 109

2. BASE MOLECULAR DE LA INTERACCIÓN CÉLULA INMUNE-HEPATOCITO 110

2.1. ICAM-1 hepático se asocia a ERM a través de su segmento citoplásmico, requerido para la localización apical del receptor

2.2. Doble rol de la maquinaria proteica ERM-ICAM-1 en células parenquimales hepáticas

3. LOS HEPATOCITOS POLARIZADOS PREVIENEN LA EXPOSICIÓN DE ICAM-1 A CÉLULAS INMUNES REDIRIGIENDO EL RECEPTOR DESDE LA MEMBRANA BASOLATERAL AL CANALÍCULO BILIAR 113

4. ASPECTOS FUNCIONALES DE LA EXPOSICIÓN HEPATOCITARIA DE ICAM-1 AL ESPACIO EXTRACELULAR 114

4.1. Función haptotáctica de ICAM-1

4.2. Rol de ICAM-1 en la tolerancia inmune y presentación antigénica

5. LA ESTIMULACIÓN POR TNF-α A LARGO PLAZO AUMENTA LA EXPOSICIÓN BASOLATERAL DE ICAM-1 A TRAVÉS DE LA ACTIVACIÓN DE ERM VÍA PKC Y ROCK 118

6. ENFERMEDAD INFLAMATORIA Y POLARIDAD 120

VII CONCLUSIONES/ CONCLUSIONS 125

VIII BIBLIOGRAFÍA 131

IX ANEXO 149

ABREVIATURAS

- **Ad**: *Adenovirus*
- **DNA**: *Del inglés deoxyribonucleic acid*
- **ALCAM**: *Del inglés activated leukocyte cell adhesión molecule*
- **aPKC**: *Del inglés atypical protein kinase C*
- **ARNm**: *Ácido ribonucleico mensajero*
- **Arp2/3**: *Del inglés actin related protein 2/3 complex*
- **BC**: *Del inglés Bile Canaliculus*
- **BSA**: *Del inglés Bovine serum albumin*
- **Cdc42**: *Del inglés cell division cycle 42*
- **CD40L**: *Ligando de CD40*
- **CHX**: *cicloheximida*
- **ConA**: *Concanavalina A*
- **C-ter**: *Región carboxilo terminal*
- **dcAMP**: *Del ingles dibutyryl-cAMP*
- **DMEM**: *Del inglés Dulbecco's Modified Eagle Medium*
- **EDTA**: *Del inglés Ethylenediaminetetraacetic acid*
- **ERK**: *Del inglés Extracelular-signal regulated kinases*
- **ERM**: *Ezrin, Radixin, Moesin*
- **F-actin**: *Actina filamentosa*
- **FERM**: *Del inglés Four point one Ezrin Radixin Moesin*
- **FHF**: *Fallo hepático fulminante*
- **GFP**: *Del inglés Green Fluorescent Protein*
- **CMV**: *Citomegalovirus*
- **GPI**: *glicofosfatidilinositol*
- **GST**: *Del inglés Glutathione S-Transferase*
- **GTP**: *Guanosín trifosfato*
- **GDP**: *Guanosín difosfato*
- **HBV**: *Virus hepatitis B*
- **HBx**: *Proteína X del virus de la hepatitis B*
- **HCV**: *Virus hepatitis C*
- **HEPES**: *Ácido 2-[4-(2-hidroxietil)-1-piperacinil-(1)] etanosulfónico*
- **HRP**: *Del inglés horseradish peroxidase*
- **HUVECs**: *Del inglés human umbilical vein endotelial cells*
- **ICAM-1**: *Del inglés intercellular adhesion molecule-1*
- **IL-1**: *Interleukina 1*
- **INF-g**: *Gamma interferón*
- **Jnk**: *Del inglés c-Jun N-terminal kinases*
- **LB**: *Medio de cultivo Luria-Bertani broth*
- **mF**: *milifaradios*

- **Mrp-2**: *Del inglés multidrug associated resistance protein-2*
- **p**: *valor p*
- **PA**: *Fotoactivación, del inglés photoactivation*
- **pa-GFP**: *Del inglés photoactivatable green fluorescence protein*
- **PAGE**: *Del inglés Polyacrylamide gel electrophoresis*
- **PAR**: *del inglés partition-defective protein*
- **PBL**: *Del inglés peripheral blood lymphocyte*
- **PBS**: *Solución salina tamponada con fosfato*
- **pERM**: *Del inglés phosphorylated ERM*
- **PIP_2**: *Fosfatidil inositol 4,5-bifosfato*
- **PIP_3**: *Fosfatidil inositol 3,4,5-trifosfato*
- **PKA**: *Del inglés protein kinase A*
- **PKC**: *Del inglés protein kinase C*
- **PMA**: *Del inglés phorbol-12 myristate-13 acetate*
- **PMSF**: *Del inglés phenylmethylsulfonyl fluoride*
- **PNS**: *Del inglés post-nuclear supernatant*
- **PS**: *pseudosustrato*
- **p38MAPK**: *Del inglés p38 Mitogen-activated protein kinases*
- **PVDF**: *Del inglés polyvinylidene fluoride*
- **Rho**: *Del inglés ras-homolog*
- **Rho-GDI**: *Del inglés Rho-GDP dissociation inhibitor*
- **ROCK**: *Del inglés Rho kinase*
- **rpm**: *revoluciones por minuto*
- **SDS**: *Del inglés Sodium Dodecyl Sulphate*
- **siRNA**: *Del inglés small interfering RNA*
- **t**: *tiempo*
- **TCA**: *Del inglés trichloroacetic acid*
- **TNF-a**: *Del inglés tumour necrosis factor alpha*
- **V**: *voltio*
- **v**: *volumen*
- **VCAM**: *Del inglés vascular adhesion molecule*
- **WAVE**: *Del inglés WASP family verproline-homologous protein*
- **WB**: *Del inglés Western-blot (Inmonoblot)*
- **YFP**: *Del inglés Yellow Fluorescent Protein*
- **Ω**: *ohmio*

RESUMEN

La polaridad apicobasal es un rasgo fundamental de los hepatocitos y resulta esencial para su correcta función. Los hepatocitos son células epiteliales especializadas que generan lúmenes apicales entre células adyacentes para formar canales encargados de la secreción biliar denominados canalículos biliares. El resto de la membrana plasmática hepatocitaria constituye el dominio basolateral, que se encuentra expuesto al espacio de Disse y es capaz de interaccionar con los leucocitos extravasados y otras células parenquimales. La pérdida de polaridad hepatocelular es distintivo de diferentes patologías hepáticas, incluyendo cáncer, hepatitis viral, trauma hepático o intoxicación crónica.

Nuestro trabajo demuestra que la pérdida de polaridad aumenta la adhesión de linfocitos a células hepáticas mediante un mecanismo dependiente de la expresión de ICAM-1. Los hepatocitos polarizados localizan ICAM-1 en su dominio apical, el cual no es accesible a los linfocitos T. En respuesta a la pérdida de polaridad, ICAM-1 y las proteínas ERM activas se exponen al espacio extracelular en proyecciones de membrana tipo microvilli capaces de contactar con los linfocitos. ICAM-1 se asocia con las proteínas ERM en la membrana plasmática hepatocelular a través de su segmento citoplásmico, el cual se requiere también para la localización apical del receptor. La citoquina TNFa regula la expression de ICAM-1 y juega un papel fundamental en la respuesta inflamatoria del hígado. Hemos comprobado que la estimulación a largo plazo con TNF-α aumenta la exposición de ICAM-1 basolateral a través de la activación en estos dominios de membrana de las proteínas ERM, la cual se encuentra regulada por ROCK y las isoformas clásicas de PKC. De acuerdo con estos resultados, hemos detectado que ICAM-1 se localiza apicalmente en parénquimas sometidos a una inflamación rápida pero que preservan su arquitectura hepatocelular, como en rechazos de hígados trasplantados, mientras que observamos una distribución mucho menos polarizada en muestras de tejido procedentes de modelos murinos de fallo hepático fulminante y en pacientes con patologías crónicas que causan inflamación hepática persistente y pérdida de polaridad hepatocelular, como por ejemplo las hepatitis virales.

En conclusión, nuestros resultados indican que la pérdida de polaridad hepatocelular y la inflamación a largo plazo aumentan la exposición de ICAM-1 y las proteínas ERM favoreciendo la interacción leucocito-hepatocito, mientras que los hepatocitos polarizados escapan del reconocimiento por el sistema inmune a través del secuestro y acumulación en su dominio apical de maquinaria proteica encargada de interaccionar con los leucocitos. Nuestra propuesta es que este mecanismo representa un paso de control inmune en el parénquima hepático que puede permitir a los leucocitos infiltrados discriminar entre hepatocitos disfuncionales y aquellos que son todavía operativos y conservan, por lo tanto, una polaridad apicobasal intacta.

Apicobasal polarity is a major feature of hepatocyte arquitecture essential for hepatocellular correct function. Hepatocytes are specialized epithelial cells that delimit lateral lumens which form channels for draining bile (the bile canaliculi) and a basolateral domain that is exposed to the space of Disse and interacts with extravasated leukocytes and other parenchymal cells. Loss of hepatocellular polarity is a hallmark of liver pathologies, including cancer and cell damage caused by virus infection, trauma or chronic intoxication.

Here we report that loss of polarity increases lymphocyte adhesion to hepatic cells in an ICAM-1-dependent manner. Polarized hepatocytes segregate ICAM-1 receptor into their apical domains. Upon depolarization, canalicular ICAM-1 and activated ERM proteins are exposed in microvilli-like membrane projections to the extracellular milieu, where they are able to contact lymphocytes. In polarized cells, ICAM-1 can reach the basolateral membrane but is rapidly redirected to apical surfaces where it remains tightly confined. ICAM-1 associates with ERM proteins at the plasma membrane through its cytoplasmic tail, which is in turn required for the receptor apical localization. Accordingly, we found ICAM-1 significantly polarized in hepatocytes from parenchymas that undergo rapid inflammatory responses but preserve their cellular architecture, as in allograft rejections, but much less polarized in samples from acute liver failure mice models and from patients suffering chronic diseases that induce persistent liver inflammation and loss of hepatocyte polarity, as in hepatitis virus infections. In addition, long-term inflammatory stimulation with TNF-α increases ICAM-1 localization at basolateral domains through ROCK and PKC classical isoforms mediated activation of ERM proteins.

In conclusion, our results indicate that loss of hepatocellular polarity and long-term inflammatory stimuli induce ICAM-1 and ERM proteins exposure and favour leukocyte-hepatocyte interactions, while polarized hepatocytes escape immune recognition by hijacking protein machinery that interacts with leukocytes through its apical confinement. We propose that this mechanism is an immune checkpoint in liver parenchymas which may help infiltrated immune cells discriminate between dysfunctional hepatocytes and those that are still operative and therefore preserve an intact apicobasal polarity.

INTRODUCCIÓN

Los primeros estudios de cultivos celulares, iniciados por Harrison en 1907, pusieron de manifiesto que los tejidos están compuestos por células individuales adheridas unas a otras (Harrison et al, 1907). A partir de ese momento la investigación sobre la adhesión celular cobra especial relevancia en biología y biomedicina, aunque no es hasta el último tercio del siglo XX cuándo se avanza en las bases moleculares de la adhesión célula-célula y célula-sustrato gracias al descubrimiento de proteínas de adhesión como las integrinas (Hynes, 1987) y las cadherinas (Takeichi, 1990). Hoy en día empezamos a comprender cómo las adhesiones celulares regulan procesos fundamentales tan diversos como la migración, la morfogénesis y la proliferación celular. La alteración patológica de las propiedades adhesivas entre distintas células o entre células y componentes de la matriz extracelular promueve la formación de tumores, su invasión y metástasis (Horwitz, 2012), enfermedades inflamatorias y autoinmunes.

La inflamación es una respuesta inmune fundamental que permite la supervivencia durante la infección o daño tisular y mantiene la homeostasis ante una variedad de circunstancias perjudiciales. La inflamación depende de eventos adhesivos específicos que van a orquestar la respuesta de distintos tipos celulares. Por ejemplo, el establecimiento de adhesiones con las células que forman los vasos sanguíneos y con la matriz extracelular permite que los leucocitos migren al lugar adecuado en el momento apropiado (Butcher, 1991). La citotoxicidad leucocitaria en el foco de inflamación requiere la adhesión a células diana y a otras células inmunes (Jaeschke and Hasegawa, 2006). A los cuatro signos cardinales de inflamación descritos por Cornelius Celsus en el siglo I D.C. (rubor et dolor cum calore et dolore), Rudolph Virchow añadió en 1858 un quinto (functio laesa) (Majno, G. 1975), indicando que cualquier respuesta inflamatoria altera la función y homeostasis celular. De hecho, una inflamación masiva, fuera de control o dirigida de forma crónica frente a lo propio puede dar lugar a patologías de la importancia de la aterosclerosis, esclerosis múltiple o cirrosis. Por ello se está invirtiendo mucho esfuerzo en comprender las señales, las moléculas y los mecanismos que causan y amplifican la respuesta inflamatoria, con el anhelo de llegar a regularlos terapéuticamente.

1. EL HÍGADO

1.1. Estructura y fisiología

El hígado es un órgano excepcional en términos metabólicos, inmunológicos y estructurales. Tiene el potencial único de regenerarse después de la lesión tisular, y cumple importantes funciones detoxificantes, sintéticas y de almacenaje. Su capacidad extraordinaria para adaptarse ante las necesidades del organismo hace del hígado un órgano imprescindible para el mantenimiento de la homeostasis corporal. El hígado participa en el metabolismo y la síntesis de proteínas, hidratos de carbono y lípidos, constituye un reservorio importante de glucógeno y vitaminas, produce y excreta la bilis hacia la vía biliar e interviene en el catabolismo de fármacos y tóxicos (Guyton y Hall 10ª ed.) (Arias I, et al. 2001) (Thomson y Knolle, 2010).

La ubicación anatómica del hígado resulta también singular, provocando que su aporte sanguíneo tenga dos orígenes distintos: desde el sistema arterial a través de las arterias hepáticas y desde el tracto gastrointestinal a través de la vena porta (Ilustración 1) (Lippert, ed. 2002). La circulación hepática y portal confluyen en una red de pequeños capilares denominados sinusoides, que atraviesan el parénquima hepático irrigando los hepatocitos circundantes y drenan finalmente a las venas hepáticas. Estas venas se denominan venas centrolobulillares por encontrarse en el centro de los lobulillos hepáticos, que son subunidades irregularmente

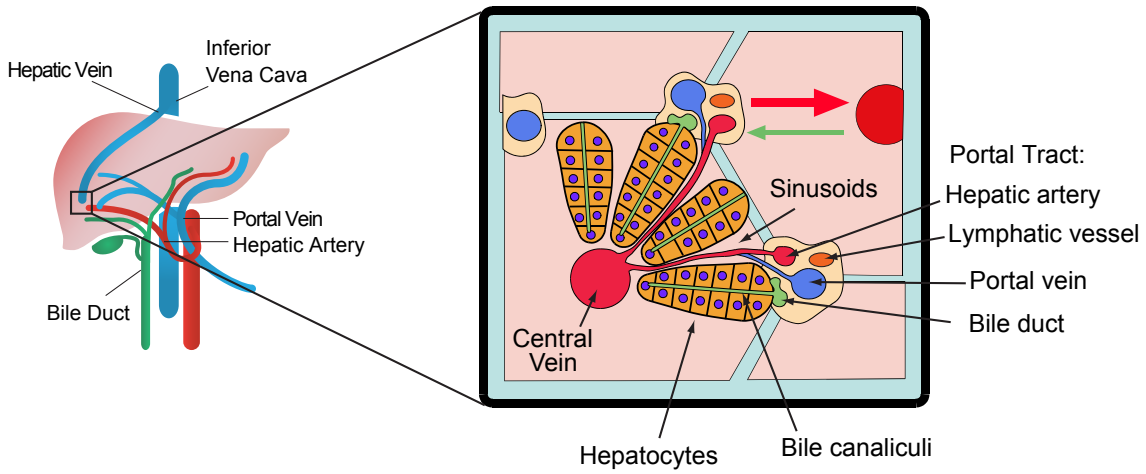

Ilustración 1. Anatomía general del hígado.

Diagrama que muestra la estructura de un lóbulo hepático. El tejido se organiza alrededor de áreas vasculares denominadas espacios porta, que contienen una rama de la vena porta, una arteriola, un canal biliar y un capilar linfático. Desde los espacios porta la sangre circula a través de una red densa de sinusoides que existe entre las láminas de hepatocitos hasta las venas centrolobulillares, mientras que la bilis secretada por los hepatocitos a los canalículos biliares fluye en dirección contraria hacia los conductos biliares de los espacios porta.

hexagonales formadas por láminas de hepatocitos. En los ángulos de los lobulillos hepáticos se sitúan los espacios porta (Ilustración1), formados por la presencia de cuatro grandes conductos: rama de la arteria hepática, rama de la vena porta, capilar linfático y canal biliar. La bilis secretada por los hepatocitos se vierte a una red de canalículos dentro de las láminas de hepatocitos y fluye, en forma centrípeta al lobulillo, hacia los conductos biliares de los espacios porta (Guyton y Hall, 10ª ed.) (Arias I, et al. 2001).

Histológicamente el hígado está compuesto de células parenquimales clásicas, los hepatocitos, y células no parenquimales o estructurales, entre las que se encuentran los colangiocitos que recubren el lumen de los canales biliares, las células endoteliales sinusoidales, células de Kupffer y células de Ito (Ilustración 2).

Los hepatocitos constituyen alrededor del 80% de la población celular del tejido hepático y son responsables de la mayoría de las funciones que cumple el hígado, incluyendo la formación de bilis, el metabolismo y síntesis de proteínas, lípidos y carbohidratos y la inactivación de sustancias extrañas. Su estructura y función se revisará más adelante. Los hepatocitos se distribuyen en el hígado cerca de los sinusoides y se disponen formando placas o láminas de hepatocitos anastomosados, de no más de dos células de grosor, que irradian desde cada espacio porta hacia las venas centrolobulillares (Ilustración 1) (Leslie P.Gartner y James L.Hiatt, 3ª ed.).

Los sinusoides son estrechos capilares de 5 a 7 um de grosor muy distintos al resto de vasos sanguíneos, ya que carecen de membrana basal y sus células endoteliales se disponen de manera discontínua, no forman uniones estrechas y se encuentran además fenestradas por poros de 100-200 nm de diámetro. Todo ello hace que el intercambio de solutos así como

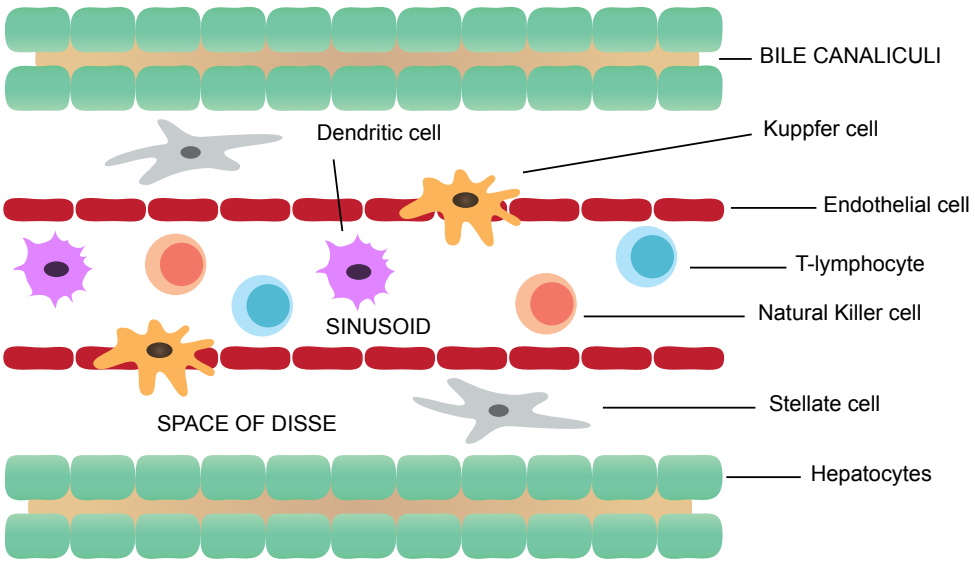

Ilustración 2. Organización de los sinusoides hepáticos.

Los sinusoides se encuentran rodeados por células endoteliales fenestradas y carecen de membrana basal. El microambiente hepático se encuentra enriquecido en células del sistema inmune innato (células de Kupffer, Natural killer cells) y en células dendríticas y linfocitos T, que participan en la respuesta inmune adaptativa. El espacio sub-endotelial que se encuentra entre los sinusiodes y las láminas de hepatocitos se conoce como espacio de Disse y es dónde residen las células de Ito o células estrelladas.

la interacción entre las células parenquimales y los componentes del torrente sanguíneo se encuentre mucho más favorecida que en el resto de los órganos (Crispe, 2003) (Adams et al., 2010). El estrecho espacio perisinusoidal que se encuentra entre la pared de los sinusoides y las láminas de hepatocitos se denomina espacio de Disse (Ilustración 2), y está ocupado por una red de fibras reticulares y plasma sanguíneo que baña libremente la superficie de los hepatocitos. Por otro lado, el hígado cuenta también con la presencia de tipos celulares exclusivos que se localizan mayoritariamente en el espacio de Disse. Las células de Kupffer son macrófagos que patrullan los sinusoides encargándose de eliminar endotoxinas sanguíneas, actúan como células presentadoras de antígenos y pueden derivar de precursores de médula ósea o ser hígado-residentes. Las células de Ito o células estrelladas hepáticas son fibroblastos que actúan como pericitos rodeando el endotelio sinusoidal. Esta células son también capaces de activar linfocitos T, aunque son más conocidas por su función pro-fibrótica debido a su capacidad de sintetizar colágeno y proliferar en respuesta a la fagocitosis de cuerpos apoptóticos o de desechos celulares (Friedman, 2000) (Friedman, 2008).

1.2. Función de defensa y tolerancia inmune.

El hígado se encuentra estratégicamente situado entre la circulación porta y sistémica, lo que confiere a este órgano una función inmunológica excepcional. Además de las células parenquimales y estructurales, el hígado cuenta con un número amplio de células inmunes que llegan al órgano a través del torrente circulatorio y resultan esenciales para que éste cumpla su función de defensa. Este ambiente inmunológico único dota al hígado del potencial para desarrollar una respuesta inmune frente a elementos perjudiciales, pero también de la capacidad para ser "inmunológicamente tolerante" frente a la exposición diaria de antígenos y microorganismos no dañinos que provienen del tracto gastrointestinal (Thomson and Knolle, 2010) (Crispe, 2003).

El hígado se encuentra enriquecido en macrófagos, células NK (Natural Killer) y células NKT (Natural killer T cells). Los macrófagos están fundamentalmente representados por las células de Kupffer y presentan capacidad fagocítica (Adams et al., 2010), mientras que las células NK se caracterizan por su acción citolítica (Krueger et al., 2011). El hígado cuenta también con una amplia población de linfocitos T que llegan a través del torrente circulatorio, patrullan el tejido y o bien lo abandonan vía vasos linfáticos o bien quedan retenidos para desempeñar la vigilancia inmune en ausencia de inflamación o como células efectoras en el contexto de enfermedad inflamatoria y daño hepático (Shetty et al., 2008) (Hiraoka, 2010) (Crispe, 2003). Las células presentadoras de antígeno (APC) profesionales en el hígado se encuentran representadas por células dendríticas inmaduras (Ilustración 2), que recorren los sinusoides y maduran en respuesta a la inflamación para migrar a los nódulos linfáticos (D'Amico et al., 2000). Todas las células inmunes descritas son capaces de liberar un amplio panel de citoquinas pro o anti-inflamatorias que van a determinar su actuación.

Para mantener su ambiente tolerogénico el hígado utiliza distintas estrategias. Las células de Kupffer retiran endotoxinas de la sangre y secretan citoquinas antiinflamatorias como interleucina 10 (IL-10), mientras que las células NK hepáticas mantienen un estado de hiporeac-

tividad y son capaces de disminuir la activación linfocitos T o incluso destruirlos (Krueger et al., 2011). Por otro lado, en ausencia de inflamación la activación de linfocitos T CD8 por hepatocitos y células endoteliales sinusoidales provoca su muerte prematura y una citotoxicidad disminuida con respecto a la activación en los nódulos linfáticos, lo que resulta en una activación ineficaz comprometiendo la respuesta inmune subsecuente (Limmer et al., 2000) (Bertolino et al., 1998) (Holz et al., 2010). Asimismo en ausencia de daño hepático los linfocitos T CD4 activados por células endoteliales sinusoidales pueden diferenciarse a células reguladoras de fenotipo antiinflamatorio y secretar IL-10 (Knolle et al., 1999). Estos procesos sugieren que la presentación de antígenos mediada por células hepáticas puede favorecer la tolerancia inmune en condiciones fisiológicas. Se ha propuesto además que estos mecanismos de tolerancia pueden ser en parte responsables del éxito obtenido en los trasplantes hepáticos sin necesidad de utilizar terapias inmunosupresoras (Qian et al., 1997), aunque también patógenos hepatotrópicos como los virus de la hepatitis C y B pueden aprovecharse de estos mecanismos para establecer infecciones persistentes (Cooper et al., 1999) (Crispe, 2003) (Thomson and Knolle, 2010).

2. INFILTRACIÓN LEUCOCITARIA EN LA RESPUESTA INFLAMATORIA HEPÁTICA

2.1. Aspectos generales de la infiltración leucocitaria

El sistema inmune se ha desarrollado para responder a los antígenos extraños de una manera rápida y específica. Durante el proceso inflamatorio las células inmunes son reclutadas al tejido dañado como mecanismo de defensa, lo que implica su salida del torrente circulatorio y migración a través de los vasos sanguíneos. El reclutamiento de leucocitos conlleva una cascada multietapa de eventos de adhesión entre el endotelio vascular y los leucocitos circulantes (Butcher, 1991). Los estímulos proinflamatorios como el TNF-α, IFN-γ o IL-1 inducen la expresión transitoria de un conjunto de receptores de superficie que median dicha adhesión y posterior transmigración de células inmunes a través de la barrera endotelial (Ilustración 3) (Osborn et al., 1989) (Pober et al., 1986) (Reglero-Real et al., 2012). Las diversas elecciones moleculares de cada etapa (receptores de adhesión, quimioquinas, etc) confieren al proceso amplias posibilidades de combinación, permitiendo que distintas clases de leucocitos con funciones diferentes puedan situarse en el lugar apropiado en el momento adecuado. El inicio de la interacción leucocito-endotelio se denomina “rolling”, y se produce principalmente por interacciones muy breves a través de la familia de las selectinas y sus ligandos carbohidratos. Estas uniones intermitentes permiten el reconocimiento por parte de receptores acoplados a proteínas G en el leucocito de quimioquinas expuestas en la membrana luminal endotelial. Las quimioquinas son potentes agentes quimiotácticos que pueden ser producidos por distintas células en respuesta a citoquinas proinflamatorias (Rot and Von Andrian, 2004) y que son

expuestas en la superficie luminal del endotelio (Alon and Ley, 2008) (Alon, Ley, 2008, Curr Op Cell Biol). Las quimoquinas a su vez activan integrinas de la familia β1 (VLA-4) y β2 (LFA-1) que se unen a receptores de adhesión endoteliales de la familia inmunoglobulina, VCAM-1 e ICAM-1 respectivamente (Alon and Ley, 2008) (Butcher, 1991). Estos receptores median el siguiente paso que es la adhesión firme del leucocito al endotelio. Durante la adhesión, el leucocito migra sobre la monocapa endotelial hasta que finalmente atraviesa el endotelio, un proceso que se denomina diapedesis o migración transendotelial, y que puede ocurrir entre las uniones celulares (migración paracelular) o a través de las células endoteliales (migración transcelular) (Carman and Springer, 2004) (Millan et al., 2006). En la mayoría de los vasos los leucocitos continúan atravesando la cubierta exterior formada por pericitos y redes de matriz extracelular (Nourshargh and Marelli-Berg, 2005) (Nourshargh et al., 2010), aunque en estos términos el hígado supone una excepción ya que los sinusoides carecen de membrana basal. Por último, durante la migración intersticial por el parénquima hacia el área dañada los leucocitos escanean la superficie de las células parenquimales buscando la presentación de antígenos, quimioquinas o receptores de adhesión que utilizarán para desplazarse mediante un mecanismo conocido como haptoquinesis (Friedl and Weigelin, 2008). Mientras que el paso de leucocitos a través de la barrera endotelial ha sido ampliamente estudiado, los mecanismos que regulan la navegación de las células inmunes por los tejidos no han sido descritos en tanto detalle.

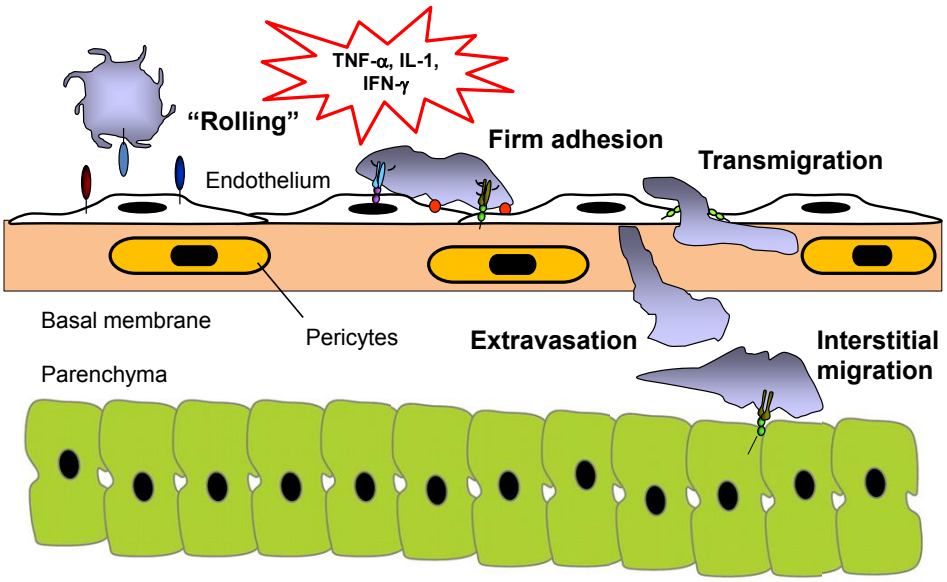

Ilustración 3. Esquema de la extravasación leucocitaria durante la inflamación.

En respuesta a estímulos proinflamatorios el endotelio expresa en su superficie una serie de receptores de adhesión que van a favorecer el "rolling", la adhesión y posterior transmigración de leucocitos a través de la monocapa endotelial. El proceso de extravasación conlleva también atravesar la membrana basal en la mayoría de los vasos sanguíneos salvo en los sinusoides hepáticos, y finaliza con la migración intersticial de las células inmunes por el parénquima hacia el área dañada.

2.2. Infiltración leucocitaria del parénquima hepático

La infiltración de leucocitos en el parénquima hepático es esencial para la vigilancia inmune, controla el desarrollo de infecciones y cáncer y facilita la regeneración tisular. Por otra parte, las interacciones aberrantes entre leucocitos y hepatocitos desencadenan el fallo hepático en enfermedades autoinmunes y rechazo hepático post-trasplante, además de exacerbar el daño hepático en respuesta a trauma severo (Adams et al., 2010) (Shetty et al., 2008).

La realización de experimentos intravitales ha permitido describir que aunque los leucocitos son capaces de adherirse y migrar a través de diferentes regiones de la microvasculatura hepática, la mayoría llegan al parénquima a través de los sinusoides (Adams et al., 2010). El estrecho diámetro de estos capilares ralentiza el flujo sanguíneo intrahepático disminuyendo el característico "rolling" de los leucocitos sobre el endotelio, favoreciendo que directamente se adhieran y repten sobre las células endoteliales. Esta peculiaridad supone que las células endoteliales sinusoidales presenten diferencias en la expresión de moléculas de adhesión respecto a otros endotelios, incluyendo una reducción en la expresión de selectinas (Adams et al., 1996) y la expresión amplia de receptores de adhesión como ICAM-1 y VCAM-1 o VAP-1 y CD44 (Crispe, 2003). Estos últimos cumplen además funciones particulares en el endotelio sinusoidal para facilitar el reclutamiento hepático de leucocitos (Shetty et al., 2008).

El estudio del tráfico leucocitario hepático se ha centrado en la interacción con el endotelio, sin embargo estas células existen en un complejo microambiente multicelular en los sinusoides y se conoce que otros tipos celulares y señales pueden influenciar el reclutamiento de leucocitos. De esta manera tanto las células de Kupffer, las células estrelladas, los colangiocitos o los hepatocitos son capaces de liberar citoquinas proinflamatorias o expresar ligandos adhesivos en su superficie para favorecer la adhesión o migración leucocitaria. Una vez dentro del tejido inflamado, los leucocitos tienen que migrar hasta el foco de daño hepático. En el carcinoma hepatocelular por ejemplo, los linfocitos llegan al tejido tumoral por migración intersticial en vez de utilizar la vasculatura dentro del tumor (Hiraoka, 2010). La migración eficiente de leucocitos hacia áreas disfuncionales en el parénquima implica diferentes pistas moleculares para guiar a las células inmunes, como citoquinas y quimioquinas secretadas por diferentes tipos celulares, sustancias liberadas por células necróticas (péptidos N-formil, lípidos, especies reactivas de oxígeno,etc) o factores haptotácticos como componentes de la matriz extracelular o receptores de adhesión expuestos en la superficie de las células parenquimales (Oo and Adams, 2010) (McDonald and Kubes, 2011). Por todo ello, el ambiente estromal hepático ayuda a establecer "códigos de direccionalidad" en la cascada de reclutamiento de leucocitos condicionando el comportamiento del endotelio sinusoidal o directamente interaccionando con las células inmunes (McGettrick et al., 2012). La transformación oncogénica, infección vírica, daño o muerte de los hepatocitos promueven la extravasación a través de los sinusoides de numerosas células inmunes que buscan la presencia de células dañadas o transformadas, desechos celulares, microorganismos o la presentación de antígenos (Kang et al., 2011) (Hiraoka, 2010) (Longhi et al., 2010). La naturaleza, extensión y localización intrahepática del infiltrado leucocitario van a determinar la progresión y severidad del daño hepático.

Los mecanismos moleculares que median la adhesión leucocitaria al parénquima hepático todavía no se han investigado en detalle. Sin embargo, la expresión diferencial de moléculas de adhesión y quimioquinas resulta clave en el reclutamiento selectivo de leucocitos. Las quimioquinas secretadas por células parenquimales son además susceptibles de su presentación por el endotelio sinusoidal, ya que pueden ser transportadas desde la membrana basolateral hasta la superficie luminal endotelial por transcitosis, o ser capturadas directamente del lento flujo sanguíneo sinusoidal por el glicocalix endotelial en caso de que hayan sido secretadas por colangiocitos en los espacios porta (Oo and Adams, 2010). El complejo sistema quimioquina-receptor determina que se recluten adecuadamente en el tiempo y en el espacio subtipos específicos de células inmunes. Así por ejemplo durante el daño hepático aumenta la expresión de las quimioquinas CXCL16 y CXCL9-11 en hepatocitos y colangiocitos, siendo capaces de reclutar al parénquima y a los ductos biliares células T que interaccionarán a través de sus receptores CXCR6 y CXCR3 respectivamente. Se ha demostrado que la unión del receptor CXCR6 en células T a su ligando en estas células epiteliales promueve su adhesión dependiente de integrinas y favorece el anclaje del linfocito sobre la célula parenquimal (Heydtmann et al., 2005). Al menos para neutrófilos y células-T, su adhesión firme sobre las células hepáticas se ha sugerido que ocurre a través de integrinas B2 en la superficie del leucocito y su ligando ICAM-1 en células hepáticas (Meijne et al., 1994) (Nagendra et al., 1997) (Jaeschke and Hasegawa, 2006). Por otra parte, la ligación de integrinas B2 en neutrófilos va a generar especies reactivas de oxígeno y la liberación de gránulos citotóxicos con enzimas proteolíticas que causan la necrosis hepatocelular (Jaeschke and Hasegawa, 2006). Por último, se ha propuesto que ICAM-1 expuesto en los microvilli de los hepatocitos puede pasar a través de las fenestraciones sinusoidales, alcanzar el torrente sanguíneo e interaccionar con los linfocitos circulantes (Warren et al., 2006) (Edwards et al., 2005) lo que sugiere que la interacción leucocito-hepatocito podría regula procesos de migración leucocitaria más allá de la infiltración parenquimal, como la migración transendotelial o la presentación antigénica a leucocitos en los sinusoides.

3. EL RECEPTOR DE ADHESIÓN ICAM-1 EN LA RESPUESTA INFLAMATORIA

3.1. Estructura

ICAM-1 (Intercellular adhesión molecule-1) pertenece a la superfamilia de las inmunoglobulinas, que engloba otras moléculas de adhesión como ICAM-2 y -3, VCAM-1 (vascular adhesion molecule), ALCAM (activated leukocyte cell adhesion molecule) (Oppenheimer-Marks et al., 1991) (de Fougerolles et al., 1991) (Cayrol et al., 2008). Estas moléculas funcionan como contra-receptores de las integrinas, receptores heterodiméricos de adhesión que se activan pasando a un estado de alta afinidad en respuesta a estímulos citoplásmicos. En concreto ICAM-1 es un ligando de las integrinas αLβ2 LFA-1 (lymphocyte associated antigen 1) y

αMβ2 Mac-1 (macrophage-1-antigen) presentes en la membrana de los leucocitos.

ICAM-1-es una proteína transmembrana tipo I con peso molecular comprendido entre 80 y 114 KDa dependiendo de su estado de glicosilación. Contiene 5 dominios extracelulares tipo inmunoglobulina (D1-D2), un dominio transmembrana y un corto segmento citoplásmico (Ilustración 4a). En su estado nativo ICAM-1 se encuentra en la superficie celular en equilibrio entre un estado monomérico y dimérico y difunde libremente por la membrana plasmática. Se han descrito dos sitios de dimerización para la molécula en los dominios extracelulares D1 y D4, y el dominio transmembrana es capaz de estabilizar dicha dimerización (Chen et al., 2007) que favorece la unión a integrinas (Miller et al., 1995). La unión y entrecruzamiento del receptor con integrinas o anticuerpos específicos provoca la disminución de su movilidad lateral, probablemente debido al aumento de la asociación a través de su segmento citoplásmico con proteínas conectoras del citoesqueleto de actina (Yang et al., 2006) (van Buul et al., 2010).

3.2. Función

ICAM-1 juega un papel importante en la respuesta inmune innata y adquirida. En la formación de la sinapsis inmune su unión a LFA-1 favorece el contacto entre la célula presentadora de antígeno y el linfocito T, permitiendo la interacción entre el receptor de células T (TCR) y las moléculas del complejo mayor de histocompatibilidad (MHC) unidas al antígeno correspondiente (Lawson and Wolf, 2009).

Por otro lado, ICAM-1 es esencial para la adhesión y transmigración leucocitaria a través de la barrera endotelial. ICAM-1 no solo forma un gradiente de adhesión que el leucocito

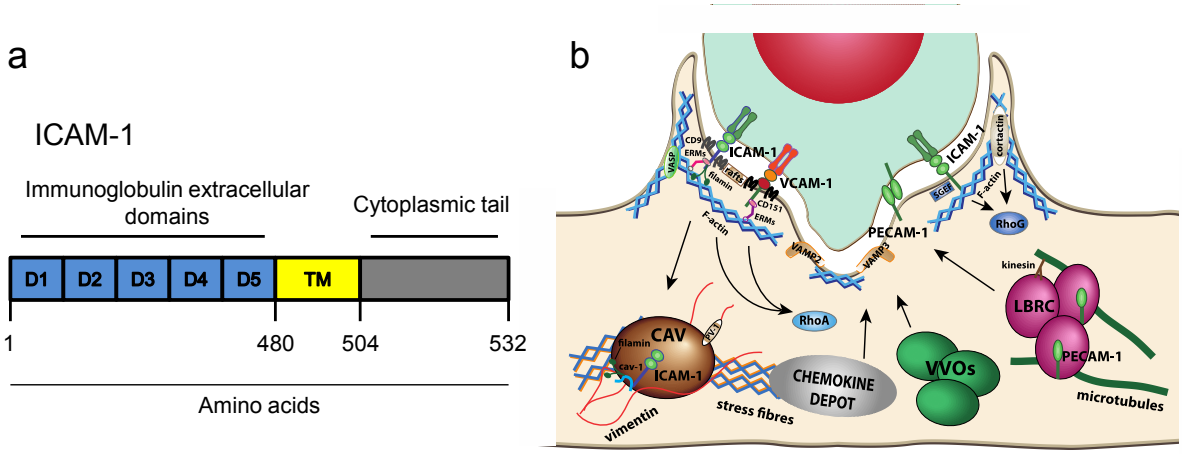

Figura 4. Estructura y función del receptor ICAM-1.

(a) Esquema de los diferentes dominios de ICAM-1. TM= Transmembrana. **(b)** Figura representativa de las estructuras de anclaje endoteliales encargadas de la adhesión y transmigración leucocitaria en las que ICAM-1 ha sido implicado. Adaptado de Reglero-Real et al, 2012.

sigue hasta encontrar el mejor lugar para su extravasación, sino que provoca también la propagación de señales necesaria para la formación de "estructuras de anclaje" endoteliales que abrazan a los leucocitos favoreciendo su transmigración (Carman and Springer, 2004) (Reglero-Real et al., 2012). Estas proyecciones de membrana son muy similares a agrupaciones de microvilli de superficie y se encuentran enriquecidas en actina y en los receptores de adhesión ICAM-1 y VCAM-1 y tetraspaninas como CD151 y CD9, que interaccionan con los receptores de adhesión agrupándolos en la superficie celular (Barreiro et al., 2002) (Carman et al., 2003) (Ilustración4b) (Reglero-Real et al., 2012).

3.3. Conexión de ICAM-1 al citoesqueleto de actina: Las proteínas ERM

Para que la transmigración leucocitaria a través de la barrera endotelial sea eficiente, resulta imprescindible la interacción del extremo citoplásmico de ICAM-1 con el citoesqueleto de actina a través de proteínas adaptadoras que regulan el agrupamiento de receptores en la superficie endotelial, como la proteína a-actinina (Carpen et al., 1992), cortactina (Tilghman and Hoover, 2002), filamina (Kanters et al., 2008) o las proteínas Ezrina/Radixina/Moesina (ERMs) (Huang et al., 2011). Durante la adhesión leucocitaria a la superficie endotelial, estas proteínas conectoras median el reclutamiento de los receptores de adhesión ICAM-1 y VCAM-1 en las estructuras de anclaje endoteliales, encargándose de unir a estos receptores al citoesqueleto de actina cortical (Ilustración4b) (Barreiro et al., 2002) (Oh et al., 2007) (Kanters et al., 2008) (Schnoor et al., 2011).

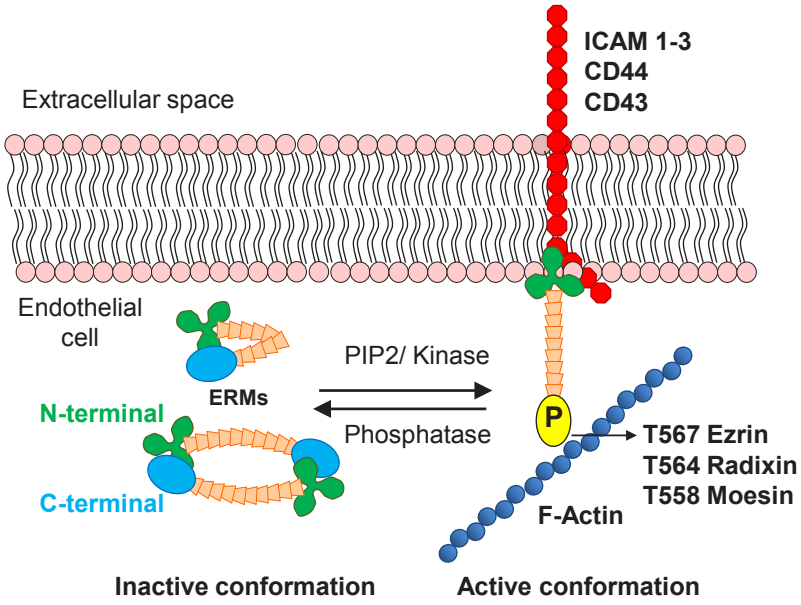

Figura 5. Esquema del mecanismo de activación de ERM.

La fosforilación de un residuo específico de treonina en el extremo C-terminal y la presencia del fosfolípido PIP2 provocan el cambio conformacional de las proteínas ERM, encargadas de unir proteínas transmembrana al citoesqueleto de actina en su conformación activa o abierta. Adaptado de (Ivetic and Ridley, 2004).

Las proteínas ERM pertenecen a la superfamilia de proteínas con dominio FERM (Four point one, Ezrin, Radixin, Moesin), presente en el extremo N-terminal de todas ellas. Este dominio es el responsable de la interacción con el segmento citoplásmico de proteínas de membrana y posee al menos tres secuencias consenso de unión a fosfoinosítidos. ERM contienen además un dominio central a-helicoidal y otro dominio de unión a actina en la región C-terminal (Ilustración 5). La interacción intramolecular de sus extremos N y C-terminal regula negativamente a ERM, enmascarando sus sitios de unión a las proteínas correspondientes. La fosforilación de un residuo de treonina conservado en el dominio C-terminal de las tres proteínas (T567 en la ezrina, T564 en la radixina, T558 en la moesina) provoca un cambio conformacional que activa a ERM y las trasloca desde el citoplasma a la membrana, de manera que el dominio de unión a actina y el dominio FERM quedan expuestos y libres para interaccionar con F-actina y proteínas de membrana respectivamente (Ilustración 5) (Bretscher et al., 2002). Distintas proteínas quinasas pueden potencialmente regular la fosforilación de ERM en este particular residuo de treonina. Entre ellas se ha identificado a PKC (en concreto PKC-α y PKCθ), p38MAPK y ROCK, el principal efector de RhoA (Ng et al., 2001) (Ivetic and Ridley, 2004) (Koss et al., 2006). Recientemente se ha descrito además que las quinasas LOK (lymphocyte orientated kinase) y SLK (Ste20-like kinase 4) son necesarais para que ezrina cicle entre su forma fosforilada y defosforilada, lo cual restringe la actividad de la proteína al dominio apical de células epiteliales placentarias (Viswanatha et al., 2012). Por otro lado, la unión a fosfoinosítidos, en especial a fosfatidilinositol 4,5 bisfosfato (PIP2), es necesaria para la activación de ERM y su reclutamiento a la membrana plasmática. Este lípido está presente en la cara citoplásmica de la membrana y actúa estabilizando la forma fosforilada en el extremo C-terminal o favoreciendo el cambio conformacional de los monómeros a la forma activa previamente a la fosforilación (Ivetic and Ridley, 2004) (Fievet et al., 2007).

3.4. Regulación de ICAM-1 por la citoquina inflamatoria TNF-α. Relevancia en enfermedades inflamatorias hepáticas.

Además de los efectos directos de las células inmunes sobre los hepatocitos, la respuesta inflamatoria hepática se encuentra ampliamente regulada por citoquinas, que funcionan como pequeños mensajeros secretados por una célula para alterar el comportamiento de células vecinas o el de la propia célula. Las citoquinas juegan un papel clave en la compleja interacción entre células inmunes y hepatocitos, ya que pueden activar funciones efectoras en leucocitos así como vías de señalización hepatocelulares necesarias para el control de la homeostasis celular. Las células de Kupffer y los macrófagos y linfocitos T infiltrados en el parénquima hepático constituyen las fuentes principales de liberación de citoquinas, entre las que se encuentran IL-1 (*Interleukin 1*), IL-6, TNF-α (*tumor-necrosis factor alpha*) e INF-γ (*interferon gamma*).

Una de las rutas de mayor relevancia en la inflamación y daño hepático es la mediada por TNF-α. Pacientes con hepatitis fulminante presentan niveles elevados en suero de TNF-α así como de sus receptores TNF-R1 y TNF-R2, y sus hígados muestran infiltrados leucocitarios

con alta producción de TNF-α y elevada expresión de TNF-R1 hepatocelular (Streetz et al., 2000).

Muchos de los efectos proinflamatorios de TNF-α se pueden explicar a través de su capacidad para inducir el reclutamiento de leucocitos al lugar dañado. Por una parte, TNF-α provoca un aumento en la permeabilidad de barreras endoteliales y epiteliales a través de la alteración de las uniones intercelulares y la remodelación dramática de su citoesqueleto de actina, procesos en los que intervienen rutas de señalización mediadas por la GTPasa RhoA, MAPK y la proteína quinasa C (PKC) (Nwariaku et al., 2003) (Ferro et al., 2000). Por otra parte, TNF-α activa vías de señalización intracelular (Tacke et al., 2009) que inducen la expresión de moléculas de adhesión como ICAM-1 y VCAM-1 en diferentes tipos celulares (Sano et al., 1999). La expresión celular del receptor ICAM-1 es moderada en el hígado, pero se induce en respuesta a TNF-α en células endoteliales, hepatocitos y células epiteliales biliares (Sano et al., 1999) (Cruickshank et al., 1998). Además, se observa marcaje hepatocelular de ICAM-1 en diversas patologías inflamatorias como hepatitis C y B (Volpes et al., 1990a) (Volpes et al., 1990b) (Doi et al., 1994), enfermedad autoinmune hepática (Adams et al., 1991) y rechazo hepático (Romero et al., 2000). Por último, la forma soluble de ICAM-1, que contiene los cinco dominios inmunoglobulina del receptor, se encuentra incrementada en plasma de pacientes con patologías hepáticas inflamatorias (Adams et al., 1993) (Thomson et al., 1994).

3.5. Función de ICAM-1 en el parénquima hepático

Aunque la función de ICAM-1 en hepatocitos no ha sido estudiada tan en detalle como en células inmunes o endoteliales, este receptor contribuye al reclutamiento de linfocitos T durante el desarrollo de hepatitis fulminante inducida por Concanavalin A en modelos murinos (Wolf et al., 2001). La severidad de la hepatitis inducida en este modelo se encuentra reducida en ratones "knockout" para ICAM-1 (Kawasuji et al., 2006). Por otro lado, existe también evidencia para sugerir un rol del receptor en la capacidad inmunogénica de hígados transplantados, ya que tanto hepatocitos como células no parenquimales deficientes en ICAM-1 generan un desarrollo defectuoso de linfocitos T citotóxicos alogénicos (Bumgardner et al., 1998).)

4. POLARIDAD HEPATOCELULAR Y FUNCIÓN

4.1. Aspectos generales de la polaridad celular epitelial

La asimetría espacial o polaridad es una propiedad fundamental de la mayoría de las células eucariotas y es esencial para el correcto desarrollo tisular de organismos complejos. Durante la adquisición de polaridad celular la célula establece y mantiene dominios en la membrana plasmática separados físicamente y de composición y función diferentes. Esta organización

espacial controla procesos celulares tan diversos como la secreción de moléculas, la respuesta inmune, la migración y diferenciación celular, el desarrollo y la morfogénesis (Wodarz and Nathke, 2007).

Uno de los mejores modelos para estudiar la polaridad celular son las células epiteliales que recubren la superficie de las cavidades de los órganos. Los epitelios constituyen una capa celular altamente organizada que sirve de barrera entre distintos compartimentos extracelulares y posee funciones muy especializadas de secreción, absorción y transporte de solutos y moléculas. Como consecuencia, las células epiteliales diferencian su membrana plasmática en un dominio apical que mira al lumen y otro basolateral en contacto con células vecinas y la circulación sanguínea, lo que se conoce como polaridad apicobasal (Ilustración 6) (McCaffrey and Macara, 2011). Ambos dominios son diferentes en función y composición (Simons and van Meer, 1988), que se mantiene gracias a la existencia de uniones estrechas encargadas de evitar la difusión de proteínas y lípidos de la membrana apical a la basolateral y viceversa (Zegers and Hoekstra, 1998).

Para generar y mantener su arquitectura polarizada, las células necesitan establecer un transporte diferencial y dirigir moléculas específicamente hacia la membrana apical o basolateral. Las proteínas de membrana pueden alcanzar su destino a través de dos mayoritarias rutas de transporte. En la ruta directa las proteínas de nueva síntesis se segregan en vesículas en la red trans-Golgi (TGN) y se dirigen directamente al dominio de membrana correspondiente (basolateral o apical). Durante la ruta indirecta, todas las proteínas llegan primero un dominio, normalmente la membrana basolateral. Desde allí las proteínas se endocitan y mediante mecanismos específicos de reparto (*sorting*) vesicular se transportan finalmente al dominio opuesto. Este transporte vesicular entre diferentes dominios de superficie se denomina transcitosis (Ilustración 6) (Zegers and Hoekstra, 1998) (Mostov et al., 2000).

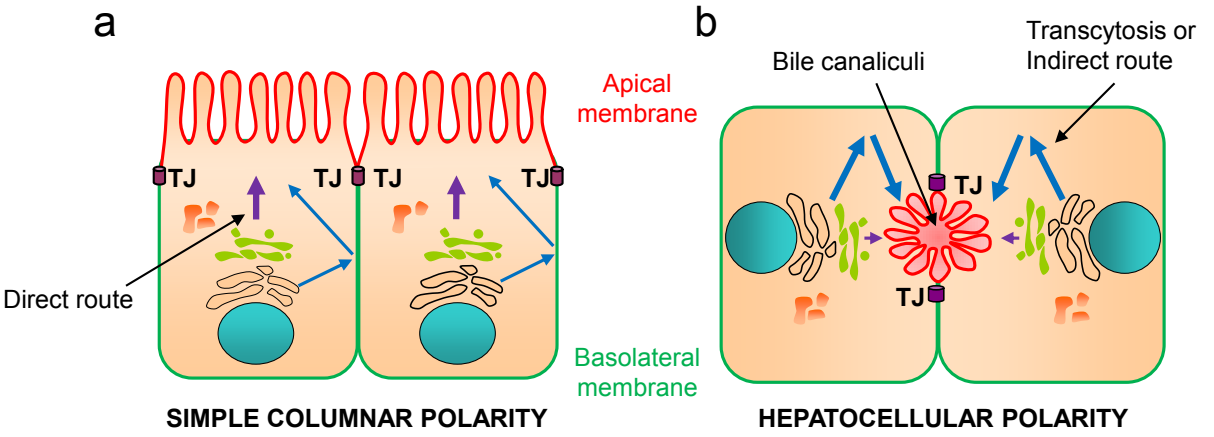

Figura 6. Polaridad celular epitelial.

Esquema representativo de células epiteliales con polaridad columnar **(a)** y hepatocitos **(b)** donde se distinguen el dominio basolateral (verde) y el dominio apical (rojo) separados por las uniones estrechas (TJ). En los hepatocitos el dominio apical forma un lumen lateral que corresponde al canalículo biliar. Las flechas moradas indican la ruta de transporte apical directo que predomina en las células con polaridad columnar, mientras que el transporte apical indirecto señalado por flechas azules abunda en los hepatocitos.

4.2. Mecanismos implicados en el establecimiento de la polaridad apicobasal del hepatocito

Los hepatocitos son células epiteliales polarizadas que difieren morfológicamente del resto de epitelios. Mientras que el dominio apical de las células epiteliales columnares forma un plano continúo en su vértice apical, los hepatocitos generan lúmenes apicales que forman canales entre células adyacentes denominados canalículos biliares (Ilustración6). Las uniones estrechas separan el dominio apical de la membrana basolateral, que queda expuesta al espacio de Disse e interacciona con los sinusoides y leucocitos extravasados. El mantenimiento de esta arquitectura polarizada resulta esencial para la correcta función del hepatocito; en su superficie basal intercambia metabolitos con la sangre, incluyendo el transporte de pequeñas moléculas a través de este dominio y la secreción de proteínas plasmáticas, mientras que en la membrana apical se secretan ácidos biliares y productos de detoxificación al lumen canalicular. La pérdida de polaridad es distintivo de disfunción, daño hepático y colestasis (Wang and Boyer, 2004).

Los principales mecanismos de polarización hepatocelulares incluyen el tráfico intracelular, las uniones intercelulares y componentes reguladores del citoesqueleto.

4.2.1. Transporte vesicular polarizado

A pesar de que los hepatocitos comparten muchas características en el tráfico polarizado de proteínas y lípidos a dominios específicos de membrana con el resto de células epiteliales, existen diferencias notorias en este aspecto. Mientras que en el modelo epiteliales con polaridad columnar, como en células derivadas de epitelios de riñon domina la ruta directa de transporte apical entre el Golgi y membrana, en los hepatocitos muchas proteínas de nueva síntesis siguen una ruta adicional transcitótica para llegar al dominio apical (Ilustración 6) (Weisz and Rodriguez-Boulan, 2009) (Zegers and Hoekstra, 1998) (Wang and Boyer, 2004).

Ruta directa

Únicamente se ha descrito un transporte apical directo en hepatocitos para los transportadores canaliculares tipo ABC (ATP-binding cassette) (Kipp and Arias, 2000). Dentro de esta familia, las proteínas se clasifican en función de las distintas sustancias que van a transportar hacia el lumen canalicular, incluyendo a MDR1 (*multidrug resistance protein*; cationes orgánicos), MDR2 (fosfolípidos), ABCB11/Bsep (*bile acid export pump*; ácidos biliares), MRP2 (*multidrug resistance associated protein*; ácidos biliares y aniones orgánicos) y ABCG5/8 (esteroles). Estos transportadores ciclan entre la membrana canalicular y un compartimento subapical de endosomas de reciclaje positivo para Rab11, y se dirigen directamente al dominio canalicular desde la TGN mediante un mecanismo dependiente de balsas lipídicas (Wakabayashi et al., 2004), (Wakabayashi et al., 2006) (Weisz and Rodriguez-Boulan, 2009) (Wang and Boyer, 2004).

Por otro lado, los hepatocitos secretan a la bilis abundantes cantidades de fosfolípidos y colesterol, por lo que el tráfico lipídico cobra especial relevancia en este tipo celular. A

pesar de que lípidos y proteínas pueden co-transportarse en las mismas vesículas hasta la membrana plasmática, en hepatocitos una parte sustancial de los lípidos totales, sobre todo esfingolípidos, se transporta directamente al dominio apical (Zegers and Hoekstra, 1998).

Ruta indirecta

En hepatocitos se ha descrito un transporte apical indirecto para proteínas transmembrana como dipeptidil peptidasa IV y el receptor polimérico de inmunoglobulina A (Bastaki et al., 2002) y proteínas unidas a grupos glicosilfosfatidilinositol (GPI) como 5'-nucleotidasa (Schell et al., 1992) y CD59 (de Marco et al., 2002). Entre la maquinaria que regula la transcitosis de proteínas apicales se encuentra la Rho GTPasa Cdc42, que actúa a través de su asociación con la formina INF-2 y la proteína residente en balsas lipídicas MAL-2 (Madrid et al., 2010). Las balsas lipídicas son dominios ordenados de membrana ricos en glicoesfingolípidos y colesterol e insolubles en detergentes no iónicos, característica que permite aislarlos bioquímicamente, y la inclusión de proteínas en balsas lipídicas constituye una señal de transporte apical en hepatocitos. La familia de proteínas MAL emerge como maquinaria clave en la regulación de estos dominios ordenados de membrana, y del transporte polarizado en diferentes epitelios (Puertollano et al., 1999) (Martin-Belmonte et al., 2000).

Mecanismos reguladores del transporte intracelular polarizado en hepatocitos

El tráfico de esfingolípidos a la membrana canalicular se encuentra regulado por las kinasas PKC y PKA, y modificaciones en este transporte se correlacionan con cambios en la polaridad hepatocelular. De esta manera la activación de PKC con ésteres de forbol como PMA inhibe el transporte apical de lípidos por la ruta directa e indirecta, además de perturbar las uniones estrechas a tiempos más tardíos, lo cual se refleja en una alteración o completa desaparición de las estructuras canaliculares (Zegers and Hoekstra, 1997) (Kubitz et al., 2004) (Mee et al., 2009). Asimismo, la secreción biliar y el transporte vesicular apical en hepatocitos de rata se inhibe al estimular PKC (Corasanti et al., 1989) (Benedetti et al., 1994). Sin embargo, la activación de PKA promueve el transporte vesicular apical de lípidos y proteínas por ambas rutas, así como el aumento de "vacuolas canaliculares" en hepatocitos no polarizados. Como consecuencia los hepatocitos con actividad incrementada de PKA presentan mayor tamaño y número de lúmenes apicales además de una elevada síntesis de ácidos biliares (Zegers and Hoekstra, 1997). Los propios ácidos biliares, por otro lado, estimulan la adquisición de polaridad hepatocelular a través de la señalización por las kinasas LKB1(*Liver kinase B1*) y AMPK (*AMP-activated protein kinase*) (Fu et al., 2011), que son claves en la regulación del metabolismo celular en condiciones de depleción energética y suponen una unión molecular entre polaridad y el estado metabólico de la célula (Williams and Brenman, 2008)..

4.2.2. Uniones intercelulares

Entre los diferentes tipos de complejos multiproteicos que forman las uniones célula-célula, las uniones intercelulares estrechas son cruciales en hepatocitos porque separan el flujo biliar de la circulación sanguínea. Las uniones estrechas se componen de proteínas integrales de

membrana incluyendo a ocludina, la familia de las claudinas y las JAMs (*Junctional Adhesion Molecules*), que se asocian a proteínas que interaccionan con el citoesqueleto de actina como ZO-1 (*Zonula Occludens protein 1*) (Benedicto et al., 2008). Estas estructuras se encuentran reguladas por diversas citoquinas y factores de crecimiento (Kojima et al., 2009) y están implicadas en la formación de canalículos biliares y en conservar la separación entre los dominios apical y basolateral (Konopka et al., 2007) (Braiterman et al., 2008) (Kojima et al., 2009), por lo que resultan esenciales para el mantenimiento de la polaridad hepatocelular.

4.2.3. Proteínas reguladoras del citoesqueleto: Rho GTPasas

La familia de Rho GTPasas está compuesta por proteínas monoméricas con un tamaño aproximado de 20 kDa. La mayoría de las Rho GTPasas ciclan entre dos estados: uno activo unidas a nucleótidos de guanosina trifosfato (GTP) y otro inactivo unido a guanosina difosfato (GDP). Su actividad está regulada por 3 tipos de proteínas: GEF (*Guanosin nucleotide Exchange Factor*) que activa las Rho GTPasas intercambiando GDP por GTP, GAP (*GTPase-Activating Protein*) que favorece la hidrólisis del GTP y por tanto inactiva a las Rho-GTPasas, y GDI (*GDP-dissociation inhibitor*) que inhibe el intercambio de GDP por GTP, manteniéndolas en estado inactivo y localización citoplásmica. Las Rho GTPasas ejercen normalmente su función en la membrana plasmática, donde pueden anclarse debido a que se encuentran modificadas postraduccionalmente por prenilación.

En la especie humana están representadas por al menos 23 miembros, de las cuales Rac, Cdc42 y Rho son las mejor caracterizadas. La activación de RhoA, a través de su efector ROCK (*Rho Kinase*) que activa a Miosina-II ATPasa, promueve la formación de fibras de estrés y el ensamblaje/desensamblaje de las adhesiones focales. En el hepatocito poralizado inhibe la morfogénesis de lúmenes apicales mediada por la matriz extracelular (Herrema et al., 2006). Rac y Cdc42 median la polimerización de actina a través de la familia de activadores del complejo Arp2/3, WASP y WAVE (Ridley et al., 2003) y en células polarizadas contribuyen a la formación de las uniones intercelulares y a establecer polaridad apicobasal a través de diferentes efectores como el complejo de polaridad PAR.

Complejo de polaridad PAR

Los complejos de polaridad funcionan determinando puntos de referencia en la membrana plasmática que irán expandiéndose por el reclutamiento de proteínas específicas a estos lugares. El complejo de polaridad PAR está formado por Par3 (*Partition defective 3*), Par6 y una Proteína kinasa C atípica (aPKC), que incluye las isoformas PKCλ/τ y PKCξ que varía dependiendo del contexto celular. Este complejo controla numerosos aspectos de la polaridad celular, entre los que se incluye el establecimiento del eje de polaridad apicobasal y la formación del lumen en células epiteliales (Martin-Belmonte and Mostov, 2008). El complejo PAR es de especial interés ya que su activación por Rho GTPasas constituye la primera pista para el inicio de la señalización de polaridad. Las formas activas de Rac1 y cdc42 se unen a Par6 abrogando su efecto inhibitorio sobre aPKC (Garrard et al., 2003), a la que se encuentra constitutivamente asociada, siendo las distintas aPKCs los mayores efectores del complejo de polaridad. De esta manera, Rac1 activo a través de su GEF

Tiam1 controla la asociación y activación del complejo Par3/Par6/aPKC para inducir la biogénesis de las uniones estrechas y el establecimiento de la polaridad en células epiteliales (Mertens et al., 2006). Por otro lado, Cdc42 también regula la formación de la membrana apical y el lumen durante la morfogénesis epitelial localizando y activando a Par6/aPKC al dominio apical de células MDCK en cultivo 3D. (Martin-Belmonte et al., 2007).

4.2.4. Proteínas reguladoras del citoesqueleto: ERMs

Como ya se ha mencionado en apartados anteriores, las proteínas ezrina, radixina y moesina interconectan proteínas de membrana en la superficie celular con el citoesqueleto de actina subyacente, contribuyendo a la formación de diversas estructuras de membrana y a numerosas rutas de señalización celular. En células epiteliales se acumulan en los microvilli del dominio apical, y son fundamentales no solo para el anclaje y transporte de proteínas apicales sino también para las funciones fisiológicas que ocurren en este dominio (Fievet et al., 2007).

Inicialmente descritas por separado, las proteínas ERM se encuentran altamente conservadas a lo largo de la evolución y su expresión es ubicua y depende del órgano y del tipo celular. Las proteínas ERMs juegan papeles redundantes en muchos procesos celulares, aunque juegan funciones específicas en ciertos tipos celulares (Serrador et al., 1997). En hepatocitos la proteína ERM dominante es la radixina, que resulta esencial para el mantenimiento de su arquitectura polarizada. La radixina se distribuye en la membrana canalicular y es necesaria para la integridad de esta estructura y una correcta secreción biliar a través del transportador Mrp2 (Wang et al., 2006), con el cual interacciona a través de su dominio C-terminal (Kikuchi et al., 2002). Los ratones con expresión deficiente de radixina presentan un cuadro de hiperbilirrubinemia conjugada que recuerda al síndrome humano de “Dubin-Johnson”, cursando con daño hepático, alteración de la superficie canalicular, disminución de microvilli y deslocalización de Mrp2 de este dominio (Kikuchi et al., 2002). La ezrina hepática se ha detectado en patologías del hígado, sobre todo en hepatocellular carcinoma (Okamura et al., 2008) y hepatocitos en áreas cirróticas (Claperon et al., 2013), y ocasionalmente en hepatocitos sanos (Gilbert et al., 2012). A pesar de que las proteínas ERM parecen ser claves para la retención de algunas proteínas canaliculares, hasta ahora no se conoce en detalle cómo estas proteínas conectoras operan en la membrana sinusoidal.

5. POLARIDAD HEPATOCELULAR Y DAÑO HEPÁTICO

Como ya se ha mencionado anteriormente, existe una correlación robusta entre pérdida de polaridad hepatocelular y disfunción hepática. No sólo la pérdida de polaridad es una característica típica de la transformación oncogénica de los epitelios polarizados, incluidos los hepatomas (McCaffrey and Macara, 2011). Los hepatocitos dañados por trauma o infectados por virus de la hepatitis B y C, pierden también su polaridad apicobasal (Benedicto et al., 2008) (Benedicto et al., 2011) (Mee et al., 2010) (Shousha et al., 2004). Por ejemplo, el virus de la hepatitis C utiliza las proteínas de uniones estrechas claudina y ocludina como vía de entrada en la célula (Evans et al., 2007) (Ploss et al., 2009) (Benedicto et al., 2011), provocando la pérdida de polaridad de los hepatocitos infectados (Mee et al., 2010), lo cual hace que estas células sean a su vez más susceptibles a la entrada de nuevos virus (Mee et al., 2009). El análisis comparativo de marcadores canaliculares en biopsias de hígados con diferentes grados de cirrosis, hepatitis C y carcinoma hepático ha demostrado la pérdida de estas estructuras apicales en condiciones de daño hepático severo, mientras que en enfermedades que cursan con componente inflamatorio leve y fibrosis suave se preserva el marcaje canalicular (Shousha et al., 2004). Puesto que todas estas alteraciones requieren el reclutamiento de células inmunes al parénquima para combatir infecciones o regenerar el tejido, la pérdida de polaridad hepatocelular se correlaciona, además, con un aumento del infiltrado leucocitario hepático (Shousha et al., 2004) (Shetty et al., 2008).

OBJETIVOS

La arquitectura polarizada de los hepatocitos resulta esencial para su correcta función. La pérdida de polaridad hepatocelular es distintivo de disfunción y daño hepático y se correlaciona además con un aumento en la infiltración de leucocitos en el tejido. Esto nos ha llevado a preguntarnos si la polaridad apicobasal de los hepatocitos es capaz de regular la interacción entre las células del sistema inmune y las células hepáticas. Para responder a esta cuestión nos planteamos los siguientes objetivos:

1. Investigar si existe relación entre polaridad apicobasal y adhesión leucocitaria a células hepáticas.

2. Caracterizar el mecanismo molecular que regula la interacción entre células inmunes y hepatocitos.

3. Investigar la distribución de receptores de adhesión hepáticos in vivo en muestras de tejido de pacientes con hepatopatías de componente inflamatorio agudo y crónico.

MATERIALES Y MÉTODOS

1. MATERIALES

1.1. Anticuerpos

1.1.1. Anticuerpos primarios

Proteína	Anticuerpo	Especie	Referencia	Dilución WB	Dilución IF	Dilución IHQ
ICAM-1	anti-ICAM1	Ratón	R&D Systems	-	1:500	-
ICAM-1	anti-ICAM1	Conejo	Santa Cruz Biotechnology	1:1000	-	-
ICAM-1	anti-ICAM1	Ratón	Santa Cruz Biotechnology	-	-	1:1000
ICAM-1	anti-ICAM1	Rata	Santa Cruz Biotechnology	-	-	1:1000
ALCAM	PAIN s-15	Ratón	Dr. C. Cabañas (CBMSO, Madrid , España)	-	1:100	-
Mrp-2	H-17	Rata	Santa Cruz Biotechnology	-	1/200	-
ERK1/2	anti-ERK	Conejo	Santa Cruz Biotechnology	1:1000	-	-
Cdc42	anti-Cdc42	Ratón	BD Transduction Laboratories	1:1000	-	-
CD10	anti-CD10	Ratón	Dako	-	-	Ninguna
TfR	anti-TfR	Conejo	ZYMED	1:1000	-	-
ERM	anti-ERM	Conejo	Cell Signaling Technology	1:1000	-	-
P-ERM	anti-P-ERM	Conejo	Cell Signaling Technology	1:1000	1:500	-
Radixin	anti-Radixin	Conejo	Cell Signaling Technology	1:1000	1:200	-
Moesin	anti-Moesin	Conejo	Cell Signaling Technology			
Ezrina	anti-Ezrin	Ratón	BD Transduction Laboratories	1:1000	-	-
GFP	anti-GFP	Ratón	Sigma	1:500	1:500	-
CD59	MEM 43/5	Ratón	Dr. V. Horejsi (Institute of Molecular Genetics, Prague, Czech Republic)	-	1:500	-

Los anticuerpos primarios empleados en inmunodetección (WB) y en inmunofluorescencia (IF), se resumen en la siguiente tabla:

Anticuerpo	Especie	Referencia	Dilución WB	Dilución IF	Dilución IHQ
Anti-IgGs ratón HRP	Cabra	Jackson Immuno-research	1:5000		-
Anti-IgGs conejo HRP	Cabra	GE Healthcare	1:5000		-

Anti-IgGs ratón 488-555	Burro	Invitrogen	-	1:500	-
Anti-IgGs conejo 488-555	Burro	Invitrogen	-	1:500	-
Anti-IgGs ratón 647	Burro	Invitrogen	-	1:200	-
Anti-IgGs conejo 647	Burro	Invitrogen	-	1:200	-
Anti-IgGs rata 488-555	Burro	Invitrogen	-	1:500	-
Faloidina-TRICT	-	Invitrogen	-	1:4000	-
Faloidina-647	-	Invitrogen	-	1:1000	-
Anti-IgGs ratón Biotinilado	Conejo	Dako	-	-	1:250
Anti-IgGs rata Biotinilado	Conejo	Dako	-	-	1:80

1.1.2. Anticuerpos secundarios

Los anticuerpos secundarios utilizados en inmunodetección (WB) y en inmunofluorescencia (IF), se resumen en la siguiente tabla:

1.2. Reactivos

El medio de montaje Fluoromont fue adquirido a Southern Biotechonology Associates Inc. (Birmingham, AL). El antibitico geneticina se obtuvo de Gibco-Life Technologies. La Sulfo-NHS-biotina y la neutravidina-agarosa fueron adquiridas a Thermo-Scientific, y la resina glutathione-sepharose a GE Healthcare. El Dibutiril-AMPcíclico (dcAMP), el Forbol 12-miristato 13-acetato (PMA) y el inhibidor PD169316 se obtuvieron de Sigma-Aldrich y el pseudosubs-

Plásmido	Expresión	Vector	Epítopo	Referencia
ICAM-1-GFP	ICAM-1	pEGFP-N1	GFP	Dr. F. Sánchez-Madrid (Hospital de la Princesa, Madrid, Spain).
paICAM-1-GFP	ICAM-1-GFP fotoactivable	pEGFP-N1	paGFP	Generado en el laboratorio
ICAM-1-Act-GFP	Dominios TM y extracelulares de ICAM-1	pEGFP-N1	GFP	Dr. Chang-Duk Jun (Gwangju Institute of Science and Technology, Korea)
GFP-ICAM-1-Δext	Dominios TM y citoplásmico de ICAM-1	pEGFP-C1	GFP	Generado en el laboratorio
GST-ICAM-1-tail	Dominio citoplásmico de ICAM-1	pGEX-2T	GST	Prof. Anne Ridley (Kings College, London, U.K.)
GST-ICAM-1 K>L	Dominio citoplásmico de ICAM-1 con la mutación K>L de las lisinas 508, 510 y 511.	pGEX-2T	GST	Prof. Anne Ridley (Kings College, London, U.K.)

RDX-YFP	Radixina	pReceiver-M16	YFP	Dr. F. Valderrama (St. George University, London, UK)
Ezrin-GFP	Ezrina	pEGFP-N1	GFP	Dra. Monique Arpin (Institut Curie-Unité Mixte de Recherche Centre National de la Recherche Scientifique, Paris, France)
EzrinTD-GFP	EzrinaT567D	pEGFP-N1	GFP	Dra. Monique Arpin (Institut Curie-Unité Mixte de Recherche Centre National de la Recherche Scientifique, Paris, France)
GFP	GFP	pEGP-N1	-	Clontech
YFP	YFP	pcDNA3-YFP	-	Addgene
Actin-cherry	Cherry	pmCherry	-	Ann Wheeler (Imperial College, London, UK)

trato de aPKC y las sondas Calceína-AM y CMTMR de Invitrogen. Los inhibidores PKCGö e Y-27632 fueron adquiridos a Calbiochem y el TNF a R&D.

1.3. Plásmidos

1.4. Oligonucleótidos

Nombre	Secuencia 5'-3'
GFP-ICAM-1-Δext 5'	GGGCCCGAATTCTGGCGGCTCCCCCCGGTATGAGATTGTC
GFP-ICAM-1-Δext 3'	CCCGGGGGATCCTCAGGGAGGCGTGGCTTGTGTGTT

Los oligonucleótidos utilizados para los clonajes de este trabajo fueron sintetizados por Isogen mientras que los oligos para los experimentos de interferencia (siRNA) fueron adquiridos a Dharmacon.

Nombre	Secuencia 5'-3'
siICAM-1 (1)	GAAGAUAGCCAACCAAUGU
si ICAM-1 (2)	GAACAGAGUGGAAGACAUAUU
si Cdc42 (1)	GAUUACGACCGCUGAGUUAUU
si Cdc42 (2)	GAUGACCCCUCUACUAUUGUU
Si Control (C) (Dharmacon)	-

1.4.1. Oligonucleótidos

1.4.2. siRNA

1.5. Enzimas

1.5.1. De restricción

Para el clonaje de las construcciones de DNA generadas durante esta tesis se emplearon las siguientes enzimas de restricción: BamHI y EcoRI.

1.5.2. Polimerasas

La polimerasa termoestable empleada en los clonajes fue la Taq DNA polimerasa de Thermus aquaticus (Promega). Asimismo, se utilizó la DNA ligasa del fago T4 de Fermentas para la ligación de los fragmentos de DNA y vectores.

2. MÉTODOS

2.1. Líneas celulares, cultivos primarios y condiciones de cultivo

HepG2 (línea epitelial de hígado humano)

Hepatocitos primarios humanos

PBLs (linfocitos T de sangre periférica)

HUVECs (células endoteliales humanas provenientes de la vena de cordón umbilical))

La línea celular HepG2 se creció en medio DMEM suplementado con glutamina al 1%, suero fetal de ternera al 5% (Sigma-Aldrich, St. Louis, MO), 50U/ml penicilina y estreptomicina 50 U/ml (Gibco-BRL, Gaithersburg, MD). Los hepatocitos primarios fueron crecidos en sándwiches de colágeno con medio HCM (LONZA) durante 5 días para inducir su polarización como se ha descrito previamente (Dunn et al., 1992) (Tolosa et al., 2011) Los linfocitos T humanos se aislaron de sangre procedente de un sujeto sano mediante gradiente de Ficoll, se estimularon con 0.5% phytohemaglutinina y durante 48h y posteriormente se cultivaron con IL-2 durante al menos 7-12 días. Los cultivos primarios de células endoteliales provenientes de la vena de cordón umbilical fueron cultivados en medio EGM-2 de Lonza.

Todos los cultivos se mantuvieron en incubadores a 37ºC, con CO2 al 5% y 95% de humedad.

2.2. Tejidos

- Tejidos humanos: En colaboración con el Hospital General de Asturias se analizaron muestras de tejido que provenían de tres casos de rechazo hepático post-transplante, tres casos de hepatitis B y tres de hepatitis C, así como de cuatro donantes sanos utilizados como control.

- Tejidos murinos: Las muestras de tejido hepático procedentes de modelos murinos de daño hepático fulminante fueron proporcionadas por el laboratorio del Prof. Prieto (CIMA, Universidad de Navarra). Se analizaron muestras de animales tratados con ConA durante 6, 12, 24 y 48 horas y con AdCD40L durante 96 horas (Fernandez-Ruiz et al., 2011).

2.3. Clonajes

El clonaje de la construcción que expresa GFP fusionado al fragmento transmembrana y citoplásmico de ICAM-1 se llevó a cabo mediante la amplificación de fragmentos de DNA por PCR en condiciones estándar utilizando los oligos GFP-ICAM-1-Δext 5´y GFP-ICAM-1-Δext 3', que contienen, además de las secuencias específicas, las dianas para EcoRI y BamHI, respectivamente. Como molde se utilizó el DNA de ICAM-1-GFP.

El fragmento obtenido se clonó en el vector de expresión pEGP-C1 (Clontech) obteniéndose la construcción GFP-ICAM-1-Δext.

2.4. Transfección de DNA y generación de clones estables

La transfección en células HepG2 de los vectores de expresión anteriormente descritos se realizó por electroporación con un electroporador Electro Cell Manipulator 600 (BTX). Las células se tripsinizaron, centrifugaron y resuspendieron en un volumen final de 200 l de medio DMEM suplementado con suero fetal bovino 10% (v/v), glutamina 1% (p/v), penicilina 100 U/ml y estreptomicina 100 g/ml, 10 mM HEPES (Sigma) y 37,5 mM NaCl. Posteriormente se mezclaron con 1-5 g del DNA plasmídico a transfectar y con 20 g de esperma de salmón (Sigma-Aldrich). Tras un pulso eléctrico de 200V, 480 y 950 mF, las células se volvieron a sembrar en placas y se procesaron a las 24 ó 48 horas posteriores a la transfección.

Para la expresión estable de proteínas exógenas, las células transfectadas fueron seleccionadas con geneticina G-418 a una concentración de 0.5mg/ml durante al menos 4 semanas. Los clones resistentes al antibiótico y positivos para la expresión de la proteína en cada caso fueron aislados y analizados por inmunotransferencia o inmunofluorescencia con anticuerpos específicos. Después de varios pases en medio sin antibiótico más del 90% de las células mantuvieron la expresión del producto exógeno.

2.5. Transfección de siRNA

Las transfecciones de oligonucleótidos pequeños de interferencia de ARN "siRNA" complementario al ARNm de la proteína diana se llevaron a cabo con oligofectamina 2000 (Invitrogen), según instrucciones del proveedor. 24 horas después de la transfección las células fueron tripsinizadas y sembradas en placas de cultivo o cubres de vidrio. 48 horas más tarde se procedió a realizar la lisis celular o los ensayos de inmunofluorescencia, biotinilación o adhesión linfocitaria.

2.6. Obtención de extractos proteicos

Los extractos totales de proteínas procedentes de cultivos celulares se obtuvieron tras el lavado de las células dos veces con PBS (solución salina tamponada con fosfato, 8 mM Na2HPO4, 1,5 mM KH2PO4 pH7,2; 137 mM NaCl y 2,7 mM KCl) y su lisis con solución de Laemmli

(Laemmli, 1970). Posteriormente, los extractos se sonicaron durante 1 minuto para romper el ADN celular.

2.7. Electroforesis de proteínas (SDS-PAGE), electrotransferencia e inmunodetección (Western-Blot)

Los extractos proteicos preparados en solución de Laemmli se hirvieron durante 5 minutos antes de analizarlos en condiciones reductoras en geles de poliacrilamida (SDS-PAGE) adaptados al sistema de electroforesis Mini-PROTEAN II (Bio-Rad). Como marcadores se utilizó la mezcla de proteínas de pesos moleculares conocidos comprendidos entre 10 y 250 kDa, Dual Color (Bio-Rad). Los geles se corrieron a un voltaje constante de 120 V durante 1 hora, en una solución tamponada con 25 mM Tris, 130 mM glicina y SDS 0,1% (p/v).

Las proteínas separadas en geles SDS-PAGE se transfirieron a una membrana de Immobilon – PVDF (Millipore) en una solución de Tris-Glicina pH 8,6 y MeOH 20% usando el sistema Mini Trans-Blot (Bio-Rad). Las transferencias se realizaron durante 1 hora a un voltaje de 100V. Las membranas se bloquearon con leche en polvo desnatada al 10% (p/v) en PBS con Tween-20 al 0,05% (v/v), durante 1 hora. Se incubaron con el anticuerpo primario durante la noche a 4ºC, y después se lavaron durante 10 minutos tres veces consecutivas en PBS con Tween-20 al 0,05% (v/v). Para la inmunodetección de los complejos antígeno-anticuerpo sobre las membranas, se usaron anticuerpos secundarios acoplados a peroxidasa (HRP). Las membranas se incubaron durante 60 minutos con los anticuerpos secundarios y se lavaron posteriormente 3 veces durante 20 minutos en PBS Tween-20 al 0,05%. La detección de las proteínas se realizó mediante la reacción quimio-luminiscente catalizada por la peroxidasa de rábano unida a los anticuerpos secundarios usando los reactivos ECL (Enhanced ChemiLuminiscence) de Amersham Pharmacia Biotech y película fotográfica de Kodak.

2.8. Modulación de la polaridad celular en HepG2

Para reducir la polaridad en células HepG2 se utilizaron diversas estrategias; además de silenciar la expresión de Cdc42, se trataron las células con PMA (100nM) durante 2 horas o con PS-aPKC (40 g/mL) durante 18 horas. El grado de polaridad en células HepG2 se aumentó mediante el tratamiento con dcAMP (100 M) durante 2 horas.

Para realizar el análisis morfológico y cuantificación del número de canalículos biliares (BC), las células HepG2 o hepatocitos primarios fueron teñidas para F-actina y CD59.

2.9. Ensayos de adhesión

Células HepG2 tratadas o no con siRNA especificos y crecidas sobre placas de cultivo M24 (2.5x105/pocillo) durante 48 horas fueron co-cultivadas durante 30 minutos con linfocitos periféricos (PBLs) que habían sido previamente marcados con una sonda fluorescente verde, calcein-AM 0,5 M, durante 30 minutos. Las HepG2 que habían sido sometidas a trata-

mientos se lavaron extensivamente antes de añandir los linfocitos (3-4x105/pocillo). Tras la incubación con los PBLs, las células HepG2 fueron lavadas tres veces con medio de cultivo y una última con PBS completo. La intensidad de fluorescencia se midió en un lector de placas (FLUOstar OPTIMA, BMG Labtech) provisto de los filtros para la emisión de 480 nm. Alternativamente los ensayos de adhesión se realizaron también usando un microscopio confocal para contar los PBLs teñidos con calceína o CMTMR y adheridos a células HepG2.

2.10. Inmunohistoquímica

Secciones de tejido de 4 m de grosor fijadas con formalina y embebidas en parafina fueron desparafinadas en xileno y rehidratadas en una batería de soluciones de alcohol de porcentaje decreciente. Tras a inhibir la peroxidasa endógena (peróxido de hidrógeno al 3% (v/v) durante 10 minutos) y desenmascarar los epítopos (hirviendo en tampón citrato 10mM, pH 6 durante 10-15 minutos), se bloquearon las muestras con suero (de la especie animal del anticuerpo secundario) al 2.5% en PBS durante 30 minutos. Posteriormente las muestras se incubaron con el anticuerpo primario durante una hora a temperatura ambiente en una cámara húmeda y seguidamente se lavaron con PBS y se incubaron con el anticuerpo secundario biotinilado correspondiente durante 30 minutos. Tras volver a lavar se incubó el complejo estreptavidina-biotina-peroxidasa (VECTASTAIN ABC Reagent, Vector Laboratories) durante otros 30 minutos y finalmente las proteínas marcadas se visualizaron utilizando DAB (Dako). Para la contratación se utilizó hematoxilina de Mayer. En cada experimento se llevó a cabo un control negativo para asegurar la especificidad de los anticuerpos incubando las muestras únicamente con el anticuerpo secundario. En este caso no se detectó tinción alguna.

2.11. Inmunofluorescencia y microscopía confocal

Las células se crecieron sobre cubreobjetos en placas de pocillos de fondo plano (Costar Corp., Cambridge, MA) y se fijaron utilizando distintos protocolos en función de los requerimientos del anticuerpo primario usado en la IF. Se emplearon 3 tipos de fijaciones:

- Formalina: Las células se incubaron en una disolución de formalina (Formaldehído al 37%; Sigma-Aldrich) al 10% (v/v) en PBS durante 20 minutos a temperatura ambiente. El exceso de formaldehído se bloqueó incubando 10 minutos con una solución 10 mM de glicina en PBS. Las células fijadas se permeabilizaron posteriormente con Tritón X-100, al 0,2% (v/v) en PBS.

- Metanol: Las células se incubaron durante 2 minutos en metanol puro (MERCK) a -20ºC.

- Ácido tricloroacético (TCA): Las células se incubaron con TCA durante 10 minutos a 4ºC y posteriormente se permeabilizaron con Tritón X-100, al 0,2% (v/v) en PBS.

Tras la fijación, las células se incubaron en una solución de bloqueo de PBS 3%BSA durante 15 minutos a temperatura ambiente. A continuación, se incubaron los cubres con los anticuer-

pos primarios y secundarios apropiados en la misma solución de bloqueo a distintos tiempos y diferentes diluciones según el anticuerpo utilizado. Finalmente se prepararon las muestras con el medio de montaje Fluoromont. Los controles para asegurar la especificidad de la inmunofluorescencia se realizaron incubando las células solamente con el primer anticuerpo o bien omitiendo el mismo e incubando únicamente con el secundario.

Las preparaciones se analizaron en un microscopio confocal LSM 510 acoplado a un microscopio invertido de Zeiss modelo Axiovert 2000. Todas las imágenes obtenidas fueron procesadas empleando los programas LSM 5 Image Browser, Adobe Photoshop 7.0, Adobe Illustrator 10 y cuantificadas con el programa FIJI.

El Índice Basolateral (Basolateral Index) de las distintas proteínas se calculó midiendo el ratio entre la intensidad de fluorescencia en áreas basolaterales y en zonas canaliculares y normalizando frente al ratio obtenido para F-actina. Se cuantificó una media de 40 células polarizadas por experiemento.

2.12. Ensayos de entrecruzamiento (*crosslinking*) y análisis de colocalización subcelular.

Células HepG2 crecidas sobre cubreobjetos fueron incubadas con anti-ICAM-1 monoclonal (0,5 g/ml) durante 30 minutos a 4ºC. Posteriormente las células se lavaron 3 veces con medio y el crosslinking se llevó a cabo añadiendo el anticuerpo secundario Alexa-633 (1mg/ml) durante 45 minutos a 37ºC (Ilustración 7). Finalmente las células se volvieron a lavar, se fijaron y se procedió a marcar las proteínas de interés por inmunofluorescencia.

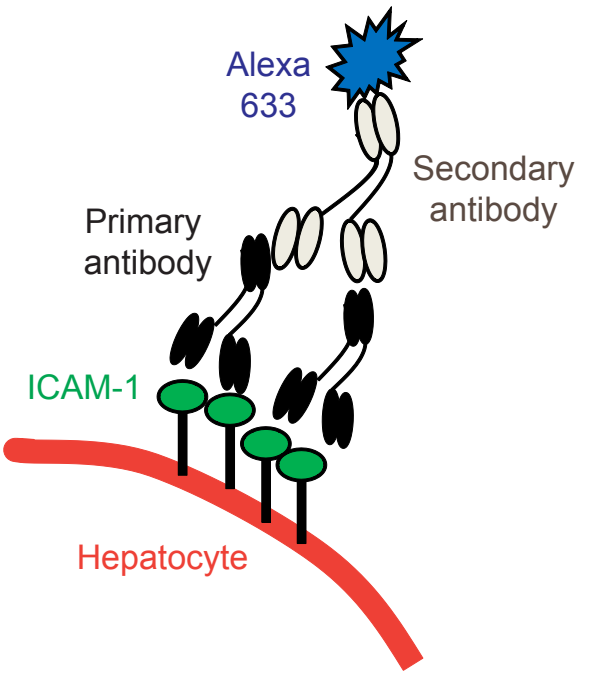

Ilustración 7. Esquema ilustrativo del entrecruzamiento (crosslinking) de ICAM-1.

El anticuerpo primario específico contra el receptor ICAM-1 es a su vez reconocido por un anticuerpo secundario fluorescente, causando el agrupamiento de ICAM-1 en acúmulos en la membrana plasmática hepatocitaria.

Para cuantificar la colocalización de los acúmulos de ICAM-1 con las proteínas de interés se tomaron 10 imágenes confocales por cubre en tres experimentos diferentes. Se cuantificaron entre 2 y 4 células por imagen. Se utilizó el programa FIJI (National Institutes of Health, Bethesda, MA) para hallar el coeficiente de colocalización de Manders en áreas que presentasen acúmulos de ICAM-1 una vez restado el fondo.

2.13. Ensayos de biotinilación

Se aplicaron distintos tratamientos sobre células HepG2 para modular su polaridad y acto seguido se lavaron con PBS Ca++/Mg++ y se incubaron durante 20 minutos con sulfo-NHS-biotina (250 g/ml). Las células se volvieron a lavar y la biotina no unida se bloqueó mediante la incubación con DMEM al 10% (v/v) de suero. La lisis de las células marcadas con biotina se realizó con Tx100 al 1% en TNE (20 mM Tris-HCL pH 8.0, 150mM NaCl, 2mM EDTA) más PMSF 0,1mM, inhibidores de proteasas (Leupeptina, Pepstatina y Aprotinina 1ug/mL), e inhibidores de fosfatasas (B-glicerolfosfato 10mM, NaF 5mM, NaVO4 10mM, caliculina 0,3ng/ul), y posteriormente se realizó un pull-down incubando los lisados una hora con neutravidina-agarosa. Todo el procedimiento se realizó a 4ºC. Finalmente la resina se lavó con tampón de lisis y las proteínas unidas se eluyeron añadiendo tampón de carga Laemmli, centrifugando 5 minutos a 12000 rpm e hirviendo las muestras. Las proteínas se separaron por SDS-PAGE y se detectaron con anticuerpos específicos.

2.14. Ensayos de asociación de proteínas por *pull-down*

Las construcciones GST-ICAM-1-tail y GST-ICAM-1 K>L fueron generadas en el laboratorio de la Dra. Anne Ridley (Kings College, London, U.K.).

Para purificar las proteínas de fusión se indujo su expresión con IPTG en bacterias Escherichia coli previamente transformadas con las construcciones antes mencionadas, que se encuentran bajo el control del promotor lac. Posteriormente las bacterias se lisaron, se solubilizó la proteína de fusión por centrifugación y se unió a la resina glutathione-sepharose. La cantidad de proteína de fusión purificada se cuantificó a través de un gel de poliacrilamida extrapolando el valor a una curva de diluciones de BSA de concentración conocida (ver resultados, Fig. 19).

Después, células HepG2 fueron lisadas en tampón de lisis (20 mM Tris-HCL pH 8.0, 150mM NaCl, 1% NP-40, 10% glicerol, inhibidores de proteasas 1ug/mL, 0,1mM PMSF, B-glicerolfosfato 10mM, NaF 5mM, NaVO4 10mM) enfriado en hielo y los lisados aclarados por centrifugación para separar el sobrenadante postnuclear (PNS). Se utilizó una centésima parte de este sobrenadante para detectar la proteína soluble y el resto del volumen se incubó con 30-50 ug de proteínas recombinantes GST-ICAM-1tail o GST-ICAM-1 K>L conjugadas a 30 ul de la resina glutatión-sepharosa durante una hora a 4ºC. Posteriormente la resina se lavó a con tampón de lisis y las proteínas unidas se eluyeron añadiendo tampón de carga Laemmli, centrifugando 5 minutos a 12000 rpm e hirviendo las muestras. Las proteínas se separaron por SDS-PAGE y se detectaron con anticuerpos específicos.

2.15. Microscopía *time-lapse* ó Microscopía de células vivas.

2.15.1. Ensayos de fotoactivación

Durante las últimas décadas los avances generados en el campo de la microscopía de fluorescencia han permitido a los biólogos celulares estudiar en profundidad el funcionamiento interno de células y tejidos. El clonaje de GFP (Green Fluorescent Protein) hace casi 20 años (Chalfie et al., 1994) revolucionó el campo de la biología celular permitiendo la visualización de una amplia variedad de mecanismos moleculares en células vivas. La utilización de proteínas fluorescentes fusionadas a la proteína de interés permite visualizar la localización subcelular de la molécula, mientras que su filmación por técnicas de videomicroscopía permite observar el movimiento de la estructura o del orgánulo dónde dicha proteína se localiza (Muzzey and van Oudenaarden, 2009). Sin embargo, para estudiar de manera precisa la dinámica molecular de proteínas a nivel celular se necesita marcar de forma exclusiva una subpoblación de moléculas en un área específica. La utilización de proteínas fotoactivables no sólo permite alcanzar estos objetivos, sino que además presenta amplias ventajas frente a otras técnicas comúnmente utilizadas para el análisis de la dinámaica molecular de proteínas como el FRAP (Fluorescence Recovery After Photobleaching) (Snapp et al., 2003) El marcaje de una población de moléculas a través de la fotoactivación mejora la señal óptica obtenida y evita además que las moléculas de nueva síntesis interfieran con los resultados, ya que éstas no son inicialmente fluorescentes como ocurre en el FRAP (Lippincott-Schwartz et al., 2003).

En concreto en este trabajo hemos utilizado la proteína GFP fotoactivable (paGFP) fusionada al extremo c-terminal del receptor ICAM-1 para estudiar su dinámica en células HepG2. El mutante paGFP resulta de la sustitución de un residuo de treonina en la posición 203 de la molécula de GFP por histidina (T203H) (Patterson and Lippincott-Schwartz, 2002). La activación de la molécula con un haz de luz ultravioleta (400 nm) provoca el cambio irreversible desde su forma neutra, no fluorescente bajo iluminación de 488 nm, a la forma aniónica que emite brillantemente a esta longitud de onda (Ilustración 8). La luz ultravioleta induce la descarboxilación de un residuo de glutámico (Glu222) que, junto con la sustitución de T203 por histidina, es responsable de un cambio en el estado de protonación del cromóforo que resulta en un incremento de 100 veces en la intensidad de fluorescencia observada bajo la excitación de luz de 488 nm respecto a su forma nativa (Henderson et al., 2009). Por todo ello, la fotoactivación resulta una técnica idónea para el análisis de la dinámica de proteínas a nivel subcelular en el tiempo y el espacio.

En los expreimentos de fotoactivación desarrollados durante este trabajo, aproximadamente 2.5x105 HepG2 expresando establemente paICAM-1-GFP se sembraron en placas p35 provistas de un cubre de cristal (MatTek, Ashland, MA, U.S.A.) y se crecieron durante 2 días. Para la filmación las células se incubaron con medio libre de rojo fenol HBSS (Hank's Balanced Salt Solution) al 0,5% (v/v) de suero y HEPES 20mM. La grabación se realizó con un objetivo de inmersión en agua 63x (Plan Apochromat; NA 1) en un microscopio invertido (AxioObserver) equipado con un sistema de escaneo confocal (LSM10; Zeiss) y provisto de una cámara cerrada con temperatura constante (37ºC). Para fotoactivar la proteína paICAM-1-GFP en el área de interés se utilizó un láser de longitud de onda de 405-nm.

Para los vídeos cortos (hasta 10 minutos de duración total), la fotoactivación se realizó usando un único pulso de luz láser a una potencia del 40%, seguido de la adquisición de imágenes confocales cada 3 segundos.

Para los vídeos largos (hasta 120 minutos), la fotoactivación en los dominios basolateral o apical se realizó utilizando varios pulsos de luz láser a una potencia del 40% o un único pulso a una potencia del 20% respectivamente, seguido de la toma de 2-3 imágenes a máxima velocidad para después adquirir las imágenes cada 10 minutos durante 1-2 horas.

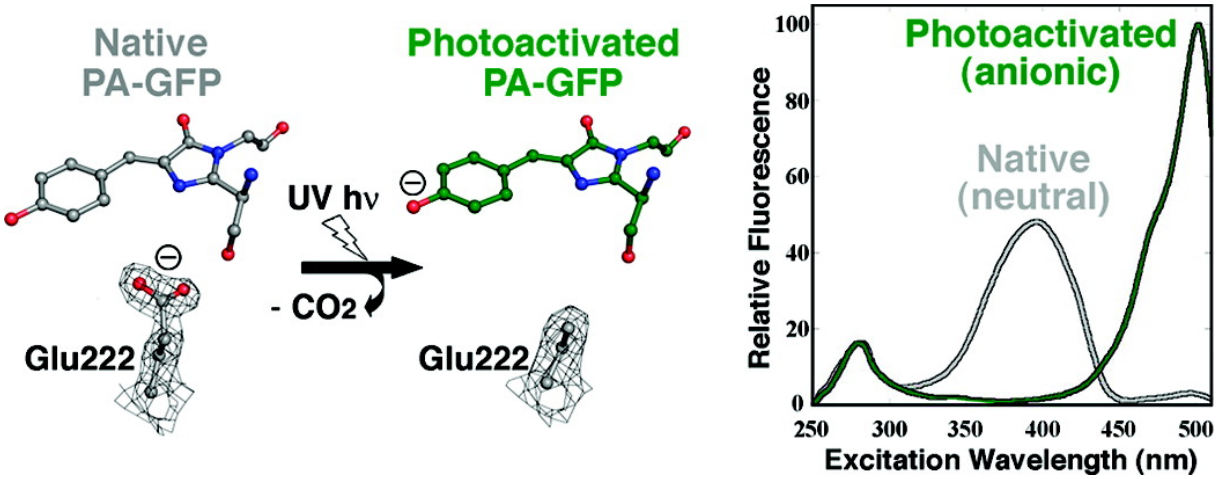

Ilustración 8. Mecanismo de fotoactivación de la proteína paGFP.

La activación por luz ultravioleta (UV) de la molécula de paGFP en su estado nativo provoca la descarboxilación del residuo Glu222 y un desplazamiento en el equilibrio del cromóforo hacia la forma aniónica. Mientras que la forma neutra de la molécula no emite fluorescencia al ser excitada con luz de una longitud de onda de 488 nm, lo cual se debe a la sustitución del residuo de treonina 203 por histidina, la conformación fotoactivada presenta un incremento de 100 veces en la intensidad de fluorescencia emitida respecto a la forma nativa. Adaptado de Henderson et al, J. Am. Chem. Soc. 2009.

En cualquier caso se adquirieron dos imágenes antes de la fotoactivación para poder restar el valor medio de su intensidad de fluorescencia como fondo al resto de las imágenes obtenidas después de la fotoactivación. El análisis de imagen se realizó con los programas ZEN (2010) y FIJI y se normalizó el valor de intensidad de fluorescencia de cada imagen a la intensidad obtenida en la primera imagen grabada después de la fotoactivación.

2.15.2. Vídeo-microscopía de las interacciones entre linfocitos T y células HepG2

1.5x105 HepG2 expresando establemente ICAM-1-GFP fueron sembradas en placas p35 provistas de un cubre de cristal. 48 horas después las células fueron tratadas durante 2 horas con PMA, lavadas extensivamente e incubadas con medio libre de rojo fenol HBSS (Hank's Balanced Salt Solution) al 0,5% (v/v) de suero y HEPES 20mM. Acto seguido se añadieron 5x105 PBLs teñidos con la sonda CMTMR por placa. Para la grabación se utilizó un objetivo

de inmersión en aceite 63x (Plan Apochromat; NA 1.4) en un microscopio invertido AF6000 LX (LEICA) provisto de una cámara cerrada con temperatura y humedad constantes (37ºC y 5% CO2). Las células fueron grabadas durante al menos una hora a intervalos de 1 minuto. Posteriormente, los videos fueron procesados utilizando el software FIJI.

2.16. Microscopía electrónica de barrido

Las células crecidas sobre cubreobjetos y sometidas o no al tratamiento con PMA se fijaron en una solución de glutaraldehído al 2% y paraformaldehído al 4% en tampón fosfato 0.1M pH 7.4 durante 2 horas a temperatura ambiente. Después de lavar extensivamente, las muestras fueron post-fijadas con tetraóxido de osmio al 1% durante 60 minutos a 4ºC, se lavaron con agua y se deshidrataron en una batería de alcoholes de graduación ascendiente (de 50 a 100%). Las células deshidratadas se secaron a punto crítico (Balzers Union, Balzers, Liechenstein) y se recubrieron con 7 nm de oro usando un Hummer X23 sputter coater (Anatech Ltd., Springfield, VA). Las muestras se analizaron con un microscopio electrónico de barrido con emisión de campo operando a 10 kV (JSM-6335-F, JEOL, Japan). Las imágenes fueron obtenidas con una cámara digital CCD.

RESULTADOS

1. LA POLARIDAD HEPATOCELULAR REGULA LA ADHESIÓN LINFOCITARIA A TRAVÉS DEL RECEPTOR DE ADHESIÓN ICAM-1

La pérdida patológica de polaridad en el parénquima hepático se correlaciona con un aumento en la infiltración de leucocitos en el tejido (Shousha et al., 2004) (Shetty et al., 2008). Esto nos ha llevado a preguntarnos si la polaridad apicobasal de los hepatocitos regula la interacción entre las células del sistema inmune y las células hepáticas.

Para el estudio de la polaridad hepatocelular en humanos se pueden utilizar diversos modelos in vitro de cultivos celulares (Zegers and Hoekstra, 1998) (Decaens et al., 2008). La extracción de hepatocitos primarios provoca la pérdida de su polaridad apicobasal, pero su cultivo entre dos capas de matriz extracelular (colágeno) consigue que vuelvan a adquirir un fenotipo polarizado en algunos días. Sin embargo, este modelo presenta las desventajas propias del trabajo con células primarias, ya que permite su utilización durante cortos períodos de tiempo y existe variabilidad entre células de diferentes individuos. La utilización de matriz extracelular además, añade mayor dificultad para discriminar entre los fenómenos de adhesión célula-célula y la adhesión célula-sustrato durante ensayos de adhesión. Para el estudio de la polaridad apicobasal hepática resulta frecuente el empleo de líneas celulares inmortalizadas que expongan un fenotipo polarizado similar al que ocurre en las células primarias en ambientes tridimensionales. Durante este trabajo se ha utilizado principalmente como modelo las células HepG2, una línea celular de hepatoma altamente diferenciada que conserva propiedades básicas de polarización de hepatocitos primarios sin necesidad de crecer en matrices tridimensionales, constituyendo así un modelo ampliamente aceptado para la investigación de la polaridad hepatocelular (de Marco et al., 2002) (Madrid et al., 2010) (van et al., 1997).

1.1. La pérdida de polaridad apicobasal aumenta la adhesión de linfocitos a células HepG2

Las células HepG2 crecen formando colonias tridimensionales con lúmenes esféricos o tubulares entre dos o más células que se encuentran sellados por uniones estrechas y se asemejan a los conductos biliares que existen entre los hepatocitos in vivo. Dependiendo del número de pases, entre un 40 y un 60% de células presentan una morfología polarizada. Como se ha mencionado, la Rho GTPasa Cdc42 resulta clave para la regulación de la polaridad celular ya que controla el tráfico vesicular polarizado, las uniones intercelulares y rutas de señalización encargadas de mantener un fenotipo polarizado (Madrid et al., 2010; Martin-Belmonte et al., 2007; Martin-Belmonte and Perez-Moreno, 2012). Como primera estrategia para alterar la polaridad, silenciamos Cdc42 con dos siRNAs distintos que redujeron significativamente la

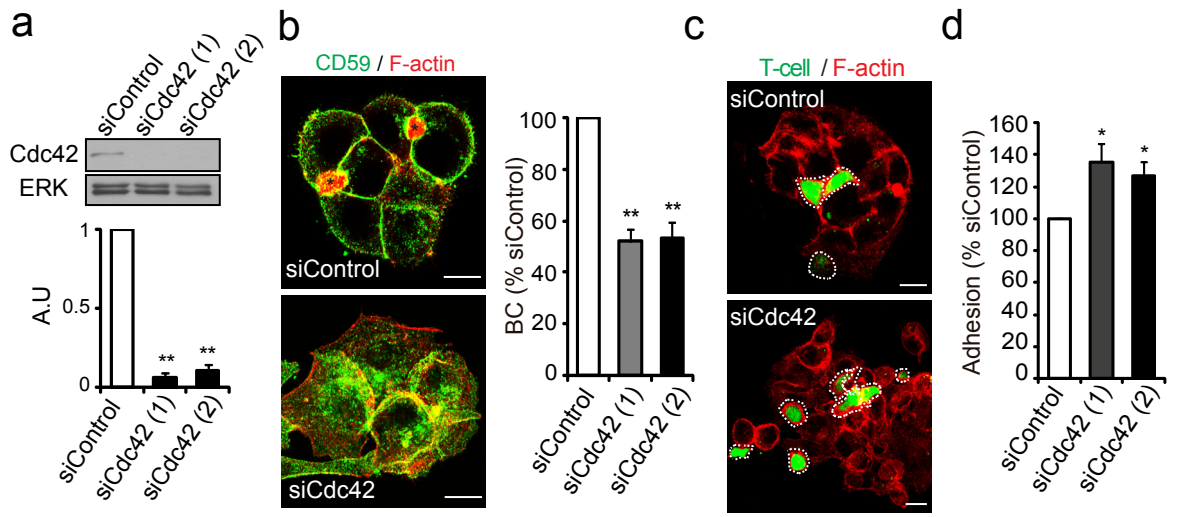

Figura 1. El silenciamiento génico de Cdc42 reduce la polaridad apicobasal y aumenta la adhesión linfocitaria de las células HepG2.

Las células HepG2 se transfectaron con un siRNA control (control) y dos siRNAs específicos para Cdc42 (siCdc42) durante 24 h y a continuación se sembraron en placas durante 48 h para formar colonias de células polarizadas. **(a)** Inmunodetección por western blot de Cdc42 y ERK y cuantificación de los niveles de expresión de Cdc42 en las células transfectadas con los siRNA indicados, expresada en unidades arbitrarias (A.U.). La inmunodetección de ERK fue usada como control de carga. **(b)** Paneles izquierdos. Identificación de los canalículos biliares (asteriscos) por inmunofluorescencia de colonias de HepG2 fijadas y teñidas para F-actina con faloidina-TRITC y para CD59 con un anticuerpo específico. Gráfico derecho. Cuantificación relativa del número de canalículos biliares (BC) en células transfectadas con los siRNA indicados. **(c)** Células HepG2 transfectadas con siRNA fueron incubadas con linfocitos T marcados con calceína durante 20-30 minutos. Tras varios lavados, las células se fijaron y se tiñeron para F-actina para visualizar las HepG2 y los linfocitos T adheridos. La fluorescencia de la calceina permitió identificar los linfocitos T (T-cell) (líneas discontinuas, paneles izquierdos). La adhesión linfocitaria se cuantificó midiendo la intensidad de fluorescencia de la calceína en un lector de placas (gráfico derecho). Barras, 10 μm. Las barras de error muestran el promedio + error estándar del promedio (SEM) de al menos tres experimentos distintos; * p<0.05; **p<0.005.

expresión de la proteína en comparación con células transfectadas con un siRNA control (Fig. 1a). Para analizar la polaridad apicobasal en HepG2 se cuantificó el número de canalículos biliares por célula por por inmunofluorescencia mediante un doble marcaje con actina filamentosa (F-actina) y la proteína CD59, que se encuentra anclada a un grupo glicofosfatidilinositol (GPI) y se acumula en la membrana apical vía transcitosis (de Marco et al., 2002) (Fig. 1b). El número de canalículos biliares en células HepG2 con niveles reducidos de Cdc42 fue el 52% y 53%, conrespecto al número de lúmenes en células transfectadas con un siRNA control (Fig. 1b),de acuerdo con resultados previos (Madrid et al., 2010).

Para analizar el efecto de la pérdida de polaridad hepática sobre la adhesión de células del sistema inmunitario utilizamos linfocitos T provenientes de sangre humana previamente diferenciados a células memoria con alta capacidad adhesiva y migratoria (Millan et al., 2006a). Además de inducir pérdida de polaridad hepática, la interferencia de la expresión deCdc42 con los dos siRNA aumentó la adhesión de linfocitos T primarios a las células HepG2 un 35% y 27%, respectivamente (Fig. 1c, d). La inhibición de aPKC con un pseudosubstrato (PS-aPKC) suprime la morfogénesis de lúmenes apicales en células epiteliales caninas cultivadas en tres dimensiones (Martin-Belmonte et al., 2007). De manera similar al silenciamiento de Cdc42, incubación con PS-aPKC en células HepG2 redujo el número de canalículos biliares al-

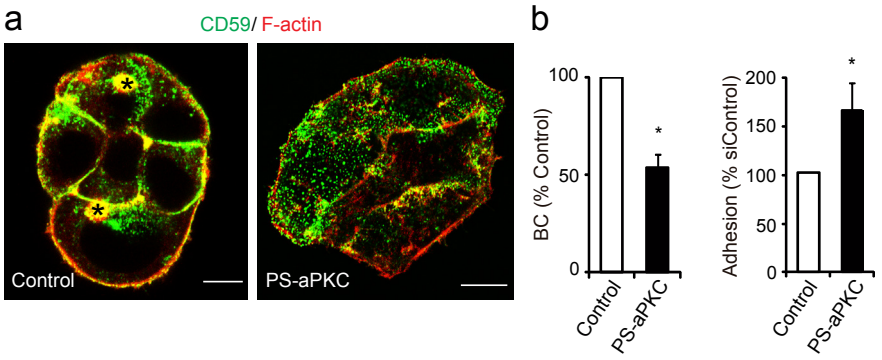

Figura 2. La inhibición de aPKC reduce la polaridad apicobasal y aumenta la adhesión linfocitaria de las células HepG2.

(a) Imágenes de microscopía confocal de colonias de células HepG2, teñidas para F-actina y CD59, sin tratar (Control) o tratadas con un pseudosustrato de aPKC (PS-aPKC) a 40 µg/ml durante 18 h. Los asteriscos indican estructuras canaliculares. **(b)** Cuantificación relativa del número de canalículos biliares (BC) (gráfico izquierdo) y de la adhesión de linfocitos T (gráfico derecho) en células control o tratadas con PS-aPKC. Barras, 10 µm. Las barras de error muestran el promedio + SEM de al menos tres experimentos distintos; * $p<0.05$.

rededor de un 50%. Tras lavados reiterados del inhibidor, las células tratadas incrementaron la adhesión de células T un 62% (Fig. 2a, b). Estos resultados en su conjunto indican por tanto que la inhibición de la ruta de señalización controlada por Cdc42-PAR reduce la polaridad apicobasal e induce la adhesión de linfocitos T a las células HepG2.

Para descartar una posible función de la ruta mediada por aPKC y cdc42, no relacionada con la polaridad apicobasal, en la interacción entre células hepáticas y leucocitos, utilizamos estrategias alternativas para modular la polaridad hepatocelular. Como ya se ha descrito en la introducción, la activación de las isoformas clásicas de PKC con ésteres de forbol como el PMA reduce la polarización de células HepG2, mientras que los análogos del cAMP promueven la formación de canalículos biliares activando PKA o EPAC (Fu et al., 2011) (Zegers and Hoekstra, 1997). La incubación de células HepG2 con PMA durante 120 min disminuyó el número de canalículos biliares un 70%, mientras que la adhesión de linfocitos T a células tratadas y posteriormente lavadas intensivamente para eliminar el PMA, aumentó un 71% con respecto al control (Fig. 3a,b). De manera opuesta, la incubación con DcAMP supuso un aumento en el número de canalículos del 23% y una disminución del 22% en la adhesión de células T (Fig. 3a-c). Debido a que las rutas de señalización implicadas en el establecimiento de la polaridad pueden regular la respuesta inflamatoria (Mashukova et al., 2011) e inducir la expresión de receptores de adhesión para los leucocitos (Delpino et al., 2010), decidimos realizar los ensayos en presencia de la droga cicloheximida para inhibir la síntesis proteica. La cicloheximida no provocó alteración del efecto del PMA sobre la adhesión linfocitaria a las células HepG2 (Fig. 3b, c), por lo que el aumento en la adhesión de células T observado en respuesta a la pérdida de polaridad inducida por PMA no se debe a la nueva síntesis de receptores hepáticos involucrados en la interacción entre leucocitos y hepatocitos.

En resumen y como primera conclusión, utilizando cuatro estrategias diferentes para modular la polaridad de células HepG2, hemos demostrado que existe una relación inversa entre la polaridad de estas células hepáticas y su habilidad para interaccionar con linfocitos T.

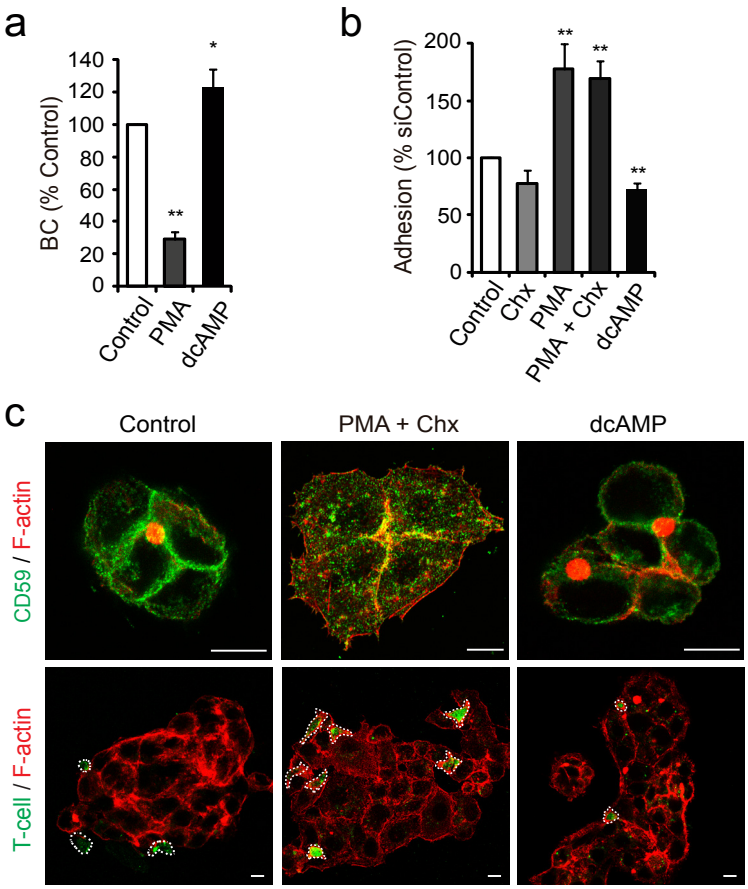

Figura 3. Correlación inversa entre la polaridad hepatocelular y la adhesión de linfocitos T en células HepG2 tratadas con PMA y dcAMP.

(a) Cuantificación relativa del número de canalículos biliares (BC) en células sin tratar (Control) y tratadas durante 2 h con PMA (100 nM) o con dcAMP (100 µM). **(b)** Cuantificación relativa de la adhesión de células T a células HepG2 tratadas con los reactivos indicados. La síntesis de proteínas se inhibió con CHX a 1 µg/ml en los puntos indicados. **(c)** Imágenes superiores. Las células HepG2 tratadas de la manera señalada fueron teñidas para F-actina y CD59 para identificar los canalículos biliares. Imágenes inferiores. Tras el ensayo de adhesión de linfocitos T marcados con calceína (T-cell), las células fueron fijadas, teñidas para F-actina y analizadas por inmunoflorescencia confocal. Barras, 10 µm. Las barras de error muestran el promedio + SEM de al menos tres experimentos distintos; * $p<0.05$; ** $p<0.005$.

1.2. ICAM-1 se acumula en el dominio apical de células HepG2 y hepatocitos humanos *in vitro* e *in vivo*

La migración intersticial de leucocitos a través del parénquima implica el desplazamiento de las células inmunes a través de interacciones de sus integrinas con el estroma y con las células parenquimales, que termina a menudo en la adhesión firme del leucocito sobre una célula diana constituyendo el destino final del trayecto migratorio (Friedl and Weigelin, 2008). Algunos resultados previos sugieren que la adhesión de leucocitos al parénquima hepático puede estar mediada por la interacción de integrinas β2 leucocitarias con el receptor hepático ICAM-1 (Meijne et al., 1994) (Nagendra et al., 1997), aunque el estudio de esta interacción en el tejido hepático está mucho menos caracterizada en comparación con otros procesos celulares, como el de adhesión y transmigración de los linfocitos a través del endotelio (Fernandez-Borja et al., 2010) (Reglero-Real et al., 2012).

Para abordar el estudio de la posible función de ICAM-1 en la interacción leucocito-hepatocito durante la pérdida de polaridad, procedimos en primer lugar a analizar la distribución de este receptor en células HepG2 polarizadas en cultivos en dos dimensiones (2D) (Fig. 4a) y en tres dimensiones (3D) (Fig. 4b). Mediante ensayos de inmunofluorescencia y microscopía confocal observamos que el receptor endógeno se acumula de forma mayoritaria en el dominio

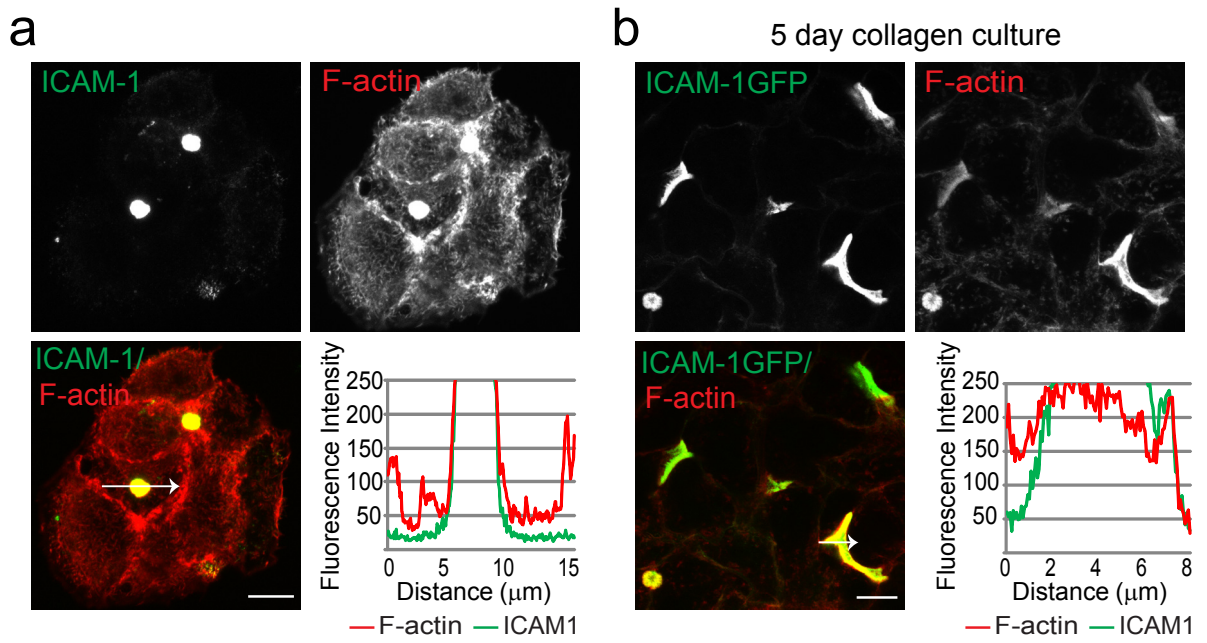

Figura 4. ICAM-1 se localiza en el canalículo biliar de células HepG2

(a) Las células HepG2 se cultivaron durante 72 h, se fijaron y se tiñeron para ICAM-1 con un anticuerpo específico y para F-actina con faloidina-TRITC. El gráfico en la esquina inferior derecha muestra el perfil de intensidad de fluorescencia de la flecha blanca marcada en la imagen. **(b)** Se cultivaron células HepG2 expresando de forma estable ICAM-1-GFP en sándwiches de colágeno durante 5 días, se fijaron y se marcaron como en (a). El gráfico inferior derecho muestra el perfil de intensidad de fluorescencia de la flecha blanca en la imagen. Barras, 10 μm.

canalicular de dichas células y colocaliza con F-actina (Fig. 4a). De manera parecida, células HepG2 polarizadas expresando de forma estable ICAM-1 conjugado desde su extremo citoplásmico con GFP (ICAM-1-GFP), acumularon también la proteína exógena en los canalículos biliares, que tras cinco días de incubación en una matriz tridimensional generada con un sándwich de colágeno aparecieron elongados y tubulares, con una morfología similar a la observada en el hígado (Fig. 4b). Para comprobar si la distribución polarizada es exclusiva de ICAM-1, analizamos la distribución de otros receptores de adhesión pertenecientes a

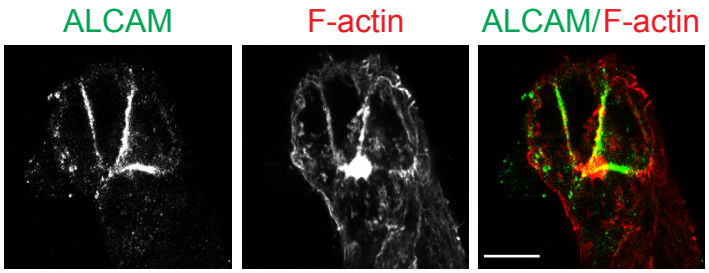

Figura 5. ALCAM no se encuentra polarizado en la membrana apical de células HepG2.

Las células HepG2 se cultivaron durante 72 h, se fijaron y se tiñeron para ALCAM con un anticuerpo específico y para F-actina con faloidina-TRITC. Barras, 10 μm.

la superfamilia de las inmunoglobulinas en nuestro modelo. De acuerdo con resultados previos en hepatocitos primarios murinos (Bumgardner et al., 1998), no se observó expresión de VCAM-1 (Vascular cell adhesión molecule-1) en células HepG2. Sin embargo observamos que ALCAM (Activated leukocyte adhesión molecule), un receptor que también participa en la adhesión leucocitaria y que se expresa en epitelios y en el endotelio vascular (Cayrol et al., 2008), así como en muchos tipos de tumores, se distribuía por la membrana basolateral y quedaba excluido del dominio apical de las células HepG2 (Fig. 5). Para corroborar la localización de ICAM-1 observada en la línea celular hepática, analizamos también su distribución en hepatocitos primarios humanos polarizados en 3D con sándwich de colágeno a distintos tiempos, comprobando que el receptor exhibía una distribución similar a la de otros marcadores canaliculares como F-actina, las proteínas ERM fosforiladas, el transportador Mrp2 y Radixina (Fig. 6a, b) (Kikuchi et al., 2002). Cabe mencionar que también se detectó tinción de ICAM-1 en la membrana basolateral de hepatocitos polarizados (Fig. 6a, b), aunque la intensidad de esta señal resultó ser mucho menor que la acumulada en el dominio apical. Por último, la tinción de muestras de tejido hepático humano provenientes de controles sanos reveló una distribución del receptor en algunas zonas del tejido compatible con una localización canalicular (Fig. 6c), lo que está de acuerdo con referencias previas que indican que, a pesar de que la expresión de ICAM-1 se incrementa en el parénquima hepático en un contexto inflamatorio, dicho receptor también se expresa en ausencia de inflamación en hepatocitos humanos (de Fougerolles et al., 1991). Nuestros datos sugieren que in vitro e in vivo, ICAM-1 se encuentra confinado al dominio canalicular de células parenquimales hepáticas, sin perjuicio de que exista también una fracción minoritaria del receptor en la región basolateral.

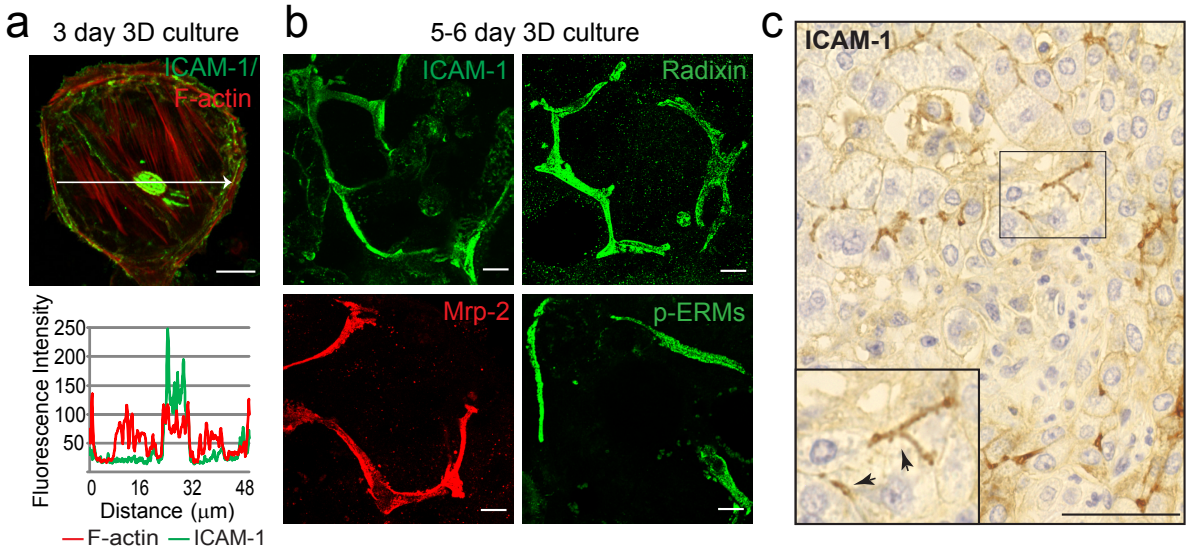

Figura 6. ICAM-1 se encuentra confinado en el canalículo biliar de hepatocitos humanos.

(a) Se cultivaron hepatocitos humanos en sándwiches de colágeno durante 72 h, se fijaron y se marcaron para ICAM-1 y F-actin. El gráfico muestra el perfil de intensidad de la flecha blanca en la imagen. **(b)** Se cultivaron hepatocitos humanos durante 6 días en sándwiches de colágeno, se fijaron y se tiñeron para ICAM-1, radixina, Mrp-2 o ERM fosforiladas (p-ERM). Barras, 10 μm. **(c)** Muestra de tejido hepático procedente de un donante sano que fue desparafinada y teñida para ICAM-1. Barras, 50 μm.

1.3. La exposición de ICAM-1 apical a células inmunes aumenta en respuesta a la pérdida de polaridad hepatocelular

En el parénquima hepático los leucocitos infiltrados establecen contactos preferentemente con la membrana basolateral de de los hepatocitos, que se encuentra expuesta al espacio de Disse y a los sinusoides (Warren et al., 2006). Puesto que la localización de ICAM-1 en este dominio es mínima en hepatocitos polarizados, quisimos investigar si este receptor aparece expuesto al espacio extracelular y media por tanto el aumento en la adhesión linfocitaria en respuesta a la pérdida de polaridad apicobasal.

Para abordar esta posibilidad hicimos uso de la estrategia anteriormente utilizada para despolarizar los hepatocitos mediante su incubación con PMA y cicloheximida, un coctel que induce pérdida de polaridad y evita la síntesis de nuevas moléculas de adhesión que puedan contribuir a un aumento de la unión linfocitaria. En paralelo a la desintegración de los canalículos biliares, el proceso de despolarización provocó la dispersión de ICAM-1 y su aparición en dominios discretos distribuidos por toda la superficie celular (Fig. 7a y vídeo 1). Estos dominios estaban enriquecidos en F-actina y recordaban a los microvilli en los que ICAM-1 se concentra en células endoteliales inflamadas (Fig. 7a, ampliación) (Millan et al., 2006a) (Oh et al., 2007). La fosforilación de un residuo específico de treonina en el dominio C-terminal de las proteínas ERM es necesaria para promover su conformación activa, abierta, que conecta proteínas de membrana a la F-actina subcortical. Las células HepG2 polarizadas acumulan las proteínas ERM fosforiladas y por tanto activas en el dominio apical (Fig. 7b), al igual que ocurre en hepatocitos primarios humanos (Fig.6b) (Kikuchi et al., 2002). Tras el estímulo despolarizante las proteínas ERM activas se relocalizaron en dominios discretos en la membrana plasmática siguiendo un patrón de distribución muy parecido al de ICAM-1 (Fig 7b). A continuación analizamos el proceso de pérdida de polaridad por microscopía electrónica de barrido. Aunque las células con una aparente organización polarizada presentaban abundantes microvilli cortos, en respuesta al tratamiento despolarizante se detectó la aparición de filamentos más largos en la superficie celular que podrían corresponder a los microvilli con distribución canalicular previa (Fig. 7c).

Con el fin de analizar de manera cuantitativa la cantidad de ICAM-1 que resulta expuesta al espacio extracelular en respuesta a la pérdida de polaridad hepatocelular, realizamos ensayos de marcaje de proteínas de superficie con sulfo-NHS-biotina. Las células control y despolarizadas se marcaron en frío con este reactivo, que al ser impermeable a la membrana plasmática únicamente reconoce el ICAM-1 expuesto en la membrana basolateral sin llegar a alcanzar el canalículo biliar. Acto seguido se aisló el ICAM-1 biotinilado mediante un pull-down con neutravidina, el ligando de la biotina, conjugada a agarosa. A pesar de que en condiciones control sólo la mitad de las células presentan un fenotipo polarizado, la ratio entre la proteína marcada y detectada en la fracción o sedimento del pull down (Exposed) respecto a la proteína en el extracto total aumentó para ICAM-1 y p-ERM en aquellas células sometidas a un estímulo despolarizante, lo que sugiere que ICAM-1 es más accesible desde el espacio extracelular

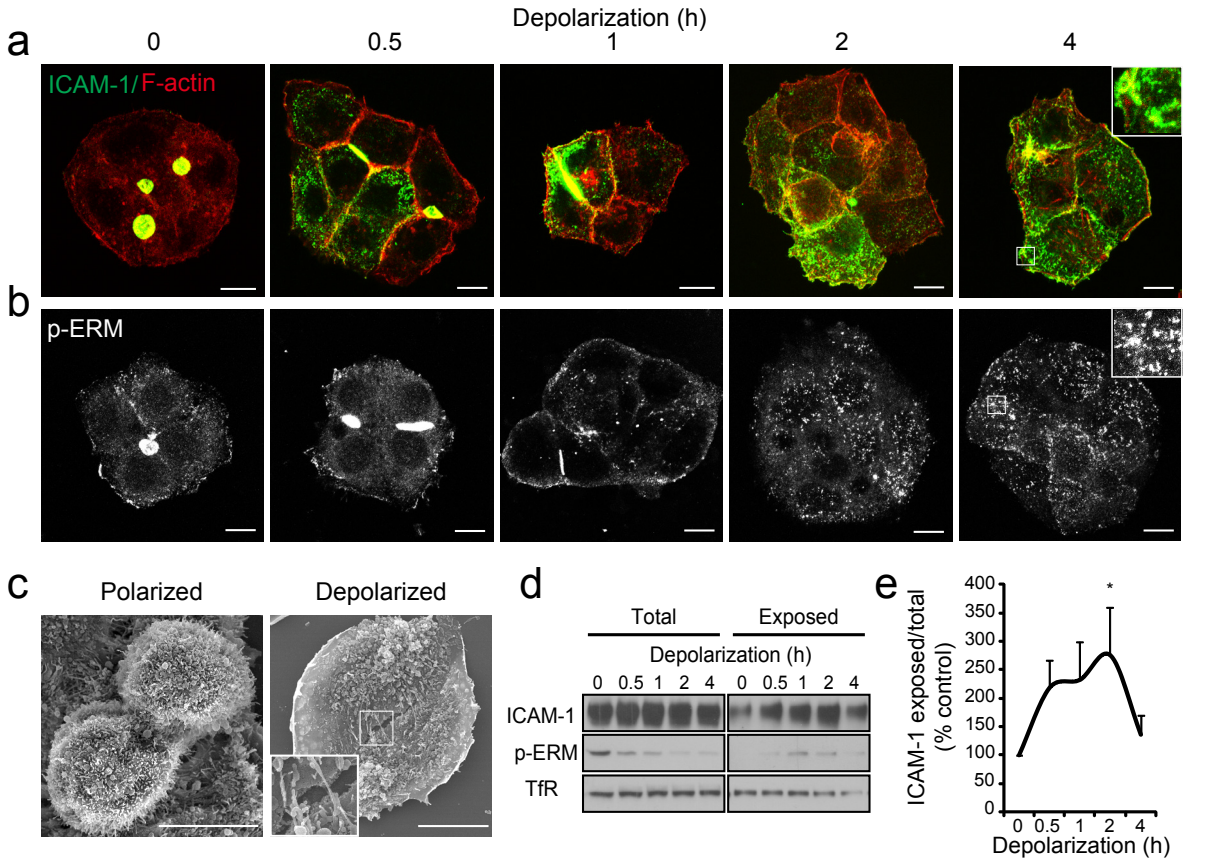

Figura 7. El receptor ICAM-1 y las proteínas ERM canaliculares se exponen a las células inmunes en respuesta a la pérdida de polaridad.

Las células HepG2 se cultivaron durante 72 h y se despolarizaron con PMA 100 nM en la presencia de CHX durante los tiempos indicados. **(a, b)** Las células se fijaron y tiñeron para F-actina e ICAM-1 (a) o para p-ERM (b). **(c)** Las células HepG2 sometidas o no al tratamiento despolarizante, se fijaron y se sometieron a los tratamientos necesarios para el análisis por microscopía electrónica de barrido. Las células despolarizadas muestran en su superficie largos filamentos que se asemejan a microvilli (ampliación). **(d)** Células HepG2 despolarizadas a distintos tiempos se marcaron con sulfo-NHS-biotina y se lisaron. Las proteínas expuestas y por tanto biotiniladas (Exposed) se aislaron mediante un ensayo de *pull-down* con neutravidina-agarosa. **(e)** El ratio de las proteínas expuestas al espacio extracelular frente al total de proteína se expresó como porcentaje del ratio de las células control sin tratar. Nótese que tras el incremento de los niveles de receptor biotinilado entre 0.5 y 2 h (d,e), los niveles totales y/o de superficie de las tres proteínas señaladas disminuyeron a 4 h por la internalización y degradación constitutiva de proteínas en células cuya síntesis proteica es inhibida con CHX. **(d).** Barras, 10 µm. Las barras de error muestran el promedio + SEM de al menos tres experimentos distintos; * $p<0.05$.

cuando las células hepáticas pierden la polaridad. Hay que destacar que el PMA produjo a menudo una disminución de los niveles de proteínas ERM fosforiladas, debido probablemente a la desorganización de la estructura canalicular. Aun así, las proteínas ERM activas fueron detectadas de forma significativa en el sedimento biotinilado durante la despolarización, lo que indica que estas proteínas se asocian desde la cara citoplásmica de la membrana a proteínas de superficie que incrementan su nivel de biotinilación (Fig.7d, e). Los ensayos de biotinilación repetidos con estrategias de despolarización alternativas como el silenciamiento de Cdc42 o la inhibición de aPKC dieron también como resultado un incremento significativo de la cantidad de receptor biotinilado en las células despolarizadas (Fig 8a-d).

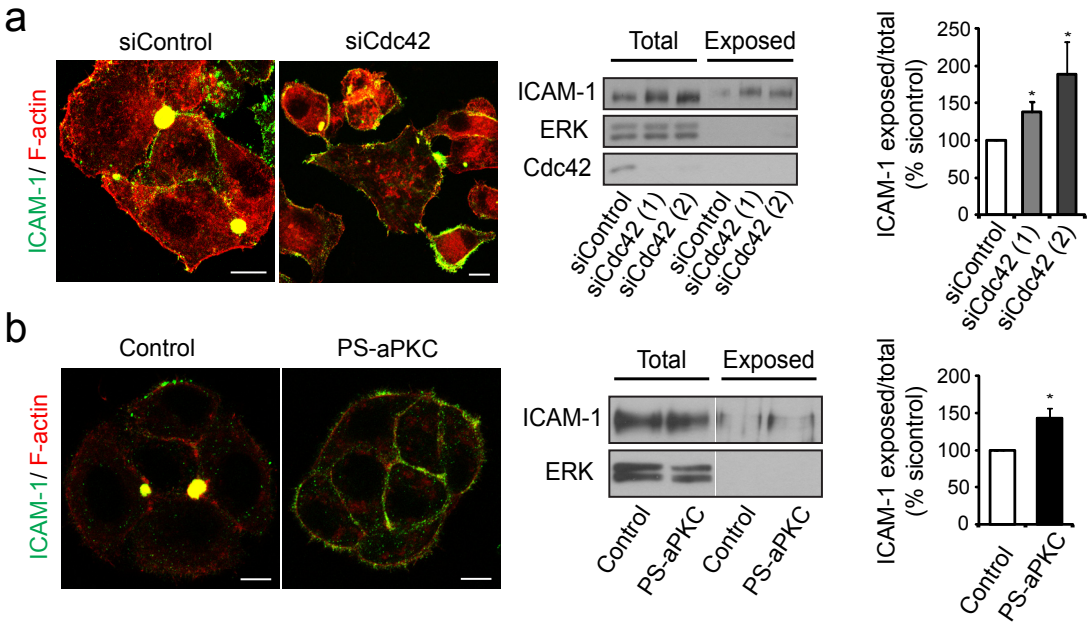

Figura 8. ICAM-1 se expone al espacio extracelular en respuesta a la inhibición de aPKC o al silenciamiento de Cdc42.

Las células HepG2 fueron despolarizadas mediante silenciamiento de Cdc42 **(a)** o incubación con PS-aPKC **(b)** A continuación se fijaron y se tiñeron para ICAM-1 y F-actina (imágenes a la izquierda), o se marcaron con sulfo-NHS-biotina para luego llevar a cabo un *pull-down* con neutravina-agarosa y un análisis por western blot con los anticuerpos indicados. La ratio entre ICAM-1 biotinilado y total fue posteriormente cuantificado (gráficos a la derecha) Barras, 10 µm. Las barras de error muestran el promedio + SEM de al menos tres experimentos distintos; * p<0.05.

En conjunto nuestros datos indican que la pérdida de polaridad hepatocelular provoca que los microvilli canaliculares, enriquecidos en F-actina, pERM e ICAM-1, aparezcan expuestos al espacio extracelular.

1.4. ICAM-1 media la adhesión de linfocitos T a células Hep G2 despolarizadas

Basándonos en estos resultados, quisimos investigar la contribución de ICAM-1 al incremento de la adhesión de leucocitos producida por la pérdida de polaridad de las células HepG2.

En primer lugar realizamos ensayos de video microscopía co-cultivando linfocitos T teñidos con la sonda CMTMR sobre células HepG2 despolarizadas que expresaban establemente ICAM-1-GFP. Unos minutos después del contacto de la célula T con la superficie del hepatocito, observamos una redistribución local del receptor en forma de protrusiones alrededor del linfocito adherido (Fig. 9, vídeo 2), lo cual es compatible con el posible papel de ICAM-1 en el reclutamiento de leucocitos cuando se encuentra expuesto en la membrana de los hepatocitos despolarizados. De manera similar, el análisis por microscopía confocal de dicha interacción, seguido de la reconstrucción tridimensional de las imágenes, reveló que ICAM-1se acumula en estructuras tipo microvilli, ricas en actina, alrededor de los linfocitos adheridos (Fig. 10a, b, vídeo 3). Esta reorganización de membrana recuerda a las “estructuras de anclaje” encargadas de mediar la migración transendotelial de leucocitos a través de los vasos sanguíneos

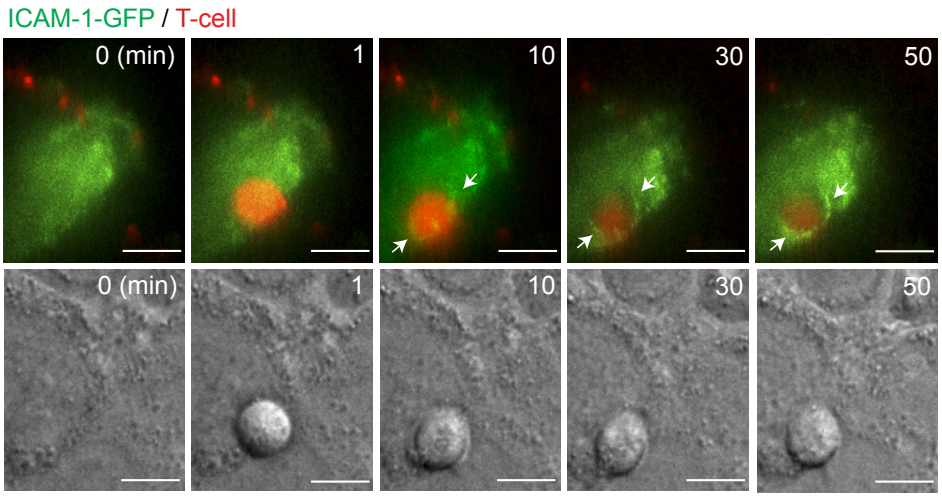

Figura 9. ICAM-1-GFP se acumula alrededor de los linfocitos T adheridos a células HepG2 despolarizadas.

Las células HepG2 previamente despolarizadas con PMA y expresando establemente ICAM-1-GFP se incubaron con linfocitos T marcados con la sonda roja CMTMR y se analizaron por videomicroscopía. Las flechas indican la acumulación de ICAM-1-GFP alrededor de un linfocito T adherido. Barras 10 µm.

(Barreiro et al., 2002) (Carman and Springer, 2004) (Reglero-Real et al., 2012), sugiriendo un paralelismo mecanístico entre el gradiente de adhesión haptotáctico que siguen los leucocitos infiltrados en el parénquima hepático y la captura y adhesión de células inmunes a la monocapa endotelial durante las primeras etapas de la extravasación.

Por último, para comprobar si la interacción leucocito-hepatocito se encuentra mediada por ICAM-1, se silenció de forma eficiente la expresión del receptor en células HepG2 con dos siRNAs diferentes (siICAM-1(1) e siICAM-1(2)) (Fig. 11a). Acto seguido, las células se despolarizaron con PMA, se lavaron de forma repetida y se llevaron a cabo ensayos de adhesión utilizando linfocitos T. Las células interferidas para ICAM-1 disminuyeron de forma significativa su capacidad de adherir de células T, la cual supuso alrededor del 50% del aumento de adhesión observado en células despolarizadas (Fig. 11b, Fig. 3b). El siRNA siICAM-1(2) tiene como diana la región 3' no traducida (3'UTR) del RNA mensajero de ICAM-1 y no afecta, por tanto, a la expresión de la proteína exógena ICAM-1-paGFP, cuyo mRNA carece de esta región. El silenciamiento de ICAM-1 endógeno en células HepG2-ICAM-1-paGFP no interfirió la expresión de la proteína exógena (Fig. 11a) y en consecuencia no tuvo efecto alguno sobre la adhesión de leucocitos a estas células. Es más, la adhesión de linfocitos T a células que expresan ICAM-1-paGFP aumentó respecto a la de células HepG2 normales transfectadas con siControl, probablemente debido a la sobreexpresión de receptor exógeno (Fig. 11b). Estos últimos resultados demuestran que la disminución de la adhesión leucocitaria observada al silenciar ICAM-1 es consecuencia exclusivamente de la reducción en la expresión del receptor.

En conclusión, los datos obtenidos indican que la adhesión de linfocitos T a células HepG despolarizadas está mediada, al menos en parte, por el receptor de adhesión ICAM-1.

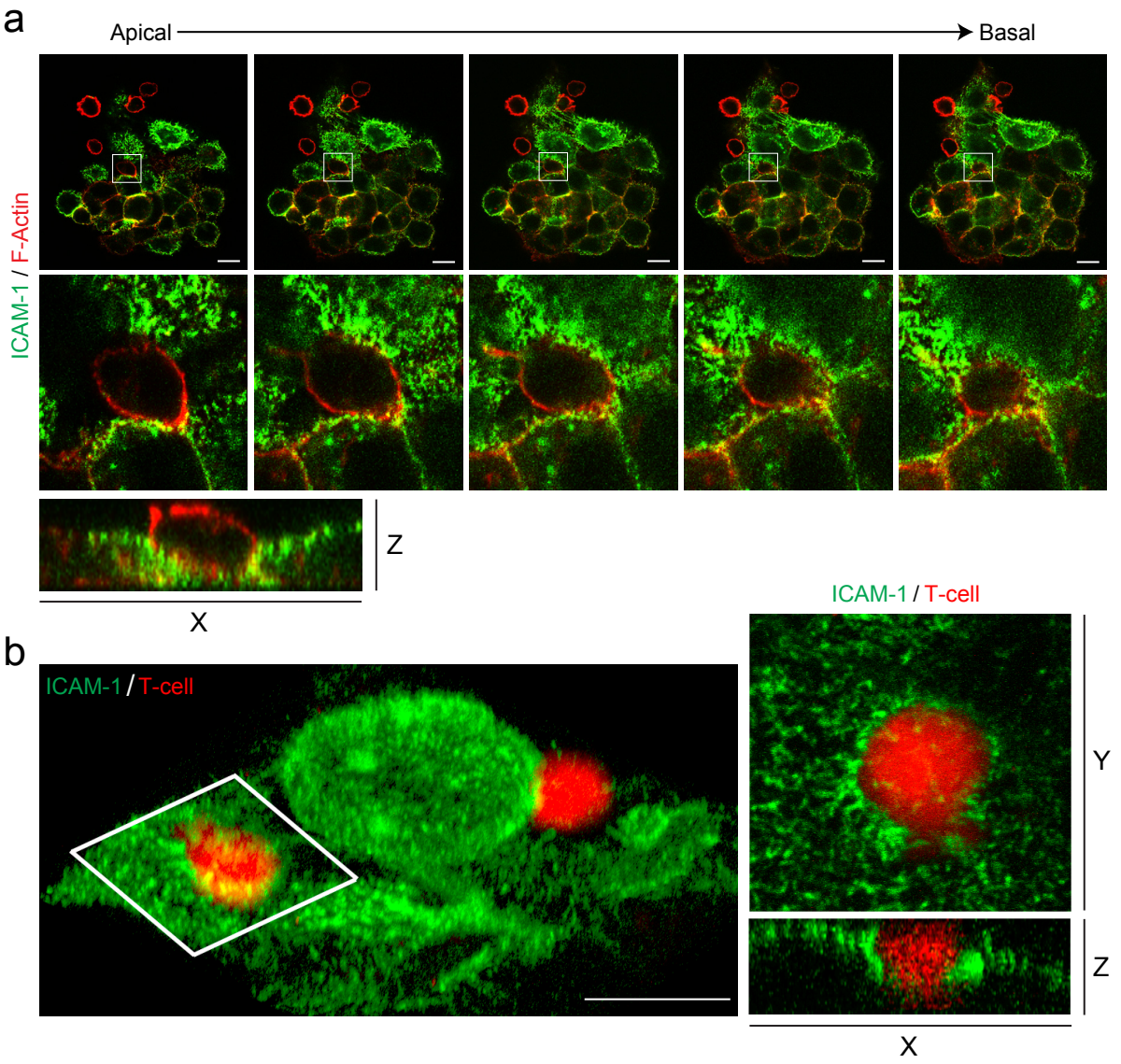

Figura 10. Protrusiones de membrana enriquecidas en ICAM-1 rodean a los linfocitos T adheridos a células HepG2 despolarizadas.

Imágenes de microscopía confocal del ICAM-1 hepático rodeando un linfocito T adherido a células HepG2 previamente despolarizadas. **(a)** Doble tinción para ICAM-1 y F-actina. Las imágenes superiores muestran diferentes cortes en el eje z; la imágenes centrales son una ampliación de la zona encuadrada. La imagen inferior muestra una vista ortogonal. **(b)** Reconstrucción 3D de una imagen confocal de ICAM-1 endógeno y células T marcadas con CMTMR (izquierda). Proyección de los diferente cortes en un plano en el eje X-Y (arriba, derecha) y plano intermedio ortogonal en el eje X-Z (abajo derecha). Barras, 10 µm.

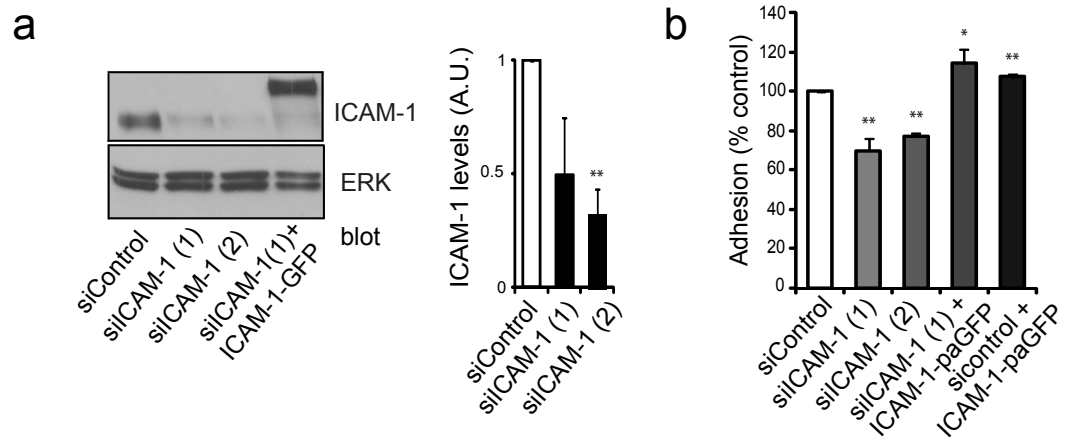

Figura 11. La adhesión de linfocitos T a células HepG2 despolarizadas es dependiente de ICAM-1.

(a) Las células HepG2 se transfectaron durante 72 h con los siRNAs indicados para silenciar la expresión de ICAM-1. En paralelo se transfectaron células que expresan establemente ICAM-1-GFP con siICAM-1(1), cuya diana se encuentra en la región 3'UTR del RNA mensajero (siICAM-1+ICAM-1-GFP). Después de 72 h las células se lisaron y se inmunodetectaron las proteínas ICAM-1 y ERK. **(b)** Efecto de la transfección de los distintos siRNA en la adhesión de linfocitos T a células HepG2 o células HepG2-ICAM-1-paGFP despolarizadas. Las barras de error muestran el promedio + SEM de al menos tres experimentos distintos; * $p<0.05$; ** $p<0.005$.

2. BASES MOLECULARES QUE DETERMINAN LA POLARIDAD APICAL DE ICAM-1 EN CÉLULAS HEPÁTICAS

2.1. ICAM-1 basolateral se redirige y confina en el canalículo biliar

Con el fin de dilucidar el mecanismo a través del cual se segrega ICAM-1 al dominio canalicular decidimos estudiar la dinámica del receptor en células HepG2. En la actualidad uno de los métodos más adecuados para monitorizar el movimiento de una población de moléculas concreta a nivel subcelular consiste en la utilización de proteínas fotoactivables fusionadas a la proteína de interés (Patterson and Lippincott-Schwartz, 2004) (ver materiales y métodos). Por ello generamos una construcción de ICAM-1 fusionado por su extremo c-terminal a la proteína GFP fotoactivable (ICAM-1-paGFP) (Patterson and Lippincott-Schwartz, 2002). Se generaron clones en células HepG2 que expresaban establemente la proteína y se comprobó que su distribución era muy similar a la de ICAM-1 endógeno e ICAM-1-GFP, acumulándose de forma significativa en la membrana apical (Fig. 12). Además, para poder identificar las regiones basolateral y apical durante los ensayos de fotoactivación se expresó de forma transitoria actina-Cherry en colonias de células ICAM-1-paGFP.

En primer lugar se fotoactivó la región canalicular y se filmaron las células durante al menos

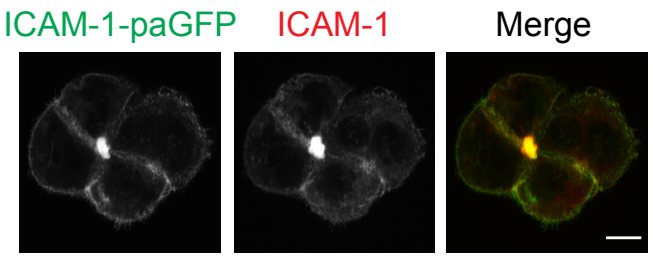

Figura 12. ICAM-1-paGFP está mayoritariamente localizado en el canalículo biliar de células HepG2.

Las células HepG2 que expresan establemente ICAM-1 fusionado a la proteína GFP fotoactivable (paGFP) fueron fijadas, permeabilizadas y teñidas con un anticuerpo anti-GFP y un anticuerpo específico para ICAM-1.

90 minutos. Tras la adquisición de imágenes confocales pudimos comprobar cómo la intensidad de fluorescencia prácticamente no disminuyó en el área fotoactivada y el aumento de fluorescencia en las regiones basolaterales adyacentes resultó insignificante al cabo de 90 minutos post-fotoactivación (Fig. 13 a, b; vídeo 4), lo que sigiere que ICAM-1 se encuentra notablemente confinado al canalículo biliar.

Como se ha mencionado en la introducción , se ha propuesto que algunas proteínas transmembrana son susceptibles de seguir una ruta de transporte indirecto desde el Golgi a la membrana apical, pasando previamente por el dominio basolateral, desde dónde son trans-

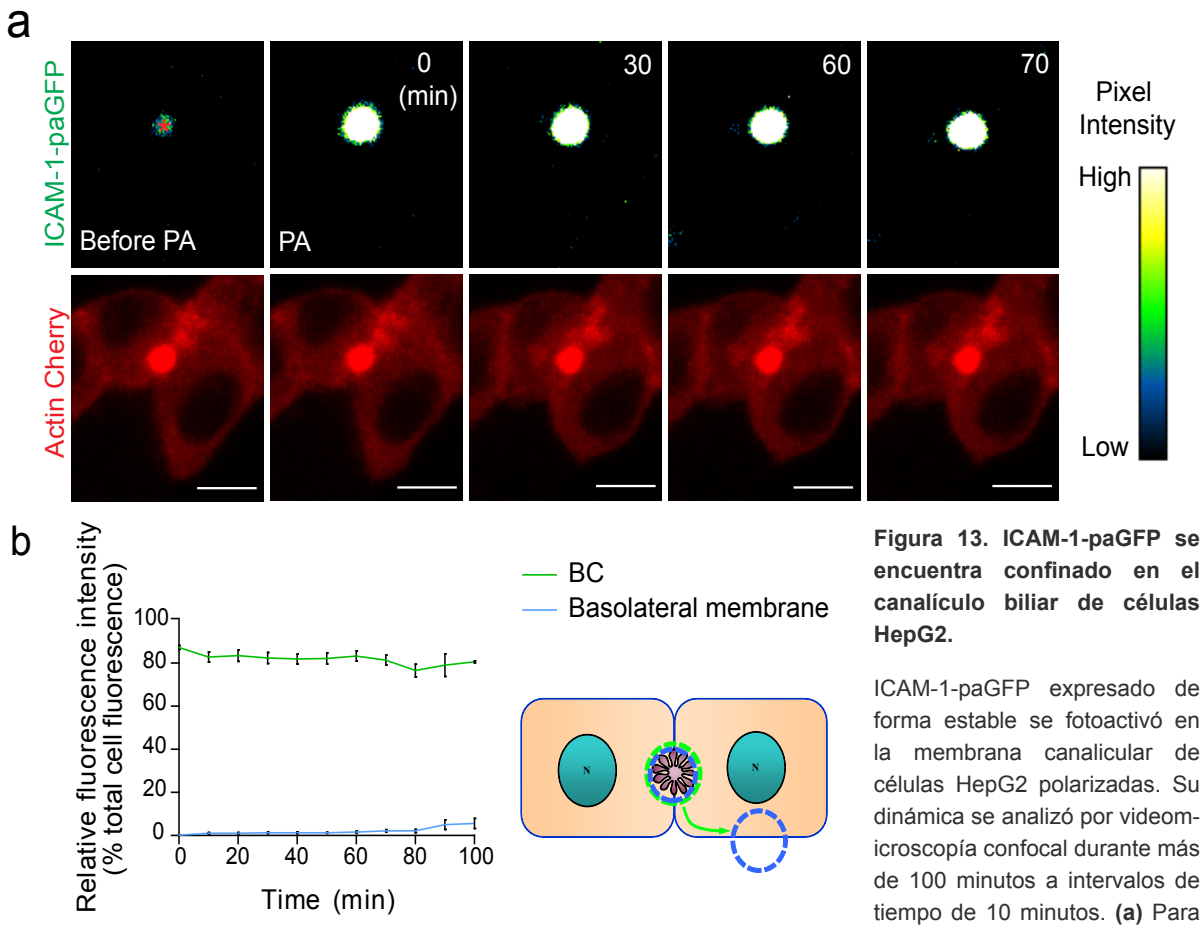

Figura 13. ICAM-1-paGFP se encuentra confinado en el canalículo biliar de células HepG2.

ICAM-1-paGFP expresado de forma estable se fotoactivó en la membrana canalicular de células HepG2 polarizadas. Su dinámica se analizó por videomicroscopía confocal durante más de 100 minutos a intervalos de tiempo de 10 minutos. **(a)** Para poder visualizar los canalículos biliares se expresó previamente actina-cherry. El asterisco marca fluorescencia de fondo previa a la fotoactivación (PA) del laser, proveniente de la fotoactivación ambiental y que es detectada por la notable acumulación del receptor en el canalículo biliar. **(b)** Cuantificación de la intensidad de fluorescencia relativa en las áreas canaliculares fotoactivadas (BC) y en dominios basolaterales adyacentes después de restar el fondo, como se indica en el dibujo (n=13 células). Barras, 10 µm.

portadas por transcitosis a la región apical (Bastaki et al., 2002) (Weisz and Rodriguez-Boulan, 2009). Siguiendo nuestra estrategia de fotoactivación selectiva en diferentes dominios de membrana, fuimos capaces de fotoactivar también la fracción minoritaria de ICAM-1-paGFP localizada en la membrana basolateral(Fig. 14a). A pesar de que la intensidad de fluorescencia obtenida en la fotoactivación basolateral fue mucho menor que en la apical, fuimos capaces de filmar la dinámica del ICAM-1-paGFP en superficie. En comparación con

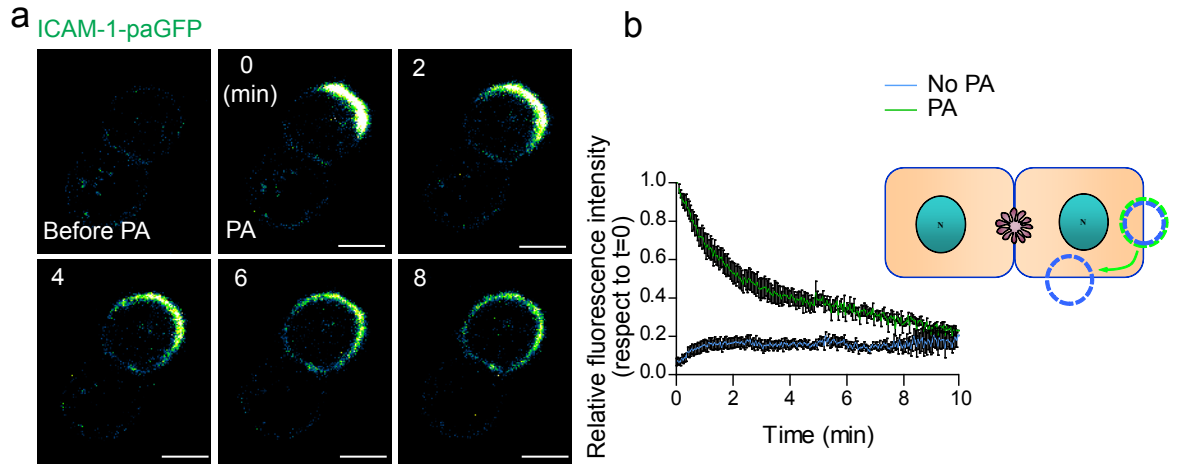

Figura 14. ICAM-1-paGFP difunde rápidamente por la membrana basolateral de células HepG2.

ICAM-1-pa-GFP se fotoactivó en la membrana basolateral y su dinámica se analizó por videomicroscopía confocal durante 10 minutos a intervalos de tiempo de 3 segundos. **(b)** Cuantificación de la intensidad de fluorescencia relativa en áreas fotoactivadas y en otras no fotoactivadas adyacentes, después de restar el fondo, como se indica en el dibujo (n=18 células). Barras, 10 µm.

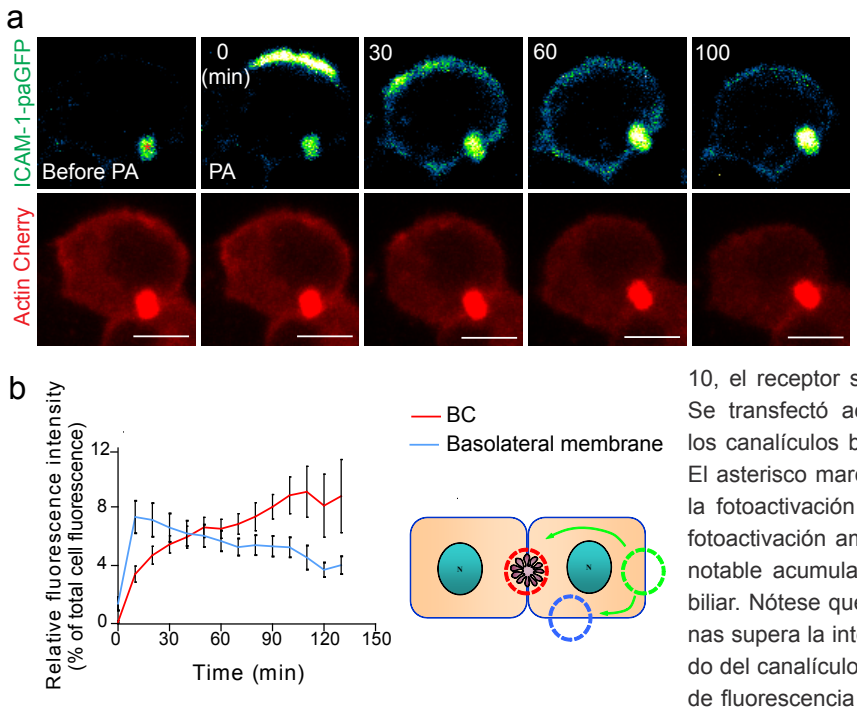

Figura 15. ICAM-1-pa-GFP se redirige desde la membrana basolateral hacia el canalículo biliar de células HepG2.

(a)ICAM-1-pa-GFP se fotoactivó en la membrana basolateral y su dinámica se analizó por videomicroscopía confocal durante 100 minutos a intervalos de tiempo de 10 minutos. Tras una difusión basolateral rápida, como ocurre en la figura 10, el receptor se acumula en el área canalicular. Se transfectó actina-cherry para poder visualizar los canalículos biliares y la membrana basolateral. El asterisco marca fluorescencia de fondo previa a la fotoactivación (PA) del laser, proveniente de la fotoactivación ambiental y que es detectada por la notable acumulación del receptor en el canalículo biliar. Nótese que la fotoactivación basolateral apenas supera la intensidad de la fluorescencia de fondo del canalículo **(b)** Cuantificación de la intensidad de fluorescencia relativa en dominios basolaterales diferentes de la región fotoactivada y en el canalículo biliar (BC), después de restar el fondo, como se indica en el dibujo (n=17 células). Barras, 10 µm.

la lenta tasa de difusión detectada en la fotoactivación apical, observamos cómo el receptor difunde rápidamente desde el área fotoactivada al resto de la membrana basolateral en los 10 minutos siguientes a la fotoactivación (Fig. 14a, b; vídeo 5). El análisis de esta dinámica a tiempos más largos reveló además que entre 90 y 130 minutos post-fotoactivación el receptor fotoactivado se acumulaba en el canalículo biliar. De manera concomitante a la acumulación canalicular, la intensidad de fluorescencia disminuyó en la dominios basolaterales adyacentes al área inicialmente fotoactivada, sugiriendo que existe un tráfico de la proteína en dirección basolateral-apical (Fig. 15a, b; vídeo 6). Colectivamente estos resultados indican que el ICAM-1 basolateral se redirige al canalículo biliar, dónde puede permanecer estable al menos durante 100 minutos. Por tanto, el confinamiento de ICAM-1 en esta estructura se debe a diferencias entre el tráfico del receptor desde el dominio basolateral al apical y viceversa.

Para corroborar los datos obtenidos mediante el análisis de la dinámica de ICAM-1-paGFP, se realizaron ensayos de marcaje basolateral, utilizados con anterioridad para analizar latranscitosis basolateral-apical de proteínas hepáticas (de Marco et al., 2002) (Hemery et al., 1996). ICAM-1-GFP o ICAM-1 endógeno fueron marcados con anticuerpos específicos en la superficie basolateral de células HepG2 en frío. A continuación, se incubaron a 37ºC, durante distin-

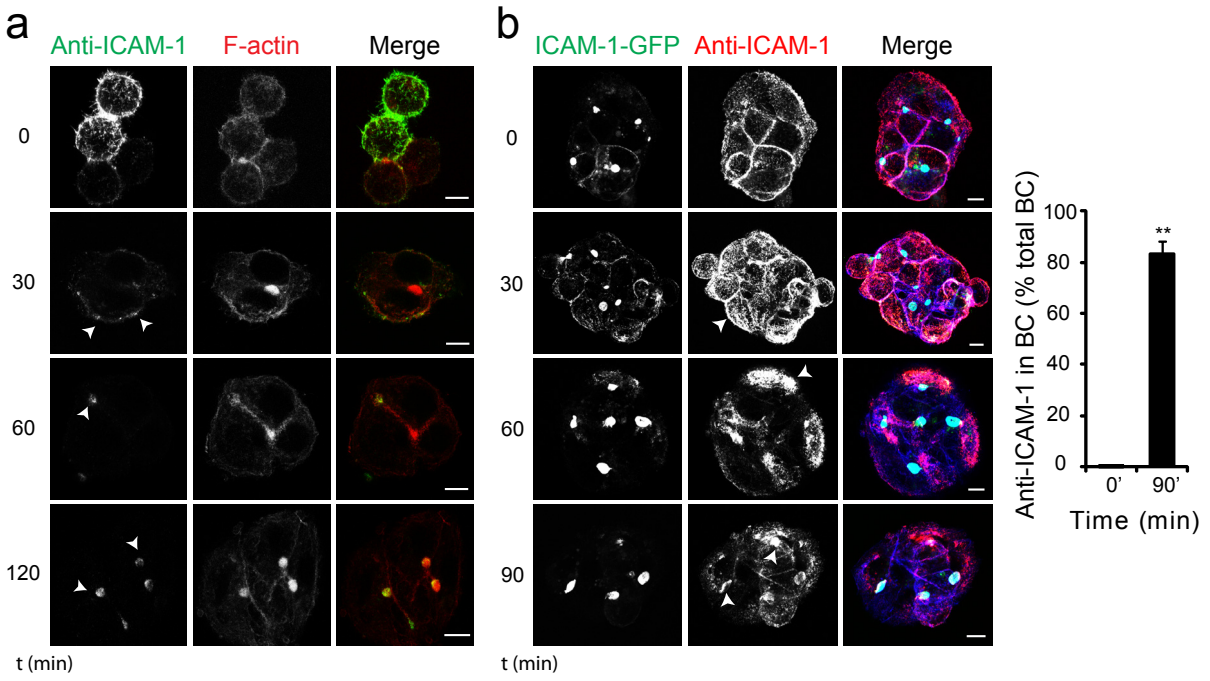

Figura 16. ICAM-1 marcado basolateralmente con anticuerpos específicos se acumula en el canalículo biliar de células HepG2.

Las células HepG2 polarizadas se incubaron con un anticuerpo específico de ratón para ICAM-1 en frio durante 30 min. A continuación se incubaron a 37oC durante los tiempos indicados, se fijaron, permeabilizaron y se tiñeron con un anticuerpo anti-ratón unido al fluoróforo Alexa 488 y con faloidina-TRITC para detectar la F-actina. **(b)** Las células HepG2 expresando establemente ICAM-1-GFP se marcaron de la misma forma que en (a). Después de la fijación y permeabilización, las células se tiñeron con un anticuerpo anti-ratón unido al fluoróforo Alexa 555. El ICAM-1 marcado basolateralmente se acumula en dominios discretos que se localizan en los canalículos biliares después de 120 min (a) y 90 min (b) de incubación a 37oC (cabezas de flecha). Nótese que la distribución total del ICAM-1-GFP, mayoritariamente canalicular, no varía significativamente durante el ensayo. **(c)** Cuantificación del porcentaje de canalículos (BC) positivos para ICAM-1 marcados con el anticuerpo específico a los tiempos indicados. Barras, 10 µm. Las barras de error muestran el promedio + SEM de al menos tres experimentos distintos; **p<0.005.

tos intervalos de tiempo, las células previamente marcadas, para permitir la internalización del receptor. Acto seguido las células se fijaron, se permeabilizaron y el anticuerpo primario se detectó con un anticuerpo secundario unido a un fluoróforo. Mientras que los anticuerpos incubados inicialmente en frío tiñeron exclusivamente la membrana basolateral, tras 90 minutos de incubación a 37oC el anticuerpo unido al receptor se acumuló de forma parcial, pero clara, en los canalículos biliares (Fig. 16a, b), sugiriendo que parte del receptor basolateral marcado había seguido una ruta transcitótica para alcanzar la membrana apical.

En conjunto nuestros datos indican que la arquietctura polarizada del hepatocito previene la acumulación basolateral de ICAM-1 redirigiéndolo hacia el canalículo biliar, impidiendo así que el receptor quede expuesto al espacio de Disse hepático y a las células inmunes.

2.2. El dominio citoplásmico de ICAM-1 es necesario para su completa polarización.

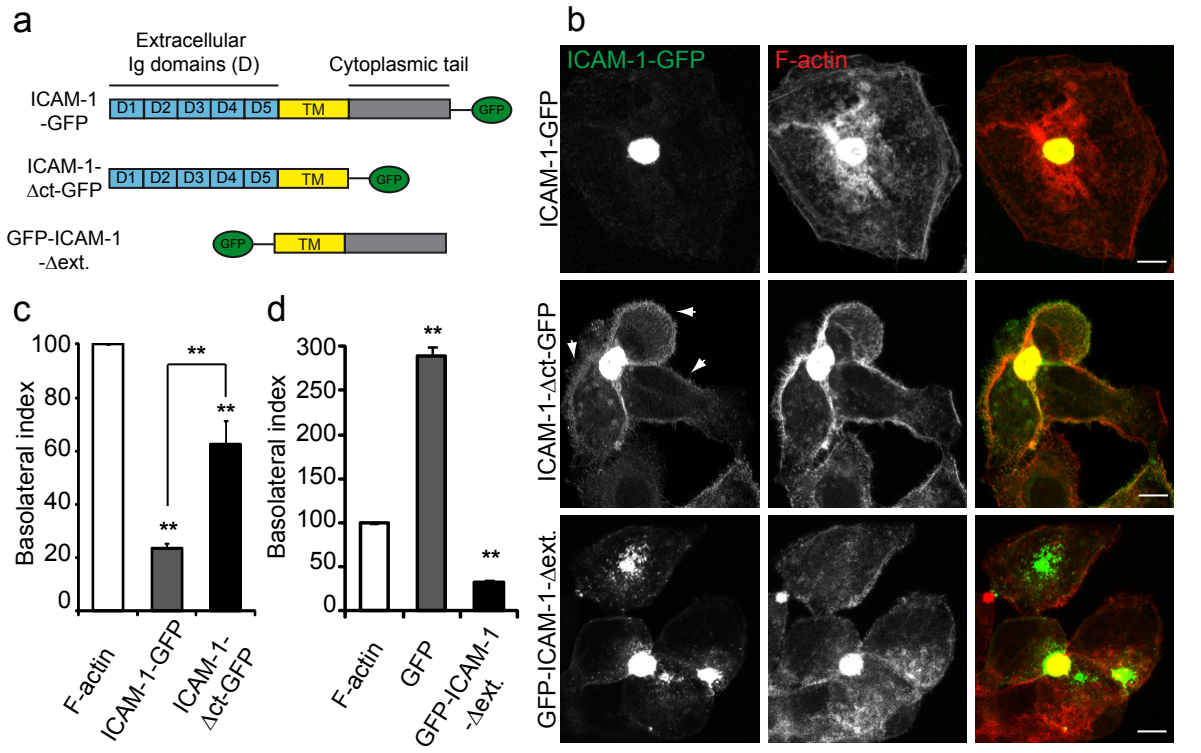

17. El dominio citoplásmico de ICAM-1 es necesario para su completa polarización.

(a) Esquemas de ICAM-1 completo y de las quimeras expresadas de manera exógena en células HepG2. **(b)** Células que expresan establemente ICAM-1-GFP o ICAM-1-Δct-GFP se crecieron durante 72h, se fijaron y se tiñeron para F-actina con faloidina-TRITC. La expresión de GFP-ICAM-1-Δext resultó ser tóxica a largo plazo, por lo que esta quimera y el control GFP se expresaron transitoriamente. **(c,d)** Cuantificación del ratio basolateral/apical (Basolateral index) de las proteínas indicadas, normalizado al índice basolateral para F-actina en cada célula polarizada. Barras, 10 μm. Las barras de error muestran el promedio + SEM de al menos tres experimentos distintos; **p<0.005, respecto a la ratio de la actina, menos cuando se indica.

A continuación comparamos la localización de una construcción ICAM-1-GFP sin su fragmento intracelular (ICAM-1-Δct-GFP) (Fig. 17 a) respecto a la de ICAM-1-GFP en clones estables silenciados para la expresión de ICAM-1 endógeno y observamos que el primero incrementa su localización basolateral respecto al segundo (Fig. 17b, c). En base a estos resultados, desarrollamos otro mutante conteniendo la proteína GFP fusionada por su extremo C-terminal al dominio transmembrana y citoplásmico de ICAM-1 (GFP-ICAM-1-Δext) (Fig. 17a), y la expresamos transitoriamente en células HepG2, ya que la generación de clones estables resultó imposible debido a la toxicidad de la quimera. La presencia del dominio citoplásmico fue suficiente para dirigir GFP a la región canalicular (Fig. 17b), y su distribución basolateral resultó similar a la de ICAM-1-GFP (Fig. 14b-d). Por tanto, la cola citoplásmica de ICAM-1 contribuye a la localización apical del receptor. Sin embargo, hay que destacar que el receptor mutante sin su segmento intracelular continúa localizándose en parte en el dominio apical (Fig. 17b), lo que sugiere la existencia de interacciones adicionales a través otros dominios que contribuyen también a la polarización del receptor.

2.3. ICAM-1 se asocia a las proteínas ERM en la membrana plasmática células HepG2

2.3.1. ICAM-1 colocaliza con ezrina y radixina en células HepG2

En otros tipos celulares, la asociación de ICAM-1 a la actina filamentosa submembranal se realiza a través de proteínas conectoras como la a-actinina (Carpen et al., 1992), cortactina (Tilghman and Hoover, 2002), filamina (Kanters et al., 2008) o las proteínas ERM (Huang et al., 2011). Las proteínas ERM son ubicuas, pero su expresión relativa depende del tipo celular analizado. Radixina constituye la ERM más abundante en hepatocitos primarios (Kikuchi et al., 2002) (Wang et al., 2006), aunque también se ha detectado expresión de ezrina en este tipo celular (Gilbert et al., 2012) y en hepatocitos transformados (Okamura et al., 2008). Por otra parte, la expresión de radixina es necesaria para la formación de la estructura canalicular y la localización de proteínas en las membranas del canalículo biliar (Kikuchi et al., 2002) (Wang et al., 2006), lo que nos llevó a formular una primera hipótesis sobre la posible asociación de las proteínas ERM al receptor ICAM-1 en células hepáticas. Para investigar esta posible asociación, primero desciframos el perfil de expresión de ERM en nuestro modelo celular. Realizamos ensayos de inmunodetección con anticuerpos específicos para ezrina, radixina y moesina en extractos de células HepG2, que se compararon con extractos de células endoteliales humanas provenientes de la vena del cordón umbilical (HUVECs), en los que es conoci-

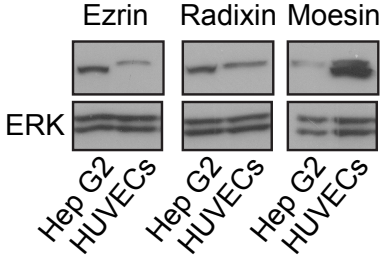

Figura 18. Las células HepG2 expresan todos los miembros de la familia ERM: Ezrina, Radixina y Moesina.

Los lisados de células HepG2 crecidas durante 72h fueron analizados por western blot con anticuerpos específicos para ezrina, radixina y moesina. En paralelo se analizó un extracto de células HUVECs. Mientras que en las células endoteliales predomina la expresión de moesina, en las células HepG2 lo hace la de ezrina y radixina respecto a la expresión endotelial.

do que la moesina y la ezrina son proteínas mayoritarias (Barreiro et al., 2002). La expresión de ezrina y radixina en las células HepG2 resultó mayor que en células HUVEC, mientras que la moesina se detectó con mucha menos intensidad en los extractos de células hepáticas que en los lisados endoteliales (Fig. 18). Estos resultados sugieren que ezrina y radixina se expresan de forma significativa en las células HepG2 y podrían ser candidatos a conectar ICAM-1 con la F-actina en las células HepG2.

A continuación analizamos la distribución de radixina-YFP o ezrina-GFP, expresadas de forma transitoria en célula hepáticas, junto con la de ICAM-1 endógeno, detectado por inmunofluorescencia. Encontramos una perfecta colocalización entre estas proteínas fluorescentes y el receptor tanto en células polarizadas como despolarizadas (Fig 19a, b).

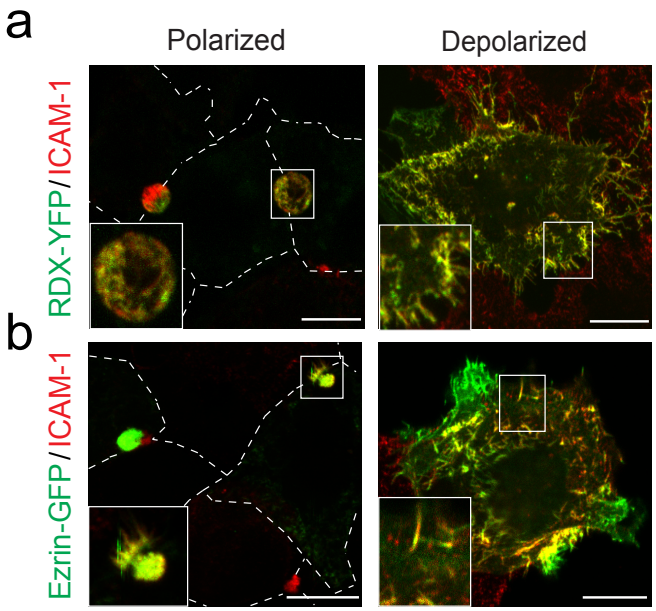

Figura 19. Radixina y Ezrina colocalizan con ICAM-1 en células HepG2 polarizadas y no polarizadas.

Las células HepG2 expresando Radixina (RDX)-YFP **(a)** o Ezrina-GFP **(b)** se trataron (depolarized) o no (polarized) con PMA 100nM durante 2 horas, se fijaron y se tiñeron para ICAM-1. Barras, 10 µm.

1.6.2. La asociación de pERM con ICAM-1 depende de su segmento citoplásmico

El entrecruzamiento (*crosslinking*) de proteínas de superficie con anticuerpos específicos es una estrategia experimental que permite analizar la asociación de otras proteínas a dichos receptores en dominios discretos de la membrana plasmática (Toomre et al., 2000) (Millan et al., 2006b). Esta estrategia presenta dos ventajas frente a técnicas bioquímicas convencionales como la inmunoprecipitación: se realiza en ausencia de detergentes, lo que permite detectar interacciones lábiles que son disociadas por éstos, y además evita artefactos producidos en los lisados celulares en los que proteínas de diferentes compartimentos contactan de forma artificial. El co-agrupamiento de proteínas en respuesta al entrecruzamiento suministra información sobre el grado de asociación entre dos proteínas, que puede ser cuantificado por técnicas de procesamiento de imagen, y no sólo sobre su proximidad, como hacen otras estrategias basadas también en la detección de fluorescencia, como el FRET (Pietraszewska-

Bogiel and Gadella, 2011).

El entrecruzamiento con anticuerpos anti-ICAM-1 (ver materiales y métodos) indujo el co-agrupamiento de radixina-YFP y ezrina-GFP en células HepG2 (Fig. 20a, c). El cálculo del coeficiente de colocalización de Manders (ver materales y métodos), que indica el grado de solapamiento existente entre los píxeles de dos canales diferentes (Dunn et al., 2011), reveló una colocalización muy significativa de ambas proteínas fluorescentes en los agrupamientos de ICAM-1. Este solapamiento resultó ser significativamente mayor que el de las proteínas control YFP y GFP, que no se enriquecieron en los acúmulos de ICAM-1 (Fig. 20b, d).

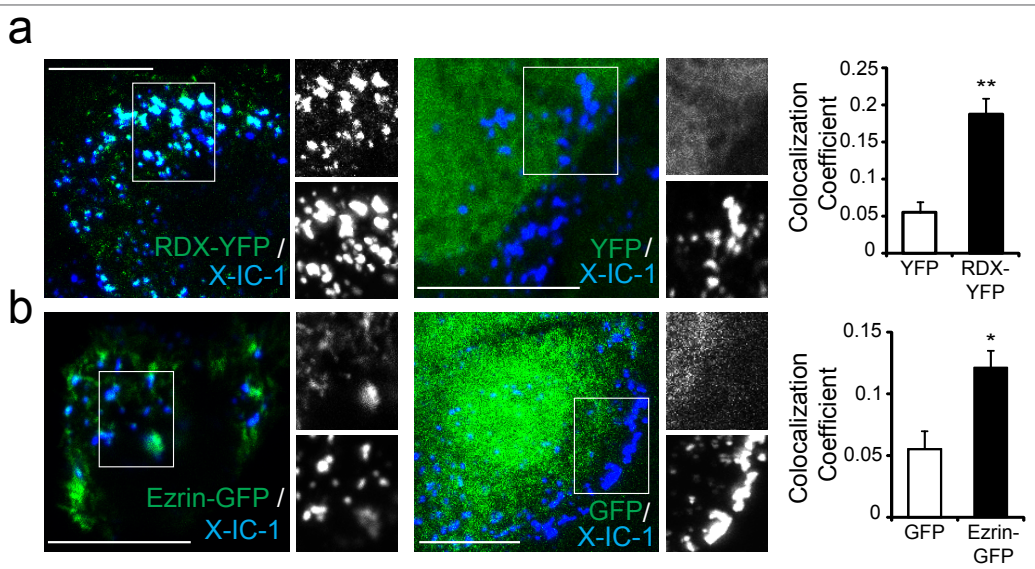

Figura 20. Radixina y Ezrina colocalizan con ICAM-1 entrecruzado en la membrana plasmática.

Las células HepG2 no polarizadas fueron incubadas con un anticuerpo frente a ICAM-1 durante 30 minutos en frío. A continuación el receptor fue entrecruzado con un anticuerpo secundario unido al fluoróforo Alexa 647 durante 40 minutos a 37oC (X-IC-1) en células que expresaban Radixina-YFP o YFP **(a)** y Ezrina-GFP o GFP **(b).** El entrecruzamiento con el segundo anticuerpo indujo la agregación del receptor en dominios discretos de membrana. Los gráficos muestran el coeficiente de colocalización de Manders, que indica el porcentaje de los píxeles del canal verde (Radixina-YFP, YFP, Ezrina-GFP o GFP) que solapan con el canal azul (X-IC-1) con valor máximo de 1. Barras, 10 µm. Las barras de error muestran el promedio + SEM de al menos tres experimentos distintos; * $p<0.05$; ** $p<0.005$.

A continuación, se realizaron ensayos de crosslinking en células HepG2 que expresaban establemente ICAM-1-GFP o ICAM-1-Δct-GFP (Fig. 18b), observándose que el enriquecimiento de ERM fosforiladas (pERM) en los acúmulos de ICAM-1 y su nivel de colocalización con el receptor era menor en los clones que expresan la construcción mutada de ICAM-1 (Fig. 21b, c). En estos experimentos, la expresión de ICAM-1 endógeno se silenció en ambos clones estables utilizando el siRNA siICAM-1(2) que no afecta a la expresión de la proteína exógena, reduciéndose así el co-agrupamiento de ERM con el receptor endógeno (Fig. 21a). Los experimentos de entrecruzamiento indican, de forma colectiva, que ICAM-1 puede asociarse a través de su dominio citoplásmico a las proteínas ERM en la membrana plasmática de las células HepG2, respaldando resultados previos que muestran la asociación entre ICAM-1 y ezrina y moesina en células endoteliales (Oh et al., 2007).

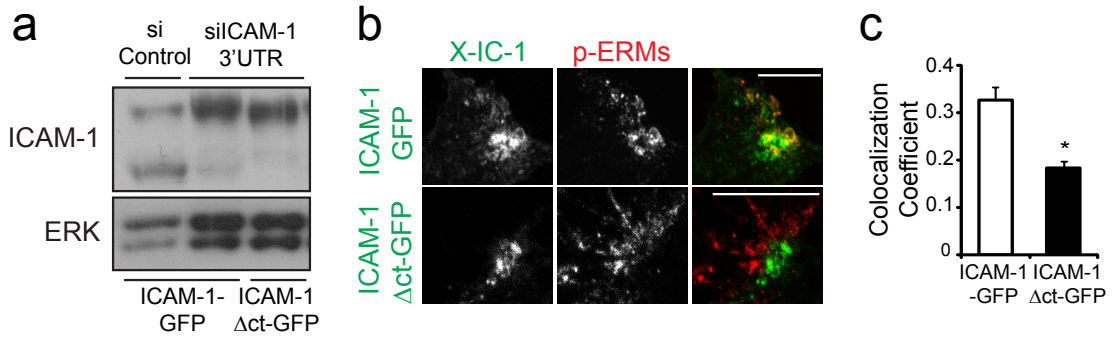

Figura 21. El dominio citoplásmico de ICAM-1 es necesario para el reclutamiento de p-ERM en los acúmulos de ICAM-1.

(a) ICAM-1 endógeno fue silenciado durante 72 h con un siRNA cuya diana se encuentra en la región 3'UTR del RNA mensajero (siRNA 3`UTR) en células HepG2 con expresión estable de ICAM-1-GFP o ICAM-1-Δct-GFP (b,c) 72 h más tarde se realizaron ensayos de entrecruzamiento de ICAM-1 (X-IC-1) como en la Figura 17, y la células se fijaron y se tiñeron para p-ERM. **(b)** Imágenes de microscopía confocal representativas. **(c)** Coeficiente de colocalización de Manders que indica el porcentaje de píxeles del canal verde (ICAM-1-GFP, ICAM-1-Δct-GFP) que solapan con el canal rojo (p-ERM). A pesar de una reducción apreciable en la señal de GFP debido al método de fijación para detectar p-ERM, se encontró una diferencia significativa entre la capacidad para reclutar a p-ERM de ICAM-1 completo e ICAM-1 sin el segmento citoplásmico. Barras, 10 μm. Las barras de error muestran el promedio + SEM de al menos tres experimentos distintos; * $p<0.05$.

1.6.3. La asociación de Ezrina y Radixina con ICAM-1 depende de tres residuos de lisina en el dominio C-terminal del receptor

A continuación se realizaron ensayos de pull-down con una proteína recombinante formada por la fusión de GST (*glutathione-S-transferase*) a la cola citoplásmica de ICAM-1 (GST-ICAM-1 tail) (Fig. 22a). Estos ensayos revelaron que este segmento del receptor es capaz de asociarse a radixina (Fig. 19b). ICAM-1 interacciona con proteínas conectoras del citoesqueleto de actina, como α-actinina y ezrina, a través de residuos básicos presentes en en su dominio citoplásmico (Carpen et al., 1992) (Oh et al., 2007). En una región cerca del segmento transmembrana del receptor, la sustitución de tres residuos aminoacídicos de lisina por tres leucinas (GST-ICAM-1 K>L) (Fig. 22a) fue suficiente para interrumpir la asociación entre radixina y la cola citoplásmica de ICAM-1 (Fig. 22b). Por último, y de forma similar, también se detectó una asociación significativa de ezrina al segmento citoplásmico del receptor y dependiente de estas tres lisinas mencionadas (Fig. 22b).

Conjuntamente, nuestros resultados indican que ICAM-1 se asocia en los microvilli a ERM activas y F-actina, una maquinaria previamente implicada en la adhesión leucocitaria cuando aparece expuesta a células inmunes (Reglero-Real et al., 2012), pero que en hepatocitos se encuentra polarizada, dado que resulta esencial para dirigir determinadas proteínas al canalículo biliar y para mantener la arquitectura polarizada (Kikuchi et al., 2002) (Wang et al., 2006). El doble papel de dicha maquinaria en polaridad y adhesión leucocitaria puede proporcionar la base molecular para explicar la relación inversa que hemos encontrado entre ambos procesos.

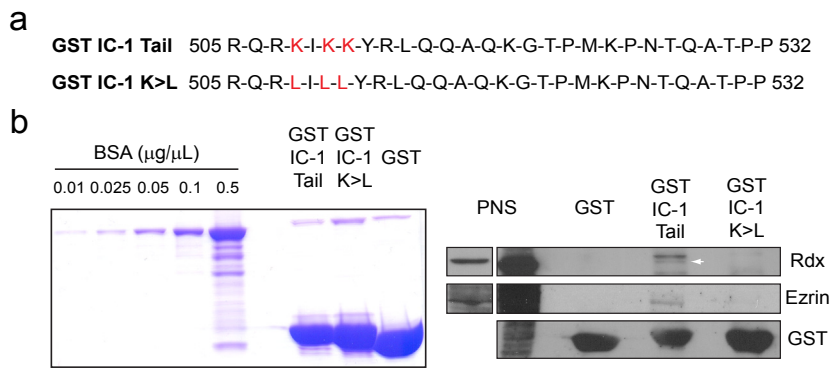

Figura 22. La asociación de radixina y ezrina con ICAM-1 depende de tres residuos de lisina en el dominio C-terminal del receptor.

(a) Esquema de la proteína recombinante GST unida al fragmento citoplásmico de ICAM-1 entero y sin mutar (arriba) o con tres residuos de lisina mutados a leucina (abajo). **(b)** Tinción de Coomassie de concentraciones crecientes de BSA y las proteínas de fusión GST. **(c)** Radixina (Rdx) y Ezrina se asocia a la cola citoplásmica entera de ICAM-1. Ensayos de pull-down de la proteína recombinante GST y GST unida al fragmento citoplásmico de ICAM-1. La sustitución de los tres residuos de lisina por leucinas es suficiente para abrogar la asociación de radixina y ezrina con la cola citoplásmica de ICAM-1.

3. EFECTO DE LA INFLAMACIÓN SOBRE LA POLARIDAD HEPATOCELULAR DE ICAM-1

3.1. La estimulación a largo plazo con TNF-α aumenta la exposición basolateral de ICAM-1

La mayoría de las patologías hepáticas agudas y crónicas se caracterizan por procesos inflamatorios que cursan con una acentuada expresión de diversas citoquinas proinflamatorias. La acción de estas citoquinas contribuye al desarrollo de muchos desórdenes hepáticos que a menudo terminan en cirrosis y fibrosis (Tilg et al., 2006). La expresión del receptor ICAM-1 se encuentra regulada en diferentes tejidos por varias citoquina proinflamatorias, entre las que destaca TNF-α (Aranda et al., 2013), una citoquina que resulta central en la respuesta inflamatoria hepática a largo plazo (Gonzalez-Amaro et al., 1994). De hecho, TNF-α es una citoquina paradigmática como inductor de adhesión leucocitaria a células endoteliales y epiteliales, incluidos los hepatocitos (Bradley, 2008) (Nagendra et al., 1997) (Sano et al., 1999). TNF-α juega un papel fundamental en la progresión de fallo hepático fulminante (Zhou et al., 2005) (Chastre et al., 2012), promueve el carcinoma hepatocelular (Grivennikov et al., 2010), aparece en hepatocitos que expresan también ICAM-1 en hepatitis alcohólica aguda (Ohlinger et al., 1993) y en infección por HBV y HCV (Gonzalez-Amaro et al., 1994), y sus niveles en suero aumentan en patologías como hepatitis C, hepatitis alcohólica aguda y rechazo he

pático (Neuman et al., 2012), (Panasiuk et al., 2007), (Imagawa et al., 1990).

Puesto que ICAM-1 es un paradigma de receptor regulado por citoquinas inflamatorias, quisimos investigar a continuación el efecto de TNF-α sobre la polaridad del receptor. Las células HepG2 fueron expuestas a TNF-α de origen humano a diferentes concentraciones y durante distintos períodos de tiempo. En nuestros ensayos inicales comprobamos que la expresión de ICAM-1 aumenta de forma óptima en respuesta a 50ng/ml de TNF-α a lo largo del tiempo, alcanzando niveles máximos tras 24 horas de estimulación (Fig. 24a, b), lo que corrobora datos previos sobre la modulación de la expresión de este receptor en hepatocitos en respuesta a citoquinas proinflamatorias obtenidos por diferentes laboratorios desde hace tiempo (Morita et al., 1994) (Sano et al., 1999) (Ohlinger et al., 1993). A continuación, investigamos el efecto de TNF-α sobre la polarización de ICAM-1 y la polaridad hepatocelular. La visualización por técnicas de inmunofluorescencia de células HepG2 inflamadas reveló un aumento de ICAM-1 en la membrana basolateral entre 4 y 24 horas post-estimulación (Fig. 23a). Tras 24 horas de tratamiento observamos además la acumulación de ICAM-1 en estructuras discretas de membrana enriquecidas en F-actina (Fig. 23a, ampliación) que se asemejan a los microvilli encontrados en células endoteliales inflamadas y que también detectamos por microscopía electrónica de barrido en células estimuladas con TNF-α (Fig 30b, ampliación).

Quisimos dilucidar a continuación si el incremento del receptor en el dominio basolateral observado por microscopía confocal se debe al aumento global en los niveles totales de proteína o si, además, TNF-α induce un cambio en la polaridad del receptor. Para ello realizamos ensayos de biotinilación en células HepG2 no transfectadas y en clones HepG2 que expresaban establemente ICAM-1-GFP, estimulados o no con la citoquina. Tras analizar los resultados hay que subrayar primero que TNF-α indujo un aumento tardío de la expresión total no sólo del receptor endógeno, sino también de ICAM-1-GFP. Puesto que la expresión ectópica de esta proteína se encuentra controlada por un promotor de citomegalovirus (CMV), del que no se ha descrito su regulación por esta citoquina, este incremento de ICAM-1-GFP podría estar revelando la existencia de una regulación post-traduccional del receptor o de la estabilidad de su RNA mensajero por parte de esta citoquina. Más importante, la razón entre la proteína expuesta respecto a la proteína total aumentó en respuesta a TNF-α tanto para ICAM-1 endógeno como para ICAM-1-GFP, indicando que ICAM-1 es más accesible desde el espacio extracelular en hepatocitos polarizados inflamados (Fig. 23c, d). El aumento de la ratio de proteína expuesta para ICAM-1 endógeno se detectó desde las cuatro horas de estimulación, mientras que el de ICAM-1-GFP se observó tras 24h de estimulación. Por tanto y en conclusión, TNF-α no sólo induce un aumento de la expresión de ICAM-1, sino también un cambio significativo en la polaridad del receptor.

TNF-α es una citoquina que puede inducir muerte celular (Tacke et al., 2009). Se conoce además que TNF-α altera la integridad de diferentes barreras endoteliales y epiteliales (McKenzie and Ridley, 2007) (Ivanov et al., 2010) (Kakiashvili et al., 2009). Por consiguiente, analizamos si el aumento de la exposición de ICAM-1 en respuesta a este estímulo era consecuencia de una pérdida de polaridad en las células hepáticas. El contaje de canalículos biliares detectados con diferentes marcadores reveló que la arquitectura polarizada de las HepG2 se mantenía durante al menos 24 horas tras la estimulación con TNF-α (Fig. 23e), lo cual sugie-

re que el aumento de la ratio basolateral/apical de ICAM-1 no es consecuencia de una pérdida de la integridad canalicular provocada por esta citoquina, aunque no se puede descartar que la separación entre los dominios apicales y basolaterales sea más permeable en los hepatocitos inflamados.

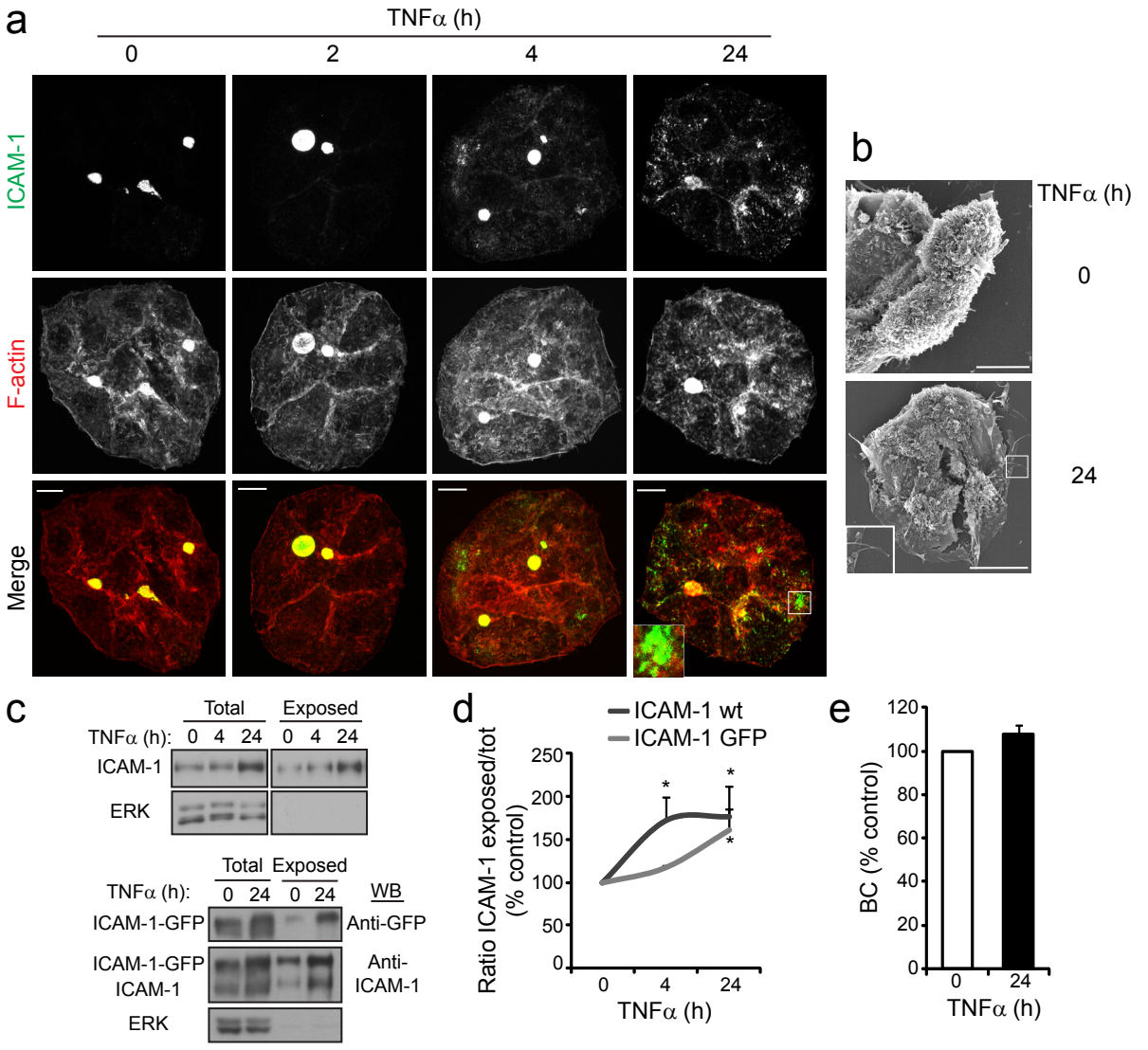

Figura 23. La exposición de ICAM-1 en microvilli basolaterales aumenta en respuesta a TNFα en células HepG2.

(a) Las células HepG2 se cultivaron durante 48 h y se estimularon con TNFα (50ng/ml) durante los tiempos indicados, se fijaron y se tiñeron para ICAM-1 y F-actina. La ampliación del área recuadrada ilustra el incremento del marcaje de ICAM-1 en los microvilli de la membrana basolateral detectado entre 4 y 24 h de estimulación. **(b)** Las células HepG2 estimuladas durante 24 h con TNFα se fijaron y se sometieron a los tratamientos necesarios para el análisis por microscopía electrónica de barrido. Las células inflamadas muestran en su superficie largos filamentos que se asemejan a microvilli. **(c)** Las células HepG2 normales (western blot superior) o expresando establemente ICAM-1-GFP (western blot inferior) estimuladas durante 4 y/o 24 h con TNFα se incubaron con sulfo-NHS-biotina y se lisaron. Las proteínas biotiniladas (Exposed) se aislaron mediante un ensayo de pull-down con neutravidina-agarosa. **(d)** El ratio de las proteínas expuestas al espacio extracelular frente al total de proteína se expresó como porcentaje de las células control sin tratar para ICAM-1 endógeno e ICAM-1-GFP. **(e)** Cuantificación del número de canalículos de células estimuladas respecto a células control. Barras, 10 µm. Las barras de error muestran el promedio + SEM de al menos tres experimentos distintos; * $p<0.05$.

3.2. La activación de ERM y su localización basolateral en hepatocitos polarizados aumentan en respuesta a la estimulación con TNF-α a largo plazo.

Nuestro grupo y otros autores han descrito que TNF-α puede activar a las proteínas ERM en células endoteliales, lo que altera la función de barrera y la expresión de receptores de adhesión en respuesta a esta citoquina (Koss et al., 2006) (Aranda et al., 2013). Como se ha mostrado anteriormente, las proteínas ERM pueden asociarse con ICAM-1 en la membrana plasmática (Fig. 16). Puesto que la localización basolateral de ICAM-1 aumenta en respuesta a TNF-α, pero no la polaridad de las células hepáticas, nos planteamos si las proteínas ERM podrían contribuir al aumento de la distribución basolateral de este receptor.

El análisis cuantitativo de cinéticas de TNF-α en HepG2 reveló un incremento global en la fosforilación de ERM que resultó significativo a 2, 4 y 8 horas post-estimulación (Fig. 24a, b). Este aumento ocurrió sin alteración aparente de los niveles de expresión de ERM (Fig. 24a). Además, el incremento de fosforilación precedió a la inducción de la expresión de ICAM-1 (Fig. 24a). En concordancia, el silenciamiento de ICAM-1 no tuvo efecto alguno sobre la fosforilación de ERM (Fig. 24a), descartando un papel del propio receptor en la activación de estas proteínas.

Además, la localización de ERM activas en células HepG2 estimuladas a distintos tiempos con TNF-α, indica que pERM se acumula en proyecciones de membrana tipo microvilli en la región basolateral a partir de 4 horas de activación (Fig. 25a). Para corroborar este dato realizamos ensayos de biotinilación, que nos permitieron detectar un incremento de pERM asociadas a receptores biotinilados en la superficie celular en células inflamadas (Fig. 25b).

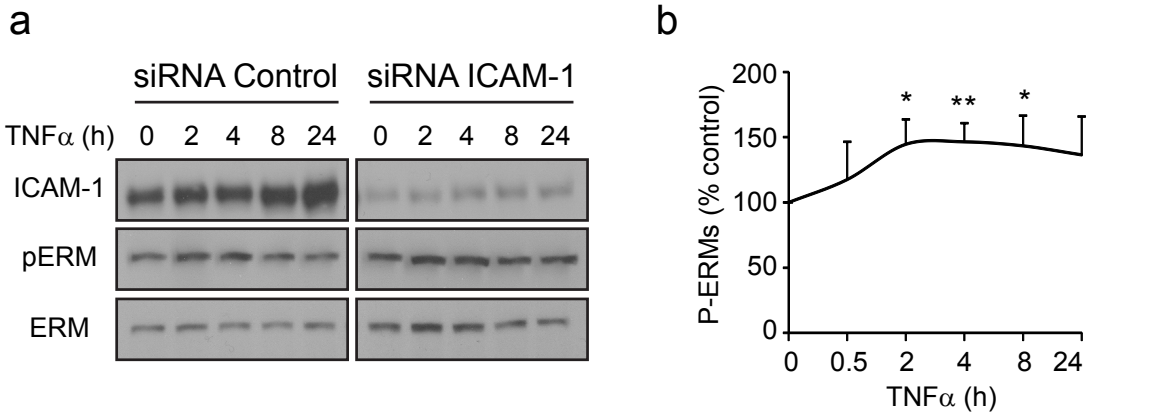

Figura 24. La fosforilación de ERM aumenta en respuesta a TNF-α en células HepG2.

(a) Las células HepG2 se transfectaron durante 72h con un siRNA control o con un siRNA específico para silenciar la expresión de ICAM-1 y se estimularon con TNFα durante los tiempos indicados. Los lisados celulares se analizaron por western blot para las proteínas pERM, ICAM-1 y ERK. **(b)** La gráfica muestra el aumento de la fosforilación de ERM en células control en respuesta a la estimulación con TNF-α. Las barras de error muestran el promedio + SEM de al menos tres experimentos distintos; * $p<0.05$; ** $p<0.005$.

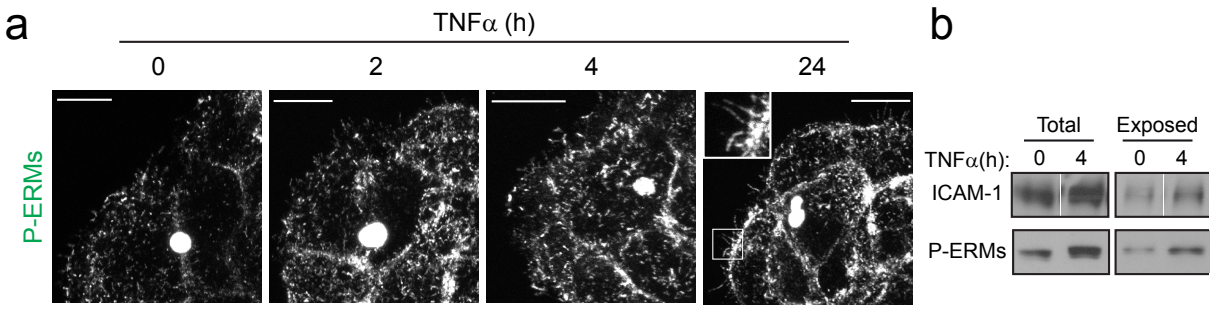

Figura 25. La fosforilación de pERM en la membrana plasmática de HepG2 aumenta en respuesta a TNFα en células HepG2 polarizadas.

Las células HepG2 se estimularon con TNFα durante los tiempos indicados, se fijaron y se tiñeron para pERM **(a)** o se marcaron con sulfo-NHS-biotina para luego desarrollar un pull-down con neutravina-agarosa **(b).** Barras, 10 µm.

3.2.1. La expresión del mutante constitutivamente activo de ezrina es suficiente para desplazar ICAM-1 hacia la membrana basolateral

Ezrina y radixina son las proteínas ERMs más abundantes en HepG2 (Fig. 18) y ambas se asocian a ICAM-1 en la membrana plasmática (Fig. 20). La interferencia de la función de ERM mediante distintos abordajes experimentales provoca una pérdida notable de la polaridad hepatocelular (Kikuchi et al., 2002), (Wang et al., 2006), lo que hace poco aconsejable estudiar la distribución de ICAM-1 siguiendo estas estrategias. Utilizamos por tanto un mutante de ezrina en el que la treonina fosforilable del extremo c-terminal (T567) había sido sustituida por ácido aspártico, mimetizando así una fosforilación constante que da lugar a la forma constitutivamente activa de la proteína (ezrinT567D-GFP). Como se observa en la figura 26, la expresión transitoria de este mutante en células HepG2 claramente polarizadas fue suficiente para incrementar la localización basolateral de ICAM-1 en comparación con células polarizadas pero no transfectadas en la misma colonia o en comparación con células que habían sido transfectadas con el plásmido GFP vacío. De esta manera, la sobreexpresión de ezrina constitutivamente activa es suficiente para despolarizar ICAM-1, aumentando su distribución basolateral en células que conservan una morfología polarizada.

3.2.2.La inhibición simultánea de PKC y ROCK reduce la fosforilación de las proteínas ERM y la exposición de ICAM-1 en la superficie basolateral en respuesta a TNF-α

Las rutas de señalización que regulan la activación de las proteínas ERM dependen de cada tipo celular y no están todavía bien definidas (Fehon et al., 2010). Entre las quinasas postuladas como activadoras de estas proteínas se encuentran la familia de las PKCs clásicas, Rho kinasa (ROCK) y p38MAPK o Jnk (Ng et al., 2001) (Ivetic and Ridley, 2004) (Koss et al., 2006) (Naydenov et al., 2009) (Aranda et al., 2013). Por otro lado, se ha descrito que en respuesta a TNF-α p38MAPK y varias isoformas típicas de PKC fosforilan a las proteínas ERM en células endoteliales microvasculares de pulmón (Koss et al., 2006), mientras que p38MAPK y ROCK lo hacen en células epiteliales sinoviales (Huang et al., 2011). Por ello, nos preguntamos si la fosforilación de ERM en respuesta a TNF-α podría estar regulada por alguna de estas quinasas en nuestro modelo. Para testar esta hipótesis incubamos las células con inhibidores selectivos

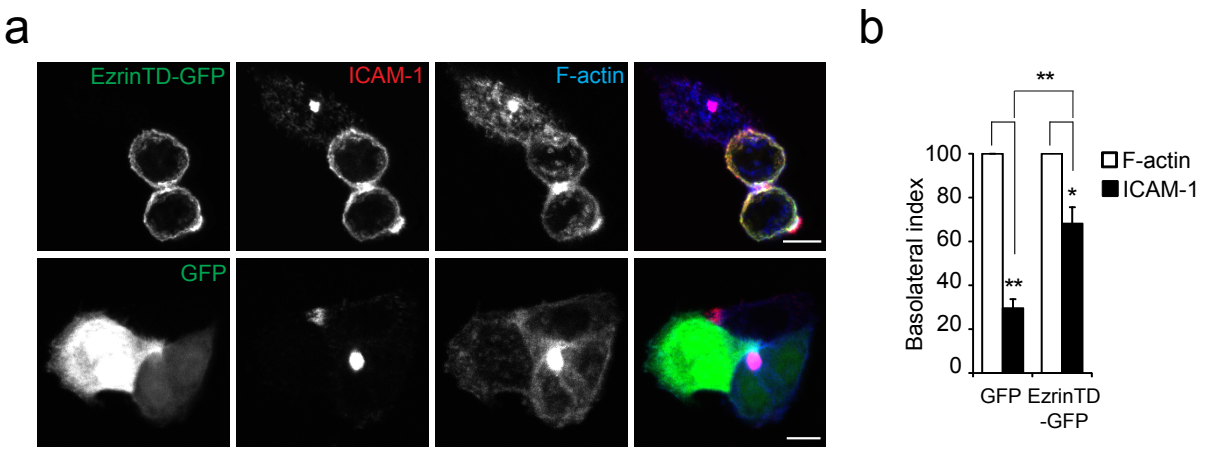

Figura 26. EzrinaTD-GFP incrementa la localización basolateral de ICAM-1 en células HepG2 polarizadas.

(a) Las células HepG2 se transfectaron con EzrinaTD-GFP o con GFP y 24 h después se fijaron y se tiñeron para ICAM-1 y F-actina. **(b)** Cuantificación del ratio basolateral/apical (Basolateral index) de las proteínas indicadas normalizado al índice basolateral para F-actina en cada célula polarizada. Barras, 10 μm. Las barras de error muestran el promedio + SEM de al menos tres experimentos distintos; * $p<0.05$.

de las isoformas clásicas de PKC (PKCGö), de ROCK (Y27632) y de p38 MAPK (PD169316) durante una hora y después procedimos a estimularlas con TNF-α durante 4 horas. El tratamiento con PD169316 no disminuyó los niveles de pERM en respuesta al estímulo (datos no mostrados), mientras que la inhibición de ROCK y PKC-α lo hizo parcialmente. La reducción de los niveles de pERM no fue significativa desde el punto de vista estadístico al inhibir las dos vías por separado, mientras que la inhibición conjunta de ambas quinasas produjo una disminución significativa del 50% respecto al aumento de la fosforilación en respuesta a TNF-α (Fig. 27a, b). Todo ello sugiere que PKC-α y ROCK regulan de forma conjunta la fosforilacion de ERM en respuesta a TNF-α en células HepG2 y que ambas quinasas regulan estas proteínas de forma paralela puesto que los inhibidores tienen un efecto aditivo. Estos datos resultan compatibles con datos de nuestro laboratorio y de otros mostrando que TNF-α activa vías de señalización mediadas tanto por PKC clásicas, como por RhoA-ROCK (Peng et al., 2011) (Nwariaku et al., 2003) (Fernandez-Martin et al., 2012) (Aranda et al., 2013).

Acto seguido, nos preguntamos si los inhibidores de la fosforilación de las proteínas ERM podrían evitar que el receptor se acumulara a este dominio en respuesta a TNF-α. Para contestar a esta pregunta analizamos los niveles de ICAM-1 basolateral (Basolateral Index) en células control o tratadas con PKC-Gö y Y27632 y estimuladas o no con TNF-α. El receptor aparece más polarizado en células con señalización deficiente para PKC clásicas y ROCK que en células control (Fig. 28a, b), mientras que los niveles totales de ICAM-1 en células inflamadas no se alteraron en respuesta al tratamiento con los inhibidores (Fig. 28c).

En conjunto, estos resultados sugieren que la activación de ERM en respuesta a la inflamación por TNF-α a largo plazo puede contribuir a la exposición basolateral de ICAM-1, sin afectar a la integridad canalicular de los hepatocitos. Esta exposición está parcialmente regulada por rutas de señalización dependientes de PKC clásicas y de ROCK, que a su vez previenen la exposición basolateral de este receptor. La exploración detallada de las rutas que favorecen la

segregación de receptores de adhesión en dominios celulares poco accesibles por células del sistema inmunitario podría desvelar nuevas oportunidades terapéuticas para atenuar disfunciones inflamatorias crónicas.

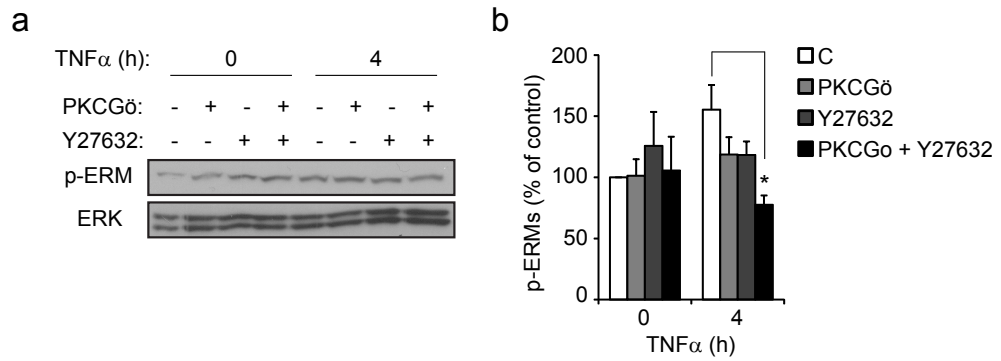

Figura 27. PKCα y ROCK participan en la fosforilación de ERM en respuesta a TNF-α en células HepG2.

(a) Las células HepG2 se cultivaron durante 48 h, se incubaron una hora con inhibidores específicos para PKCα (PKCGö) y/o ROCK (Y27632) y se estimularon durante 4 horas con TNF-α. Los lisados se analizaron por inmunodetección para pERM y ERK con anticuerpos específicos. **(b)** Cuantificación de los niveles de P-ERM para las condiciones detalladas en (a). C, control sin tratamiento. Las barras de error muestran el promedio + SEM de al menos tres experimentos distintos; * p<0.05.

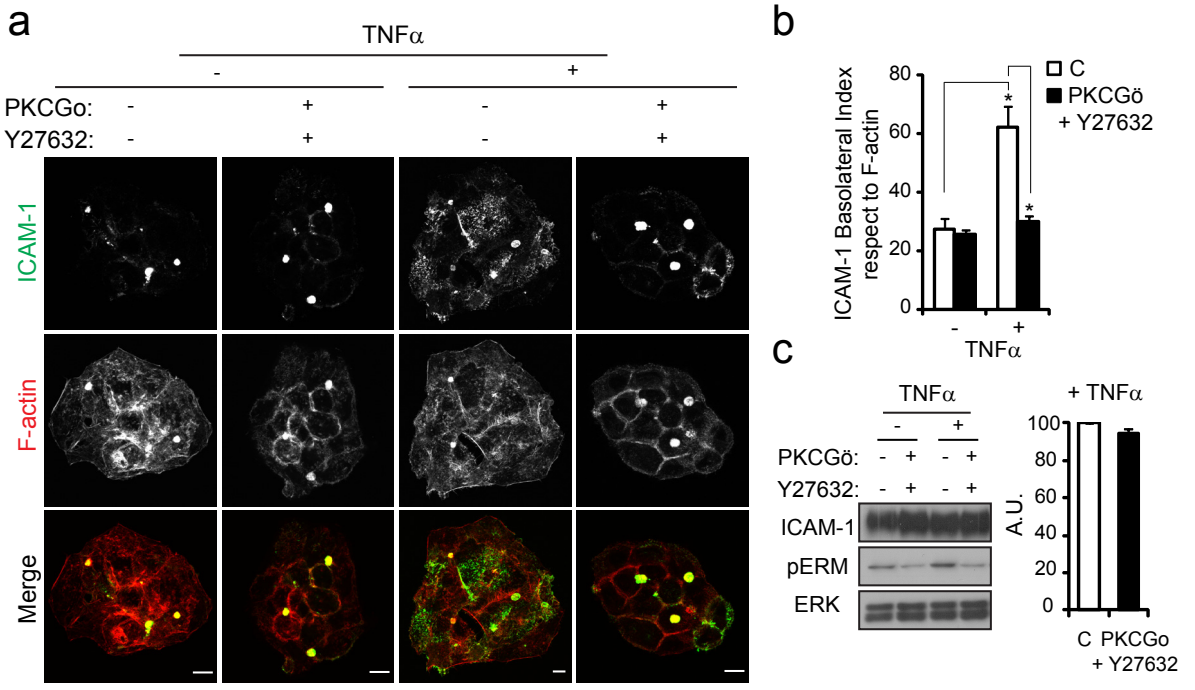

Figura 28. La inhibición de PKCα y ROCK reduce la exposición de ICAM-1 basolateral en respuesta a TNFα.

(a) Las células HepG2 se cultivaron durante 48 h, se incubaron 60 min con inhibidores específicos para PKCα (PKCGö) y ROCK (Y27632) y se estimularon durante 4 h con TNFα. Las células fijadas se marcaron para ICAM-1 y F-actina y se analizaron por inmunofluorescencia. **(b)** Cuantificación del ratio basolateral/apical (Basolateral Index) de ICAM-1 normalizado al índice basolateral para F-actina en cada célula polarizada tratada como se indica. C, control sin tratamiento. **(c)** Células estimuladas con TNF-α y tratadas como se indica fueron lisadas y analizadas por western blot con anticuerpos específicos para ICAM-1, pERM y ERK. Gráfico derecho. Cuantificación de los niveles totales de ICAM-1 en respuesta al tratamiento con inhibidores. A.U., unidades arbitrarias. Barras, 10 μm. Las barras de error muestran el promedio + SEM de al menos tres experimentos distintos; * p<0.05.

4. DISTRIBUCIÓN DE ICAM-1 IN VIVO EN PATOLOGÍAS HEPÁTICAS CON DISTINTO COMPONENTE INFLAMATORIO

Tras nuestros resultados obtenidos *in vitro* indicando que la polarización de ICAM-1 puede contribuir a la respuesta inflamatoria, decidimos estudiar la distribución de ICAM-1 *in vivo* en muestras de modelos animales y de pacientes con diferentes patologías hepáticas inflamatorias en las que este receptor podría jugar un papel relevante (Romero et al., 2000) (Doi et al., 1994) (Volpes et al., 1990) (Kawasuji et al., 2006) (Fernandez-Ruiz et al., 2011).

4.1. El receptor ICAM-1 hepatocítico pierde polaridad durante daño hepático agudo en modelos murinos

En primer lugar quisimos investigar la distribución de ICAM-1 en hepatopatías relacionadas con un daño hepático fulminante, para lo que recurrimos a modelos murinos que mimetizan la situación de fallo hepático fulminante (FHF) humano. El FHF es un síndrome que suele aparecer en pacientes sin necesidad de una enfermedad hepática pre-existente y su etiología es muy variada, incluyendo orígenes víricos, tóxicos o isquémicos (Karlmark et al., 2008). El resultado es una destrucción masiva del parénquima hepático, que puede tener lugar por mecanismos mediados inmunológicamente o por daño directo del hepatocito. Los modelos experimentales de FHF en ratón nos permiten controlar el tiempo y la intensidad del daño hepático. Decidimos, por tanto, analizar la distribución de ICAM-1 el el paréquima hepático de dos modelos murinos de inducción de FHF por tratamiento con Concanavalina A (ConA) o por infección con adenovirus que expresa el ligando del receptor CD40 (AdCD40L).

La administración de ConA, una lectina derivada de la judía, desencadena la activación de células T y NKT de manera intensa, lo que da lugar a la producción masiva de citoquinas hepatotóxicas y a un aumento en la citotoxicidad celular que desemboca en la aparición de numerosas zonas necrosadas en el tejido hepático murino (Zhou et al., 2005) (Fernandez-Ruiz et al., 2011). Se ha demostrado que ICAM-1 juega un papel importante en el reclutamiento de linfocitos CD4 positivos (Wolf et al., 2001) y en el progreso de esta patología inducida (Kawasuji et al., 2006). Como se puede observar en la figura 29a, ICAM-1 se distribuye mayoritariamente en los sinusoides a tiempos cortos de daño hepático (6-24 horas ConA), mientras que apenas se detectó marcaje en los hepatocitos. Sin embargo, entre 12 y 24 horas tras la inyección de ConA, se observaron zonas dónde ICAM-1 se acumula en estructuras inter-hepatocíticas que recuerdan a canalículos biliares (Fig. 29a, imágenes 12 y 24h, ampliación). A las 48 horas de inducción de daño hepático, se detectó un aumento en la expresión de ICAM-1 tanto

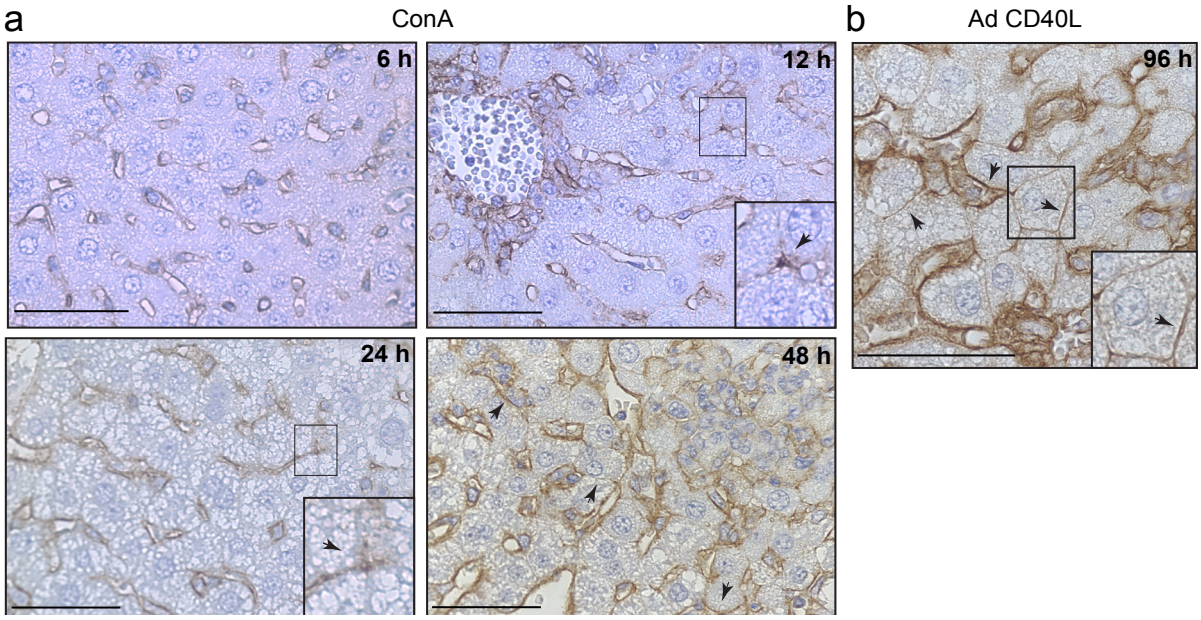

Figura 29. Distribución de ICAM-1 en modelos murinos de daño hepático fulminante.

(a) Muestras embebidas en parafina de tejido hepático de ratones tratados durante 6-48h con ConA fueron desparafinadas y teñidas para ICAM-1. El receptor marca los sinusoides hepáticos (S) y los hepatocitos entre 12 y 48 h tras la inducción de daño hepático (flechas). Las áreas recuadradas ampliadas muestran una distribución del receptor en la membrana canalicular. **(b)** Muestras embebidas en parafina de tejido hepático de ratones tratados durante 96h con AdCD40L fueron desparafinadas y teñidas para ICAM-1. El receptor marca los sinusoides hepáticos (S) y la membrana hepatocítica (área recuadrada ampliada y flechas). En ambos tratamientos se puede observar la pérdida de integridad

en los sinusoides como en los hepatocitos. En estos últimos el receptor se localizó de manera difusa y no polarizada por toda la superficie hepatocelular (Fig. 29a, imagen 48h).

El tratamiento con AdCD40L induce un cuadro de hepatitis fulminante con denso infiltrado leucocitario causado por la activación de células inmunes a diferentes niveles debido a la interacción CD40-CD40L (Fernandez-Ruiz et al., 2011). De modo similar a lo observado dos días después de la inducción del daño hepático por administración de ConA, ICAM-1 se detectó también por todo el perímetro celular de los hepatocitos de ratones tratados durante 96 horas con AdCD40L, incluso en áreas en las que la integridad hepática se encontraba aparentemente conservada (Fig. 29b).

En conjunto, los datos obtenidos de los modelos murinos sugieren que en respuesta a trauma hepático severo ICAM-1 aumenta su expresión hepatocítica y pierde su polaridad canalicular a largo plazo, exponiéndose hacia otras células del prénquima y los sinusoides.

4.2. ICAM-1 se encuentra confinado en el dominio apical en hepatocitos y células epiteliales de los ductos biliares en muestras humanas de rechazo hepático

Durante el rechazo hepático post-transplante la disparidad genética existente entre donante y receptor causa una inflamación del aloinjerto que afecta primordialmente a los canales

biliares y venas porta y hepáticas, con frecuente infiltrado inflamatorio que se extiende al parénquima hepático. Durante esta condición existe un aumento de expresión de ICAM-1 en los hepatocitos (Romero et al., 2000), y el reclutamiento de leucocitos en la microvasculatura hepática de los aloinjertos rechazados es dependiente de dicho receptor (Wong et al., 2002). Al tratarse de una respuesta inmune aguda relativamente corta, se conserva la integridad del tejido en muchas áreas, por lo que decidimos analizar la distribución de ICAM-1 en muestras de pacientes que presentaban esta patología. Además de expresarse en el endotelio sinusoidal, pudimos observar la distribución de ICAM-1 en los canalículos biliares entre hepatocitos en zonas desprovistas de infiltrado leucocitario y sin daño tisular aparente, (Fig. 30, imágenes P1-3). La expresión del receptor en hepatocitos sanos resultó ser muy baja (Fig. 30, imágen Ct) o suficiente, en algunas áreas del parénquima, para detectar una localización canalicular de ICAM-1 como ya se ha señalado anteriormente (Fig. 6c). Hay que destacar que también observamos una distribución apical del receptor en colangiocitos de los ductos biliares intralobulares coincidiendo con el marcador apical CD10 en las muestras de pacientes (Fig. 31,

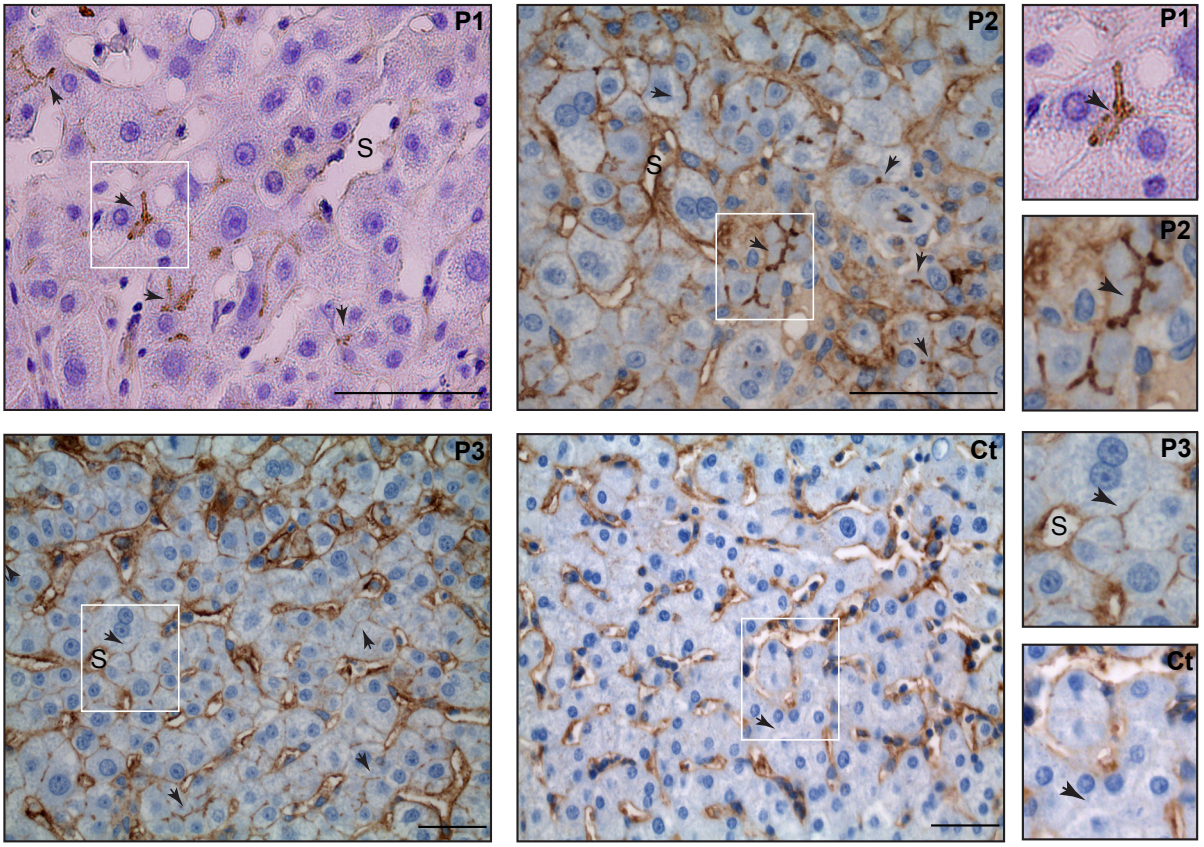

Figura 30. ICAM-1 se localiza en los canalículos biliares de hepatocitos en muestras humanas de rechazo hepático agudo.

Muestras incluidas en parafina de biopsias de tres pacientes (P1-P3) que sufrían rechazo agudo después de transplante hepático fueron desparafinadas y teñidas para ICAM-1. Las imágenes son representativas de áreas sin aparente infiltrado leucocitario ni daño hepático. ICAM-1 aparece marcando los sinusoides hepáticos (S) y los canalículos biliares (BC) (flechas y áreas recuadradas). La imagen inferior derecha muestra una tinción en paralelo de una muestra de tejido hepático procedente de un donante sano (Ct), en la que ICAM-1 se detecta únicamente en los sinusoides. Las imágenes a la derecha muestran ampliaciones de las áreas recuadradas.Barras, 50 µm.

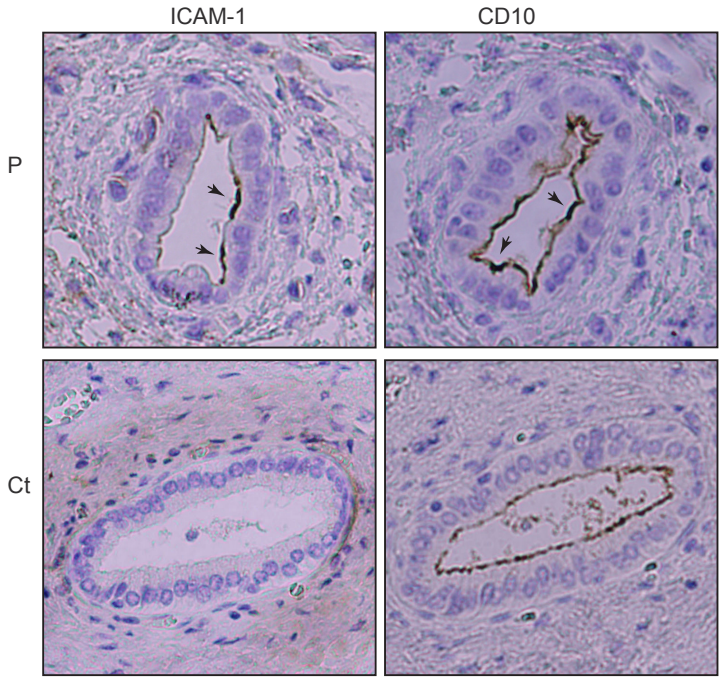

Figura 31. ICAM-1 se localiza en el dominio apical de células epiteliales de ductos biliares en muestras humanas de rechazo hepático agudo.

Cortes seriados de muestras de biopsias de un paciente (P) que sufría rechazo agudo después de transplante hepático y de un donante sano (Ct) fueron desparafinadas y teñidas para ICAM-1 y CD10 con el fin de identificar las células epiteliales biliares. ICAM-1 se localiza en el área apical de los colangiocitos que miran al lumen del ducto biliar en el paciente con rechazo mientras que no se detecta tinción en el control sano (flechas).

imágenes P), mientras que no se detectó expresión de ICAM-1 en ductos biliares de controles sanos (Fig. 31, imágen Ct). De acuerdo a estos resultados, podemos concluir que los hepatocitos que mantienen su arquitectura polarizada segregan ICAM-1 en el canalículo biliar impidiendo por tanto que el receptor sea accesible a los leucocitos infiltrados, corroborando así los datos obtenidos anteriormente en condiciones *in vitro*.

2.2. ICAM-1 presenta una distribución heterogénea en el parénquima hepático en muestras humanas de hígados infectados de forma crónica por los virus de la hepatitis B y C.

La infección por virus de la hepatitis B y C induce una respuesta inmune sostenida en el tiempo que genera daño hepático progresivo y desemboca frecuentemente en fibrosis o carcinoma hepatocelular, causando un deterioro irreversible del parénquima hepático (Kew, 2011) (Wilson et al., 2012). Para analizar in vivo la distribución de ICAM-1 en condiciones de inflamación crónica elegimos por tanto muestras de pacientes que presentasen estas patologías. Además del diagnóstico clínico, se realizó una interpretación anatomopatológica de las biopsias hepáticas para confirmar la existencia de hepatitis crónica (Tabla I). Para ello se detectó la actividad necroinflamatoria (grado) y el índice de fibrosis (estadío) de cada biopsia según el método de Scheuer (Scheuer, 1991). Este método permite expresar los parámetros de actividad y fibrosis de forma semicuantitativa a través de valores numéricos en una escala del 0 (valor mínimo) al 4 (valor máximo). La necroinflamación, que indica la actividad del proceso, se evaluó en el intersticio portal y en la interfase periportal (grado de inflamación portal/periportal) y en el lobulillo (grado de daño hepatocelular). La fibrosis es consecuencia del proceso progresivo necroinflamatorio, que conduce a una remodelación patológica de la arquitectura tisular hepática, y valora el momento evolutivo y la cronicidad de la patología.

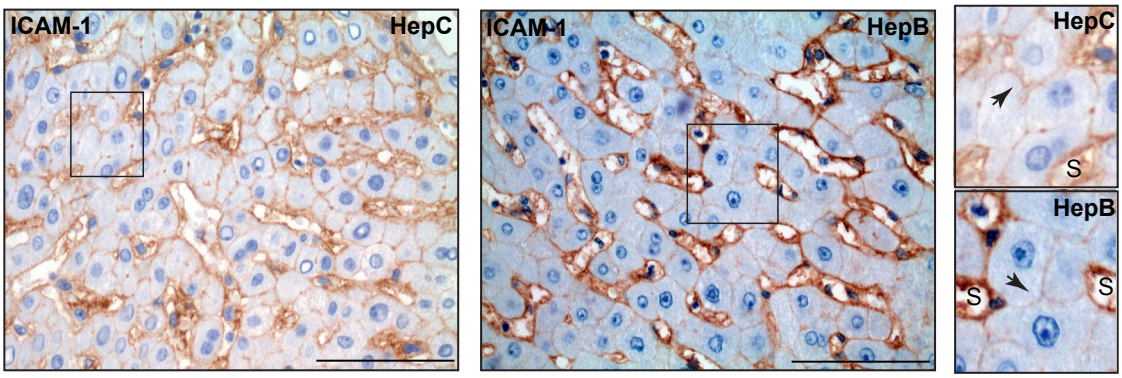

Figura 32. ICAM-1 se distribuye de forma no polarizada en la membrana hepatocítica en muestras humanas de hepatitis B y C.

Muestras incluidas en parafina de biopsias de dos pacientes que sufrían hepatitis C y hepatitis B fueron desparafinadas y teñidas para ICAM-1. El receptor aparece marcando los sinusoides hepáticos (S) y la membrana hepatocítica (flechas y áreas recuadradas). Las imágenes a la derecha muestran ampliaciones de las áreas recuadradas. Barras 50 µm.

Además de la clásica tinción sinusoidal, detectamos un marcaje pericelular de ICAM-1 por la superficie de los hepatocitos en la mayoría de los hígados infectados por virus de hepatitis B (HBV) y hepatitis C (HCV) (Fig. 32), lo que sugiere una pérdida de la polarización del receptor en comparación con las muestras de rechazo hepático (Tabla III). La infección por HBV y HCV reduce la polaridad de los hepatocitos y se ha sugerido por algunos autores que incrementa la transición epitelio-mesénquima, lo que podría contribuir al desarrollo del carcinoma hepatocelular (Akkari et al., 2012) (Kew, 2011; Wilson et al., 2012). En este sentido, un análisis exhaustivo de la polaridad hepatocelular en diferentes patologías hepáticas ha revelado la pérdida de marcadores canaliculares en estados avanzados de hepatitis B y hepatitis C (Shousha et al., 2004). Al examinar la distribución del marcador canalicular CD10 por inmunohistoquímica en muestras de hepatitis B y C fuimos capaces de encontrar zonas con pérdida moderada o totalmente desprovistas de estructuras canaliculares (Fig. 33, Tabla III), lo que corrobora el efecto descrito previamente. El análisis de cortes seriados del mismo tejido seguido de un patrón preciso de reconocimiento de estructuras sinusoidales y canaliculares confirmó una buena correlación entre la acumulación de ICAM-1 y CD10. De esta manera ICAM-1 se distribuye por la superficie hepatocelular en ausencia de estructura canalicular (Fig. 33), mientras que se acumula en el dominio apical cuando se mantiene intacta la arquitectura polarizada de los hepatocitos (Fig. 34a). Al igual que ocurre en las muestras de rechazo hepático post-transplante, ICAM-1 tiñe apicalmente las células epiteliales que recubren el lumen de los ductos biliares en muestras de hepatitis C (Fig. 34b). No obstante, fuimos capaces de encontrar también un número significativo de hepatocitos que aparentemente no polarizan ICAM-1, pero aún así concentran CD10 en estructuras canaliculares (Fig. 35), sugiriendo la existencia in vivo de mecanismos que inducen la exposición basolateral de ICAM-1 sin afectar la integridad canali cular, como por ejemplo la exposición a una inflamación persistente.

En conjunto, nuestros datos in vivo sugieren que la pérdida de polaridad o el incremento de la polaridad basolateral de este receptor en células hepáticas juegan un papel relevante en respuestas inflamatorias agudas, en enfermedades inflamatorias crónicas y en hepatocitos dañados durante fallo hepático fulminante. El análisis de patologías hepáticas de diversa

Paciente	Etiología hepatitis crónica	Grado de actividad portal/ periportal	Grado de daño hepatocelular/ actividad lobulillar	Índice de fibrosis/ estadío
1	HBV	1	2	3
2	HBV	0/1	2	4/3
3	HBV	3	1	4
4	HCV	2	2	3
5	HCV	2/3	2	2/3
6	HCV	2	1/2	3/4

Tabla I. Datos anatomopatológicos de las biopsias con hepatitis B y C.

Tejido	Vena	Arteria	Ducto Biliar	Sinusoide	Hepatocito
HepB	-	-	-	+++	++
HepC	-	-	+	++++	+++
Rechazo	+	+	+	+++	++
Normal	-	-	-	++	-/+

Tabla II. Intensidad del marcaje de ICAM-1 en las biopsias hepáticas analizadas.

Tejido	Grado polaridad (CD10)	ICAM-1 canalicular
HepB	+	+
HepC	+	+
Rechazo	+++	+++
Normal	+++	-/+

Tabla III. Marcaje canalicular de CD10 (Grado de polaridad del tejido) y marcaje canalicular de ICAM-1 en las biopsias hepáticas analizadas.

etiología y prolongación en el tiempo nos permite concluir que los hepatocitos con una arquitectura polarizada intacta son capaces de segregar ICAM-1 a su dominio apical, dónde se encuentra inaccesible a células inmunes sinusoidales y parenquimales. El receptor puede perder su polaridad en respuesta a trauma hepático severo así como en hepatopatías crónicas que afectan a la polaridad hepatocelular. Sin embargo, hay que destacar que también hemos detectado pérdida de polaridad del receptor cuando se mantiene la integridad canalicular encondiciones de inflamación cróewnica y persistente (Fig. 35), lo que sugiere que podrían existir mecanismos que inducen la exposición basolateral de ICAM-1 al margen de la pérdida de polaridad apicobasal hepatocitaria. Nuestros resultados *in vitro* indican que las células hepáticas acumulan ICAM-1 en su membrana basolateral en respuesta a la estimulación prolongada con TNF-α, por lo que resulta plausible que la intensidad del estímulo inflamatorio, en concreto de la citoquina TNF-α, regule la polaridad del receptor en patologías hepáticas crónicas.

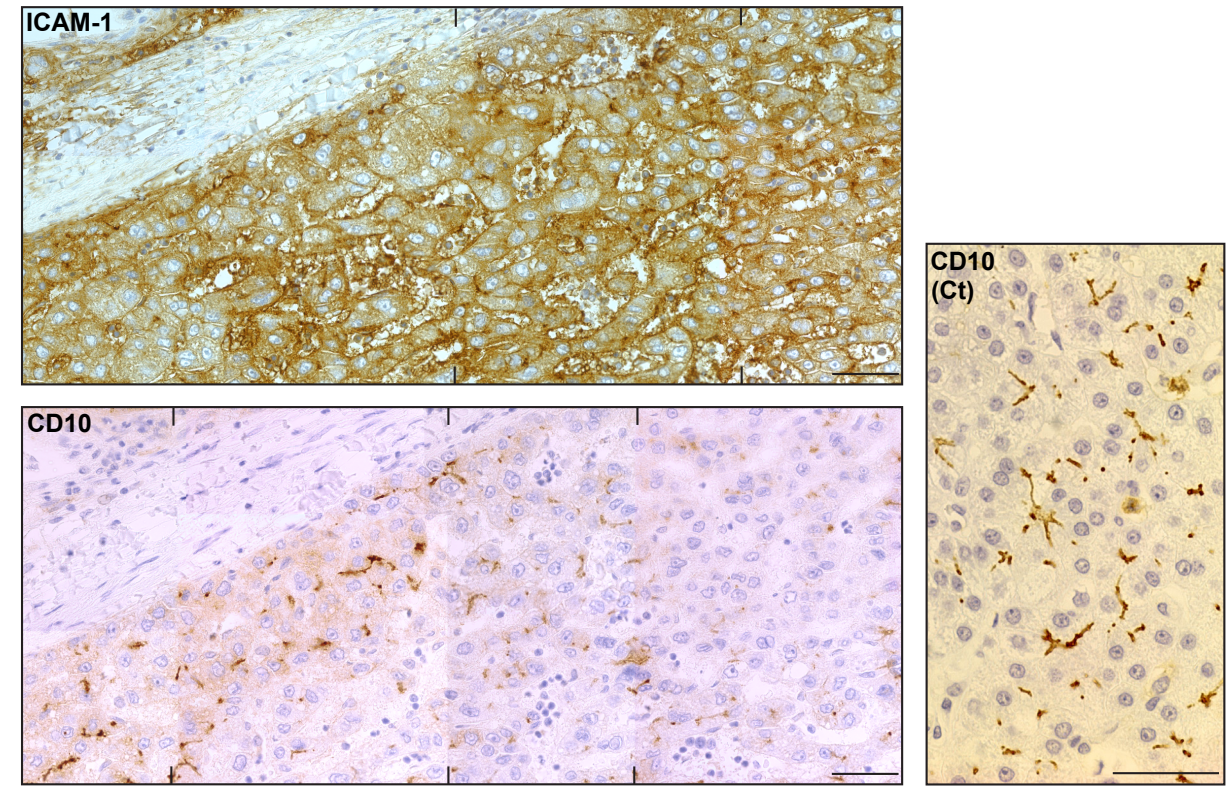
ICAM-1
CD10
CD10
(Ct)

a

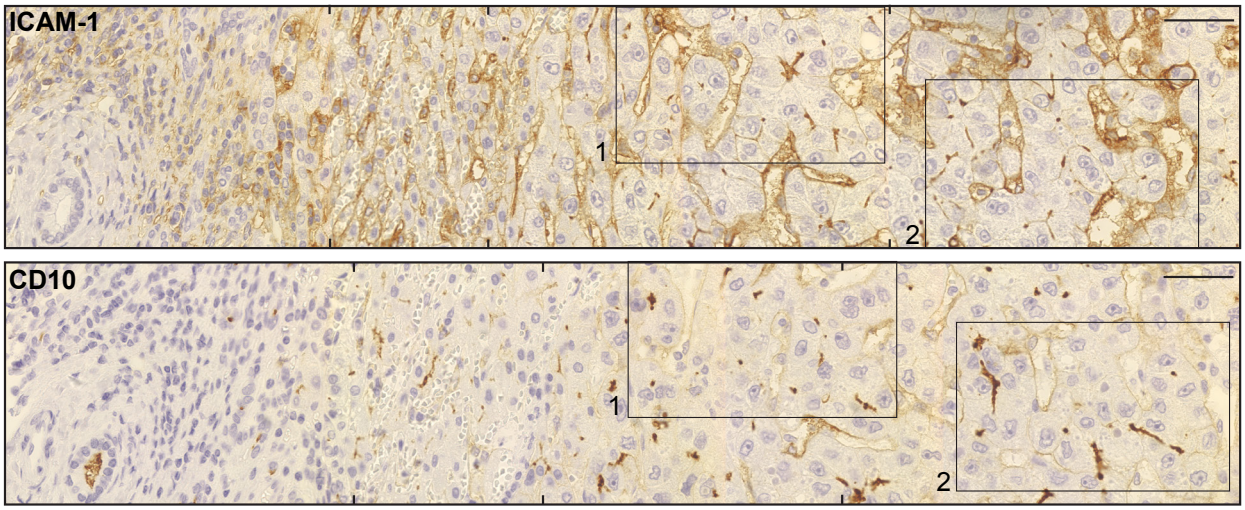
ICAM-1
1
2
CD10
1
2

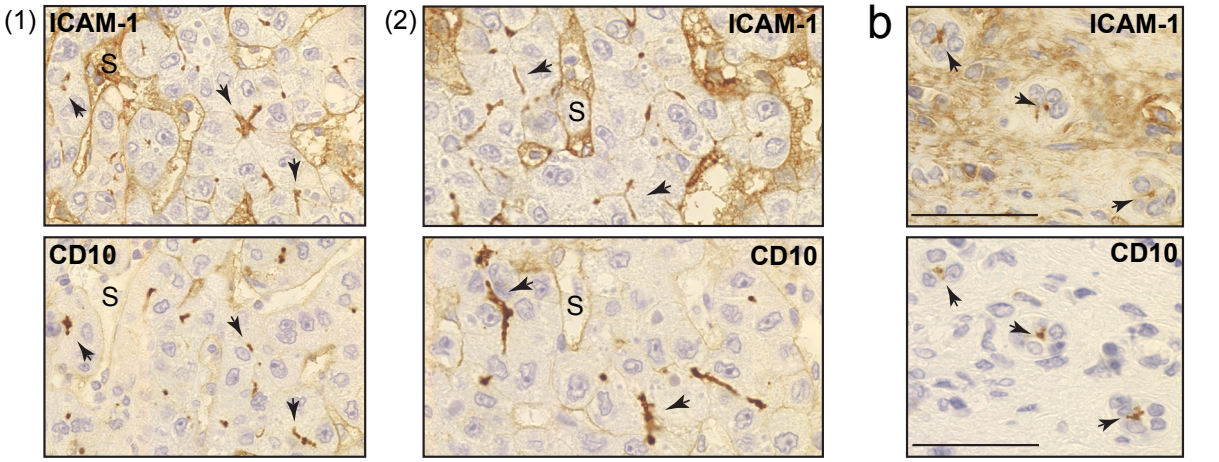
(1)
ICAM-1
S
CD10
S
(2)
ICAM-1
S
CD10
S
b
ICAM-1
CD10

Figura 33. ICAM-1 se distribuye por la superficie de hepatocitos despolarizados en muestras humanas de hepatitis C.

Cortes seriados de muestras de pacientes que sufrían hepatitis C fueron teñidas para ICAM-1 y CD10. La imagen inferior derecha muestra una tinción de CD10 de tejido procedente de un donante sano (Ct). El marcaje de CD10 en las muestras de pacientes presenta áreas con patrón canalicular disminuido respecto al donante sano (zona izquierda) o totalmente ausente (zona derecha). ICAM-1 aparece marcando la mayoría de la superficie parenquimal. Barras, 50 µm.

Figura 34. ICAM-1 se localiza en los canalículos biliares de hepatocitos polarizados y en el dominio apical de colangiocitos de ductos biliares en muestras humanas de hepatitis C.

(a) Cortes seriados de muestras de pacientes que sufrían hepatitis C fueron teñidas para ICAM-1 y CD10. ICAM-1 aparece marcando los sinusoides hepáticos (S) y se acumula en los canalículos biliares teñidos por CD10 (flechas y áreas recuadradas). Las imágenes inferiores muestran ampliaciones de las áreas recuadradas. **(b)** Cortes consecutivos de la misma región del tejido mostrando que ICAM-1 se distribuye apicalmente en colangiocitos de ductos biliares en muestras de hepatitis C (flechas). Barras, 50 µm.

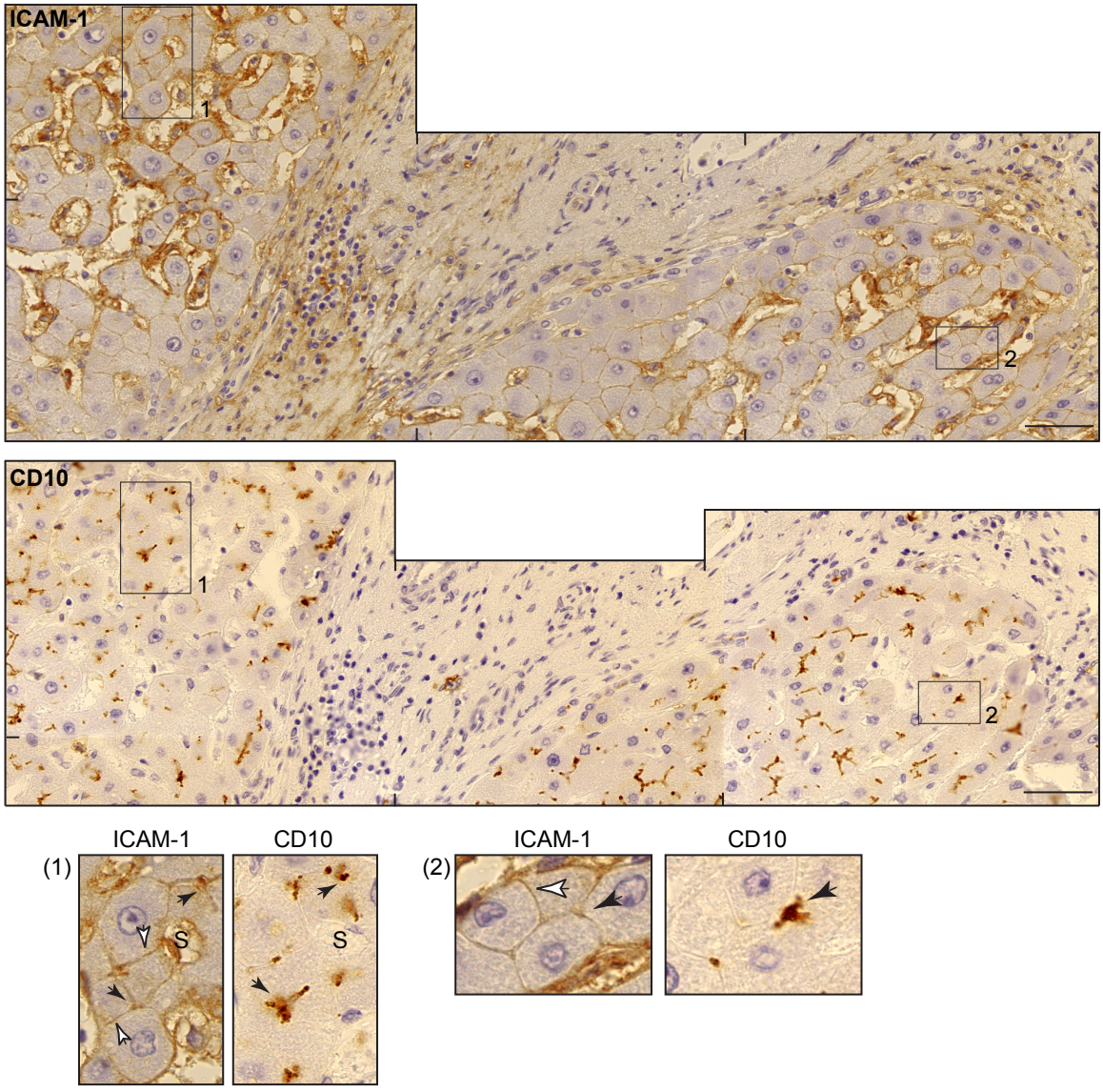

Figura 35. ICAM-1 se distribuye en la membrana basolateral de hepatocitos polarizados en muestras humanas de hepatitis C.

Cortes seriados de muestras de pacientes que sufrían hepatitis C fueron teñidas para ICAM-1 y CD10. En zonas del tejido que mantienen su polaridad, ICAM-1 se localiza en la membrana basolateral de hepatocitos que concentran CD10 en su dominio apical (flechas y áreas recuadradas). Las imágenes inferiroes muestran ampliaciones de las áreas recuadradas. Barras, 50 µm.

DISCUSIÓN

1. LA PÉRDIDA DE POLARIDAD HEPATOCELULAR AUMENTA LA ADHESIÓN LEUCOCITARIA A TRAVÉS DE UN MECANISMO DEPENDIENTE DE ICAM-1

Los hepatocitos son células epiteliales especializadas responsables de la secreción biliar y de las funciones de depuración y detoxificación hepáticas. Como consecuencia de esta última función, las células parenquimales hepáticas se encuentran notablemente expuestas a agentes carcinógenos, tóxicos o infecciosos que causan daño celular, muerte o transformación oncogénica, por lo que el hígado se encuentra estrechamente vigilado por el sistema inmune, y la infiltración leucocitaria del parénquima hepático es distintivo de una amplia gama de patologías hepáticas (Shetty et al., 2008). Mientras que las lesiones histopatológicas de muchas de estas enfermedades se han descrito en detalle en la literatura científica, el mecanismo molecular que regula la comunicación entre células inmunes y células parenquimales hepáticas no se ha investigado en profundidad.

Nuestros resultados indican que la pérdida de polaridad apicobasal aumenta la adhesión leucocitaria a células hepáticas a través de un mecanismo dependiente del receptor de adhesión ICAM-1. Durante este trabajo demostramos que los hepatocitos polarizados segregan ICAM-1 a su dominio apical in vivo e in vitro, impidiendo que sea accesible a los leucocitos infiltrados. Sin embargo, en respuesta a la pérdida de polaridad y a estímulos proinflamatorios ICAM-1 aumenta su exposición al espacio extracelular en contacto con los sinusoides y las células inmunes extravasadas. Estos datos concuerdan con resultados previos obtenidos in vivo que relacionan la expresión de ICAM-1 en la superficie hepatocítica con la infiltración de neutrófilos y linfocitos en hígados con hepatitis alcohólica o inflamación severa causada por HBV (Ohlinger et al., 1993) (Doi et al., 1994). Asimismo existe evidencias in vitro de que la interacción entre ICAM-1 y las integrinas β2 es esencial en la adhesión hepatocito-leucocito, aunque hasta el momento estos estudios se han realizado en hepatocitos primarios estimulados con cócteles de citoquinas proinflamatorias (IFN-γ y TNF-α) (Sano et al., 1999) o cultivados sobre una única capa de matriz extracelular, que no es suficiente para inducir polaridad en cultivos primarios (Meijne et al., 1994), lo que sugiere que la distribución polarizada de ICAM-1 o la polaridad celular hepática pudieran estar disminuidas en estas condiciones. En este contexto, nuestros resultados son los primeros en relacionar la polaridad de este receptor con su capacidad para mediar la adhesión leucocitaria. Nuestros resultados indican que no sólo los niveles de expresión de ICAM-1, sino también su localización en células parenquimales, son capaces de regular la interacción hepatocito-leucocito y, potencialmente, la inflamación hepática.

Los ensayos de adhesión presentados en la primera parte de esta memoria revelan un aumento de la adhesión de linfocitos T sobre células HepG2 despolarizadas. Como se ha co-

mentado anteriormente, en condiciones normales de cultivo entre el 40% y el 60% de las células HepG2 no se encuentran polarizadas. Esto hace que las alteraciones detectadas en la adhesión leucocitaria en respuesta a la modulación de la polaridad apicobasal sean aún más significativas desde el punto de vista cuantitativo, ya que corresponden a cambios producidos en aproximadamente la mitad de la población celular estudiada. Por otro lado, a pesar de que los experimentos de pérdida de función de ICAM-1 hepatocelular a través del silenciamiento de su expresión con siRNAs específicos disminuyeron significativamente la adhesión linfocitaria sobre células HepG2 despolarizadas, ésta no se abolió por completo. Este efecto se debe probablemente a que los hepatocitos expresan otras moléculas de adhesión capaces de interaccionar con los leucocitos además de ICAM-1. En células HepG2 hemos comprobado la expresión de otros receptores de la superfamilia de las inmunoglobulinas como ALCAM, aunque éste no aparece polarizado en nuestro sistema celular. Existe asimismo evidencia de la expresión de distintas moléculas de adhesión como JAM-A (Konopka et al., 2007), CD44 (Seelentag et al., 1995), LFA-3 y CD40 (Cruickshank et al., 1998). Sin embargo el rescate de la adhesión linfocitaria debido a la expresión exógena de ICAM-1-paGFP en células HepG2 silenciadas para la expresión de ICAM-1 endógeno realizado en este trabajo demuestra que este receptor cumple una función relevante en la adhesión de linfocitos T a células parenquimales hepáticas que pierden la polaridad apicobasal.

2. BASE MOLECULAR DE LA INTERACCIÓN CÉLULA INMUNE-HEPATOCITO

2.1. ICAM-1 hepático se asocia a ERM a través de su segmento citoplásmico, requerido para la localización apical del receptor.

Se han descrito múltiples proteínas de membrana que pueden asociarse a ERM, entre ellas receptores de adhesión presentes en leucocitos y/o células endoteliales como ICAM-1-3, CD44, CD43 y L-Selectina (Heiska et al., 1998) (Bretscher et al., 2002). En concreto para ICAM-1, se ha identificado una secuencia de cinco aminoácidos básicos (RKIKK) en su segmento citoplásmico crítica para la interacción del receptor con ERMs, su localización en los microvilli endoteliales y la adhesión y transmigración leucocitaria (Oh et al., 2007). Mediante ensayos de asociación hemos demostrado que los tres residuos de lisina comprendidos en el motivo RKIKK son fundamentales para la interacción de ICAM-1 con ezrina y radixina en células hepáticas. Sin embargo ICAM-1 hepatocitario no sólo requiere su dominio citoplásmico para asociarse a las proteínas ERM en la membrana plasmática, sino también para localizarse en el dominio apical enriquecido en ERM fosforiladas. Nuestros datos sugieren que, además de estabilizar ICAM-1 en la membrana basolateral en condiciones de daño hepático o inflamación, las proteínas ERM sean probablemente también necesarias para la retención apical de ICAM-1 en hepatocitos polarizados, al igual que se ha descrito para otras proteínas transmembrana

como Mrp2 (Kikuchi et al., 2002). A pesar de ello, la construcción de ICAM-1 sin el segmento citoplásmico continúa localizándose en parte en el dominio apical, por lo que no puede descartarse la existencia de interacciones a través de su extremo extracelular que contribuyan también a la polarización del receptor. Otros candidatos a unirse al dominio extracelular de ICAM-1 en los lúmenes apicales hepáticos podrían pertenecer a las familias de las mucinas, como MUC-1. Las mucinas son glicoproteínas de localización apical, sintetizadas por las células epiteliales, que pueden actuar como receptores transmembrana señalizando a través de sus extremos citoplásmicos o bien ser secretadas al espacio intraluminal para proteger la superficie mucosa de sustancias tóxicas presentes en fluidos corporales como la bilis. La interacción entre ICAM-1 y la mucina transmembrana MUC-1 se ha descrito en otros tipos celulares (Shen et al., 2008) y su expresión se ha detectado in vivo en muestras humanas de carcinomas hepatocelulares (Cao et al., 1999) y en colangiocitos (Vandenhaute et al., 1997), por lo que resulta tentador especular sobre una posible interacción entre ambas proteínas en el lumen apical de estas células. Aunque en hepatocitos no transformados su expresión es negativa, MUC-1 es una mucina cuya expresión se incrementa en respuesta a TNF-α, por lo que su posible interacción con ICAM-1 en células epiteliales polarizadas podría depender de su estimulación inflamatoria.

2.2. Doble rol de la maquinaria proteica ERM-ICAM-1 en células parenquimales hepáticas.

En hepatocitos polarizados las proteínas ERM cumplen roles muy diferentes a aquellos descritos para la transmigración leucocitaria a través de la monocapa endotelial. ERM regulan la polaridad hepatocelular: se localizan en el canalículo biliar modulando los microvilli canaliculares y la localización apical de transportadores como Mrp2 (Kikuchi et al., 2002) (Wang et al., 2006). Sin embargo, como se ha explicado anteriormente, nuestros resultados sugieren que la interacción de ERM con ICAM-1 podría participar en la interacción entre leucocitos y hepatocitos. Nuestra propuesta es que este doble rol constituye la base molecular de la relación inversa encontrada entre polaridad hepatocelular y adhesión leucocitaria. Cuando se encuentran confinadas a los microvilli canaliculares, las proteínas ERM regulan la polaridad hepatocelular y la secreción biliar a la vez que contribuyen a atenuar la respuesta inmune confinando receptores de adhesión. En respuesta a daño hepático o inflamación persistente, dicha maquinaria deja de jugar un papel en el mantenimento de la polaridad canalicular, se expone al espacio extracelular y cumple funciones haptotácticas de manera similar a lo que ocurre en el endotelio (Barreiro et al., 2002) (Reglero-Real et al., 2012) (Fig. 36). Los futuros estudios sobre la función de ERM hepáticas pueden contribuir a dilucidar nuevas posibilidades terapéuticas para controlar la función hepática durante la respuesta inflamatoria.

Probablemente la doble función descrita para ERM e ICAM-1 puede extenderse a otra maquinaria proteica, y sería interesante comprobar si los hepatocitos sanos utilizan el mismo mecanismo para mantener "ocultos" a las células inmunes distintos receptores de adhesión. JAM-A, por ejemplo, es un componente de las uniones estrechas que pertenece a la superfamilia de las inmunoglobulinas y media la transmigración leucocitaria endotelial (Bradfield et

al., 2007). Este receptor resulta además clave en la regulación de la polaridad en células inmunes y epiteliales (Bradfield et al., 2007), y tanto la ausencia como la sobreexpresión de JAM-A impiden la adquisición por los hepatocitos de un fenotipo polarizado (Braiterman et al., 2008) (Konopka et al., 2007). Además de regular la polaridad hepatocelular resulta plausible que este receptor intervenga en la interacción leucocito-hepatocito en células parenquimales dañadas que hayan perdido la integridad canalicular. Otro candidato a desempeñar una función similar a la de ICAM-1 en el parénquima hepático es el receptor CD44. Al igual que ICAM-1, CD44 es una proteína transmembrana tipo I que se localiza apicalmente en células epiteliales y señaliza al citoesqueleto de actina a través de su interacción con las proteínas ERM (Yonemura and Tsukita, 1999) (Pure and Cuff, 2001). Este receptor está implicado en las interacciones célula-célula y célula-matriz, siendo el ácido hialurónico su ligando principal. CD44 presenta una distribución ubicua, y su expresión hepatocelular ha sido descrita en líneas celulares derivadas de hepatoma como HepG2 (Mi et al., 2012) (Phillips et al., 2012) e in vivo en hepatocitos transformados, mientras que no se ha llegado a detectar en hígados de controles sanos (Seelentag et al., 1995). Es más, la interacción entre CD44 y las proteínas ERMs parece mediar la migración de células hepáticas inducida por la proteína X del virus de la hepatitis B (Lara-Pezzi et al., 2001). Por otra parte, además de participar en la migración y

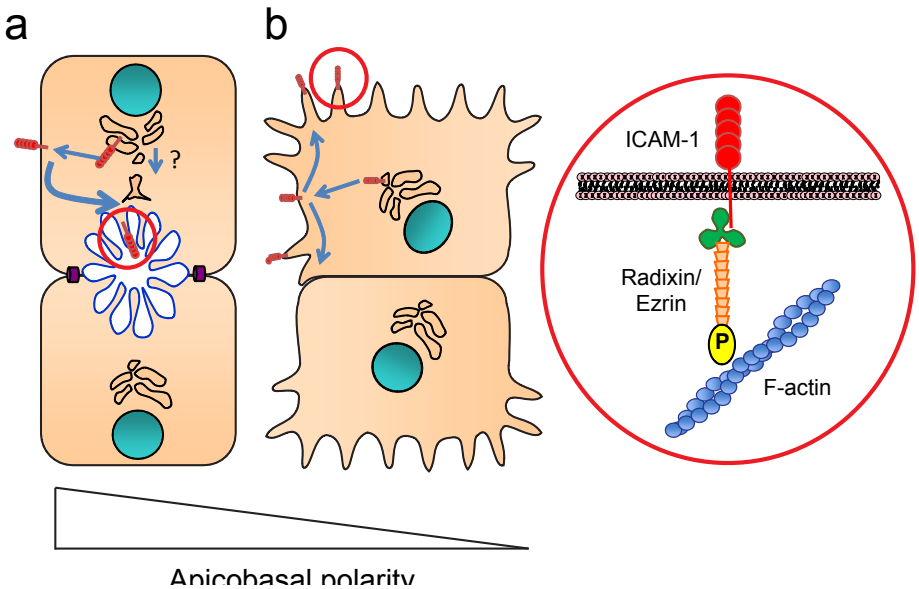

Figura 36. Doble rol de la maquinaria proteica ERM-ICAM-1 en el parénquima hepático.

(a) En hepatocitos polarizados ICAM-1 es capaz de alcanzar la membrana basolateral pero es redirigido al canalículo biliar, dónde probablemente juegue un papel en el mantenimiento de la integridad canalicular junto con las proteínas ERM. (b) En respuesta a la despolarización ICAM-1 y ERM aparecen expuestos al espacio extracelular favoreciendo la interacción entre leucocitos y hepatocitos. ICAM-1 se encuentra anclado al citoesqueleto de actina a través de la interacción de su cola citoplásmica con las proteínas ERM.

proliferación celular, procesos asociados a la remodelación tisular y a la metástasis tumoral, CD44 regula el desanclaje de linfocitos adheridos a la superficies epiteliales (Brazil et al., 2010). Por tanto, en el contexto de la trasformación de células hepáticas, la regulación de la polaridad y/o expresión de este receptor también podría ayudar a las células del sistema inmune a reconocer células parenquimales despolarizadas y con una capacidad migratoria patológica.

3. LOS HEPATOCITOS POLARIZADOS PREVIENEN LA EXPOSICIÓN DE ICAM-1 A CÉLULAS INMUNES REDIRIGIENDO EL RECEPTOR DESDE LA MEMBRANA BASOLATERAL AL CANALÍCULO BILIAR

Se ha propuesto que en hepatocitos polarizados algunos receptores transmembrana como la dipeptidil peptidasa IV, o el receptor de inmunoglobulina polimérica A (pIgA-R) son confinados en la membrana apical mediante una ruta de transporte denominada indirecta que incluye la localización basolateral inicial seguida de transcitosis desde el dominio basolateral hasta el apical (Bastaki et al., 2002). A través de diferentes estrategias experimentales hemos demostrado la existencia de un transporte en la dirección basolateral-apical para ICAM-1 en células HepG2. La fotoactivación selectiva de ICAM-1-paGFP en el dominio apical nos ha permitido además demostrar que el receptor se encuentra firmemente confinado en el canalículo biliar, probablemente a través a su interacción con el citoesqueleto de actina descrita en el apartado anterior. Por tanto, el transporte desde la región basolateral hasta la membrana apical y el posterior confinamiento del receptor en este dominio explican la segregación de ICAM-1 fuera de la membrana basolateral hepatocitaria, que es accesible desde los sinusoides y el resto del parénquima, a pesar de que la existencia de una ruta de transporte apical directo para ICAM-1 no se puede descartar con estos experimentos. Por consiguiente, además de las proteínas conectoras que estabilizan ICAM-1 en distintos dominios de membrana, la maquinaria de transcitosis que gobierna el tráfico basolateral-apical en hepatocitos proporcionaría un segundo conjunto de potenciales dianas terapéuticas para modular la exposición de receptores de adhesión a células inmunes infiltradas en el parénquima hepático. Esta maquinaria hepática incluye la proteína MAL2, un miembro de la familia de proteínas MAL que se caracteriza por residir en balsas lipídicas de membrana. MAL2 está involucrada en el transporte vesicular polarizado e interacciona con la formina invertida INF2, regulada por la Rho-GTPasa Cdc42 (de Marco et al., 2002) (Madrid et al., 2010). INF2 emite cometas de actina desde la región apical a la basolateral que guían el compartimento sub-apical de MAL2 y provocan su encuentro con el material internalizado desde la membrana basolateral (Madrid et al., 2010). Por otra parte, ICAM-1 se recluta a balsas lipídicas de membrana en respuesta a la unión de sus ligandos o de anticuerpos específicos en células endoteliales (Tilghman and Hoover, 2002), localizándose particularmente en dominios ordenados de membrana deno-

minados caveolas, que son vesículas recubiertas por la proteína caveolina. La transcitosis del receptor en estas vesículas desde la superficie luminal a la región basal regula la vía de transmigración endotelial transcelular (Millan et al., 2006). Tanto la maquinaria asociada a MAL-2 como el sistema caveolar son potenciales reguladores de la localización polarizada de ICAM-1 y, por tanto, de las interacciones leucocito-hepatocito.

4. ASPECTOS FUNCIONALES DE LA EXPOSICIÓN HEPATOCITARIA DE ICAM-1 AL ESPACIO EXTRACELULAR

4.1. Función haptotáctica de ICAM-1

Durante la migración intersticial por el parénquima los leucocitos desarrollan un movimiento ameboide que permite escanear la superficie de las células parenquimales y detectar la presencia de receptores de adhesión que utilizarán para desplazarse mediante un mecanismo conocido como haptoquinesis (Friedl and Weigelin, 2008). Tanto la función inmune innata como adquirida dependen de la migración intersticial leucocitaria, por lo que la regulación de este proceso puede suprimir la inflamación innecesaria o estimular respuestas inmunes insuficientes. Recientemente se ha demostrado además que la inmunovigilancia hepática cumple un papel central en la eliminación de células transformadas, para lo que resulta imprescindible que las células inmunes reciban información de los hepatocitos no funcionales en el parénquima (Kang et al., 2011).

Nuestros resultados in vitro y el análisis de diversas muestras de tejido indican que, además de la existencia de gradientes quimiotácticos, la polaridad hepatocelular y la extensión de la respuesta inflamatoria pueden contribuir a proporcionar pistas haptotácticas para los leucocitos infiltrados a través de la exposición de receptores de adhesión por parte de los hepatocitos. Este mecanismo permitiría a las células inmunes discriminar entre hepatocitos despolarizados y disfuncionales y aquellos que conserven su polaridad y se encuentren todavía operativos (Fig. 37). De acuerdo a esta hipótesis, la interacción de ICAM-1 expuesto en la membrana sinusoidal de hepatocitos disfuncionales con las integrinas β2 de linfocitos T CD8 activos o neutrófilos permitiría el contacto cercano entre célula diana y efectora, facilitando, por ejemplo, la liberación de gránulos citotóxicos y especies reactivas de oxígeno al citoplasma de los hepatocitos, lo que causaría la muerte por necrosis de la célula parenquimal despolarizada (Jaeschke and Hasegawa, 2006). Además se ha propuesto que los microvilli de los hepatocitos pueden pasar a través de las fenestraciones sinusoidales, alcanzar el torrente sanguíneo y así contribuir a la transmigración de leucocitos (Warren et al., 2006) (Edwards et al., 2005), por lo que, según

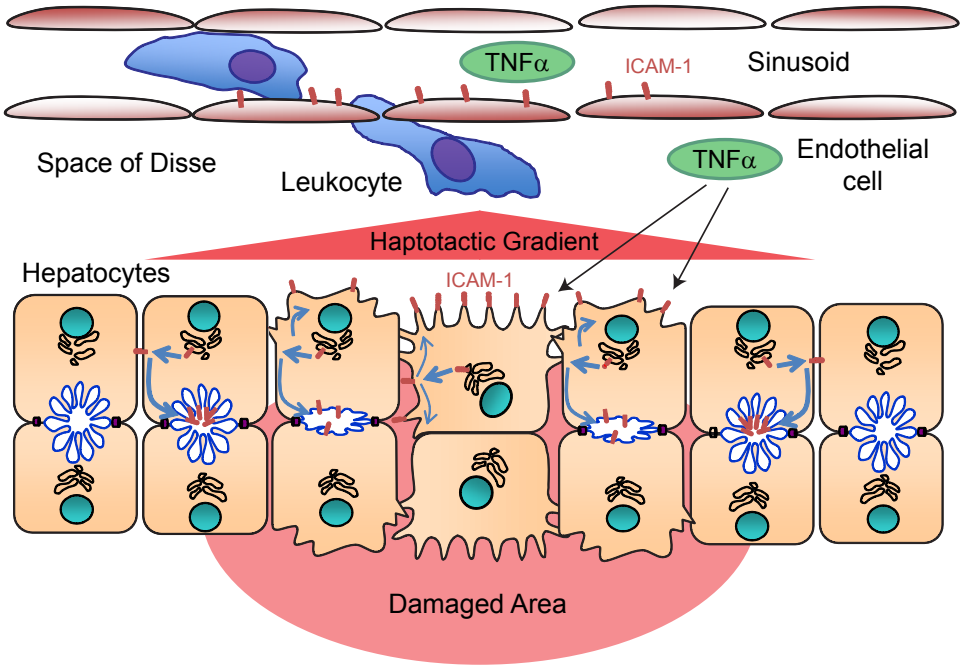

Figura 37. La polaridad apicobasal de células hepáticas regula la respuesta inflamatoria en el hígado.

Nuestra propuesta es que la polaridad hepatocelular y la inflamación crónica pueden contribuir generar un gradiente haptotáctico para los leucocitos infiltrados a través de la exposición de receptores de adhesión por parte de los hepatocitos. Este mecanismo permitiría a las células inmunes discriminar entre hepatocitos despolarizados y disfuncionales y aquellos que conserven su polaridad y se encuentren todavía operativos.

este modelo, la despolarización de ICAM- l en hepatocitos dañados o inflamados intervendría directamente en el reclutamiento de nuevas células inmunes desde los sinusoides.

In vivo, la identificación de las estructuras canaliculares por CD10 y el marcaje de ICAM-1 en cortes seriados de tejido hepático con hepatitis B y C crónica nos ha permitido observar que el receptor se acumula en los canalículos biliares en áreas donde todavía se conserva la integridad tisular, mientras que los hepatocitos con pérdida de polaridad apicobasal exhiben una distribución de ICAM-1 por toda la superficie celular. También hemos detectado hepatocitos con una distribución despolarizada de ICAM-1 pero donde CD10 todavía marca estructuras canaliculares, lo que sugiere que, en un contexto de inflamación crónica, existen mecanismos adicionales que inducen la acumulación de ICAM-1 en la membrana basolateral hepatocítica. Estos datos, además, concuerdan con estudios previos de hígados infectados por HBV donde se describe el confinamiento canalicular de ICAM-1 en hígados con infección de HBV leve, mientras que en condiciones de inflamación severa y notable infiltrado leucocitario ICAM-1 presenta una distribución no polarizada (Doi et al., 1994). Las infecciones agudas por HBV y HCV reducen la polaridad hepatocelular y contribuyen al desarrollo de un fenotipo hepatocelular transformado (Akkari et al., 2012) (Kew, 2011; Wilson et al., 2012), por lo que hipotetizamos que la exposición basolateral de ICAM-1 puede ayudar a las células inmunes a detectar hepatocitos en estados avanzados de infección viral. Por otra parte, nuestros resultados acerca del efecto de la estimulación a largo plazo con TNF-α sobre la polaridad de ICAM-1, que se discuten en más detalle en apartados posteriores, sugieren que una inflamación persistente, como la que ocurre

en hígados con infección crónica de hepatitis B y C, podría subyacer a la mencionada localización basolateral de ICAM-1 que se detecta en hepatocitos polarizados en estados avanzados de estas patologías.

4.2. Rol de ICAM-1 en la tolerancia inmune y presentación antigénica.

Además de contribuir al gradiente haptotáctico que favorece la migración intersticial de los leucocitos a través del parénquima hepático, la exposición de ICAM-1 hepatocelular al espacio extracelular puede tener otras consecuencias. Se ha propuesto que el hígado cumple un papel único en el sistema inmune y que podría competir con los nódulos linfáticos en la activación de linfocitos T "naive" o vírgenes (Holz et al., 2010) en procesos de tolerancia inmunológica. La activación de linfocitos T vírgenes requiere el entrecruzamiento de su receptor, TCR (T cell receptor) por moléculas del complejo mayor de histocompatibilidad (MHC) unidas al antígeno correspondiente, así como la interacción entre moléculas coestimuladoras en la superficie de las células presentadoras de antígeno y sus ligandos linfocitarios (Dubey and Croft, 1996). En el hígado existen numerosas células con capacidad de presentación antigénica, pero en concreto los hepatocitos exponen en su membrana basolateral moléculas MHC capaces de activar linfocitos T. Los hepatocitos expresan MHC tipo I bajo condiciones normales (Warren et al., 2006) que aumentan en respuesta a citoquinas proinflamatorias (Cruickshank et al., 1998), mientras que la expresión de MHC tipo II únicamente se ha detectado en higados infectados con virus de la hepatitis (Franco et al., 1988). Además, la interacción entre el TCR y el complejo antígeno-MHC es de baja afinidad y la adhesión entre la célula T y célula presentadora debe ser estabilizada para alcanzar el umbral de activación adecuado en cada caso (Dubey and Croft, 1996). En los hepatocitos, la unión de ICAM-1 a las integrinas LFA-1 y Mac-1 linfocitarias contribuiría a estabilizar esta interacción linfocito-hepatocito implicando que la célula hepática desempeñe un papel en la activación linfocitaria además de actuar como diana inmunológica. Los linfocitos T vírgenes carecen de las moléculas necesarias para atravesar las barreras endoteliales, pero, como se ha mencionado la arquitectura singular del sinusoide facilita el contacto a través de sus fenestraciones entre las células inmunes y las parenquimales. (Warren et al., 2006). Esto permitiría que los linfocitos T escaneen directamente la superficie hepatocitaria en busca de la presentación de antígenos sin la necesidad de abandonar los sinusoides, favorecidos por el estrecho diámetro sinusoidal, el lento flujo sanguíneo y la ausencia de membrana basal.

Se ha comprobado que los linfocitos T CD8 pueden ser activados por MHC de clase I hepatocíticas de un modo en que las células inicialmente proliferan pero mueren de forma temprana por apoptosis (Bertolino et al., 1998). Esta activación se ha relacionado con la función del hígado como órgano que fomenta la tolerancia inmune hacia antígenos inocuos procedentes del tracto gastrointestinal (Holz et al., 2010). Hay que subrayar que la proliferación de células T mediada por hepatocitos es independiente de CD28, pero depende del papel coestimulador de la interacción ICAM-1/LFA-1 (Bertolino et al., 1998). La coestimulación por ICAM-1/LFA-1 induce en células T vírgenes una proliferación inicial y una muerte posterior por apoptosis

(Zuckerman et al., 1998), como la observada tras la estimulación por hepatocitos, mientras que en células T Th1 induce anergia (Zuckerman et al., 1998), unas respuestas en el linfocito que se consideran de tipo tolerogénico. Por tanto, puesto que los hepatocitos carecen de moléculas coestimuladoras B7 para interaccionar con el coestimulador linfocítico CD28 (Holz et al., 2010), la presencia de ICAM-1 en el dominios basolaterales de membrana podría contribuir a regular la tolerancia inmune coestimulando durante la presentación antigénica por hepatocitos. Aunque nuestros resultados indican que la exposición de ICAM-1 hepatocítico a las células inmunes ocurre en respuesta a la pérdida de polaridad apicobasal o a la inflamación, hemos detectado una fracción del receptor que se sitúa en la membrana basolateral de células hepáticas en condiciones normales, probablemente en su ruta transcitótica hacia el dominio apical. Por otro lado, desconocemos si ICAM-1 es capaz de acumularse en el dominio basolateral de los hepatocitos en condicones de presentación antigénica. Se ha demostrado que la retención de linfocitos que reconocen específicamente un antígeno presentado por hepatocitos puede ser bloqueada con anticuerpos bloqueantes de ICAM-1 e ICAM-2 (Warren et al., 2006), aunque la función de estos coreceptores expresados por el hepatocito en la regulación de la tolerancia inmunológica mediada por el hígado no ha sido formalmente demostrada *in vivo* por el momento.

Los hepatocitos intervienen también en la tolerancia inmune provocando la eliminación de células T autoreactivas activadas en el hígado. Se ha demostrado que la trasferencia de linfocitos T autoreactivos en modelos murinos de autoinmunidad no induce ninguna patología autoinmune porque dichos linfocitos son eliminados en el hígado por las células hepáticas (Benseler et al., 2011). Los hepatocitos eliminan estas células mediante un proceso denominado emperipolesis, en el que el linfocito se adhiere y penetra en la célula hepática para terminar degradándose en el compartimento lisosomal (Benseler et al., 2011). La emperopolesis presenta muchas similitudes con la migración transendotelial transcelular en el que los linfocitos emiten podosomas que invaden y abren canales en las células endoteliales para posteriormente atravesarlas (Carman et al., 2007). Este mecanismo implica la internalización de ICAM-1 en caveolas y su transcitosis desde la región luminal a la basal (Millan et al., 2006). Puesto que el paralelismo entre ambos procesos parece evidente, resulta tentador especular que, para guiar la internalización de linfocitos T autoreactivos adheridos al hepatocito, estos utilicen el tráfico de ICAM-1 desde la región basolateral a la apical descrito en este trabajo para guiar el proceso de invasión intracelular de modo parecido a l diapédesis transcelular. Por otro lado, la emperipolesis se ha observado también en muestras de pacientes con hepatitis B y C (Dienes, 1989), y se ha descrito que distintas líneas celulares tumorales, entre ellas HepG2, pueden internalizar células NK sanas y producir intracelularmente su muerte por apoptosis (Wang et al., 2009b). En estos casos la célula tumoral internaliza al leucocito mediante un mecanismo dependiente de ezrina (Wang et al., 2009b). ICAM-1 expuesto al espacio extracelular en los hepatocitos dañados o transformados podría intervenir en este proceso mediante su interacción con ERM y la formación de “estructuras de anclaje” que hemos descrito en células parenquimales y que se asemejan a las proyecciones de membrana

endoteliales encargadas de rodear a los leucocitos durante su transmigración. Proponemos por tanto que la polaridad hepatocelular y el tráfico del receptor ICAM-1 podrían regular el fenómeno de la emperipolesis controlando la localización de receptores de adhesión y, una vez más, la respuesta inmune hepática.

5. LA ESTIMULACIÓN POR TNF-α A LARGO PLAZO AUMENTA LA EXPOSICIÓN BASOLATERAL DE ICAM-1 A TRAVÉS DE LA ACTIVACIÓN DE ERM VÍA PKC Y ROCK.

Durante este trabajo hemos comprobado que la estimulación a largo plazo de hepatocitos con citoquinas proinflamatorias como el TNF-α aumenta la exposición basolateral de ICAM-1 y ERM manteniendo la integridad canalicular. Esto explicaría la distribución de ICAM-1 observada en muestras humanas de hepatopatías crónicas como hepatitis B y C, donde el receptor se localiza tanto en la membrana basolateral como en el dominio apical hepatocíticos, sugiriendo que la intensidad de la respuesta inflamatoria puede regular la accesibilidad de la maquinaria de adhesión a las células inmunes.

Nuestros resultados sugieren que la activación basolateral de ERM en respuesta a TNF-α es responsable de la acumulación de ICAM-1 en este dominio, probablemente reteniendo el receptor a través de su anclaje al citoesqueleto de actina por su extremo citoplásmico. Asimismo hemos comprobado que las quinasas ROCK y PKC clásica regulan la fosforilación de ERM hepatocelulares en respuesta a TNF-α. Estos datos concuerdan con resultados previos obtenidos en otros tipos celulares que demuestran la implicación de esta maquinaria en la fosforilación de las proteínas ERM (Aranda et al., 2013) (Hirao et al., 1996) y la activación de las rutas de señalización mediadas por RhoA-ROCK y PKC en respuesta a TNF-α (Nwariaku et al., 2003) (Ferro et al., 2000) (Fernandez-Martin et al., 2012). Para conseguir una disminución estadísticamente significativa de la fosforilación de ERM fue necesario inhibir ROCK y PKC clásica de manera conjunta, lo que sugiere que las dos quinasas tienen efecto aditivo y descarta que ambas estén implicadas en la misma ruta de señalización activada por TNF-α como ocurre en otros contextos celulares (Peng et al., 2011). A pesar de ello estos experimentos no excluyen la posibilidad de que otra maquinaria regule la actividad de ERM en hepatocitos en respuesta a la inflamación. Nuestra hipótesis es que el tratamiento de hepatocitos con TNF-α probablemente incremente la activación y localización en membrana de PKC-α al igual que sucede en células endoteliales (Ross and Joyner, 1997). El mecanismo por el que esta citoquina activa PKC-α no está descrito al detalle, aunque se ha demostrado que TNF-α puede activar PC-PLC (fosfatidilcolina fosfolipasa C) (Schutze et al., 1991) a través de su

receptor p55 (Schutze et al., 1992) (Machleidt et al., 1996) lo que activaría PKC-α a través de la unión de diacilglicerol y calcio intracelular a sus dominios reguladores. Por otro lado, tampoco se conoce en detalle la ruta por la que TNF-α activa la ruta de Rho-ROCK. Es probable que GEF-H1 sea la GEF más relevante RhoA en respuesta a esta citoquina (Kakiashvili et al., 2009) (Kakiashvili et al., 2011), aunque se desconoce si en el epitelio hepático juega una función central en la activación de Rho durante la inflamación. Por otra parte, las proteínas ERM son capaces de activar RhoA a través de su unión a RhoGDI (Rho-GDP dissociation inhibitor) (Takahashi et al., 1997) (Ivetic and Ridley, 2004), una conexión molecular que permitiría que la activación de ERM dependiente de PKC clásicas contribuyera a la activación de Rho-ROCK en el contexto inflamatorio, estableciendo un posible mecanismo de retroalimentación en el que las proteínas ERM regularían su propia activación y la de la rutas de señalización dependientes de Rho.

Por otra parte, existe cierta controversia acerca de si estas quinasas, y en particular ROCK, fosforilan directamente la treonina en el dominio citoplásmico que induce una conformación abierta en las ERMs. Mientras que el dominio catalítico ROCK puede fosforilar estas proteínas in vitro (Matsui et al., 1998), estudios posteriores sugieren que RhoA controla la fosforilación de proteínas ERM a través de otro efector, fosfatidilinositol 4-fosfato 5-quinasa tipo 1 alfa (PI4P5K) que regula la generación de PIP2, que a su vez induciría la fosforilación de ERMs por una quinasa diferente a ROCK (Matsui et al., 1999). Sin embargo, otros grupos han demostrado un efecto claro de la inhibición de ROCK en la fosforilación y activación de estas proteínas (Hebert et al., 2008) (Wang et al., 2009a), por lo que es probable que la regulación de su fosforilación dependa del tipo celular y del estímulo. En células endoteliales, TNF-α induce las fosforilación de ERM por mecanismos dependientes de PKC y p38MAPK (Koss et al., 2006). Sin embargo, en HepG2, la inhibición de p38 no parece tener un efecto significativo sobre la fosforilación de estas proteínas (datos no mostrados).

Puesto que la inhibición de PKCa y ROCK en presencia de TNF-α recupera la polaridad de ICAM-1 en hepatocitos, futuros estudios sobre la modulación de la actividad de estas quinasas y su efecto sobre las proteínas ERM pueden contribuir a dilucidar nuevas posibilidades terapéuticas para controlar la exposición de receptores de adhesión leucocitarios durante la respuesta inflamatoria hepática.

A pesar de que la estimulación durante 24 horas con TNF-α tuvo efectos mínimos sobre la polaridad de las células HepG2, existe evidencia indicando que la permeabilidad de las uniones estrechas hepatocitarias se altera tras este tratamiento (Mee et al., 2009). La integridad de las uniones estrechas es esencial para el mantenimiento de los lúmenes canaliculares (Braiterman et al., 2008), y tanto la modificación directa de sus componentes como su regulación indirecta a través del citoesqueleto de actina pueden perturbar la permeabilidad de estas estructuras. La estimulación de células epiteliales con citoquinas proinflamatorias que provoca la formación de fibras de estrés. Esto genera un aumento de la contracción mediada por actomiosina que lleva a la desorganización de las uniones intercelulares por tensión mecánica y al aumento de la permeabilidad (Harhaj and Antonetti, 2004) (Ivanov et al., 2010). Aunque en esta tesis se ha analizado la integridad de las uniones estrechas hepatocelulares tras 24 horas de estimulación con TNF-α, encontrándose diferencias poco significativas (datos no mostrados), no

se puede descartar un efecto de la citoquina sobre la remodelación del citoesqueleto de actina que aumente la permeabilidad de las uniones estrechas y, en respuesta a una estimulación más prolongada, sea responsable de ocasionar la pérdida de las estructuras canaliculares. La activación por TNF-α de las proteínas ERM en la membrana basolateral podría favorecer este proceso aumentando la tensión del anillo contráctil de F-actina en esta región. De acuerdo con esta hipótesis se ha descrito que la sobreexpresión durante más de 24 horas del mutante constitutivamente fosforilado de radixina altera la polaridad apicobasal en células WIF-B (Suda et al., 2011), y el aumento de fosforilación de las proteínas ERM se ha relacionado con el colapso de las uniones estrechas en células epiteliales (Naydenov et al., 2009). Por otra parte, además de regular la fosforilación de las proteínas ERM en hepatocitos como hemos podido comprobar aquí, la activación de las isoformas clásicas de PKC provocan colestasis y pérdida de polaridad hepatocelular a través de la alteración del tráfico intracelular polarizado (Kubitz et al., 2001) (Zegers and Hoekstra, 1997). Ya sea como consecuencia de la reorganización del citoesqueleto de actina, de la modificación o relocalización de elementos de las uniones estrechas o de su efecto pro-apoptótico (Tacke et al., 2009), no se puede descartar un efecto despolarizante de una inflamación crónica mediada por TNF-α.

6. ENFERMEDAD INFLAMATORIA Y POLARIDAD.

El objetivo de muchas aproximaciones terapéuticas para combatir una inflamación hepática exacerbada o inadecuada consiste en bloquear la respuesta inmune de manera inespecífica antagonizando el efecto de distintas citoquinas proinflamatorias. Esto implica una inmunosupresión no deseada del individuo con la consiguiente susceptibilidad a sufrir nuevas infecciones. Sin embargo, nuestro trabajo revela que las células parenquimales hepáticas no son dianas pasivas del ataque leucocitario, sino que a través de la exposición de moléculas de adhesión son capaces de regular el reclutamiento de células inmunes. La inflamación provoca que estas moléculas de adhesión se hagan más accesibles a los leucocitos infiltrados, sugiriendo que los hepatocitos desempeñan un rol crítico en la regulación de la migración y el posicionamiento de células inmunes sobre el parénquima hepático. La disección de las rutas celulares y moleculares que advierten al sistema inmune durante el daño hepático, incluyendo aquellas que coreografían el reclutamiento de leucocitos y su migración intersticial hacia el lugar dañado, tienen el potencial de permitir el desarrollo de nuevas estrategias terapéuticas que modulen la inflamación hepática sin comprometer la respuesta inmune global. Basándonos en nuestros resultados, el confinamiento de ICAM-1 al canalículo biliar a través de estrategias polarizantes como el tratamiento con análogos del cAMP podría disminuir la destrucción innecesaria del parénquima. Por ello, el desarrollo de fármacos que modulen la polaridad hepatocelular resultaría útil en un contexto de daño hepático fulminante causado por la infiltración masiva de neutrófilos en el parénquima, así como en enfermedad autoinmune o rechazo de un aloinjerto hepático para evitar la acción citolítica linfocitaria sobre los hepatocitos reconocidos como extraños. De igual modo esta estrategia podría ser adecuada

para reducir la infección por HCV, ya que la polaridad hepatocelular restringe la entrada del virus en hepatocitos (Mee et al., 2009). Por otra parte, además de activar vías intracelulares específicas influenciando el destino celular de los hepatocitos (Tacke et al., 2009), este trabajo demuestra que TNF-α puede modular la distribución polarizada de receptores de adhesión. Por ello moléculas que se encuentren en la cascada de señalización de TNF-α, como PKC clásicas o ERM, representan también posibles dianas terapéuticas para regular la exposición de receptores de adhesión hepatocitarios a células inmunes infiltradas. De modo interesante se ha implicado a ERM en la regulación de Epac y PKA (Dransfield et al., 1997) (Gloerich et al., 2010), maquinaria que se activan por AMPc y modula la polaridad hepatocelular (Zegers and Hoekstra, 1997) (Fu et al., 2011). Las proteínas ERM activas controlan la distribución y función de Epac y PKA, anclándolas a la membrana plasmática y contribuyendo a la formación de plataformas de señalización en distintas localizaciones de membrana. La modulación específica de la actividad de ERM hepatocitarias permitiría regular tanto la polaridad hepatocelular en un contexto de daño hepático agudo como la exposición de receptores de adhesión en hepatopatías de componente inflamatorio crónico.

Los mecanismos de polaridad apicobasal se encuentran conservados en distintos epitelios, dónde la accesibilidad de células inmunes al lumen de las cavidades internas es menor que en el espacio parenquimal (Weisz and Rodriguez-Boulan, 2009). Por tanto, la polarización de receptores epiteliales que intervengan en la adhesión y activación de células inmunes puede constituir un mecanismo para prevenir la exacerbación de la respuesta inmune que no se encuentra únicamente restringido al tejido hepático. La distribución apical de ICAM-1 en un contexto inflamatorio se ha descrito también en el epitelio intestinal, donde este receptor media la adhesión a la membrana apical de neutrófilos presentes en el lumen intestinal y su posterior transmigración en dirección apical-basolateral (Parkos et al., 1996). Durante la enfermedad inflamatoria intestinal, un síndrome idiopático que cursa con inflamación crónica y se caracteriza por un aumento de la permeabilidad de la barrera epitelial intestinal, se alteran componentes implicados en mantener la polaridad de las células epiteliales (Wald et al., 2011). Una de las aproximaciones terapéuticas actuales para tratar esta patología se basa en el uso de anticuerpos monoclonales dirigidos contra TNF-α (Infliximab), que presentan amplios efectos secundarios como consecuencia de la supresión de la respuesta inmune (Bradley, 2008). La regulación de la polaridad del parénquima intestinal puede suponer una estrategia terapéutica alternativa para esta enfermedad libre de efectos inmunosupresores. Puesto que la pérdida de polaridad es un rasgo general de disfunción epitelial, nuestra propuesta es que la exposición diferencial de receptores de adhesión, que ocurre como consecuencia de este proceso, constituye un paso de control inmune para mantener los tejidos epiteliales libres de células dañadas o transformadas. En el futuro, el tratamiento de patologías inflamatorias crónicas deberá incluir dianas terapéuticas que regulen la respuesta inflamatoria tanto en leucocitos como en células parenquimales.

CONCLUSIONES

1. La pérdida de polaridad apicobasal aumenta la adhesión de linfocitos T a células hepáticas.
2. El receptor ICAM-1 se localiza en el canalículo biliar de hepatocitos polarizados in vitro e in vivo.
3. En respuesta a la pérdida de polaridad, los hepatocitos exponen ICAM-1 y ERM activas desde el dominio canalicular al espacio extracelular accesible a linfocitos T, en proyecciones de membrana tipo microvilli.
4. La adhesión de linfocitos a hepatocitos despolarizados depende de la expresión de ICAM-1.
5. ICAM-1 puede alcanzar la membrana basolateral en hepatocitos polarizados pero se redirige rápidamente al canalículo biliar, dónde se encuentra estrechamente confinado.
6. ICAM-1 se asocia con las proteínas ERM en la membrana plasmática hepatocelular a través de su segmento citoplásmico, el cual se requiere también para la localización apical del receptor.
7. La estimulación a largo plazo con TNF-a aumenta la exposición de ICAM-1 basolateral a través de la activación de las proteínas ERM, la cual se encuentra regulada por ROCK y las isoformas clásicas de PKC.
8. ICAM-1 pierde su polaridad apical en condiciones de fallo hepático agudo y en hepatopatías crónicas que afectan a la arquitectura hepatocelular y cursan con una inflamación persistente.

1. Loss of hepatocellular polarity increases lymphocyte adhesion to hepatic cells.
2. Polarized hepatocytes segregate the ICAM-1 receptor into bile canaliculi in vitro and *in vivo*.
3. Upon hepatic cell depolarization, canalicular ICAM-1 and activated ERM proteins are exposed to immune cells in microvilli-like membrane projections.
4. Lymphocyte adhesion to depolarized hepatocytes depends on ICAM-1 expression.
5. In polarized HepG2 cells, ICAM-1 can reach the basolateral membrane but is rapidly redirected to the apical domain, where it remains tightly confined.
6. ICAM-1 associates with ERM proteins at the plasma membrane through its cytoplasmic tail, which is in turn required for ICAM-1 apical localization.
7 Long-term TNFa stimulation increases ICAM-1 basolateral exposure through activation of ERM proteins, which is mediated by ROCK and classical PKC.
9. ICAM-1 losses its apical polarity in acute liver failure and chronic liver diseases that affect hepatocyte architecture and are subjected to persistent inflammatory upset.

BIBLIOGRAFÍA

Adams, D.H., S.G. Hubscher, N.C. Fisher, A. Williams, and M. Robinson. 1996. Expression of E-selectin and E-selectin ligands in human liver inflammation. Hepatology. 24:533-538.

Adams, D.H., S.G. Hubscher, J. Shaw, G.D. Johnson, C. Babbs, R. Rothlein, and J.M. Neuberger. 1991. Increased expression of intercellular adhesion molecule 1 on bile ducts in primary biliary cirrhosis and primary sclerosing cholangitis. Hepatology. 14:426-431.

Adams, D.H., C. Ju, S.K. Ramaiah, J. Uetrecht, and H. Jaeschke. 2010. Mechanisms of immune-mediated liver injury. Toxicol Sci. 115:307-321.

Adams, D.H., E. Mainolfi, E. Elias, J.M. Neuberger, and R. Rothlein. 1993. Detection of circulating intercellular adhesion molecule-1 after liver transplantation--evidence of local release within the liver during graft rejection. Transplantation. 55:83-87.

Akkari, L., D. Gregoire, N. Floc'h, M. Moreau, C. Hernandez, Y. Simonin, A.R. Rosenberg, P. Lassus, and U. Hibner. 2012. Hepatitis C viral protein NS5A induces EMT and participates in oncogenic transformation of primary hepatocyte precursors. Journal of hepatology. 57:1021-1028.

Alon, R., and K. Ley. 2008. Cells on the run: shear-regulated integrin activation in leukocyte rolling and arrest on endothelial cells. Curr Opin Cell Biol. 20:525-532.

Aranda, J.F., N. Reglero-Real, B. Marcos-Ramiro, A. Ruiz-Saenz, L. Fernandez-Martin, M. Bernabe-Rubio, L. Kremer, A.J. Ridley, I. Correas, M.A. Alonso, and J. Millan. 2013. MYADM controls endothelial barrier function through ERM-dependent regulation of ICAM-1 expression. Mol Biol Cell. 24:483-494.

Arias,I., A. Wolkoff, J. Boyer, D. Shafritz, N. Fausto, H. Alter, D. Cohen. The Liver: Biology and Pathobiology. (Fith edition, Wiley-Blackwell).

Barreiro, O., M. Yanez-Mo, J.M. Serrador, M.C. Montoya, M. Vicente-Manzanares, R. Tejedor, H. Furthmayr, and F. Sanchez-Madrid. 2002. Dynamic interaction of VCAM-1 and ICAM-1 with moesin and ezrin in a novel endothelial docking structure for adherent leukocytes. J Cell Biol. 157:1233-1245.

Bastaki, M., L.T. Braiterman, D.C. Johns, Y.H. Chen, and A.L. Hubbard. 2002. Absence of direct delivery for single transmembrane apical proteins or their "Secretory" forms in polarized hepatic cells. Molecular biology of the cell. 13:225-237.

Battaglia, S., N. Benzoubir, S. Nobilet, P. Charneau, D. Samuel, A.L. Zignego, A. Atfi, C. Brechot, and M.F. Bourgeade. 2009. Liver cancer-derived hepatitis C virus core proteins shift TGF-beta responses from tumor suppression to epithelial-mesenchymal transition. PLoS One. 4:e4355.

Benedetti, A., M. Strazzabosco, O.C. Ng, and J.L. Boyer. 1994. Regulation of activity and apical targeting of the Cl-/HCO3- exchanger in rat hepatocytes. Proc Natl Acad Sci U S A.

91:792-796.

Benedicto, I., F. Molina-Jimenez, O. Barreiro, A. Maldonado-Rodriguez, J. Prieto, R. Moreno-Otero, R. Aldabe, M. Lopez-Cabrera, and P.L. Majano. 2008. Hepatitis C virus envelope components alter localization of hepatocyte tight junction-associated proteins and promote occludin retention in the endoplasmic reticulum. Hepatology. 48:1044-1053.

Benedicto, I., F. Molina-Jimenez, R. Moreno-Otero, M. Lopez-Cabrera, and P.L. Majano. 2011. Interplay among cellular polarization, lipoprotein metabolism and hepatitis C virus entry. World journal of gastroenterology : WJG. 17:2683-2690.

Benseler, V., A. Warren, M. Vo, L.E. Holz, S.S. Tay, D.G. Le Couteur, E. Breen, A.C. Allison, N. van Rooijen, C. McGuffog, H.J. Schlitt, D.G. Bowen, G.W. McCaughan, and P. Bertolino. 2011. Hepatocyte entry leads to degradation of autoreactive CD8 T cells. Proc Natl Acad Sci U S A. 108:16735-16740.

Bertolino, P., M.C. Trescol-Biemont, and C. Rabourdin-Combe. 1998. Hepatocytes induce functional activation of naive CD8+ T lymphocytes but fail to promote survival. Eur J Immunol. 28:221-236.

Bradfield, P.F., S. Nourshargh, M. Aurrand-Lions, and B.A. Imhof. 2007. JAM family and related proteins in leukocyte migration (Vestweber series). Arterioscler Thromb Vasc Biol. 27:2104-2112.

Bradley, J.R. 2008. TNF-mediated inflammatory disease. J Pathol. 214:149-160.

Braiterman, L.T., S. Heffernan, L. Nyasae, D. Johns, A.P. See, R. Yutzy, A. McNickle, M. Herman, A. Sharma, U.P. Naik, and A.L. Hubbard. 2008. JAM-A is both essential and inhibitory to development of hepatic polarity in WIF-B cells. Am J Physiol Gastrointest Liver Physiol. 294:G576-588.

Brazil, J.C., W.Y. Lee, K.N. Kolegraff, A. Nusrat, C.A. Parkos, and N.A. Louis. 2010. Neutrophil migration across intestinal epithelium: evidence for a role of CD44 in regulating detachment of migrating cells from the luminal surface. J Immunol. 185:7026-7036.

Bretscher, A., K. Edwards, and R.G. Fehon. 2002. ERM proteins and merlin: integrators at the cell cortex. Nat Rev Mol Cell Biol. 3:586-599.

Bumgardner, G.L., J. Li, S. Apte, M. Heininger, and W.L. Frankel. 1998. Effect of tumor necrosis factor alpha and intercellular adhesion molecule-1 expression on immunogenicity of murine liver cells in mice. Hepatology. 28:466-474.

Butcher, E.C. 1991. Leukocyte-endothelial cell recognition: three (or more) steps to specificity and diversity. Cell. 67:1033-1036.

Cao, Y., U. Karsten, G. Otto, and P. Bannasch. 1999. Expression of MUC1, Thomsen-Friedenreich antigen, Tn, sialosyl-Tn, and alpha2,6-linked sialic acid in hepatocellular carcinomas and preneoplastic hepatocellular lesions. Virchows Arch. 434:503-509.

Carman, C.V., C.D. Jun, A. Salas, and T.A. Springer. 2003. Endothelial cells proactively form

microvilli-like membrane projections upon intercellular adhesion molecule 1 engagement of leukocyte LFA-1. J Immunol. 171:6135-6144.

Carman, C.V., P.T. Sage, T.E. Sciuto, M.A. de la Fuente, R.S. Geha, H.D. Ochs, H.F. Dvorak, A.M. Dvorak, and T.A. Springer. 2007. Transcellular diapedesis is initiated by invasive podosomes. Immunity. 26:784-797.

Carman, C.V., and T.A. Springer. 2004. A transmigratory cup in leukocyte diapedesis both through individual vascular endothelial cells and between them. J Cell Biol. 167:377-388.

Carpen, O., P. Pallai, D.E. Staunton, and T.A. Springer. 1992. Association of intercellular adhesion molecule-1 (ICAM-1) with actin-containing cytoskeleton and alpha-actinin. J Cell Biol. 118:1223-1234.

Cayrol, R., K. Wosik, J.L. Berard, A. Dodelet-Devillers, I. Ifergan, H. Kebir, A.S. Haqqani, K. Kreymborg, S. Krug, R. Moumdjian, A. Bouthillier, B. Becher, N. Arbour, S. David, D. Stanimirovic, and A. Prat. 2008. Activated leukocyte cell adhesion molecule promotes leukocyte trafficking into the central nervous system. Nat Immunol. 9:137-145.

Claperon, A., D. Debray, M.J. Redon, M. Mergey, T.H. Nguyen Ho-Bouldoires, C. Housset, M. Fabre, and L. Fouassier. 2013. Immunohistochemical profile of ezrin and radixin in human liver epithelia during fetal development and pediatric cholestatic diseases. Clin Res Hepatol Gastroenterol. 37:142-151.

Cooper, S., A.L. Erickson, E.J. Adams, J. Kansopon, A.J. Weiner, D.Y. Chien, M. Houghton, P. Parham, and C.M. Walker. 1999. Analysis of a successful immune response against hepatitis C virus. Immunity. 10:439-449.

Corasanti, J.G., N.D. Smith, E.R. Gordon, and J.L. Boyer. 1989. Protein kinase C agonists inhibit bile secretion independently of effects on the microcirculation in the isolated perfused rat liver. Hepatology. 10:8-13.

Crispe, I.N. 2003. Hepatic T cells and liver tolerance. Nat Rev Immunol. 3:51-62.

Cruickshank, S.M., J. Southgate, P.J. Selby, and L.K. Trejdosiewicz. 1998. Expression and cytokine regulation of immune recognition elements by normal human biliary epithelial and established liver cell lines in vitro. J Hepatol. 29:550-558.

Chalfie, M., Y. Tu, G. Euskirchen, W.W. Ward, and D.C. Prasher. 1994. Green fluorescent protein as a marker for gene expression. Science. 263:802-805.

Chastre, A., M. Belanger, E. Beauchesne, B.N. Nguyen, P. Desjardins, and R.F. Butterworth. 2012. Inflammatory cascades driven by tumor necrosis factor-alpha play a major role in the progression of acute liver failure and its neurological complications. PLoS One. 7:e49670.

Chen, X., T.D. Kim, C.V. Carman, L.Z. Mi, G. Song, and T.A. Springer. 2007. Structural plasticity in Ig superfamily domain 4 of ICAM-1 mediates cell surface dimerization. Proc Natl Acad Sci U S A. 104:15358-15363.

D'Amico, G., G. Frascaroli, G. Bianchi, P. Transidico, A. Doni, A. Vecchi, S. Sozzani, P. Alla-

vena, and A. Mantovani. 2000. Uncoupling of inflammatory chemokine receptors by IL-10: generation of functional decoys. Nat Immunol. 1:387-391.

de Fougerolles, A.R., S.A. Stacker, R. Schwarting, and T.A. Springer. 1991a. Characterization of ICAM-2 and evidence for a third counter-receptor for LFA-1. The Journal of experimental medicine. 174:253-267.

de Fougerolles, A.R., S.A. Stacker, R. Schwarting, and T.A. Springer. 1991b. Characterization of ICAM-2 and evidence for a third counter-receptor for LFA-1. J Exp Med. 174:253-267.

de Marco, M.C., F. Martin-Belmonte, L. Kremer, J.P. Albar, I. Correas, J.P. Vaerman, M. Marazuela, J.A. Byrne, and M.A. Alonso. 2002. MAL2, a novel raft protein of the MAL family, is an essential component of the machinery for transcytosis in hepatoma HepG2 cells. J Cell Biol. 159:37-44.

Decaens, C., M. Durand, B. Grosse, and D. Cassio. 2008. Which in vitro models could be best used to study hepatocyte polarity? Biol Cell. 100:387-398.

Delpino, M.V., P. Barrionuevo, R. Scian, C.A. Fossati, and P.C. Baldi. 2010. Brucella-infected hepatocytes mediate potentially tissue-damaging immune responses. Journal of hepatology. 53:145-154.

Dienes, H.P. 1989. Viral and autoimmune hepatitis. Morphologic and pathogenetic aspects of cell damage in hepatitis with potential chronicity. Veroff Pathol. 132:1-107.

Doi, T., G. Yamada, M. Mizuno, and T. Tsuji. 1994. Immunohistochemical study of the distribution of intercellular adhesion molecule-1 and lymphocyte function-associated antigen-1 in chronic type B hepatitis. Journal of gastroenterology. 29:164-171.

Dransfield, D.T., A.J. Bradford, J. Smith, M. Martin, C. Roy, P.H. Mangeat, and J.R. Goldenring. 1997. Ezrin is a cyclic AMP-dependent protein kinase anchoring protein. EMBO J. 16:35-43.

Dubey, C., and M. Croft. 1996. Accessory molecule regulation of naive CD4 T cell activation. Immunol Res. 15:114-125.

Dunn, J.C., R.G. Tompkins, and M.L. Yarmush. 1992. Hepatocytes in collagen sandwich: evidence for transcriptional and translational regulation. The Journal of cell biology. 116:1043-1053.

Dunn, K.W., M.M. Kamocka, and J.H. McDonald. 2011. A practical guide to evaluating colocalization in biological microscopy. Am J Physiol Cell Physiol. 300:C723-742.

Edwards, S., P.F. Lalor, G.B. Nash, G.E. Rainger, and D.H. Adams. 2005. Lymphocyte traffic through sinusoidal endothelial cells is regulated by hepatocytes. Hepatology. 41:451-459.

Evans, M.J., T. von Hahn, D.M. Tscherne, A.J. Syder, M. Panis, B. Wolk, T. Hatziioannou, J.A. McKeating, P.D. Bieniasz, and C.M. Rice. 2007. Claudin-1 is a hepatitis C virus co-receptor required for a late step in entry. Nature. 446:801-805.

Fehon, R.G., A.I. McClatchey, and A. Bretscher. 2010. Organizing the cell cortex: the role of ERM proteins. Nat Rev Mol Cell Biol. 11:276-287.

Fernandez-Borja, M., J.D. van Buul, and P.L. Hordijk. 2010. The regulation of leucocyte transendothelial migration by endothelial signalling events. Cardiovascular research. 86:202-210.

Fernandez-Martin, L., B. Marcos-Ramiro, C.L. Bigarella, M. Graupera, R.J. Cain, N. Reglero-Real, A. Jimenez, E. Cernuda-Morollon, I. Correas, S. Cox, A.J. Ridley, and J. Millan. 2012. Crosstalk between reticular adherens junctions and platelet endothelial cell adhesion molecule-1 regulates endothelial barrier function. Arteriosclerosis, thrombosis, and vascular biology. 32:e90-e102.

Fernandez-Ruiz, V., M. Kawa, C. Berasain, M. Iniguez, V. Schmitz, E. Martinez-Anso, M. Inarrairaegui, I. Herrero, B. Sangro, D. D'Avola, J. Quiroga, C. Qian, and J. Prieto. 2011. Treatment of murine fulminant hepatitis with genetically engineered endothelial progenitor cells. J Hepatol. 55:828-837.

Ferro, T., P. Neumann, N. Gertzberg, R. Clements, and A. Johnson. 2000. Protein kinase C-alpha mediates endothelial barrier dysfunction induced by TNF-alpha. Am J Physiol Lung Cell Mol Physiol. 278:L1107-1117.

Fievet, B., D. Louvard, and M. Arpin. 2007. ERM proteins in epithelial cell organization and functions. Biochim Biophys Acta. 1773:653-660.

Franco, A., V. Barnaba, P. Natali, C. Balsano, A. Musca, and F. Balsano. 1988. Expression of class I and class II major histocompatibility complex antigens on human hepatocytes. Hepatology. 8:449-454.

Friedl, P., and B. Weigelin. 2008. Interstitial leukocyte migration and immune function. Nat Immunol. 9:960-969.

Friedman, S.L. 2000. Molecular regulation of hepatic fibrosis, an integrated cellular response to tissue injury. J Biol Chem. 275:2247-2250.

Friedman, S.L. 2008. Hepatic stellate cells: protean, multifunctional, and enigmatic cells of the liver. Physiol Rev. 88:125-172.

Fu, D., Y. Wakabayashi, J. Lippincott-Schwartz, and I.M. Arias. 2011. Bile acid stimulates hepatocyte polarization through a cAMP-Epac-MEK-LKB1-AMPK pathway. Proceedings of the National Academy of Sciences of the United States of America. 108:1403-1408.

Garrard, S.M., C.T. Capaldo, L. Gao, M.K. Rosen, I.G. Macara, and D.R. Tomchick. 2003. Structure of Cdc42 in a complex with the GTPase-binding domain of the cell polarity protein, Par6. EMBO J. 22:1125-1133.

Gartner L.P., J. L. Hiatt. 2008. Texto Atlas de Histología. (Tercera edición, McGraw-Hill Interamericana).

Gilbert, S., A. Loranger, J.N. Lavoie, and N. Marceau. 2012. Cytoskeleton keratin regulation of FasR signaling through modulation of actin/ezrin interplay at lipid rafts in hepatocytes.

Apoptosis. 17:880-894.

Gloerich, M., B. Ponsioen, M.J. Vliem, Z. Zhang, J. Zhao, M.R. Kooistra, L.S. Price, L. Ritsma, F.J. Zwartkruis, H. Rehmann, K. Jalink, and J.L. Bos. 2010. Spatial regulation of cyclic AMP-Epac1 signaling in cell adhesion by ERM proteins. Mol Cell Biol. 30:5421-5431.

Gonzalez-Amaro, R., C. Garcia-Monzon, L. Garcia-Buey, R. Moreno-Otero, J.L. Alonso, E. Yague, J.P. Pivel, M. Lopez-Cabrera, E. Fernandez-Ruiz, and F. Sanchez-Madrid. 1994. Induction of tumor necrosis factor alpha production by human hepatocytes in chronic viral hepatitis. J Exp Med. 179:841-848.

Grivennikov, S.I., F.R. Greten, and M. Karin. 2010. Immunity, inflammation, and cancer. Cell. 140:883-899.

Guyton & Hall. Tratado de fisiología médica. (Décima edición, Elsevier Saunders).

Harhaj, N.S., and D.A. Antonetti. 2004. Regulation of tight junctions and loss of barrier function in pathophysiology. Int J Biochem Cell Biol. 36:1206-1237.

Harrison, R.G. 1907. Observations on the livining developing nerve fiber. Proceedings of the society for experimental biology and medicine. 4:140-143.

Hebert, M., S. Potin, M. Sebbagh, J. Bertoglio, J. Breard, and J. Hamelin. 2008. Rho-ROCK-dependent ezrin-radixin-moesin phosphorylation regulates Fas-mediated apoptosis in Jurkat cells. J Immunol. 181:5963-5973.

Heiska, L., K. Alfthan, M. Gronholm, P. Vilja, A. Vaheri, and O. Carpen. 1998. Association of ezrin with intercellular adhesion molecule-1 and -2 (ICAM-1 and ICAM-2). Regulation by phosphatidylinositol 4, 5-bisphosphate. J Biol Chem. 273:21893-21900.

Hemery, I., A.M. Durand-Schneider, G. Feldmann, J.P. Vaerman, and M. Maurice. 1996. The transcytotic pathway of an apical plasma membrane protein (B10) in hepatocytes is similar to that of IgA and occurs via a tubular pericentriolar compartment. J Cell Sci. 109 (Pt 6):1215-1227.

Henderson, J.N., R. Gepshtein, J.R. Heenan, K. Kallio, D. Huppert, and S.J. Remington. 2009. Structure and mechanism of the photoactivatable green fluorescent protein. J Am Chem Soc. 131:4176-4177.

Herrema, H., D. Czajkowska, D. Theard, J.M. van der Wouden, D. Kalicharan, B. Zolghadr, D. Hoekstra, and S.C. van Ijzendoorn. 2006. Rho kinase, myosin-II, and p42/44 MAPK control extracellular matrix-mediated apical bile canalicular lumen morphogenesis in HepG2 cells. Mol Biol Cell. 17:3291-3303.

Heydtmann, M., P.F. Lalor, J.A. Eksteen, S.G. Hubscher, M. Briskin, and D.H. Adams. 2005. CXC chemokine ligand 16 promotes integrin-mediated adhesion of liver-infiltrating lymphocytes to cholangiocytes and hepatocytes within the inflamed human liver. J Immunol. 174:1055-1062.

Hirao, M., N. Sato, T. Kondo, S. Yonemura, M. Monden, T. Sasaki, Y. Takai, and S. Tsukita.

1996. Regulation mechanism of ERM (ezrin/radixin/moesin) protein/plasma membrane association: possible involvement of phosphatidylinositol turnover and Rho-dependent signaling pathway. J Cell Biol. 135:37-51.

Hiraoka, N. 2010. Tumor-infiltrating lymphocytes and hepatocellular carcinoma: molecular biology. International journal of clinical oncology / Japan Society of Clinical Oncology. 15:544-551.

Holz, L.E., A. Warren, D.G. Le Couteur, D.G. Bowen, and P. Bertolino. 2010. CD8+ T cell tolerance following antigen recognition on hepatocytes. Journal of autoimmunity. 34:15-22.

Horwitz, A.R. 2012. The origins of the molecular era of adhesion research. Nat Rev Mol Cell Biol. 13:805-811.

Huang, H., Y. Xiao, H. Lin, D. Fu, Z. Zhan, L. Liang, X. Yang, J. Fan, Y. Ye, L. Sun, and H. Xu. 2011. Increased phosphorylation of ezrin/radixin/moesin proteins contributes to proliferation of rheumatoid fibroblast-like synoviocytes. Rheumatology (Oxford). 50:1045-1053.

Hynes, R.O. 1987. Integrins: a family of cell surface receptors. Cell. 48:549-554.

Imagawa, D.K., J.M. Millis, K.M. Olthoff, L.J. Derus, D. Chia, L.R. Sugich, M. Ozawa, R.A. Dempsey, Y. Iwaki, P.J. Levy, and et al. 1990. The role of tumor necrosis factor in allograft rejection. I. Evidence that elevated levels of tumor necrosis factor-alpha predict rejection following orthotopic liver transplantation. Transplantation. 50:219-225.

Ivanov, A.I., C.A. Parkos, and A. Nusrat. 2010. Cytoskeletal regulation of epithelial barrier function during inflammation. Am J Pathol. 177:512-524.

Ivetic, A., and A.J. Ridley. 2004. Ezrin/radixin/moesin proteins and Rho GTPase signalling in leucocytes. Immunology. 112:165-176.

Jaeschke, H., and T. Hasegawa. 2006. Role of neutrophils in acute inflammatory liver injury. Liver Int. 26:912-919.

Kakiashvili, E., Q. Dan, M. Vandermeer, Y. Zhang, F. Waheed, M. Pham, and K. Szaszi. 2011. The epidermal growth factor receptor mediates tumor necrosis factor-alpha-induced activation of the ERK/GEF-H1/RhoA pathway in tubular epithelium. J Biol Chem. 286:9268-9279.

Kakiashvili, E., P. Speight, F. Waheed, R. Seth, M. Lodyga, S. Tanimura, M. Kohno, O.D. Rotstein, A. Kapus, and K. Szaszi. 2009. GEF-H1 mediates tumor necrosis factor-alpha-induced Rho activation and myosin phosphorylation: role in the regulation of tubular paracellular permeability. J Biol Chem. 284:11454-11466.

Kang, T.W., T. Yevsa, N. Woller, L. Hoenicke, T. Wuestefeld, D. Dauch, A. Hohmeyer, M. Gereke, R. Rudalska, A. Potapova, M. Iken, M. Vucur, S. Weiss, M. Heikenwalder, S. Khan, J. Gil, D. Bruder, M. Manns, P. Schirmacher, F. Tacke, M. Ott, T. Luedde, T. Longerich, S. Kubicka, and L. Zender. 2011. Senescence surveillance of pre-malignant hepatocytes limits liver cancer development. Nature. 479:547-551.

Kanters, E., J. van Rijssel, P.J. Hensbergen, D. Hondius, F.P. Mul, A.M. Deelder, A. Sonnen-

berg, J.D. van Buul, and P.L. Hordijk. 2008. Filamin B mediates ICAM-1-driven leukocyte transendothelial migration. J Biol Chem. 283:31830-31839.

Karlmark, K.R., H.E. Wasmuth, C. Trautwein, and F. Tacke. 2008. Chemokine-directed immune cell infiltration in acute and chronic liver disease. Expert Rev Gastroenterol Hepatol. 2:233-242.

Kawasuji, A., M. Hasegawa, M. Horikawa, T. Fujita, Y. Matsushita, T. Matsushita, M. Fujimoto, D.A. Steeber, T.F. Tedder, K. Takehara, and S. Sato. 2006. L-selectin and intercellular adhesion molecule-1 regulate the development of Concanavalin A-induced liver injury. J Leukoc Biol. 79:696-705.

Kew, M.C. 2011. Hepatitis B virus x protein in the pathogenesis of hepatitis B virus-induced hepatocellular carcinoma. Journal of gastroenterology and hepatology. 26 Suppl 1:144-152.

Kikuchi, S., M. Hata, K. Fukumoto, Y. Yamane, T. Matsui, A. Tamura, S. Yonemura, H. Yamagishi, D. Keppler, and S. Tsukita. 2002. Radixin deficiency causes conjugated hyperbilirubinemia with loss of Mrp2 from bile canalicular membranes. Nature genetics. 31:320-325.

Kipp, H., and I.M. Arias. 2000. Newly synthesized canalicular ABC transporters are directly targeted from the Golgi to the hepatocyte apical domain in rat liver. J Biol Chem. 275:15917-15925.

Knolle, P.A., E. Schmitt, S. Jin, T. Germann, R. Duchmann, S. Hegenbarth, G. Gerken, and A.W. Lohse. 1999. Induction of cytokine production in naive CD4(+) T cells by antigen-presenting murine liver sinusoidal endothelial cells but failure to induce differentiation toward Th1 cells. Gastroenterology. 116:1428-1440.

Kojima, T., M. Murata, T. Yamamoto, M. Lan, M. Imamura, S. Son, K. Takano, H. Yamaguchi, T. Ito, S. Tanaka, H. Chiba, K. Hirata, and N. Sawada. 2009. Tight junction proteins and signal transduction pathways in hepatocytes. Histol Histopathol. 24:1463-1472.

Konopka, G., J. Tekiela, M. Iverson, C. Wells, and S.A. Duncan. 2007. Junctional adhesion molecule-A is critical for the formation of pseudocanaliculi and modulates E-cadherin expression in hepatic cells. J Biol Chem. 282:28137-28148.

Koss, M., G.R. Pfeiffer, 2nd, Y. Wang, S.T. Thomas, M. Yerukhimovich, W.A. Gaarde, C.M. Doerschuk, and Q. Wang. 2006. Ezrin/radixin/moesin proteins are phosphorylated by TNF-alpha and modulate permeability increases in human pulmonary microvascular endothelial cells. J Immunol. 176:1218-1227.

Krueger, P.D., M.G. Lassen, H. Qiao, and Y.S. Hahn. 2011. Regulation of NK cell repertoire and function in the liver. Critical reviews in immunology. 31:43-52.

Kubitz, R., C. Huth, M. Schmitt, A. Horbach, G. Kullak-Ublick, and D. Haussinger. 2001. Protein kinase C-dependent distribution of the multidrug resistance protein 2 from the canalicular to the basolateral membrane in human HepG2 cells. Hepatology. 34:340-350.

Kubitz, R., N. Saha, T. Kuhlkamp, S. Dutta, S. vom Dahl, M. Wettstein, and D. Haussinger.

2004. Ca2+-dependent protein kinase C isoforms induce cholestasis in rat liver. J Biol Chem. 279:10323-10330.

Laemmli, U.K. 1970. Cleavage of structural proteins during the assembly of the head of bacteriophage T4. Nature. 227:680-685.

Lara-Pezzi, E., J.M. Serrador, M.C. Montoya, D. Zamora, M. Yanez-Mo, M. Carretero, H. Furthmayr, F. Sanchez-Madrid, and M. Lopez-Cabrera. 2001. The hepatitis B virus X protein (HBx) induces a migratory phenotype in a CD44-dependent manner: possible role of HBx in invasion and metastasis. Hepatology. 33:1270-1281.

Lawson, C., and S. Wolf. 2009. ICAM-1 signaling in endothelial cells. Pharmacological reports : PR. 61:22-32.

Limmer, A., J. Ohl, C. Kurts, H.G. Ljunggren, Y. Reiss, M. Groettrup, F. Momburg, B. Arnold, and P.A. Knolle. 2000. Efficient presentation of exogenous antigen by liver endothelial cells to CD8+ T cells results in antigen-specific T-cell tolerance. Nat Med. 6:1348-1354.

Lippert. 2002. Anatomía. Estructura y morfología del cuerpo humano. (Cuarta edición, Marbán).

Lippincott-Schwartz, J., N. Altan-Bonnet, and G.H. Patterson. 2003. Photobleaching and photoactivation: following protein dynamics in living cells. Nat Cell Biol. Suppl:S7-14.

Longhi, M.S., Y. Ma, G. Mieli-Vergani, and D. Vergani. 2010. Adaptive immunity in autoimmune hepatitis. Digestive diseases. 28:63-69.

Machleidt, T., B. Kramer, D. Adam, B. Neumann, S. Schutze, K. Wiegmann, and M. Kronke. 1996. Function of the p55 tumor necrosis factor receptor “death domain” mediated by phosphatidylcholine-specific phospholipase C. J Exp Med. 184:725-733.

Madrid, R., J.F. Aranda, A.E. Rodriguez-Fraticelli, L. Ventimiglia, L. Andres-Delgado, M. Shehata, S. Fanayan, H. Shahheydari, S. Gomez, A. Jimenez, F. Martin-Belmonte, J.A. Byrne, and M.A. Alonso. 2010. The formin INF2 regulates basolateral-to-apical transcytosis and lumen formation in association with Cdc42 and MAL2. Dev Cell. 18:814-827.

Majno, G. 1975. The Healing Hand - Man and wound in the ancient world. (Cambridge, MA: Harvard University Press).

Martin-Belmonte, F., A. Gassama, A. Datta, W. Yu, U. Rescher, V. Gerke, and K. Mostov. 2007. PTEN-mediated apical segregation of phosphoinositides controls epithelial morphogenesis through Cdc42. Cell. 128:383-397.

Martin-Belmonte, F., and K. Mostov. 2008. Regulation of cell polarity during epithelial morphogenesis. Current opinion in cell biology. 20:227-234.

Martin-Belmonte, F., and M. Perez-Moreno. 2012. Epithelial cell polarity, stem cells and cancer. Nature reviews. Cancer. 12:23-38.

Martin-Belmonte, F., R. Puertollano, J. Millan, and M.A. Alonso. 2000. The MAL proteolipid

is necessary for the overall apical delivery of membrane proteins in the polarized epithelial Madin-Darby canine kidney and fischer rat thyroid cell lines. Mol Biol Cell. 11:2033-2045.

Mashukova, A., F.A. Wald, and P.J. Salas. 2011. Tumor necrosis factor alpha and inflammation disrupt the polarity complex in intestinal epithelial cells by a posttranslational mechanism. Molecular and cellular biology. 31:756-765.

Matsui, T., M. Maeda, Y. Doi, S. Yonemura, M. Amano, K. Kaibuchi, and S. Tsukita. 1998. Rho-kinase phosphorylates COOH-terminal threonines of ezrin/radixin/moesin (ERM) proteins and regulates their head-to-tail association. J Cell Biol. 140:647-657.

Matsui, T., S. Yonemura, S. Tsukita, and S. Tsukita. 1999. Activation of ERM proteins in vivo by Rho involves phosphatidyl-inositol 4-phosphate 5-kinase and not ROCK kinases. Curr Biol. 9:1259-1262.

McCaffrey, L.M., and I.G. Macara. 2011. Epithelial organization, cell polarity and tumorigenesis. Trends Cell Biol. 21:727-735.

McDonald, B., and P. Kubes. 2011. Cellular and molecular choreography of neutrophil recruitment to sites of sterile inflammation. J Mol Med (Berl). 89:1079-1088.

McGettrick, H.M., L.M. Butler, C.D. Buckley, G.E. Rainger, and G.B. Nash. 2012. Tissue stroma as a regulator of leukocyte recruitment in inflammation. Journal of leukocyte biology. 91:385-400.

McKenzie, J.A., and A.J. Ridley. 2007. Roles of Rho/ROCK and MLCK in TNF-alpha-induced changes in endothelial morphology and permeability. Journal of cellular physiology. 213:221-228.

Mee, C.J., M.J. Farquhar, H.J. Harris, K. Hu, W. Ramma, A. Ahmed, P. Maurel, R. Bicknell, P. Balfe, and J.A. McKeating. 2010. Hepatitis C virus infection reduces hepatocellular polarity in a vascular endothelial growth factor-dependent manner. Gastroenterology. 138:1134-1142.

Mee, C.J., H.J. Harris, M.J. Farquhar, G. Wilson, G. Reynolds, C. Davis, I.S.C. van, P. Balfe, and J.A. McKeating. 2009. Polarization restricts hepatitis C virus entry into HepG2 hepatoma cells. J Virol. 83:6211-6221.

Meijne, A.M., M.H. Driessens, G. La Riviere, D. Casey, C.A. Feltkamp, and E. Roos. 1994. LFA-1 integrin redistribution during T-cell hybridoma invasion of hepatocyte cultures and manganese-induced adhesion to ICAM-1. Journal of cell science. 107 (Pt 9):2557-2566.

Mertens, A.E., D.M. Pegtel, and J.G. Collard. 2006. Tiam1 takes PARt in cell polarity. Trends in cell biology. 16:308-316.

Mi, W., W. Jia, Z. Zheng, J. Wang, Y. Cai, W. Ying, and X. Qian. 2012. Surface glycoproteomic analysis of hepatocellular carcinoma cells by affinity enrichment and mass spectrometric identification. Glycoconj J. 29:411-424.

Millan, J., L. Hewlett, M. Glyn, D. Toomre, P. Clark, and A.J. Ridley. 2006a. Lymphocyte transcellular migration occurs through recruitment of endothelial ICAM-1 to caveola- and

F-actin-rich domains. Nat Cell Biol. 8:113-123.

Millan, J., L. Williams, and A.J. Ridley. 2006b. An in vitro model to study the role of endothelial rho GTPases during leukocyte transendothelial migration. Methods Enzymol. 406:643-655.

Miller, J., R. Knorr, M. Ferrone, R. Houdei, C.P. Carron, and M.L. Dustin. 1995. Intercellular adhesion molecule-1 dimerization and its consequences for adhesion mediated by lymphocyte function associated-1. J Exp Med. 182:1231-1241.

Morita, M., Y. Watanabe, and T. Akaike. 1994. Inflammatory cytokines up-regulate intercellular adhesion molecule-1 expression on primary cultured mouse hepatocytes and T-lymphocyte adhesion. Hepatology. 19:426-431.

Mostov, K.E., M. Verges, and Y. Altschuler. 2000. Membrane traffic in polarized epithelial cells. Curr Opin Cell Biol. 12:483-490.

Muzzey, D., and A. van Oudenaarden. 2009. Quantitative time-lapse fluorescence microscopy in single cells. Annu Rev Cell Dev Biol. 25:301-327.

Nagendra, A.R., J.K. Mickelson, and C.W. Smith. 1997. CD18 integrin and CD54-dependent neutrophil adhesion to cytokine-stimulated human hepatocytes. The American journal of physiology. 272:G408-416.

Naydenov, N.G., A.M. Hopkins, and A.I. Ivanov. 2009. c-Jun N-terminal kinase mediates disassembly of apical junctions in model intestinal epithelia. Cell Cycle. 8:2110-2121.

Neuman, M.G., H. Schmilovitz-Weiss, N. Hilzenrat, M. Bourliere, P. Marcellin, C. Trepo, T. Mazulli, G. Moussa, A. Patel, A.A. Baig, and L. Cohen. 2012. Markers of inflammation and fibrosis in alcoholic hepatitis and viral hepatitis C. Int J Hepatol. 2012:231210.

Ng, T., M. Parsons, W.E. Hughes, J. Monypenny, D. Zicha, A. Gautreau, M. Arpin, S. Gschmeissner, P.J. Verveer, P.I. Bastiaens, and P.J. Parker. 2001. Ezrin is a downstream effector of trafficking PKC-integrin complexes involved in the control of cell motility. The EMBO journal. 20:2723-2741.

Nourshargh, S., P.L. Hordijk, and M. Sixt. 2010. Breaching multiple barriers: leukocyte motility through venular walls and the interstitium. Nature reviews. Molecular cell biology. 11:366-378.

Nourshargh, S., and F.M. Marelli-Berg. 2005. Transmigration through venular walls: a key regulator of leukocyte phenotype and function. Trends Immunol. 26:157-165.

Nwariaku, F.E., P. Rothenbach, Z. Liu, X. Zhu, R.H. Turnage, and L.S. Terada. 2003. Rho inhibition decreases TNF-induced endothelial MAPK activation and monolayer permeability. J Appl Physiol. 95:1889-1895.

Oh, H.M., S. Lee, B.R. Na, H. Wee, S.H. Kim, S.C. Choi, K.M. Lee, and C.D. Jun. 2007. RKIKK motif in the intracellular domain is critical for spatial and dynamic organization of ICAM-1: functional implication for the leukocyte adhesion and transmigration. Mol Biol Cell.

18:2322-2335.

Ohlinger, W., H.P. Dinges, K. Zatloukal, S. Mair, F. Gollowitsch, and H. Denk. 1993. Immunohistochemical detection of tumor necrosis factor-alpha, other cytokines and adhesion molecules in human livers with alcoholic hepatitis. Virchows Arch A Pathol Anat Histopathol. 423:169-176.

Okamura, D., M. Ohtsuka, F. Kimura, H. Shimizu, H. Yoshidome, A. Kato, and M. Miyazaki. 2008. Ezrin expression is associated with hepatocellular carcinoma possibly derived from progenitor cells and early recurrence after surgical resection. Mod Pathol. 21:847-855.

Oo, Y.H., and D.H. Adams. 2010. The role of chemokines in the recruitment of lymphocytes to the liver. J Autoimmun. 34:45-54.

Oppenheimer-Marks, N., L.S. Davis, D.T. Bogue, J. Ramberg, and P.E. Lipsky. 1991. Differential utilization of ICAM-1 and VCAM-1 during the adhesion and transendothelial migration of human T lymphocytes. J Immunol. 147:2913-2921.

Osborn, L., C. Hession, R. Tizard, C. Vassallo, S. Luhowskyj, G. Chi-Rosso, and R. Lobb. 1989. Direct expression cloning of vascular cell adhesion molecule 1, a cytokine-induced endothelial protein that binds to lymphocytes. Cell. 59:1203-1211.

Panasiuk, A., J. Pogorzelska, and D. Prokopowicz. 2007. [Growth factors in chronic hepatitis C]. Przegl Epidemiol. 61:559-566.

Parkos, C.A., S.P. Colgan, M.S. Diamond, A. Nusrat, T.W. Liang, T.A. Springer, and J.L. Madara. 1996. Expression and polarization of intercellular adhesion molecule-1 on human intestinal epithelia: consequences for CD11b/CD18-mediated interactions with neutrophils. Mol Med. 2:489-505.

Patterson, G.H., and J. Lippincott-Schwartz. 2002. A photoactivatable GFP for selective photolabeling of proteins and cells. Science. 297:1873-1877.

Patterson, G.H., and J. Lippincott-Schwartz. 2004. Selective photolabeling of proteins using photoactivatable GFP. Methods. 32:445-450.

Peng, J., F. He, C. Zhang, X. Deng, and F. Yin. 2011. Protein kinase C-alpha signals P115RhoGEF phosphorylation and RhoA activation in TNF-alpha-induced mouse brain microvascular endothelial cell barrier dysfunction. J Neuroinflammation. 8:28.

Phillips, R.J., K.J. Helbig, K.H. Van der Hoek, D. Seth, and M.R. Beard. 2012. Osteopontin increases hepatocellular carcinoma cell growth in a CD44 dependant manner. World J Gastroenterol. 18:3389-3399.

Pietraszewska-Bogiel, A., and T.W. Gadella. 2011. FRET microscopy: from principle to routine technology in cell biology. J Microsc. 241:111-118.

Ploss, A., M.J. Evans, V.A. Gaysinskaya, M. Panis, H. You, Y.P. de Jong, and C.M. Rice. 2009. Human occludin is a hepatitis C virus entry factor required for infection of mouse cells. Nature. 457:882-886.

Pober, J.S., M.A. Gimbrone, Jr., L.A. Lapierre, D.L. Mendrick, W. Fiers, R. Rothlein, and T.A. Springer. 1986. Overlapping patterns of activation of human endothelial cells by interleukin 1, tumor necrosis factor, and immune interferon. J Immunol. 137:1893-1896.

Puertollano, R., F. Martin-Belmonte, J. Millan, M.C. de Marco, J.P. Albar, L. Kremer, and M.A. Alonso. 1999. The MAL proteolipid is necessary for normal apical transport and accurate sorting of the influenza virus hemagglutinin in Madin-Darby canine kidney cells. J Cell Biol. 145:141-151.

Pure, E., and C.A. Cuff. 2001. A crucial role for CD44 in inflammation. Trends Mol Med. 7:213-221.

Qian, S., L. Lu, F. Fu, Y. Li, W. Li, T.E. Starzl, J.J. Fung, and A.W. Thomson. 1997. Apoptosis within spontaneously accepted mouse liver allografts: evidence for deletion of cytotoxic T cells and implications for tolerance induction. J Immunol. 158:4654-4661.

Reglero-Real, N., B. Marcos-Ramiro, and J. Millan. 2012. Endothelial membrane reorganization during leukocyte extravasation. Cellular and molecular life sciences : CMLS.

Ridley, A.J., M.A. Schwartz, K. Burridge, R.A. Firtel, M.H. Ginsberg, G. Borisy, J.T. Parsons, and A.R. Horwitz. 2003. Cell migration: integrating signals from front to back. Science. 302:1704-1709.

Romero, M., C. Garcia Monzon, G. Clemente, M. Salcedo, R. Banares, E. Alvarez, A. de Diego, L. Santos, and R. Moreno Otero. 2000. Modulation of ICAM-1 tissue expression in patients with liver transplantation (LT) and acute rejection (AR) after glucocorticoid treatment. Transpl Int. 13 Suppl 1:S456-460.

Ross, D., and W.L. Joyner. 1997. Resting distribution and stimulated translocation of protein kinase C isoforms alpha, epsilon and zeta in response to bradykinin and TNF in human endothelial cells. Endothelium. 5:321-332.

Rot, A., and U.H. Von Andrian. 2004. Chemokines in Innate and Adaptive Host Defense: Basic Chemokinese Grammar for Immune Cells. Annu Rev Immunol. 22:891-928.

Sano, K., M. Nagaki, A. Sugiyama, H. Hatakeyama, H. Ohnishi, Y. Muto, and H. Moriwaki. 1999. Effects of cytokines on the binding of leukocytes to cultured rat hepatocytes and on the expression of ICAM-1 by hepatocytes. Dig Dis Sci. 44:796-805.

Schell, M.J., M. Maurice, B. Stieger, and A.L. Hubbard. 1992. 5'nucleotidase is sorted to the apical domain of hepatocytes via an indirect route. The Journal of cell biology. 119:1173-1182.

Scheuer, P.J. 1991. Classification of chronic viral hepatitis: a need for reassessment. J Hepatol. 13:372-374.

Schnoor, M., F.P. Lai, A. Zarbock, R. Klaver, C. Polaschegg, D. Schulte, H.A. Weich, J.M. Oelkers, K. Rottner, and D. Vestweber. 2011. Cortactin deficiency is associated with reduced neutrophil recruitment but increased vascular permeability in vivo. The Journal of experi-

mental medicine. 208:1721-1735.

Schutze, S., D. Berkovic, O. Tomsing, C. Unger, and M. Kronke. 1991. Tumor necrosis factor induces rapid production of 1'2'diacylglycerol by a phosphatidylcholine-specific phospholipase C. J Exp Med. 174:975-988.

Schutze, S., K. Potthoff, T. Machleidt, D. Berkovic, K. Wiegmann, and M. Kronke. 1992. TNF activates NF-kappa B by phosphatidylcholine-specific phospholipase C-induced "acidic" sphingomyelin breakdown. Cell. 71:765-776.

Seelentag, W.K., R. Flury, M. Schmid, P. Komminoth, P. Saremaslani, U. Gunthert, P.U. Heitz, and J. Roth. 1995. [Expression of CD44 isoforms in normal human liver and also in regenerative and neoplastic liver changes]. Verh Dtsch Ges Pathol. 79:144-147.

Serrador, J.M., J.L. Alonso-Lebrero, M.A. del Pozo, H. Furthmayr, R. Schwartz-Albiez, J. Calvo, F. Lozano, and F. Sanchez-Madrid. 1997. Moesin interacts with the cytoplasmic region of intercellular adhesion molecule-3 and is redistributed to the uropod of T lymphocytes during cell polarization. J Cell Biol. 138:1409-1423.

Shen, Q., J.J. Rahn, J. Zhang, N. Gunasekera, X. Sun, A.R. Shaw, M.J. Hendzel, P. Hoffman, A. Bernier, and J.C. Hugh. 2008. MUC1 initiates Src-CrkL-Rac1/Cdc42-mediated actin cytoskeletal protrusive motility after ligating intercellular adhesion molecule-1. Mol Cancer Res. 6:555-567.

Shetty, S., P.F. Lalor, and D.H. Adams. 2008. Lymphocyte recruitment to the liver: molecular insights into the pathogenesis of liver injury and hepatitis. Toxicology. 254:136-146.

Shousha, S., F. Gadir, D. Peston, D. Bansi, A.V. Thillainaygam, and I.M. Murray-Lyon. 2004. CD10 immunostaining of bile canaliculi in liver biopsies: change of staining pattern with the development of cirrhosis. Histopathology. 45:335-342.

Simons, K., and G. van Meer. 1988. Lipid sorting in epithelial cells. Biochemistry. 27:6197-6202.

Snapp, E.L., N. Altan, and J. Lippincott-Schwartz. 2003. Measuring protein mobility by photobleaching GFP chimeras in living cells. Curr Protoc Cell Biol. Chapter 21:Unit 21 21.

Streetz, K., L. Leifeld, D. Grundmann, J. Ramakers, K. Eckert, U. Spengler, D. Brenner, M. Manns, and C. Trautwein. 2000. Tumor necrosis factor alpha in the pathogenesis of human and murine fulminant hepatic failure. Gastroenterology. 119:446-460.

Suda, J., L. Zhu, and S. Karvar. 2011. Phosphorylation of radixin regulates cell polarity and Mrp-2 distribution in hepatocytes. American journal of physiology. Cell physiology. 300:C416-424.

Tacke, F., T. Luedde, and C. Trautwein. 2009. Inflammatory pathways in liver homeostasis and liver injury. Clin Rev Allergy Immunol. 36:4-12.

Takahashi, K., T. Sasaki, A. Mammoto, K. Takaishi, T. Kameyama, S. Tsukita, and Y. Takai. 1997. Direct interaction of the Rho GDP dissociation inhibitor with ezrin/radixin/moesin

initiates the activation of the Rho small G protein. J Biol Chem. 272:23371-23375.

Takeichi, M. 1990. Cadherins: a molecular family important in selective cell-cell adhesion. Annu Rev Biochem. 59:237-252.

Thomson, A.W., and P.A. Knolle. 2010. Antigen-presenting cell function in the tolerogenic liver environment. Nat Rev Immunol. 10:753-766.

Thomson, A.W., S. Satoh, A.K. Nussler, K. Tamura, J. Woo, J. Gavaler, and D.H. van Thiel. 1994. Circulating intercellular adhesion molecule-1 (ICAM-1) in autoimmune liver disease and evidence for the production of ICAM-1 by cytokine-stimulated human hepatocytes. Clin Exp Immunol. 95:83-90.

Tilg, H., A. Kaser, and A.R. Moschen. 2006. How to modulate inflammatory cytokines in liver diseases. Liver Int. 26:1029-1039.

Tilghman, R.W., and R.L. Hoover. 2002a. E-selectin and ICAM-1 are incorporated into detergent-insoluble membrane domains following clustering in endothelial cells. FEBS Lett. 525:83-87.

Tilghman, R.W., and R.L. Hoover. 2002b. The Src-cortactin pathway is required for clustering of E-selectin and ICAM-1 in endothelial cells. Faseb J. 16:1257-1259.

Tolosa, L., A. Bonora-Centelles, M.T. Donato, V. Mirabet, E. Pareja, A. Negro, S. Lopez, J.V. Castell, and M.J. Gomez-Lechon. 2011. Influence of platelet lysate on the recovery and metabolic performance of cryopreserved human hepatocytes upon thawing. Transplantation. 91:1340-1346.

Toomre, D., J.A. Steyer, P. Keller, W. Almers, and K. Simons. 2000. Fusion of constitutive membrane traffic with the cell surface observed by evanescent wave microscopy. J Cell Biol. 149:33-40.

van Buul, J.D., J. van Rijssel, F.P. van Alphen, M. Hoogenboezem, S. Tol, K.A. Hoeben, J. van Marle, E.P. Mul, and P.L. Hordijk. 2010. Inside-out regulation of ICAM-1 dynamics in TNF-alpha-activated endothelium. PLoS ONE. 5:e11336.

van, I.S.C., M.M. Zegers, J.W. Kok, and D. Hoekstra. 1997. Segregation of glucosylceramide and sphingomyelin occurs in the apical to basolateral transcytotic route in HepG2 cells. The Journal of cell biology. 137:347-357.

Vandenhaute, B., M.P. Buisine, V. Debailleul, B. Clement, N. Moniaux, M.C. Dieu, P. Degand, N. Porchet, and J.P. Aubert. 1997. Mucin gene expression in biliary epithelial cells. J Hepatol. 27:1057-1066.

Viswanatha, R., P.Y. Ohouo, M.B. Smolka, and A. Bretscher. 2012. Local phosphocycling mediated by LOK/SLK restricts ezrin function to the apical aspect of epithelial cells. J Cell Biol. 199:969-984.

Volpes, R., J.J. van den Oord, and V.J. Desmet. 1990a. Hepatic expression of intercellular adhesion molecule-1 (ICAM-1) in viral hepatitis B. Hepatology. 12:148-154.

Volpes, R., J.J. van den Oord, and V.J. Desmet. 1990b. Immunohistochemical study of adhesion molecules in liver inflammation. Hepatology. 12:59-65.

Wakabayashi, Y., H. Kipp, and I.M. Arias. 2006. Transporters on demand: intracellular reservoirs and cycling of bile canalicular ABC transporters. J Biol Chem. 281:27669-27673.

Wakabayashi, Y., J. Lippincott-Schwartz, and I.M. Arias. 2004. Intracellular trafficking of bile salt export pump (ABCB11) in polarized hepatic cells: constitutive cycling between the canalicular membrane and rab11-positive endosomes. Mol Biol Cell. 15:3485-3496.

Wald, F.A., R. Forteza, R. Diwadkar-Watkins, A. Mashukova, R. Duncan, M.T. Abreu, and P.J. Salas. 2011. Aberrant expression of the polarity complex atypical PKC and non-muscle myosin IIA in active and inactive inflammatory bowel disease. Virchows Arch. 459:331-338.

Wang, J.P., X.H. Guo, L.J. Wang, Q. Li, B. Chen, W. Wu, X.L. Huang, and Q.B. Huang. 2009a. [Effects of Rho/ROCK signal pathway on AGEs-induced morphological and functional changes in human dermal microvascular endothelial cells.]. Sheng Li Xue Bao. 61:132-138.

Wang, L., and J.L. Boyer. 2004. The maintenance and generation of membrane polarity in hepatocytes. Hepatology. 39:892-899.

Wang, S., Z. Guo, P. Xia, T. Liu, J. Wang, S. Li, L. Sun, J. Lu, Q. Wen, M. Zhou, L. Ma, X. Ding, X. Wang, and X. Yao. 2009b. Internalization of NK cells into tumor cells requires ezrin and leads to programmed cell-in-cell death. Cell Res. 19:1350-1362.

Wang, W., C.J. Soroka, A. Mennone, C. Rahner, K. Harry, M. Pypaert, and J.L. Boyer. 2006. Radixin is required to maintain apical canalicular membrane structure and function in rat hepatocytes. Gastroenterology. 131:878-884.

Warren, A., D.G. Le Couteur, R. Fraser, D.G. Bowen, G.W. McCaughan, and P. Bertolino. 2006. T lymphocytes interact with hepatocytes through fenestrations in murine liver sinusoidal endothelial cells. Hepatology. 44:1182-1190.

Weisz, O.A., and E. Rodriguez-Boulan. 2009. Apical trafficking in epithelial cells: signals, clusters and motors. Journal of cell science. 122:4253-4266.

Wilson, G.K., C.L. Brimacombe, I.A. Rowe, G.M. Reynolds, N.F. Fletcher, Z. Stamataki, R.H. Bhogal, M.L. Simoes, M. Ashcroft, S.C. Afford, R.R. Mitry, A. Dhawan, C.J. Mee, S.G. Hubscher, P. Balfe, and J.A. McKeating. 2012. A dual role for hypoxia inducible factor-1alpha in the hepatitis C virus lifecycle and hepatoma migration. Journal of hepatology. 56:803-809.

Williams, T., and J.E. Brenman. 2008. LKB1 and AMPK in cell polarity and division. Trends Cell Biol. 18:193-198.

Wodarz, A., and I. Nathke. 2007. Cell polarity in development and cancer. Nat Cell Biol. 9:1016-1024.

Wolf, D., R. Hallmann, G. Sass, M. Sixt, S. Kusters, B. Fregien, C. Trautwein, and G. Tiegs. 2001. TNF-alpha-induced expression of adhesion molecules in the liver is under the control of TNFR1--relevance for concanavalin A-induced hepatitis. J Immunol. 166:1300-1307.

Wong, J., P. Kubes, Y. Zhang, Y. Li, S.J. Urbanski, C.F. Bennett, and S.S. Lee. 2002. Role of ICAM-1 in chronic hepatic allograft rejection in the rat. Am J Physiol Gastrointest Liver Physiol. 283:G196-203.

Yang, L., J.R. Kowalski, P. Yacono, M. Bajmoczi, S.K. Shaw, R.M. Froio, D.E. Golan, S.M. Thomas, and F.W. Luscinskas. 2006. Endothelial cell cortactin coordinates intercellular adhesion molecule-1 clustering and actin cytoskeleton remodeling during polymorphonuclear leukocyte adhesion and transmigration. Journal of immunology. 177:6440-6449.

Yonemura, S., and S. Tsukita. 1999. Direct involvement of ezrin/radixin/moesin (ERM)-binding membrane proteins in the organization of microvilli in collaboration with activated ERM proteins. J Cell Biol. 145:1497-1509.

Zegers, M.M., and D. Hoekstra. 1997. Sphingolipid transport to the apical plasma membrane domain in human hepatoma cells is controlled by PKC and PKA activity: a correlation with cell polarity in HepG2 cells. The Journal of cell biology. 138:307-321.

Zegers, M.M., and D. Hoekstra. 1998. Mechanisms and functional features of polarized membrane traffic in epithelial and hepatic cells. The Biochemical journal. 336 (Pt 2):257-269.

Zhou, F., M.N. Ajuebor, P.L. Beck, T. Le, C.M. Hogaboam, and M.G. Swain. 2005. CD154-CD40 interactions drive hepatocyte apoptosis in murine fulminant hepatitis. Hepatology. 42:372-380.

Zuckerman, L.A., L. Pullen, and J. Miller. 1998. Functional consequences of costimulation by ICAM-1 on IL-2 gene expression and T cell activation. J Immunol. 160:3259-3268.

ANEXO

Cell. Mol. Life Sci. (2012) 69:3079–3099
DOI 10.1007/s00018-012-0987-4

Cellular and Molecular Life Sciences

REVIEW

Endothelial membrane reorganization during leukocyte extravasation

Natalia Reglero-Real · Beatriz Marcos-Ramiro · Jaime Millán

Received: 23 December 2011 / Revised: 22 March 2012 / Accepted: 29 March 2012 / Published online: 10 May 2012

Abstract Leukocyte trafficking from the bloodstream to inflamed tissues across the endothelial barrier is an essential response in innate immunity. Leukocyte adhesion, locomotion, and diapedesis induce signaling in endothelial cells and this is accompanied by a profound reorganization of the endothelial cell surfaces that is only starting to be unveiled. Here we review the current knowledge on the leukocyte-mediated alterations of endothelial membrane dynamics and their role in promoting leukocyte extravasation. The formation of protein- and lipid-mediated cell adhesion nanodomains at the endothelial apical surface, the extension of micrometric apical membrane docking structures, which are derived from microvilli and embrace adhered leukocytes, as well as the vesicle-trafficking pathways that are required for efficient leukocyte diapedesis, are discussed. The coordination between these different endothelial membrane-remodeling events probably provides the road map for transmigrating leukocytes to find exit points in the vessel wall, in a context of severe mechanical and inflammatory stress. A better understanding of how vascular endothelial cells respond to immune cell adhesion should enable new therapeutic strategies to be developed that can abrogate uncontrolled leukocyte extravasation in inflammatory diseases.

Keywords Diapedesis · Tetraspanins · Microvilli · Docking structures · Transcellular · Caveolae · PECAM-1 · ICAM-1

N. Reglero-Real and B. Marcos-Ramiro contributed equally to this work.

N. Reglero-Real · B. Marcos-Ramiro · J. Millán (✉)
Centro de Biología Molecular Severo Ochoa,
CSIC-Universidad Autónoma de Madrid,
C/Nicolás Cabrera 1, Cantoblanco, 28049 Madrid, Spain
e-mail: jmillan@cbm.uam.es

Abbreviations

PMN	Polymorphonuclear
FCS	Fluorescence correlation spectroscopy
TIRF	Total internal reflection fluorescence
FRET	Fluorescent resonance energy transfer
FRAP	Fluorescence recovery after photobleaching
TEM	Transendothelial migration
BBB	Blood–brain barrier
LBR	Lateral border recycling
DRM	Detergent-resistant membranes

Introduction

Endothelial cells line the inner surface of the vascular wall, where they form a selective barrier that controls the passage of cells and small solutes between the blood and the tissue. In response to tissue injury, the endothelium from vessels surrounding the damaged area undergoes a local increase of permeability to cells and solutes that is essential for the inflammatory response [1, 2]. The increase in cell extravasation is not a passive event, but involves the active retention of blood cells, mainly leukocytes, on the endothelial surface, and the subsequent promotion by the endothelium of leukocyte extravasation toward the interstitial space [3]. Leukocyte transmigration, when pathologically altered, contributes to the development of a range of proinflammatory diseases, such as atherosclerosis, multiple sclerosis, and rheumatoid arthritis [4–6].

In the current paradigm of leukocyte transmigration, different subsets of leukocyte and endothelial receptors establish a cascade of interactions that involve initial leukocyte tethering and rolling, firm adhesion, crawling or locomotion on the luminal endothelial surface, and a final

step of transendothelial migration (TEM), which is also known as diapedesis [3, 7]. Loss-of-function strategies, like blocking antibodies and genetic ablation, have enabled the identification of many surface receptors involved in the leukocyte–endothelial cell interaction [5, 8–15]. Intravital microscopy studies have also provided clarification of the chronological and hierarchical order of these interactions at each step of the cascade [16, 17]. The most important endothelial receptors involved in leukocyte transmigration through blood vessels have been extensively reviewed elsewhere and their roles often depend on the vascular bed and the leukocyte type implicated in the interaction [17–20]. In general, and from the endothelial side, initial leukocyte tethering and rolling are mediated by E- and P-selectin, and by carbohydrates exposed on the endothelial surface that are able to engage leukocyte (L)-selectin [21]. Intercellular adhesion molecule (ICAM)-1 and vascular adhesion molecule (VCAM)-1 are adhesion receptors of the immunoglobulin superfamily that are central players in the subsequent step: leukocyte firm adhesion [22]. ICAM-1 and VCAM-1 also mediate locomotion of adhered leukocytes on the endothelium and some features of diapedesis [23]. Diapedesis mostly occurs through junctions between two endothelial cells, in what is called a paracellular route. However, there exists an alternative transcellular route in which leukocytes can traverse the body of single endothelial cells [24]. A range of surface receptors localized at endothelial cell–cell junctions interacts with and facilitates extravasation of leukocytes following paracellular diapedesis. The way each of these receptors promotes local gap opening has been a matter of intense investigation in recent years [25, 26]. For instance, ICAM-1, VCAM-1, and some junctional proteins that interact with the transmigrating leukocyte have the ability to signal to and destabilize adherens junctions and, as a consequence, promote a local increase in permeability [27–29]. Some others, namely platelet endothelial cell adhesion molecule (PECAM-1), promote plasma membrane extensions at endothelial cell borders that also facilitate diapedesis. Expression levels of ICAM-1 and probably VCAM-1, also contribute to diapedesis by regulating the balance between the paracellular and transcellular routes of TEM [24, 30]. The molecular basis of this regulation will be discussed in this review.

A basal rate of leukocyte trafficking through the circulatory system is necessary for immuno-surveillance. However, leukocyte transmigration through vessels in the proximity of an inflammatory focus is increased in a spatiotemporally restricted manner. This increase is mediated by inflammatory cytokines, such as TNF-α or IL-1β, which are released by interstitial cells in response to the inflammatory upset. These stimuli upregulate the expression of E-selectin, ICAM-1, VCAM-1, and chemokines that are deposited in the luminal endothelial glycocalyx, all of which promote leukocyte capture and extravasation in the surroundings of the inflammatory focus. In addition, in response to some of these proinflammatory cytokines, junctional proteins involved in diapedesis are partially dispersed from cell–cell contacts and localize all over the luminal endothelial surface. This suggests that these proteins may play a role away from junctions in a proinflammatory context [31, 32].

Far from being passive agents exposing a plethora of receptors on their surface, endothelial cells determine the successful accomplishment of leukocyte extravasation by eliciting crucial signaling responses upon leukocyte contact [33]. In the multistep paradigm of leukocyte–endothelial interaction, the first steps (tethering, rolling, and firm adhesion) are more dependent on leukocyte behavior, whereas endothelial cell responses contribute more to modulate subsequent leukocyte locomotion and diapedesis. So, near-physiological levels of leukocyte tethering, rolling, and firm adhesion can be achieved in vitro in the absence of endothelium by providing the correct combination of laminar flow and recombinant endothelial molecules immobilized on a solid substrate [21, 34]. In contrast, endothelial adhesion receptors can be individually blocked with no apparent effect on leukocyte adhesion, but with significant consequences for the ability of leukocytes to crawl and find a passage for extravasation, indicating that the role of these endothelial receptors goes beyond their adhesive properties [30, 35]. Furthermore, altering the signaling properties of some of these receptors, for example ICAM-1, also has no effect on leukocyte adhesion but impairs posterior leukocyte transmigration [36]. In addition, once the leukocyte is engaged in crossing the endothelium, paracellular diapedesis can still be abrogated or even reversed simply by blocking the endothelial receptors involved in this step of transmigration [37]. These and several other lines of evidence indicate that leukocytes can proactively initiate the sequence of interactions that lead to the first immune reaction against tissue injury, but also that endothelial cell responses are crucial for the final outcome of this reaction, an efficient leukocyte extravasation and arrival to the focus of the inflammation.

Leukocyte interaction with the endothelial cell must be strong enough to overcome the shear stress from the blood flow and transient enough to allow leukocyte locomotion and egress from the vessel. The organization of the endothelial cell surface, the biological fence facing the vessel lumen, is thus essential to integrate signals from different sources, such as mechanical forces, cytokine signaling and cell–cell interactions. Research focused on the analysis of leukocyte–endothelial interactions at the molecular level, combining high-resolution and analytical microscopy with sophisticated in vitro settings, has been developed over recent years. These studies are finding that endothelial

responses to leukocyte interaction involve a remarkable reorganization of endothelial membranes, ranging from the formation of nanodomains of adhesion receptors, based on protein–protein and protein–lipid interactions, to the extension of microvillus-like structures that engulf the leukocyte, or the formation of invaginations when leukocytes push down endothelial membranes during locomotion Importantly, this endothelial remodeling does not seem important for leukocyte adhesion itself but is essential for diapedesis. Here we provide an overview of the effect of leukocyte binding on the organization of the endothelial surface.

Submicron organization of adhesion receptors at the endothelial plasma membrane in response to leukocyte interactions

The endothelial adhesion receptors ICAM-1 and VCAM-1 are glycoproteins with an N-terminal extracellular domain containing five and seven immunoglobulin domains, respectively. They have a single transmembrane span and a short C-terminal cytoplasmic domain. ICAM-1 binding to leukocyte β2-integrins and VCAM-1 binding to β1-integrins mediate leukocyte adhesion to endothelial cells in most vascular beds [38, 39]. The structure, localization, role and dynamics of ICAM-1 and VCAM-1 are very similar, so it is conceivable that they associate and form heteroligomers or homoligomers. Using latex beads covered with anti-ICAM-1 or anti-VCAM-1 antibodies as surrogate leukocytes, van Buul and colleagues [40] have demonstrated that one receptor engagement induces association with the bead of the other. Using a different strategy, Barreiro and colleagues [41] have shown that cells overexpressing one type of integrin, and therefore engaging mainly one adhesion receptor, can indeed induce the recruitment of the other receptor to leukocyte-endothelial contacts. Interestingly, FRET studies have revealed the existence of ICAM-1 homotypic interactions but not of VCAM-1 or of ICAM-1-VCAM-1 heterotypic complexes on the endothelial surface in the absence of leukocytes. Accordingly, co-immunoprecipitation experiments of unengaged ICAM-1 and VCAM-1 have found only a negligible association between the two receptors [42]. Collectively, these data indicate that VCAM-1 and ICAM-1 follow similar dynamics upon leukocyte engagement, and become part of the same macromolecular complex in the area of contact with the leukocyte. However, in the absence of ligation, despite having a similar distribution on the endothelial surface, these two receptors are not directly associated with each other on the endothelial surface.

ICAM-1 and VCAM-1 reside in preformed tetraspanin platforms at the endothelial plasma membrane

Tetraspanins form a large group of proteins with some shared structural features: four transmembrane domains that comprise a very short intracellular segment, a first small extracellular loop or domain (SEL/SED) or EC1, and a large extracellular loop (LEL, LED) or EC2. LED contains four to eight cysteine residues, including those in a CCG motif that is conserved in all tetraspanins. LED cysteines form disulphide bonds that are necessary to maintain the structure of this domain, which is responsible for most tetraspanin interactions with other proteins [43–45]. Tetraspanins have the ability to associate with each other, forming remarkable macromolecular complexes known as tetraspanin webs [43, 46]. Cysteine residues found in close contact with the cytoplasmic leaflet of the membrane undergo palmitoylation, which is required for the formation of tetraspanin microdomains [47]. Tetraspanins interact with several other molecules, including VCAM-1 and ICAM-1 [48]. The tetraspanin web contributes to establish physical connections in large membrane domains between associate receptors that are at relatively low density within the membrane. Given the size of the contact area between the leukocyte and the endothelial cell during leukocyte adhesion, tetraspanins may form large endothelial macromolecular platforms mediated by ICAM-1 and VCAM-1 interactions with leukocyte integrins. A detailed analysis of the molecular platforms formed between tetraspanins CD9 and CD151 and VCAM-1 and ICAM-1 has been carried out using analytical microscopy techniques. By combining FRET, FRAP and FCS spectroscopy, the existence of preformed tetraspanin platforms and adhesion receptors on the endothelial surface has been suggested [41]. In contrast to the lack of association between ICAM-1 and VCAM-1, CD9 and CD51 have been linked with both receptors in immunoprecipitation experiments performed in the absence of engagement, consistent with the analytical microscopy data [41, 42]. Moreover, FRAP and FCS analyses of tetraspanins and adhesion receptors indicate that tetraspanin-receptor platforms are stabilized in the endothelial area of contact with the adhered leukocyte. Notably, a soluble recombinant protein carrying the tetraspanin LED decreased the clustering of ICAM-1 and VCAM-1 [41], and inhibited leukocyte adhesion, detachment and diapedesis. Taken together, these data indicate that ICAM-1 and VCAM-1 are pre-embedded in endothelial tetraspanin platforms, which are required for proper adhesion receptor function in leukocyte extravasation (Fig. 1).

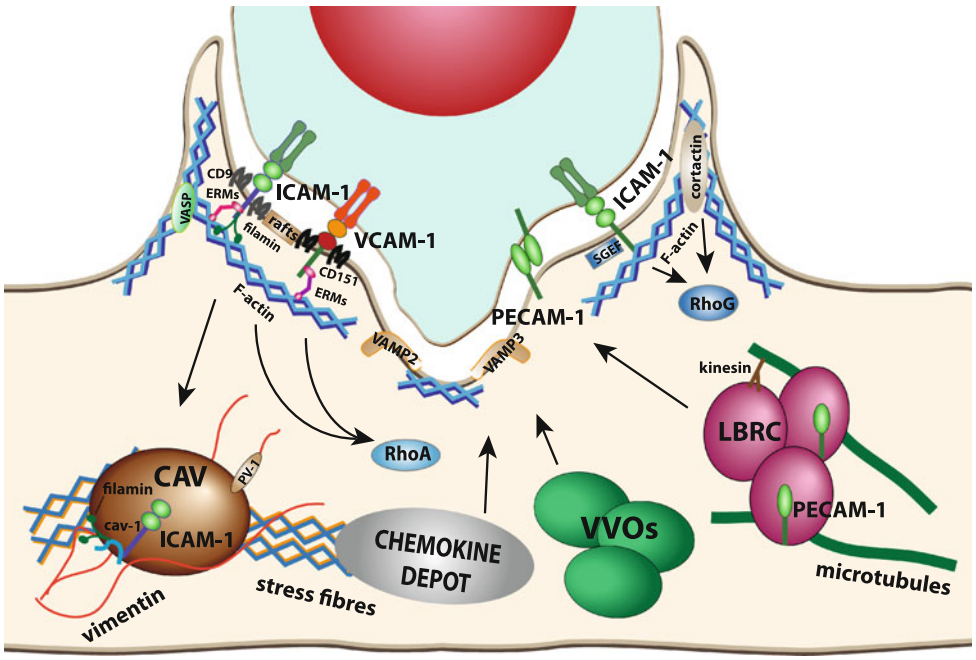

Fig. 1 Proteins involved in endothelial apical membrane reorganization upon leukocyte interaction. ICAM-1, VCAM-1, and PECAM-1 are the three best characterized receptors that modulate the endothelial cell surfaces in contact with leukocytes. ICAM-1 and VCAM-1 are embedded into tetraspanin webs. Both receptors and E-selectin can be transiently recruited to membrane rafts upon engagement. ICAM-1 and VCAM-1 are connected to subcortical actin through different protein connectors such as ERM proteins or filamins. These receptors form signaling platforms in apical microvillar reorganization called docking structures. ICAM-1 and VCAM-1 signal to different Rho GTPases and cortactin to tune actin dynamics in the surrounding of endothelial cell-leukocyte contact areas and facilitate diapedesis. When apical ICAM-1 is engaged in caveola-rich cellular areas, can be internalized into basolateral caveolae. It has been proposed that PECAM-1 is translocated from the LBR compartment to endothelial contact areas. On the ventral side of the leukocyte, endothelial SNARE machinery participates in membrane remodeling in response to leukocytes emitting pseudopods/podosomes that scan for gateways to traverse the endothelial monolayer. VVOs participate in the formation of endothelial invaginations surrounding podosomes. Chemokine depots are intracellular compartments, still uncharacterized, which translocate chemokines to endothelial surface upon leukocyte adhesion. Actin stress fibers determine the localization of caveolae and chemokine depots. The vimentin network is associated with caveolae through PV-1. Microtubules and kinesins regulate LBRC dynamics

Coalescence of endothelial adhesion receptors into membrane rafts upon leukocyte adhesion

Membrane lipids and proteins do not diffuse freely in the bilayer, but are laterally constrained by mechanisms such as hydrophobic compatibility, membrane protein–protein interactions, or interactions between membrane proteins and the submembrane cytoskeleton. The intrinsic heterogeneity of the plasma membrane has been explained by the differential miscibility of lipids that spontaneously form microdomains of distinctive membrane order or compaction, which in turn are able to compartmentalize subsets of membrane proteins. The term "membrane rafts" designates the most popular model of membrane microdomains, which proposes the existence of liquid-ordered nano-scale assemblies of cholesterol and sphingolipids that exclude most transmembrane proteins, and preferentially include those with lipid modifications, such as glycosylphosphatidylinositol or palmitoylation. The size (10–200 nm) and dynamics of membrane rafts depend on the physiological context. Signaling events can induce the coalescence of transient and small membrane clusters into larger and more stable platforms and vice versa [49]. Crude biochemical approaches based on the different solubility properties of membrane proteins in non-ionic detergents [50] have given way to novel biophysical and microscopy techniques to investigate membrane rafts. These novel approaches are yielding evidence that confirms the partition of certain proteins into small membrane platforms regulated by cholesterol content [49]. However, the true nature of membrane rafts remains elusive, due mainly to the difficulties of clearly visualizing these domains within the cell, and this has generated skepticism and controversy [51].

Compact membrane domains of cholesterol and sphingolipids are less sensitive to detergent extraction than are fluid, non-raft membranes, so the former can be biochemically isolated as detergent-resistant membranes (DRMs).

As already mentioned, this has been criticized as a strategy to characterize membrane rafts [51], but it is a simple method that provides qualitative evidence of changes occurring in the lipid context of particular proteins. On the other hand, receptor engagement with antibodies has proved to be a powerful strategy for investigating leukocyte-endothelial interactions because it enables signaling events from one cell type or the other to be identified. These can subsequently be validated by more physiological experimental approaches. Antibody-mediated engagement of E-selectin induces receptor confinement into DRMs in endothelial cells [52]. Leukocyte- or antibody-induced clustering also increases E-selectin colocalization with caveolin-1 [53], the scaffolding protein of caveolae [54–57], a vesicular compartment quite abundant in endothelial cells [58]. Caveolin-1 binds cholesterol, and caveolae are considered as specialized membrane raft domains [57]. Furthermore, endothelial raft disruption with cholesterol-sequestering reagents decreases neutrophil rolling on E-selectin and reduce the ability of E-selectin to transduce signals [59]. These findings suggest that cholesterol-rich domains may regulate leukocyte rolling by modulating signaling mediated by, at least, E-selectin. However, experimental strategies that can specifically disrupt E-selectin microdomains, or the identification of the protein signals and scaffolds responsible for the partition of E-selectin into ordered membranes, are necessary to clarify the real role of ordered membranes in these first steps in leukocyte transmigration.

Similarly, in response to leukocyte interaction or antibody crosslinking, ICAM-1 is partially confined within DRMs [52, 60]. Time-lapse analysis of ICAM-1 trafficking reveals unusual dynamics for this receptor. Following antibody clustering, ICAM-1 is translocated from actin-rich microvilli to actin stress fibers and is then partially segregated to the cell poles. Engaged ICAM-1 accumulates in areas close to, but distinct from the cell–cell junctions, where several actin bundles converge [60]. Interestingly, these areas are also enriched in caveolin-1 (Fig. 2a, b). A more detailed analysis by electron microscopy and total internal reflection fluorescence (TIRF) microscopy, which detects fluorescence at the very basal region of the cell and in close contact with the substrate, has revealed that a fraction of ICAM-1 is internalized into caveolar-like structures and is transcytosed to the abluminal endothelial membrane [60]. Thus, upon ligation, ICAM-1 is not only recruited to DRMs but is also partially segregated in a vesicular compartment enriched in membrane rafts. VCAM-1 dynamics has not been studied in such detail, but the available data suggest it is comparable to that of ICAM-1. Crosslinked VCAM-1 also segregates into membrane rafts, then aligns with stress fibers and is subsequently is partially localized in caveolin-1-rich structures [60]. Cholesterol-sequestering reagents reduce E-selectin and ICAM-1 clustering [52, 53]. However, since disruption of cholesterol-rich membrane domains inhibits the previous step of leukocyte rolling, the role of raft domains in leukocyte adhesion and locomotion has been difficult to assess using this strategy. More artificial approaches, such as analyzing apical detachment of anti-ICAM-1-bearing beads in response to the shear stress, show that cholesterol extraction increases leukocyte de-adhesion, which is also dependent on actin polymerization [61]. The role of caveolae-like domains in diapedesis has been investigated in more detail. Some groups have found that leukocytes follow a route of transcellular diapedesis preferentially in areas enriched in caveolin-1 and other caveolar components [60, 62, 63]. This suggests that clustering of at least ICAM-1 into raft-like microdomains may help guide the leukocyte towards points of extravasation. Membrane remodeling during diapedesis is reviewed in more detail below.

Relationship between tetraspanin domains and rafts at the endothelial surface

Several lines of evidence have shown that most of the interactions between tetraspanins and other molecules are not dependent on cholesterol. However, tetraspanins can be partially recruited into DRMs isolated in isopycnic sucrose gradients using mild lysis conditions that preserve tetraspanin–tetraspanin interactions. Tetraspanin domains are though only partially sensitive to cholesterol depletion compared to membrane domains rich in prototypical raft-proteins such as GPI-linked proteins [47, 64]. Detailed measurement of the diffusion coefficient of the tetraspanin CD9 by single-molecule fluorescence microscopy indicated that cholesterol extraction affects its membrane dynamics [47]. This effect was attributed to a general alteration in membrane fluidity caused by cholesterol extraction, which also affected the dynamics of raft and non-raft protein markers. Notwithstanding a possible role of raft-lipids in the organization of tetraspanin webs [65], these webs form domains that largely depend on protein–protein interactions, with features that make them clearly distinguishable from membrane rafts [43]. Overall, distinct but complementary roles for tetraspanin and raft domains can be envisaged from a consideration of all the published evidence regarding endothelial ICAM-1 and VCAM-1 function and clustering. Data strongly support the confinement of ICAM-1 and VCAM-1 in tetraspanin nanodomains, but not in cholesterol-rich DRMs, in the absence of receptor engagement [52, 60, 66]. However, size measurements of ICAM-1 and VCAM-1 nanoclusters

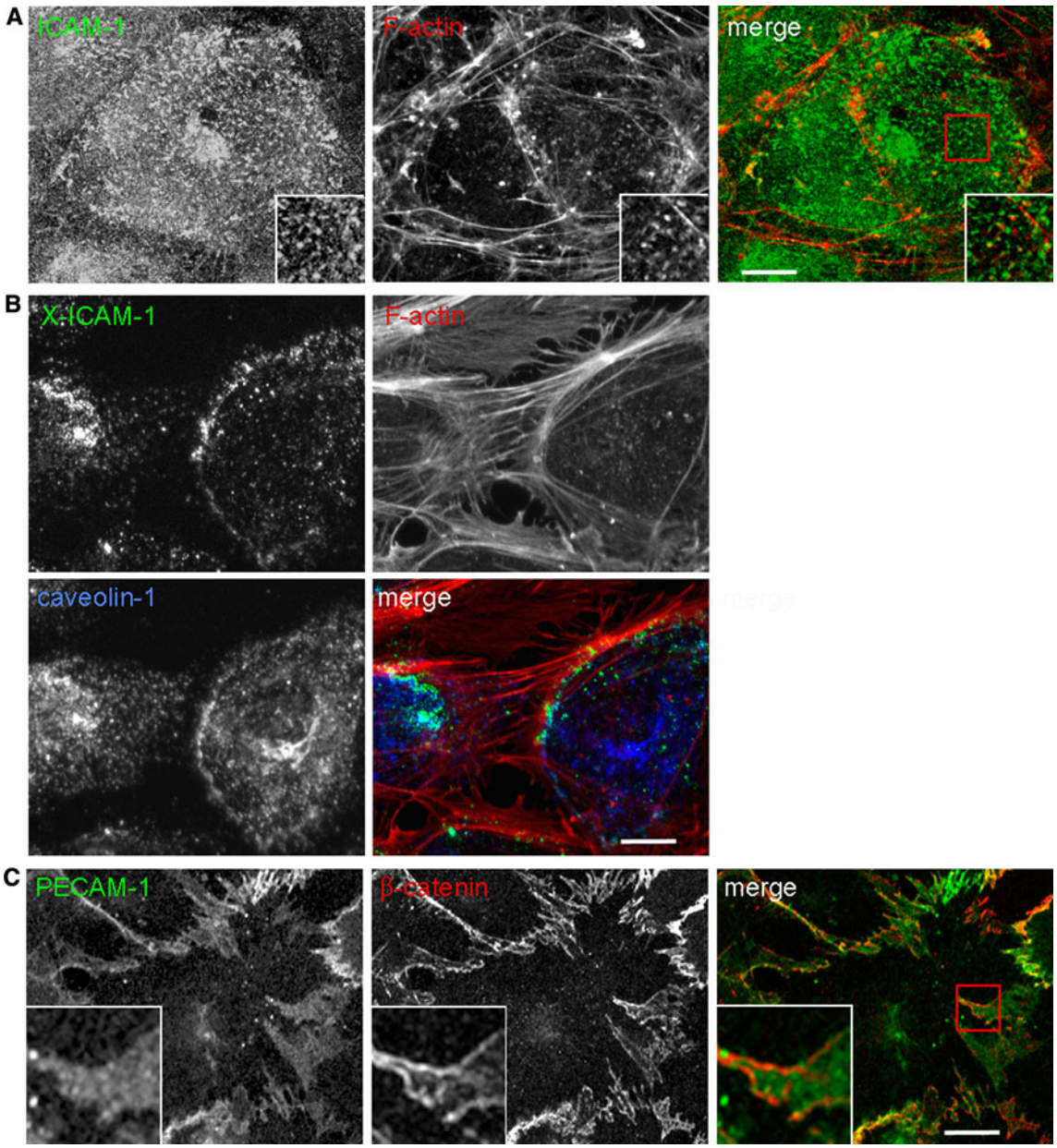

Fig. 2 Endothelial membrane domains involved in adhesion receptor dynamics. **a** Microvilli. Confocal images of HUVECs stained for ICAM-1 and F-actin (phalloidin) showing the accumulation of this receptor in apical microvilli, involved in the formation of docking structures in response to leukocyte adhesion **b** Caveolae. Upon antibody-mediated ICAM-1 clustering (X-ICAM-1), actin stress fibers are increased, ICAM-1 aligns with actin filaments and partially colocalizes with caveolin-1. Leukocytes transmigrate transcellularly through areas rich in caveolin-1. **c** Lateral border recycling (LBR) compartment. PECAM-1 is diffusely localized at cell borders, labeled with anti-β-catenin antibody, in an internal compartment that is translocated to the cell surface upon leukocyte interaction. The LBR compartment is required for both paracellular and transcellular diapedesis. *Bar* 10 μm

indicate that they coalesce and are more stable in the leukocyte contact area [41]. This coalescence parallels ICAM-1 recruitment into ordered domains, so it could well be mediated by cholesterol-enriched rafts [60]. In fact, examples of coalescence between tetraspanin and membrane rafts can be found in different cellular contexts, such as cell infection by HIV, *Plasmodium* sporozoite invasion, or during engagement of the B-cell receptor or the MHC-II complex [67–70]. Thus, future investigation of the relationship between the tetraspanin web, which constitutively accommodates transmembrane receptors, and membrane rafts, which can merge platforms based on protein–protein interactions, may complete the picture of how endothelial adhesion

receptors are organized in the contact area between leukocyte and endothelium.

Ups and downs of the endothelial response to leukocyte interaction

Endothelial ICAM-1 and VCAM-1 can be organized into submicron membrane platforms in response to leukocyte interaction. However, leukocytes also induce supramolecular remodeling of the endothelial membrane, with the contribution of subcortical cytoskeleton, which is essential for achieving successful extravasation (Fig. 1).

Ups: endothelial membrane structures derived from microvilli embrace adhered leukocytes

With the advent of modern microscopy, cell surfaces have been shown to be uneven and able to emit dynamic protrusions necessary for motility and communication. Cells decorate their respective surfaces exposed to extracellular milieu with small actin-dependent projections, bearing different subsets of surface receptors and ion channels, known as microvilli (Fig. 2a) [71]. These surface organelles are important for cell communication with the extracellular space. F-actin, the cytoskeletal scaffold of the microvilli, is associated with the plasma membrane through different protein linkers that connect membrane receptors to the actin filament. In endothelial cells, ICAM-1 and VCAM-1 are enriched in microvilli and are connected to the underlying F-actin via interactions through their cytoplasmic tails with ezrin, radixin and moesin (ERM) proteins, which belong to the 4.1 superfamily of proteins. This superfamily is formed by proteins containing an N-terminal four point one, ezrin, radixin, moesin (FERM) domain that interacts with the lipids and basic amino acids in intracellular segments of membrane proteins [72]. ICAM-1 interacts preferentially with ezrin [73, 74] and VCAM-1 with moesin [66]. In their active, open conformation, ERM proteins are linked to the plasma membrane through N-terminal FERM domains and to submembrane F-actin through their C-terminal domains [75]. ERM proteins are required for microvillar elongation [74, 76–78]. Mutation of a short segment in the cytoplasmic region of ICAM-1, rich in basic amino acids, abrogates ICAM-1 interaction with ERM protein as well as the ability of this receptor to elongate microvilli [74]. ICAM-1 bearing these mutations also failed to promote leukocyte transmigration [74]. Moreover, incubation of endothelial cells with a permeable peptide blocking ICAM-1-ERM interaction did not affect leukocyte adhesion but significantly diminished leukocyte transmigration. This again supports the idea that expression of endothelial adhesion receptors is sufficient to capture and adhere leukocytes bearing active integrins, whereas ICAM-1 and probably VCAM-1 interactions with subcortical actin in microvillar structures are essential for leukocyte extravasation. The detailed molecular mechanism whereby microvilli control leukocyte transmigration is not completely understood, but probably involves substantial remodeling in response to leukocyte adhesion of the apical endothelial plasma membrane in the so-called microvillar cups or docking structures.

In 1999, Wojciak-Stothard and colleagues [79] showed that ICAM-1, VCAM-1, and E-selectin accumulated along the edges of attached monocytes, outlining fine protrusions formed by the monocyte-endothelial interface. These protrusions were positive for F-actin and morphologically reminiscent of microvilli. Barreiro and colleagues [66] subsequently reported for the first time a detailed analysis of these microvillar protrusions that surrounded adhered leukocytes, and named them docking structures. Docking structures contained F-actin, vinculin, α-actinin, VASP and phosphorylated, active ERM proteins. Analyzing various fluorescent probes suggested that the phosphoinositide $PI(4,5)P_2$, which anchors ERM proteins to the plasma membrane, was also enriched at the tip of the protrusions [66]. Additional reports have provided substantial evidence that endothelial cup-shaped membrane projections embracing leukocytes are derived from microvilli [74, 80, 81]. Like microvilli, docking structures are sensitive to actin and microtubule depolymerization [66, 79, 80] In addition, the accumulation of VASP in these membrane projections strongly suggests that de novo actin polymerization is required for their formation, similarly to what has been found for other surface membrane extensions, such as those occurring during phagocytosis [66, 82, 83].

The investigation of the signaling pathways involved in the formation of docking structures has provided confusing information about the role of these protrusions in leukocyte extravasation. Rho family GTPases are master regulators of cytoskeletal networks. Most Rho GTPases are molecular switches that cycle between an inactive GDP-bound state and an active GTP-bound state that regulates a plethora of effectors [84]. RhoA, Rac and Cdc42 are the three most extensively studied Rho GTPases in the family, but there are many other Rho members poorly characterized [85]. In endothelial cells, RhoA controls actomyosin-mediated contractility mainly through the activation of its effector ROC kinase (ROCK) [18]. Rho and probably ROCK, activate ERM proteins, which can promote microvillar elongation [75]. Thus, the Rho-ROCK pathway could regulate the formation of docking structures, leukocyte adhesion, and transmigration. This pathway is however fundamental to endothelial architecture and function,

including barrier function, so data regarding the effect of Rho or ROCK inhibition on endothelial docking structures and on leukocyte transmigration are not conclusive. For instance, treatment of endothelial cells with the toxin C3 transferase, a potent inhibitor of Rho, impairs leukocyte transmigration [79, 86, 87], but its effect on leukocyte adhesion is still unclear [86, 88]. C3 transferase has been shown to prevent [79] or not prevent [80] adhesion receptor clustering around adhered leukocytes. There is also disagreement about the role of the ROCK in leukocyte adhesion and in the formation of docking structures. Pharmacological inhibition of this kinase clearly reduced leukocyte adhesion, transmigration and formation of these microvillus-derived cups in some conditions [66], or had no effect on adhesion and formation of docking structures in others [80]. A stronger consensus has been reached concerning the effect of ROCK inhibition on leukocyte extravasation, which is clearly hampered. Taken together, these findings provide evidence of an essential role for the Rho-ROCK pathway in leukocyte transmigration in general and, probably, in the formation of docking structures in particular.

Clearer information has come from studies about the proteins in endothelial plasma membrane that are responsible for the formation of these cups. K562 cells overexpressing LFA-1 [80] or VLA-4 [66] have been used to preferentially engage ICAM-1 or VCAM-1, respectively, in endothelial cells. Both cell clones were able to promote the formation of docking structures upon adhesion to endothelial cells, which suggests that single engagement of each adhesion receptor is sufficient to generate microvillar cups. However, the blocking of the interaction of ICAM-1 with LFA-1, but not of VCAM-1 with VLA-4, reduced the formation of docking structures surrounding MCP-1-activated monocytes, suggesting a predominant role for ICAM-1 in this process [80]. Although the relative contribution of each receptor to these membrane extensions probably depends on their relative abundance, leukocyte population and type of vascular bed, further investigation of the role of adhesion receptors in microvillar cups has been mainly focused on ICAM-1. The aforementioned mutation of a domain rich in polybasic amino acids in the ICAM-1 cytoplasmic tail, which decreases ICAM-1-induced microvilli and leukocyte transmigration, also reduces the formation of endothelial docking structures upon leukocyte adhesion. This reinforces the similarities between microvilli and docking structures. ICAM-1-mediated signaling or interaction with subcortical actin thus appears to be necessary for the formation of docking complexes. Analysis of ICAM-1-mediated signaling in response to antibody engagement has revealed a major activation of a RhoA-regulated pathway [89, 90]. This, together with the fact that Rho pathway inhibition reduces the formation of the microvillar cups, further supports a role for Rho in coordinating signals originating from ICAM-1, which promote the eventual reorganization of the microvilli to embrace adhered leukocytes.

ICAM-1 can also signal to other Rho GTPases. van Buul and colleagues [81] have reported that ICAM-1 crosslinking activates RhoA, Rac1, Cdc42, and RhoG, suggesting that leukocyte adhesion orchestrates several Rho-dependent pathways to promote a profound reorganization of the endothelial apical membrane. RhoG had previously been found to be involved in the formation of the phagocytic cup [91]. Following the parallelism with the endothelial microvillus-derived cups, the role of this small GTPase has been investigated. RhoG and its guanine-nucleotide exchange factor (GEF), SH3-GEF (SGEF), were found enriched in dorsal ruffles and in membrane projections surrounding the leukocyte upon adhesion. Expression of active mutants of RhoG increased the emission of these projections, whereas RhoG or SGEF knockdown with small interfering RNA (siRNA) decreased them. It is of note that SGEF was found to be associated with the ICAM-1 cytoplasmic tail and that a tail-less ICAM-1 mutant failed to recruit RhoG to the docking structures. Future studies of the crosstalk between RhoG and other Rho GTPases will probably shed light on the signaling networks that mediate the formation of docking structures. For instance, siRNA-mediated knockdown of RhoA reduces RhoG activation upon ICAM-1 engagement, suggesting that the former GTPase is an upstream regulator of the latter [81]. VCAM-1 and ICAM-1 clustering activates Rac1 in endothelial cells [27, 81]. Analysis of the effect of Rac1 dominant negative mutants in human endothelial cells indicates that Rac1 is not required for firm adhesion of monocytes [79]. However, inhibition of Rac1 function with permeable blocking peptides or Rac1 knockdown strongly supports a role for this Rho GTPase in leukocyte extravasation [27, 92]. Notably, RhoG has the potential to regulate Rac1 activity through common GEF protein complexes [93, 94] and Rac and its effectors are in turn required for dorsal membrane dynamics such as the formation of ruffles and macropinocytosis [95–97]. Hence, a role can be envisaged for adhesion receptor-mediated Rac activation in the formation of the endothelial docking structure and in leukocyte diapedesis. Rac could contribute to RhoG or RhoA signaling pathways, as has already been observed in other cellular contexts [93, 95]. In summary, although the architecture of these docking structures seems well defined, the protein machinery recruited to these membrane protrusions and the signaling pathways emanating from these domains are still poorly defined. Nevertheless, in light of the current knowledge about the proteins that regulate

microvillar cups, these structures could be also considered as hubs where supramolecular organization of protein complexes formed by adhesion receptors, tetraspanins, ERM proteins and Rho GTPases, can signal and determine the additional endothelial remodeling necessary for diapedesis. This may include microvillar elongation to ensure dynamic leukocyte retention against blood flow, but also RhoA-mediated cell contraction or Rac1-mediated weakening of cell–cell junctions.

The ability of ICAM-1 to bring together signaling machinery in the docking structure through its cytoplasmic tail seems to be of fundamental importance. Thus, the role of this receptor domain in leukocyte diapedesis may somehow denote the function of docking structures in extravasation. The reconstitution of a brain endothelioma cell line, derived from ICAM-1 and ICAM-2 double-knockout mice, with ICAM-1 mutants has elegantly demonstrated that the extracellular domain of ICAM-1 is sufficient to support T-cell adhesion, while its cytoplasmic tail is necessary for diapedesis. Truncation of this cytoplasmic domain prevented not only TEM in these cell lines but also ICAM-1-mediated RhoA activation [35]. Therefore, there are strong correlations between ICAM-1-mediated signaling, docking structures and leukocyte diapedesis, but not adhesion, which implies that the remodeling of the endothelial apical membrane helps to establish signaling platforms that facilitate the passage of leukocytes across the endothelium.

However, it is of note that docking structures have not been always observed in vitro. Luscinksas's group has reported clustering of ICAM-1 and LFA-1 around transmigrating neutrophils under laminar flow, but not microvillus-derived structures [30, 98]. In vivo, these structures have been also difficult to detect [99]. This disagreement may be related to the different experimental settings used, which may determine different levels of integrin activation. Higher integrin activation could result in greater recruitment of endothelial counter-receptors and the subsequent stimulation of signaling pathways related to phagocytosis. This has been more extensively discussed in a previous review [100]. Further investigation into mechanisms regulating the formation of docking structures and their in vivo relevance is still required.

Downs: leukocyte-induced endothelial membrane invaginations

The scanning by adhered leukocytes for suitable areas of transmigration on the endothelial luminal membrane is defined as locomotion [23]. In this step, leukocytes search for clues to initiate diapedesis in the presence of shear stress forces from the bloodstream. Pioneering electron microscopy studies in the 1960s showed leukocytes emitting pseudopods and remodeling endothelial cells during extravasation [101–103]. Modern in vitro approaches, which combine settings reproducing leukocyte transmigration under near-physiological conditions with high-resolution fluorescent microscopy, have enabled the fine-scale analysis of leukocyte locomotion dynamics on the endothelial cells. Experiments using blocking antibodies specific for β1 and β2 integrins, VCAM-1 and ICAM-1, strongly suggest that ICAM-1 plays a predominant role in leukocyte lateral displacement on the endothelium, at least in the cases of T cells [104] and monocytes [23]. Neutrophil locomotion has been also observed in vivo in inflamed venules. Neutrophils from knockout mice of Mac-1 integrin, ligand of ICAM-1 and ICAM-2, adhered extremely well but failed to crawl on the vessel. ICAM-1, but not ICAM-2 blocking, also inhibited in vivo locomotion [105]. On the other hand, the analysis of ICAM-1 and LFA-1 distribution during leukocyte locomotion revealed that the active leukocyte integrin and endothelial ICAM-1 accumulate in the ventral area of migrating T cells. These areas of intense leukocyte–endothelial interaction were termed focal zones [106]. The formation of focal zones seems to be dependent on the association in the leukocyte of integrins with actin through talin [106]. Thus, ICAM-1 not only concentrates in membrane projections that surround leukocytes, but also accumulates beneath them, where leukocytes form integrin-dependent adhesion structures. Additional analysis of leukocyte endothelial interactions with more sophisticated in vitro approaches, including laminar shear stress and the presence of chemokines exposed on the apical surface of endothelial cells, confirmed the existence of these ventral clusters of ICAM-1 [104]. This study also shows a different distribution for VCAM-1, which surrounded preferentially the uropod pole of the adhered leukocyte, instead of accumulating in the ventral focal zone. Scanning electron microscopy also revealed the presence in crawling T cells of small and invasive filopodia that penetrate the endothelial cell. The number and size of these filopodia were increased by the shear flow and were dependent on Cdc42 activity [104]. On the other hand, visualization of ICAM-1-GFP dynamics by TIRF microscopy has shown that protrusions emitted by T cells migrating on the apical endothelial surface can reach the endothelial basal membrane [60]. In all these analyses, endothelial invaginations observed under the lymphocyte occurred during apical locomotion, before and independently of the diapedesis step.

Leukocyte protrusions penetrating endothelial cells have been found to be controlled by the Src kinase and the actin regulatory protein WASP, which has led Carman and colleagues [107, 108] to propose these structures to be similar

to invasive podosomes, the adhesive basal structures found in invading cancer cells. Interestingly, these authors have also found active endothelial SNARE machinery, such as VAMP2 and VAMP3, within the endothelial podoprints that surround these cognate podosomes [107], which indicates that endothelial cells provide trafficking and membrane fusion machinery to the areas where leukocytes extend their podosomes. It is of note that the treatment of endothelial cells with *N*-ethylmaleimide, which prevents SNARE-mediated membrane fusion [109], has a specific effect on the transcellular route of diapedesis, suggesting that proactive endothelial membrane fusion mediated by these endothelial SNARE proteins during the locomotion step is a prerequisite for the subsequent leukocyte transcellular TEM [107]. In accordance, grape-like clusters of vesicles resembling the vesiculo-vacuolar organelle (VVO) were found accumulated close to endothelial podoprints. Taken together, these findings indicate that leukocytes moving on the apical endothelial surface in search of an extravasation route induce ICAM-1-enriched endothelial invaginations that require active endothelial intracellular machinery. These invaginations have the potential to reach endothelial basolateral domains and thereby initiate transcellular diapedesis. Nonetheless, whereas most leukocytes crawling on the endothelium induce this membrane remodeling in the endothelial cell, only around 10 % of them in human vascular endothelial cells and 30 % in microvascular endothelial cells, follow transcellular diapedesis, implying that additional endothelial events may be required to facilitate the opening of a transcellular pore.

Endothelial membrane remodeling during diapedesis

Docking structures and diapedesis routes

The docking structures embracing leukocytes that adhere to the apical endothelial membrane are also observed when leukocytes undergo paracellular and transcellular diapedesis [63]. Although these membrane extensions play a role in leukocyte retention and signaling that is essential for leukocyte diapedesis, to date, no evidence has been found to suggest a function for docking structures in leukocyte guidance towards a specific route of diapedesis. Figure 3 illustrates endothelial membrane remodeling during diapedesis.

The lateral border recycling (LBR) compartment during paracellular diapedesis

Comprehensive reviews of the endothelial signaling induced by leukocyte adhesion that control paracellular diapedesis have recently been published [24, 33, 110, 111].

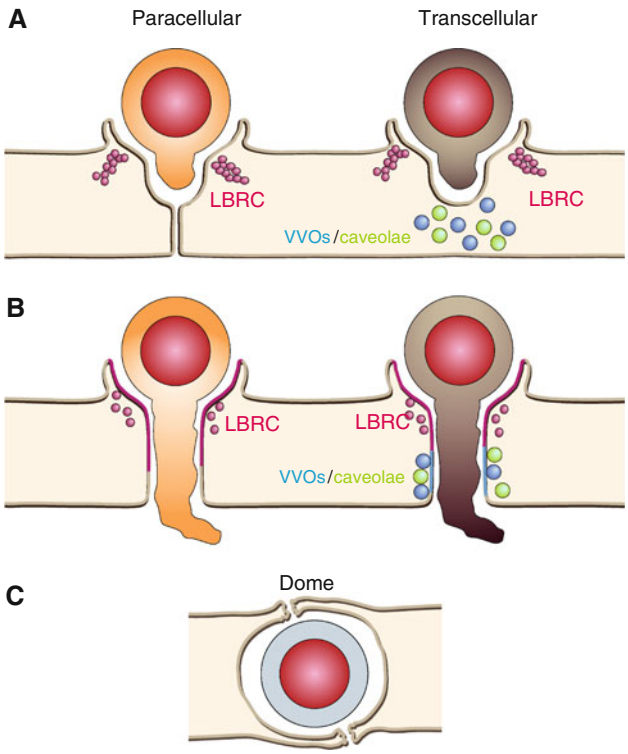

Fig. 3 Endothelial membrane reorganization during diapedesis. Leukocytes probe the endothelial surface emitting pseudopods/podosomes (**a**). Once they find appropriate areas for paracellular or transcellular diapedesis (**b**), effective docking structures derived from microvilli must embrace apically adhered leukocytes and PECAM-1 must be relocated from the LBR compartment to leukocyte-endothelial contact areas. In paracellular diapedesis, actin-mediated cell contraction, and cell–cell junction disruption induce gap opening. In transcellular diapedesis, coordination of events described in Fig. 1 can occasionally lead to the formation of transcellular passages, in which LBR-compartment, VVOs and caveolae can potentially supply intracellular membranes. **c** Endothelial domes that encapsulate transmigrating leukocytes have been observed in vivo

Paracellular diapedesis involves disruption of cell–cell junctions, opening of intercellular gaps and reconstitution of cell–cell contacts. Adhesion receptor engagement elicits Rho- and Rac-dependent signaling pathways that induce cell contraction and junctional destabilization [27, 89, 90, 112]. This engagement also activates Src kinases and generation of reactive oxygen species (ROS) that have a direct effect on phosphorylation of junctional molecules, such as VE-cadherin [27, 28, 113–115]. In addition, endothelial cells selectively express an additional set of receptors that can be partially confined at cell borders and support paracellular diapedesis. CD99, PECAM-1 and the junctional adhesion molecules (JAMs) are the best-characterized receptors mediating diapedesis, although endothelial cell-selective adhesion molecules (ESAMs), nectins and ICAM-2 also mediate leukocyte paracellular TEM [20, 116–119]. Receptors localized at cell borders facilitate TEM by establishing new homotypic or

heterotypic molecular dimers between the leukocyte and the endothelial cell, which replace interactions between two adjacent endothelial cells and thereby induce local disruption of cell–cell junctions.

With the exception of the cuboidal endothelium in high endothelial venules [120, 121], endothelial cells form relatively thin monolayers where junctions distribute in overlapping cell borders, in clear contrast with the paradigmatic straight junctional complexes found in vertical borders of columnar epithelial cells [122, 123]. One of the best characterized junctional receptors involved in diapedesis, PECAM-1, has been found in a novel intracellular compartment situated at overlapping areas of endothelial cell–cell junctions known as the LBR compartment (Fig. 2c) [124]. Electron microscopy and PECAM-1 recycling experiments suggest that this compartment is composed of concatenated vesicles that are connected to the exterior through the junction. Analysis of PECAM-1 trafficking within this compartment during monocyte paracellular diapedesis suggests that PECAM-1 is translocated from LBR vesicles towards the external contact area with the leukocyte [124]. In an attempt to characterize PECAM-1 trafficking in paracellular diapedesis, an essential role has been reported in this trafficking for the kinesin family of motor proteins, which move along the microtubular network [125]. Microtubule depolymerizing drugs or blocking antibodies against kinesins had no apparent effect on the steady-state distribution of junctional PECAM-1, but inhibited PECAM-1 trafficking during leukocyte diapedesis, blocking the passage of leukocytes through the junction. Quantitatively, the effects of these treatments were comparable to that of PECAM-1-blocking antibodies on diapedesis. JAM-A and CD99 have also been observed on the LBR, although their trafficking has yet to be investigated [126].

The protein machinery involved in the formation of LBR vesicles and the molecular clues that keep this compartment associated with cell borders have not been elucidated. Regarding the nature of the LBR compartment, endothelial cells contain unique membrane compartments involved in solute transport, such as fenestrae, caveolae and VVOs, which may potentially contribute to the LBR compartment [55, 127, 128]. Previous electron microscopy studies had suggested that PECAM-1 is concentrated in the VVOs, which are formed by numerous caveolae-like connected vesicles. However, VVOs are not restricted to perijunctional areas and are morphologically different from LBR vesicles [124, 129]. Biochemical and morphological analyses also indicate that the LBR compartment is different from caveolae [124]. The identification of the vesicle machinery and the junctional proteins involved in the genesis and regulation of the LBR compartment, and the molecular mechanisms that mediate kinesin-dependent PECAM-1 trafficking should clarify the importance of this structure in paracellular diapedesis.

The LBR compartment during transcellular diapedesis

Some junctional receptors involved in paracellular diapedesis, such as JAM-A and PECAM-1, are redistributed and localized apically, away from junctions, in response to proinflammatory cytokines such as TNF-α and INF-γ [31, 32, 130]. JAM-family proteins have the ability to establish *cis* and *trans* homophilic and heterophilic interactions between their members. In addition, JAM-A is an alternative cognate receptor for leukocyte β2-integrins that is involved in leukocyte adhesion and TEM [131–133]. JAM-C can also interact with β2-integrins [134–136], whereas JAM-B can bind β1-integrins [137], although these interactions have been less thoroughly explored. In TNF-α-stimulated HUVECs, JAM-A, CD99, and PECAM-1 accumulated within docking structures surrounding leukocytes undergoing transcellular diapedesis, away from cell–cell junctions [126]. Carman and colleagues [107] have also detected a remarkable accumulation of PECAM-1 in microvillus-derived cups embracing adhered memory T cells, although much less in the case of cups adhering monocytes [63]. Importantly, function-blocking antibodies against PECAM-1 and CD99, but not against JAM-A, can significantly diminish paracellular and transcellular diapedesis, indicating that these junctional proteins also play a role away from cell borders [107, 126]. Based on these data, Mamdouh and colleagues have proposed that the LBR compartment might supply adhesion receptors such as JAM-A, CD99 or PECAM-1 to the transcellular pores. It is of note that this unselective inhibition of both routes of diapedesis seems quite similar to the inhibition resulting from the previously enumerated strategies that target the formation of docking structures [63]. Moreover, microtubule-dependent PECAM-1 recycling from the LBR compartment was also detected in membrane extensions resembling docking structures, which surrounded leukocytes undergoing transcellular diapedesis [125, 126]. So far, the potential relationship between the LBR compartment and the docking structures in the transcellular passage has not been addressed, and may be an interesting avenue of investigation in the future.

ICAM-1 and caveolae in transcellular diapedesis

In accordance with the predominant role that ICAM-1 plays in endothelial membrane remodeling upon leukocyte adhesion and locomotion, this receptor seems also to be central for the route of transcellular extravasation in vitro.

Modulation of endothelial ICAM-1 levels has an important effect on the rate of transcellular diapedesis for PMN leukocytes [30]. In endothelial cells, caveolin-1, the scaffolding protein of the caveolae, is enriched in areas where several actin stress fibers converge. Notably, in response to antibody ligation, ICAM-1 is slowly translocated to these areas along actin filaments, where the receptor is transcytosed to the endothelial basal membrane through caveolae [60]. Confocal and time-lapse microscopy reveals that engaged ICAM-1 moves to the cell periphery, whereas caveolin-1- and F-actin domains remain comparatively static (Fig. 2b). TIRF analysis of T cells crawling on the endothelial membrane reveals their capacity to step down caveolin-1 clusters that contact the basal membrane. Three research groups have found that leukocytes preferentially migrate transcellularly in areas enriched in caveolin-1 [60, 62, 63], although this has not been always observed [126]. Comparative analysis of docking structures and caveolin-1 accumulation at the transcellular pore shows that they are differently localized. Caveolae are found in a more basal plane than apical microvillar protrusions [60]. *Caveolin-1* gene silencing specifically impairs the transcellular diapedesis but does not affect total or paracellular diapedesis [60, 138].

Some other caveolar components have been found in the transcellular pore, such as the protein plasmalemmal vesicle-associated protein (PV-1) [62, 139]. PV-1 is localized in stomatal diaphragms of endothelial caveolae and fenestrae [139, 140], where it is essential for the formation of these diaphragms [141]. Although the role of these structures is not well understood, stomata are thought to participate in the transcellular exchange of liquids and macromolecules [142]. PV-1-blocking antibody reduced leukocyte transmigration in vivo and in vitro, whereas adhesion was not affected. Under experimental settings that favor paracellular over transcellular TEM, anti-PV-1 antibodies had little effect on either adhesion or transmigration, suggesting that PV-1 preferentially regulates transcellular diapedesis [62]. However, further analysis of the relative contribution of PV-1 to diapedesis in cells that can follow both the transcellular and paracellular transmigration routes would definitively elucidate the true role of this protein in leukocyte egress from vessels.

Part of the machinery involved in endothelial membrane remodeling caused by apical leukocyte locomotion, such as VAMP3 [107], has been found to form transcytotic complexes with caveolin-1 in endothelial cells [143]. Stimuli like EGF can induce caveolin-1 relocalization to VAMP3-positive internal compartments, implying that the association of caveolin-1 with the SNARE machinery can be transient and regulated by extracellular stimuli [144]. Furthermore, in a series of in vitro experiments, Predescu and colleagues [145] have elegantly demonstrated the involvement of t-SNARE machinery in caveolar fusion events at the endothelial plasma membrane. On the other hand, electron microscopy of endothelial membranes in contact with pseudopods emitted by leukocytes during locomotion has revealed the accumulation of arrays of vesicles that resemble the VVO [107]. There is an unclear relationship between VVOs and caveolae. The two vesicular compartments are morphologically very similar, although VVOs form grape-like clusters of up to several hundred interconnected vesicles of heterogeneous diameter, whereas caveolar clusters are formed by the linking of a few vesicles that are more homogenous in size. Analysis of caveolin-1 distribution shows that 30–50 % of VVOs contain this signature protein of caveolae. VVO fusion events, like caveolae, are sensitive to *N*-ethylmaleimide (NEM) [146]. Additionally, the SNARE protein VAMP-2 has been found in VVOs and caveolae [146, 147]. However, electron microscopy studies of endothelium from caveolin-1 knockout mice revealed a comparable number of VVOs, whereas caveolar-like vesicles in contact with the apical or basolateral plasma membrane were significantly reduced in number. This indicates that caveolin-1 is not required for maintaining the morphological integrity of VVOs, but that the two compartments share molecular features. In summary, although caveolin-1 does not seem involved in the translocation of vesicle machinery found surrounding the leukocyte podosomes [107] there exists an evident molecular link between this machinery and caveolae.

Collectively, these data suggest a mechanism by which leukocytes may initiate transcellular migration. Leukocytes continuously induce transient ICAM-1 clustering, searching for sites where they can transmigrate by pushing down pseudopods or podosomes that constantly probe the endothelial surface. Leukocyte-induced endothelial invaginations recruit machinery with the potential to induce fusion of caveolae, VVOs, or both. When ICAM-1 is invaginated in areas with a high density of these intracellular compartments and F-actin, then the receptor induces vesicle fusion, resulting in the formation of a transcellular pore (Fig. 3).

Taken together, these results also indicate that the machinery involved in transcytosis of small molecules may contribute to the transcellular route of leukocyte transmigration, mediated mostly by the ICAM-1 receptor. Interestingly, Hu and colleagues have formally demonstrated that leukocyte transmigration regulates transcytosis in vitro and in vivo. PMN leukocyte adhesion through ICAM-1 or antibody-mediated ICAM-1 crosslinking induced caveolin-1-dependent albumin endocytosis and

Src-mediated caveolin-1 phosphorylation in endothelial cells, which is suggestive of caveolin internalization [148].

Role of endothelial actin and vimentin networks in diapedesis

Actin stress fibers are associated with focal adhesion or cell–cell junctions in confluent endothelial cells [149]. As mentioned above, ICAM-1 and VCAM-1 clustering promotes receptor alignment with stress fibers. In addition, this clustering induces RhoA activation and stress fibers formation, which suggest that these receptors facilitate paracellular diapedesis by promoting cell contraction [27, 89]. On the other hand most transcellular pores opened by transmigrating T-cells appear in contact with stress fibers [60]. The role of these actin filaments in the formation of these passages is currently unclear. They may help to determine the cellular region that is most robust for the opening of the transcellular gap or, complementarily, they could contribute to establish a physical barrier that controls the size of the pore and preserves cell integrity. Stress fibers determine caveolae accumulation in the endothelial cell [60]. Caveolae are linked to F-actin through a direct interaction of caveolin-1 with filamin proteins [150]. Filamins coalign with caveolin-1 and stress fibers in response to activation of Rho GTPases [150]. In addition, filamin-A regulates caveolin-1 localization and dynamics [150–152]. Filamin-A, -B and caveolin-1 proteins have been found in ICAM-1 immunoprecipitates from endothelial cells [153]. The expression of filamin-B determines ICAM-1 lateral mobility, recruitment of ICAM-1 to endothelial docking structures upon leukocyte adhesion as well as leukocyte adhesion and transmigration [61, 153]. However, the particular contribution of filamins to different routes of leukocyte TEM has not yet been investigated. Cortactin, a multidomain scaffold protein involved in cortical actin assembly, also regulates ICAM-1 clustering around adhered PMN leukocytes as well as their transmigration, but had not effect on PMN cell adhesion [154, 155]. In vivo, cortactin-deficient mice display a reduced rate of neutrophil extravasation, despite vascular permeability is enhanced. This extravasation defect seems general and affects neutrophil rolling, adhesion and diapedesis [156]. These authors also observed in vitro that cortactin knockdown abrogated the formation of docking structures upon PMN leukocyte adhesion and, importantly, inhibited ICAM-1-mediated activation of RhoG. Therefore, cortactin regulates signaling pathways that are induced in response to leukocyte adhesion and are required for efficient diapedesis. Whereas filamins induce long-term stabilization of actin filaments, cortactin probably contributes to a rapid and more transient F-actin rearrangement at sites of leukocyte adhesion and transmigration through the stabilization of the Arp2/3 complex [157–159].

Finally, a complementary role has been recently proposed for actin stress fibers. Intracellular stores of chemokines that translocate to the cell surface upon leukocyte interaction have been found associated with stress fibers. Chemokines on the apical endothelial surface signal into adhered leukocytes and induce an inside-out, local activation of leukocyte integrins, thereby orientating leukocyte motility. This opens up the interesting possibility of stress fibers functioning as a railways that provide cues for leukocytes to find areas of extravasation [160].

Endothelial cells are enriched in intermediate filaments of vimentin [161, 162]. Endothelial vimentin networks mediate leukocyte transcellular TEM, probably through their association with caveolar PV-1 [163]. It is of note that vimentin is highly enriched in endothelial caveolae [164]. The relationship between endothelial F-actin, vimentin and caveolin has not been adequately addressed. However, given that the formation of a transcellular pore is likely to involve considerable mechanical stress, it is quite plausible that coordination between the different cytoskeletal scaffolds may be required.

In vivo observation of endothelial membrane reorganization and diapedesis

Technical improvement of in vivo microscopy, in combination with electron microscopy, is enabling the analysis of leukocyte-endothelial cell contact areas in animal models with a remarkable resolution. Adhesion receptor clustering or endothelial membrane remodeling in response to leukocyte interaction have been already detected in mice [165, 166]. The ratio between paracellular and transcellular diapedesis has been quantitated in venules from inflamed cremaster muscle and is similar to that found in vitro in HUVECs, but lower that in microvascular endothelial cells [60, 107, 165]. Accumulation of PECAM-1 around transcellular pores, compared to that detected in paracellular gaps opened by extravasating leukocytes, is, however, reduced in these microvessels [165]. Knock-in mice expressing VE-cadherin fused with α-catenin have highly stabilized endothelial adherens junctions and reduced capillary permeability. These mice showed a remarkable inhibition of total neutrophil extravasation and an impairment of paracellular but not transcellular diapedesis [167]. This confirms that most of leukocyte transmigration also occurs paracellularly in in vivo mouse models. The fact that levels of caveolin-1 expression in mouse venules do not correlate with increased neutrophil transmigration also supports the predominance of the paracellular transmigratory route [138].

Most of the high-resolution microscopy analysis of leukocyte transmigration has been performed in the cremaster muscle, but the molecular mechanisms regulating leukocyte diapedesis may differ depending on the endothelial bed and the inflammatory challenge. For instance, leukocyte homing to lymph nodes is not affected in the VE-cadherin-α-catenin chimeric mouse model [167], which suggests that adherens junction integrity may not be so relevant during leukocyte diapedesis through high endothelial venules. In a pioneering work on in vivo leukocyte diapedesis, Feng and colleagues [99] showed that rabbit neutrophils can emigrate from venules by a transcellular pathway in response to *N*-formyl-methionyl-leucyl-phenylalanine (FMLP). The endothelium of the blood–brain barrier (BBB) presents tight cell–cell junctions and low paracellular permeability [168]. In a model of experimental autoimmune encephalomyelitis, detailed electron microscopy studies suggest that mononuclear leukocytes have the ability to traverse post capillary venules of the BBB, leaving endothelial junctions intact [169]. This suggests that in vivo transcellular TEM may occur at higher rate in the BBB. The mechanisms mediating leukocyte diapedesis and endothelial membrane remodeling in these in vivo models have not been properly addressed yet. In general, detailed studies on the reorganization of endothelial adhesion receptors and the relevance of tetraspanin domains, rafts, LBR compartment dynamics, apical docking structures or endothelial membrane invaginations upon leukocyte interaction are still not available in in vivo systems.

Different endothelial membrane structures that almost completely encapsulate transmigrating leukocytes have been observed in vivo and termed "domes" [166, 170]. Domes are formed by basolateral and apical endothelial domains and may constitute the final outcome of all the different processes of membrane reorganization that are individually observed in vitro. Although little is known about the molecular players that are important for these structures, leukocyte-specific protein 1 (LSP1), an F-actin-binding protein recently shown to be expressed in the endothelium, seems essential for effective neutrophil transmigration and dome formation, supporting again the idea of a central role for subcortical actin in endothelial surface reorganization [170].

Concluding remarks

Leukocytes induce the simultaneous engagement of a plethora of endothelial receptors that orchestrate intracellular signaling pathways in order to facilitate diapedesis. The molecular complexity of diapedesis, revealed in recent years, is probably a consequence of the central and multitasking role of the endothelium in preserving the integrity of small vessels. Control of mechanical stress, plasma leakage and leukocyte transmigration all happen simultaneously in the initial inflammatory response and must be regulated by the endothelium. One important feature in this response is membrane dynamics, which has been summarized in this review that has been focused on the endothelial side. In the future, the major challenge for a deeper understanding of endothelial membrane remodeling upon leukocyte interaction will be the integration between the information on nanoscale membrane reorganization, such as the coalescence of tetraspanin-adhesion receptor domains, with that on microscale events, in which the submembrane cytoskeleton plays a complementary and scaffolding function. In this regard, both tetraspanin webs and lipid rafts have been shown to be involved in the dynamics of microvilli or in vesicle trafficking in other cellular processes [171–173], so they may well participate in the formation of docking structures or endothelial invaginations in response to leukocyte locomotion and diapedesis. It can also be noticed that the studies reviewed here have mainly been performed using sophisticated in vitro experimental techniques, whereas in vivo analyses of these endothelial responses are still rare. Thus, the in vivo validation of these in vitro results is clearly another main challenge in this exciting field. It is to be hoped that further insight into these aspects of endothelial cell–leukocyte interactions will help us to gain control of dysfunctional leukocyte extravasation in the origin of several inflammatory pathologies.

Acknowledgments We would like to thank M.A. Alonso, E. Cernuda-Morollón and S. Gharbi for critical reading of the manuscript. We also appreciate the help of F. Belio with the design of the figures. Dr. J. Millán is supported by grants SAF2008-01936, SAF2011-22624 from Ministerio de Ciencia e Innovación, Spain, and received research support from Biogen-Idec. B. Marcos-Ramiro is supported by an FPI fellowship from Ministerio de Ciencia e Innovación. N. Reglero-Real is supported by a JAE fellowship from CSIC.

KEY POINTS
Tetraspanin platforms: Supramolecular membrane protein complexes formed by tetraspanins and other surface proteins, such as receptors from the immunoglobulin (Ig) superfamily or integrins. These complexes are based on protein–protein interactions. Tetraspanin form pre assembled platforms with ICAM-1 and VCAM-1 in endothelial cells.
Membrane rafts: Supramolecular membrane protein complexes based on lipid–protein and lipid–lipid interactions. Rafts are liquid ordered membrane domains, enriched in sphingolipids and cholesterol, which confine proteins based on hydrophobic compatibility. Membrane rafts participate in membrane trafficking or in coalescence of signaling proteins. In endothelial cells, E-selectin, ICAM-1, and VCAM-1 are partially segregated into membrane rafts upon engagement.
Microvilli: Small apical membrane projections with a subcortical F-actin scaffold that concentrates surface proteins. Endothelial microvilli accumulate adhesion receptors, such as ICAM-1 and VCAM-1, to facilitate leukocyte adhesion and transmigration.
Docking structures: Microvillus-derived membrane structures in endothelial cells that embrace adhered leukocytes. Enriched in ICAM-1, VCAM-1, and in proteins that connect these receptors to F-actin, such as ezrin, radixin, moesin.
Focal zones: Areas of intense interaction between endothelial ICAM-1 and β2-integrins in the ventral area of the leukocyte when is firmly adhered to the endothelium.
Podosomes: Plasma membrane adhesive complexes that contain integrins, adaptors, and concentrate actin polymerization. Podosomes share components with focal adhesions but are more dynamic. During crawling on the endothelium, prior to transmigration, leukocyte can form podosome-like domains, rich in β2-integrins, which induce invaginations into endothelial cell. Such invaginations contain the cognate ICAM-1 and fusogenic machinery and have been termed podoprints.
Vesiculo-vacuolar organelle (VVO): Grape-like clusters of vesicles, of uncertain nature, which are abundant in endothelial cells. VVOs contain SNARE machinery, have been found close to endothelial podoprints and thus, may contribute to the membrane fusion events necessary to trigger the formation of a transcellular pore during diapedesis.
Lateral border recycling (LBR) compartment: Novel intracellular membrane compartment associated with endothelial cell borders that concentrates PECAM-1. PECAM-1 translocation to the endothelial surface is required for an efficient paracellular and transcellular diapedesis. PECAM-1 dynamics depends on microtubule-associated motor proteins called kinesins.
Caveolae: Vesicular compartment, abundant in endothelial cells, which contains the scaffolding protein caveolin-1 and is involved in trafficking and signaling. Upon clustering, ICAM-1 is partially transcytosed to the basal endothelial membrane through caveolae. Caveolin-1 reduction decreases transcellular diapedesis in vitro. Some leukocytes follow transcellular diapedesis through areas enriched in caveolin-1 and PV-1, another caveolar component.
Chemokine depots: Endothelial intracellular vesicle stores of chemokines that are associated with actin stress fibers and are required for leukocyte integrin activation and leukocyte transmigration.
Endothelial domes: Endothelial membrane extensions that encapsulate adherent neutrophils in vivo and are proposed to contribute to control vascular permeability in paracellular and transcellular diapedesis. Leukocyte-specific protein 1 (LSP1), an F-actin-binding protein, is required for dome formation and neutrophil transmigration.

References

1. Pober JS, Sessa WC (2007) Evolving functions of endothelial cells in inflammation. Nat Rev Immunol 7(10):803–815
2. Davignon J, Ganz P (2004) Role of endothelial dysfunction in atherosclerosis. Circulation 109(23 Suppl 1):III27–III32
3. Butcher EC (1991) Leukocyte-endothelial cell recognition: three (or more) steps to specificity and diversity. Cell 67(6):1033–1036
4. Libby P (2002) Inflammation in atherosclerosis. Nature 420(6917):868–874
5. McMurray RW (1996) Adhesion molecules in autoimmune disease. Semin Arthritis Rheum 25(4):215–233
6. Compston A, Coles A (2008) Multiple sclerosis. Lancet 372(9648):1502–1517
7. Nourshargh S, Hordijk PL, Sixt M (2010) Breaching multiple barriers: leukocyte motility through venular walls and the interstitium. Nat Rev Mol Cell Biol 11(5):366–378. doi:10.1038/nrm2889
8. Mayadas TN, Johnson RC, Rayburn H, Hynes RO, Wagner DD (1993) Leukocyte rolling and extravasation are severely compromised in P selectin-deficient mice. Cell 74(3):541–554
9. Frenette PS, Mayadas TN, Rayburn H, Hynes RO, Wagner DD (1996) Susceptibility to infection and altered hematopoiesis in mice deficient in both P- and E-selectins. Cell 84(4):563–574
10. Labow MA, Norton CR, Rumberger JM, Lombard-Gillooly KM, Shuster DJ, Hubbard J, Bertko R, Knaack PA, Terry RW, Harbison ML et al (1994) Characterization of E-selectin-deficient mice: demonstration of overlapping function of the endothelial selectins. Immunity 1(8):709–720
11. Oppenheimer-Marks N, Davis LS, Bogue DT, Ramberg J, Lipsky PE (1991) Differential utilization of ICAM-1 and VCAM-1 during the adhesion and transendothelial migration of human T lymphocytes. J Immunol 147(9):2913–2921
12. Jones DA, McIntire LV, Smith CW, Picker LJ (1994) A two-step adhesion cascade for T cell/endothelial cell interactions under flow conditions. J Clin Invest 94(6):2443–2450
13. Bowden RA, Ding ZM, Donnachie EM, Petersen TK, Michael LH, Ballantyne CM, Burns AR (2002) Role of alpha4 integrin and VCAM-1 in CD18-independent neutrophil migration across mouse cardiac endothelium. Circ Res 90(5):562–569
14. Bochner BS, Luscinskas FW, Gimbrone MA Jr, Newman W, Sterbinsky SA, Derse-Anthony CP, Klunk D, Schleimer RP (1991) Adhesion of human basophils, eosinophils, and neutrophils to interleukin 1-activated human vascular endothelial cells: contributions of endothelial cell adhesion molecules. J Exp Med 173(6):1553–1557
15. Nandi A, Estess P, Siegelman M (2004) Bimolecular complex between rolling and firm adhesion receptors required for cell arrest; CD44 association with VLA-4 in T cell extravasation. Immunity 20(4):455–465
16. Zarbock A, Ley K (2009) New insights into leukocyte recruitment by intravital microscopy. Curr Top Microbiol Immunol 334:129–152. doi:10.1007/978-3-540-93864-4_6
17. Ley K, Laudanna C, Cybulsky MI, Nourshargh S (2007) Getting to the site of inflammation: the leukocyte adhesion cascade updated. Nat Rev Immunol 7(9):678–689. doi:10.1038/nri2156
18. Millan J, Ridley AJ (2005) Rho GTPases and leucocyte-induced endothelial remodelling. Biochem J 385(Pt 2):329–337
19. Muller WA (2003) Leukocyte-endothelial-cell interactions in leukocyte transmigration and the inflammatory response. Trends Immunol 24(6):327–334
20. Weber C, Fraemohs L, Dejana E (2007) The role of junctional adhesion molecules in vascular inflammation. Nat Rev Immunol 7(6):467–477
21. Zarbock A, Ley K, McEver RP, Hidalgo A (2011) Leukocyte ligands for endothelial selectins: specialized glycoconjugates that mediate rolling and signaling under flow. Blood 118(26):6743–6751. doi:10.1182/blood-2011-07-343566
22. Barreiro O, de la Fuente H, Mittelbrunn M, Sanchez-Madrid F (2007) Functional insights on the polarized redistribution of leukocyte integrins and their ligands during leukocyte migration and immune interactions. Immunol Rev 218:147–164
23. Schenkel AR, Mamdouh Z, Muller WA (2004) Locomotion of monocytes on endothelium is a critical step during extravasation. Nat Immunol 5(4):393–400
24. Wittchen ES (2009) Endothelial signaling in paracellular and transcellular leukocyte transmigration. Front Biosci 14:2522–2545
25. Vestweber D, Broermann A, Schulte D (2010) Control of endothelial barrier function by regulating vascular endothelial-cadherin. Curr Opin Hematol 17(3):230–236. doi:10.1097/MOH.0b013e328338664b
26. Vestweber D (2007) Adhesion and signaling molecules controlling the transmigration of leukocytes through endothelium. Immunol Rev 218:178–196. doi:10.1111/j.1600-065X.2007.00533.x
27. van Wetering S, van den Berk N, van Buul JD, Mul FP, Lommerse I, Mous R, ten Klooster JP, Zwaginga JJ, Hordijk PL (2003) VCAM-1-mediated Rac signaling controls endothelial cell–cell contacts and leukocyte transmigration. Am J Physiol Cell Physiol 285(2):C343–C352
28. Allingham MJ, van Buul JD, Burridge K (2007) ICAM-1-mediated, Src- and Pyk2-dependent vascular endothelial cadherin tyrosine phosphorylation is required for leukocyte transendothelial migration. J Immunol 179(6):4053–4064
29. Turowski P, Martinelli R, Crawford R, Wateridge D, Papageorgiou AP, Lampugnani MG, Gamp AC, Vestweber D, Adamson P, Dejana E, Greenwood J (2008) Phosphorylation of vascular endothelial cadherin controls lymphocyte emigration. J Cell Sci 121(Pt 1):29–37
30. Yang L, Froio RM, Sciuto TE, Dvorak AM, Alon R, Luscinskas FW (2005) ICAM-1 regulates neutrophil adhesion and transcellular migration of TNF-{alpha} activated vascular endothelium under flow. Blood 106(2):584–592
31. Romer LH, McLean NV, Yan HC, Daise M, Sun J, DeLisser HM (1995) IFN-gamma and TNF-alpha induce redistribution of PECAM-1 (CD31) on human endothelial cells. J Immunol 154(12):6582–6592
32. Martinez-Estrada OM, Manzi L, Tonetti P, Dejana E, Bazzoni G (2005) Opposite effects of tumor necrosis factor and soluble fibronectin on junctional adhesion molecule-A in endothelial cells. Am J Physiol Lung Cell Mol Physiol 288(6):L1081–L1088
33. Fernandez-Borja M, van Buul JD, Hordijk PL (2010) The regulation of leucocyte transendothelial migration by endothelial signalling events. Cardiovasc Res 86(2):202–210. doi:10.1093/cvr/cvq003
34. Shulman Z, Alon R (2012) Real-time analysis of integrin-dependent transendothelial migration and integrin-independent interstitial motility of leukocytes. Methods Mol Biol 757:31–45. doi:10.1007/978-1-61779-166-6_3
35. Lyck R, Reiss Y, Gerwin N, Greenwood J, Adamson P, Engelhardt B (2003) T-cell interaction with ICAM-1/ICAM-2 double-deficient brain endothelium in vitro: the cytoplasmic tail of endothelial ICAM-1 is necessary for transendothelial migration of T cells. Blood 102(10):3675–3683
36. Greenwood J, Amos CL, Walters CE, Couraud PO, Lyck R, Engelhardt B, Adamson P (2003) Intracellular domain of brain endothelial intercellular adhesion molecule-1 is essential for T lymphocyte-mediated signaling and migration. J Immunol 171(4):2099–2108
37. Schenkel AR, Mamdouh Z, Chen X, Liebman RM, Muller WA (2002) CD99 plays a major role in the migration of monocytes through endothelial junctions. Nat Immunol 3(2):143–150

38. Rahman A, Fazal F (2009) Hug tightly and say goodbye: role of endothelial ICAM-1 in leukocyte transmigration. Antioxid Redox Signal 11(4):823–839. doi:10.1089/ARS.2008.2204
39. Wang J, Springer TA (1998) Structural specializations of immunoglobulin superfamily members for adhesion to integrins and viruses. Immunol Rev 163:197–215
40. van Buul JD, van Rijssel J, van Alphen FP, van Stalborch AM, Mul EP, Hordijk PL (2010) ICAM-1 clustering on endothelial cells recruits VCAM-1. J Biomed Biotechnol 2010:120328. doi:10.1155/2010/120328
41. Barreiro O, Zamai M, Yanez-Mo M, Tejera E, Lopez-Romero P, Monk PN, Gratton E, Caiolfa VR, Sanchez-Madrid F (2008) Endothelial adhesion receptors are recruited to adherent leukocytes by inclusion in preformed tetraspanin nanoplatforms. J Cell Biol 183(3):527–542
42. Edwards S, Lalor PF, Nash GB, Rainger GE, Adams DH (2005) Lymphocyte traffic through sinusoidal endothelial cells is regulated by hepatocytes. Hepatology 41(3):451–459. doi:10.1002/hep.20585
43. Charrin S, le Naour F, Silvie O, Milhiet PE, Boucheix C, Rubinstein E (2009) Lateral organization of membrane proteins: tetraspanins spin their web. Biochem J 420(2):133–154. doi:10.1042/BJ20082422
44. Stipp CS, Kolesnikova TV, Hemler ME (2003) Functional domains in tetraspanin proteins. Trends Biochem Sci 28(2):106–112
45. Kitadokoro K, Bordo D, Galli G, Petracca R, Falugi F, Abrignani S, Grandi G, Bolognesi M (2001) CD81 extracellular domain 3D structure: insight into the tetraspanin superfamily structural motifs. EMBO J 20(1–2):12–18. doi:10.1093/emboj/20.1.12
46. Yang X, Claas C, Kraeft SK, Chen LB, Wang Z, Kreidberg JA, Hemler ME (2002) Palmitoylation of tetraspanin proteins: modulation of CD151 lateral interactions, subcellular distribution, and integrin-dependent cell morphology. Mol Biol Cell 13(3):767–781. doi:10.1091/mbc.01-05-0275
47. Espenel C, Margeat E, Dosset P, Arduise C, Le Grimellec C, Royer CA, Boucheix C, Rubinstein E, Milhiet PE (2008) Single-molecule analysis of CD9 dynamics and partitioning reveals multiple modes of interaction in the tetraspanin web. J Cell Biol 182(4):765–776. doi:10.1083/jcb.200803010
48. Yanez-Mo M, Barreiro O, Gordon-Alonso M, Sala-Valdes M, Sanchez-Madrid F (2009) Tetraspanin-enriched microdomains: a functional unit in cell plasma membranes. Trends Cell Biol 19(9):434–446. doi:10.1016/j.tcb.2009.06.004
49. Simons K, Gerl MJ (2010) Revitalizing membrane rafts: new tools and insights. Nat Rev Mol Cell Biol 11(10):688–699
50. Brown DA, Rose JK (1992) Sorting of GPI-anchored proteins to glycolipid-enriched membrane subdomains during transport to the apical cell surface. Cell 68(3):533–544
51. Munro S (2003) Lipid rafts: elusive or illusive? Cell 115(4):377–388
52. Tilghman RW, Hoover RL (2002) E-selectin and ICAM-1 are incorporated into detergent-insoluble membrane domains following clustering in endothelial cells. FEBS Lett 525(1–3):83–87
53. Kiely JM, Hu Y, Garcia-Cardena G, Gimbrone MA Jr (2003) Lipid raft localization of cell surface E-selectin is required for ligation-induced activation of phospholipase C gamma. J Immunol 171(6):3216–3224
54. Lajoie P, Goetz JG, Dennis JW, Nabi IR (2009) Lattices, rafts, and scaffolds: domain regulation of receptor signaling at the plasma membrane. J Cell Biol 185(3):381–385
55. Parton RG (2003) Caveolae—from ultrastructure to molecular mechanisms. Nat Rev Mol Cell Biol 4(2):162–167
56. Chidlow JH Jr, Sessa WC (2010) Caveolae, caveolins, and cavins: complex control of cellular signalling and inflammation. Cardiovasc Res 86(2):219–225
57. Lajoie P, Nabi IR (2010) Lipid rafts, caveolae, and their endocytosis. Int Rev Cell Mol Biol 282:135–163. doi:10.1016/S1937-6448(10)82003-9
58. Li XA, Everson WV, Smart EJ (2005) Caveolae, lipid rafts, and vascular disease. Trends Cardiovasc Med 15(3):92–96
59. Setiadi H, McEver RP (2008) Clustering endothelial E-selectin in clathrin-coated pits and lipid rafts enhances leukocyte adhesion under flow. Blood 111(4):1989–1998. doi:10.1182/blood-2007-09-113423
60. Millan J, Hewlett L, Glyn M, Toomre D, Clark P, Ridley AJ (2006) Lymphocyte transcellular migration occurs through recruitment of endothelial ICAM-1 to caveola- and F-actin-rich domains. Nat Cell Biol 8(2):113–123
61. van Buul JD, van Rijssel J, van Alphen FP, Hoogenboezem M, Tol S, Hoeben KA, van Marle J, Mul EP, Hordijk PL (2010) Inside-out regulation of ICAM-1 dynamics in TNF-alpha-activated endothelium. PLoS One 5(6):e11336. doi:10.1371/journal.pone.0011336
62. Keuschnigg J, Henttinen T, Auvinen K, Karikoski M, Salmi M, Jalkanen S (2009) The prototype endothelial marker PAL-E is a leukocyte trafficking molecule. Blood 114(2):478–484
63. Carman CV, Springer TA (2004) A transmigratory cup in leukocyte diapedesis both through individual vascular endothelial cells and between them. J Cell Biol 167(2):377–388
64. Rodriguez-Fraticelli AE, Vergarajauregui S, Eastburn DJ, Datta A, Alonso MA, Mostov K, Martin-Belmonte F (2010) The Cdc42 GEF Intersectin 2 controls mitotic spindle orientation to form the lumen during epithelial morphogenesis. J Cell Biol 189(4):725–738. doi:10.1083/jcb.201002047
65. Xu C, Zhang YH, Thangavel M, Richardson MM, Liu L, Zhou B, Zheng Y, Ostrom RS, Zhang XA (2009) CD82 endocytosis and cholesterol-dependent reorganization of tetraspanin webs and lipid rafts. FASEB J 23(10):3273–3288. doi:10.1096/fj.08-123414
66. Barreiro O, Yanez-Mo M, Serrador JM, Montoya MC, Vicente-Manzanares M, Tejedor R, Furthmayr H, Sanchez-Madrid F (2002) Dynamic interaction of VCAM-1 and ICAM-1 with moesin and ezrin in a novel endothelial docking structure for adherent leukocytes. J Cell Biol 157(7):1233–1245
67. Hogue IB, Grover JR, Soheilian F, Nagashima K, Ono A (2011) Gag induces the coalescence of clustered lipid rafts and tetraspanin-enriched microdomains at HIV-1 assembly sites on the plasma membrane. J Virol 85(19):9749–9766. doi:10.1128/JVI.00743-11
68. Silvie O, Charrin S, Billard M, Franetich JF, Clark KL, van Gemert GJ, Sauerwein RW, Dautry F, Boucheix C, Mazier D, Rubinstein E (2006) Cholesterol contributes to the organization of tetraspanin-enriched microdomains and to CD81-dependent infection by malaria sporozoites. J Cell Sci 119(Pt 10):1992–2002. doi:10.1242/jcs.02911
69. Zilber MT, Setterblad N, Vasselon T, Doliger C, Charron D, Mooney N, Gelin C (2005) MHC class II/CD38/CD9: a lipid-raft-dependent signaling complex in human monocytes. Blood 106(9):3074–3081. doi:10.1182/blood-2004-10-4094
70. Cherukuri A, Shoham T, Sohn HW, Levy S, Brooks S, Carter R, Pierce SK (2004) The tetraspanin CD81 is necessary for partitioning of coligated CD19/CD21-B cell antigen receptor complexes into signaling-active lipid rafts. J Immunol 172(1):370–380
71. Lange K (2011) Fundamental role of microvilli in the main functions of differentiated cells: outline of an universal regulating and signaling system at the cell periphery. J Cell Physiol 226(4):896–927. doi:10.1002/jcp.22302
72. Diakowski W, Grzybek M, Sikorski AF (2006) Protein 4.1, a component of the erythrocyte membrane skeleton and its related homologue proteins forming the protein 4.1/FERM superfamily. Folia Histochem Cytobiol 44(4):231–248

73. Heiska L, Alfthan K, Gronholm M, Vilja P, Vaheri A, Carpen O (1998) Association of ezrin with intercellular adhesion molecule-1 and -2 (ICAM-1 and ICAM-2). Regulation by phosphatidylinositol 4, 5-bisphosphate. J Biol Chem 273(34): 21893–21900
74. Oh HM, Lee S, Na BR, Wee H, Kim SH, Choi SC, Lee KM, Jun CD (2007) RKIKK motif in the intracellular domain is critical for spatial and dynamic organization of ICAM-1: functional implication for the leukocyte adhesion and transmigration. Mol Biol Cell 18(6):2322–2335
75. Ivetic A, Ridley AJ (2004) Ezrin/radixin/moesin proteins and Rho GTPase signalling in leucocytes. Immunology 112(2): 165–176
76. Fehon RG, McClatchey AI, Bretscher A (2010) Organizing the cell cortex: the role of ERM proteins. Nat Rev Mol Cell Biol 11(4):276–287
77. Saotome I, Curto M, McClatchey AI (2004) Ezrin is essential for epithelial organization and villus morphogenesis in the developing intestine. Dev Cell 6(6):855–864. doi:10.1016/j.devcel.2004.05.007
78. Yonemura S, Tsukita S, Tsukita S (1999) Direct involvement of ezrin/radixin/moesin (ERM)-binding membrane proteins in the organization of microvilli in collaboration with activated ERM proteins. J Cell Biol 145(7):1497–1509
79. Wojciak-Stothard B, Williams L, Ridley AJ (1999) Monocyte adhesion and spreading on human endothelial cells is dependent on Rho-regulated receptor clustering. J Cell Biol 145(6): 1293–1307
80. Carman CV, Jun CD, Salas A, Springer TA (2003) Endothelial cells proactively form microvilli-like membrane projections upon intercellular adhesion molecule 1 engagement of leukocyte LFA-1. J Immunol 171(11):6135–6144
81. van Buul JD, Allingham MJ, Samson T, Meller J, Boulter E, Garcia-Mata R, Burridge K (2007) RhoG regulates endothelial apical cup assembly downstream from ICAM1 engagement and is involved in leukocyte trans-endothelial migration. J Cell Biol 178(7):1279–1293
82. Clancy RM, Abramson SB (2000) Acetylcholine prevents intercellular adhesion molecule 1 (CD54)-induced focal adhesion complex assembly in endothelial cells via a nitric oxide-cGMP-dependent pathway. Arthritis Rheum 43(10):2260–2264
83. Booth JW, Trimble WS, Grinstein S (2001) Membrane dynamics in phagocytosis. Semin Immunol 13(6):357–364
84. Heasman SJ, Ridley AJ (2008) Mammalian Rho GTPases: new insights into their functions from in vivo studies. Nat Rev Mol Cell Biol 9(9):690–701
85. Ridley AJ (2006) Rho GTPases and actin dynamics in membrane protrusions and vesicle trafficking. Trends Cell Biol 16(10):522–529. doi:10.1016/j.tcb.2006.08.006
86. Martin-Belmonte F, Mostov K (2008) Regulation of cell polarity during epithelial morphogenesis. Curr Opin Cell Biol 20(2): 227–234. doi:10.1016/j.ceb.2008.01.001
87. Martin-Belmonte F, Gassama A, Datta A, Yu W, Rescher U, Gerke V, Mostov K (2007) PTEN-mediated apical segregation of phosphoinositides controls epithelial morphogenesis through Cdc42. Cell 128(2):383–397. doi:10.1016/j.cell.2006.11.051
88. Saito H, Minamiya Y, Saito S, Ogawa J (2002) Endothelial Rho and Rho kinase regulate neutrophil migration via endothelial myosin light chain phosphorylation. J Leukoc Biol 72(4):829–836
89. Thompson PW, Randi AM, Ridley AJ (2002) Intercellular adhesion molecule (ICAM)-1, but not ICAM-2, activates RhoA and stimulates c-fos and rhoA transcription in endothelial cells. J Immunol 169(2):1007–1013
90. Etienne S, Adamson P, Greenwood J, Strosberg AD, Cazaubon S, Couraud PO (1998) ICAM-1 signaling pathways associated with Rho activation in microvascular brain endothelial cells. J Immunol 161(10):5755–5761
91. deBakker CD, Haney LB, Kinchen JM, Grimsley C, Lu M, Klingele D, Hsu PK, Chou BK, Cheng LC, Blangy A, Sondek J, Hengartner MO, Wu YC, Ravichandran KS (2004) Phagocytosis of apoptotic cells is regulated by a UNC-73/TRIO-MIG-2/RhoG signaling module and armadillo repeats of CED-12/ELMO. Curr Biol 14(24):2208–2216. doi:10.1016/j.cub.2004.12.029
92. Cain RJ, Vanhaesebroeck B, Ridley AJ (2010) The PI3K p110alpha isoform regulates endothelial adherens junctions via Pyk2 and Rac1. J Cell Biol 188(6):863–876
93. Katoh H, Negishi M (2003) RhoG activates Rac1 by direct interaction with the Dock180-binding protein Elmo. Nature 424(6947):461–464. doi:10.1038/nature01817
94. Katoh H, Hiramoto K, Negishi M (2006) Activation of Rac1 by RhoG regulates cell migration. J Cell Sci 119(Pt 1):56–65. doi:10.1242/jcs.02720
95. Ridley AJ, Paterson HF, Johnston CL, Diekmann D, Hall A (1992) The small GTP-binding protein rac regulates growth factor-induced membrane ruffling. Cell 70(3):401–410
96. Dharmawardhane S, Sanders LC, Martin SS, Daniels RH, Bokoch GM (1997) Localization of p21-activated kinase 1 (PAK1) to pinocytic vesicles and cortical actin structures in stimulated cells. J Cell Biol 138(6):1265–1278
97. Takenawa T, Suetsugu S (2007) The WASP-WAVE protein network: connecting the membrane to the cytoskeleton. Nat Rev Mol Cell Biol 8(1):37–48. doi:10.1038/nrm2069
98. Shaw SK, Ma S, Kim MB, Rao RM, Hartman CU, Froio RM, Yang L, Jones T, Liu Y, Nusrat A, Parkos CA, Luscinskas FW (2004) Coordinated redistribution of leukocyte LFA-1 and endothelial cell ICAM-1 accompany neutrophil transmigration. J Exp Med 200(12):1571–1580
99. Feng D, Nagy JA, Pyne K, Dvorak HF, Dvorak AM (1998) Neutrophils emigrate from venules by a transendothelial cell pathway in response to FMLP. J Exp Med 187(6):903–915
100. Muller WA (2011) Mechanisms of leukocyte transendothelial migration. Annu Rev Pathol 6:323–344. doi:10.1146/annurev-pathol-011110-130224
101. Holz LE, Warren A, Le Couteur DG, Bowen DG, Bertolino P (2010) CD8+ T cell tolerance following antigen recognition on hepatocytes. J Autoimmun 34(1):15–22. doi:10.1016/j.jaut.2009.08.005
102. Williamson JR, Grisham JW (1960) Leucocytic emigration from inflamed capillaries. Nature 188:1203
103. Williamson JR, Grisham JW (1961) Electron microscopy of leukocytic margination and emigration in acute inflammation in dog pancreas. Am J Pathol 39:239–256
104. Shulman Z, Shinder V, Klein E, Grabovsky V, Yeger O, Geron E, Montresor A, Bolomini-Vittori M, Feigelson SW, Kirchhausen T, Laudanna C, Shakhar G, Alon R (2009) Lymphocyte crawling and transendothelial migration require chemokine triggering of high-affinity LFA-1 integrin. Immunity 30(3): 384–396. doi:10.1016/j.immuni.2008.12.020
105. Phillipson M, Heit B, Colarusso P, Liu L, Ballantyne CM, Kubes P (2006) Intraluminal crawling of neutrophils to emigration sites: a molecularly distinct process from adhesion in the recruitment cascade. J Exp Med 203(12):2569–2575. doi:10.1084/jem.20060925
106. Smith A, Carrasco YR, Stanley P, Kieffer N, Batista FD, Hogg N (2005) A talin-dependent LFA-1 focal zone is formed by rapidly migrating T lymphocytes. J Cell Biol 170(1):141–151. doi:10.1083/jcb.200412032
107. Carman CV, Sage PT, Sciuto TE, de la Fuente MA, Geha RS, Ochs HD, Dvorak HF, Dvorak AM, Springer TA (2007) Transcellular diapedesis is initiated by invasive podosomes. Immunity 26(6):784–797

108. Carman CV, Springer TA (2008) Trans-cellular migration: cell–cell contacts get intimate. Curr Opin Cell Biol 20(5):533–540
109. Malsam J, Kreye S, Sollner TH (2008) Membrane fusion: SNAREs and regulation. Cell Mol Life Sci 65(18):2814–2832. doi:10.1007/s00018-008-8352-3
110. Lawson C, Wolf S (2009) ICAM-1 signaling in endothelial cells. Pharmacol Rep 61(1):22–32
111. van Buul JD, Kanters E, Hordijk PL (2007) Endothelial signaling by Ig-like cell adhesion molecules. Arterioscler Thromb Vasc Biol 27(9):1870–1876
112. Etienne-Manneville S, Manneville JB, Adamson P, Wilbourn B, Greenwood J, Couraud PO (2000) ICAM-1-coupled cytoskeletal rearrangements and transendothelial lymphocyte migration involve intracellular calcium signaling in brain endothelial cell lines. J Immunol 165(6):3375–3383
113. van Buul JD, Voermans C, van den Berg V, Anthony EC, Mul FP, van Wetering S, van der Schoot CE, Hordijk PL (2002) Migration of human hematopoietic progenitor cells across bone marrow endothelium is regulated by vascular endothelial cadherin. J Immunol 168(2):588–596
114. Dejana E, Orsenigo F, Lampugnani MG (2008) The role of adherens junctions and VE-cadherin in the control of vascular permeability. J Cell Sci 121(Pt 13):2115–2122
115. Wang Q, Pfeiffer GR 2nd, Gaarde WA (2003) Activation of SRC tyrosine kinases in response to ICAM-1 ligation in pulmonary microvascular endothelial cells. J Biol Chem 278(48): 47731–47743
116. Bixel MG, Li H, Petri B, Khandoga AG, Khandoga A, Zarbock A, Wolburg-Buchholz K, Wolburg H, Sorokin L, Zeuschner D, Maerz S, Butz S, Krombach F, Vestweber D (2010) CD99 and CD99L2 act at the same site as, but independently of, PECAM-1 during leukocyte diapedesis. Blood 116(7):1172–1184. doi:10.1182/blood-2009-12-256388
117. Wegmann F, Petri B, Khandoga AG, Moser C, Khandoga A, Volkery S, Li H, Nasdala I, Brandau O, Fassler R, Butz S, Krombach F, Vestweber D (2006) ESAM supports neutrophil extravasation, activation of Rho, and VEGF-induced vascular permeability. J Exp Med 203(7):1671–1677. doi:10.1084/jem.20060565
118. Reymond N, Imbert AM, Devilard E, Fabre S, Chabannon C, Xerri L, Farnarier C, Cantoni C, Bottino C, Moretta A, Dubreuil P, Lopez M (2004) DNAM-1 and PVR regulate monocyte migration through endothelial junctions. J Exp Med 199(10): 1331–1341
119. Woodfin A, Reichel CA, Khandoga A, Corada M, Voisin MB, Scheiermann C, Haskard DO, Dejana E, Krombach F, Nourshargh S (2007) JAM-A mediates neutrophil transmigration in a stimulus-specific manner in vivo: evidence for sequential roles for JAM-A and PECAM-1 in neutrophil transmigration. Blood 110(6):1848–1856. doi:10.1182/blood-2006-09-047431
120. Aird WC (2003) Endothelial cell heterogeneity. Crit Care Med 31(4 Suppl):S221–S230
121. Garlanda C, Dejana E (1997) Heterogeneity of endothelial cells. Specific markers. Arterioscler Thromb Vasc Biol 17(7):1193–1202
122. Albelda SM (1991) Endothelial and epithelial cell adhesion molecules. Am J Respir Cell Mol Biol 4(3):195–203
123. Dejana E (2004) Endothelial cell–cell junctions: happy together. Nat Rev Mol Cell Biol 5(4):261–270
124. Mamdouh Z, Chen X, Pierini LM, Maxfield FR, Muller WA (2003) Targeted recycling of PECAM from endothelial surface-connected compartments during diapedesis. Nature 421(6924): 748–753
125. Mamdouh Z, Kreitzer GE, Muller WA (2008) Leukocyte transmigration requires kinesin-mediated microtubule-dependent membrane trafficking from the lateral border recycling compartment. J Exp Med 205(4):951–966. doi:10.1084/jem.20072328
126. Mamdouh Z, Mikhailov A, Muller WA (2009) Transcellular migration of leukocytes is mediated by the endothelial lateral border recycling compartment. J Exp Med 206(12):2795–2808
127. Braet F, Riches J, Geerts W, Jahn KA, Wisse E, Frederik P (2009) Three-dimensional organization of fenestrae labyrinths in liver sinusoidal endothelial cells. Liver Int 29(4):603–613. doi:10.1111/j.1478-3231.2008.01836.x
128. Vasile E, Qu H, Dvorak HF, Dvorak AM (1999) Caveolae and vesiculo-vacuolar organelles in bovine capillary endothelial cells cultured with VPF/VEGF on floating Matrigel-collagen gels. J Histochem Cytochem 47(2):159–167
129. Feng D, Nagy JA, Pyne K, Dvorak HF, Dvorak AM (2004) Ultrastructural localization of platelet endothelial cell adhesion molecule (PECAM-1, CD31) in vascular endothelium. J Histochem Cytochem 52(1):87–101
130. Ozaki H, Ishii K, Horiuchi H, Arai H, Kawamoto T, Okawa K, Iwamatsu A, Kita T (1999) Cutting edge: combined treatment of TNF-alpha and IFN-gamma causes redistribution of junctional adhesion molecule in human endothelial cells. J Immunol 163(2):553–557
131. Manes TD, Pober JS (2011) Identification of endothelial cell junctional proteins and lymphocyte receptors involved in transendothelial migration of human effector memory CD4+ T cells. J Immunol 186(3):1763–1768. doi:10.4049/jimmunol.1002835
132. Ostermann G, Weber KS, Zernecke A, Schroder A, Weber C (2002) JAM-1 is a ligand of the beta(2) integrin LFA-1 involved in transendothelial migration of leukocytes. Nat Immunol 3(2):151–158
133. Wojcikiewicz EP, Koenen RR, Fraemohs L, Minkiewicz J, Azad H, Weber C, Moy VT (2009) LFA-1 binding destabilizes the JAM-A homophilic interaction during leukocyte transmigration. Biophys J 96(1):285–293. doi:10.1529/biophysj.108.135491
134. Santoso S, Sachs UJ, Kroll H, Linder M, Ruf A, Preissner KT, Chavakis T (2002) The junctional adhesion molecule 3 (JAM-3) on human platelets is a counterreceptor for the leukocyte integrin Mac-1. J Exp Med 196(5):679–691
135. Zen K, Babbin BA, Liu Y, Whelan JB, Nusrat A, Parkos CA (2004) JAM-C is a component of desmosomes and a ligand for CD11b/CD18-mediated neutrophil transepithelial migration. Mol Biol Cell 15(8):3926–3937. doi:10.1091/mbc.E04-04-0317
136. Lamagna C, Meda P, Mandicourt G, Brown J, Gilbert RJ, Jones EY, Kiefer F, Ruga P, Imhof BA, Aurrand-Lions M (2005) Dual interaction of JAM-C with JAM-B and alpha(M)beta2 integrin: function in junctional complexes and leukocyte adhesion. Mol Biol Cell 16(10):4992–5003. doi:10.1091/mbc.E05-04-0310
137. Ludwig RJ, Hardt K, Hatting M, Bistrian R, Diehl S, Radeke HH, Podda M, Schon MP, Kaufmann R, Henschler R, Pfeilschifter JM, Santoso S, Boehncke WH (2009) Junctional adhesion molecule (JAM)-B supports lymphocyte rolling and adhesion through interaction with alpha4beta1 integrin. Immunology 128(2):196–205. doi:10.1111/j.1365-2567.2009.03100.x
138. Marmon S, Hinchey J, Oh P, Cammer M, de Almeida CJ, Gunther L, Raine CS, Lisanti MP (2009) Caveolin-1 expression determines the route of neutrophil extravasation through skin microvasculature. Am J Pathol 174(2):684–692. doi:10.2353/ajpath.2009.080091
139. Stan RV, Ghitescu L, Jacobson BS, Palade GE (1999) Isolation, cloning, and localization of rat PV-1, a novel endothelial caveolar protein. J Cell Biol 145(6):1189–1198
140. Stan RV, Kubitza M, Palade GE (1999) PV-1 is a component of the fenestral and stomatal diaphragms in fenestrated endothelia. Proc Natl Acad Sci USA 96(23):13203–13207
141. Stan RV, Tkachenko E, Niesman IR (2004) PV1 is a key structural component for the formation of the stomatal and

fenestral diaphragms. Mol Biol Cell 15(8):3615–3630. doi:10.1091/mbc.E03-08-0593
142. Stan RV (2007) Endothelial stomatal and fenestral diaphragms in normal vessels and angiogenesis. J Cell Mol Med 11(4):621–643. doi:10.1111/j.1582-4934.2007.00075.x
143. Predescu SA, Predescu DN, Palade GE (2001) Endothelial transcytotic machinery involves supramolecular protein–lipid complexes. Mol Biol Cell 12(4):1019–1033
144. Pol A, Lu A, Pons M, Peiro S, Enrich C (2000) Epidermal growth factor-mediated caveolin recruitment to early endosomes and MAPK activation. Role of cholesterol and actin cytoskeleton. J Biol Chem 275(39):30566–30572. doi:10.1074/jbc.M001131200
145. Predescu SA, Predescu DN, Shimizu K, Klein IK, Malik AB (2005) Cholesterol-dependent syntaxin-4 and SNAP-23 clustering regulates caveolar fusion with the endothelial plasma membrane. J Biol Chem 280(44):37130–37138. doi:10.1074/jbc.M505659200
146. Schnitzer JE, Allard J, Oh P (1995) NEM inhibits transcytosis, endocytosis, and capillary permeability: implication of caveolae fusion in endothelia. Am J Physiol 268(1 Pt 2):H48–H55
147. Dvorak AM, Feng D (2001) The vesiculo-vacuolar organelle (VVO). A new endothelial cell permeability organelle. J Histochem Cytochem 49(4):419–432
148. Hu G, Vogel SM, Schwartz DE, Malik AB, Minshall RD (2008) Intercellular adhesion molecule-1-dependent neutrophil adhesion to endothelial cells induces caveolae-mediated pulmonary vascular hyperpermeability. Circ Res 102(12):e120–e131. doi:10.1161/CIRCRESAHA.107.167486
149. Millan J, Cain RJ, Reglero-Real N, Bigarella C, Marcos-Ramiro B, Fernandez-Martin L, Correas I, Ridley AJ (2010) Adherens junctions connect stress fibres between adjacent endothelial cells. BMC Biol 8:11
150. Stahlhut M, van Deurs B (2000) Identification of filamin as a novel ligand for caveolin-1: evidence for the organization of caveolin-1-associated membrane domains by the actin cytoskeleton. Mol Biol Cell 11(1):325–337
151. Muriel O, Echarri A, Hellriegel C, Pavon DM, Beccari L, Del Pozo MA (2011) Phosphorylated filamin A regulates actin-linked caveolae dynamics. J Cell Sci 124(Pt 16):2763–2776. doi:10.1242/jcs.080804
152. Sverdlov M, Shinin V, Place AT, Castellon M, Minshall RD (2009) Filamin A regulates caveolae internalization and trafficking in endothelial cells. Mol Biol Cell 20(21):4531–4540. doi:10.1091/mbc.E08-10-0997
153. Kanters E, van Rijssel J, Hensbergen PJ, Hondius D, Mul FP, Deelder AM, Sonnenberg A, van Buul JD, Hordijk PL (2008) Filamin B mediates ICAM-1-driven leukocyte transendothelial migration. J Biol Chem 283(46):31830–31839
154. Yang L, Kowalski JR, Zhan X, Thomas SM, Luscinskas FW (2006) Endothelial cell cortactin phosphorylation by Src contributes to polymorphonuclear leukocyte transmigration in vitro. Circ Res 98(3):394–402. doi:10.1161/01.RES.0000201958.59020.1a
155. Yang L, Kowalski JR, Yacono P, Bajmoczi M, Shaw SK, Froio RM, Golan DE, Thomas SM, Luscinskas FW (2006) Endothelial cell cortactin coordinates intercellular adhesion molecule-1 clustering and actin cytoskeleton remodeling during polymorphonuclear leukocyte adhesion and transmigration. J Immunol 177(9):6440–6449
156. Schnoor M, Lai FP, Zarbock A, Klaver R, Polaschegg C, Schulte D, Weich HA, Oelkers JM, Rottner K, Vestweber D (2011) Cortactin deficiency is associated with reduced neutrophil recruitment but increased vascular permeability in vivo. J Exp Med 208(8):1721–1735. doi:10.1084/jem.20101920
157. Uruno T, Liu J, Zhang P, Fan Y, Egile C, Li R, Mueller SC, Zhan X (2001) Activation of Arp2/3 complex-mediated actin polymerization by cortactin. Nat Cell Biol 3(3):259–266. doi:10.1038/35060051
158. Flanagan LA, Chou J, Falet H, Neujahr R, Hartwig JH, Stossel TP (2001) Filamin A, the Arp2/3 complex, and the morphology and function of cortical actin filaments in human melanoma cells. J Cell Biol 155(4):511–517
159. Viola A, Gupta N (2007) Tether and trap: regulation of membrane-raft dynamics by actin-binding proteins. Nat Rev Immunol 7(11):889–896
160. Shulman Z, Cohen SJ, Roediger B, Kalchenko V, Jain R, Grabovsky V, Klein E, Shinder V, Stoler-Barak L, Feigelson SW, Meshel T, Nurmi SM, Goldstein I, Hartley O, Gahmberg CG, Etzioni A, Weninger W, Ben-Baruch A, Alon R (2011) Transendothelial migration of lymphocytes mediated by intraendothelial vesicle stores rather than by extracellular chemokine depots. Nat Immunol. doi:10.1038/ni.2173
161. Eriksson JE, Dechat T, Grin B, Helfand B, Mendez M, Pallari HM, Goldman RD (2009) Introducing intermediate filaments: from discovery to disease. J Clin Investig 119(7):1763–1771. doi:10.1172/JCI38339
162. Pallari HM, Eriksson JE (2006) Intermediate filaments as signaling platforms. Sci STKE 2006(366):pe53. doi:10.1126/stke.3662006pe53
163. Nieminen M, Henttinen T, Merinen M, Marttila-Ichihara F, Eriksson JE, Jalkanen S (2006) Vimentin function in lymphocyte adhesion and transcellular migration. Nat Cell Biol 8(2):156–162
164. Sprenger RR, Fontijn RD, van Marle J, Pannekoek H, Horrevoets AJ (2006) Spatial segregation of transport and signalling functions between human endothelial caveolae and lipid raft proteomes. Biochem J 400(3):401–410. doi:10.1042/BJ20060355
165. Woodfin A, Voisin MB, Beyrau M, Colom B, Caille D, Diapouli FM, Nash GB, Chavakis T, Albelda SM, Rainger GE, Meda P, Imhof BA, Nourshargh S (2011) The junctional adhesion molecule JAM-C regulates polarized transendothelial migration of neutrophils in vivo. Nat Immunol 12(8):761–769. doi:10.1038/ni.2062
166. Phillipson M, Kaur J, Colarusso P, Ballantyne CM, Kubes P (2008) Endothelial domes encapsulate adherent neutrophils and minimize increases in vascular permeability in paracellular and transcellular emigration. PLoS One 3(2):e1649. doi:10.1371/journal.pone.0001649
167. Schulte D, Kuppers V, Dartsch N, Broermann A, Li H, Zarbock A, Kamenyeva O, Kiefer F, Khandoga A, Massberg S, Vestweber D (2011) Stabilizing the VE-cadherin-catenin complex blocks leukocyte extravasation and vascular permeability. EMBO J 30(20):4157–4170. doi:10.1038/emboj.2011.304
168. Coisne C, Engelhardt B (2011) Tight junctions in brain barriers during central nervous system inflammation. Antioxid Redox Signal 15(5):1285–1303. doi:10.1089/ars.2011.3929
169. Wolburg H, Wolburg-Buchholz K, Engelhardt B (2005) Diapedesis of mononuclear cells across cerebral venules during experimental autoimmune encephalomyelitis leaves tight junctions intact. Acta Neuropathol 109(2):181–190. doi:10.1007/s00401-004-0928-x
170. Petri B, Kaur J, Long EM, Li H, Parsons SA, Butz S, Phillipson M, Vestweber D, Patel KD, Robbins SM, Kubes P (2011) Endothelial LSP1 is involved in endothelial dome formation, minimizing vascular permeability changes during neutrophil transmigration in vivo. Blood 117(3):942–952. doi:10.1182/blood-2010-02-270561
171. Wang HX, Kolesnikova TV, Denison C, Gygi SP, Hemler ME (2011) The C-terminal tail of tetraspanin protein CD9

contributes to its function and molecular organization. J Cell Sci 124(Pt 16):2702–2710. doi:10.1242/jcs.085449

172. Bari R, Guo Q, Xia B, Zhang YH, Giesert EE, Levy S, Zheng JJ, Zhang XA (2011) Tetraspanins regulate the protrusive activities of cell membrane. Biochem Biophys Res Commun 415(4): 619–626. doi:10.1016/j.bbrc.2011.10.121

173. van Niel G, Charrin S, Simoes S, Romao M, Rochin L, Saftig P, Marks MS, Rubinstein E, Raposo G (2011) The tetraspanin CD63 regulates ESCRT-independent and -dependent endosomal sorting during melanogenesis. Dev Cell 21(4):708–721. doi: 10.1016/j.devcel.2011.08.019

MYADM controls endothelial barrier function through ERM-dependent regulation of ICAM-1 expression

Juan F. Aranda[a], Natalia Reglero-Real[a], Beatriz Marcos-Ramiro[a], Ana Ruiz-Sáenz[a], Laura Fernández-Martín[a], Miguel Bernabé-Rubio[a], Leonor Kremer[b], Anne J. Ridley[c], Isabel Correas[a], Miguel A. Alonso[a,*], and Jaime Millán[a,*]

[a]Centro de Biología Molecular Severo Ochoa, Consejo Superior de Investigaciones Científicas and Universidad Autónoma de Madrid, Cantoblanco, 28049 Madrid, Spain; [b]Centro Nacional de Biotecnología. Consejo Superior de Investigaciones Científicas, Cantoblanco, 28049 Madrid, Spain; [c]Randall Division of Cell and Molecular Biophysics, King's College London, London SE1 1UL, United Kingdom

ABSTRACT **The endothelium maintains a barrier between blood and tissue that becomes more permeable during inflammation. Membrane rafts are ordered assemblies of cholesterol, glycolipids, and proteins that modulate proinflammatory cell signaling and barrier function. In epithelial cells, the MAL family members MAL, MAL2, and myeloid-associated differentiation marker (MYADM) regulate the function and dynamics of ordered membrane domains. We analyzed the expression of these three proteins in human endothelial cells and found that only MYADM is expressed. MYADM was confined in ordered domains at the plasma membrane, where it partially colocalized with filamentous actin and cell–cell junctions. Small interfering RNA (siRNA)-mediated MYADM knockdown increased permeability, ICAM-1 expression, and leukocyte adhesion, all of which are features of an inflammatory response. Barrier function decrease in MYADM-silenced cells was dependent on ICAM-1 expression. Membrane domains and the underlying actin cytoskeleton can regulate each other and are connected by ezrin, radixin, and moesin (ERM) proteins. In endothelial cells, MYADM knockdown induced ERM activation. Triple-ERM knockdown partially inhibited ICAM-1 increase induced by MYADM siRNA. Importantly, ERM knockdown also reduced ICAM-1 expression in response to the proinflammatory cytokine tumor necrosis factor-α. MYADM therefore regulates the connection between the plasma membrane and the cortical cytoskeleton and so can control the endothelial inflammatory response.**

Monitoring Editor
J. Silvio Gutkind
National Institutes of Health

Received: Nov 14, 2011
Revised: Nov 15, 2012
Accepted: Dec 14, 2012

This article was published online ahead of print in MBoC in Press (http://www.molbiolcell.org/cgi/doi/10.1091/mbc.E11-11-0914) on December 21, 2012.

*These authors contributed equally to this work.

Address correspondence to: Jaime Millán (jmillan@cbm.uam.es) or Miguel A. Alonso (maalonso@cbm.uam.es).

Abbreviations used: BCR, B-cell receptor; DRM, detergent-resistant membrane; ERM, ezrin, radixin, and moesin; FERM, 4.1 ezrin–radixin–moesin; GFP, green fluorescent protein; HA, hemagglutinin; HUVEC, human umbilical vein endothelial cell; ICAM-1, intercellular adhesion molecule-1; mAb, monoclonal antibody; MARVEL, MAL and related proteins for vesicle trafficking and membrane link; MYADM, myeloid-associated differentiation marker; PBS, phosphate-buffered saline; PIP2, phosphatidylinositol 4,5-bisphosphate; PKC, protein kinase C; qPCR, quantitative PCR; S1P, sphingosine 1-phosphate; siRNA, small interfering RNA; TEER, transendothelial electrical resistance; TNF-α, tumor necrosis factor-α.

INTRODUCTION

The endothelium lines the inner side of blood vessels, forming a barrier between the blood and the surrounding tissue that is essential for vascular homeostasis. The endothelium mediates the passage of small molecules and cells from the bloodstream to the tissues, without compromising its integrity, in the presence of continuous osmotic and shear stress. The organization of the endothelial cell surface, the biological fence facing the vessel lumen, is thus essential for integrating signals from different sources that modulate selective permeability, such as mechanical forces, cytokine signaling, and cell–cell interactions (Millán and Ridley, 2005; Simionescu, 2007; Vandenbroucke *et al*., 2008; Reglero-Real *et al*., 2012).

The architecture of the endothelial surface is determined by the links between the plasma membrane, surface proteins, and underlying cytoskeleton. In the current paradigm, lipids and transmembrane proteins are connected to the underlying cytoskeleton like a

picket fence that controls the stiffness of the cell surface and the ability of lipids and proteins to diffuse and signal (Ritchie *et al.*, 2003). The 4.1 family proteins, ezrin, radixin, and moesin (ERM), are the best-known connectors between plasma membrane, transmembrane receptors, and the subcortical actin cytoskeleton (Bretscher *et al.*, 2002; Viola and Gupta, 2007). An additional level of complexity in cell surfaces arises from the fact that the complex mixture of lipids forming the plasma membrane does not distribute homogeneously but can form microdomains with specific subsets of proteins. The model that best explains this heterogeneity, although it is still under debate, posits the existence of liquid-ordered membrane domains enriched in glycolipids and cholesterol, termed *membrane rafts*. Raft-mediated plasma membrane condensation would regulate signaling, protein trafficking, and compartmentalization (Lingwood and Simons, 2010; Simons and Gerl, 2010).

Some evidence suggests a mutual regulation between ERM proteins and ordered membrane rafts (Viola and Gupta, 2007). On activation, ERMs acquire an open conformation in which the N-terminal Four point one, ezrin, radixin-moesin (FERM) domain interacts directly or indirectly with the cytoplasmic tails of transmembrane receptors, and the C-terminal domain binds to actin filaments (Fehon *et al.*, 2010). The FERM domain binds the raft lipid phosphatidylinositol 4,5-bisphosphate (PIP2) and some transmembrane proteins that also partition into ordered membranes (Wojciak-Stothard *et al.*, 1999; Tilghman and Hoover, 2002; Johnson *et al.*, 2008; Kwiatkowska, 2010). ERMs themselves have also been found compartmentalized into ordered membrane domains (Tomas *et al.*, 2002; Gupta *et al.*, 2006; Heyraud *et al.*, 2007). Finally, active ERMs have been shown to regulate membrane raft content (Prag *et al.*, 2007) and prevent membrane raft coalescence (Gupta *et al.*, 2006).

Inflammatory cytokines have the ability to alter the endothelial barrier to cells and solutes by mechanisms that are not completely understood (Vandenbroucke *et al.*, 2008). Disruption of cholesterol-rich membrane rafts has been shown to either promote or ameliorate inflammation in different cell types (Legler *et al.*, 2003; Flemming *et al.*, 2004; Meng *et al.*, 2010). In addition, cytokines such as tumor necrosis factor-α (TNF-α) and interleukin-1β (IL-1β) activate ERM proteins. This activation mediates the increase in endothelial permeability or the transcriptional regulation in response to TNF-α (Kishore *et al.*, 2005; Koss *et al.*, 2006). However, the full role of ERM activation in the endothelial inflammatory response is still not well defined. It is of note that ERM proteins play an important role localizing receptors involved not only in leukocyte adhesion but also in the regulation of endothelial permeability in an inflammatory context, for example, intercellular adhesion molecule (ICAM)-1 or vascular cell adhesion molecule (VCAM)-1 (van Wetering *et al.*, 2003; Clark *et al.*, 2007; Sumagin *et al.*, 2008).

In the current model of ordered membrane domains or rafts, protein machinery associated with these platforms is required to specify their function in the cell (Bauer and Pelkmans, 2006; Lingwood and Simons, 2010). The MAL family consists of integral proteins with several transmembrane domains involved in membrane dynamics (Sanchez-Pulido *et al.*, 2002). Several lines of evidence support a role for these proteins in events related to organization of membrane domains, such as polarized membrane trafficking or plasma membrane reorganization in response to extracellular signaling (Puertollano *et al.*, 1999; Anton *et al.*, 2008; Goldstein Magal *et al.*, 2009; Anton *et al.*, 2011; Aranda *et al.*, 2011). Myeloid-associated differentiation marker (MYADM) is a MAL family protein that regulates membrane order in migrating epithelial cells (Aranda *et al.*, 2011). In this paper, we report that MYADM is a component of endothelial surface rafts. MYADM knockdown induces an inflammatory-like phenotype, altering barrier function through the increase of the adhesion receptor ICAM-1. The rise in ICAM-1 levels is mediated by MYADM-regulated activation of ERM proteins. Collectively our results strongly suggest that the interaction between the plasma membrane and the submembrane actin cytoskeleton at the endothelial surface controls the inflammatory response.

RESULTS

MYADM is confined into ordered domains in the endothelial plasma membrane

Specific types of highly polarized epithelial cells express the MAL family members MAL and MAL2, which are involved in specialized, raft-dependent, apical vesicular trafficking (Puertollano *et al.*, 1999; de Marco *et al.*, 2002). MYADM, in contrast, is expressed ubiquitously and organizes membrane rafts at the epithelial cell surface, thereby affecting cell spreading and motility (Aranda *et al.*, 2011). The endothelium can be considered as a simple squamous epithelium (Palade *et al.*, 1979). Because ordered membrane domains have been shown to be central to endothelial barrier function and signaling (Muppidi *et al.*, 2004; Heyraud *et al.*, 2007; Chidlow and Sessa, 2010; Triantafilou *et al.*, 2010), we wondered whether these MAL proteins are expressed and play a role in primary human endothelial cells. Detergent-resistant membrane (DRM) fractions were isolated from confluent human umbilical vein endothelial cells (HUVECs) and blotted with antibodies against MAL, MAL2, and MYADM, together with a panel of cell lines used as positive and negative controls. Endogenous MYADM was clearly detected in DRM fractions from all the analyzed cell types, including HUVECs, consistent with the ubiquitous expression pattern previously reported (Aranda *et al.*, 2011). In contrast, MAL and MAL2 were detected only in DRM fractions from epithelial PC3 and Madin-Darby canine kidney (MDCK) cells (Figure 1A). Quantitative PCR (qPCR) assays confirmed that expression of MAL and MAL2 was negligible in HUVECs (Figure 1B). Further analysis of MYADM fractionation in HUVECs showed that this protein is almost exclusively found in DRMs (Figure 1, C and D). The 2B12 monoclonal antibody (mAb), raised against human MYADM is not suitable for immunofluorescence analysis (Aranda *et al.*, 2011). For the study of MYADM distribution, MYADM-green fluorescent protein (GFP) was expressed in human endothelial cells and analyzed by confocal microscopy. MYADM-GFP also partitioned in DRMs, indicating that the GFP tag does not alter MYADM insertion in plasma membrane domains (Figure 1E). MYADM-GFP was localized at the plasma membrane and in cell–cell junctions in confluent endothelial cells, and this distribution overlapped with the staining for filamentous actin and junctional markers, such as vascular endothelial (VE)-cadherin (Figure 1F, insets). A partial colocalization of MYADM-GFP at cell–cell junctions was also found with platelet endothelial cell adhesion molecule (PECAM)-1, p120-catenin, occludin, and nectin-2 (Supplemental Figure S1). In contrast, MYADM-GFP showed little colocalization with caveolin-1, a raft-associated protein essential for vascular homeostasis (Chidlow and Sessa, 2010), or with CD59, a glycosylphosphatidylinositol (GPI)-anchored protein often used as a marker of membrane rafts (Millán *et al.*, 2006), which suggests that MYADM could organize ordered membrane domains differently from caveolae or CD59 in human endothelial cells (Figure 1F).

MYADM knockdown induces an inflammatory-like phenotype by inducing ICAM-1 expression

To gain insight into the role of MYADM in endothelial cells, we investigated the effects of three different small interfering RNAs (siRNAs) that targeted MYADM with low (siMYADM 1), medium

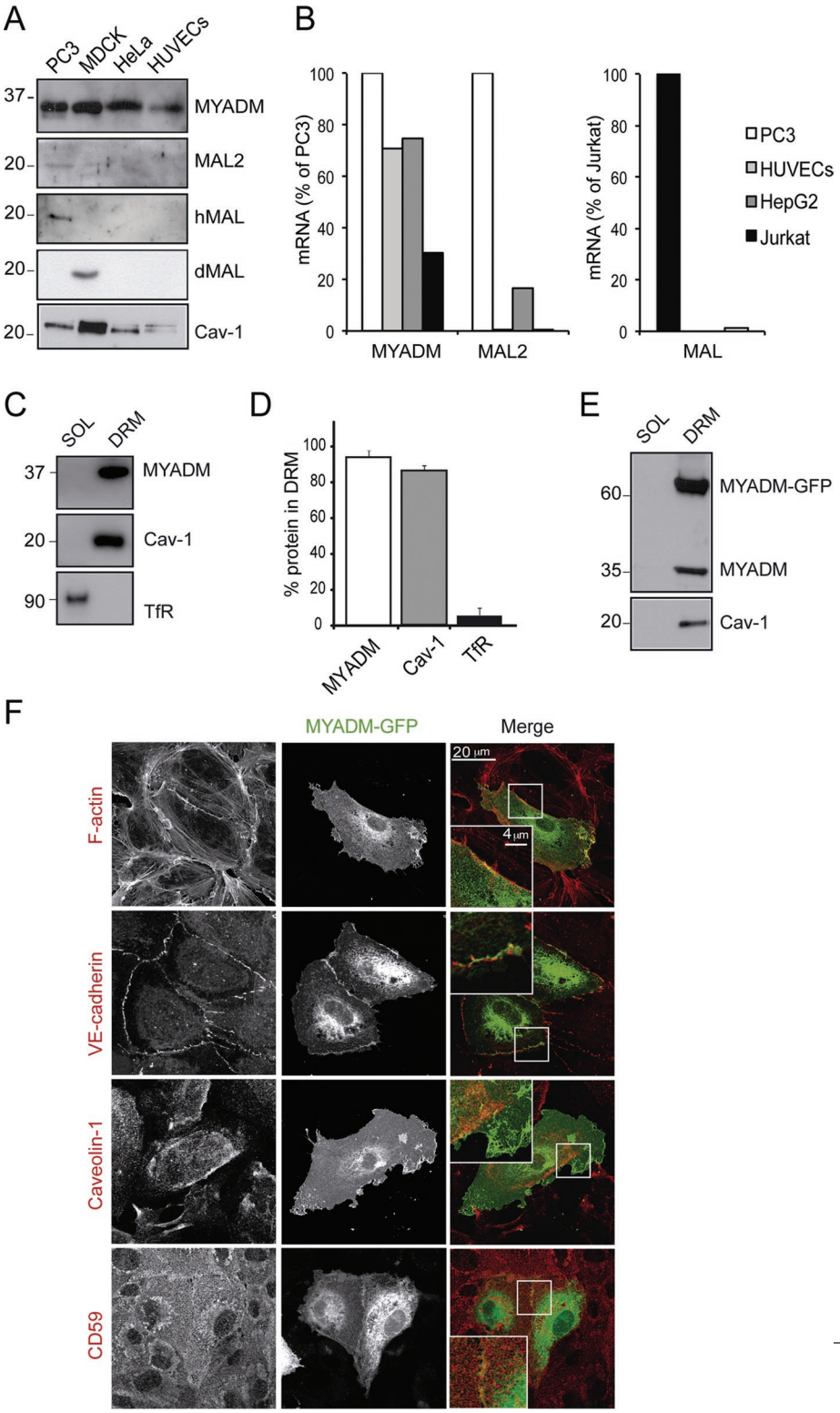

FIGURE 1: MYADM is a transmembrane protein associated with endothelial DRMs. (A) The indicated cell types were extracted with 1% Triton X-100 at 4°C and centrifuged to equilibrium in sucrose density gradients. Aliquots from DRMs were immunoblotted for MYADM, MAL2, human MAL (hMAL), canine MAL (dMAL), and caveolin-1 (Cav-1). (B) RNA from the indicated cells was isolated and the expression of MYADM, MAL2 and MAL transcripts was analyzed by qPCR. Results were normalized to mRNA levels of housekeeping genes (β-actin and GADPH) and represented as percentage of PC3 mRNA levels for MYADM and MAL2 transcripts (left) or Jurkat mRNA levels for the MAL transcript (right). (C) Aliquots from soluble (SOL) and DRM fractions from HUVECs were immunoblotted for MYADM, Cav-1 (as a control of endothelial DRMs), and transferrin receptor (TfR; as a control of transmembrane proteins in the soluble fraction). (D) Quantitation of DRM segregation of the indicated protein from three independent experiments. (E) DRMs were isolated from cells expressing MYADM-GFP for 24 h and immunoblotted for MYADM with anti-MYADM mAb 2B12 and for caveolin-1. (F) MYADM-GFP distributes at the plasma membrane of HUVECs and partially colocalizes with subcortical F-actin and with VE-cadherin. Caveolin-1 and CD59 staining reveals little colocalization of MYADM-GFP with caveolae or with GPI-protein rich-rafts in endothelial cells. Scale bar: 20 μm.

(siMYADM 2), and high efficiency (siMYADM 3; Figure 2, A and B). MYADM silencing caused a clear disruption of the endothelial monolayer and partially disorganized cell–cell junctions, as shown by staining of β-catenin, VE-cadherin, or PECAM-1 (Figure 2, C and D). MYADM reduction induced the appearance of intercellular gaps (Figure 2, C and D, asterisks, and E) and increased both filamentous (F)-actin (Figures 2, C and F, and S2) and permeability in Transwell assays (Figure 2G). Collectively these results indicate that MYADM knockdown caused endothelial barrier dysfunction.

Increased permeability and polymerization of actin are prototypical endothelial responses to several inflammatory stimuli (Pober and Sessa, 2007). We tested whether MYADM knockdown was inducing an inflammatory-like response by following the expression of different receptors previously involved in leukocyte adhesion and permeability and considered typical inflammatory markers (Albelda, 1991; Clark *et al.*, 2007; Sumagin *et al.*, 2008). Western blot analysis indicated that reduction of MYADM levels induced the expression of the adhesion receptor ICAM-1, but not of E-selectin or VCAM-1 (Figure 3, A and B). MYADM knockdown also increased ICAM-1 mRNA, as shown by qPCR experiments (Figure 3C). Immunofluorescence assays revealed the surface accumulation of this receptor in MYADM-depleted cells (Figure 3D). In contrast, no difference was found in the expression of different components of cell–cell junctions involved in modulation of barrier function in an inflammatory context (Fernandez-Martin *et al.*, 2012; Reglero-Real *et al.*, 2012), such as VE-cadherin, β-catenin, p120-catenin, and PECAM-1 (Figure 3A). The Rho GTPases RhoA, Rac1, and Cdc42 have been involved in permeability and F-actin regulation. No statistically significant changes were detected in their activity upon MYADM knockdown (Figure S3, A and B). Also, no significant alteration was detected in the phosphorylation of regulatory myosin

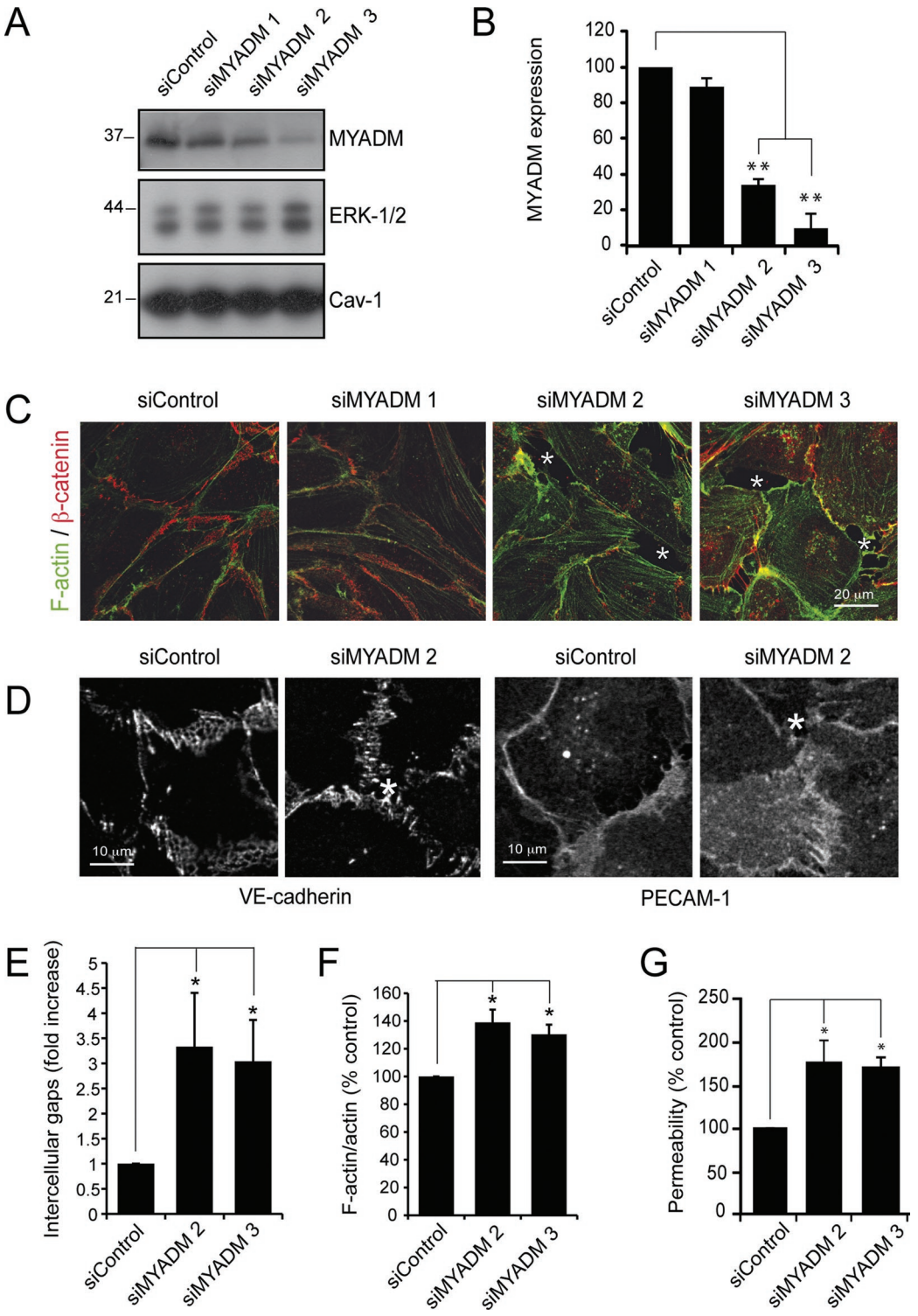

FIGURE 2: MYADM knockdown alters endothelial barrier function. (A) HUVECs were transfected in parallel with control siRNA (siControl) or with three different siRNAs targeting MYADM (siMYADM). At 72 h after transfection, MYADM levels were analyzed by immunoblotting. ERK-1/2 and caveolin-1 (Cav-1) levels are shown as loading controls. (B) Quantitation of MYADM reduction in response to siRNA transfection. The mean + SEM from three independent experiments is presented. (C and D) HUVECs were transfected with the indicated siRNAs and plated at confluence on fibronectin-coated coverslips. After 72 h, cells were fixed and stained for F-actin and β-catenin (C) or VE-cadherin or PECAM-1 (D) to detect cell–cell junctions. Asterisks in the images indicate intercellular gaps. Scale bar: 20 μm for (C) and 10 μm for (D). (E) Quantitation of intercellular gaps in cells transfected with the indicated siRNAs. (F) Cells were fixed and stained with antibody against total actin or with TRITC–phalloidin. Quantitation of the ratio F-actin/total actin (see Figure S2). (G) HUVECs were transfected with the indicated siRNAs and plated at confluence on Transwells, and permeability assays were performed 72 h after transfection. The mean + SEM from three independent experiments is shown. *, $p < 0.05$; **, $p < 0.01$.

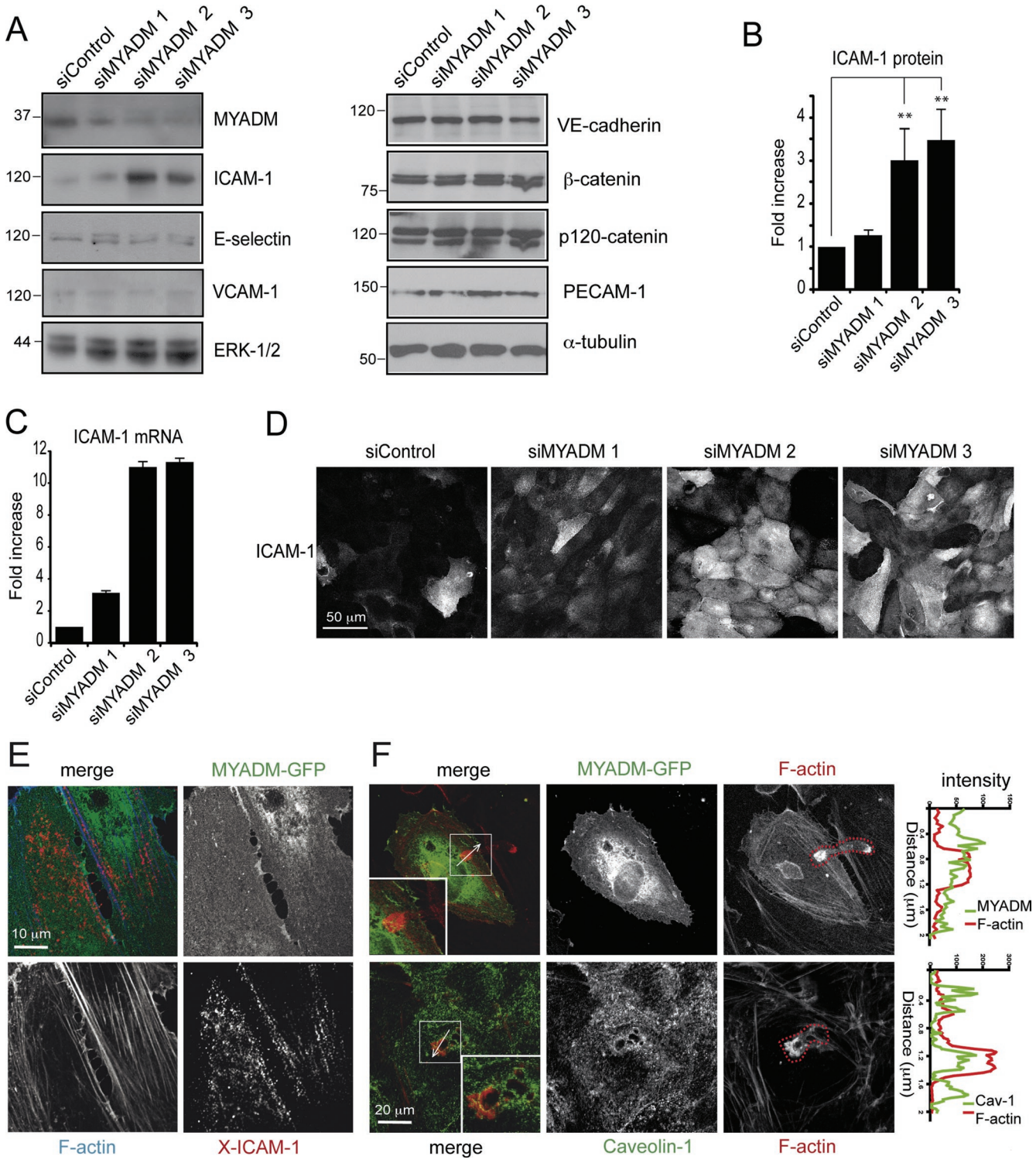

FIGURE 3: MYADM knockdown induces ICAM-1 expression. HUVECs were transfected with the indicated siRNAs for 72 h, and the expression of different proteins involved in endothelial barrier function was analyzed by Western blot (A). Quantitation of ICAM-1 protein (B) and mRNA by qPCR (C). The mean + SEM from three (B) and two (C) independent experiments is shown. **, $p < 0.01$. (D) Localization of ICAM-1 in siRNA-transfected cells by immunofluorescence analysis. (E) HUVECs expressing MYADM-GFP for 36 h were stimulated with TNF-α (10 ng/ml) for 6 h to induce detectable levels of ICAM-1. Subsequently the receptor was cross-linked with specific antibodies (X-ICAM-1). Cells were fixed, permeabilized, and stained with TRITC–phalloidin to visualize F-actin. (F) HUVECs expressing MYADM-GFP were starved, stimulated with TNF-α (10 ng/ml) for 6 h to induce expression of adhesion receptors, and then incubated with T-cells for 15 min. Cells were fixed and stained with TRITC–phalloidin to visualize F-actin (top panels) or with TRITC–phalloidin and anti–caveolin-1 antibody (bottom panels). T-cells adhering or transmigrating were morphologically distinguishable by the F-actin staining (red dotted line). Right graphs show intensity profiles across the T-cell–endothelial cell interaction area along the indicated white arrows.

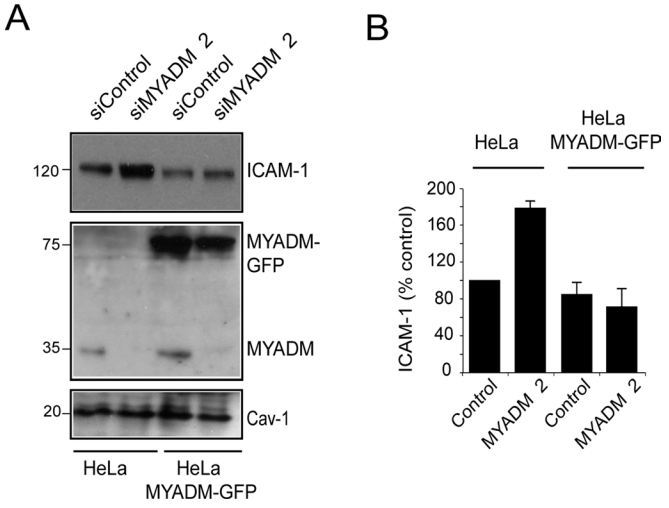

FIGURE 4: Exogenous expression of MYADM prevents ICAM-1 increase in response to MYADM siRNA transfection. (A) Parental HeLa cells or HeLa cells stably expressing MYADM-GFP were transfected with siControl or siMYADM 2 for 48 h. Cell extracts were then immunoblotted with anti–ICAM-1, anti-GFP, anti-MYADM, and anti–caveolin-1 (Cav-1) antibodies. (B) Quantitation of ICAM-1 levels in HeLa and HeLa-MYADM-GFP transfected with the indicated siRNAs. The mean + SEM is shown.

light chain, which indicates that actomyosin-mediated contractility downstream of RhoA is not affected by MYADM depletion (Figure S3C). Although MYADM knockdown induces intercellular gaps, no increase in VE-cadherin tyrosine phosphorylation or decrease in β-catenin association to VE-cadherin was detected upon MYADM knockdown (Figure S4), which suggests the stability of adherens junctions is not regulated by MYADM expression. Collectively these experiments indicate that MYADM plays a role in barrier function and ICAM-1 transcriptional regulation.

MYADM did not appear to associate with ICAM-1, in either ICAM-1 immunoprecipitation (unpublished data) or cross-linking experiments (Figure 3E). In addition, MYADM did not distribute around either adhered or transmigrating leukocytes (Figure 3F), in contrast with caveolin-1, which is enriched in areas where T-cells are transmigrating transcellularly, as previously described (Carman and Springer, 2004; Millán *et al.*, 2006; Keuschnigg *et al.*, 2009). Altogether these data suggest that MYADM depletion induces an increase in ICAM-1 expression but that MYADM is not directly associated with ICAM-1 or involved in ICAM-1 function. To rule out the possibility of an off-target effect of the siRNA oligonucleotides, we followed a rescue-of-function strategy by transfecting siMYADM 2, which targets the 3′ untranslated region of MYADM mRNA, in wild-type HeLa cells or in HeLa cells stably expressing MYADM-GFP (Aranda *et al.*, 2011). The MYADM-GFP transcript lacks the 3′ untranslated region and is thus resistant to siMYADM 2–mediated knockdown. siMYADM 2 transfection induced ICAM-1 expression only in parental HeLa cells, whereas, as predicted, no changes were observed in cells stably expressing MYADM-GFP (Figure 4).

MYADM controls endothelial barrier function and ICAM-1 expression. We next addressed whether alteration of endothelial barrier function in MYADM knockdown (KD) cells is a consequence of such receptor increase. HUVECs were transfected with control siRNA, siRNA targeting either MYADM (siMYADM 2) or ICAM-1, or both simultaneously (Figure 5A), and subjected to calcium-switch experiments in an ECIS platform in order to analyze barrier dynamics (Figure 5B). Barrier formation was impaired in MYADM knockdown cells, whereas cells undergoing double silencing for MYADM and ICAM-1 restored endothelial barrier upon calcium replenishment, with dynamics comparable with control cells. In accordance, analysis of β-catenin staining showed that ICAM-1 reduction ameliorates the loss of cell–cell junction integrity in MYADM knockdown cells (Figure 5, C and D). These experiments indicate that increased ICAM-1 expression mediates endothelial barrier reduction upon MYADM knockdown.

MYADM knockdown increases ERM phosphorylation

MYADM colocalizes with the cortical actin cytoskeleton and regulates ordered membrane domains at the plasma membrane (Aranda *et al.*, 2011). We hypothesized that MYADM controls the inflammatory status by regulating proteins involved in plasma membrane and/or cortical actin organization of endothelial cells (Viola and Gupta, 2007). Activation of ERM proteins, connectors between the plasma membrane and the cytoskeleton, increases permeability in microvascular endothelial cells during the inflammatory response (Koss *et al.*, 2006), so we tested the effect of MYADM knockdown on ERM phosphorylation at a specific threonine residue that is required for their conformational change and subsequent activation. Western blotting with an antibody recognizing phosphorylated ezrin (T567), radixin (T564), and moesin (T558) revealed that MYADM silencing increased ERM phosphorylation two- to threefold (Figure 6, A and B). Confocal analysis of MYADM-depleted cells confirmed an increase in phosphorylated ERMs at the plasma membrane (Figure 6C). Both in control and MYADM-depleted cells, pERM appeared particularly enriched in junctional membrane projections, often connecting two adjacent cells. The length of these border protrusions increased in response to MYADM knockdown (Figure 6C, arrowheads, and D). We then examined whether ERM phosphorylation can contribute to endothelial barrier dysfunction. Transfection of a constitutive active form of ERMs (moesin T558D) caused a moderate decrease of cell–cell junction integrity, whereas moesin T558A mutant, which is proposed to be in a closed, inactive conformation, did not significantly alter the distribution of the junctional marker β-catenin (Figure 6, E and F).

ICAM-1 expression increases in response to MYADM reduction or TNF-α requires ERM expression

We then examined whether ERM proteins mediate ICAM-1 protein increase caused by MYADM knockdown. Cells were transfected with control siRNA or siRNA targeting MYADM (siMYADM 2), ERM proteins (siE+R+M), or both (Figures 7A and S5, A and B). MYADM single knockdown increased ICAM-1, whereas simultaneous silencing of MYADM and ERM proteins reduced ICAM-1 to control levels (Figure 7, A and B). In MYADM-depleted cells, single knockdown of ezrin, radixin, and moesin reduced ICAM-1 expression to a lesser extent than simultaneous triple-ERM silencing (Figure S5C). These findings indicate that the three proteins are playing additive roles. Accordingly, ERM knockdown diminished the increase in leukocyte adhesion caused by MYADM depletion (Figure 7C). Triple-ERM knockdown diminished barrier integrity in control cells, due probably to the essential role of these cross-linker proteins in connecting membrane to subcortical cytoskeleton, so no rescue of function could be performed following this strategy. Together our data indicate that MYADM reduction induces a proinflammatory-like phenotype by regulating ERM protein phosphorylation and ICAM-1 expression. Several protein kinases can potentially regulate ERM phosphorylation in this particular threonine residue. Among them, classical protein kinase C (PKC) family members, serine/threonine kinases that require a proper translocation from the cytosol to the plasma membrane and

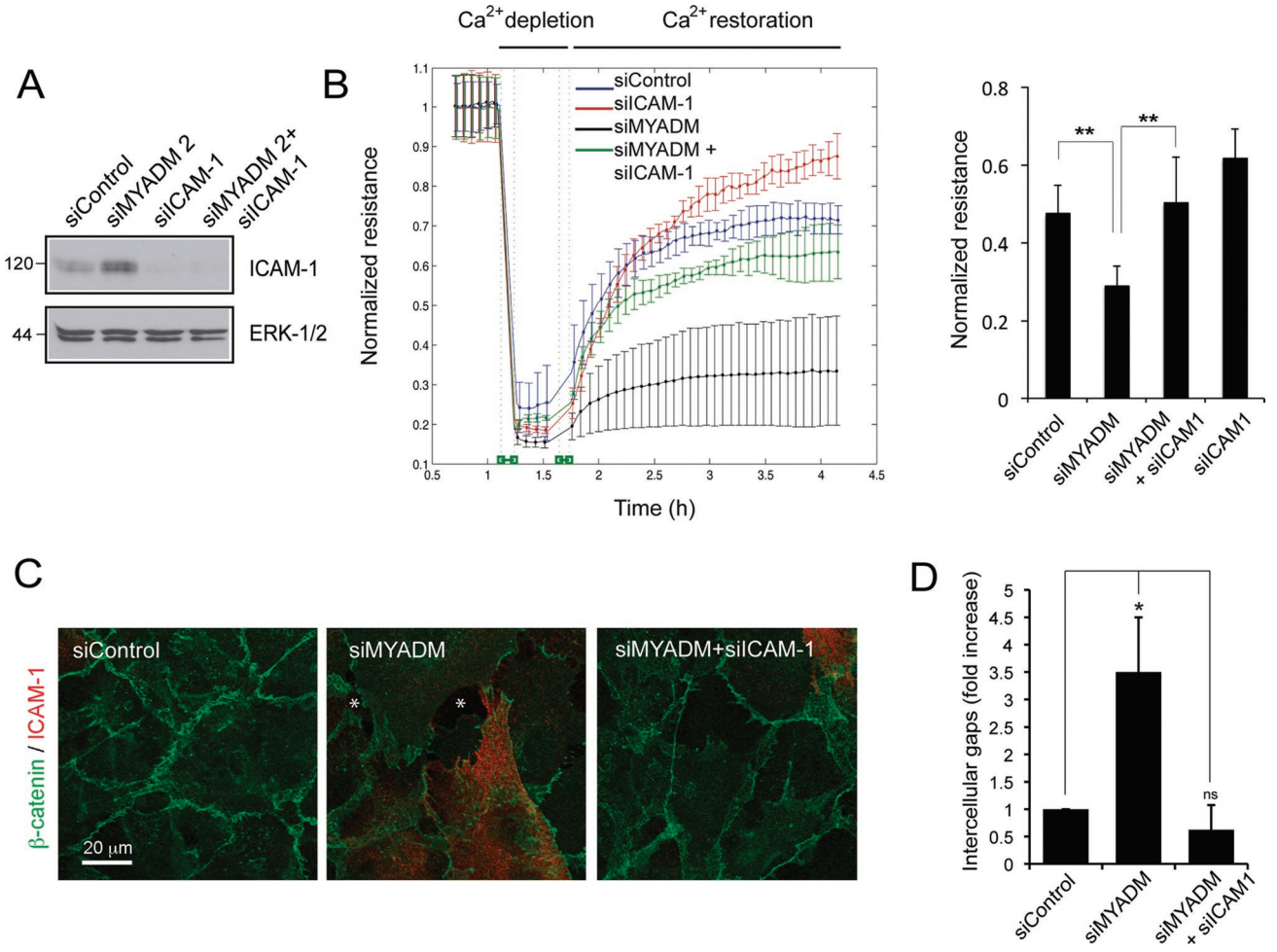

FIGURE 5: ICAM-1 knockdown prevents alteration of endothelial barrier function in response to MYADM reduction. HUVECs were transfected with the indicated siRNAs for 72 h. (A) Western blot analysis of ICAM-1 expression. ERK 1/2 is shown as a loading control. (B) Dynamics of barrier function in siRNA-transfected cells. Normalized transendothelial electrical resistance (TEER) of cells subjected to calcium switch in order to observe barrier formation. Right, quantitation of normalized resistance 60 min after calcium switch. The mean + SEM of three independent experiments with duplicate readings is shown. **, $p > 0.02$. (C) Cells were fixed and stained with β-catenin– and ICAM-1–specific antibodies. Asterisks in images indicate intercellular gaps. (D) Quantitation of intercellular gaps found in siRNA-transfected cells. Thirty images containing around 30 cells each were quantitated. The mean + SEM is shown. *, $p < 0.05$.

control endothelial barrier function (Hempel *et al.*, 1997), have been shown to phosphorylate ERM proteins in different cellular contexts (Ng *et al.*, 2001; Ivetic and Ridley, 2004; Adyshev *et al.*, 2011). We addressed whether increased ERM phosphorylation in response to MYADM reduction is dependent on PKC by using a specific inhibitor for this family of kinases. Incubation with Gö6976 for 8 h partially reduced ERM phosphorylation increase in MYADM siRNA–transfected cells, which suggests that MYADM is involved in regulating classical PKC-mediated activation of ERM proteins at the plasma membrane (Figure 7D). Together these results are compatible with a role for MYADM organizing endothelial plasma membrane and thereby regulating the membrane targeting of proteins, such as classical PKCs, that control subcortical protein machinery. Finally, we investigated whether ERM can also regulate ICAM-1 expression in a more physiological context. TNF-α is a proinflammatory cytokine that induces ICAM-1 expression and ERM phosphorylation (Koss *et al.*, 2006; Figure 7, E and F). Triple-ERM knockdown reduced ICAM-1 increment upon TNF-α exposure (Figure 7, G and H). In contrast, MYADM knockdown did not exacerbate ICAM-1 increase in response to this cytokine (Figure 7, I and J), and TNF-α did not significantly alter MYADM levels (Figure S6). Therefore these results indicate that ERM also regulates ICAM-1 expression in response to physiological inflammatory signaling. Collectively our data suggest that a connection between endothelial membrane and cortical actin cytoskeleton modulates the inflammatory response.

DISCUSSION

Membrane rafts are cholesterol-enriched ordered domains that regulate a plethora of signaling pathways. Cytokines such as TNF-α (Muppidi *et al.*, 2004) and IL-1β (Oakley *et al.*, 2009) or bacterial ligands of Toll-like-receptors (Soong *et al.*, 2004; Triantafilou *et al.*, 2010) induce proinflammatory signals through membrane rafts. Moreover, modulation of cholesterol content in these domains can induce or decrease inflammatory signaling in different cell models (Legler *et al.*, 2003; Flemming *et al.*, 2004; Meng *et al.*, 2010). Collectively these observations suggest that modulation of membrane condensation may itself contribute to the endothelial inflammatory response, probably by mimicking those changes in

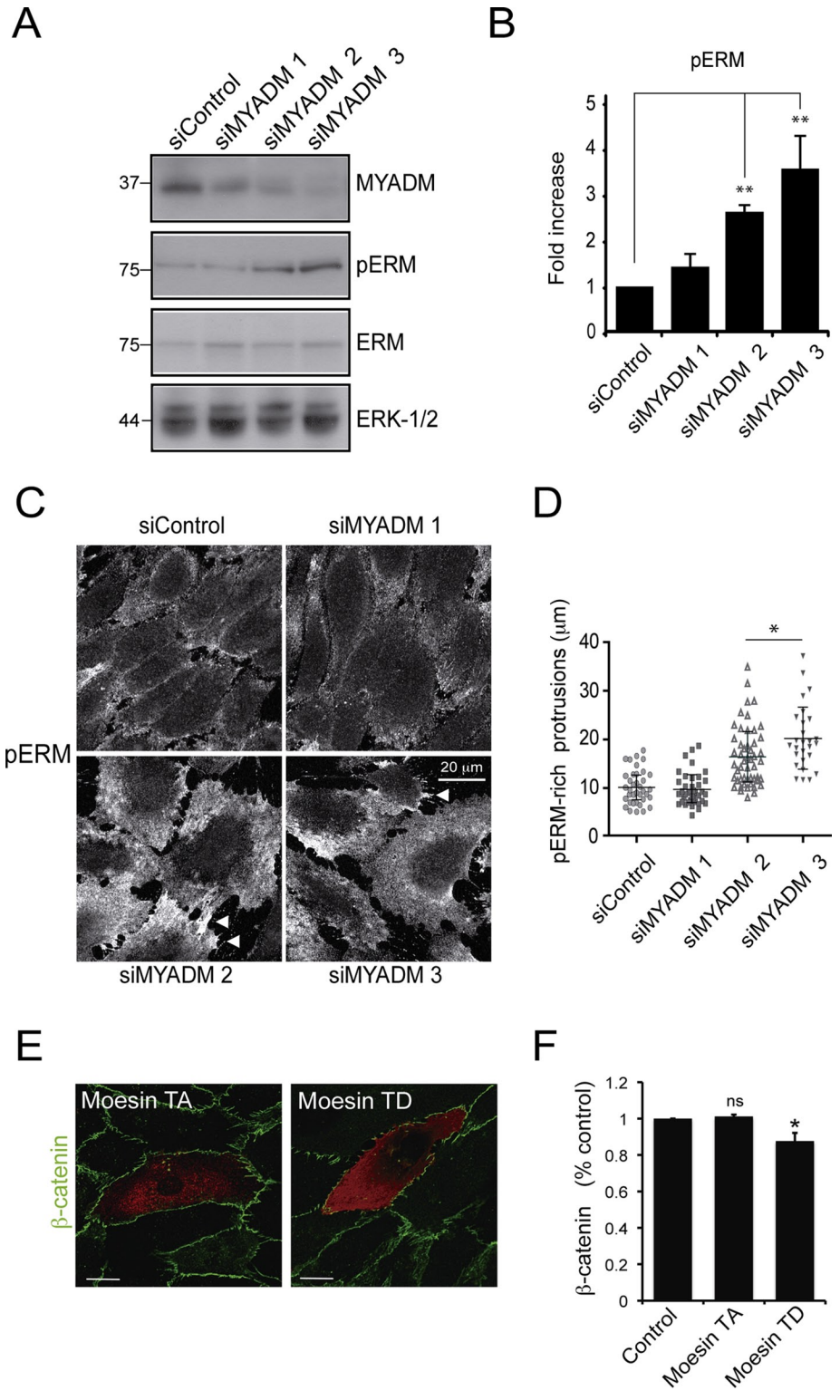

FIGURE 6: MYADM knockdown activates ERM proteins. (A) HUVECs were transfected with the indicated siRNAs for 72 h, and ERM activation was monitored by Western blot with anti-pE(T567)R(T564)M(T558)–specific antibody (pERM) and anti-ERM protein antibody. (B) Quantitation of pERM activation was performed by measuring the ratio of anti-pERM to ERM blotting signal. The mean + SEM from three independent experiments is shown. (C and D) HUVECs were transfected as in (A) and fixed with 10% trichloroacetic acid, and pERM distribution was analyzed by immunofluorescence. Arrowheads indicate the pERM-rich protrusions (C), with their lengths quantitated in (D). (E) The HA-tagged moesin mutants, moesin T558A (TA), in an inactive conformation, or moesin T558D (TD), constitutively active, were transiently expressed in HUVECs for 48 h. Cells were fixed and stained with anti-HA and anti–β-catenin antibodies to detect transfected cells and cell–cell junctions, respectively. (F) Quantitation of β-catenin intensity of transfected cells normalized to the intensity of adjacent cells (control). Five hundred thirty regions from 53 transfected cells were analyzed in three different experiments. The mean + SEM is shown. *, $p < 0.05$.

clustering or diffusion that different stimuli can induce on protein signaling machinery associated with the plasma membrane. This could be important for chronic inflammatory diseases such as arteriosclerosis, which is triggered by deregulation of homeostasis of raft lipids, as is seen in hypercholesterolemia (Libby, 2002). However, ordered membrane microdomains require protein scaffolds to play specific roles within the cell (Bauer and Pelkmans, 2006). The MAL proteins contain one or two tetra-spanning MARVEL (MAL and related proteins for vesicle trafficking and membrane link) domains that are involved in membrane apposition (Sanchez-Pulido *et al.*, 2002). Different experimental strategies have shown that these proteins have the ability to modulate membrane order or dynamics in a variety of cell types (Puertollano *et al.*, 1997; Goldstein Magal *et al.*, 2009; Aranda *et al.*, 2011). As a consequence, these proteins control the segregation into membrane rafts of signaling proteins, such as the tyrosine kinase Lck (Anton *et al.*, 2008) or the Rho GTPase Rac-1 (Aranda *et al.*, 2011). In this paper, we show that, of the three MAL family proteins with a reported role in raft-mediated function, only MYADM is expressed in endothelial cells. MYADM is also the only member of the MAL family containing two MARVEL domains, rather than one. This feature seems to determine its predominant localization at the plasma membrane, rather than in vesicular compartments (Aranda *et al.*, 2011), although MYADM trafficking has yet to be defined. On the other hand, colocalization analysis clearly shows that MYADM-containing domains are different than those of caveolae or GPI-anchored proteins in endothelial cells, in agreement with our previous studies in other cell types or with other MAL family proteins (Millán *et al.*, 1997; Aranda *et al.*, 2011).

ERM proteins are cross-linkers between transmembrane receptors and cortical actin filaments that regulate the structure and function of specific domains at the cell surface, namely microvilli or filopodia, and fundamental signaling processes involved in cell shape, junctional stability, motility, and cytokinesis (Fehon *et al.*, 2010). Cytokines, such as IL-1β

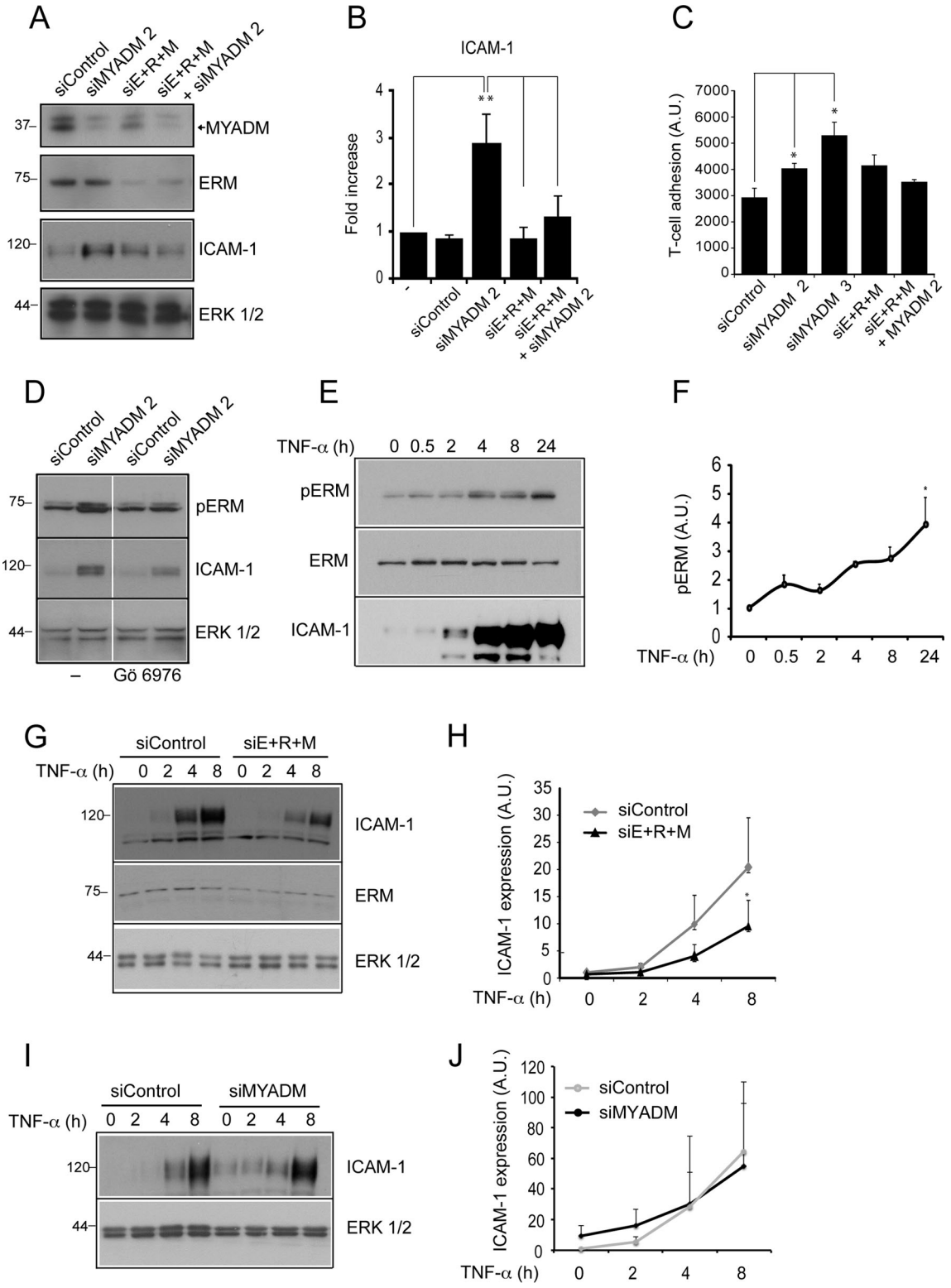

FIGURE 7: ERM knockdown prevents ICAM-1 induction mediated by MYADM knockdown or TNF-α. (A) HUVECs were transfected with the indicated siRNAs for 72 h, and MYADM, ERM, and ICAM-1 expression was analyzed by Western blotting. (B) Quantitation of ICAM-1 levels in siRNA-transfected cells. (C) siRNA-transfected HUVECs were plated at confluence, and adhesion assays were performed 72 h after transfection. The mean + SEM from three independent experiments is shown. (D) HUVECs were transfected with the indicated siRNAs for 72 h. Eight hours before lysis, cells were incubated or not with 100 nm of the PKC inhibitor Gö6976. Subsequently MYADM, ERM, and ICAM-1 expression was analyzed by Western blotting. (E and F) HUVECs were stimulated at different times with TNF-α, lysed, and immunoblotted for the indicated antibodies. (G–J) siRNA-transfected HUVECs were stimulated at different times with TNF-α, lysed, and immunoblotted for the indicated antibodies. Graphs show the mean ± SEM from three independent experiments (H and J). *, $p < 0.05$; **, $p < 0.01$.

and TNF-α, or sphingosine 1-phosphate (S1P), all of which are involved in the regulation of the inflammatory response, can also activate ERM proteins (Koss *et al.*, 2006; Adyshev *et al.*, 2011; Huang *et al.*, 2011). This activation, at least for TNF-α and S1P, mediates changes in endothelial barrier function, with different outcomes depending on the stimulus. Ordered domains at the plasma membrane and ERM proteins have thus been independently implicated in inflammation. In this study, we demonstrate that siRNA-mediated modulation of MYADM is sufficient to induce activation of ERM proteins, and this can act as a signal to alter barrier function and to provoke an inflammatory-like response in the absence of inflammatory stimuli. As the immunofluorescence analysis indicates, ERM activation occurs at the plasma membrane and at cell borders. A previous example of cross-regulation between rafts and ERM proteins at the plasma membrane has been reported in B-cells, in which ezrin can modulate the dynamics of ordered domains and their ability to contribute to B-cell receptor (BCR) signaling (Gupta *et al.*, 2006; Viola and Gupta, 2007). Gupta *et al.* (2006) proposed that, in resting B-cells, active ezrin maintains small raft domains that contain signaling molecules and are linked to cortical F-actin and dispersed on the cell surface. On BCR activation, ezrin becomes transiently inactivated and uncouples actin from the plasma membrane domains. These small rafts then coalesce and promote downstream B-cell signaling. It is therefore plausible that membrane rafts, which are regulated by MYADM, in coordination with the ERM proteins, which connect rafts to the subcortical cytoskeleton, could mediate clustering, diffusion or localization of proteins involved in signaling from inflammatory agonists in endothelial or epithelial cells. In accordance, we have found that, at least for TNF-α, a complete inflammatory response requires ERM protein expression. MYADM was not modulated by TNF-α, and its reduction had no effect on TNF-α–mediated ICAM-1 induction. The identification of the stimuli that act through MYADM and ERM proteins to promote or inhibit inflammation will be important to increase our understanding of the endothelial inflammatory response.

ERMs are involved in the inflammatory control of protein expression (Kishore *et al.*, 2005) and in connecting adhesion receptors, such as the ICAM family, to subcortical actin (Viola and Gupta, 2007; Reglero-Real *et al.*, 2012). In this paper, we show that ERM expression is required for ICAM-1 expression in response to MYADM suppression or TNF-α. ICAM-1 is a paradigmatic adhesion receptor that regulates leukocyte adhesion. However, its role as a protein essential for controlling endothelial permeability both in vivo and in vitro is emerging (Clark *et al.*, 2007; Sumagin *et al.*, 2008). MYADM knockdown selectively increases ICAM-1 expression, but not many other proteins involved in barrier function, which indicates this protein selectively controls some but not all of the pathways involved in the endothelial inflammatory response. ICAM-1 increase is necessary for MYADM-mediated alteration of barrier properties, which is in agreement with previous reports that link leukocyte adhesion and permeability through dual roles played by ICAM-1 (Clark *et al.*, 2007; Sumagin *et al.*, 2008), VCAM-1 (van Wetering *et al.*, 2003), or PECAM-1 (Graesser *et al.*, 2002; Fernandez-Martin *et al.*, 2012) receptors.

Regulation of the interaction between the plasma membrane and the underlying cytoskeleton is also essential in mechanotransduction (Chien, 2007). Cholesterol-rich membrane domains are required for signaling propagated by mechanic forces induced by shear stress (Yamamoto *et al.*, 2003) or stretch (Zeidan *et al.*, 2003). Laminar shear stress elicits proinflammatory signals that promote ICAM-1 up-regulation in vitro (Tzima *et al.*, 2002). Pathological alteration of these forces in vivo, such as disturbed blood flow, are proinflammatory and proatherogenic (Chien, 2007). It is therefore possible that membrane and actin reorganization induced by MYADM knockdown regulates pathways related to cell stiffness and mechanotransduction. Finally, further understanding of the structure of membrane ordered domains, their protein machinery, and their involvement in inflammatory signaling could lead to the design of new therapies for chronic inflammatory diseases.

MATERIALS AND METHODS

Materials

Monoclonal antibody to human MYADM (mAb 2B12) was generated as previously described (Aranda *et al.*, 2011). Rabbit anti–ICAM-1, anti–caveolin-1 (N-20), and anti-ERK1/2 antibodies were obtained from Santa Cruz Biotechnology (Santa Cruz, CA). Mouse anti–ICAM-1 antibody was from R&D Systems (Abingdon, UK). Mouse monoclonal anti–VE-cadherin antibody was from BD Biosciences (San Jose, CA). Rabbit anti–β-catenin and TRITC/FITC–phalloidin was from Sigma-Aldrich (St. Louis, MO). Anti–transferrin receptor antibodies were purchased from Zymed (San Francisco, CA). Anti-ERM, anti–phospho-ERM, and specific anti-ezrin, anti-radixin, and anti-moesin antibodies were from Cell Signaling Technology (Boston, MA). Hemagglutinin (HA)-tagged moesin-TD (T558D) and moesin-TA (T558A) were from J. Dêlon (Université René Descartes, Paris, France).

Cell culture and transfection

HUVECs were obtained and cultured as previously described (Millán *et al.*, 2010) and were always plated at confluency on fibronectin-coated dishes for 24–72 h. HeLa, MDCK, and PC3 cells were obtained from the American Type Culture Collection (Manassas, VA) and grown in DMEM supplemented with 5% fetal bovine serum. Isolation of HeLa clones stably expressing MYADM-GFP and human memory T-cells for adhesion assays has been described elsewhere (Millán *et al.*, 2006; Aranda *et al.*, 2011). HUVECs were transiently transfected with 1–5 μg plasmid DNA/10^6 cells with calcium phosphate and used for experiments 24–72 h after transfection. For siRNA transfection, we devised a protocol for delivery of siRNA with high efficiency into primary endothelial cells that is a modification of our previous method (Millán *et al.*, 2006). HUVECs were plated at subconfluence (10^5 cells on each well of a six-well dish) in EBM-2 medium (Lonza, Walkersville, MD) with no antibiotics. The following day, cells were transfected by mixing 4 μl of oligofectamine (Invitrogen, Carlsbad, CA) with siRNA to a final concentration of 100 nM. At 24 h after transfection, cells were trypsinized and plated at confluence onto different dishes for parallel assays, such as permeability, adhesion, immunofluorescence, or Western blotting. Assays were performed 72 h after transfection. Sequences of siRNA duplexes targeting MYADM were 5′-CGAGATCACTGGCTATATG-3′ (siMYADM 1), 5′-GATGTAAGCTGCAGCCGCA-3′ (siMYADM 2), and 5′GGTCTAAGACTCTCCCAAG-3′ (siMYADM 3). Ezrin was targeted with the siRNA oligonucleotide 5′-CAAGAAGGCACCUGACUUU-3′, moesin with 5′-AUAAGGAAGUGCAUAAGUC-3′, and radixin with 5′-GAACUGGCAUGAAGAACAU-3′. Sequences of siRNA controls were obtained from Dharmacon (Lafayette, CO)

DRM isolation

Different cell lines and HUVECs grown to confluence in 100-mm dishes were lysed for 20 min in 1 ml of 25 mM Tris-HCl (pH 7.5), 150 mM NaCl, 5 mM EDTA, 1% Triton X-100, 4°C, as indicated (Millán *et al.*, 2002). DRM fraction was isolated by centrifugation to equilibrium in a sucrose discontinuous density gradient in a swinging bucket SW40 rotor (Beckman Coulter, Brea, CA) at 39,000 rpm (188,000 × *g*) for 20 h (Brown and Rose, 1992; Millán *et al.*, 2006). Fractions were harvested from the bottom sucrose layer (40%; soluble) and from the above interphase between 5 and 30% sucrose

layers (DRMs). Equivalent aliquots were subjected to immunoblot analysis with the appropriate antibodies.

ICAM-1 cross-linking and immunofluorescence

Anti–ICAM-1 antibody (1 µg/ml) was added to TNF-α–stimulated HUVECs for 45 min. Cells were rinsed and incubated with 1 µg/ml of fluorophore-coupled secondary antibody for 30 min to induce receptor clustering. Cells were rinsed and fixed with 4% paraformaldehyde for 20 min, blocked with TBS (25 mM Tris, pH 7.4, 150 mM NaCl) for 10 min, permeabilized for 5 min with phosphate-buffered saline (PBS) containing 0.2% Triton X-100 at 4°C, and incubated at 37°C with tetramethylrhodamine isothiocyanate (TRITC)-labeled phalloidin to visualize F-actin. Specimens were mounted in DAKO fluorescent mounting medium (DAKO, Ely, UK). For immunofluorescence analysis of adhered T-cells, unlabeled T-cells were added to transfected HUVECs stimulated with TNF-α for 6 h. Cells were fixed and stained with the indicated antibodies and with TRITC–phalloidin to visualize T-cells. For F-actin quantification, confocal images from cells stained for TRITC-labeled phalloidin were exported in formats compatible with ImageJ software (http://rsb.info.nih.gov/ij). ImageJ was used to obtain the mean fluorescence intensities from different images of confluent cells.

Adhesion assays

Starved memory T-cells were labeled with 2′,7′,-*bis*-(2-carboxyethyl)-5-(and-6)-carboxyfluorescein, acetoxymethyl ester (Molecular Probes, Eugene, OR) in serum-free medium for 20 min, washed with medium containing 1% BSA, and incubated for 15 min at 37°C with confluent HUVECs previously transfected with different siRNAs. Nonadhered cells were washed off, and adhesion was determined by fluorescence measurement in a Fusion α-FS fluorimeter (Perkin Elmer-Cetus, Waltham, MA). Data were processed and statistical significance was determined using Student's *t* test (Microsoft Excel; Redmond, WA). For immunofluorescence analysis of adhered T-cells, unlabeled T-cells were added to transfected HUVECs stimulated with TNF-α for 6 h. Cells were fixed and stained with TRITC–phalloidin (to visualize T-cells) and with the indicated antibodies.

Permeability assays

Permeability assays were carried out as previously described (McKenzie and Ridley, 2007). siRNA-transfected HUVECs were plated at confluence on fibronectin-coated Transwells of 0.4-µm diameter. FITC-dextran (Mr 42,000; Sigma–Aldrich) was applied apically at 0.1 mg/ml and allowed to equilibrate for 60 min before a sample of the medium was removed from the lower chamber to measure fluorescence in the Fusion α-FS fluorimeter. The arithmetic mean, SE, and statistical significance corresponding to a Student's *t* test were calculated in Microsoft Excel. Alternatively, real-time permeability assays were performed using an electric cell-substrate impedance sensing system (ECIS 1600R; Applied Biophysics, Troy, NY) as previously described (Fernandez-Martin *et al.*, 2012). Briefly, 2×10^5 cells/cm^2, previously transfected with the indicated siRNA oligonucleotides, were plated in a well precoated with fibronectin (200 mg/ml) and containing 10 small-fold electrodes and a counter-electrode (8W10E arrays; IBIDI, Martinsried, Germany). After 48 h at confluency, transendothelial electrical resistance (TEER) was measured in each well (4000-Hz frequency). The TEER analysis included basal measurements during the first 2 to 4 h, followed by a calcium-switch assay in which cells were incubated in PBS for 20 min and the calcium levels were subsequently restored by replenishment with normal EBM-2 medium. Data were normalized to the mean resistance detected before the calcium switch.

qPCR analysis

One microgram of RNA from HUVECs, PC3, Jurkat, and HepG2 cell lines was subjected to reverse transcription with the High Capacity RNA-cDNA kit (Applied Biosystems, Bedford, MA). qPCR was performed from the resulting cDNA in a thermocycler CFX 384 (Bio-Rad, Hercules, CA) using the SsoFast EvaGreen Supermix (Bio-Rad) and the following forward and reverse primers, previously designed with Probefinder software (Roche Diagnostics, Indianapolis, IN): MAL2, 5′-GACATCCTGCGGACCTACTC-3′; 5′-AGACAAGACCCCCGAACAG-3′. MYADM, 5′-GCCATCTGCTTCATCCTAGC-3′; 5′-TAGCACGTTGGTGCACTCC-3′. MAL, 5′-AGACTTCCTGGGTCACCTTG-3′; 5′-CGTCTTGCATCGTGATGGT-3′. Parallel qPCR from β-actin and GADPH was performed to normalize data from each cell type with the following primers: β-actin, 5′-CAGGCACCAGGGCGTG-3′; 5′-GTGAGGATGCCTCTCTTGCTCT-3′. GADPH, 5′-AGCCACATCGCTCAGACAC-3′; 5′-CGCCCAATACGACCAAAT-3′.

ACKNOWLEDGMENTS

This work was supported by grants SAF2011–22624 (to J.M.), BFU2012–32532 and CSD2009–00016 (to M.A.A.), and BFU2011-22859 (to I.C.) from the Ministerio de Ciencia e Innovación; and grant S2010/BMD-2305 from the Comunidad de Madrid (to I.C.). J.F.A. was the recipient of an EMBO short-term fellowship in A.J.R.'s laboratory. We thank Severine Gharbi for the critical reading of the manuscript. The expert technical advice of the personnel of the Optical and Confocal Microscopy and Genomic Facilities (CBMSO, Madrid) is gratefully acknowledged.

REFERENCES

Adyshev DM, Moldobaeva NK, Elangovan VR, Garcia JG, Dudek SM (2011). Differential involvement of ezrin/radixin/moesin proteins in sphingosine 1-phosphate-induced human pulmonary endothelial cell barrier enhancement. Cell Signal 23, 2086–2096.

Albelda SM (1991). Endothelial and epithelial cell adhesion molecules. Am J Respir Cell Mol Biol 4, 195–203.

Anton O, Batista A, Millán J, Andres-Delgado L, Puertollano R, Correas I, Alonso MA (2008). An essential role for the MAL protein in targeting Lck to the plasma membrane of human T lymphocytes. J Exp Med 205, 3201–3213.

Anton OM, Andres-Delgado L, Reglero-Real N, Batista A, Alonso MA (2011). MAL protein controls protein sorting at the supramolecular activation cluster of human T lymphocytes. J Immunol 186, 6345–6356.

Aranda JF, Reglero-Real N, Kremer L, Marcos-Ramiro B, Ruiz-Saenz A, Calvo M, Enrich C, Correas I, Millán J, Alonso MA (2011). MYADM regulates Rac1 targeting to ordered membranes required for cell spreading and migration. Mol Biol Cell 22, 1252–1262.

Bauer M, Pelkmans L (2006). A new paradigm for membrane-organizing and -shaping scaffolds. FEBS Lett 580, 5559–5564.

Bretscher A, Edwards K, Fehon RG (2002). ERM proteins and merlin: integrators at the cell cortex. Nat Rev Mol Cell Biol 3, 586–599.

Brown DA, Rose JK (1992). Sorting of GPI-anchored proteins to glycolipid-enriched membrane subdomains during transport to the apical cell surface. Cell 68, 533–544.

Carman CV, Springer TA (2004). A transmigratory cup in leukocyte diapedesis both through individual vascular endothelial cells and between them. J Cell Biol 167, 377–388.

Chidlow JH, Jr., Sessa WC (2010). Caveolae, caveolins, and cavins: complex control of cellular signalling and inflammation. Cardiovasc Res 86, 219–225.

Chien S (2007). Mechanotransduction and endothelial cell homeostasis: the wisdom of the cell. Am J Physiol Heart Circ Physiol 292, H1209–H1224.

Clark PR, Manes TD, Pober JS, Kluger MS (2007). Increased ICAM-1 expression causes endothelial cell leakiness, cytoskeletal reorganization and junctional alterations. J Invest Dermatol 127, 762–774.

de Marco MC, Martin-Belmonte F, Kremer L, Albar JP, Correas I, Vaerman JP, Marazuela M, Byrne JA, Alonso MA (2002). MAL2, a novel raft protein of the MAL family, is an essential component of the machinery for transcytosis in hepatoma HepG2 cells. J Cell Biol 159, 37–44.

Fehon RG, McClatchey AI, Bretscher A (2010). Organizing the cell cortex: the role of ERM proteins. Nat Rev Mol Cell Biol 11, 276–287.
Fernandez-Martin L, Marcos-Ramiro B, Bigarella CL, Graupera M, Cain RJ, Reglero-Real N, Jimenez A, Cernuda-Morollon E, Correas I, Cox S, Ridley AJ, Millán J (2012). Crosstalk between reticular adherens junctions and platelet endothelial cell adhesion molecule-1 regulates endothelial barrier function. Arterioscler Thromb Vasc Biol 32, e90–e102.
Flemming JA, Perkins KH, Luus L, Ferguson AR, Corley RB (2004). Disruption of membrane cholesterol stimulates MyD88-dependent NF-κB activation in immature B cells. Cell Immunol 229, 68–77.
Goldstein Magal L, Yaffe Y, Shepshelovich J, Aranda JF, de Marco MD, Gaus K, Alonso MA, Hirschberg K (2009). Clustering and lateral concentration of raft lipids by the MAL protein. Mol Biol Cell 20, 3751–3762.
Graesser D, Solowiej A, Bruckner M, Osterweil E, Juedes A, Davis S, Ruddle NH, Engelhardt B, Madri JA (2002). Altered vascular permeability and early onset of experimental autoimmune encephalomyelitis in PECAM-1-deficient mice. J Clin Invest 109, 383–392.
Gupta N, Wollscheid B, Watts JD, Scheer B, Aebersold R, DeFranco AL (2006). Quantitative proteomic analysis of B cell lipid rafts reveals that ezrin regulates antigen receptor-mediated lipid raft dynamics. Nat Immunol 7, 625–633.
Hempel A, Maasch C, Heintze U, Lindschau C, Dietz R, Luft FC, Haller H (1997). High glucose concentrations increase endothelial cell permeability via activation of protein kinase Cα. Circ Res 81, 363–371.
Heyraud S, Jaquinod M, Durmort C, Dambroise E, Concord E, Schaal JP, Huber P, Gulino-Debrac D (2007). Contribution of annexin 2 to the architecture of mature endothelial adherens junctions. Mol Cell Biol 28, 1657–1668.
Huang H *et al.* (2011). Increased phosphorylation of ezrin/radixin/moesin proteins contributes to proliferation of rheumatoid fibroblast-like synoviocytes. Rheumatology (Oxford) 50, 1045–1053.
Ivetic A, Ridley AJ (2004). Ezrin/radixin/moesin proteins and Rho GTPase signalling in leucocytes. Immunology 112, 165–176.
Johnson CM, Chichili GR, Rodgers W (2008). Compartmentalization of phosphatidylinositol 4,5-bisphosphate signaling evidenced using targeted phosphatases. J Biol Chem 283, 29920–29928.
Keuschnigg J, Henttinen T, Auvinen K, Karikoski M, Salmi M, Jalkanen S (2009). The prototype endothelial marker PAL-E is a leukocyte trafficking molecule. Blood 114, 478–484.
Kishore R, Qin G, Luedemann C, Bord E, Hanley A, Silver M, Gavin M, Yoon YS, Goukassian D, Losordo DW (2005). The cytoskeletal protein ezrin regulates EC proliferation and angiogenesis via TNF-alpha-induced transcriptional repression of cyclin A. J Clin Invest 115, 1785–1796.
Koss M, Pfeiffer GR, II, Wang Y, Thomas ST, Yerukhimovich M, Gaarde WA, Doerschuk CM, Wang Q (2006). Ezrin/radixin/moesin proteins are phosphorylated by TNF-α and modulate permeability increases in human pulmonary microvascular endothelial cells. J Immunol 176, 1218–1227.
Kwiatkowska K (2010). One lipid, multiple functions: how various pools of PI(4,5)P(2) are created in the plasma membrane. Cell Mol Life Sci 67, 3927–3946.
Legler DF, Micheau O, Doucey MA, Tschopp J, Bron C (2003). Recruitment of TNF receptor 1 to lipid rafts is essential for TNFα-mediated NF-κB activation. Immunity 18, 655–664.
Libby P (2002). Inflammation in atherosclerosis. Nature 420, 868–874.
Lingwood D, Simons K (2010). Lipid rafts as a membrane-organizing principle. Science 327, 46–50.
McKenzie JA, Ridley AJ (2007). Roles of Rho/ROCK and MLCK in TNF-α-induced changes in endothelial morphology and permeability. J Cell Physiol 213, 221–228.
Meng G, Liu Y, Lou C, Yang H (2010). Emodin suppresses lipopolysaccharide-induced pro-inflammatory responses and NF-κB activation by disrupting lipid rafts in CD14-negative endothelial cells. British J Pharmacol 161, 1628–1644.
Millán J, Cain RJ, Reglero-Real N, Bigarella C, Marcos-Ramiro B, Fernandez-Martin L, Correas I, Ridley AJ (2010). Adherens junctions connect stress fibres between adjacent endothelial cells. BMC Biol 8, 11.
Millán J, Hewlett L, Glyn M, Toomre D, Clark P, Ridley AJ (2006). Lymphocyte transcellular migration occurs through recruitment of endothelial ICAM-1 to caveola- and F-actin-rich domains. Nat Cell Biol 8, 113–123.
Millán J, Montoya MC, Sancho D, Sanchez-Madrid F, Alonso MA (2002). Lipid rafts mediate biosynthetic transport to the T lymphocyte uropod subdomain and are necessary for uropod integrity and function. Blood 99, 978–984.
Millán J, Puertollano R, Fan L, Alonso MA (1997). Caveolin and MAL, two protein components of internal detergent-insoluble membranes, are in distinct lipid microenvironments in MDCK cells. Biochem Biophys Res Commun 233, 707–712.
Millán J, Ridley AJ (2005). Rho GTPases and leucocyte-induced endothelial remodelling. Biochem J 385, 329–337.
Muppidi JR, Tschopp J, Siegel RM (2004). Life and death decisions: secondary complexes and lipid rafts in TNF receptor family signal transduction. Immunity 21, 461–465.
Ng T *et al.* (2001). Ezrin is a downstream effector of trafficking PKC-integrin complexes involved in the control of cell motility. EMBO J 20, 2723–2741.
Oakley FD, Smith RL, Engelhardt JF (2009). Lipid rafts and caveolin-1 coordinate interleukin-1β (IL-1β)-dependent activation of NFκB by controlling endocytosis of Nox2 and IL-1β receptor 1 from the plasma membrane. J Biol Chem 284, 33255–33264.
Palade GE, Simionescu M, Simionescu N (1979). Structural aspects of the permeability of the microvascular endothelium. Acta Physiol Scand 463, 11–32.
Pober JS, Sessa WC (2007). Evolving functions of endothelial cells in inflammation. Nat Rev Immunol 7, 803–815.
Prag S *et al.* (2007). Activated ezrin promotes cell migration through recruitment of the GEF Dbl to lipid rafts and preferential downstream activation of Cdc42. Mol Biol Cell 18, 2935–2948.
Puertollano R, Li S, Lisanti MP, Alonso MA (1997). Recombinant expression of the MAL proteolipid, a component of glycolipid-enriched membrane microdomains, induces the formation of vesicular structures in insect cells. J Biol Chem 272, 18311–18315.
Puertollano R, Martin-Belmonte F, Millán J, de Marco MC, Albar JP, Kremer L, Alonso MA (1999). The MAL proteolipid is necessary for normal apical transport and accurate sorting of the influenza virus hemagglutinin in Madin-Darby canine kidney cells. J Cell Biol 145, 141–151.
Reglero-Real N, Marcos-Ramiro B, Millán J (2012). Endothelial membrane reorganization during leukocyte extravasation. Cell Mol Life Sci 69, 3079–3099.
Ritchie K, Iino R, Fujiwara T, Murase K, Kusumi A (2003). The fence and picket structure of the plasma membrane of live cells as revealed by single molecule techniques (review). Mol Membr Biol 20, 13–18.
Sanchez-Pulido L, Martin-Belmonte F, Valencia A, Alonso MA (2002). MARVEL: a conserved domain involved in membrane apposition events. Trends Biochem Sci 27, 599–601.
Simionescu M (2007). Implications of early structural-functional changes in the endothelium for vascular disease. Arterioscler Thromb Vasc Biol 27, 266–274.
Simons K, Gerl MJ (2010). Revitalizing membrane rafts: new tools and insights. Nat Rev Mol Cell Biol 11, 688–699.
Soong G, Reddy B, Sokol S, Adamo R, Prince A (2004). TLR2 is mobilized into an apical lipid raft receptor complex to signal infection in airway epithelial cells. J Clin Invest 113, 1482–1489.
Sumagin R, Lomakina E, Sarelius IH (2008). Leukocyte-endothelial cell interactions are linked to vascular permeability via ICAM-1-mediated signaling. Am J Physiol Heart Circulat Physiol 295, H969–H977.
Tilghman RW, Hoover RL (2002). E-selectin and ICAM-1 are incorporated into detergent-insoluble membrane domains following clustering in endothelial cells. FEBS Lett 525, 83–87.
Tomas EM, Chau TA, Madrenas J (2002). Clustering of a lipid-raft associated pool of ERM proteins at the immunological synapse upon T cell receptor or CD28 ligation. Immunol Lett 83, 143–147.
Triantafilou M, Lepper PM, Olden R, Dias Ide S, Triantafilou K (2010). Location, location, location: is membrane partitioning everything when it comes to innate immune activation? Mediators Inflamm 2011, 186093.
Tzima E, Del Pozo MA, Kiosses WB, Mohamed SA, Li S, Chien S, Schwartz MA (2002). Activation of Rac1 by shear stress in endothelial cells mediates both cytoskeletal reorganization and effects on gene expression. EMBO J 21, 6791–6800.
Vandenbroucke E, Mehta D, Minshall R, Malik AB (2008). Regulation of endothelial junctional permeability. Ann NY Acad Sci 1123, 134–145.
van Wetering S, van den Berk N, van Buul JD, Mul FP, Lommerse I, Mous R, ten Klooster JP, Zwaginga JJ, Hordijk PL (2003). VCAM-1-mediated Rac signaling controls endothelial cell-cell contacts and leukocyte transmigration. Am J Physiol Cell Physiol 285, C343–C352.
Viola A, Gupta N (2007). Tether and trap: regulation of membrane-raft dynamics by actin-binding proteins. Nat Rev Immunol 7, 889–896.
Wojciak-Stothard B, Williams L, Ridley AJ (1999). Monocyte adhesion and spreading on human endothelial cells is dependent on Rho-regulated receptor clustering. J Cell Biol 145, 1293–1307.
Yamamoto K, Sokabe T, Ohura N, Nakatsuka H, Kamiya A, Ando J (2003). Endogenously released ATP mediates shear stress-induced Ca2+ influx into pulmonary artery endothelial cells. Am J Physiol Heart Circ Physiol 285, H793–H803.
Zeidan A, Broman J, Hellstrand P, Sward K (2003). Cholesterol dependence of vascular ERK1/2 activation and growth in response to stretch: role of endothelin-1. Arterioscler Thromb Vasc Biol 23, 1528–1534.

Arteriosclerosis, Thrombosis, and Vascular Biology
JOURNAL OF THE AMERICAN HEART ASSOCIATION

Crosstalk Between Reticular Adherens Junctions and Platelet Endothelial Cell Adhesion Molecule-1 Regulates Endothelial Barrier Function

Laura Fernández-Martín, Beatriz Marcos-Ramiro, Carolina L. Bigarella, Mariona Graupera, Robert J. Cain, Natalia Reglero-Real, Anaïs Jiménez, Eva Cernuda-Morollón, Isabel Correas, Susan Cox, Anne J. Ridley and Jaime Millán

Arterioscler Thromb Vasc Biol. 2012;32:e90-e102; originally published online June 21, 2012;
doi: 10.1161/ATVBAHA.112.252080
Arteriosclerosis, Thrombosis, and Vascular Biology is published by the American Heart Association, 7272 Greenville Avenue, Dallas, TX 75231

Print ISSN: 1079-5642. Online ISSN: 1524-4636

Crosstalk Between Reticular Adherens Junctions and Platelet Endothelial Cell Adhesion Molecule-1 Regulates Endothelial Barrier Function

Laura Fernández-Martín, Beatriz Marcos-Ramiro, Carolina L. Bigarella, Mariona Graupera, Robert J. Cain, Natalia Reglero-Real, Anaïs Jiménez, Eva Cernuda-Morollón, Isabel Correas, Susan Cox, Anne J. Ridley, Jaime Millán

Objective—Endothelial cells provide a barrier between the blood and tissues, which is reduced during inflammation to allow selective passage of molecules and cells. Adherens junctions (AJ) play a central role in regulating this barrier. We aim to investigate the role of a distinctive 3-dimensional reticular network of AJ found in the endothelium.

Methods and Results—In endothelial AJ, vascular endothelial-cadherin recruits the cytoplasmic proteins β-catenin and p120-catenin. β-catenin binds to α-catenin, which links AJ to actin filaments. AJ are usually described as linear structures along the actin-rich intercellular contacts. Here, we show that these AJ components can also be organized in reticular domains that contain low levels of actin. Reticular AJ are localized in areas where neighboring cells overlap and encompass the cell adhesion receptor platelet endothelial cell adhesion molecule-1 (PECAM-1). Superresolution microscopy revealed that PECAM-1 forms discrete structures distinct from and distributed along AJ, within the voids of reticular domains. Inflammatory tumor necrosis factor-α increases permeability by mechanisms that are independent of actomyosin-mediated tension and remain incompletely understood. Reticular AJ, but not actin-rich linear AJ, were disorganized by tumor necrosis factor-α. This correlated with PECAM-1 dispersal from cell borders. PECAM-1 inhibition with blocking antibodies or small interfering RNA specifically disrupted reticular AJ, leaving linear AJ intact. This disruption recapitulated typical tumor necrosis factor-α–induced alterations of barrier function, including increased β-catenin phosphorylation, without altering the actomyosin cytoskeleton.

Conclusion—We propose that reticular AJ act coordinately with PECAM-1 to maintain endothelial barrier function in regions of low actomyosin-mediated tension. Selective disruption of reticular AJ contributes to permeability increase in response to tumor necrosis factor-α. **(*Arterioscler Thromb Vasc Biol*. 2012;32:e90-102.)**

Key Words: vascular endothelial-cadherin ■ platelet endothelial cell adhesion molecule-1 ■ F-actin ■ tumor necrosis factor-α ■ endothelial barrier function

Intercellular junctions in the endothelium regulate the permeability between blood and tissues and thereby play an essential role in tissue homeostasis and inflammatory responses.[1–4] Endothelial cell–cell contacts contain tight junctions and adherens junctions (AJ), which are also found in epithelium, as well as some junctional proteins that are unique to endothelial cells, such as platelet endothelial cell adhesion molecule-1 (PECAM-1), intercellular adhesion molecule-2, and S-endo I.[1] Vascular endothelial (VE)-cadherin is a transmembrane homophilic adhesion receptor specific to endothelial AJ. Like E-cadherin, the VE-cadherin intracellular tail interacts with β-catenin, γ-catenin, and p120-catenin. β-catenin binds to α-catenin that has the potential to link the AJ complex to the actin cytoskeleton.[5–7] In epithelial cells, α-catenin also binds to actin-interacting proteins, such as zonula occludens-1, vinculin, and α-actinin, acting as a mechanosensor that regulates AJ stability.[8–10] However, a direct link between cortical F-actin and α-catenin in epithelial AJ has been called into question by data demonstrating that the binding of α-catenin to β-catenin and F-actin is mutually exclusive. It has been proposed that α-catenin instead stabilizes AJ by regulating actin polymerization.[11,12]

Endothelial cell–cell junctions are regulated by inflammatory stimuli, which often act by inducing reorganization of the actin cytoskeleton. Acute inflammatory stimuli, such as histamine and thrombin, activate the RhoA GTPase, and

Received on: March 11, 2011; final version accepted on: June 4, 2012.

From the Centro de Biología Molecular Severo Ochoa, CSIC-UAM, Madrid, Spain (L.F.-M., B.M.-R., N.R.-R., A.J., I.C., J.M.); Developmental and Regenerative Biology Department, Mount Sinai School of Medicine, New York, NY (C.L.B.); Grup de Angiogènesi, Laboratori d'Oncologia Molecular (LOM), Institut d´Investigació Biomèdica de Bellvitge (IDIBELL), Hospital Duran i Reynals, L´Hospitalet de Llobregat, Barcelona, Spain (M.G.); King's College London, Randall Division of Cell and Molecular Biophysics, Guy's Campus, London, UK (R.J.C., S.C.); and Facultad de Medicina, Universidad de Oviedo, Oviedo, Spain (E.C.-M.).

The online-only Data Supplement is available with this article at http://atvb.ahajournals.org/lookup/suppl/doi:10.1161/ATVBAHA.112.252080/-/DC1.

Correspondence to Jaime Millán, PhD, Centro de Biología Molecular Severo Ochoa, Universidad Autónoma de Madrid, Cantoblanco, 28049 Madrid, Spain. E-mail jmillan@cbm.uam.es

Arterioscler Thromb Vasc Biol **is available at http://atvb.ahajournals.org** **DOI: 10.1161/ATVBAHA.112.252080**

its targets, the Rho-serine/threonine kinases (ROCK), stimulate actomyosin-based contractility and thereby contribute to a rapid increase in endothelial permeability.[13,14] In contrast, stimuli such as tumor necrosis factor-α (TNF-α) induce slower but more prolonged changes in actin stress fibers and a parallel slow increase in permeability. This long-term permeability induction, however, neither correlates with the activation of RhoA-ROCK-myosin pathway nor is reduced by ROCK or myosin inhibition.[15–17] This indicates that TNF-α alters the endothelial barrier by mechanisms independent of actomyosin-based contractility. Alternatively, other signaling proteins, including the phosphoinositide 3-kinase isoform p110α, Rac1, and the tyrosine kinase Pyk2, affect TNF-α–induced permeability.[18,19]

PECAM-1 is a transmembrane receptor of the immunoglobulin superfamily that forms homophilic interactions between adjacent endothelial cells or between endothelial cells and leukocytes. PECAM-1 is not only important for efficient leukocyte transmigration[20–23] but can also modulate endothelial permeability in response to acute contraction through regulation of β-catenin function.[22,24–26] It has been reported that PECAM-1 is localized in a subjunctional compartment from where it constitutively recycles to the junctional plasma membrane.[21] This localization is necessary for PECAM-1 function in leukocyte transendothelial migration, although the nature and regulation of this compartment are still unclear.

In cuboidal epithelial cells, tight junctions are localized close to the apical membrane, and AJ are situated beneath them in the junctional cleft. Tight junctions and AJ are associated with a subcortical actin ring that stabilizes these complexes. Here, we investigate the properties of AJ that are distributed in a distinctive 3-dimensional reticular network, which is selectively found in quiescent endothelial cells. Reticular AJ are localized in regions where neighboring endothelial cells overlap, which contain low levels of actin and are enriched in PECAM-1. We demonstrate that VE-cadherin and PECAM-1 are interdependent within these reticular structures. Reticular AJ disorganization in response to PECAM-1 inhibition is sufficient to mimic typical TNF-α–mediated alterations of the endothelial barrier. As an alternative to actomyosin-based tension, regulation of PECAM-1 and AJ crosstalk could contribute to vascular permeability increase in response to TNF-α.

Methods

Cell Culture and Transfection

Human umbilical vein endothelial cells (HUVECs) and human dermal microvascular endothelial cells were obtained and cultured as previously described[27] and always plated at confluency on fibronectin-coated dishes for 24 to 48 hours, then stimulated with 10 ng/mL TNF-α for 15 to 18 hours before experiments. HUVECs were transiently transfected with 1 to 5 μg plasmid DNA/10^6 cells with a Nucleofector kit (VPB-1002) (Amaxa Biosystems, Cologne, Germany) according to the manufacturer's instructions and were used for experiments 24 to 72 hours after transfection. For small interfering RNA (siRNA) transfection, we devised a protocol for delivery of siRNA with high efficiency into primary endothelial cells, which is a modification of our previous method[27] (see Methods in the online-only Data Supplement). For rescue experiments, 24 hours after transfection of siRNA, the indicated plasmids were transfected by the phosphate calcium method.

Barrier Function Assays

An electric cell-substrate impedance sensing system (ECIS 1600R; Applied Biophysics, Troy, NY) was used to measure transendothelial electrical resistance (a measure of endothelial barrier integrity and permeability) of HUVEC monolayers seeded on gold electrode arrays (IBIDI, Martinsried, Germany) as previously described.[28] Permeability assays were carried out as previously described[16,29] (see Methods in the online-only Data Supplement).

Results

AJ Form Reticular Structures in Endothelial Cells

Endothelial cell–cell junctions exhibit a remarkable morphological heterogeneity. This reflects the functional requirements for barrier function, which differ according to the physiological context and the type of vessel in the vascular tree.[30–32] In quiescent HUVECs, VE-cadherin is linearly distributed along cell borders, similar to what occurs in epithelial AJ (Figure 1A and 1B, arrows), but it also appears distributed in reticular structures that cover significant areas at cell borders (Figure 1A, boxed area).[21,33] The fact that AJ displaying this characteristic 3-dimensional distribution have hitherto been poorly characterized prompted us to investigate their functional properties. The AJ proteins α-catenin, β-catenin, and p120-catenin all localized in reticular structures, which we therefore named reticular AJ (Figure 1B, arrowhead). In contrast, the junctional protein zonula occludens-1[34] did not have a reticular distribution but was localized linearly along cell–cell borders and also in linear discontinuous domains, together with AJ components, as previously described (Figure 1B, arrowhead).[35] Reticular AJ were also present in human dermal microvascular endothelial cells, but they were not found in epithelial Madin-Darby canine kidney cells or in the endothelial cell line Ey.ha.926, formed by fusion of HUVECs with the human lung adenocarcinoma A549 (Figure 1C).[36] In these cell types, AJ localization was linear along cell–cell borders. These results suggest that reticular AJ structures are restricted to primary endothelial cells.

Expression of p120-catenin-dsRed and p120-catenin-GFP in adjacent cells indicated that reticular AJ formed where neighboring cells overlapped and that AJ proteins from both cells contributed to the structures (Figure 1D, arrowhead). Transmission electron microscopy images showed that adjacent HUVECs frequently overlapped, and multiple electron-dense regions resembling cell–cell junctions were localized where membranes from overlapping cells were closely apposed (Figure 1E, arrowheads), consistent with the presence of reticular AJ. Although the possibility that part of reticular AJ are located in a subjunctional internal compartment cannot be ruled out, these experiments strongly suggest that reticular AJ are formed by homotypic interactions occurring at the surfaces of 2 neighboring cells that superpose.

AJ have the potential to associate with actin filaments via α-catenin,[37] although it has been proposed that epithelial cadherin/catenin complexes are not directly linked to F-actin.[12] In HUVECs, linear AJ colocalized with cortical F-actin at cell borders as expected (Figure 2A, arrow). In contrast, F-actin did not form reticular structures, and little F-actin was detected in regions of reticular AJ in comparison with linear AJ. F-actin was instead localized along the edges of reticular AJ (Figure 2A, arrowheads). Intensity profiles of F-actin in linear AJ and reticular AJ (Figure 2A, right

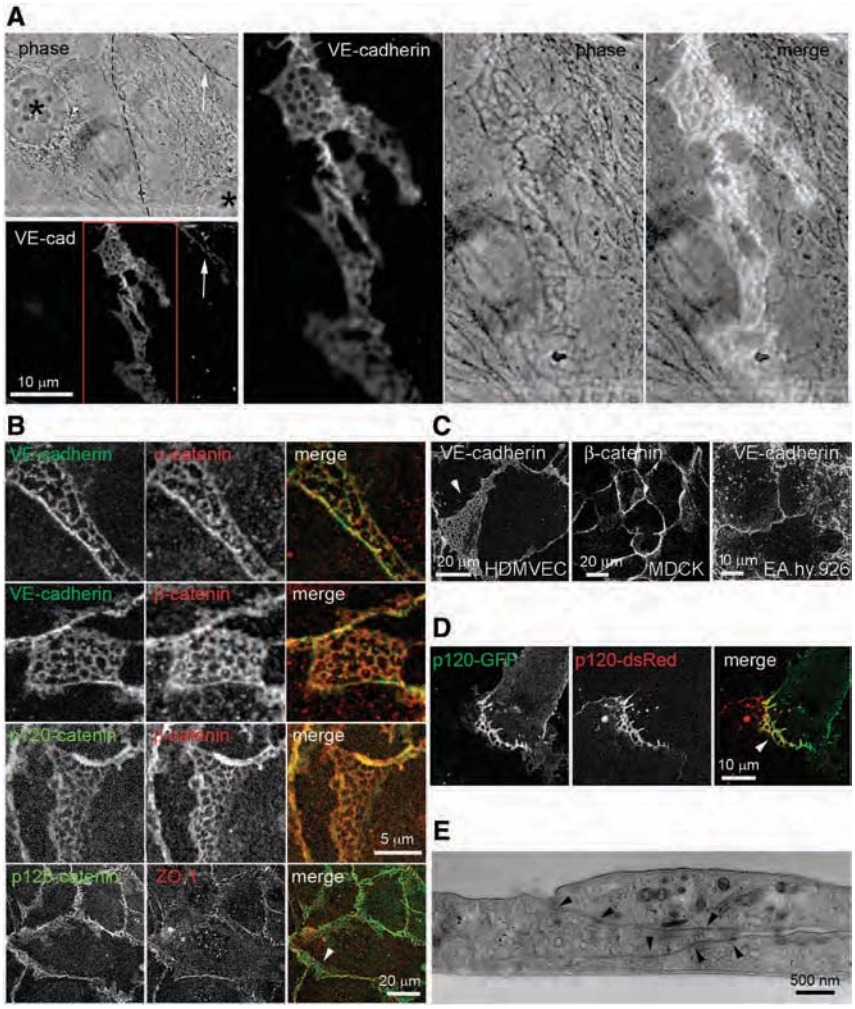

Figure 1. Endothelial adherens junctions (AJ) are distributed in linear and reticular domains. **A** and **B**, Confluent human umbilical vein endothelial cells (HUVECs) were fixed, permeabilized, and stained with antibodies to the indicated proteins. Vascular endothelial (VE)-cadherin, α-catenin, β-catenin, and p120-catenin are distributed in reticular structures (enlarged boxed area and arrowheads), which are morphologically distinguishable in phase contrast images (**A**). They also distributed linearly along cell–cell junctions (**arrow**) or in linear discontinuous junctions away from cell borders[30] (**open arrowheads**). Note that zonula occludens-1 (ZO-1) does not have a reticular distribution. **C**, Confluent human dermal microvascular endothelial cells (HDMVECs), Madin-Darby canine kidney (MDCK) cells, and EA.hy.926 cells were stained with antibodies to the indicated proteins. **Arrowheads** indicate reticular AJ. **D**, Reticular AJ are localized in areas where 2 adjacent cells overlap. HUVECs were nucleofected with expression vectors containing p120-catenin-dsRed (p120-dsRed) or p120-catenin-green fluorescent protein (GFP) (p120-GFP), mixed, and plated at confluence for 24 hours in growth medium before fixation. p120-catenin from each cell colocalizes in an overlapping reticular AJ (**arrowhead**). **E**, Confluent HUVECs grown as in **A** were fixed and processed for electron microscopy. Overlapping areas at junctions are shown. **Arrowheads** indicate electrodense junctional complexes. Scale bars, 10 or 20 μm, as indicated (**A–D**); 500 nm (**E**). VE-cad indicates VE-cadherin.

graphs) showed that F-actin content in reticular AJ is similar to the intensity found in cytoplasmic areas. Consistent with low levels of F-actin within reticular AJ, in cells transfected with actin-mCherry, mCherry fluorescence was less intense in areas where endogenous β-catenin and p120-catenin were in reticular AJ than in surrounding regions (Figure 2B, arrowhead, inset, right graph). Expression of actin-mCherry and actin-green fluorescent protein (GFP) in neighboring cells showed F-actin filaments (Figure IA in the online-only Data Supplement, arrow) at the edge but not within reticular AJ (Figure IA in the online-only Data Supplement, arrowheads). Double immunofluorescence of β-catenin with an antibody against an epitope common to all actin isoforms also indicated that actin levels were low in reticular AJ (Figure 2C, right graph). Finally, stimulated emission depletion superresolution microscopy of F-actin at junctions also revealed no significant actin accumulation in reticular AJ structures (Figure IB in the online-only Data Supplement). Time-lapse movies of confluent cells coexpressing actin-GFP and p120-catenin-dsRed showed that, compared with other regions at cell borders, reticular AJ contain lower levels of actin-GFP (Figure 2D). These domains underwent morphological remodeling (Movie I in the online-only Data Supplement, arrowheads) but looked as stable as actin-rich AJ (Movie I in the online-only Data Supplement, arrows). It, therefore, appears that endothelial AJ can form reticular structures that are stable at cell–cell contacts without associating with large F-actin domains. Furthermore, markers of actomyosin-based tension transduction such as myosin light chain phosphorylation at Ser-19 or vinculin[9] were not enriched in reticular AJ (Figure IIA in the online-only Data Supplement, arrowheads, boxed area). Myosin light chain phosphorylation staining was found distributed not only in linear structures, suggestive of alignment with actin filaments (Figure IIA in the online-only Data Supplement, brackets), but also in linear AJ (Figure IIA in the online-only Data Supplement, arrows). Vinculin localized to focal adhesions in subconfluent regions, but it was mostly diffuse in confluent endothelial cells (Figure IIB in the online-only Data Supplement), similar to the previously described distribution of other focal adhesion proteins such as paxillin.[35] Our results thus suggest that reticular AJ are in regions of low actomyosin-mediated tension.

PECAM-1 Localizes Within Reticular AJ

PECAM-1 has been described as localizing to an internal subjunctional compartment called lateral border recycling compartment (LBRC),[21] which appears to resemble the distribution of reticular AJ. We, therefore, analyzed the distribution of PECAM-1 in relation to reticular AJ. PECAM-1

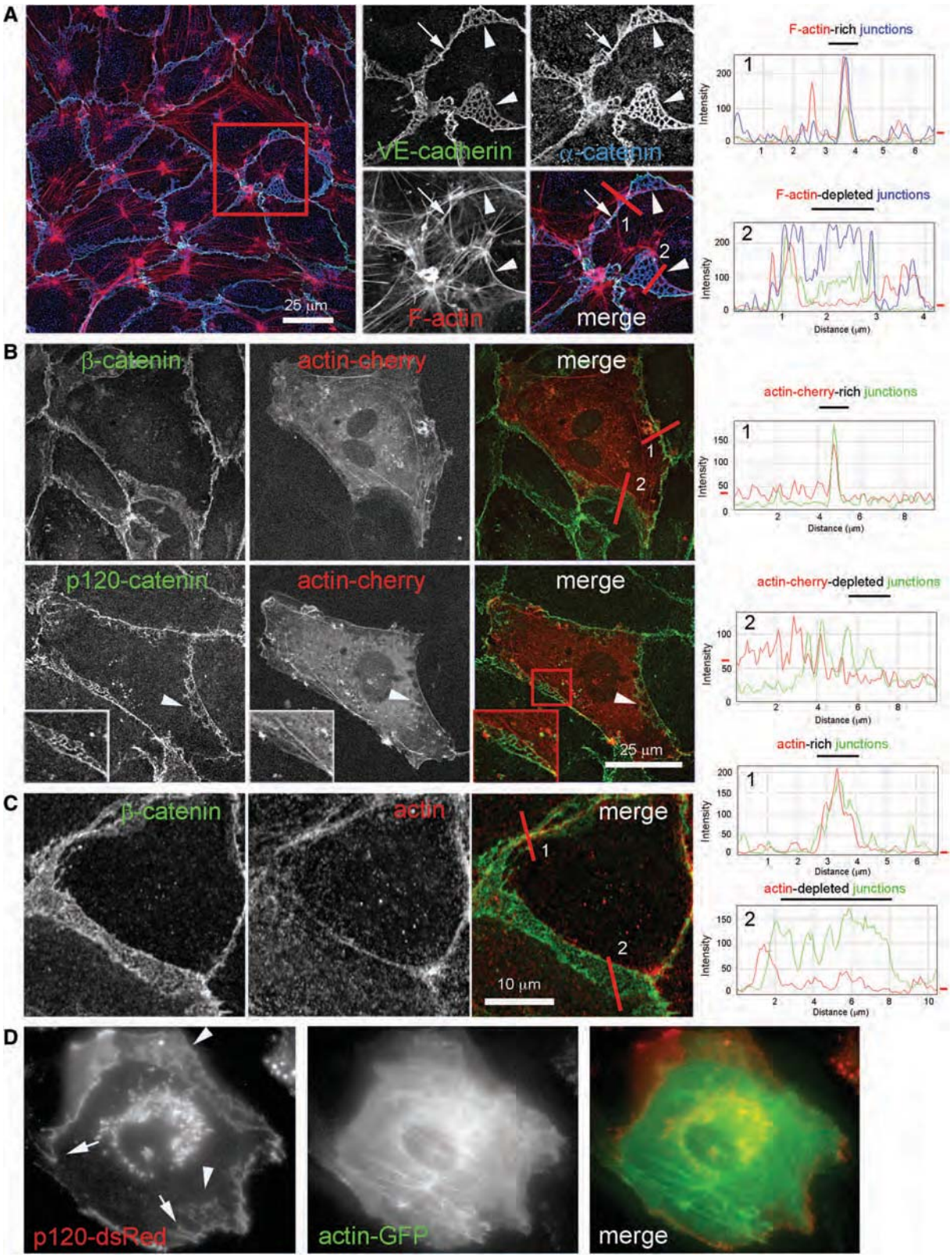

Figure 2. Actin filaments do not localize in reticular domains. **A**, Unstimulated confluent human umbilical vein endothelial cells (HUVECs) in growth medium were stained for F-actin (phalloidin-TRITC) and antibodies to VE-cadherin or α-catenin. **Arrowheads** indicate reticular adherens junctions (AJ) surrounded by F-actin, whereas **arrows** indicate linear AJ that colocalize with F-actin. **B**, HUVECs were nucleofected with actin-cherry (red) and plated at confluence for 24 to 48 hours in growth medium. Cells were fixed and stained for β-catenin or p120-catenin (green). **Arrowheads** and the enlarged boxed area show reticular AJ. **C**, Cells were grown and fixed as in **A** and stained with antibodies against actin and β-catenin. Right graphs in **A–D** show the intensity profiles of lines 1 and 2 or each merge panel. Red **mark** in graphs marks the level of actin intensity in the cytoplasmic region. **D**, Dynamics of reticular AJ. HUVECs were nucleofected with plasmids coding for actin-green fluorescent protein (GFP) and p120-catenin-dsRed (p120-dsRed) and plated at confluence for 24 hours in growth medium. Cell images were acquired by fluorescence time-lapse microscopy, 2 frame/min. **Arrows** point at actin-rich cell junctions, whereas **arrowheads** point to actin-depleted junctions. Scale bars, 25 μm (**A**, **B**); 10 μm (**C**).

and VE-cadherin had a similar localization along linear junctions (Figure 3). In areas of cell–cell overlap, PECAM-1 was often enclosed within the VE-cadherin reticular lattice (Figure 3A and 3B, see staining intensity profiles) or in some areas was more uniformly distributed, localizing throughout the reticular area (Figure 3B). However, a detailed analysis

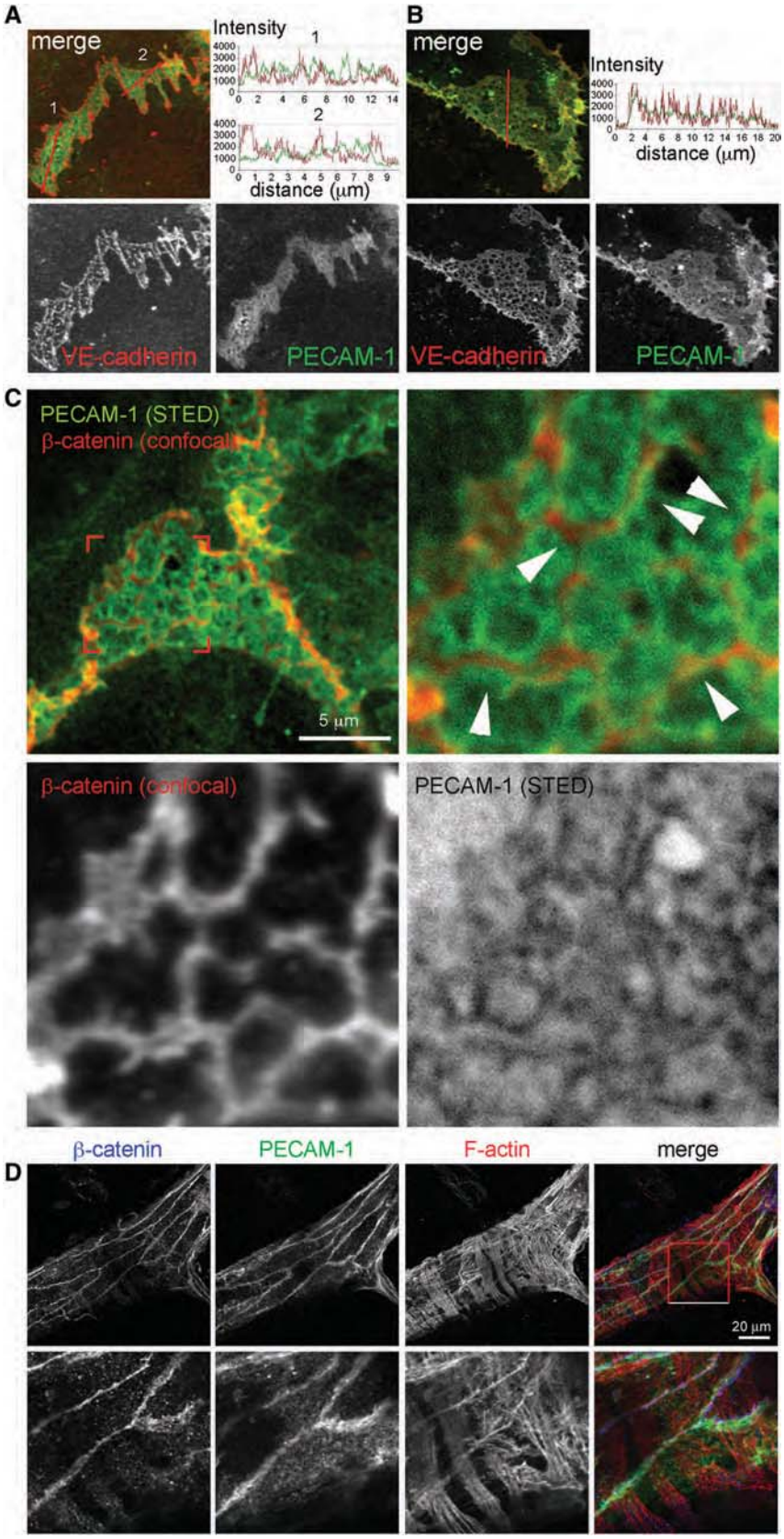

Figure 3. Platelet endothelial cell adhesion molecule-1 (PECAM-1) localizes within reticular adherens junctions (AJ). Confocal images of human umbilical vein endothelial cells (HUVECs) (**A**) or human dermal microvascular endothelial cells (HDMVECs) (**B**) stained for vascular endothelial (VE)-cadherin and PECAM-1. Graphs show intensity profiles across the reticular area along the indicated **red lines**. Note how the VE-cadherin profile is different from the PECAM-1 profile and more intense at the borders in **A**. In HDMVECs (**B**), VE-cadherin and PECAM-1 overlap more than in HUVECs. VE-cadherin staining is clearly reticular, whereas PECAM-1 is more evenly distributed across reticular areas. **C**, Superresolution stimulated emission depletion (STED) confocal microscopy of PECAM-1. Cells were grown and fixed as in **A** and stained for β-catenin and PECAM-1 antibodies. Anti–PECAM-1 was visualized with a secondary antibody conjugated to ATTO-647N fluorophore, for STED detection. **Arrowheads** show PECAM-1 structures surrounding β-catenin in the honeycomb structures of reticular AJ. Scale bar, 5 μm. **D**, Reticular junction structures in blood vessels in vivo. Mouse tissue was stained for β-catenin, PECAM-1, and F-actin. Confocal z-stacks of 15 planes are projected as a single image. Image of a vessel surrounded by pericytes (detected by F-actin staining). Bottom images show the boxed area from the top images at higher magnification and are taken from a single image of the z-stack. Scale bar, 20 μm.

of PECAM-1 and reticular AJ by stimulated emission depletion superresolution microscopy revealed that PECAM-1 was organized in tubule-like structures that were distinct from and ran parallel to AJ within the voids of the reticulum (Figure 3C; Figure IB in the online-only Data Supplement). PECAM-1 structures often surrounded AJ in these reticular domains (Figure 3C, arrowheads). In accordance, and as previously reported,[38] PECAM-1 and AJ components did not coimmunoprecipitate (Figure III in the online-only Data Supplement). Altogether, these results support the existence of 2 different, albeit related, structures in these reticular areas. We also found that PECAM-1 showed less colocalization with junction markers that did not display a reticular distribution, such as nectin-2 (Figure IVA in the online-only Data Supplement). To further investigate the nature of the PECAM-1 tubules detected by superresolution microscopy, PECAM-1-GFP was expressed. Similar to endogenous PECAM-1, PECAM-1-GFP was localized in reticular areas. However, in cells expressing high levels of PECAM-1-GFP, the ectopic protein accumulated in internal structures, displaying a pattern similar to that at cell junctions (Figure IVB in the online-only Data Supplement). AJ components did not accumulate in these internal structures, suggesting that they are independent of reticular AJ. Overexpression of VE-cadherin did not induce appearance of intracellular reticular structures (Figure IVB in the online-only Data Supplement, bottom panels). The ability of PECAM-1 to form intracellular structures with a tubular or reticular pattern upon overexpression suggests that endogenous PECAM-1 has an intrinsic ability to organize these structures, without requirement of cell–cell contacts. These tubular structures, detected endogenously at junctions and away from them upon PECAM-1 ectopic expression, may share features with or may be the proposed LBRC,[21] which would be embedded in reticular AJ. Junctional adhesion molecule-A, which has been also proposed to be part of this compartment, displayed a clear reticular pattern, with the AJ marker plakoglobin different from that of PECAM-1 (Figure IVA in the online-only Data Supplement). Thus, junctional adhesion molecule-A may also be involved in the organization of reticular domains at junctions. Finally, PECAM-1 and AJ also localized in regions where cells appeared to overlap in mouse blood vessels in vivo, both in small capillaries (Figure IVC in the online-only Data Supplement) and in bigger vessels surrounded by pericytes (Figure 3D), suggesting that our observations in vitro reflect the organization of AJ and PECAM-1 in vivo.

TNF-α Disrupts Reticular AJ Independently of Actomyosin-Mediated Tension

TNF-α is a proinflammatory stimulus that induces a gradual increase in permeability, stress fiber formation, and cell elongation in HUVECs.[16] TNF-α increases association of actin with AJ.[35] RhoA and ROCK are required for TNF-α–mediated increase of actin fibers,[39,40] but their role in the TNF-α–induced increase in permeability[40,41] has been challenged, suggesting the existence of an additional mechanism that regulates barrier function.[16,42] We found that reticular AJ were lost in TNF-α–stimulated cells. Instead, AJ were mostly linear or discontinuous, and there was little overlap between adjacent cells (Figure 4A). Quantification of the junctional area, stained for the AJ markers VE-cadherin and β-catenin, showed a strong decrease in reticular AJ (Figure 4A, right graph). The ROCK inhibitor Y-27632 impaired TNF-α–induced stress fiber formation but did not prevent reticular AJ disruption. Interestingly, in the presence of the inhibitor, endothelial cells still significantly overlapped, but the pattern of AJ distribution in overlapping areas of cells treated with TNF-α and Y-27632 was different from that of control cells: VE-cadherin had a nonreticular, punctate distribution (Figure 4A, boxed areas). Indeed, Y-27632 did not prevent the TNF-α–induced reduction in total junctional area (Figure 4A, right graph). An analysis of transendothelial electrical resistance in real time showed no effect of Y-27632 on either early or late TNF-α–induced barrier disruption (Figure 4B, left graph). Similarly, siRNA-mediated silencing of RhoA, the main upstream regulator of ROCK activity, did not affect barrier function (Figure VA–VC in the online-only Data Supplement). In contrast, thrombin, which is well known to act via ROCK to induce barrier disruption[43] (Figure 4B, right graph), also decreased reticular AJ, but this reduction was prevented by Y-27632 (Figure 4C; Figure VD in the online-only Data Supplement). In accordance with these results, RhoA activity was strongly stimulated by thrombin compared with the minor increase detected upon long-term stimulation with TNF-α (Figure VE and VF in the online-only Data Supplement). Collectively, these data suggest that the contribution of RhoA-ROCK to the TNF-α–induced permeability increase is negligible. Interestingly, although AJ staining intensity decreased at the remaining overlapping areas between adjacent cells in response to TNF-α, it was not diminished in response to thrombin (Figure 4A and 4D; Figure VD in the online-only Data Supplement), suggesting that thrombin reduces reticular AJ by inducing ROCK-mediated cell contraction, whereas TNF-α disruption of reticular AJ, like the permeability increase, is ROCK independent and involves a decrease of AJ density at cell–cell contacts (Figure 4D). These data suggest that an additional mechanism regulates junctional integrity in response to TNF-α.

PECAM-1 Is Necessary for Maintaining Reticular But Not Linear AJ

Concomitant with the disappearance of reticular AJ, TNF-α stimulation led to dispersal of PECAM-1 from the junctions and increased PECAM-1 in internal vesicles, although it did not decrease total PECAM-1 levels (Figure 5) or the ratio of surface to total PECAM-1 and VE-cadherin (Figure VIA in the online-only Data Supplement). Biochemical fractionation showed that the levels of PECAM-1, β-catenin, or VE-cadherin in the detergent-insoluble pellet, which contains actin filaments,[44] were not altered by TNF-α stimulation (Figure VIB in the online-only Data Supplement, pellet). This implies that the presence or absence of reticular AJ does not affect the association of AJ with F-actin. It has been proposed that AJ components and PECAM-1 can also be fractionated into buoyant detergent-resistant membranes, suggestive of confinement into lipid rafts.[45,46] Neither PECAM-1, β-catenin, nor VE-cadherin was found to be significantly associated with the detergent-resistant membrane fraction in unstimulated cells, rich in reticular AJ, or TNF-α–stimulated cells, with few reticular AJ (Figure VIB in the online-only Data Supplement, rafts). It is, therefore, unlikely that reticular AJ and PECAM-1 are enriched in lipid rafts.

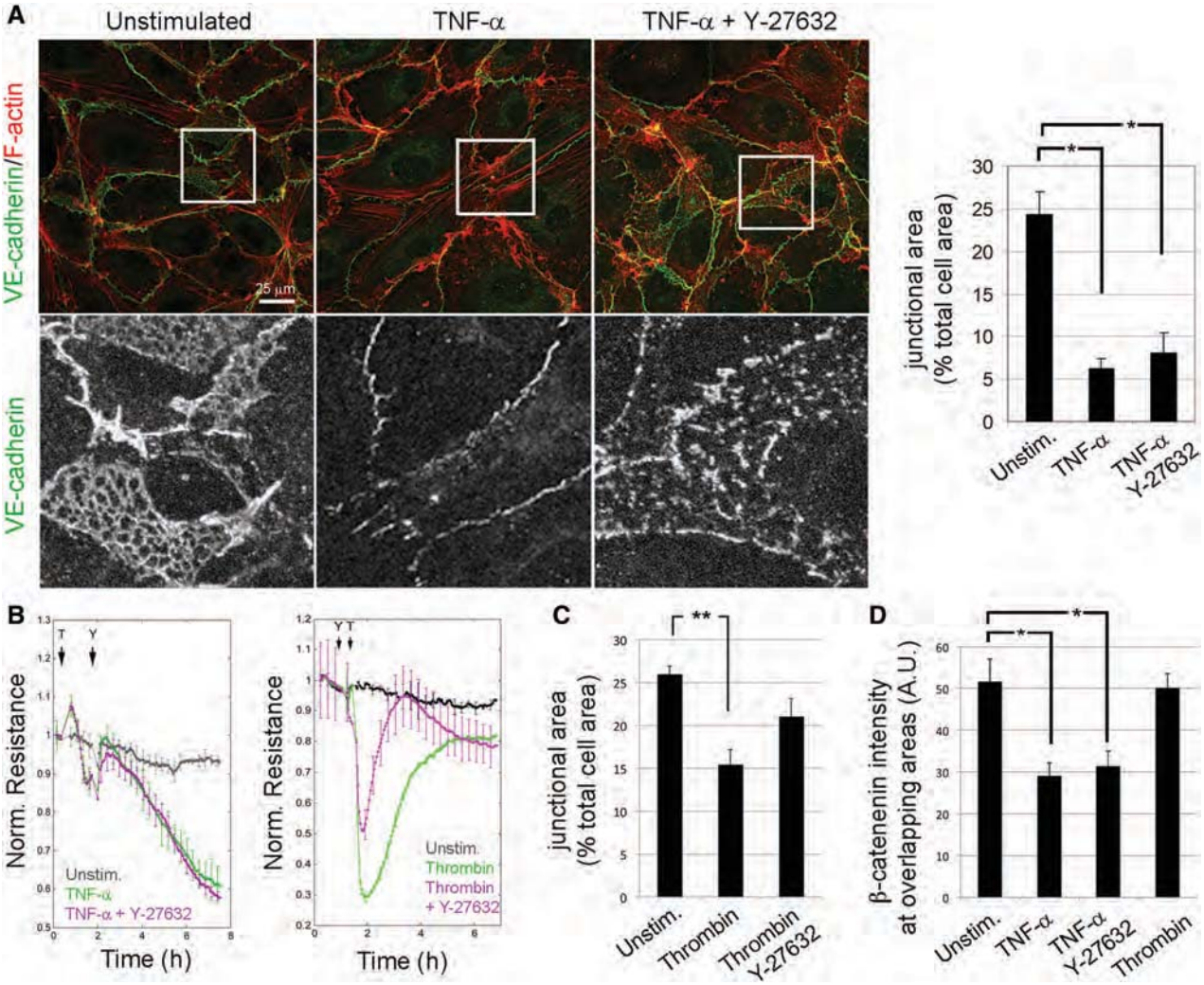

Figure 4. Tumor necrosis factor-α (TNF-α) disrupts reticular adherens junctions (AJ) independently of ROCK. **A**, Confluent human umbilical vein endothelial cells (HUVECs) were incubated in starving medium for 4 hours and then left unstimulated or stimulated for 24 hours with TNF-α. Thirty minutes after TNF-α addition, 5 μmol/L Y-27632 was added where indicated (TNF-α+Y-27632). Cells were fixed, permeabilized, and stained for F-actin (phalloidin, **red**) and VE-cadherin (**green**) (top panels). Scale bar, 25 μm. Bottom panels show the vascular endothelial (VE)-cadherin staining from the boxed area of the top panels at higher magnification. Right graph shows quantification of area covered by AJ. Junctional area was expressed as percentage of total cell area. Bars show mean±SEM; *P<0.001. **B**, Transendothelial electrical resistance of confluent HUVECs. **Left**, HUVECs were incubated in starving medium for 2 hours and then left unstimulated or stimulated for 8 hours with TNF-α (T). Thirty minutes after TNF-α addition, 5 μmol/L Y-27632 (Y) was added where indicated (TNF-α+Y-27632). **Right**, HUVECs in starving medium were left unstimulated or stimulated with thrombin in the presence or absence of 5 μmol/L Y-27632. **C**, Quantification of junctional area as in **A**. Bars show mean ± SEM; **P<0.0005. **D**, Quantification of β-catenin intensity at overlapping junctional areas of cells in the presence or absence of the indicated stimuli and Y-27632. Bars show mean±SEM; *P<0.001.

We then hypothesized that reticular AJ, which were not apparently connected to an F-actin belt, may be stabilized in an alternative manner. PECAM-1 domains surround reticular AJ and TNF-α disperses PECAM-1 from junctions, so we also hypothesized that these domains could stabilize AJ and that PECAM-1 dispersion could contribute to permeability increase in response to TNF-α. The HEC-7 antibody has been shown to block PECAM-1 function and abrogate PECAM-1–mediated leukocyte transendothelial migration.[20] When cells were incubated with HEC-7 at 37°C (Figure 6A) or PECAM-1 was knocked down by siRNA (Figure 6B; Figure VII in the online-only Data Supplement), reticular AJ were disrupted and fragmented even in areas where cells clearly overlapped (Figure 6A and 6B, insets). In contrast, linear AJ were not altered by HEC-7 or PECAM-1 knockdown. In some regions, HEC-7–treated cells showed linear AJ clearly decorating the edges of these overlapping areas (Figure 6A, insets). The cell area covered by AJ upon PECAM-1 inhibition with antibodies or siRNA was reduced to levels similar to that of TNF-α–stimulated cells (Figure 6, right panels). PECAM-1 inhibition disorganized reticular structures and decreased β-catenin levels at the remaining overlapping areas by 50% (Figure 6C). However, disrupting PECAM-1 function had little effect on AJ distribution in endothelial cells already stimulated with TNF-α, where AJ are distributed in F-actin–rich linear or discontinuous junctions[35] (Figure 6A, 6B, right; Figure VIII in the online-only Data Supplement), and PECAM-1 is dispersed from cell borders (Figure 5). To rule out the possibility of an

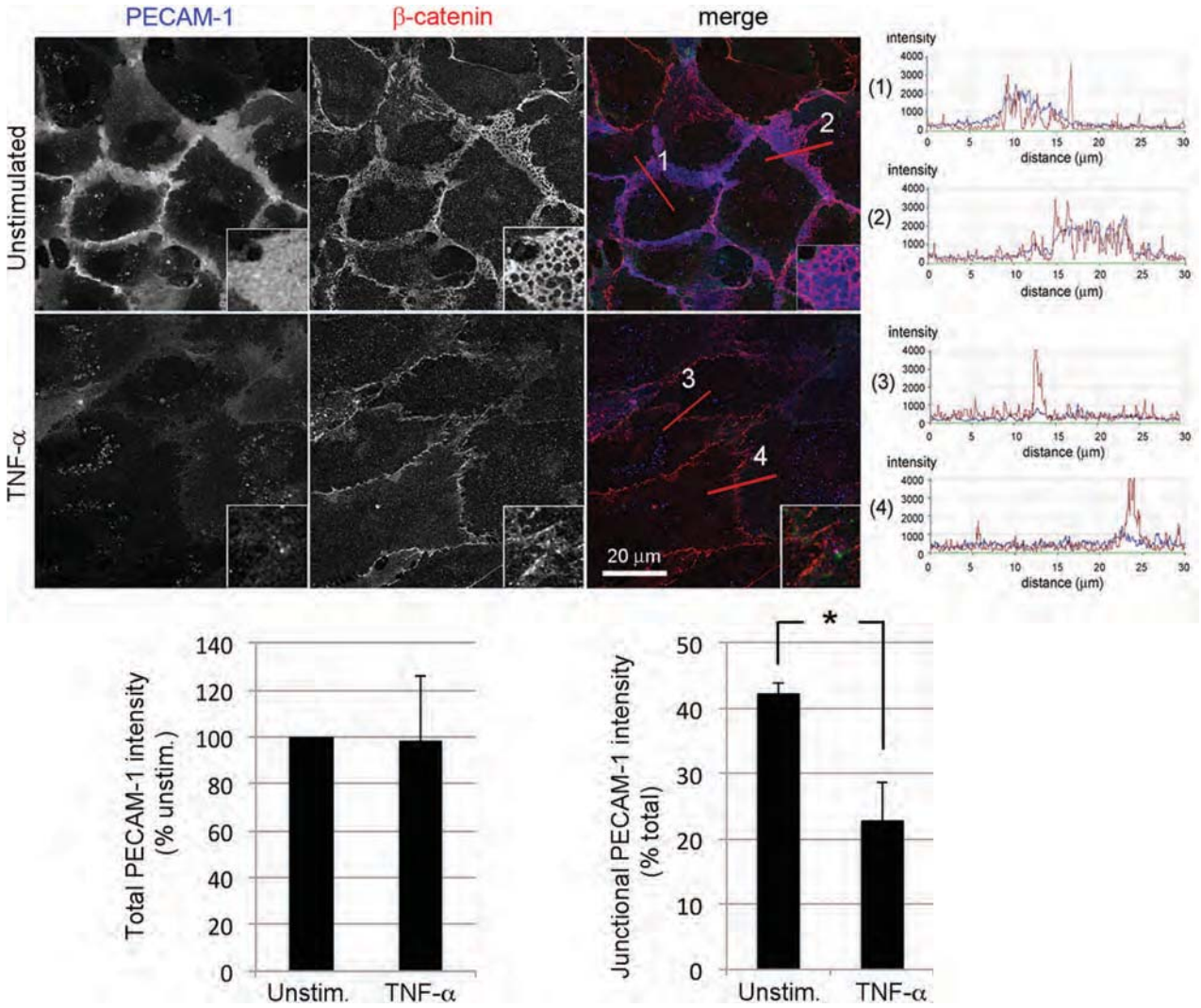

Figure 5. Tumor necrosis factor-α (TNF-α) disperses platelet endothelial cell adhesion molecule-1 (PECAM-1) from cell–cell contacts. PECAM-1 and β-catenin distribution in control and TNF-α–stimulated cells. **Right**, Graphs show intensity profiles across the reticular area along the indicated red lines. Note that, compared with β-catenin (red), PECAM-1 staining (blue) at junctions diminishes upon TNF-α stimulation. **Bottom graphs**, Quantification of total PECAM-1 staining and PECAM-1 staining at cell–cell junctions. Bars show mean±SEM; n=3; **P*<0.02.

off-target effect of the siRNA oligonucleotides for PECAM-1, a third siRNA targeting the 3′ untranslated region of PECAM-1 mRNA was transfected, and 24 hours later, GFP or PECAM-1-GFP was expressed. This siRNA-reduced PECAM-1 expression (Figure VIIIB in the online-only Data Supplement) also disrupted reticular AJ (Figure 6D). Expression of PECAM-1-GFP but not of GFP partially rescued the formation of reticular AJ (Figure 6D).

To determine whether AJ also affect the localization of PECAM-1, we disrupted them with anti–VE-cadherin blocking antibodies or by transfecting VE-cadherin siRNA (Figures VII and IX in the online-only Data Supplement). In contrast to PECAM-1 inhibition, antibody-mediated VE-cadherin inhibition was not restricted to reticular domains but affected all cell–cell contacts, inducing numerous intercellular gaps (Figure IXA in the online-only Data Supplement). Similarly, VE-cadherin knockdown also led to loss of most β-catenin from intercellular junctions, although some PECAM-1 remained at cell–cell contacts displaying a nonreticular distribution (Figure IXB in the online-only Data Supplement). VE-cadherin knockdown reduced junctional area more dramatically than did PECAM-1 silencing and induced disruption of cell–cell junctions in unstimulated and TNF-α–stimulated cells (Figure 6B, right panel).

PECAM-1 Inhibition Recapitulates the Effects of TNF-α on Barrier Function But Not on F-Actin Remodeling or Adhesion Receptor Expression

We tested whether disorganization of reticular AJ via PECAM-1 inhibition could mimic TNF-α effects on endothelial barrier function. TNF-α induced a 3-fold increase in permeability (Figure 7A). VE-cadherin blocking antibody significantly increased permeability in unstimulated and TNF-α–stimulated cells (Figure 7A, left graph), consistent with a widespread effect of the antibody on junctional architecture. In contrast, HEC-7 increased permeability in unstimulated HUVECs but had no effect on cells already stimulated with TNF-α (Figure 7A, right graph). This is in agreement with a selective effect of PECAM-1 inhibition on reticular AJ,

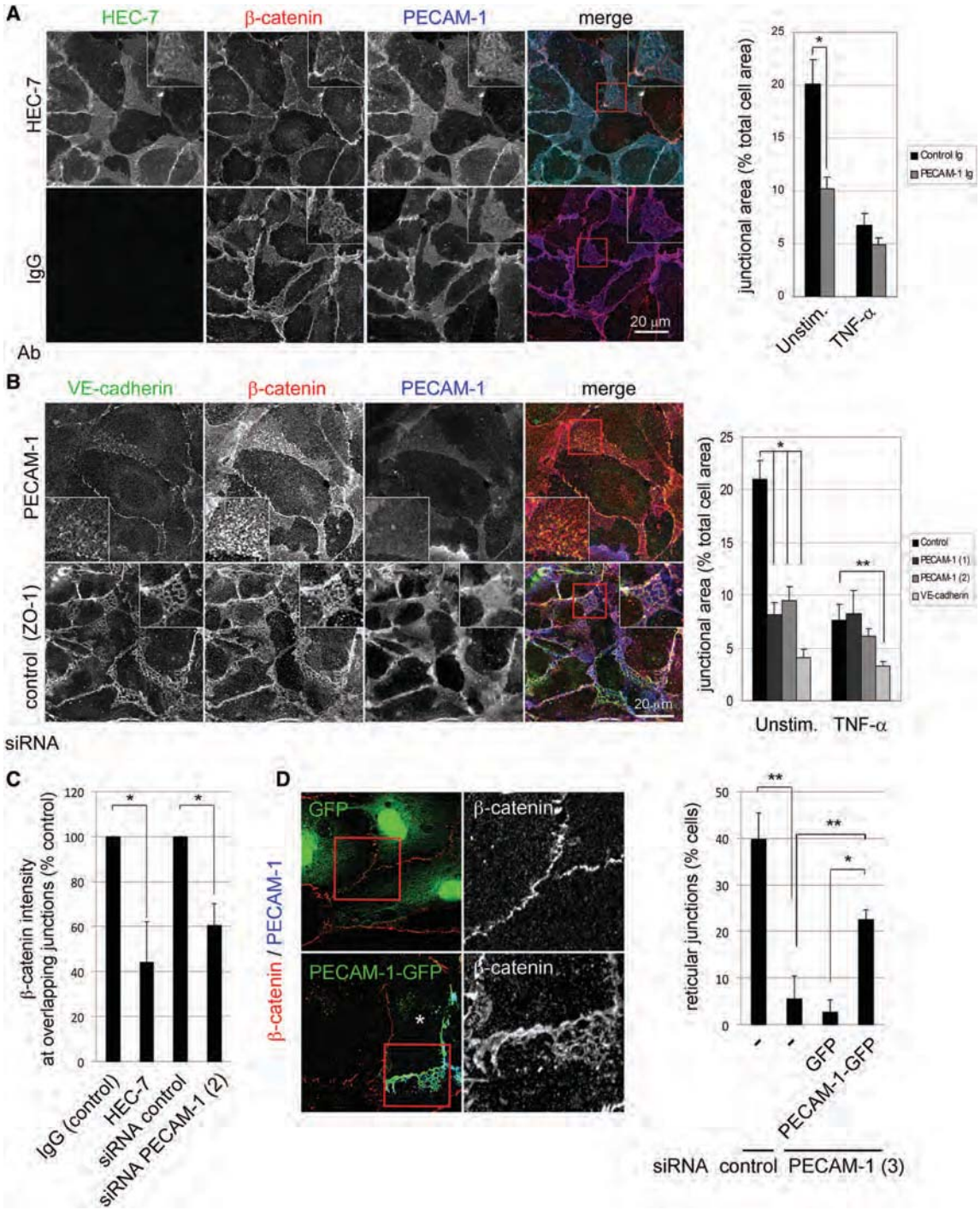

Figure 6. Platelet endothelial cell adhesion molecule-1 (PECAM-1) is required for organization of adherens junctions (AJ) into reticular but not into linear domains. Human umbilical vein endothelial cells (HUVECs) were plated at confluence for 70 hours. **A**, Cells were incubated with control IgG mouse antibody or anti–PECAM-1 blocking antibody HEC-7 (green) at 20 μg/mL for 90 minutes before fixation and stained for PECAM-1 and β-catenin to detect AJ. Note the absence of β-catenin reticulum in nonstimulated cells in the presence of HEC-7. Scale bar, 25 μm. Details of the distribution of junctional proteins are shown in the enlarged boxed areas. **B**, HUVECs were transfected with small interfering RNA (siRNA) oligonucleotides targeting PECAM-1 or the tight junction protein ZO-l. After 24 hours, cells were trypsinized and plated at confluence and analyzed 48 hours later (72 hours after transfection) by immunofluorescence for the indicated proteins. Scale bars, 20 μm. **Right graphs**, Quantification of junctional area in unstimulated cells and cells stimulated with tumor necrosis factor-α (TNF-α) for 20 hours includes cells transfected with vascular endothelial (VE)-cadherin siRNA. Bars show mean±SEM; **P*<0.0005; ***P*<0.02. **C**, Quantification of β-catenin intensity at overlapping junction areas of cells incubated with the indicated antibodies or transfected with the indicated siRNA oligonucleotides. Bars show mean±SEM; **P*<0.05. **D**, HUVECs were transfected with siRNA oligonucleotides targeting the 3′ untranslated region sequence of platelet endothelial cell adhesion molecule-1 (PECAM-1) mRNA (PECAM-1 (3)) or control. Twenty-four hours later, cells were transfected with green fluorescent protein (GFP) or PECAM-GFP and left confluent for 60 hours. Cells were fixed and stained for β-catenin and PECAM-1. Percentage of cells containing reticular AJ is quantified in the right graph. Bars show mean±SEM; n=3. ***P*<0.02; **P*<0.005.

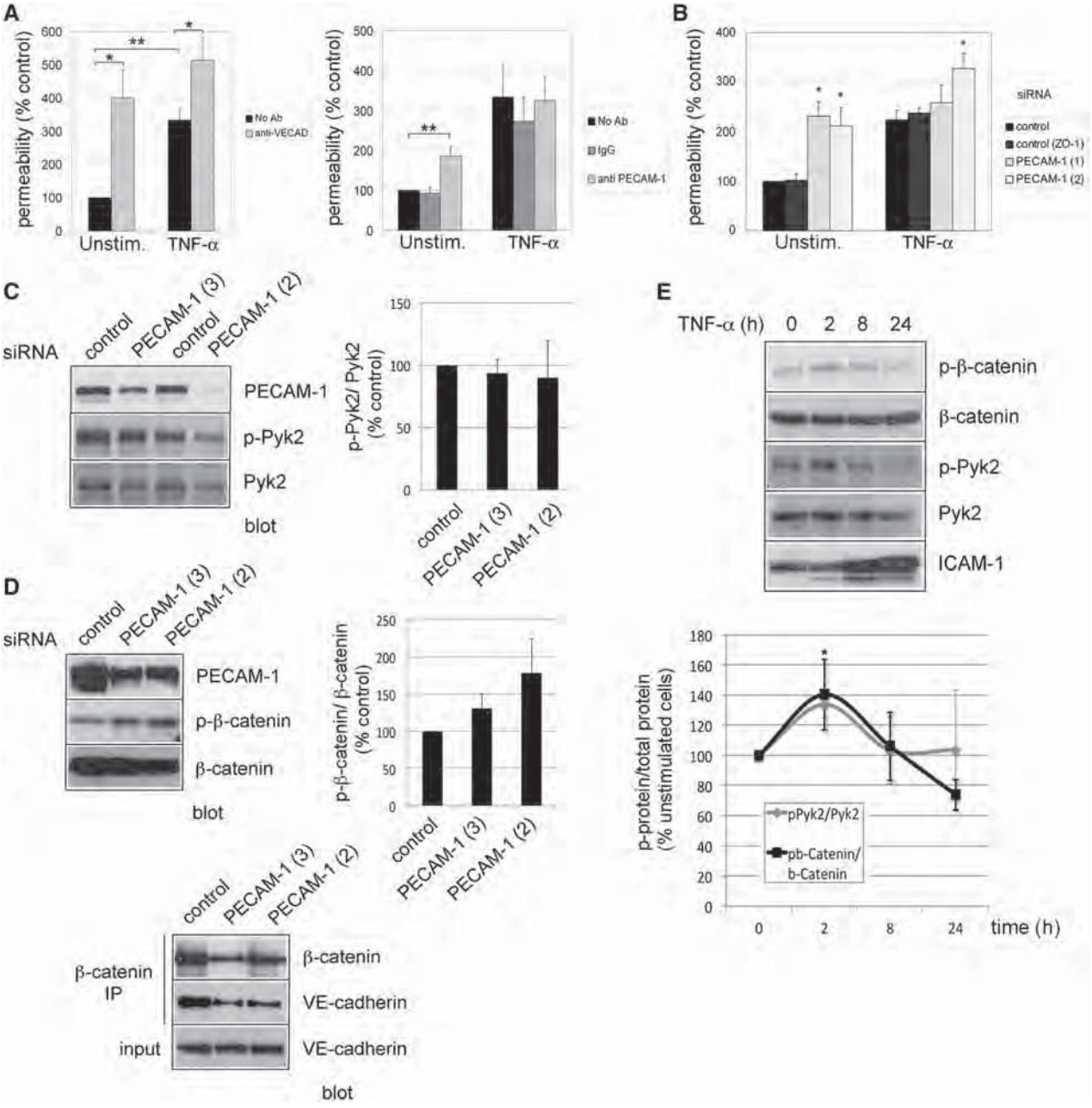

Figure 7. Platelet endothelial cell adhesion molecule-1 (PECAM-1) inhibition increases permeability and β-catenin phosphorylation. **A**, Human umbilical vein endothelial cells (HUVECs) were plated at confluence on transwells for 24 hours and then stimulated with or without 10 ng/mL tumor necrosis factor (TNF-α) in growth medium for 20 hours. Vascular endothelial (VE)-cadherin blocking antibody (5 μg/mL; **left**), PECAM-1 blocking antibody (20 μg/mL; **right**), or control IgG was added to the transwells 30 minutes before adding fluorescein isothiocyanate-dextran to measure monolayer permeability. **B**, HUVECs were transfected with small interfering RNAs (siRNAs) targeting PECAM-1, zonula occludens-1, or a nonspecific siRNA control. Permeability was analyzed 72 hours after transfection in unstimulated or TNF-α–stimulated cells. Bars show mean±SEM, n=3; **P*<0.05; ***P*<0.006. **C**, Effect of PECAM-1 siRNA on PECAM-1, pY402-Pyk2, and Pyk2 levels. **Right graph**, Bars show mean±SEM; n=3. **D**, Effect of PECAM-1 siRNA on PECAM-1, pT41/S45-β-catenin, and β-catenin levels. **Right graph**, Bars show mean±SEM; n=3. **E**, HUVECs were either stimulated with TNF-α or left unstimulated before lysis, SDS-PAGE, and immunoblotting with pT41/S45-β-catenin and β-catenin pY402-Pyk2, Pyk2, and ICAM-1 as a positive control of TNF-α activation. Graph shows mean±SEM; n=3; **P*<0.04.

present only in resting cells. Because TNF-α disperses PECAM-1 from junctions, PECAM-1 blocking antibody does not cause a further permeability increase. Similarly, PECAM-1 knockdown increased permeability >2-fold in unstimulated cells, whereas it had a reduced effect in TNF-α–stimulated cells, with low levels of PECAM-1 at cell borders (Figure 7B). In addition, the increase in permeability obtained with 2 siRNAs that strongly depleted PECAM-1 was similar to that induced by TNF-α (Figure 7B). We then investigated the possible mechanisms whereby PECAM-1 may regulate ROCK-independent permeability increase in response to TNF-α stimulation. The phosphoinositide 3-kinase isoform p110α regulates TNF-α–mediated barrier function through activation of the tyrosine kinase Pyk2.[18,19] Pyk2 activation is initiated

byY402 phosphorylation.[47] PECAM-1 knockdown induced no significant changes in pPyk2/Pyk2 ratio (Figure 7C), whereas TNF-α transiently increased Pyk2 phosphorylation, as previously reported (Figure 7E).[18] This indicates that PECAM-1 is not involved in Pyk2-mediated increase of permeability upon TNF-α exposure. On the other hand, VE-cadherin and PECAM-1 crosstalk within reticular domains might be mediated by β-catenin. PECAM-1 cytosolic tail binds the SHP2 phosphatase[25] and thereby controls glycogen synthase kinase 3β-mediated phosphorylation and a decrease in the stability of β-catenin.[25] Casein kinase-1α phosphorylates β-catenin at S45, which primes this N-terminal region for subsequent phosphorylation by glycogen synthase kinase 3β at T41, S37, and S33.[48] β-catenin phosphorylation can be also controlled by the kinase c-Jun N-terminal kinase.[49] Upon phosphorylation, β-catenin is uncoupled from cadherins and can be found in the cytosol, complexed with other proteins, which can lead to eventual proteasome degradation.[50] Indeed, PECAM-1 null mice exhibit a prolonged increase in permeability in response to histamine.[22,26] siRNA-mediated decrease of PECAM-1 in HUVECs significantly increased T41/S45 phosphorylation of β-catenin, in agreement with previous bibliography (Figure 7D, top panel).[25] No major decrease in β-catenin total levels was found though, which could be because of the fact that PECAM-1 siRNA only decreases partial PECAM-1 levels compared with the total elimination of the protein in PECAM-1 knockout cells.[25] Alternatively, PECAM-1 may control β-catenin phosphorylation, but additional signals could be required to promote its final degradation, because both events are not always coupled.[49] Indeed, nondegraded, phosphorylated β-catenin can be found accumulated in different nonjunctional areas in the cell.[49,51,52] Concomitantly, and in agreement with the AJ dispersion observed in Figure 6A and 6B, β-catenin association with VE-cadherin decreased (Figure 7D, bottom panel). Interestingly, similar to PECAM-1 knockdown, TNF-α also induced a transient phosphorylation of β-catenin (Figure 7E), which suggests that such phosphorylation may contribute to AJ alteration observed in response to this cytokine and this could be promoted by PECAM-1 dispersion from junctions.

Although the effect of TNF-α on permeability does not involve actomyosin-mediated contractility, TNF-α induces an increase in stress fibers and cell elongation. PECAM-1 knockdown, however, had no effect on F-actin levels or cell elongation (Figure XA in the online-only Data Supplement). In addition, myosin light chain phosphorylation at Ser-19 also remained unaffected upon PECAM-1 depletion, suggesting that general actomyosin-mediated contraction does not explain the permeability increase upon PECAM-1 reduction (Figure XB in the online-only Data Supplement). Finally, PECAM-1 or downstream glycogen synthase kinase 3β have been proposed as regulators of the nuclear factor-κB pathway during inflammatory responses.[53–55] We explored the possibility that PECAM-1 knockdown had no specific effect on cell junctions but instead increased permeability by inducing a proinflammatory phenotype. The expression of the adhesion receptor intercellular adhesion molecule-1 was analyzed as a marker of inflammation (Figure XB in the online-only Data Supplement). No increase was found in intercellular adhesion molecule-1 levels in response to PECAM-1 depletion, suggesting no role for PECAM-1 in inflammatory induction, in agreement with a previous report.[56] Taken together, these results indicate that inhibiting PECAM-1 in reticular AJ domains only reproduces the effects of TNF-α stimulation on cell–cell junctions but does not cause a general proinflammatory phenotype. PECAM-1 dispersal may, therefore, contribute to the TNF-α–mediated, actomyosin-independent, permeability increase through the control of β-catenin phosphorylation and reticular AJ stability.

Discussion

Cadherins and their binding partners interact to form AJ between neighboring cells. In addition to forming linear AJ at cell–cell borders, we show here that VE-cadherin has a reticular distribution in areas where adjacent endothelial cells overlap. Peripheral F-actin and stress fibers surround these reticular AJ but do not colocalize with them, in contrast to linear and discontinuous AJ that are always found associated with F-actin.[35] The possibility of reticular AJ being associated with some other undetectable cortical F-actin structures cannot be ruled out, but, in epithelial cells, an indirect link between AJ and F-actin has previously been proposed in confluent resting monolayers.[12,57] The role of α-catenin would consist of regulating local actin polymerization rather than directly bridging F-actin to AJ. This is consistent with the existence of a subset of endothelial AJ that is not in contact with perijunctional F-actin. In addition, nonmuscle myosins[58,59] and vinculin[9,60] mediate AJ stability and binding to perijunctional F-actin, playing a role as sensors of tension during epithelial remodeling. Here, we show that neither phosphorylated myosin light chain nor vinculin was enriched in reticular AJ. On the other hand, several reports have convincingly demonstrated a direct interaction between F-actin and AJ.[9,59–61] We have recently reported that endothelial cells can also form discontinuous AJ, which are orthogonal to cell–cell borders and associated with actin stress fibers, providing a connection between stress fibers in neighboring cells, which increases upon TNF-α stimulation.[35] The most plausible explanation for all these findings is that some AJ are associated with F-actin, whereas others, such as endothelial reticular AJ, do not require direct interaction with F-actin and are formed in areas of low mechanical tension.

In small blood vessels in vivo, we have observed endothelial junctional areas that resemble the reticular distribution of AJ and PECAM-1 observed in vitro, implying that reticular AJ exist in vivo. Junctional PECAM-1 has been localized in the LBRC, an internal vesicular compartment localized at cell–cell junctions.[21] We cannot exclude the possibility of the existence of a subset of AJ that is distributed in this LBRC. However, expression of AJ components bearing different fluorescent tags in adjacent cells clearly shows that most of reticular AJ are formed between VE-cadherin homophilic complexes from 2 different cells at overlapping junctional areas (Figure 1D). A comprehensive confocal analysis of reticular AJ shows that PECAM-1 and VE-cadherin stainings overlap, but that VE-cadherin reticular domains are more discrete and encompass PECAM-1. AJ and PECAM-1 are not physically associated in endothelial cell–cell junctions.[38] Superresolution microscopy confirmed that PECAM-1 and AJ are organized into different domains. PECAM-1 appeared distributed in discrete domains in the voids of reticular AJ, running along AJ

and often almost surrounded them. These PECAM-1–rich structures could be the proposed internal LBRC,[21] although further investigation into the nature of these domains in endothelial cell borders will shed light into this unique organization at junctions. Interestingly, the distribution of these PECAM-1 domains suggests that they may well be regulating the access of AJ to machinery involved in AJ trafficking or actin-mediated tension and thereby regulate their stability. Upon ectopic overexpression, PECAM-1-GFP, but not VE-cadherin, accumulated into internal domains, displaying a morphology that resembled that of reticular junctions (Figure IVB in the online-only Data Supplement). This would suggest that PECAM-1 has the intrinsic ability to form organized domains independently of AJ.

VE-cadherin and PECAM-1 crosstalk within reticular domains might be mediated by β-catenin. PECAM-1–null mice exhibit a prolonged increase in permeability in response to histamine,[22] which correlates with a phosphorylation increase and a decrease of β-catenin stability.[25] It has been proposed that PECAM-1 molecules in the proximity of AJ recruit SRC homology 2 domain-containing phosphatase, which maintains β-catenin in a dephosphorylated state, thereby stabilizing AJ. Here, we have found that TNF-α induces PECAM-1 dispersion from junctions and that this correlates with an increase in permeability, β-catenin phosphorylation, and with a decrease in reticular AJ. PECAM-1 knockdown is sufficient to reproduce all these alterations in HUVECs. It is of note that regulation of SRC homology 2 domain-containing phosphatase activity by TNF-α has been reported,[62] so, in the future, it would be of interest to address whether this cytokine regulates the presence and role of SRC homology 2 domain-containing phosphatase in reticular AJ or in PECAM-1 domains. On the other hand, we have also tested other pathways potentially involved in barrier function decrease, such as actomyosin-mediated tension, Pyk2 activation, or a general inflammatory response, and found no evidence of PECAM-1 role in these events. This suggests that the role of PECAM-1 in TNF-α stimulation is limited to the control of reticular AJ through the regulation of β-catenin phosphorylation, and not to a general regulation of inflammatory pathways, as it had been previously proposed.[53] Finally, there could exist additional crosstalk of AJ or PECAM-1 with other junctional components also found in these reticular areas, such as junctional adhesion molecule-A.

PECAM-1 could also contribute to transient AJ disruption to allow leukocyte diapedesis in noninflammatory conditions. Endothelial PECAM-1 engages in homophilic interactions with leukocytes.[25] PECAM-1 located in the LBRC mediates this paracellular route of transmigration.[21] We predict that recruitment of reticular PECAM-1 to sites of leukocyte interaction would locally disassemble reticular AJ, allowing leukocyte diapedesis with no need of general cell contraction. PECAM-1 return to reticular areas could subsequently facilitate reassembly of reticular AJ. Last, reticular AJ could also provide a source of additional membrane to allow endothelial remodeling to occur during leukocyte diapedesis or during changes in vessel diameter in response to stimuli that induce vasoconstriction or vasodilation.

In conclusion, we have characterized the properties of reticular AJ domains, which are distinctive of quiescent endothelium. These domains contain low levels of F-actin, suggesting that junctional actin filaments do not contribute to their formation. PECAM-1 is localized in a linear compartment that is interspersed within the voids of reticular AJ structures and may contribute to stabilize AJ and thereby regulate barrier function. Loss of reticular AJ by PECAM-1 inhibition mimics TNF-α–induced changes in reticular AJ and in endothelial barrier function but not in F-actin or intercellular adhesion molecule-1 expression. Further investigation of these reticular domains could identify specific targets to control barrier function without altering other important properties of endothelial cells during inflammation.

Acknowledgments

We are grateful to the members of the Ridley laboratory, as well as to Juan Francisco Aranda, Miguel A. Alonso, and Severine Gharbi for helpful discussions. We thank Pedro L. Majano for providing reagents. We thank Dr Santiago Lamas's laboratory for providing HUVECs and the confocal microscopy facility of the CBMSO.

Sources of Funding

This work was supported by the Ludwig Institute for Cancer Research, Cancer Research UK, the Association for International Cancer Research, and the EC FP6 project LSHG-CT-2003-502935 (MAIN). J. Millan was supported by a Marie Curie fellowship (HPMF-CT-2000-01061), a British Heart Foundation intermediate fellowship (FS/04/006), and grants from the Spanish Government SAF2008-01936 and SAF2011-22624. I. Correas was supported by grant BFU2011-22859. B. Marcos-Ramiro is supported by an FPI fellowship from Spanish government. N. Reglero-Real is supported by a JAE pre fellowship from Consejo Superior de Investigaciones Científicas and a grant from Biogen. S. Cox is supported by a Royal Society University Research Fellowship and the Wellcome Trust. The stimulated emission depletion microscope was funded by the British Heart Foundation.

Disclosures

None.

References

1. Bazzoni G, Dejana E. Endothelial cell-to-cell junctions: molecular organization and role in vascular homeostasis. *Physiol Rev*. 2004;84:869–901.
2. Yan X, Lin Y, Yang D, Shen Y, Yuan M, Zhang Z, Li P, Xia H, Li L, Luo D, Liu Q, Mann K, Bader BL. A novel anti-CD146 monoclonal antibody, AA98, inhibits angiogenesis and tumor growth. *Blood*. 2003;102:184–191.
3. Muller WA. The role of PECAM-1 (CD31) in leukocyte emigration: studies *in vitro* and in vivo. *J Leukoc Biol*. 1995;57:523–528.
4. Dejana E. Endothelial cell-cell junctions: happy together. *Nat Rev Mol Cell Biol*. 2004;5:261–270.
5. Harris ES, Nelson WJ. VE-cadherin: at the front, center, and sides of endothelial cell organization and function. *Curr Opin Cell Biol*. 2010;22:651–658.
6. Vincent PA, Xiao K, Buckley KM, Kowalczyk AP. VE-cadherin: adhesion at arm's length. *Am J Physiol, Cell Physiol*. 2004;286:C987–C997.
7. Spindler V, Schlegel N, Waschke J. Role of GTPases in control of microvascular permeability. *Cardiovasc Res*. 2010;87:243–253.
8. Rajasekaran AK, Hojo M, Huima T, Rodriguez-Boulan E. Catenins and zonula occludens-1 form a complex during early stages in the assembly of tight junctions. *J Cell Biol*. 1996;132:451–463.
9. Yonemura S, Wada Y, Watanabe T, Nagafuchi A, Shibata M. alpha-Catenin as a tension transducer that induces adherens junction development. *Nat Cell Biol*. 2010;12:533–542.
10. Knudsen KA, Soler AP, Johnson KR, Wheelock MJ. Interaction of alpha-actinin with the cadherin/catenin cell-cell adhesion complex via alpha-catenin. *J Cell Biol*. 1995;130:67–77.
11. Drees F, Pokutta S, Yamada S, Nelson WJ, Weis WI. Alpha-catenin is a molecular switch that binds E-cadherin-beta-catenin and regulates actin-filament assembly. *Cell*. 2005;123:903–915.
12. Yamada S, Pokutta S, Drees F, Weis WI, Nelson WJ. Deconstructing the cadherin-catenin-actin complex. *Cell*. 2005;123:889–901.
13. Wojciak-Stothard B, Ridley AJ. Rho GTPases and the regulation of endothelial permeability. *Vascul Pharmacol*. 2002;39:187–199.

14. Pober JS, Sessa WC. Evolving functions of endothelial cells in inflammation. *Nat Rev Immunol*. 2007;7:803–815.
15. Partridge CA, Horvath CJ, Del Vecchio PJ, Phillips PG, Malik AB. Influence of extracellular matrix in tumor necrosis factor-induced increase in endothelial permeability. *Am J Physiol*. 1992;263(6 Pt 1):L627–L633.
16. McKenzie JA, Ridley AJ. Roles of Rho/ROCK and MLCK in TNF-alpha-induced changes in endothelial morphology and permeability. *J Cell Physiol*. 2007;213:221–228.
17. Förster C, Burek M, Romero IA, Weksler B, Couraud PO, Drenckhahn D. Differential effects of hydrocortisone and TNFalpha on tight junction proteins in an *in vitro* model of the human blood-brain barrier. *J Physiol (Lond)*. 2008;586:1937–1949.
18. Cain RJ, Vanhaesebroeck B, Ridley AJ. The PI3K p110alpha isoform regulates endothelial adherens junctions via Pyk2 and Rac1. *J Cell Biol*. 2010;188:863–876.
19. Angelini DJ, Hyun SW, Grigoryev DN, Garg P, Gong P, Singh IS, Passaniti A, Hasday JD, Goldblum SE. Tnf-alpha increases tyrosine phosphorylation of vascular endothelial cadherin and opens the paracellular pathway through fyn activation in human lung endothelia. *Am J Physiol Lung Cell Mol Physiol*. 2006;291:L1232–L1245.
20. Muller WA, Weigl SA, Deng X, Phillips DM. PECAM-1 is required for transendothelial migration of leukocytes. *J Exp Med*. 1993;178:449–460.
21. Mamdouh Z, Chen X, Pierini LM, Maxfield FR, Muller WA. Targeted recycling of PECAM from endothelial surface-connected compartments during diapedesis. *Nature*. 2003;421:748–753.
22. Graesser D, Solowiej A, Bruckner M, Osterweil E, Juedes A, Davis S, Ruddle NH, Engelhardt B, Madri JA. Altered vascular permeability and early onset of experimental autoimmune encephalomyelitis in PECAM-1-deficient mice. *J Clin Invest*. 2002;109:383–392.
23. Schenkel AR, Chew TW, Muller WA. Platelet endothelial cell adhesion molecule deficiency or blockade significantly reduces leukocyte emigration in a majority of mouse strains. *J Immunol*. 2004;173:6403–6408.
24. Ferrero E, Ferrero ME, Pardi R, Zocchi MR. The platelet endothelial cell adhesion molecule-1 (PECAM1) contributes to endothelial barrier function. *FEBS Lett*. 1995;374:323–326.
25. Biswas P, Canosa S, Schoenfeld D, Schoenfeld J, Li P, Cheas LC, Zhang J, Cordova A, Sumpio B, Madri JA. PECAM-1 affects GSK-3beta-mediated beta-catenin phosphorylation and degradation. *Am J Pathol*. 2006; 169:314–324.
26. Privratsky JR, Paddock CM, Florey O, Newman DK, Muller WA, Newman PJ. Relative contribution of pecam-1 adhesion and signaling to the maintenance of vascular integrity. *J Cell Sci*. 2011;124:1477–1485.
27. Millán J, Hewlett L, Glyn M, Toomre D, Clark P, Ridley AJ. Lymphocyte transcellular migration occurs through recruitment of endothelial ICAM-1 to caveola- and F-actin-rich domains. *Nat Cell Biol*. 2006;8:113–123.
28. Tiruppathi C, Malik AB, Del Vecchio PJ, Keese CR, Giaever I. Electrical method for detection of endothelial cell shape change in real time: assessment of endothelial barrier function. *Proc Natl Acad Sci USA*. 1992;89:7919–7923.
29. Wójciak-Stothard B, Potempa S, Eichholtz T, Ridley AJ. Rho and Rac but not Cdc42 regulate endothelial cell permeability. *J Cell Sci*. 2001; 114:1343–1355.
30. Schnittler HJ. Structural and functional aspects of intercellular junctions in vascular endothelium. *Basic Res Cardiol*. 1998;93(Suppl):30–39.
31. Garlanda C, Dejana E. Heterogeneity of endothelial cells. Specific markers. *Arterioscler Thromb Vasc Biol*. 1997;17:1193–1202.
32. Tse D, Stan RV. Morphological heterogeneity of endothelium. *Semin Thromb Hemost*. 2010;36:236–245.
33. Ukropec JA, Hollinger MK, Woolkalis MJ. Regulation of VE-cadherin linkage to the cytoskeleton in endothelial cells exposed to fluid shear stress. *Exp Cell Res*. 2002;273:240–247.
34. Mitic LL, Anderson JM. Molecular architecture of tight junctions. *Annu Rev Physiol*. 1998;60:121–142.
35. Millán J, Cain RJ, Reglero-Real N, Bigarella C, Marcos-Ramiro B, Fernández-Martín L, Correas I, Ridley AJ. Adherens junctions connect stress fibres between adjacent endothelial cells. *BMC Biol*. 2010;8:11.
36. Edgell CJ, McDonald CC, Graham JB. Permanent cell line expressing human factor VIII-related antigen established by hybridization. *Proc Natl Acad Sci USA*. 1983;80:3734–3737.
37. Mège RM, Gavard J, Lambert M. Regulation of cell-cell junctions by the cytoskeleton. *Curr Opin Cell Biol*. 2006;18:541–548.
38. Kronstein R, Seebach J, Grossklaus S, Minten C, Engelhardt B, Drab M, Liebner S, Arsenijevic Y, Taha AA, Afanasieva T, Schnittler HJ. Caveolin-1 opens endothelial cell junctions by targeting catenins. *Cardiovasc Res*. 2012;93:130–140.
39. Campos SB, Ashworth SL, Wean S, Hosford M, Sandoval RM, Hallett MA, Atkinson SJ, Molitoris BA. Cytokine-induced f-actin reorganization in endothelial cells involves rhoa activation. *Am J Physiol Renal Physiol*. 2009;296:F487–F495.
40. Mong PY, Petrulio C, Kaufman HL, Wang Q. Activation of rho kinase by tnf-alpha is required for jnk activation in human pulmonary microvascular endothelial cells. *J Immunol*. 2008;180:550–558.
41. Nwariaku FE, Rothenbach P, Liu Z, Zhu X, Turnage RH, Terada LS. Rho inhibition decreases TNF-induced endothelial MAPK activation and monolayer permeability. *J Appl Physiol*. 2003;95:1889–1895.
42. Petrache I, Verin AD, Crow MT, Birukova A, Liu F, Garcia JG. Differential effect of MLC kinase in TNF-alpha-induced endothelial cell apoptosis and barrier dysfunction. *Am J Physiol Lung Cell Mol Physiol*. 2001;280:L1168–L1178.
43. Komarova YA, Mehta D, Malik AB. Dual regulation of endothelial junctional permeability. *Sci STKE*. 2007;2007:re8.
44. Millán J, Montoya MC, Sancho D, Sánchez-Madrid F, Alonso MA. Lipid rafts mediate biosynthetic transport to the T lymphocyte uropod subdomain and are necessary for uropod integrity and function. *Blood*. 2002;99:978–984.
45. Heyraud S, Jaquinod M, Durmort C, Dambroise E, Concord E, Schaal JP, Huber P, Gulino-Debrac D. Contribution of annexin 2 to the architecture of mature endothelial adherens junctions. *Mol Cell Biol*. 2008;28:1657–1668.
46. Florey O, Durgan J, Muller W. Phosphorylation of leukocyte pecam and its association with detergent-resistant membranes regulate transendothelial migration. *J Immunol*. 2010;185:1878–1886.
47. Mitra SK, Hanson DA, Schlaepfer DD. Focal adhesion kinase: in command and control of cell motility. *Nat Rev Mol Cell Biol*. 2005;6:56–68.
48. Liu C, Li Y, Semenov M, Han C, Baeg GH, Tan Y, Zhang Z, Lin X, He X. Control of beta-catenin phosphorylation/degradation by a dual-kinase mechanism. *Cell*. 2002;108:837–847.
49. Lee MH, Koria P, Qu J, Andreadis ST. Jnk phosphorylates beta-catenin and regulates adherens junctions. *FASEB J*. 2009;23:3874–3883.
50. MacDonald BT, Tamai K, He X. Wnt/beta-catenin signaling: Components, mechanisms, and diseases. *Dev Cell*. 2009;17:9–26.
51. Maher MT, Mo R, Flozak AS, Peled ON, Gottardi CJ. Beta-catenin phosphorylated at serine 45 is spatially uncoupled from beta-catenin phosphorylated in the GSK3 domain: implications for signaling. *PLoS ONE*. 2010;5:e10184.
52. Faux MC, Coates JL, Kershaw NJ, Layton MJ, Burgess AW. Independent interactions of phosphorylated β-catenin with E-cadherin at cell-cell contacts and APC at cell protrusions. *PLoS ONE*. 2010;5:e14127.
53. Privratsky JR, Newman DK, Newman PJ. PECAM-1: conflicts of interest in inflammation. *Life Sci*. 2010;87:69–82.
54. Cepinskas G, Savickiene J, Ionescu CV, Kvietys PR. PMN transendothelial migration decreases nuclear NFkappaB in IL-1beta-activated endothelial cells: role of PECAM-1. *J Cell Biol*. 2003;161:641–651.
55. Eto M, Kouroedov A, Cosentino F, Lüscher TF. Glycogen synthase kinase-3 mediates endothelial cell activation by tumor necrosis factor-alpha. *Circulation*. 2005;112:1316–1322.
56. Privratsky JR, Tourdot BE, Newman DK, Newman PJ. The anti-inflammatory actions of platelet endothelial cell adhesion molecule-1 do not involve regulation of endothelial cell NF-kappa B. *J Immunol*. 2010;184:3157–3163.
57. Weis WI, Nelson WJ. Re-solving the cadherin-catenin-actin conundrum. *J Biol Chem*. 2006;281:35593–35597.
58. Ivanov AI, Bachar M, Babbin BA, Adelstein RS, Nusrat A, Parkos CA. A unique role for nonmuscle myosin heavy chain IIA in regulation of epithelial apical junctions. *PLoS ONE*. 2007;2:e658.
59. Smutny M, Cox HL, Leerberg JM, Kovacs EM, Conti MA, Ferguson C, Hamilton NA, Parton RG, Adelstein RS, Yap AS. Myosin II isoforms identify distinct functional modules that support integrity of the epithelial zonula adherens. *Nat Cell Biol*. 2010;12:696–702.
60. le Duc Q, Shi Q, Blonk I, Sonnenberg A, Wang N, Leckband D, de Rooij J. Vinculin potentiates E-cadherin mechanosensing and is recruited to actin-anchored sites within adherens junctions in a myosin II-dependent manner. *J Cell Biol*. 2010;189:1107–1115.
61. Kametani Y, Takeichi M. Basal-to-apical cadherin flow at cell junctions. *Nat Cell Biol*. 2006;9:92–98.
62. Lerner-Marmarosh N, Yoshizumi M, Che W, Surapisitchat J, Kawakatsu H, Akaike M, Ding B, Huang Q, Yan C, Berk BC, Abe J. Inhibition of tumor necrosis factor-[alpha]-induced shp-2 phosphatase activity by shear stress: A mechanism to reduce endothelial inflammation. *Arterioscler Thromb Vasc Biol*. 2003;23:1775–1781.

THE JOURNAL OF IMMUNOLOGY

MAL Protein Controls Protein Sorting at the Supramolecular Activation Cluster of Human T Lymphocytes

Olga M. Antón, Laura Andrés-Delgado, Natalia Reglero-Real, Alicia Batista and Miguel A. Alonso

J Immunol 2011; 186:6345-6356; Prepublished online 20 April 2011;
doi: 10.4049/jimmunol.1003771
http://www.jimmunol.org/content/186/11/6345

The Journal of Immunology is published twice each month by
The American Association of Immunologists, Inc.,
9650 Rockville Pike, Bethesda, MD 20814-3994.

Print ISSN: 0022-1767 Online ISSN: 1550-6606.

MAL Protein Controls Protein Sorting at the Supramolecular Activation Cluster of Human T Lymphocytes

Olga M. Antón, Laura Andrés-Delgado, Natalia Reglero-Real, Alicia Batista, and Miguel A. Alonso

T cell membrane receptors and signaling molecules assemble at the immunological synapse (IS) in a supramolecular activation cluster (SMAC), organized into two differentiated subdomains: the central SMAC (cSMAC), with the TCR, Lck, and linker for activation of T cells (LAT), and the peripheral SMAC (pSMAC), with adhesion molecules. The mechanism of protein sorting to the SMAC subdomains is still unknown. MAL forms part of the machinery for protein targeting to the plasma membrane by specialized mechanisms involving condensed membranes or rafts. In this article, we report our investigation of the dynamics of MAL during the formation of the IS and its role in SMAC assembly in the Jurkat T cell line and human primary T cells. We observed that under normal conditions, a pool of MAL rapidly accumulates at the cSMAC, where it colocalized with condensed membranes, as visualized with the membrane fluorescent probe Laurdan. Mislocalization of MAL to the pSMAC greatly reduced membrane condensation at the cSMAC and redistributed machinery involved in docking microtubules or transport vesicles from the cSMAC to the pSMAC. As a consequence of these alterations, the raft-associated molecules Lck and LAT, but not the TCR, were missorted to the pSMAC. MAL, therefore, regulates membrane order and the distribution of microtubule and transport vesicle docking machinery at the IS and, by doing so, ensures correct protein sorting of Lck and LAT to the cSMAC. ***The Journal of Immunology*****, 2011, 186: 6345–6356.**

In response to appropriate Ags presented by an APC, T cells polarize, forming a surface subdomain at the T cell–APC interface known as the immunological synapse (IS) (1, 2). Membrane receptors and signaling molecules are not randomly distributed at the IS but, instead, assemble into a well-defined structure known as the supramolecular activation cluster (SMAC), which is subcompartmented into two differentiated concentric zones, termed the central SMAC (cSMAC) and peripheral SMAC (pSMAC) (3). The cSMAC contains the T cell Ag receptor/CD3 complex (TCR), Lck, and the linker for activation of T cells (LAT) adapter. pSMAC contains adhesion molecules, such as LFA-1 and ICAM-1, and cytoskeletal proteins, such as actin and talin. The actin cytoskeleton and intracellular protein trafficking are important for SMAC assembly (4, 5). The precise mechanism by which the cSMAC and pSMAC are formed is still unknown, but is believed to depend on signals generated by the TCR. Although its exact role remains a mystery, the IS is thought to be a focal point for endocytosis, exocytosis (6), and signaling (7).

One of the mechanisms proposed for compartmentation in biological membranes is the clustering of specific lipids, such as cholesterol and sphingolipids, into highly condensed domains. The use of the membrane fluorescent probe Laurdan has allowed visualization of cholesterol-dependent membrane domains with different degrees of condensation in living cells (8, 9). Condensed membranes are probably equivalent to liquid-ordered membrane assemblies of glycolipid and cholesterol, also referred to as membrane rafts, which play a role in the recruitment of specific proteins for membrane trafficking or signaling events and in the formation of membrane compartments such as caveolae (10, 11). Paralleling the elucidation of the SMAC architecture, membrane rafts emerged as putative functional platforms for the assembly of signaling machinery around the TCR at the IS. However, although raft lipids translocate to the IS (12), the IS contains condensed membranes (13), and TCR activation domains accumulate raft lipids (14), protein–protein interactions seem to be sufficient for the assembly of the signaling machinery (15). Therefore, the role of raft membranes at the IS remains unknown.

MAL is a highly hydrophobic integral membrane protein of 17 kDa consisting of four hydrophobic segments separated by short hydrophilic loops. MAL is expressed in normal human T lymphocytes and polarized epithelia as well as in representative cell lines, such as human Jurkat T cells and epithelial Madin-Darby canine kidney cells, respectively. A highly peculiar feature of MAL is its selective partitioning into detergent-resistant membrane (DRM) fractions that are enriched in compact membranes (16, 17). MAL silencing in Madin-Darby canine kidney cells severely impairs the targeting of influenza virus hemagglutinin (HA) to the apical surface and produces its intracellular retention and missorting to the basolateral surface (17, 18). Similarly, MAL silencing in human T cells blocks transport of Lck to the cell surface and induces its intracellular accumulation (19). Remarkably, the

Centro de Biología Molecular Severo Ochoa, Consejo Superior de Investigaciones Científicas and Universidad Autónoma de Madrid, Cantoblanco, 28049 Madrid, Spain

Received for publication November 15, 2010. Accepted for publication March 22, 2011.

This work was supported by Grants BFU2009-07886 and CONSOLIDER CSD2009-00016 (to M.A.A.) from the Ministerio de Ciencia e Innovación, Spain.

Address correspondence and reprint requests to Dr. Miguel A. Alonso, Centro de Biologia Molecular Severo Ochoa, Nicolas Cabrera, 1, Madrid 28049, Spain. E-mail address: maalonso@cbm.uam.es

The online version of this article contains supplemental material.

Abbreviations used in this article: cSMAC, central supramolecular activation cluster; DRM, detergent-resistant membrane; GP, generalized polarization; HA, hemagglutinin; IS, immunological synapse; LAT, linker for activation of T cells; NA, numerical aperture; PKC, protein kinase C; pSMAC, peripheral supramolecular activation cluster; SEB, staphylococcal enterotoxin B; SEE, staphylococcal enterotoxin E; SMAC, supramolecular activation cluster; *t*-SNARES, target-membrane SNARES.

www.jimmunol.org/cgi/doi/10.4049/jimmunol.1003771

effect on HA and Lck targeting strictly correlates with the exclusion of both cargo molecules from DRMs. MAL clustering has been shown to create specifically large, condensed membrane domains in the plasma membrane (20). MAL is, therefore, considered a component of the machinery for organization and function of condensed membranes in epithelial cells and human T lymphocytes (17, 20).

Although the requirement of MAL for Lck transport in resting T cells is established, its possible role at the IS has not been explored. In this study, we examined the dynamics of MAL during the formation of the IS and observed that a pool of MAL rapidly redistributed to the cSMAC. Remarkably, the expression of a modified MAL protein mistargeted to the pSMAC causes mislocalization of the raft-associated Lck and LAT molecules to the pSMAC. The missorting of MAL, Lck, and LAT was accompanied by a redistribution of condensed membranes and docking machinery for transport vesicle (syntaxin-4 and SNAP-23) or microtubules (EB1 and adenomatous polyposis coli protein) from the cSMAC to the pSMAC. Moreover, ectopically expressed HA, which is normally targeted to the cSMAC, was misrouted to the pSMAC under those conditions, reflecting the profound alternations in protein sorting at the SMAC primarily caused by MAL mislocalization. In summary, our results strongly argue for a role of MAL in the organization of the IS by targeting condensed membranes, docking machinery for transport vesicles and microtubules, and proteins specific to the cSMAC.

Materials and Methods

Materials

The mAb 6D9 to human MAL was previously described (16). The rabbit Abs to CD3ζ and ZAP70 and the mAbs to ICAM-3 and CD45 were kindly provided by Dr. Alarcón (Centro de Biología Molecular "Severo Ochoa," Madrid, Spain) and Dr. Sánchez-Madrid (Hospital de la Princesa, Madrid, Spain). The rabbit polyclonal Ab to Lck and mAb MEM-43/5 to CD59 were kindly provided by Dr. Veillette (McGill University, Montreal, Canada) and Dr. Horejsi (Institute of Molecular Genetics, Prague, Czech Republic), respectively. The Abs to phospholipase Cγ1, protein kinase C (PKC)-θ, EB1, syntaxin-4, and phosphotyrosine PY20 were from Transduction Labs (Lexington, KY); the mouse hybridoma producing anti-myc mAb 9E10 was purchased from the American Type Culture Collection; the Abs to total or phosphorylated Erk were from Promega (Madison, WI); the Abs to LAT were purchased from Upstate Biotechnology (Lake Placid, NY); the Abs to SNAP-23 and adenomatous polyposis coli protein we obtained from Santa Cruz Biotechnology(Santa Cruz, CA); anti-FLAG Ab M2 and anti–α-tubulin mAb DM1A were from Sigma-Aldrich (St. Louis, MO). We obtained staphylococcal enterotoxin E (SEE) and B (SEB) superantigens from Toxin Technology (Sarasota, FL). HRP-conjugated secondary Abs were obtained from Pierce. Cell Tracker orange-fluorescent tetramethylrhodamine, secondary goat Abs coupled to Alexa 488, Alexa 594, or Alexa-647, and TRITC-phalloidin were purchased from Molecular Probes (Eugene, OR).

Cell-culture conditions and conjugate-formation procedure

Human T lymphoblastoid Jurkat cells were grown in RPMI 1640 supplemented with 5% FBS (Sigma-Aldrich), 50 U/ml penicillin, and 50 μg/ml streptomycin at 37˚C in an atmosphere of 5% CO_2/95% air. To distinguish Raji cells from Jurkat cells in the conjugates, Raji cells (3.0×10^6 cells/ml) were stained with the appropriate fluorescent cell tracker for 20 min at 37˚C, washed, and resuspended in RPMI 1640/5% FBS. The cells were then incubated for 20 min in the presence or absence of 4 μg/ml SEE and mixed with an equal number of Jurkat cells (5.0×10^5 cells/well) in a final volume of 50 μl, incubated at 37˚C for 15 min, and plated onto poly-L-lysine–coated slides. After incubation for 15 min at 37˚C, cells were processed for immunofluorescence. Jurkat CH7C17 cells expressing exogenous TCRα- and TCRβ- (Vβ3)chains specific for HA were conjugated to HOM2 cells in the presence of 200 μg/ml HA peptide 307–319 (PKYVKQNTLKLAT), a control inactive peptide (PKYVKQNTLELAT), or 4 μg/ml SEB. For conjugation of primary T cells, freshly isolated T lymphocytes from healthy donors were incubated with SEE-pulsed Raji cells and processed as described for the Jurkat–APC conjugates. The experiments with human cells were done following the guidelines of the Bioethics Committee of the Spanish Research Council and were approved by the institutional Management Committee of the Centro de Biología Molecular Severo Ochoa.

DNA constructs and transfection conditions

The MAL-FLAG DNA construct, encoding MAL with its final extracellular loop modified by insertion of the 13-aa sequence DYKDDDDKAANLT, which contains the FLAG epitope (DYKD), was described previously (21). The DNA constructs expressing intact MAL or MAL-FLAG molecules with N-terminal myc, GFP, or cherry tags were generated by standard techniques, as were the constructs expressing GFP or cherry appended to the C terminus of Lck or LAT (Lck-GFP, Lck-cherry). The pSuperhMAL/GFP construct expressing GFP and the shRNA targeted to MAL mRNA from the same plasmid were described previously (19). To interfere with MAL expression and simultaneously express GFP fusions of Lck or LAT, the coding sequences of these proteins were inserted in-frame with the GFP coding sequence in the pSuperhMAL/GFP DNA construct. The plasmid expressing the transmembrane HA protein fused to GFP (22) was a kind gift from Dr. Lippincott-Schwartz (National Institutes of Health, Bethesda, MD). The Lck10-GFP DNA construct (23) was generously provided by Dr. Rodgers (Oklahoma Medical Research Foundation). Jurkat cells were transfected by electroporation using the Gene Pulser system (Bio-Rad, Hercules, CA). For transfection of human primary T cells, we used Amaxa nucleofector equipment (Lonza).

Immunofluorescence analysis

Cells were fixed in formalin for 20 min, rinsed, and treated with 10 mM glycine in PBS for 5 min to quench the aldehyde groups. Cells were then washed, permeabilized or not with 0.2% Triton X-100 in PBS at 4˚C for 5 min, rinsed, incubated with 3% (w/v) BSA for 15 min, and incubated with the primary Ab. After 1 h at room temperature, cells were washed and incubated with the appropriate fluorescent secondary Ab. For double-labeling experiments, the same procedure was repeated for the second primary Ab. Controls to assess the specificity of the labeling included incubations with control primary Abs and omission of the primary Abs. Immunofluorescence images were obtained using a Meta LSM 510 Confocal Laser microscope (Carl Zeiss, Oberkochen, Germany). For single-color time-lapse confocal fluorescence microscopy, Jurkat cells expressing stably myc-tagged MAL or MAL-FLAG proteins were transfected with GFP fusions of Lck, LAT, or EB3. For dual-color time-lapse microscopy, normal Jurkat cells stably expressing GFP-MAL or GFP-MAL-FLAG were used for the expression of cherry fusions of Lck or LAT. Images were captured using a Zeiss LSM 510 confocal microscope equipped with a 63× objective (1.2 numerical aperture [NA] water objective or 1.4 NA oil immersion objective for live or fixed cells, respectively; Carl Zeiss) and transferred to a computer workstation running MetaMorph imaging software (Molecular Devices, Downington, PA). Three-dimensional reconstruction and colocalization images representing only the pixels in which the staining of the two analyzed proteins coincided were done using the Image J program (National Institutes of Health; http://rsb.info.nih.gov/ij). The level of colocalization was represented by a pseudocolored scale (0, no colocalization; +1, maximal colocalization). For deconvolution, we used the Huygens 3.0 program (Scientific Volume Imaging, Hilversum, The Netherlands).

Laurdan staining

Live cells were labeled with the Laurdan fluorescent probe (5 μM), the microscope was calibrated, and two-photon microscopy was performed as described elsewhere (8) using an LSM 710 NLO Multiphoton coupled to an AxioObserver inverted microscope (Carl Zeiss MicroImaging, Thornwood, NY) with a 63× water objective and NA 1.3. In brief, Laurdan was excited at 800 nm, and emission intensities were recorded simultaneously in the 400–460 nm and 470–530 nm ranges. Intensity images were converted into a generalized polarization (GP) index defined as I(400–460) − I(470–530)/I(400–460) + I(I(470–530), in which I is the emission intensity, as previously described (8). GP values range from −1 (fluid domains) to +1 (highly ordered domains); membranes with GP values >0.3 were considered to be ordered membrane domains. The GP distributions and mean GP values obtained from GP images were normalized and represented using the GraphPad Prism program (GraphPad, San Diego, CA).

Detergent extraction procedures, immunoblot, and immunoprecipitation analyses

Jurkat cells (5.0×10^7 cells) were lysed for 15 min in 25 mM Tris-HCl (pH 7.2), 150 mM NaCl, and 0.2% Triton X-100 at 4˚C in the presence of

phosphatase and protease inhibitors. The extract was brought to 40% sucrose (w/w) and placed at the bottom of two sequential layers of 30% and 5% sucrose. Gradients were centrifuged to equilibrium, and the soluble and low-density insoluble fractions were harvested (24). Equivalent aliquots from the soluble and insoluble fractions were subjected to SDS-PAGE and transferred to Immobilon-P membranes (Millipore, Bedford, MA). After blocking with 5% nonfat dry milk and 0.05% Tween-20 in PBS, blots were incubated with the appropriate Abs for 1 h. After several washes, blots were incubated for 30 min with secondary Abs coupled to HRP and developed using a commercial kit (Amersham Biosciences, Buckinghamshire, U.K.). For immunoprecipitation studies, cells were lysed in 25 mM Tris-HCl (pH 7.4), 150 mM NaCl, 5 mM EDTA, 0.5% Triton X-100, and a mixture of phosphatase and protease inhibitors. The lysates were precleared for 1 h at 4˚C with protein G-Sepharose, centrifuged, and the supernatant incubated with the indicated specific Abs for 1 h at 4˚C. After incubation with protein G-Sepharose for 1 h, the immunoprecipitates were collected by centrifugation, washed six times, and analyzed by immunoblotting with the appropriate Abs.

Statistical analysis

Data are expressed as mean ± SEM. A paired Student *t* test was used to establish the statistical significance of differences between the means.

Results

MAL translocates to the cSMAC

In resting Jurkat T cells, MAL distributes in distinct pools at different locations (Fig. 1*A*, Supplemental Fig. 1*A*). One such pool is present at the plasma membrane. A second pool is found in pericentriolar endosomes, where MAL shows a high level of colocalization with the recycling endosome markers Rab11 and internalized transferrin. The colocalization of MAL with EEA1 and Rab5, which label early endosomes, or CD63, a late endosome marker, was much lower. Finally, a third pool decorates part of the radial microtubule cytoskeleton. A quantitative analysis of the colocalizations is shown in Supplemental Fig. 1*B*. To analyze

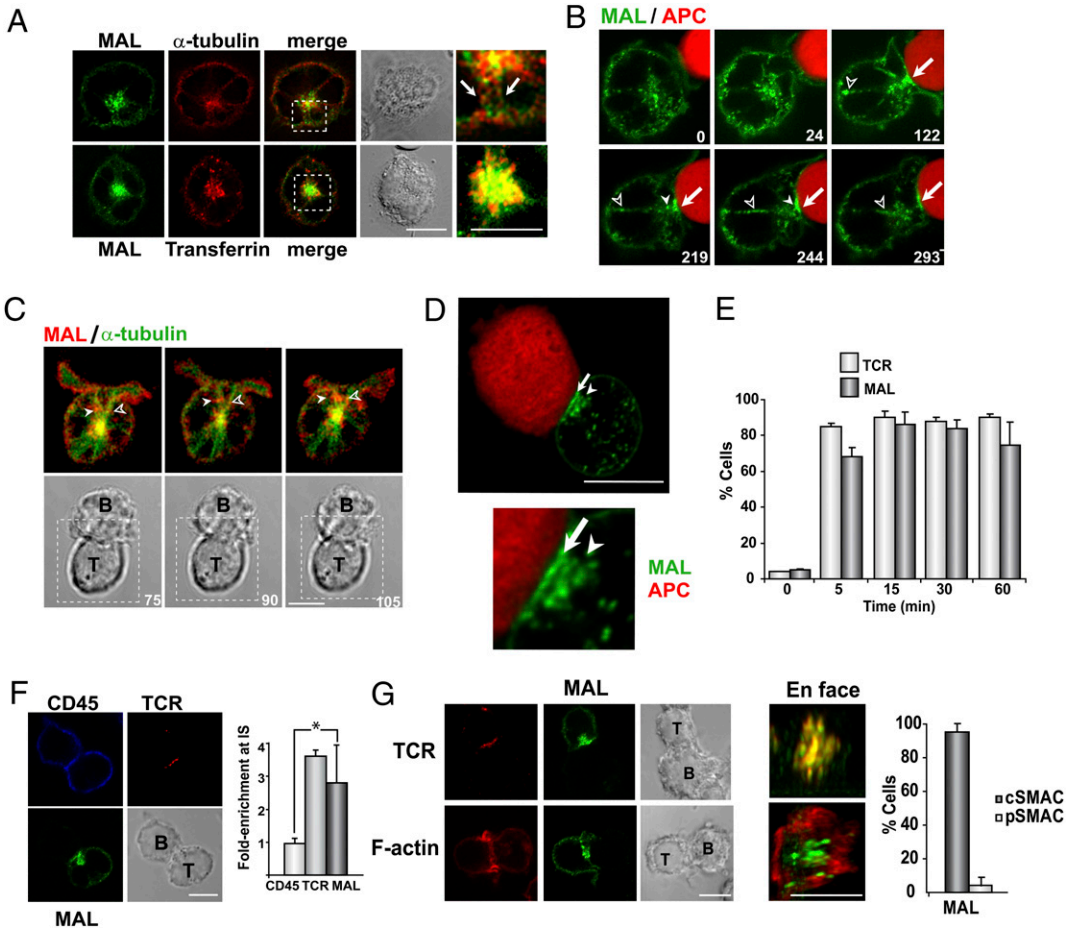

FIGURE 1. MAL translocates to the cSMAC in T cell–APC conjugates. *A*, Jurkat cells stably expressing myc-tagged MAL were loaded with human transferrin for 15 min, washed, and were processed 20 min later for double-label immunofluorescence analysis of MAL and transferrin or α-tubulin. A magnification of the boxed region is shown in the *right panels*. The arrows point to microtubules positive for MAL staining. *B*, Jurkat cells stably expressing GFP-MAL were conjugated to SEE-pulsed APCs and subjected to time-lapse videomicroscopy. Solid and clear arrowheads indicate vesicles/tubules transporting MAL from the Golgi region to the IS or from the cell periphery to the Golgi region, respectively. Arrows indicate sites of MAL accumulation at the IS. Numbers indicate time in seconds. *C*, Jurkat cells stably expressing cherry-MAL were transfected with a DNA construct expressing α-tubulin–GFP. After 24 h, cells were conjugated to SEE-pulsed APCs and subjected to time-lapse videomicroscopy. Solid and clear arrowheads indicate two vesicles transporting MAL from the Golgi to the IS. Numbers indicate time in seconds. *D*, Side view of a T cell–APC interface. The arrow and arrowhead indicate the MAL pools at the IS and the centrosomal region, respectively. *E*, Quantification of the number of T cells with MAL or TCR at the IS at different times of T cell–APC conjugation. *F*, Jurkat cells stably expressing myc-tagged MAL were conjugated to SEE-loaded APCs for 15 min. Cell were fixed, permeabilized, and stained for TCR, CD45, and MAL. The histogram represents the fluorescence intensity of the TCR, CD45, and MAL at the contact zone relative to that in the opposite region of the cell surface. *G*, Jurkat cells expressing myc-tagged MAL were conjugated to SEE-loaded APCs for 15 min. Cells were fixed, permeabilized, and processed for double-label immunofluorescence analysis for MAL and TCR or F-actin (*left panels*). A reconstruction image of the plane at the contact zone is shown (*right panels*). The histogram represents the percentage of T cells with MAL at the cSMAC or pSMAC. Means ± SEM of three independent experiments are represented in *E*–*G*. Scale bars, 5 μm.

dynamically the response of MAL to T cell stimulation, we used Jurkat J77 vβ8$^+$ cells stably expressing GFP-MAL as T cells and the Raji B cell line loaded with SEE as an APC (25). Time-lapse videomicroscopy revealed that soon after the T cell encountered an APC, a pool of MAL rapidly concentrated at the IS (Fig. 1*B*, Supplemental Video 1). A detailed analysis of the initial events during formation of the conjugates revealed that MAL rapidly distributed in the T cell lamellipodia embracing the APC and, a few seconds later, concentrated at the center of the contacting membranes. Almost simultaneously, the internal MAL pool reoriented, probably with the centrosome, to face the IS. In addition, numerous MAL-positive vesicles were visualized trafficking bidirectionally between the centrosomal region and the plasma membrane along tracks made of microtubules (Fig. 1*B*, 1*C*). We reconstructed three-dimensional images and rotated them to view the IS from the side, which allowed the MAL pool present at the contact membrane to be distinguished from that at the pericentriolar region, which is very close to the T cell–APC interface (Fig. 1*D*). The number of conjugates with MAL at the IS increased and had kinetics similar to that of TCR, with >80% of conjugates with MAL concentrated at the IS after 15 min of conjugation (Fig. 1*E*). Quantitative analysis showed an ~2.8-fold enrichment of MAL and an ~3.7-fold of TCR at the IS, whereas CD45 was evenly distributed at the plasma membrane (Fig. 1*F*). The accumulation of MAL at the IS occurred preferentially at the cSMAC, as revealed by double-label immunofluorescence analysis of MAL

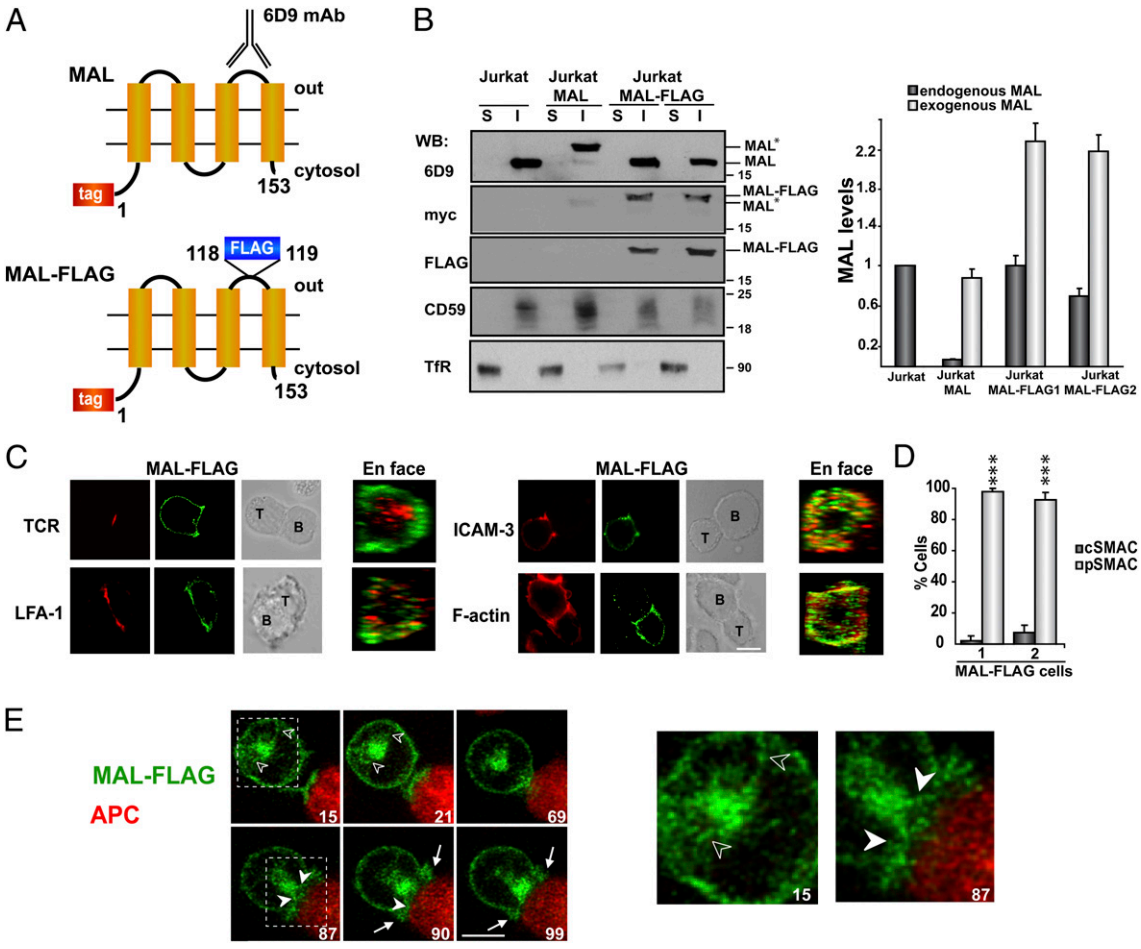

FIGURE 2. Modification of the last extracellular loop of MAL missorts the protein to the pSMAC. *A*, Schematic model of the MAL proteins for which exogenous expression was analyzed. Exogenous MAL molecules were modified with a tag (myc or GFP) at the N terminus (MAL) or also with a FLAG epitope at the last hydrophilic loop of the molecule (MAL-FLAG). The anti-MAL mAb 6D9 recognizes that loop in MAL but not in MAL-FLAG because it is disrupted by the insertion of the FLAG sequence. The anti-myc Ab recognizes the two types of exogenous MAL, and the anti-FLAG Ab only the MAL-FLAG molecule. *B*, The soluble (S) and the DRM (I) fractions from control Jurkat, Jurkat MAL, or Jurkat MAL-FLAG cells were immunoblotted with anti-MAL mAb 6D9 or Abs to the myc or FLAG epitopes (*left panels*). The position of endogenous MAL (MAL), myc-MAL (MAL*), and myc-MAL-FLAG (MAL-FLAG) as well as that of molecular mass markers is shown. The distributions of transferrin receptor (TfR) and CD59 were used as markers of the S and I fractions, respectively. A quantitative analysis of the levels of the endogenous and exogenous MAL molecules is shown (*right panel*). Two different clones of Jurkat MAL-FLAG cells (clones 1 and 2) were analyzed. *C*, Jurkat MAL-FLAG cells were conjugated to SEE-pulsed APCs for 15 min. Cells were fixed and, without the permeabilization step, stained with anti-FLAG Abs and anti-TCR, LFA-1, or ICAM-3 Abs. F-actin staining was performed after permeabilization once the cells were stained with anti-FLAG Abs. An en face view of the contact zone is also shown. The same result was obtained with MAL-FLAG cell clones 1 and 2. *D*, The histogram represents the percentage of T cells with MAL-FLAG at the cSMAC or pSMAC. Clones 1 and 2 of Jurkat MAL-FLAG cells were analyzed. For analysis of statistical significance, these values were compared with the corresponding values obtained for MAL in Jurkat MAL cells (Fig. 1*G*). Jurkat MAL-FLAG cell clone 1 was used in the rest of the experiments in this work. *E*, Jurkat MAL-FLAG cells were conjugated to SEE-pulsed APCs and subjected to time-lapse videomicroscopy. Solid and clear arrowheads indicate vesicles transporting MAL-FLAG from the Golgi region to the IS and from the cell periphery to the Golgi region, respectively. Arrows point to sites of MAL-FLAG accumulation at the IS. A higher magnification of the boxed areas is shown in the *right panels*. Numbers indicate time in seconds. Means ± SEM of three independent experiments are represented in *B* and *D*. Scale bars, 5 μm. ***$p < 0.001$.

and TCR or F-actin, which were used as markers of the cSMAC or pSMAC, respectively (Fig. 1*G*). Therefore, to summarize Fig. 1, a pool of MAL translocates rapidly to the T cell–APC interface and localizes at the cSMAC in the mature IS, and a second pool of MAL reorients to the IS, accompanying the movement of the centrosome.

MAL targeting to the cSMAC requires integrity of its last extracellular loop

Our anti-MAL Ab (6D9 mAb, Fig. 2*A*), which was made to the last hydrophilic loop of the MAL molecule, is not of use in immunofluorescence analysis. Because the proximity of the internal pool to the contact membrane often obscures the detection of the pool of MAL at the IS in permeabilized cells using cytosolically oriented tags, we expressed a modified MAL molecule (MAL-FLAG), which, in addition to the cytoplasmic myc tag present at the amino terminal end, bears a FLAG epitope in its last hydrophilic loop to allow staining in unpermeabilized cells (Fig. 2*A*). That loop was demonstrated previously to be extracellular (21). We generated stable transfectants expressing MAL-FLAG in Jurkat J77 cells (Jurkat MAL-FLAG) to prevent massive overexpression and compared these cells with transfectants expressing the MAL molecule with only the myc tag (Jurkat MAL) and with control, parental Jurkat J77 cells. Curiously, whereas Jurkat-MAL cells downmodulated the expression of endogenous MAL to compensate for the expression of exogenous MAL, this was not true in MAL-FLAG cells, resulting in the expression of approximately twice as much total MAL relative to parental cells (Fig. 2*B*).

The subcellular distribution of exogenous MAL (Supplemental Fig. 2*A*), the ability of exogenous MAL or MAL-FLAG to replace the endogenous MAL protein in the processes of Lck transport to the plasma membrane (Supplemental Fig. 2*B*), targeting of TCR to the IS (Supplemental Fig. 2*C*, 2*D*) and activation of signaling pathways in response to TCR triggering (Supplemental Fig. 2*E*–*H*), and the internalization of TCR (Supplemental Fig. 2*I*) were all mostly similar in the MAL and MAL-FLAG Jurkat cell transfectants, although a delay in ERK activation was observed in MAL-FLAG cells. Importantly, MAL-FLAG mostly localized to the pSMAC, as revealed by double-label immunofluorescence analysis with Abs to the FLAG epitope and TCR, LFA-1, ICAM-3, or F-actin staining in unpermeabilized cells (Fig. 2*C*, 2*D*). This result contrasts with the cSMAC distribution of MAL observed in Jurkat MAL cells (Fig. 1*G*). The missorting of MAL-FLAG to the pSMAC was confirmed in the T cell–APC conjugates formed using a second stable Jurkat MAL-FLAG cell clone (Fig. 2*D*). Time-lapse videomicroscopy of conjugates of cells stably expressing GFP-tagged MAL-FLAG revealed that, similar to MAL, MAL-FLAG was detected at the T cell lamellipodium surrounding the APC, at the centrosome region, and in trafficking vesicles (Fig. 2*E*, Supplemental Video 2). However, unlike MAL, which was evenly distributed along the edge of the embracing

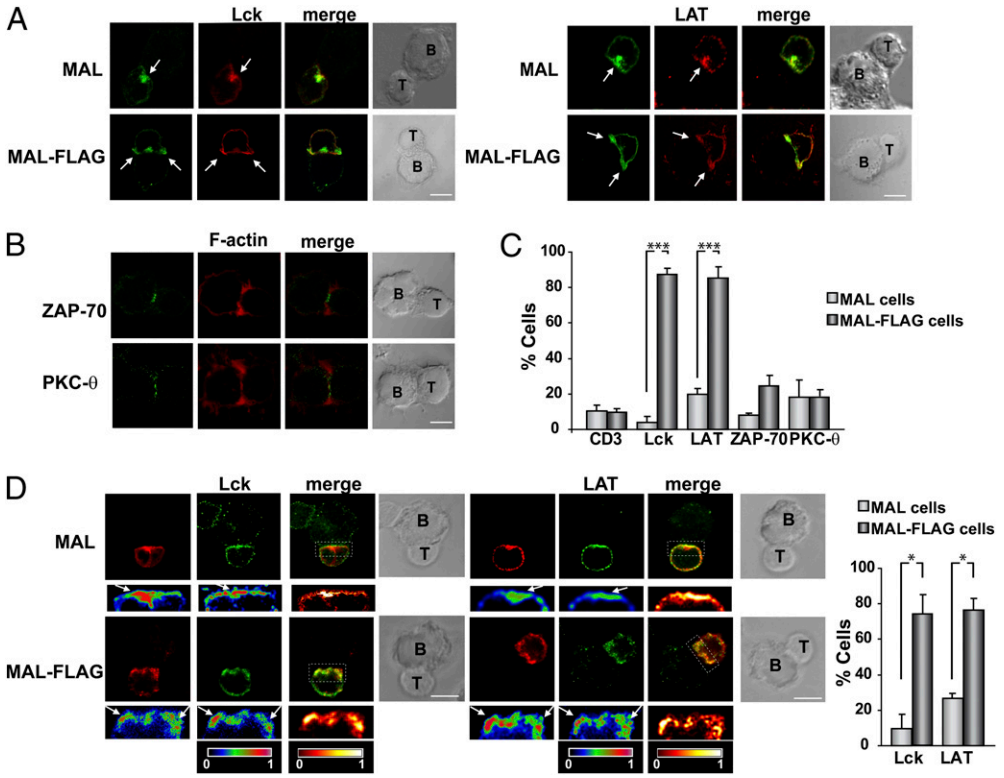

FIGURE 3. MAL distribution controls sorting of Lck and LAT at the SMAC. *A*, Jurkat MAL or Jurkat MAL-FLAG cells were conjugated to SEE-loaded APCs for 15 min. Cells were fixed, permeabilized, and stained for MAL and Lck (*left panels*) or LAT (*right panels*). Arrows point to sites of accumulation of the indicated proteins at the IS. *B*, Conjugates formed by Jurkat MAL-FLAG cells were stained for F-actin and ZAP70 or PKC-θ. *C*, Quantitative analysis of the percentage of Jurkat MAL or Jurkat MAL-FLAG cells with distribution of the indicated molecules to the pSMAC. *D*, Human primary T cells transiently expressing MAL or MAL-FLAG were conjugated to SEE-loaded APCs for 15 min. Cells were fixed, permeabilized, and analyzed for the distribution of Lck (*left panels*) or LAT (*right panels*). The *small panels* show a magnification of the contact area (boxed regions). The single-color images and the colocalization images, which represent only the pixels in which the staining of the two proteins coincides, corresponding to the magnifications were pseudocolored using the color scales indicated in each case. Arrows point to sites of accumulation of the indicated proteins at the IS. The histogram represents the percentage of cells with Lck or LAT at the pSMAC in the cells expressing MAL or MAL-FLAG. Mean values ± SEM of three (*C*) or two (*D*) independent experiments are represented. Scale bars, 5 μm. $*p < 0.05$, $***p < 0.001$.

lamellipodium, MAL-FLAG accumulated at the lamellipodium sides and remained there for a long time. The results presented in Figs. 1 and 2 show that a pool of MAL is targeted to cSMAC soon after contact of the T cell with the APC and that this targeting requires the integrity of the last extracellular loop of MAL, because its disruption caused missorting of MAL to the pSMAC.

MAL distribution controls sorting of Lck and LAT to specific SMAC subdomains

The observation that MAL-FLAG was missorted to the pSMAC prompted us to investigate whether the targeting of other SMAC proteins was affected. Although the distribution of TCR, LFA-1, or F-actin was unaltered, it is of note that both Lck and LAT were mistargeted to the pSMAC in Jurkat MAL-FLAG cells (Fig. 3*A*, 3*C*). ZAP70 and PKC-θ maintained their correct targeting to the cSMAC regardless of the distribution of exogenous MAL (Fig. 3*B*, 3*C*). The missorting of Lck and LAT induced by the presence of exogenous MAL at the pSMAC was corroborated by analyzing the distribution of transiently expressed GFP fusions of both molecules (Supplemental Fig. 3*A*). It is apparent that the targeting of MAL to the pSMAC or its effect on Lck and LAT mislocalization was not restricted to the use of the superantigen SEE, given that similar results were observed in T cell–APC conjugates formed with Jurkat CH7C17 cells (26) in the presence of SEB or the peptide-encompassing aa 307–319 of the HA molecule (Supplemental Fig. 3*B*, 3*C*). Finally, similar to the case of Jurkat MAL-FLAG cells, expression of MAL-FLAG in primary T lymphocytes resulted in mislocalization of Lck and LAT but not TCR to the IS periphery (Fig. 3*D*). In summary, the missorting of exogenous MAL to the pSMAC was accompanied by that of the raft-associated molecules Lck and LAT.

MAL is required for transport of Lck to the plasma membrane of resting T lymphocytes (19). Therefore, it is plausible that this could be also the case for Lck transport to the cSMAC in T cell–APC conjugates. To examine this hypothesis, we monitored the movement of MAL and Lck during IS formation by time-lapse videomicroscopy in Jurkat MAL cells and compared it with that in Jurkat MAL-FLAG cells (Fig. 4*A*–*D*). MAL and Lck were found to travel in the same or closely related transport carriers destined for the cSMAC in Jurkat MAL cells (Fig. 4*A*, Supplemental Fig. 4, Supplemental Video 3). In addition, we observed that whereas Lck and MAL were evenly distributed at the cell-to-cell interface after the initial contact between the T cell and APC (stage I), the levels of both proteins at the central part of IS gradually increased afterward (stages II to III) without sustained accumulation at peripheral sites (Fig. 4*C*). Lck and exogenous MAL were also found in the same transport vesicles in Jurkat MAL-FLAG cells (Fig. 4*B*, Supplemental Video 4), but, unlike Jurkat MAL cells, Lck and

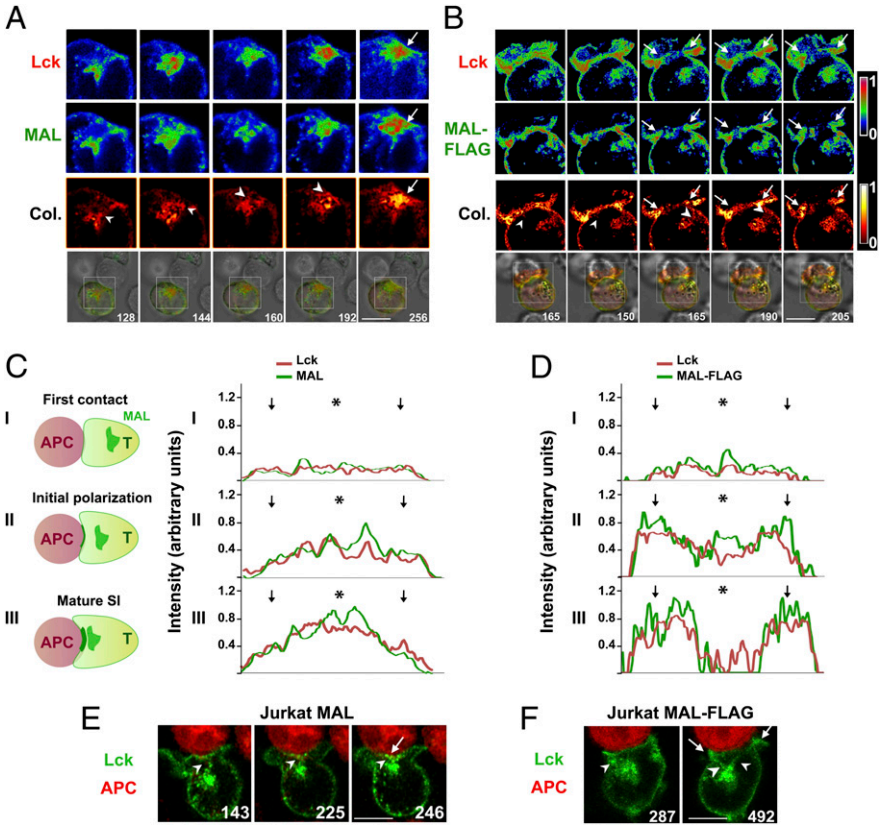

FIGURE 4. Effect of MAL distribution on Lck dynamics during IS formation. Jurkat MAL (*A*) or Jurkat MAL-FLAG (*B*) cells were transfected with a DNA construct encoding Lck-cherry. After 16 h, cells were conjugated to SEE-pulsed APCs and subjected to time-lapse videomicroscopy. The processes occurring within the boxed region in the differential contrast images (*bottom panels*) are shown at higher magnification in the *top panels*. The single-color images and the images representing only the pixels in which the staining of the two proteins coincides (Col.) were pseudocolored using the color scales indicated in each case. Arrows point to sites of accumulation of the indicated proteins at the IS. Arrowheads indicate vesicles that emerge from the Golgi region and travel to the IS. Numbers indicate time in seconds. *C* and *D*, The schematics on the left represent three stages (I–III) of IS formation defined by the progressive accumulation of MAL at the IS and the proximity of the centrosome to the contact zone. Graphs represent the fluorescence intensity of MAL (*C*) or MAL-FLAG (*D*) and Lck at the contact site at the indicated stages of IS formation obtained by analysis of Supplemental Videos 3 and 4, respectively. The arrows and the asterisk point to the periphery and the central part of the IS, respectively. Details of vesicles (arrowheads) transporting Lck to IS in Jurkat MAL (*E*) or Jurkat MAL-FLAG cells (*F*). Arrows point to sites of accumulation of Lck at the IS. Arrowheads indicate vesicles/tubules that transport Lck to the IS. Scale bars, 5 μm.

MAL accumulated at peripheral parts of the IS (stage II) and were excluded from the central part (stage III) (Fig. 4*D*). We visualized tubular connections between the centrosomal region and the IS that served as tracks for transport of Lck (Fig. 4*E*, 4*F*, Supplemental Video 5). It is of note that the connections ended at the central part of the IS in Jurkat MAL cells (Fig. 4*E*) or at its periphery in Jurkat MAL-FLAG cells (Fig. 4*F*). The results in Fig. 4 therefore indicate that MAL targets Lck directly to the cSMAC in Jurkat MAL cells or to the pSMAC in Jurkat MAL-FLAG cells and that this differential targeting takes place by vesicles and tubules that follow linear tracks connecting the centrosomal region with the cSMAC or pSMAC, respectively.

Although LAT colocalized extensively with MAL in pericentriolar endosomes (Supplemental Fig. 4), no colocalization of LAT with MAL-positive transport vesicles was found in Jurkat MAL or Jurkat MAL-FLAG cells forming an IS (Fig. 5*A*, 5*B*, Supplemental Fig. 4, Supplemental Videos 6, 7). Apparently, the initial accumulation of LAT to the IS does not involve vesicular transport from the centrosomal region in any of the two types of Jurkat cell, but, rather, LAT appears to redistribute mostly from a surface pool. Consistent with the lack of a role for MAL in targeting LAT to the cell surface, LAT transport to the plasma membrane of resting T cells occurred equally well regardless of MAL expression (Supplemental Fig. 5*A*) and took place in vesicular structures that were mostly devoid of MAL (Supplemental Fig. 5*B*). When we analyzed the redistribution of LAT to the IS in detail (Fig. 5*C*, 5*D*), we observed that initially LAT accumulated preferentially at the sides of the contact with the APC in Jurkat MAL and Jurkat MAL-FLAG cells (stage II). Later on, LAT disappeared from the IS sides and accumulated at the central part in Jurkat MAL cells (Fig. 5*C*, stage III), whereas in Jurkat MAL-FLAG cells, the levels of LAT at the IS sides increased continuously, with no evidence of redistribution to the central part (Fig. 5*D*, stage III). The results shown in Fig. 5 indicate that LAT follows a mechanism different from that of Lck for IS targeting, given that LAT appears to redistribute from a surface pool, but, similar to Lck, the accumulation of MAL at the cSMAC or pSMAC dictates the final location for concentration of LAT.

Mistargeting of MAL to the pSMAC causes reduced membrane condensation at the cSMAC and missorting of raft markers to the pSMAC

The N-terminal 10-aa sequence of Lck is sufficient to confer myristoylation and double palmitoylation on a GFP chimera (Lck10-GFP) and to incorporate it into DRMs (23, 27). Lck10-GFP has been used as a probe to monitor the distribution of specific compact membranes in T cells (23). Similar to Lck and LAT, Lck10-GFP accumulated at the cSMAC or pSMAC depending on the place of exogenous MAL accumulation (Fig. 6*A*, 6*B*). The distribution of ganglioside GM1, a raft marker normally

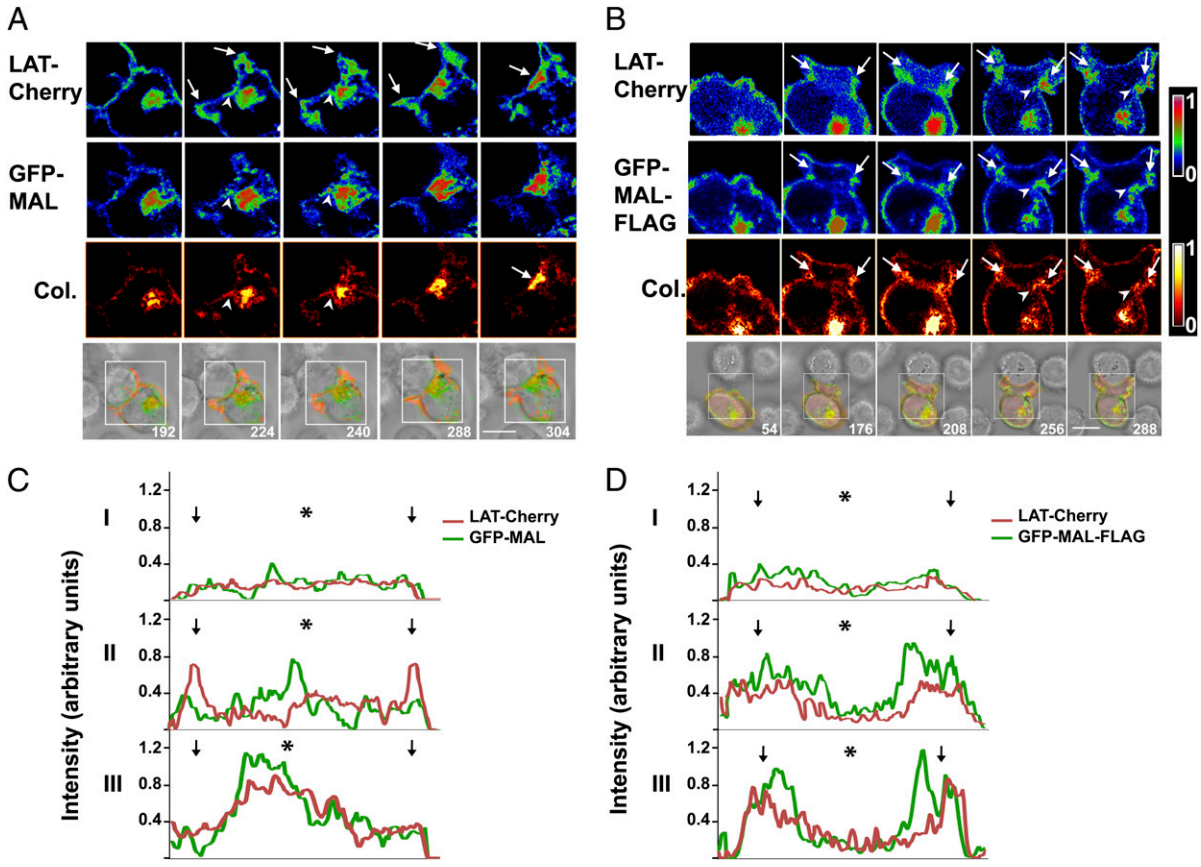

FIGURE 5. Effect of MAL distribution on LAT dynamics during IS formation. Jurkat MAL cells (*A*) or Jurkat MAL-FLAG cells (*B*) expressing LAT-cherry for 16 h were conjugated to SEE-pulsed APCs and subjected to time-lapse videomicroscopy. The processes occurring within the boxed region in the differential contrast images (*bottom panels*) are shown at higher magnification in the *top panels*. The single-color images and the images representing only the pixels in which the staining of the two proteins coincides (Col.) were pseudocolored using the color scales indicated in each case. Arrows point to sites of accumulation of the indicated proteins at the IS. Arrowheads indicate vesicles that emerge from the Golgi region and travel to IS. Numbers indicate time in seconds. Graphs representing the fluorescence intensity of LAT and MAL (*C*) or MAL-FLAG (*D*) staining at the contact site at the indicated stages of IS formation obtained by analysis of Supplemental Videos 6 and 7, respectively. The arrows and the asterisk point to the periphery and the central part of the IS, respectively. Scale bars, 5 μm.

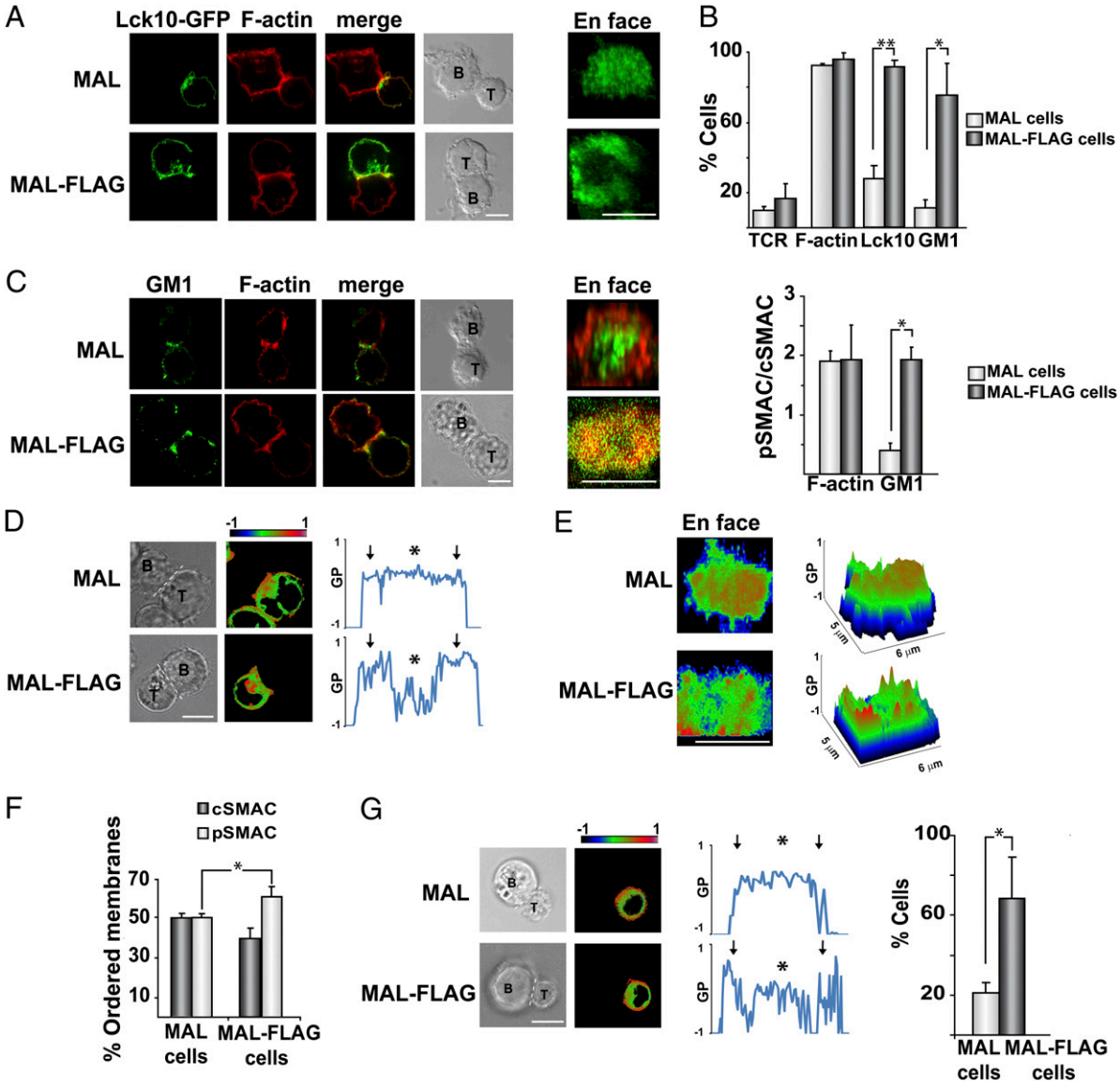

FIGURE 6. MAL missorting to the pSMAC causes redistribution of raft markers and condensed membranes within the IS. *A–C*, Jurkat MAL or MAL-FLAG cells were transiently transfected with Lck10-GFP for 18 h (*A*) or remained untransfected (*C*). Cells were then conjugated to SEE-loaded APCs for 15 min, fixed, permeabilized, and stained for actin and Lck10-GFP (*A*) or GM1 (*C*). An en face view of the IS is also shown. The histogram in *B* shows the percentage of cells with TCR, F-actin, Lck10-GFP, or GM1 preferentially distributed in the pSMAC in Jurkat MAL or MAL-FLAG cells. The histogram in *C* shows the ratio of the intensity of actin or GM1 staining at the pSMAC relative to that at the cSMAC in the two types of Jurkat cell. *D*, Jurkat MAL and Jurkat MAL-FLAG cells were labeled with Laurdan and then conjugated to SEE-loaded APCs for 15 min. The intensity of fluorescence emission in living cells was determined in two channels (400–460 nm and 470–530 nm), and the resulting intensity images were transformed to GP images and pseudocolored (see scale of GP). The graphics represent the GP values along the IS (white line in the differential contrast images) for each type of Jurkat cell. The arrows point to the IS periphery, and the asterisk indicates the central region. *E*, An en face view of the IS is shown in pseudocolor (*left panels*). A three-dimensional histogram of the GP values at the IS is also presented (*E*, *right panels*). *F*, The histogram represents the percentage of ordered membranes at the cSMAC or the pSMAC in Jurkat MAL or MAL-FLAG cells. *G*, Conjugates of human primary T cells transiently expressing MAL or MAL-FLAG were analyzed as in *D*. The histogram shows the number of cells with higher GP values at the pSMAC than at the cSMAC. Means ± SEM of three (*B*, *C*, *F*) or two (*G*) independent experiments are represented. Scale bars, 5 μm. $*p < 0.05$, $**p < 0.01$.

moderately enriched at the cSMAC, showed the same dependence on exogenous MAL as Lck10-GFP did (Fig. 6*B*, 6*C*). The packing density of biological membranes can be directly measured using the Laurdan fluorescent membrane dye (8). This does not preferentially partition into a particular type of membrane, but its fluorescence emission spectrum shifts depending on the degree of condensation and order of its membrane environment, making it possible to distinguish densely packed, ordered membranes from those with a loosely packed, disordered structure. This experimental approach has also been used to visualize the distribution of ordered domains of various cell systems, including T cells (9, 28). In Jurkat MAL cells, highly condensed domains accumulated along the entire contact zone, whereas in Jurkat MAL-FLAG cells, condensed domains were restricted to the IS periphery (Fig. 6*D*). This difference is better visualized in the en face view of the IS (Fig. 6*E*, *left panels*), where it can be clearly seen that MAL-FLAG caused depletion of highly condensed domains at the central zone of the IS, augmented membrane order (Fig. 6*E*, *right panels*), and increased the percentage of ordered membranes at the IS periphery (Fig. 6*F*). The loss of highly condensed domains from the cSMAC was confirmed in conjugates formed by primary human T lymphocytes expressing MAL-FLAG (Fig. 6*G*). There-

fore, the results in Fig. 6 indicate that misplacement of exogenous MAL to the pSMAC produces parallel missorting of raft markers and highly condensed membrane domains.

MAL distribution controls correct targeting of machinery involved in docking of microtubules or transport vesicles at the SMAC

We previously showed that MAL travels to the IS along linear tracks made of microtubules that connect the centrosome with the cSMAC (Fig. 1*B*, 1*C*). As transport vesicles and microtubules are docked at the plasma membrane using specific machineries, we decided to investigate the distribution of elements of such machineries in T cell–APC conjugates formed by Jurkat MAL and Jurkat MAL-FLAG cells. The appropriate combination of SNARES on vesicle and target membranes (*t*-SNARES) determines the docking of the transport vesicles at specific sites in cellular membranes and their subsequent fusion (29). Exocytosis in nonneuronal cells may involve two plasma membrane *t*-SNARES, syntaxin-3 or -4, and SNAP-23 (30). Consistent with previous work reporting syntaxin-4 and SNAP-23 localization (4), both proteins distributed along the entire IS in Jurkat MAL cells, but, in contrast, they preferentially accumulated at the IS periphery in Jurkat MAL-FLAG cells (Fig. 7*A–C*). Consistent with this alteration, most of SNAP-23 and a fraction of syntaxin-4 were found in compact membranes (Fig. 7*D*). Microtubule docking to the cell cortex involves interactions between specific proteins at

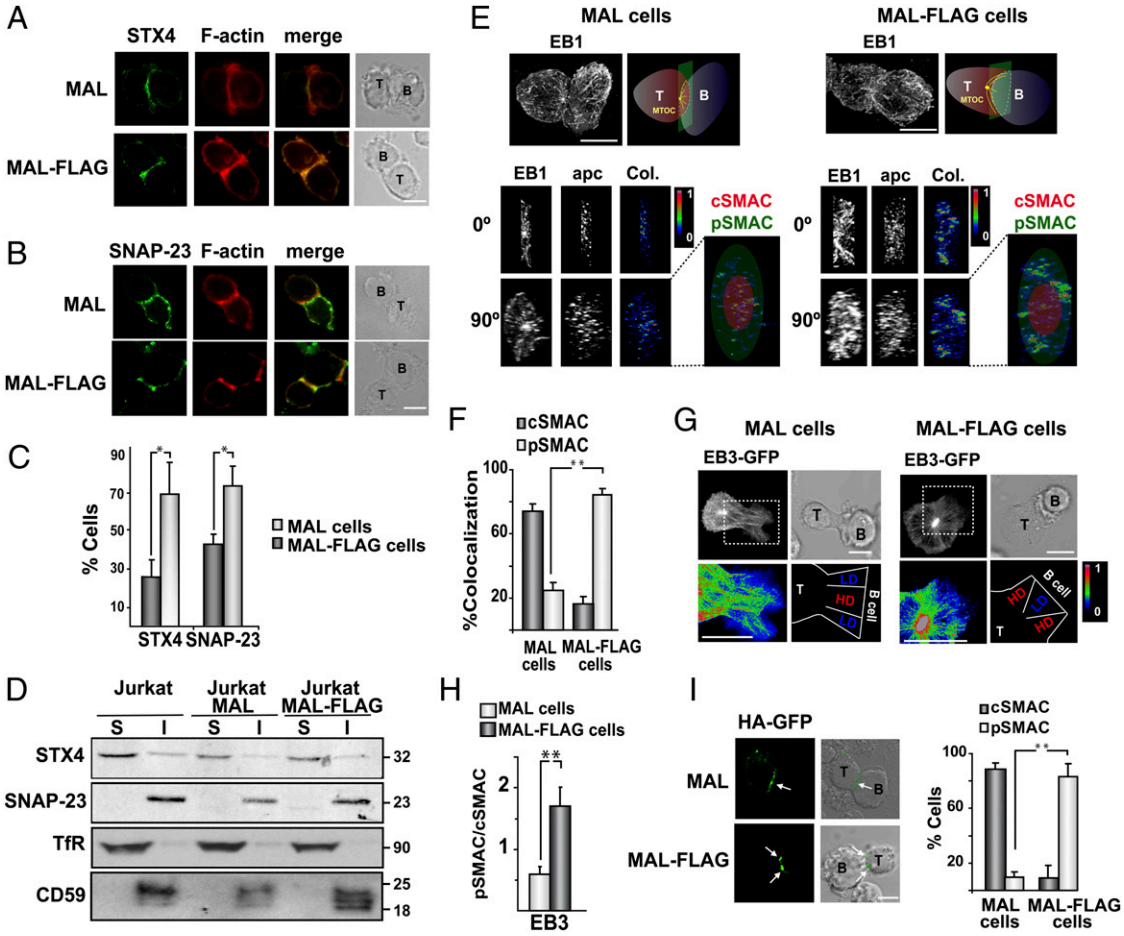

FIGURE 7. MAL distribution controls sorting to SMAC subdomains of protein machinery involved in the docking of transport carriers or microtubules to the plasma membrane. *A–C*, Jurkat MAL or Jurkat MAL-FLAG cells were conjugated with SEE-loaded APCs for 15 min. Cells were fixed, permeabilized, and stained with Abs to syntaxin-4 (STX4) (*A*) or SNAP-23 (*B*). The histogram shows the percentage of cells with STX4 or SNAP-23 enriched at the IS periphery (*C*). *D*, The soluble (S) fraction and the DRM fractions (I) from control Jurkat, Jurkat MAL, or Jurkat MAL-FLAG cells were immunoblotted with Abs to STX4 or SNAP-23. Transferrin receptor (TfR) and CD59 were used as markers of the S and I fractions, respectively. *E*, Jurkat MAL or Jurkat MAL-FLAG cells were conjugated to SEE-loaded APCs for 15 min. Cells were fixed, permeabilized, and stained with Abs to EB1 or adenomatous polyposis coli (apc) protein. The images resulting from the reconstruction of the confocal stacks obtained for EB1 staining are shown (*top panels*). The reconstructed images of EB1 and apc staining were used to obtain 0.4-μm-wide sections at the cell-to-cell contact, as shown in the schematics in the *bottom panels*. These sections were viewed from the side (0°) or rotated through 90°. The single-color images are shown in gray. The images showing only the pixels in which the staining of the two proteins coincides (Col.) were pseudocolored using the indicated color scale. An enlargement of the boxed region is also shown. Concentric rings were drawn to facilitate visualization of the place on the IS where the colocalization dots were concentrated. *F*, The histogram represents the percentage of pixels showing colocalization of EB1 and adenomatous polyposis coli protein at the pSMAC and the cSMAC. *G*, EB3-GFP was expressed in Jurkat MAL or Jurkat MAL-FLAG cells for 16 h. Cells were then conjugated with SEE-loaded APC and subjected to time-lapse videomicroscopy in a confocal microscope. The images show the reconstruction of 31 frames (*top panels*). The boxed region was enlarged and pseudocolored using the indicated scale (*bottom panels*). The schematics show the regions with a high (HD) or low density (LD) of EB3-labeled tubules traveling to the contact with the B cell. *H*, The histogram represents the ratio of EB3 intensity at the pSMAC versus that at the cSMAC. *I*, HA-GFP was expressed in Jurkat MAL or Jurkat MAL-FLAG cells for 16 h. Cells were then conjugated with SEE-loaded Raji cells for 15 min and fixed. The arrows indicate sites of HA accumulation at the IS. The histogram represents the percentage of cells with HA targeted to the cSMAC or pSMAC. Means ± SEM of three (*C*) or two (*F*, *H*, *I*) independent experiments are represented. Scale bars, 5 μm. $*p < 0.05$, $**p < 0.01$.

the growing end of microtubules, such as proteins EB1 and EB3, and proteins attached to the subcortical cytoskeleton, such as the adenomatous polyposis coli protein (31, 32). By obtaining three-dimensional reconstruction images, we observed that the colocalization between EB1 and the adenomatous polyposis coli protein was greatest at the central region or at a peripheral ring of the IS, depending on the place of accumulation of exogenous MAL (Fig. 7*E*, 7*F*). Moreover, consistent with this finding, we found a similar dependence for the place of concentration of newly formed microtubules, as monitored with EB3-GFP (Fig. 7*G*, 7*H*). Finally, we examined whether the abnormal arrangement of condensed membranes and docking machinery for vesicles and microtubules at the IS caused by missorting of exogenous MAL to the pSMAC also affects the targeting of an ectopic protein. We observed that the transmembrane HA protein, a prototypical raft-associated cargo molecule distributed preferentially to the cSMAC or to the pSMAC, depending on the place of exogenous MAL accumulation (Fig. 7*I*). In conclusion, the results in Fig. 7 indicate that MAL regulates the distribution of machinery involved in docking transport vesicles and microtubules and targeting proteins to specific regions of the IS (Fig. 8).

Discussion

The assembly of IS requires the translocation of specific molecules to the contact zone of the T cell with an APC and the effective sorting of these molecules in distinct SMAC subdomains. The precise mechanism by which protein sorting to the cSMAC and pSMAC takes place is unknown. In the absence of MAL expression, Lck is retained intracellularly and cannot be targeted to the IS, and, as a consequence, TCR, LAT, and other signaling molecules are not translocated either (19). This early effect on IS formation precluded the use of MAL knockdown for investigating the possible direct role of MAL in SMAC assembly. In this study, we show that MAL translocates rapidly to the IS and concentrates at the cSMAC. Later on, a pericentrosomal pool of MAL moves to the IS, accompanying microtubule-organizing center reorientation, as was previously observed for Lck (33). We focused our investigation on the initial recruitment of MAL to the IS and its role in protein sorting to the IS. By using a modified MAL molecule that is missorted to the pSMAC, we observed that correct MAL distribution at the IS is crucial for correct targeting of Lck and LAT, but not TCR, to the cSMAC. Missorting of MAL, in addition to mislocalizing Lck and LAT to the pSMAC, reduced membrane condensation at the cSMAC, misplaced raft markers to the pSMAC, and provoked a profound change in the distribution of machinery for docking transport vesicles and microtubules at the IS. Therefore, MAL plays a role at IS by organizing condensed membranes and controlling the targeting of proteins specifically to the cSMAC.

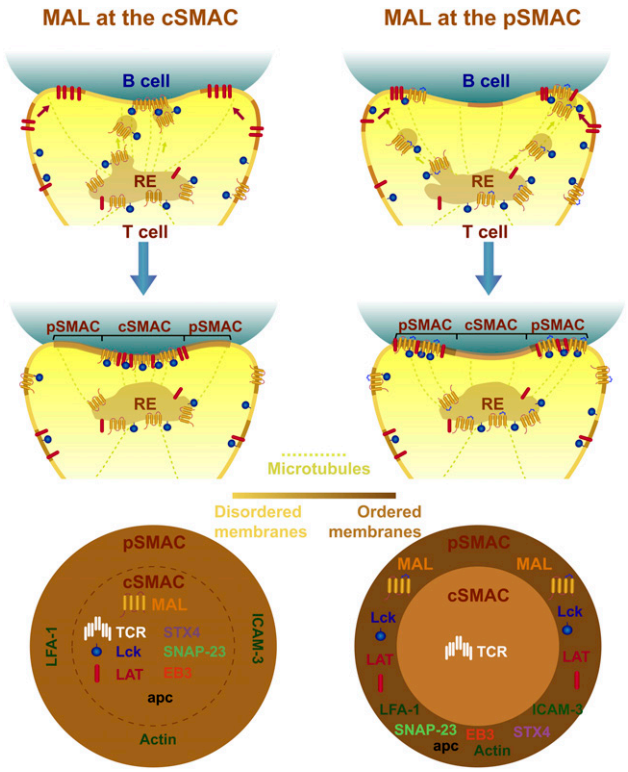

FIGURE 8. Schematics of the proposed role of MAL in the assembly of the SMAC. MAL is normally sorted to the cSMAC, where it colocalizes with highly ordered membranes. MAL mediates vesicular transport of Lck from pericentriolar endosomes directly to the cSMAC using microtubule tracks docked at the cSMAC. LAT, however, translocates to the cSMAC mainly from a plasma membrane pool. Mislocalization of MAL to the pSMAC produces loss of highly ordered membranes from the cSMAC, increased membrane condensation at the pSMAC, and missorting of Lck, LAT, and machinery for microtubule or vesicle transport docking to the pSMAC. As a result of these changes, Lck is transported directly to the pSMAC instead of to the cSMAC. Both Lck and LAT segregate at the IS into the ordered membranes organized by MAL regardless of the distribution of MAL.

Size exclusion and membrane-bending effects have long been considered as possible contributors to protein sorting within the SMAC (34). Large ectodomains in transmembrane proteins can prevent these proteins localizing in the cSMAC where the close proximity of the plasma membrane, the T cell, and the APC is needed for the TCR to recognize the Ag presented by the MHC molecule (35). The clustering state of the molecules can also affect their sorting within the SMAC, as observed for LFA-1 (36). Membrane rafts are postulated as being specialized platforms for the specific compartmentation of receptors and signaling molecules in all types of cell (37). The possible involvement of raft membranes in assembling the signaling machinery in T cells (11, 38–41) was challenged by single-molecule microscopic studies, indicating that protein–protein interactions are sufficient to explain the assembly (15). This observation, however, does not allow us to rule out the possibility that, in keeping with the existence of condensed domains and raft lipids at the contact zone (13, 14), raft membranes are the milieu where at least part of the signaling machinery is normally assembled at the IS. If this were the case, raft membranes at the IS could help to regulate the spatial organization of the SMAC by segregating specific molecules to different SMAC subdomains.

Using the Laurdan technique, we observed that MAL localization regulates the distribution of condensed membranes within the SMAC in Jurkat cells and primary T lymphocytes. Highly ordered membranes were distributed along the IS in cells expressing MAL at the cSMAC. However, in cells in which MAL was missorted to the pSMAC, membrane order, as measured by GP value, was diminished at the cSMAC and increased at the pSMAC. The missorting of ordered membranes to the pSMAC was corroborated by the parallel misdistribution of raft markers, such as ganglioside GM1 and Lck10-GFP. Despite the changes in the distribution of condensed membranes at the IS, signaling occurred efficiently in response to TCR triggering in both types of Jurkat cell. This result is consistent with previous observations showing that most of the signaling occurs in dynamic microclusters well before SMAC assembly takes place (42–44) and that microclusters form independently of raft clustering (45). The delay on ERK activation observed in the cells with MAL missorted to the pSMAC might indicate a modest contribution of the SMAC to the

signaling process. It is of particular note that the abnormal distribution of highly ordered membranes at the IS arising from the presence of MAL at the pSMAC caused missorting of Lck and LAT to the pSMAC. Therefore, the distribution of highly ordered membranes at the cSMAC and that of the raft-associated proteins Lck and LAT are strictly dependent on MAL targeting to the cSMAC. The proposed role of MAL as machinery for membrane order organization at the IS is supported by the observation of that MAL clustering creates specifically large, condensed membrane domains in the plasma membrane (20).

Lateral diffusion, cytoskeleton-mediated movement, and intracellular trafficking are different mechanisms that serve to concentrate specific membrane proteins at the IS. Consistent with this diversity, we found remarkable differences in the targeting of Lck and LAT to the IS. LAT accumulation at the IS appears to take place mainly by translocation from a surface pool that concentrated initially at the IS sides. LAT then segregated to a central position or remained at the IS sides depending on the place where MAL and the condensed domains accumulated. This observation indicates that LAT targeting to the cSMAC occurs once it has arrived at the IS by selective retention into MAL-enriched membranes. This retention might be reminiscent of the MAL-dependent stabilization of specific apical proteins described in polarized epithelial cells (46, 47). Unlike LAT, Lck was transported in MAL-positive vesicles from pericentriolar endosomes to the place where MAL accumulates, regardless of whether it was the cSMAC or the pSMAC. Importantly, the MAL-positive vesicular carriers moved to the IS along microtubule tracks that connect the centrosome with the IS, although they were differentially docked at the central part or at the sides of the cell-to-cell contact, depending on the place of exogenous MAL accumulation. Supporting this observation, we found that EB1, a protein present at the growing end of microtubules, colocalized with adenomatous polyposis coli, a protein involved in microtubule docking to the cell cortex, preferentially at the center of IS or at a peripheral ring coinciding with the place of MAL concentration. Therefore, in contrast to lytic granule movement, which takes place by minus-end directed movement along long microtubules that curve after contacting the IS (48, 49), MAL-mediated vesicular transport of Lck to the IS relies on plus-end directed traffic along short microtubules.

A role for microtubule docking at the IS in SMAC architecture has been proposed on the basis of the effect of the disruption of the dynein–dynactin complex by the overexpression of p50 dynamitin, a subunit of dynactin (50). Under those conditions, TCR disperses at the pSMAC instead of being clustered at the cSMAC, and LFA-1 becomes partially mistargeted to the cSMAC (50). Tumor suppressor gene 101, a component of the endosomal sorting complex required for transport, is essential for correct sorting of the TCR to the cSMAC. Unlike in control cells, where TCR and PKC-θ colocalize in peripheral microclusters but become segregated in the cSMAC (51), in tumor suppressor gene 101-knockdown cells, TCR and PKC-θ fail to segregate and remain together in large microclusters at the pSMAC (52). We have observed TCR concentration at the cSMAC regardless of the location of MAL accumulation at the IS, consistent with TCR following a pathway for targeting to the cSMAC that is distinct from that of Lck or LAT. Confirming this, in addition to controlling microtubule docking to the IS, MAL regulates the transport vesicle targeting site, we found that syntaxin-4 and SNAP-23, two *t*-SNARES involved in docking transport vesicles to the plasma membrane, distributed preferentially to cSMAC or pSMAC in a MAL localization-dependent manner. Therefore, in addition to transporting Lck directly to the IS, MAL appears to regulate membrane order at the IS in such a way that Lck, LAT, syntaxin-4, and SNAP-23 segregate into the ordered membranes organized by MAL (Fig. 8). Reflecting the profound alternations at the SMAC primarily caused by MAL mislocalization, the transmembrane HA protein, a prototypical raft-associated cargo protein, is also targeted to either SMAC subdomain depending on the pattern of MAL distribution.

In polarized epithelial cells, MAL mediates direct vesicular transport of cargo to the apical surface (17, 18) and stabilization of specific proteins at the apical membrane (46, 47). Our present results indicate that, in polarized T cells, MAL regulates membrane order at the IS and uses both direct vesicular transport and plasma membrane retention mechanisms to ensure correct sorting of Lck and LAT to the cSMAC.

Acknowledgments

We thank A. Jiménez and J.A. Rodríguez for technical help and Drs. I. Correas, J. Millán, and F. Martín-Belmonte for helpful comments. We also thank Drs. C. Enrich, C. Rentero, and M. Calvo (University of Barcelona, Barcelona, Spain) for expert advice about the analysis of Laurdan staining, C.C. Combs and D. Malide of the Light Microscopy Facility of the National Institutes of Health (Bethesda, MD) for expert technical advice on the time-lapse experiments and image processing, and C. Sánchez, M.A. Muñoz, T. Villalba, and V. Labrador of the Optical and Confocal Microscopy Unit of the Centro de Biologia Molecular Severo Ochoa.

Disclosures

The authors have no financial conflicts of interest.

References

1. Huppa, J. B., and M. M. Davis. 2003. T-cell-antigen recognition and the immunological synapse. *Nat. Rev. Immunol.* 3: 973–983.
2. Fooksman, D. R., S. Vardhana, G. Vasiliver-Shamis, J. Liese, D. A. Blair, J. Waite, C. Sacristán, G. D. Victora, A. Zanin-Zhorov, and M. L. Dustin. 2010. Functional anatomy of T cell activation and synapse formation. *Annu. Rev. Immunol.* 28: 79–105.
3. Monks, C. R. F., B. A. Freiberg, H. Kupfer, N. Sciaky, and A. Kupfer. 1998. Three-dimensional segregation of supramolecular activation clusters in T cells. *Nature* 395: 82–86.
4. Das, V., B. Nal, A. Dujeancourt, M.-I. Thoulouze, T. Galli, P. Roux, A. Dautry-Varsat, and A. Alcover. 2004. Activation-induced polarized recycling targets T cell antigen receptors to the immunological synapse; involvement of SNARE complexes. *Immunity* 20: 577–588.
5. Dustin, M. L., and J. A. Cooper. 2000. The immunological synapse and the actin cytoskeleton: molecular hardware for T cell signaling. *Nat. Immunol.* 1: 23–29.
6. Griffiths, G. M., A. Tsun, and J. C. Stinchcombe. 2010. The immunological synapse: a focal point for endocytosis and exocytosis. *J. Cell Biol.* 189: 399–406.
7. Lin, J., M. J. Miller, and A. S. Shaw. 2005. The c-SMAC: sorting it all out (or in). *J. Cell Biol.* 170: 177–182.
8. Gaus, K., E. Gratton, E. P. W. Kable, A. S. Jones, I. Gelissen, L. Kritharides, and W. Jessup. 2003. Visualizing lipid structure and raft domains in living cells with two-photon microscopy. *Proc. Natl. Acad. Sci. USA* 100: 15554–15559.
9. Gaus, K., S. Le Lay, N. Balasubramanian, and M. A. Schwartz. 2006. Integrin-mediated adhesion regulates membrane order. *J. Cell Biol.* 174: 725–734.
10. Lingwood, D., and K. Simons. 2010. Lipid rafts as a membrane-organizing principle. *Science* 327: 46–50.
11. Alonso, M. A., and J. Millán. 2001. The role of lipid rafts in signalling and membrane trafficking in T lymphocytes. *J. Cell Sci.* 114: 3957–3965.
12. Burack, W. R., K.-H. Lee, A. D. Holdorf, M. L. Dustin, and A. S. Shaw. 2002. Cutting edge: quantitative imaging of raft accumulation in the immunological synapse. *J. Immunol.* 169: 2837–2841.
13. Gaus, K., E. Chklovskaia, B. Fazekas de St Groth, W. Jessup, and T. Harder. 2005. Condensation of the plasma membrane at the site of T lymphocyte activation. *J. Cell Biol.* 171: 121–131.
14. Zech, T., C. S. Ejsing, K. Gaus, B. de Wet, A. Shevchenko, K. Simons, and T. Harder. 2009. Accumulation of raft lipids in T-cell plasma membrane domains engaged in TCR signalling. *EMBO J.* 28: 466–476.
15. Douglass, A. D., and R. D. Vale. 2005. Single-molecule microscopy reveals plasma membrane microdomains created by protein-protein networks that exclude or trap signaling molecules in T cells. *Cell* 121: 937–950.
16. Millán, J., and M. A. Alonso. 1998. MAL, a novel integral membrane protein of human T lymphocytes, associates with glycosylphosphatidylinositol-anchored proteins and Src-like tyrosine kinases. *Eur. J. Immunol.* 28: 3675–3684.
17. Puertollano, R., F. Martín-Belmonte, J. Millán, M. C. de Marco, J. P. Albar, L. Kremer, and M. A. Alonso. 1999. The MAL proteolipid is necessary for

normal apical transport and accurate sorting of the influenza virus hemagglutinin in Madin-Darby canine kidney cells. *J. Cell Biol.* 145: 141–151.
18. Cheong, K. H., D. Zacchetti, E. E. Schneeberger, and K. Simons. 1999. VIP17/MAL, a lipid raft-associated protein, is involved in apical transport in MDCK cells. *Proc. Natl. Acad. Sci. USA* 96: 6241–6248.
19. Antón, O., A. Batista, J. Millán, L. Andrés-Delgado, R. Puertollano, I. Correas, and M. A. Alonso. 2008. An essential role for the MAL protein in targeting Lck to the plasma membrane of human T lymphocytes. *J. Exp. Med.* 205: 3201–3213.
20. Magal, L. G., Y. Yaffe, J. Shepshelovich, J. F. Aranda, Mdel. C. de Marco, K. Gaus, M. A. Alonso, and K. Hirschberg. 2009. Clustering and lateral concentration of raft lipids by the MAL protein. *Mol. Biol. Cell* 20: 3751–3762.
21. Puertollano, R., and M. A. Alonso. 1999. MAL, an integral element of the apical sorting machinery, is an itinerant protein that cycles between the trans-Golgi network and the plasma membrane. *Mol. Biol. Cell* 10: 3435–3447.
22. Kenworthy, A. K., B. J. Nichols, C. L. Remmert, G. M. Hendrix, M. Kumar, J. Zimmerberg, and J. Lippincott-Schwartz. 2004. Dynamics of putative raft-associated proteins at the cell surface. *J. Cell Biol.* 165: 735–746.
23. Van Komen, J. S., S. Mishra, J. Byrum, G. R. Chichili, J. C. Yaciuk, A. D. Farris, and W. Rodgers. 2007. Early and dynamic polarization of T cell membrane rafts and constituents prior to TCR stop signals. *J. Immunol.* 179: 6845–6855.
24. Brown, D. A., and J. K. Rose. 1992. Sorting of GPI-anchored proteins to glycolipid-enriched membrane subdomains during transport to the apical cell surface. *Cell* 68: 533–544.
25. Niedergang, F., A. Dautry-Varsat, and A. Alcover. 1997. Peptide antigen or superantigen-induced down-regulation of TCRs involves both stimulated and unstimulated receptors. *J. Immunol.* 159: 1703–1710.
26. Hewitt, C. R., J. R. Lamb, J. Hayball, M. Hill, M. J. Owen, and R. E. O'Hehir. 1992. Major histocompatibility complex independent clonal T cell anergy by direct interaction of *Staphylococcus aureus* enterotoxin B with the T cell antigen receptor. *J. Exp. Med.* 175: 1493–1499.
27. Shenoy-Scaria, A. M., L. K. Gauen, J. Kwong, A. S. Shaw, and D. M. Lublin. 1993. Palmitylation of an amino-terminal cysteine motif of protein tyrosine kinases p56lck and p59fyn mediates interaction with glycosyl-phosphatidylinositol-anchored proteins. *Mol. Cell. Biol.* 13: 6385–6392.
28. Fitzner, D., A. Schneider, A. Kippert, W. Möbius, K. I. Willig, S. W. Hell, G. Bunt, K. Gaus, and M. Simons. 2006. Myelin basic protein-dependent plasma membrane reorganization in the formation of myelin. *EMBO J.* 25: 5037–5048.
29. Ungermann, C., and D. Langosch. 2005. Functions of SNAREs in intracellular membrane fusion and lipid bilayer mixing. *J. Cell Sci.* 118: 3819–3828.
30. Hay, J. C. 2001. SNARE complex structure and function. *Exp. Cell Res.* 271: 10–21.
31. Akhmanova, A., and M. O. Steinmetz. 2008. Tracking the ends: a dynamic protein network controls the fate of microtubule tips. *Nat. Rev. Mol. Cell Biol.* 9: 309–322.
32. Aoki, K., and M. M. Taketo. 2007. Adenomatous polyposis coli (APC): a multi-functional tumor suppressor gene. *J. Cell Sci.* 120: 3327–3335.
33. Ehrlich, L. I. R., P. J. R. Ebert, M. F. Krummel, A. Weiss, and M. M. Davis. 2002. Dynamics of p56lck translocation to the T cell immunological synapse following agonist and antagonist stimulation. *Immunity* 17: 809–822.
34. Qi, S. Y., J. T. Groves, and A. K. Chakraborty. 2001. Synaptic pattern formation during cellular recognition. *Proc. Natl. Acad. Sci. USA* 98: 6548–6553.
35. Choudhuri, K., D. Wiseman, M. H. Brown, K. Gould, and P. A. van der Merwe. 2005. T-cell receptor triggering is critically dependent on the dimensions of its peptide-MHC ligand. *Nature* 436: 578–582.
36. Hartman, N. C., J. A. Nye, and J. T. Groves. 2009. Cluster size regulates protein sorting in the immunological synapse. *Proc. Natl. Acad. Sci. USA* 106: 12729–12734.
37. Simons, K., and E. Ikonen. 1997. Functional rafts in cell membranes. *Nature* 387: 569–572.
38. Horejsí, V. 2003. The roles of membrane microdomains (rafts) in T cell activation. *Immunol. Rev.* 191: 148–164.
39. Montixi, C., C. Langlet, A.-M. Bernard, J. Thimonier, C. Dubois, M. A. Wurbel, J. P. Chauvin, M. Pierres, and H. T. He. 1998. Engagement of T cell receptor triggers its recruitment to low-density detergent-insoluble membrane domains. *EMBO J.* 17: 5334–5348.
40. Xavier, R., T. Brennan, Q. Li, C. McCormack, and B. Seed. 1998. Membrane compartmentation is required for efficient T cell activation. *Immunity* 8: 723–732.
41. Zhang, W., R. P. Trible, and L. E. Samelson. 1998. LAT palmitoylation: its essential role in membrane microdomain targeting and tyrosine phosphorylation during T cell activation. *Immunity* 9: 239–246.
42. Varma, R., G. Campi, T. Yokosuka, T. Saito, and M. L. Dustin. 2006. T cell receptor-proximal signals are sustained in peripheral microclusters and terminated in the central supramolecular activation cluster. *Immunity* 25: 117–127.
43. Yokosuka, T., K. Sakata-Sogawa, W. Kobayashi, M. Hiroshima, A. Hashimoto-Tane, M. Tokunaga, M. L. Dustin, and T. Saito. 2005. Newly generated T cell receptor microclusters initiate and sustain T cell activation by recruitment of Zap70 and SLP-76. *Nat. Immunol.* 6: 1253–1262.
44. Lasserre, R., S. Charrin, C. Cuche, A. Danckaert, M.-I. Thoulouze, F. de Chaumont, T. Duong, N. Perrault, N. Varin-Blank, J.-C. Olivo-Marin, et al. 2010. Ezrin tunes T-cell activation by controlling Dlg1 and microtubule positioning at the immunological synapse. *EMBO J.* 29: 2301–2314.
45. Hashimoto-Tane, A., T. Yokosuka, C. Ishihara, M. Sakuma, W. Kobayashi, and T. Saito. 2010. T-cell receptor microclusters critical for T-cell activation are formed independently of lipid raft clustering. *Mol. Cell. Biol.* 30: 3421–3429.
46. Carmosino, M., F. Rizzo, G. Procino, D. Basco, G. Valenti, B. Forbush, N. N. Schaeren-Wiemers, M. J. Caplan, and M. Svelto. 2010. MAL/VIP17, a new player in the regulation of NKCC2 in the kidney. *Mol. Biol. Cell* 21: 3985–3997.
47. Kamsteeg, E.-J., A. S. Duffield, I. B. M. Konings, J. Spencer, P. Pagel, P. M. T. Deen, and M. J. Caplan. 2007. MAL decreases the internalization of the aquaporin-2 water channel. *Proc. Natl. Acad. Sci. USA* 104: 16696–16701.
48. Stinchcombe, J. C., E. Majorovits, G. Bossi, S. Fuller, and G. M. Griffiths. 2006. Centrosome polarization delivers secretory granules to the immunological synapse. *Nature* 443: 462–465.
49. Kuhn, J. R., and M. Poenie. 2002. Dynamic polarization of the microtubule cytoskeleton during CTL-mediated killing. *Immunity* 16: 111–121.
50. Martín-Cófreces, N. B., J. Robles-Valero, J. R. Cabrero, M. Mittelbrunn, M. Gordón-Alonso, C.-H. Sung, B. Alarcón, J. Vázquez, and F. Sánchez-Madrid. 2008. MTOC translocation modulates IS formation and controls sustained T cell signaling. *J. Cell Biol.* 182: 951–962.
51. Yokosuka, T., W. Kobayashi, K. Sakata-Sogawa, M. Takamatsu, A. Hashimoto-Tane, M. L. Dustin, M. Tokunaga, and T. Saito. 2008. Spatiotemporal regulation of T cell costimulation by TCR-CD28 microclusters and protein kinase C theta translocation. *Immunity* 29: 589–601.
52. Vardhana, S., K. Choudhuri, R. Varma, and M. L. Dustin. 2010. Essential role of ubiquitin and TSG101 protein in formation and function of the central supramolecular activation cluster. *Immunity* 32: 531–540.

MYADM regulates Rac1 targeting to ordered membranes required for cell spreading and migration

Juan F. Aranda[a], Natalia Reglero-Real[a], Leonor Kremer[b], Beatriz Marcos-Ramiro[a], Ana Ruiz-Sáenz[a], María Calvo[c], Carlos Enrich[d], Isabel Correas[a], Jaime Millán[a,*], and Miguel A. Alonso[a,*]

[a]Centro de Biología Molecular Severo Ochoa and [b]Centro Nacional de Biotecnología Consejo Superior de Investigaciones Científicas and Universidad Autónoma de Madrid, Cantoblanco, 28049 Madrid, Spain; [c]Unidad de Microscopía Confocal Servicios Científico-técnicos and [d]Departament de Biologia Celular Immunologia i Neurociències, Institut d'Investigacions Biomèdiques August Pi i Sunyer (IDIBAPS), Facultat de Medicina Universidad de Barcelona, 08036 Barcelona, Spain

ABSTRACT **Membrane organization into condensed domains or rafts provides molecular platforms for selective recruitment of proteins. Cell migration is a general process that requires spatiotemporal targeting of Rac1 to membrane rafts. The protein machinery responsible for making rafts competent to recruit Rac1 remains elusive. Some members of the MAL family of proteins are involved in specialized processes dependent on this type of membrane. Because condensed membrane domains are a general feature of the plasma membrane of all mammalian cells, we hypothesized that MAL family members with ubiquitous expression and plasma membrane distribution could be involved in the organization of membranes for cell migration. We show that myeloid-associated differentiation marker (MYADM), a protein with unique features within the MAL family, colocalizes with Rac1 in membrane protrusions at the cell surface and distributes in condensed membranes. MYADM knockdown (KD) cells had altered membrane condensation and showed deficient incorporation of Rac1 to membrane raft fractions and, similar to Rac1 KD cells, exhibited reduced cell spreading and migration. Results of rescue-of-function experiments by expression of MYADM or active Rac1L61 in cells knocked down for Rac1 or MYADM, respectively, are consistent with the idea that MYADM and Rac1 act on parallel pathways that lead to similar functional outcomes.**

Monitoring Editor
J. Silvio Gutkind
National Institutes of Health

Received: Nov 22, 2010
Revised: Jan 19, 2011
Accepted: Feb 8, 2011

INTRODUCTION

Cell migration can be defined as a cyclical process of assembly/disassembly of integrin-based adhesive structures coordinated by the underlying cytoskeleton. Such adhesive turnover is usually oriented toward spatiotemporal cues in the environment and mediates vital processes, such as organism development, wound repair angiogenesis, and immune responses (Ridley *et al.*, 2003). A pathological deregulation of cell migration contributes to serious diseases like cancer and metastasis atherosclerosis and autoimmunity (Rolfe *et al.*, 2005; Yamazaki *et al.*, 2005).

Oriented motility requires mechanisms of compartmentalization at the plasma membrane to generate asymmetry in signaling pathways that drive forward movement at the leading edge or contraction at the back of the cell (Manes *et al.*, 2003; Ridley *et al.*, 2003). One such mechanism arises from the existence of membrane heterogeneity that favors the selective recruitment of protein complexes (Manes *et al.*, 2003; Golub and Pico, 2005). Cholesterol-dependent membrane domains with varying degrees of condensation can be visualized in living cells by staining with the fluorescent probe Laurdan (Gaus *et al.*, 2003, 2006a). Condensed membranes are probably equivalent to liquid-ordered membrane assemblies of glycolipids and cholesterol (also referred to as membrane rafts),

This article was published online ahead of print in MBoC in Press (http://www.molbiolcell.org/cgi/doi/10.1091/mbc.E10-11-0910) on February 16, 2011.

*These authors contributed equally to this work.

Address correspondence to: J. Millan (jmillan@cbm.uam.es) and M. A. Alonso (maalonso@cbm.uam.es).

Abbreviations used: DRM, detergent-resistant membrane; GFP, green fluorescent protein; GP, general polarization; GST-PBD, GTPase-binding domain of PAK1; GST-RBD, GTPase-binding domain of Rhotekin; GTP, guanosine triphosphatase; HA, hemagglutinin; KD, knockdown; mAb, monoclonal antibody; MARVEL, MAL and related proteins for vesicle trafficking and membrane link; MYADM, myeloid-associated differentiation marker; TfR, transferrin receptor.

which are involved in recruiting specific proteins for membrane trafficking or signaling events and in forming membrane compartments, such as caveolae (Simons and Ikonen, 1997; Lingwood and Simons, 2010). The Rho-family guanosine triphosphatase (GTPase) Rac1 is distributed in ordered membranes of appropriate microviscosity (Ghosh *et al.*, 2002; del Pozo *et al.*, 2004; Vilhardt and van Deurs, 2004) and regulates spreading and actin-mediated extension of lamellipodia, where nascent adhesive structures initiate oriented movement (Ridley *et al.*, 2003; del Pozo *et al.*, 2004; Heasman and Ridley, 2008). The machinery responsible for making condensed membranes competent to recruit Rac1 has remained elusive.

Members of the MAL protein family play a role in raft membranes (Cheong *et al.*, 1999; Puertollano *et al.*, 1999; Magal *et al.*, 2009). The best documented proteins of this family (MAL, BENE, MAL2, and plasmolipin) contain four transmembrane segments expressed in a restricted range of tissues and are involved in specialized membrane-trafficking processes (Puertollano *et al.*, 1999; de Marco et al., 2001, 2002; Bosse *et al.*, 2003). Because condensed membrane domains are a general feature of the plasma membrane of all mammalian cells, we hypothesized that MAL family members with ubiquitous expression and plasma membrane distribution could be involved in the function of raft membranes for cell migration. Here we report the functional characterization of the myeloid-associated differentiation marker (MYADM), a member of the MAL family with the unique features of having eight transmembrane regions and a ubiquitous pattern of expression and of being localized at the plasma membrane. Using a combination of RNA interference and rescue-of-function experimental analysis of condensed domains by Laurdan staining and isolation of detergent-insoluble membranes and different functional analyses, we found MYADM to be important for the organization of membrane domains crucial for appropriate targeting of Rac1 and hence for lamellipodium extension and cell motility.

RESULTS

MYADM is broadly expressed, partitions into compact membranes, and distributes to cell lamellipodia

The tetra-spanning MARVEL (MAL and related proteins for vesicle trafficking and membrane link) membrane domain (Sanchez-Pulido *et al.*, 2002) is present in 28 human integral proteins grouped into different families, including the MAL family (Figure 1A). The best documented proteins of the MAL family contain four transmembrane segments expressed in a restricted range of tissues and are involved in specialized membrane-trafficking processes (Puertollano *et al.*, 1999; de Marco *et al.*, 2001, 2002; Bosse *et al.*, 2003). The other three members—MYADM, MYADM-like1 (MYADML1), and MYADM-like2 (MYADML2)—contain additional transmembrane segments and form an independent branch. To search for MAL-family proteins with ubiquitous expression plasma membrane localization and association with ordered membranes, we have analyzed the expression and distribution of the three MYADM proteins. An initial expression analysis of the *MYADM, MYADML1,* and *MYADML2* genes revealed that only *MYADM* expression was detected in all the human cell lines tested (Figure 1B). The widespread range of expression of *MYADM,* which is consistent with a previous analysis (Cui *et al.*, 2001), was confirmed by Northern blot analysis (Supplemental Figure S1A). Whereas the MYADML1 and MYADML2 proteins distributed intracellularly (Supplemental Figure S1B), as do other members of the MAL family (Puertollano *et al.*, 1999; de Marco *et al.*, 2001, 2002; Bosse *et al.*, 2003), MYADM localized to the plasma membrane (Figure 1C), where it overlapped extensively with F-actin in membrane ruffles. MYADM is the only member of the MARVEL domain–containing superfamily that has two MARVEL domains (Figure 1D). The two MARVEL domains were necessary for targeting MYADM to the plasma membrane (Supplemental Figure S1C). Using a newly generated antibody (Supplemental Figure S1D), we confirmed at the protein level the widespread expression of MYADM (Figure 1D) and found that, similar to all the MAL family members analyzed to date, endogenous MYADM (Figure 1E) partitioned preferentially into detergent-resistant membranes (DRMs) enriched in compact membrane domains (Brown and Rose, 1992) as well as did exogenous MYADM-green fluorescent protein (GFP) (Supplemental Figure S1E). The domains organized by MYADM appear to be different from those organized by caveolin as a low level of colocalization was detected between both proteins (Supplemental Figure S1F). The widespread expression pattern of MYADM (Figure 1, B and D, and Supplemental Figure S1A), its presence at the plasma membrane (Figure 1C), and its partitioning into compact membranes (Figure 1E and Supplemental Figure S1E) are compatible with a general role of MYADM in raft-mediated events at the plasma membrane.

MYADM regulates cell spreading and migration

To gain insight into MYADM function, we adopted a loss-of-function strategy using specific shRNA or siRNA to generate transient knockdown (KD) of MYADM expression. First, cells were transfected with constructs expressing shRNA1 or shRNA2 that were targeted to the coding sequence or the 3′ untranslated region, respectively, of MYADM mRNA (Figure 2A). Cells expressing shRNA1 or shRNA2 were shown to maintain or severely reduce (~85–90%) MYADM levels, respectively, and were subsequently used as control or MYADM KD cells. We prepared stable transfectants expressing MYADM-GFP as a control of the specificity of shRNA2. MYADM-GFP transcript lacks the entire 3′ untranslated region of MYADM mRNA and thus is insensitive to shRNA2 (Figure 2A). Morphological analysis of MYADM KD cells revealed a reduction in the spreading area (Figure 2, B and C) and cell shape as measured by the elliptical factor (length/breadth) (Figure 2D) but not in the adhesion to the substratum (Figure 2E). Importantly, spreading and elongation defects were not observed in MYADM KD cells expressing exogenous MYADM-GFP (Figure 2, B–D). Further membrane dynamic analysis by time-lapse video microscopy revealed constant extension and retraction of the plasma membrane in subconfluent control cells undergoing random migration. In contrast, protrusive-retractile activity appeared remarkably lower at the edges of MYADM KD cells (Figure 2F). To test whether the defects in membrane dynamics affect the migratory capacity of the cells, we then compared control and MYADM KD cells in random migration assays (Figure 2G). The average velocity was significantly lower in MYADM KD cells than in control cells and in MYADM KD cells expressing MYADM-GFP (Figure 2H). In addition, the index of directionality (the net distance divided by the total distance traveled by the cell) measured on tracked cell trajectories diminished by ~50% in MYADM KD cells and was restored by expression of MYADM-GFP (Figure 2I).

To confirm the data obtained by shRNA expression in a second approach, HeLa cells were transiently transfected with specific siRNAs targeted to MYADM mRNA. siRNA1 did not significantly reduce MYADM expression and was chosen as a control siRNA whereas siRNA2 and siRNA3 knocked down MYADM levels by more than 90% and 80%, respectively, at 48 h posttransfection (Supplemental Figure S2A). The expression of siRNA2 recapitulated the effects on cell spreading and morphology and on velocity and directionality during random migration observed in shRNA2-transfected cells (Supplemental Figure S2, B–G). A milder effect on cell

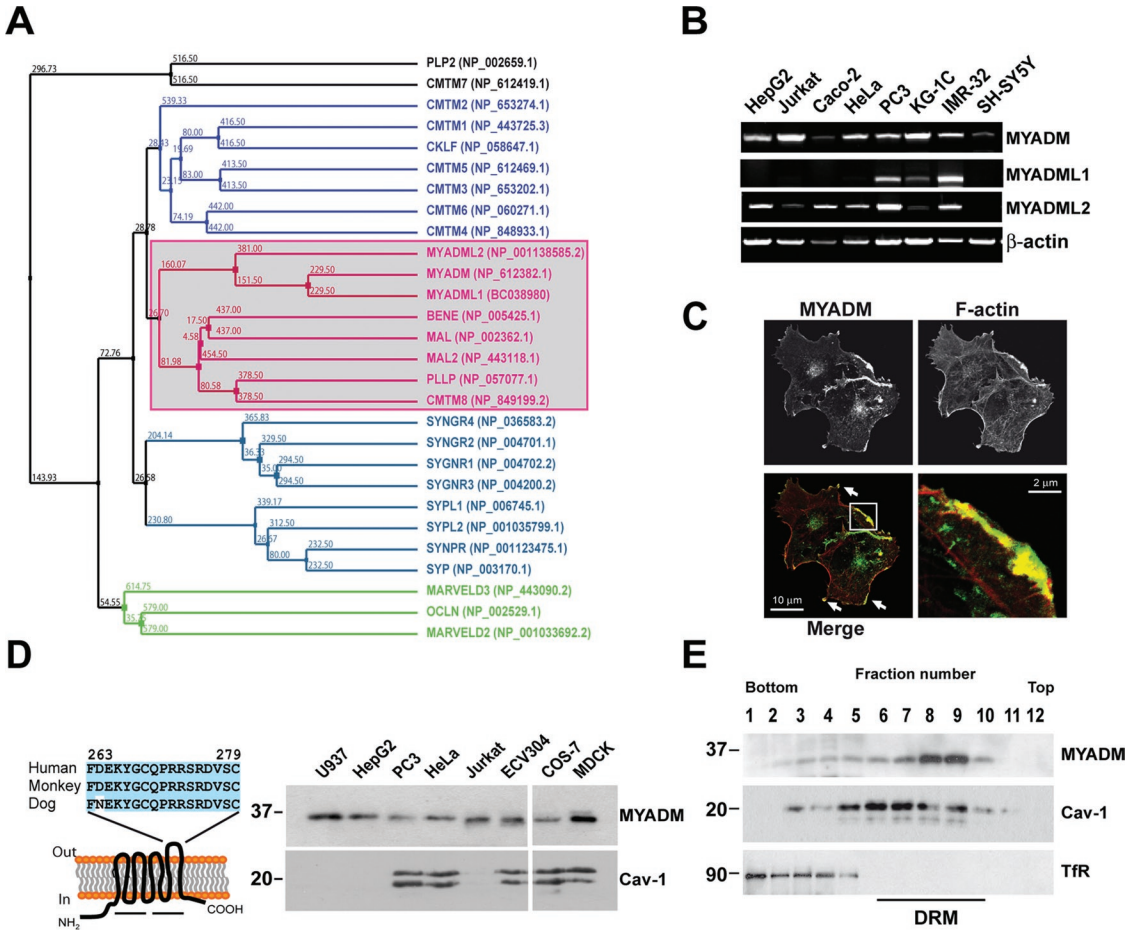

FIGURE 1: Characterization of the MYADM protein and analysis of its subcellular distribution. (A) Complete phylogenetic tree of human MARVEL domain-containing proteins. The sequences of the cytoplasmic amino- and carboxyl-terminal tails were not considered in the alignment used to generate the tree. The protein accession numbers of the corresponding sequences are indicated in brackets; the nucleotide accession number is indicated in the case of MYADML1. The MAL protein family is boxed. (B) RT-PCR analysis of the expression of the *MYADM, MYADML1,* and *MYADML2* genes in various human cell lines. (C) Cos-7 cells expressing human MYADM-GFP were stained for F-actin and analyzed by confocal microscopy. The enlargement shows the colocalization of MYADM and F-actin in the lamellipodia indicated in the boxed area. (D) Left panel: schematic model of the predicted structure of MYADM indicating the human peptide used for the generation of mAb2B12. The two lines below the model indicate the two MARVEL domains present in the MYADM molecule. Right panel: total membrane fractions from the indicated cell lines were subjected to immunoblotting with anti-MYADM mAb 2B12 or anti-caveolin-1 (Cav-1) antibodies. (E) HeLa cells were extracted with 1% Triton X-100 at 4°C and centrifuged to equilibrium in sucrose-density gradients. Aliquots from each fraction were immunoblotted for MYADM with 2B12 mAb or for caveolin-1 (Cav-1) and TfR used as markers of the DRM and soluble fractions, respectively.

morphology was observed in siRNA3-transfected cells (Supplemental Figure S2, C and D). Double staining of α-tubulin and F-actin revealed no major cytoskeletal alterations in siRNA2-transfected cells compared with control cells, although F-actin–enriched protrusions appeared to be reduced in extension and instead a thick F-actin belt decorated the cell periphery (Supplemental Figure S2B). Importantly, MYADM silencing in epithelial prostate PC3 cells reproduced the main findings obtained in HeLa cells (Supplemental Figure S2, H–K). In summary, the results in Figure 2 and Supplemental Figure S2 indicate that MYADM is necessary for normal cell spreading and migration.

MYADM regulates membrane condensation

To analyze the role of MYADM on membrane organization, we stained the cells with Laurdan. The Laurdan probe penetrates the cell membrane and aligns parallel to the phospholipids (Bagatolli *et al.*, 2003) undergoing a shift in its peak emission wavelength from ~500 nm in fluid membranes to ~440 nm in ordered membranes (Gaus *et al.*, 2006). A normalized ratio of the two emission regions given by the general polarization (GP) index, which ranges between –1 and 1 provides a relative measure of membrane order. Analysis of Laurdan fluorescence under a two-photon confocal microscope has revealed that membranes at lamellipodial adhesions are highly ordered (Gaus *et al.*, 2006a), consistent with previous findings showing the requirement of membrane rafts in these adhesive complexes for correct cell spreading (del Pozo *et al.*, 2004). To analyze the order in MYADM-enriched membrane regions, we stained HeLa cells expressing MYADM-cherry with Laurdan and used the MYADM-cherry images to mask the GP images to visualize membrane order only at the regions containing MYADM. Using this procedure, we observed MYADM-enriched membrane protrusions to be highly ordered (Figure 3A). GP images were then used to compare membrane

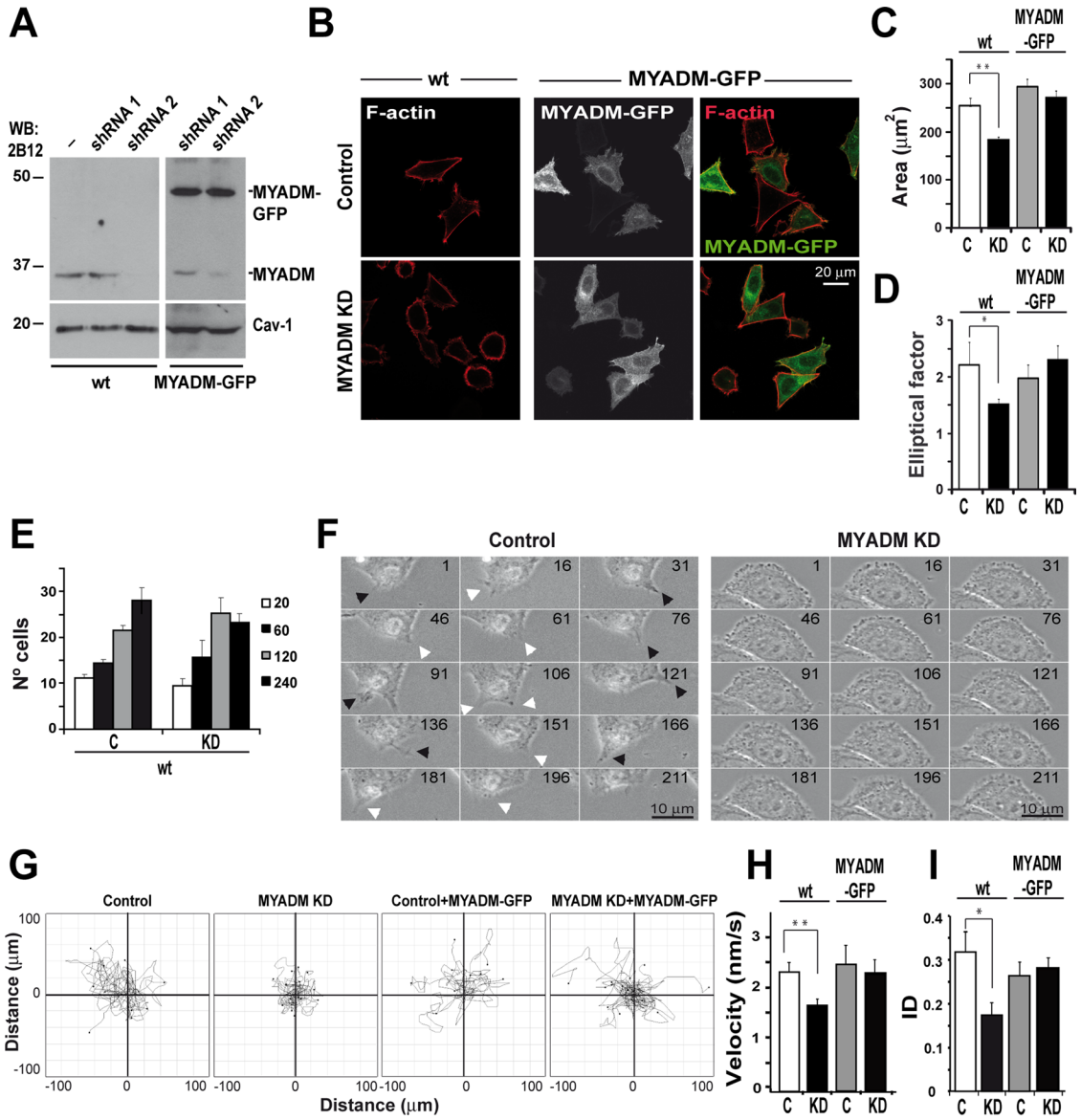

FIGURE 2: MYADM regulates cell spreading and migration. (A) Normal HeLa cells (wt) or HeLa cells stably expressing MYADM-GFP were transfected or not with plasmids expressing shRNA1 or shRNA2 for 48 h. Cell extracts were then immunoblotted with anti-MYADM 2B12 mAb or anti-caveolin-1 (Cav-1) antibodies. (B–E) Control or MYADM KD cells expressing or not MYADM-GFP were plated onto glass coverslips. After 4 h, cells were stained for F-actin (B) and analyzed for their spreading area (C) and elliptical factor (D) or used immediately to determine adhesion kinetics by measuring the number of cells attached 20, 60, 120, or 240 min after plating (E). Twenty fields for each condition were analyzed in (E). (F) Control or MYADM KD cells were subjected to time-lapse videomicroscopy. Filled and unfilled arrowheads indicate extension and retraction of cell protrusions, respectively, at the plasma membrane. Numbers indicate time in minutes. (G–I) The movement of control or MYADM KD cells stably expressing or not MYADM-GFP was recorded by time-lapse videomicroscopy at 15-min intervals in random migration assays. The migration tracks of 12–16 cells from a representative experiment (G), the migration velocity of cells (H), and the index of directionality (ID) (I) are shown. The mean ± SEM from three independent experiments is shown in (C–E, H, and I). 120–150 cells per condition were analyzed in each experiment; *$p < 0.05$; **$p < 0.01$.

order in control MYADM KD cells and cells treated with the cholesterol-sequestering agent methyl-β-cyclodextrin by quantifying their respective GP value. Remarkably, MYADM KD significantly reduced the GP value concomitantly with cell rounding to a similar extent to the effect observed in cells treated with methyl-β-cyclodextrin (Figure 3, B–D). Thus our results indicate that MYADM regulates cell membrane condensation and that alteration of membrane condensation either by cholesterol depletion or MYADM silencing had a similar effect on cell spreading in HeLa cells (Figures 2C and 3E).

It is well documented that, in addition to GTP loading, correct targeting to the plasma membrane is required for efficient signaling of Rac1 (del Pozo *et al.*, 2000). A close connection between Rac1 function and the presence of Rac1 in raft membranes has been established (del Pozo *et al.*, 2004; Vilhardt and van Deurs, 2004). Laurdan staining confirmed that Rac1 preferentially localizes to ordered membranes with a high GP value (Figure 4A). Consistent with this observation, Rac1 was detected in MYADM-enriched DRMs isolated from HeLa cells, whereas RhoA or Cdc42 was excluded (Figure 4B).

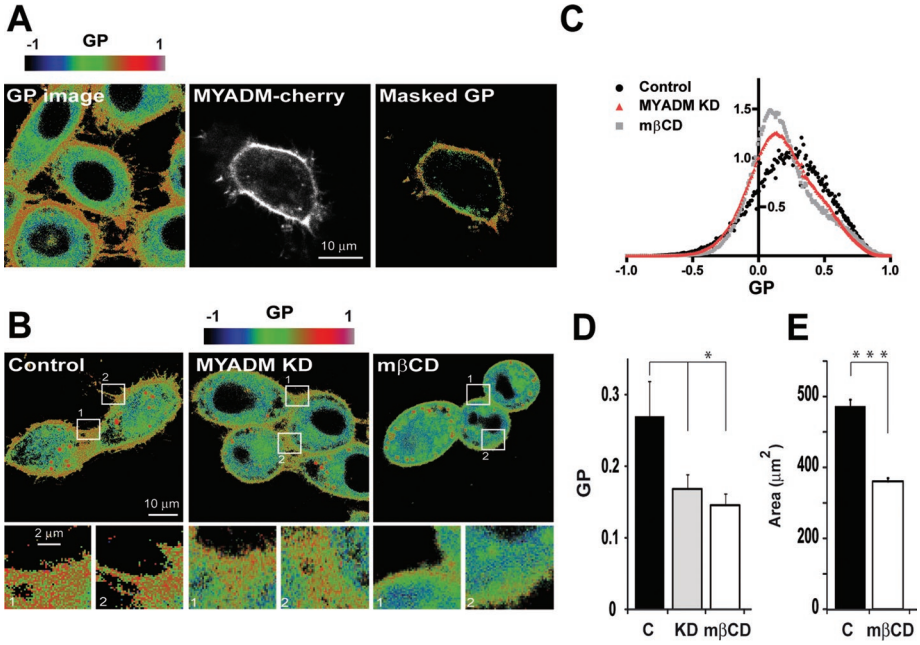

FIGURE 3: MYADM KD reduces membrane condensation. (A) HeLa cells transiently expressing MYADM-cherry were stained with Laurdan for 30 min. Cells were then imaged for MYADM-cherry (middle panel) and for the Laurdan intensity in two channels (400–460 nm and 470–530 nm). Laurdan intensity images were converted to GP images and pseudocolored using the indicated scale (left panel) to represent low-to-high GP values (see scale). The masked GP image corresponding to the membrane regions labeled for MYADM-cherry was then obtained (right panel). (B–E) Control MYADM KD cells or normal cells the cholesterol content of which was reduced by treatment with 10 mM methyl-β-cyclodextrin (mβCD) for 15 min were stained with Laurdan. The GP distribution obtained in each case is represented as pseudocolored images (B, top panels) or normalized histograms (C). In (C), The *x*-axis represents GP values, and the *y*-axis shows the percentage of pixels found for each GP value. An enlargement of the boxed regions is also shown (B, bottom panels). The GP and spreading area are presented in (D) and (E), respectively. The mean ± SEM from three independent experiments is shown (D and E). 16–20 images for each condition (16–20 cells per image) were analyzed in three independent experiments; *p < 0.05; ***p < 0.001.

Remarkably, expression of constitutively active GFP-Rac1L61 increased lamellipodial extensions where MYADM and active Rac1 colocalized extensively (Figure 4C).

MYADM mediates Rac1 targeting to ordered membranes

To investigate the requirement for MYADM in targeting Rac1 to compact membranes, we compared the partitioning of Rac1 into DRMs of control and MYADM KD cells (Figure 5, A and B). The absence of MYADM expression clearly prevented Rac1 from segregating into DRMs compared with control cells. As a control for the specificity of the effect on Rac1, we observed that the partitioning of caveolin-1 and glycosylphosphatidylinositol-anchored protein CD59 was unaltered in MYADM KD cells. Importantly, the presence of Rac1 in DRMs was rescued by the expression of exogenous MYADM-GFP in MYADM KD cells (Figure 5, A and B). Paralleling the changes observed in the association of Rac1 with DRMs, the even distribution of Rac1 at the plasma membrane found in control cells changed to a more discrete pattern in MYADM KD cells (Figure 5C). Interestingly, the levels of neither active GTP-loaded Rac1 nor RhoA nor Cdc42 were significantly altered in MYADM KD cells (Figure 5D), indicating that MYADM regulates Rac1 by mediating its targeting to condensed membranes without affecting its state of GTP loading. These results evoked the effect previously observed for Rac1 activity in cells the membrane raft integrity of which was disrupted by cholesterol sequestration with methyl-β-cyclodextrin (del Pozo *et al.*, 2004), and are consistent with previous findings showing not only that the state of GTP loading contributes to regulate the function of Rac1 but that its correct targeting to specialized raft membranes is also required (Michaely *et al.*, 1999; Ghosh *et al.*, 2002; del Pozo *et al.*, 2004; Vilhardt and van Deurs, 2004; Golub and Pico, 2005).

To further investigate the role of MYADM in Rac1 function, we performed rescue-of-function experiments using MYADM KD or Rac1 KD cells expressing or not constitutively active Rac1L61 or MYADM-GFP, respectively (Figure 6A). Cell spreading, a hallmark of Rac1 function, was taken as the output (Figure 6B). As a control, we observed dominant-negative Rac1N17, which, similar to Rac1 KD, also reduced cell spreading and did not restore cell spreading in MYADM KD cells. Remarkably, active Rac1L61 increased cell spreading regardless of MYADM expression, whereas MYADM-GFP failed to restore the cell-spreading defect of the Rac1 KD cells. The effect of Rac1L61 expression in MYADM KD cells on cell spreading is consistent with previous observations indicating that constitutively active Rac1 can partially exert its functions without being properly targeted to the plasma membrane (del Pozo *et al.*, 2000). In conclusion, the results in Figure 6 suggest that MYADM and Rac1 act on parallel pathways that lead to similar spreading outcomes.

DISCUSSION

The existence of cellular membrane heterogeneity has been widely reported by different experimental strategies that measure parameters as varied as stiffness (Wang *et al.*, 2001; Roduit *et al.*, 2008), microviscosity (Ghosh *et al.*, 2002; Vasanji *et al.*, 2004), or order (Gaus *et al.*, 2006b; Jacobson *et al.*, 2007). Mechanisms contributing to plasma membrane organization are however still poorly understood and somewhat controversial. The initial concept of preexisting auto-assembled lipid domains regulating membrane protein function has now evolved. Membrane rafts mediating localized signaling from different membrane regions are now envisaged as protein-based macromolecular assemblies that organize and are dependent on interactions with neighboring membrane lipids, such as cholesterol or phosphoinositides (Mayor *et al.*, 2006).

All members of the MAL family characterized so far have a tissue-restricted pattern of expression and have been involved in raft-mediated specialized trafficking. The MAL protein founder of the family and its best characterized member appears to organize raft lipids as platforms for apical transport of influenza virus hemagglutinin (HA) in epithelial cells (Cheong *et al.*, 1999; Puertollano *et al.*, 1999; Magal *et al.*, 2009) and Lck transport to the plasma membrane in T lymphocytes (Anton *et al.*, 2008). In the absence of MAL expression, these cargoes are no longer able to partition into DRMs and travel to its destination, whereas exogenous expression of MAL restores both cargo trafficking and partitioning (Puertollano *et al.*, 1999; Anton *et al.*, 2008). Consistent with a role in the organization of raft lipids to generate condensed membranes (Puertollano *et al.*, 1999;

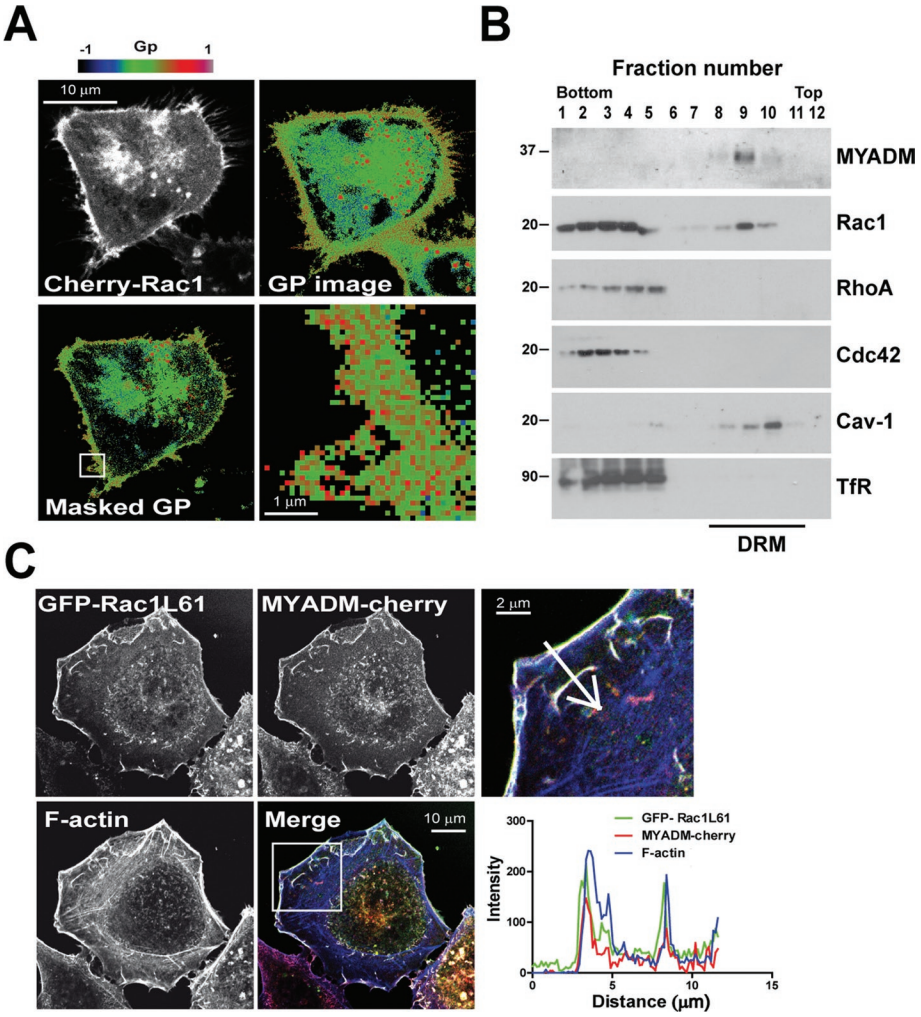

FIGURE 4: Rac1 colocalizes with MYADM at the plasma membrane and accumulates into compact membranes. (A) HeLa cells transiently expressing cherry-Rac1 were stained with Laurdan for 30 min. Cells were then imaged for cherry-Rac1 (top right panel) and for the Laurdan intensity in two channels (400–460 and 470–530 nm). Laurdan intensity images were converted to GP images and pseudocolored using the indicated scale (top left panel). The masked GP image corresponding to the membrane regions labeled for cherry-Rac1 was then obtained (bottom left panel). An enlargement of the boxed region is shown (bottom right panel). (B) HeLa cells were extracted with 0.2% Triton X-100 at 4°C, and the extracts were centrifuged to equilibrium in sucrose density gradients. The different fractions were analyzed for their content of the indicated proteins. The DRM fractions are indicated. (C) HeLa cells stably expressing MYADM-cherry were transfected with GFP-Rac1L61. After 24 h, cells were stained for F-actin and analyzed under a confocal microscope. An enlargement of the boxed region is shown. The plot shows the intensity of the staining of GFP-Rac1L61, MYADM-cherry, and F-actin along the line indicated by the arrow in the enlarged image.

Anton *et al.*, 2008), Laurdan staining has shown that MAL clustering induces the formation of large domains with specific sorting properties (Magal *et al.*, 2009). The four membrane-spanning segments of MAL constitute the MARVEL domain (Sanchez-Pulido *et al.*, 2002), which is thought to play a role in membrane domain organization (Magal *et al.*, 2009).

MYADM was identified as a gene the expression of which is upregulated during myeloid differentiation (Pettersson *et al.*, 2000). Alteration of MYADM expression also has been found in human melanoma metastasis samples (de Wit *et al.*, 2005) and during salt susceptibility–related hypertension (Yagil *et al.*, 2005). Notwithstanding that MYADM levels may be modulated in different cell contexts, we and others have shown the widespread pattern of expression of this MAL family member, which suggests a possible role of MYADM as an organizer of plasma membrane microdomains that play general or even housekeeping rather than specialized roles. In addition, MYADM has features such as displaying eight transmembrane segments organized as a tandem array of two MARVEL domains and being preferentially distributed at plasma membrane lamellipodia suggestive of a role organizing cell surface domains. Using different strategies to silence the *MYADM* gene in combination with the use of the membrane fluorescent Laurdan probe to measure membrane order, we have demonstrated here that MYADM regulates plasma membrane condensation. As a consequence, Rac1, which is loosely bound to ordered membranes in control cells, becomes excluded from those membranes in MYADM KD cells, whereas other more tightly attached proteins, such as caveolin-1 and CD59, are retained. Ectopic expression of MYADM in MYADM KD cells rescues Rac1 clustering into DRMs. Preventing Rac1 recruitment into DRMs has an effect on cell spreading and migration—a general cell function that is dependent on membrane condensation (Manes *et al.*, 2003) or microviscosity (Ghosh *et al.*, 2002; Vasanji *et al.*, 2004). We cannot discount the possibility that the presence in rafts of proteins other than Rac1 might also be affected in MYADM KD cells. Nevertheless, based on the rescue experiments with constitutively active Rac1, we think that our hypothesis that the deficient targeting of Rac1 is a major cause of the defects of cell shape and motility observed in MYADM KD cells is a plausible one. Our results are consistent with previous reports showing that Rac1 is targeted to membrane-ordered domains upon adhesion and that integrity of cholesterol-enriched membranes is essential for Rac1 localization and cell migration (del Pozo *et al.*, 2004; Palazzo *et al.*, 2004). In our experimental model, pharmacological disruption of cholesterol membranes recapitulates the effect of MYADM knockdown.

On de-adhesion, Rac1 is translocated from surface cholesterol-enriched domains to an intracellular compartment. This trafficking is controlled by actin cholesterol and caveolin-1 (del Pozo *et al.*, 2004, 2005). By following the glycolipid GM1 as a membrane raft marker, it also has been reported that subsequent cell adhesion regulates exocist- and Arf6-dependent traffic of membrane rafts from recycling endosomes to the cell surface. This process is in turn essential for proper integrin and growth factor signaling (Balasubramanian *et al.*, 2007, 2010). In contrast, Rac1 activity also requires Arf6- and Rab5-dependent recycling from endosomes to plasma membrane necessary for cell migration (Radhakrishna *et al.*, 1999; Zhang *et al.*, 1999; del Pozo *et al.*, 2004; Palamidessi *et al.*, 2008). Given the parallels between membrane rafts and Rac1 dynamics upon adhesion, it can

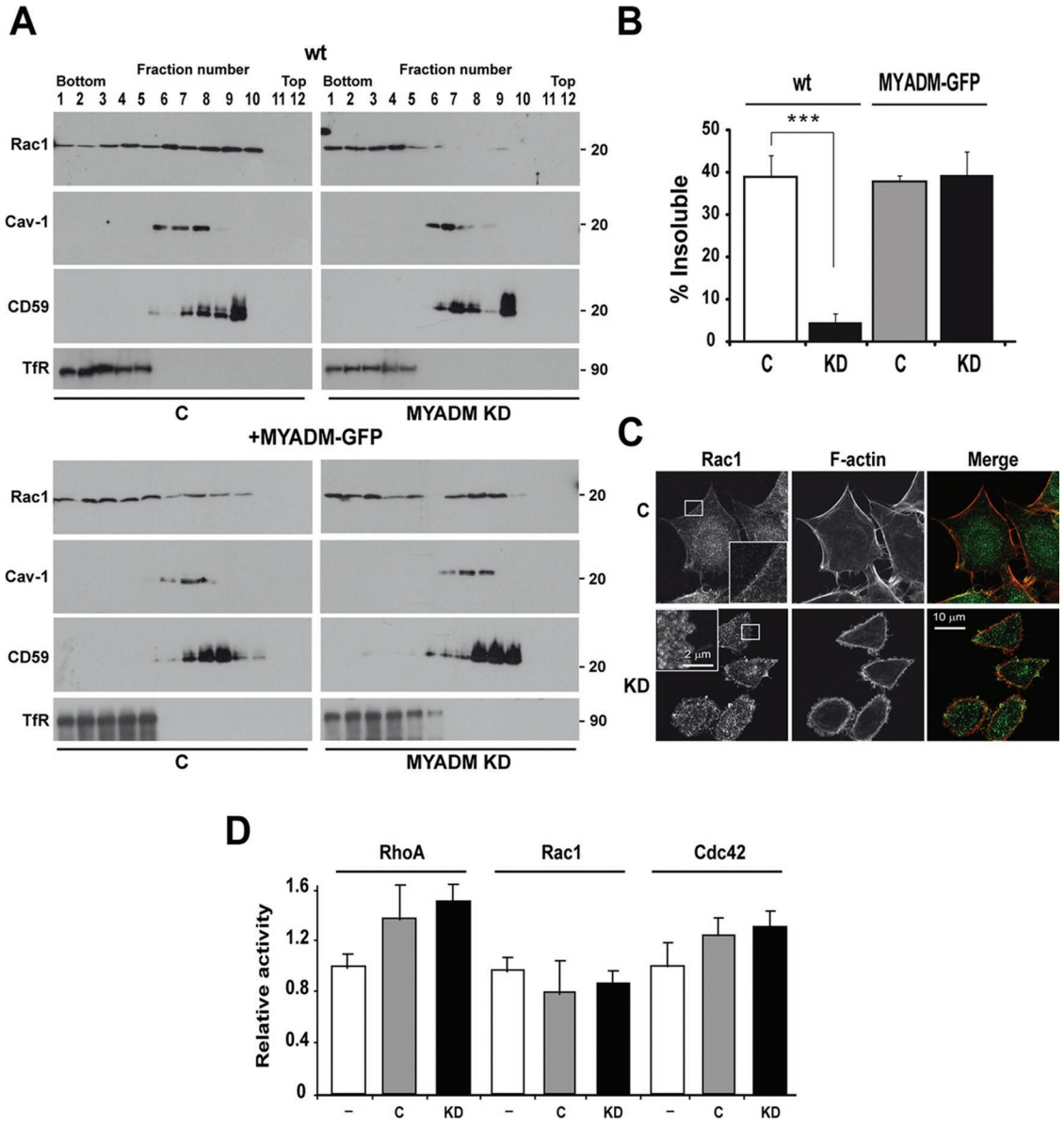

FIGURE 5: MYADM KD inhibits recruitment of Rac1 into compact membranes and alters the distribution of Rac1 at the plasma membrane. (A) Control or MYADM KD HeLa cells stably expressing or not MYADM-GFP were extracted with 0.2% Triton X-100 at 4°C, and the extracts were centrifuged to equilibrium in sucrose density gradients. The Rac1, caveolin-1, CD59, and TfR content of the different fractions was analyzed. (B) The histogram represents the percentage of insoluble Rac1 under the different conditions used in (A). (C) Control or MYADM KD cells were stained for endogenous Rac1 and F-actin. The insets show an enlargement of the boxed regions of the plasma membrane to illustrate the different pattern of distribution of Rac1 at the plasma membrane of control and MYADM KD cells. (D) The histograms show the levels of active Cdc42, Rac1, and RhoA in control and MYADM KD cells as determined in pull-down assays. The mean ± SEM from three independent experiments is shown in (B and D); ***$p < 0.001$.

be speculated that Rac1 trafficking from endosome compartments to cell surface during cell migration also occurs via ordered domains the presence of which in endosomes has been previously established (Puertollano *et al.*, 2001; Masuyama *et al.*, 2009; Nada *et al.*, 2009). Formerly characterized members of the MAL family play central roles in specialized trafficking (Puertollano *et al.*, 1999; de Marco *et al.*, 2002; Anton *et al.*, 2008) and have been found in this intracellular compartment (Puertollano *et al.*, 2001). Thus it would be interesting to address in the future whether MYADM or other MAL family members could also participate in the endosome circuitry necessary for spatially restricted Rac1 function. It is of note that no physical link has been reported for these other proteins that determine Rac1 localization to membrane compartments such as Rab5 (Palamidessi *et al.*, 2008) or caveolin-1 (del Pozo *et al.*, 2005). Like that of MYADM, the role of these proteins is to regulate membrane compartments required for proper location and function of this GTPase.

MYADM expression is modulated in two processes highly related to cell migration, such as haematopoiesis and melanoma metastasis (Pettersson *et al.*, 2000; de Wit *et al.*, 2005). MYADM transcripts appear reduced in melanoma metastasis samples compared with benign nevocellular nevi (de Wit *et al.*, 2005). This observation may apparently be inconsistent with a positive role proposed here of MYADM regulating Rac-dependent migration. Interestingly, melanoma cell lines have been studied as cell models that

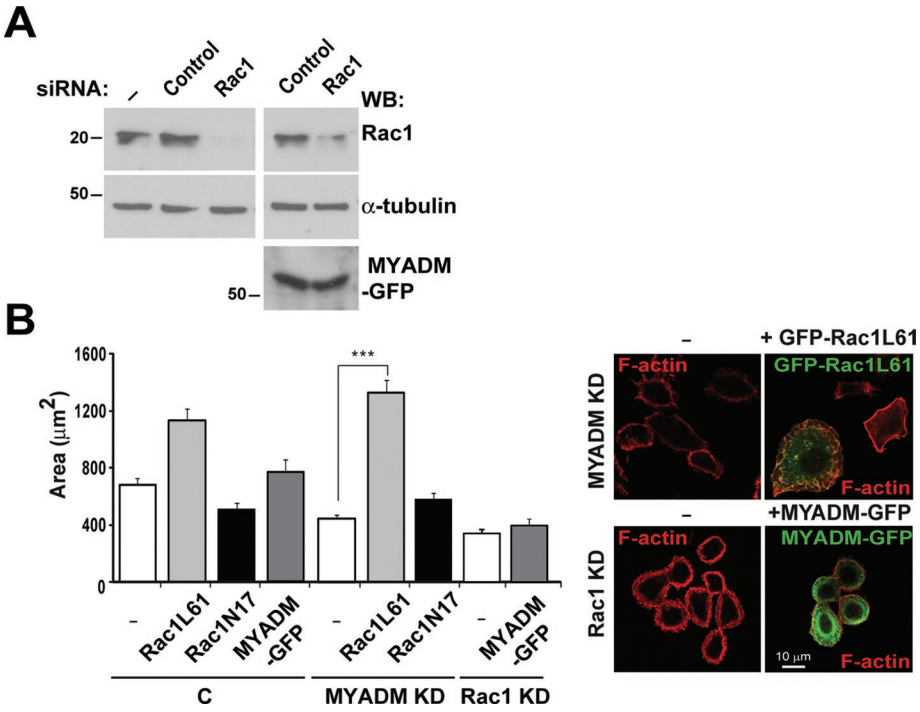

FIGURE 6: Rescue-of-function experiments in MYADM KD or Rac1 KD cells. (A) Normal HeLa cells or HeLa cells stably expressing MYADM-GFP were transfected with control siRNA or siRNA targeted to Rac1 and processed for immunoblotting for Rac1, MYADM-GFP, and α-tubulin, which was used as a loading control. (B) Control MYADM KD or Rac1 KD cells were transfected with Rac1L61 or Rac1N17 or with MYADM-GFP, respectively, as indicated. Cells were then fixed, and their spreading area was determined 24 h later. The mean ± SEM is represented (left panel). Representative images of cells stained for F-actin of MYADM KD or Rac1 KD cells transfected or not with GFP-Rac1L61 or MYADM-GFP, respectively, are shown (right panel). At least three independent experiments were performed. 100–120 cells for each condition were analyzed; ***$p < 0.001$.

spontaneously adopt two distinct modes of movement during migration in three-dimensional extracellular matrices (Sanz-Moreno *et al.*, 2008, 2010). The one called amoeboid or rounded movement is driven by high Rho activity and actomyosin contractility. This mode allows cells to squeeze forward through gaps present in the extracellular matrix in the absence of proteolytic activity. The alternative manner of tumor migration called mesenchymal or elongated is driven by extension of Rac-dependent lamellipodia and requires proteolytic processing of the extracellular matrix to allow cell movement across wider gaps. Both modes of three-dimensional migration are interconvertible; when Rac activity is kept low, cells switch to rounded migratory mode, which may confer additional plasticity to melanoma cells (Sanz-Moreno *et al.*, 2010). In vivo comparative analysis of both modes of movement strongly suggests that amoeboid movement with low Rac activity favors invasion and metastasis of these cells (Sanz-Moreno *et al.*, 2008). This observation is consistent with human melanoma metastasis samples containing cells with low levels of MYADM favoring invasive amoeboid movement and opens an attractive and unexplored possibility to MYADM playing a role in cell migration in a pathological context, such as cancer invasion.

In summary, unlike the previously characterized MAL members, MYADM is present at the plasma membrane and widely expressed, suggestive of a general raft-dependent role at the cell surface. Our results show that MYADM is necessary for correct membrane structure and appropriate targeting of Rac1 to specialized membrane rafts and subsequently for cell spreading and migration.

MATERIALS AND METHODS

Reagents

The rabbit polyclonal antibodies to caveolin-1 and the monoclonal antibody (mAb)s to RhoA, Rac1, and Cdc42 were obtained from BD Biosciences (San Jose, CA). Methyl-β-cyclodextrin and the mAb to α-tubulin or transferrin receptor (TfR) were purchased from Sigma-Aldrich (St. Louis, MO) and Zymed Laboratories (South San Francisco, CA), respectively. The anti-HA antibody 12CA5 and the anti-CD59 antibody MEM-43/5 were obtained from Roche (Indianapolis, IN) and Abcam (Cambridge, MA), respectively. Secondary goat antibodies coupled to Alexa 488 tetramethylrhodamine isothiocyanate–labeled phalloidin and the fluorescent probe Laurdan (6-acyl-2-dimethylaminonapthalene) were purchased from Molecular Probes (Eugene, OR). Secondary antibodies coupled to horseradish peroxidase were obtained from Jackson ImmunoResearch (West Grove, PA).

Cell culture conditions

Human epithelial HeLa and PC3 cells were obtained from the American Type Culture Collection and maintained in Petri dishes in DMEM supplemented with 5% fetal bovine serum (Sigma-Aldrich), penicillin (50 U/ml), and streptomycin (50 μg/ml) at 37°C in an atmosphere of 5% CO_2/95% air.

DNA constructs, siRNA, and transfection conditions

The DNA constructs expressing MYADM tagged with HA, GFP, or cherry were generated by PCR using 5′ and 3′ oligonucleotide primers with the appropriate modifications and MYADM cDNA (IMAGE clone 3627858) as the template. The amplified MYADM coding sequence was cloned in-frame for the GFP or cherry open reading frame using the pEGFP-N1 or pmCherry-N1 plasmids (Clontech, Mountain View, CA) in the case of the fluorescent chimeras or in the PCR3.1 plasmid (Invitrogen, Carlsbad, CA) in the case of HA-tagged MYADM. The DNA constructs expressing GFP-tagged MYADML1 and MYADML2 were generated by cloning in pEGFP-N1 the DNA fragments obtained by PCR using 5′ and 3′ oligonucleotide-specific primers with the appropriate modifications and MYADML1 cDNA (IMAGE clone 5297847) or MYADML2 cDNA (IMAGE clone 5172276) as template, respectively. The DNA constructs in pEGFP-C1 or pmCherry-C1 for expression of GFP fused to the amino terminus of Rac1 Rac1L61 or Rac1N17 and the DNA constructs for expression of the Rho GTPase-binding domain of PAK1 (GST-PBD) or Rhotekin (GST-RBD) fused to GST were generous gifts from A. Ridley (King's College, London, UK). The 5′-ATGCCAGTGACGGTAACCCGC-3′ and 5′-GGTGCTGAGCTCACATCCA-3′ sequences, which target the AUG translation initiation site and immediately downstream sequences and the 3′ untranslated region of MYADM mRNA, respectively, separated by a short spacer (5′-TTCAAGAGA-3′) from their reverse complement were cloned under the control of the H1-RNA promoter in the pSuper DNA vector (Brummelkamp *et al.*, 2002), thereby generating the shRNA1 and shRNA2 expression constructs.

Transfection of HeLa cells with plasmid DNA was performed by electroporation using an Electro Cell Manipulator 600 electroporation instrument (BTX, San Diego, CA). More than 90% of HeLa cells were transfected. To select stable transfectants, cells were treated with 0.5 mg/ml G-418 sulfate (Roche) for at least 4 wk after transfection. Cell clones were screened by immunoblot analysis. The clones that proved to be positive were maintained in drug-free medium. The siRNA duplexes 5′-ATCACTGGCTATATGGCC-3′ (siRNA1), 5′-GGTGCTGAGCTCACATCCA-3′ (siRNA2), and 5′-GGTCTAAGACTCTCCCAAG-3′ (siRNA3) targeted to MYADM mRNA and 5′-AGACGGAGCUGUAGGUAAAUU-3′ targeted to Rac1 mRNA were purchased from Dharmacon (Chicago, IL). The sequences of all the siRNAs used were subjected to a Basic Local Alignment *Search* Tool (BLAST) search to ensure targeting specificity. siRNA was introduced into HeLa or PC3 cells using oligofectamine 2000 (Invitrogen).

Generation of mAbs to the MYADM protein

The peptide FDEKYGCQPRRSRDVSC corresponding to amino acids 263–279 of human MYADM was coupled to keyhole limpet hemocyanin (Thermo Fisher Scientific, Rockford, IL). Spleen cells from mice immunized with the peptide were fused to myeloma cells and plated onto microtiter plates. The hybridoma clone 2B12, which produces antibodies that recognize MYADM in membrane extracts from Cos-7 cells transiently expressing HA-tagged MYADM, was selected.

Laurdan staining

Labeling of live cells with the fluorescent probe Laurdan (5 μM) microscope calibration and two-photon microscopy were performed as described (Gaus *et al*., 2003) using an LSM 710 NLO Multiphoton coupled to an AxioObserver inverted microscope (Carl Zeiss, Jena, Germany) with a 63× water objective NA 1.3. In brief, Laurdan was excited at 800 nm, and emission intensities were recorded simultaneously in the 400–460 nm and 470–530 nm ranges. Intensity images were converted into a GP index defined as I(400–460) – I(470–530) / I(400–460) + I(I(470–530), where I is the emission intensity as previously described (Gaus *et al*., 2003). Images of a standard solution of 5 μM Laurdan in dimethyl sulfoxide at room temperature (22°C) were acquired to obtain the G factor as described (Gaus *et al*., 2006b). The G factor was then used to correct the experimental GP values. GP values range from –1 (fluid domains) to +1 (highly ordered domains); membranes with GP values >0.3 are considered to be ordered membrane domains. The GP distributions and mean GP values were obtained from GP images normalized and represented using GraphPad Prism Software (San Diego, CA).

Confocal microscopy

Cells were fixed in 4% paraformaldehyde for 15 min, rinsed, and treated with 10 mM glycine for 5 min. The cells were then permeabilized with 0.2% Triton X-100, rinsed, and incubated with 3% bovine serum albumin in phosphate-buffered saline (PBS) for 15 min. Cells were incubated for 1 h with the indicated primary antibodies, rinsed several times, and incubated for 1 h with the appropriate Alexa 488–labeled secondary antibodies or with fluorescent phalloidin. Controls to assess labeling specificity included incubations with control primary antibodies or omission of the primary antibodies. Confocal fluorescence micrographs were taken using a Carl Zeiss LSM 510 microscope equipped with a 63× oil objective NA 1.3. Images were exported in TIFF format, and their brightness and contrast were optimized with Adobe Photoshop.

Random migration assays

Cells were plated onto fibronectin-coated coverslips and then immediately placed on the stage of a Carl Zeiss Axiovert 200 microscope equipped with a heated stage and CO_2 circulator to maintain cells at 37°C and 5% CO_2. Time-lapse analysis was performed at 15-min intervals for 17.5 h. Cell trajectories were manually tracked and analyzed from recorded images using MetaMorph 6.2r6 (Molecular Devices, Downingtown, PA) and ImageJ 1.43m software (http://rsb.info.nih.gov/ij). Briefly, the centroid of each cell was followed to calculate the index of directionality and velocity of individual cells correcting trajectories of overlapping cells during their movement and ruling out dividing cells from the analysis. We obtained similar results with both programs. Plots of directionality and the quantitative analysis of the elliptical factor and the area of the cells were obtained using in-house plug-ins for the ImageJ program.

RT-PCR and Northern blot analyses

The expression of MYADM, MYADML1, and MYADML2 in different cell lines was analyzed by RT-PCR using the Titan One-Tube kit (Roche) and 5′ and 3′ oligonucleotide primer pairs specific to each mRNA species. For Northern blot analysis, 20 μg of total RNA was hybridized under standard conditions to ^{32}P-labeled MYADM and β-actin cDNA probes.

DRM isolation

HeLa cells grown to confluence in 100-mm dishes were rinsed with PBS and lysed for 20 min in 1 ml of 25 mM Tris-HCl, pH 7.5; 150 mM NaCl, 5 mM EDTA, and 0.2% or 1% Triton X-100 as indicated at 4°C. The insoluble membrane fraction was isolated by centrifugation to equilibrium in a sucrose density gradient in a swinging bucket SW40 rotor (Beckman Coulter, Brea, CA) at 39,000 rpm (188,000 × *g*) for 20 h (Brown and Rose, 1992). Twelve 1-ml fractions were harvested from the bottom to the top of the centrifuge tube, and equivalent aliquots were subjected to immunoblot analysis with the appropriate antibodies.

Pull-down assays

HeLa cells were lysed in 50 mM Tris-HCl, pH 7.4; 1 mM $MgCl_2$; 2 mM EDTA; 300 mM NaCl; 0.5% Nonidet P-40; and 10% glycerol containing a cocktail of protease inhibitors. Recombinant GST, GST-PBD, or GST-RBD proteins (10 μg) immobilized on GSH-Sepharose beads (GE Life Sciences, Piscataway, NJ) were incubated with the lysates for 1 h at 4°C in lysis buffer containing 10 mM $MgCl_2$. The beads were washed three times in interaction buffer, and bound proteins were analyzed by immunoblotting with anti-RhoA-Rac1 or -Cdc42 mAbs.

Bioinformatics analysis

Protein information was retrieved from Universal Protein Resource (UniProt; http://www.expasy.uniprot.org) using the Batch Retrieval function available at the Protein Information Resource Web site (http://pir.georgetown.edu). Protein sequences were aligned, and the resulting phylogenetic tree of MARVEL domain-containing proteins was derived using JALVIEW (University of Dundee, UK).

Statistical analysis

Quantitative data are expressed as the mean ± SEM. A paired Student's *t* test was used to establish the statistical significance of differences between the means.

ACKNOWLEDGMENTS

We thank A. Jiménez, J.A. Rodríguez, and L. Fernández for their technical assistance and F. Martín-Belmonte for his helpful comments. We thank D. Abia for his helpful advice about the bioinformatic analysis of MARVEL domain-containing proteins. This work

was supported by grants BFU2009–07886 (to M.A.A.), SAF-2008–01936 and SAF2008–01158-E (to J.M.), BFU2008–02460 (to I.C.), BFU2009–10335 (to C.E.), CONSOLIDER COAT CSD2009–00016 (to M.A.A. and C.E.), all grants from the Ministerio de Ciencia e Innovación, and grants GEN-0166/2006 from the Comunidad de Madrid (to I.C.), CSIC-200920I016 from Consejo Superior de Investigaciones Científicas (to L.K.), and PI040236 from Fundació Marató TV3 (to C.E.).

REFERENCES

Anton O, Batista A, Millan J, Andres-Delgado L, Puertollano R, Correas I, Alonso MA (2008). An essential role for the MAL protein in targeting Lck to the plasma membrane of human T lymphocytes. J Exp Med 205, 3201–3213.

Bagatolli LA, Sanchez SA, Hazlett T, Gratton E (2003). Giant vesicles Laurdan and two-photon fluorescence microscopy: evidence of lipid lateral separation in bilayers. Meth Enzymol 360, 481–500.

Balasubramanian N, Meier JA, Scott DW, Norambuena A, White MA, Schwartz MA (2010). RalA-exocyst complex regulates integrin-dependent membrane raft exocytosis and growth signaling. Curr Biol 20, 75–79.

Balasubramanian N, Scott DW, Castle JD, Casanova JE, Schwartz MA (2007). Arf6 and microtubules in adhesion-dependent trafficking of lipid rafts. Nat Cell Biol 9, 1381–1391.

Bosse F, Hasse B, Pippirs U, Greiner-Petter R, Muller HW (2003). Proteolipid plasmolipin: localization in polarized cells regulated expression and lipid raft association in CNS and PNS myelin. J Neurochem 86, 508–518.

Brown DA, Rose JK (1992). Sorting of GPI-anchored proteins to glycolipid-enriched membrane subdomains during transport to the apical cell surface. Cell 68, 533–544.

Brummelkamp TR, Bernards R, Agami R (2002). A system for stable expression of short interfering RNAs in mammalian cells. Science 296, 550–553.

Cheong KH, Zacchetti D, Schneeberger EE, Simons K (1999). VIP17/MAL, a lipid raft-associated protein, is involved in apical transport in MDCK cells. Proc Natl Acad Sci USA 96, 6241–6248.

Cui W, Yu L, He H, Chu Y, Gao J, Wan B, Tang L, Zhao S (2001). Cloning of human myeloid-associated differentiation marker (MYADM) gene whose expression was up-regulated in NB4 cells induced by all-trans retinoic acid. Mol Biol Rep 28, 123–138.

de Marco MC, Kremer L, Albar JP, Martinez-Menarguez JA, Ballesta J, Garcia-Lopez MA, Marazuela M, Puertollano R, Alonso MA (2001). BENE a novel raft-associated protein of the MAL proteolipid family interacts with caveolin-1 in human endothelial-like ECV304 cells. J Biol Chem 276, 23009–23017.

de Marco MC, Martin-Belmonte F, Kremer L, Albar JP, Correas I, Vaerman JP, Marazuela M, Byrne JA, Alonso MA (2002). MAL2 a novel raft protein of the MAL family is an essential component of the machinery for transcytosis in hepatoma HepG2 cells. J Cell Biol 159, 37–44.

de Wit NJ, Rijntjes J, Diepstra JH, van Kuppevelt TH, Weidle UH, Ruiter DJ, van Muijen GN (2005). Analysis of differential gene expression in human melanocytic tumour lesions by custom made oligonucleotide arrays. Br J Cancer 92, 2249–2261.

del Pozo MA, Alderson NB, Kiosses WB, Chiang HH, Anderson RG, Schwartz MA (2004). Integrins regulate Rac targeting by internalization of membrane domains. Science 303, 839–842.

del Pozo MA, Balasubramanian N, Alderson NB, Kiosses WB, Grande-Garcia A, Anderson RG, Schwartz MA (2005). Phospho-caveolin-1 mediates integrin-regulated membrane domain internalization. Nat Cell Biol 7, 901–908.

del Pozo MA, Price LS, Alderson NB, Ren XD, Schwartz MA (2000). Adhesion to the extracellular matrix regulates the coupling of the small GTPase Rac to its effector PAK. EMBO J 19, 2008–2014.

Gaus K, Gratton E, Kable EP, Jones AS, Gelissen I, Kritharides L, Jessup W (2003). Visualizing lipid structure and raft domains in living cells with two-photon microscopy. Proc Natl Acad Sci USA 100, 15554–15559.

Gaus K, Le Lay S, Balasubramanian N, Schwartz MA (2006a). Integrin-mediated adhesion regulates membrane order. J Cell Biol 174, 725–734.

Gaus K, Zech T, Harder T (2006b). Visualizing membrane microdomains by Laurdan 2-photon microscopy. Mol Membr Biol 23, 41–48.

Ghosh PK, Vasanji A, Murugesan G, Eppell SJ, Graham LM, Fox PL (2002). Membrane microviscosity regulates endothelial cell motility. Nat Cell Biol 4, 894–900.

Golub T, Pico C (2005). Spatial control of actin-based motility through plasmalemmal PtdIns(4,5)P2-rich raft assemblies. Biochem Soc Symp 72, 119–127.

Heasman SJ, Ridley AJ (2008). Mammalian Rho GTPases: new insights into their functions from in vivo studies. Nat Rev Mol Cell Biol 9, 690–701.

Jacobson K, Mouritsen OG, Anderson RG (2007). Lipid rafts: at a crossroad between cell biology and physics. Nat Cell Biol 9, 7–14.

Lingwood D, Simons K (2010). Lipid rafts as a membrane-organizing principle. Science 327, 46–50.

Magal LG, Yaffe Y, Shepshelovich J, Aranda JF, de Marco MdC, Gaus K, Alonso MA, Hirschberg K (2009). Clustering and lateral concentration of raft lipids by the MAL protein. Mol Biol Cell 20, 3751–3762.

Manes S, Ana Lacalle R, Gomez-Mouton C, Martinez AC (2003). From rafts to crafts: membrane asymmetry in moving cells. Trends Immunol 24, 320–326.

Masuyama N, Kuronita T, Tanaka R, Muto T, Hirota Y, Takigawa A, Fujita H, Aso Y, Amano J, Tanaka Y (2009). HM1.24 is internalized from lipid rafts by clathrin-mediated endocytosis through interaction with alpha-adaptin. J Biol Chem 284, 15927–15941.

Mayor S, Viola A, Stan RV, del Pozo MA (2006). Flying kites on slippery slopes at Keystone. Symposium on Lipid Rafts and Cell Function. EMBO Rep 7, 1089–1093.

Michaely PA, Mineo C, Ying YS, Anderson RG (1999). Polarized distribution of endogenous Rac1 and RhoA at the cell surface. J Biol Chem 274, 21430–21436.

Nada S, Hondo A, Kasai A, Koike M, Saito K, Uchiyama Y, Okada M (2009). The novel lipid raft adaptor p18 controls endosome dynamics by anchoring the MEK-ERK pathway to late endosomes. EMBO J 28, 477–489.

Palamidessi A, Frittoli E, Garre M, Faretta M, Mione M, Testa I, Diaspro A, Lanzetti L, Scita G, Di Fiore PP (2008). Endocytic trafficking of Rac is required for the spatial restriction of signaling in cell migration. Cell 134, 135–147.

Palazzo AF, Eng CH, Schlaepfer DD, Marcantonio EE, Gundersen GG (2004). Localized stabilization of microtubules by integrin- and FAK-facilitated Rho signaling. Science 303, 836–839.

Pettersson M, Dannaeus K, Nilsson K, Jonsson JI (2000). Isolation of MYADM a novel hematopoietic-associated marker gene expressed in multipotent progenitor cells and up-regulated during myeloid differentiation. J Leukoc Biol 67, 423–431.

Puertollano R, Martin-Belmonte F, Millan J, de Marco MC, Albar JP, Kremer L, Alonso MA (1999). The MAL proteolipid is necessary for normal apical transport and accurate sorting of the influenza virus hemagglutinin in Madin-Darby canine kidney cells. J Cell Biol 145, 141–151.

Puertollano R, Martinez-Menarguez JA, Batista A, Ballesta J, Alonso MA (2001). An intact dilysine-like motif in the carboxyl terminus of MAL is required for normal apical transport of the influenza virus hemagglutinin cargo protein in epithelial Madin-Darby canine kidney cells. Mol Biol Cell 12, 1869–1883.

Radhakrishna H, Al-Awar O, Khachikian Z, Donaldson JG (1999). ARF6 requirement for Rac ruffling suggests a role for membrane trafficking in cortical actin rearrangements. J Cell Sci 112, 855–866.

Ridley AJ, Schwartz MA, Burridge K, Firtel RA, Ginsberg MH, Borisy G, Parsons JT, Horwitz AR (2003). Cell migration: integrating signals from front to back. Science 302, 1704–1709.

Roduit C, Van Der Goot FG, De Los Rios P, Yersin A, Steiner P, Dietler G, Catsicas S, Lafont F, Kasas S (2008). Elastic membrane heterogeneity of living cells revealed by stiff nanoscale membrane domains. Biophys J 94, 1521–1532.

Rolfe BE, Worth NF, World CJ, Campbell JH, Campbell GR (2005). Rho and vascular disease. Atherosclerosis 183, 1–16.

Sanchez-Pulido L, Martin-Belmonte F, Valencia A, Alonso MA (2002). MARVEL: a conserved domain involved in membrane apposition events. Trends Biochem Sci 27, 599–601.

Sanz-Moreno V, Gadea G, Ahn J, Paterson H, Marra P, Pinner S, Sahai E, Marshall CJ (2008). Rac activation and inactivation control plasticity of tumor cell movement. Cell 135, 510–523.

Sanz-Moreno V, Marshall CJ (2010). The plasticity of cytoskeletal dynamics underlying neoplastic cell migration. Curr Opin Cell Biol 22, 690–696.

Simons K, Ikonen E (1997). Functional rafts in cell membranes. Nature 387, 569–572.

Vasanji A, Ghosh PK, Graham LM, Eppell SJ, Fox PL (2004). Polarization of plasma membrane microviscosity during endothelial cell migration. Dev Cell 6, 29–41.

Vilhardt F, van Deurs B (2004). The phagocyte NADPH oxidase depends on cholesterol-enriched membrane microdomains for assembly. EMBO J 23, 739–748.

Wang Q, Chiang ET, Lim M, Lai J, Rogers R, Janmey PA, Shepro D, Doerschuk CM (2001). Changes in the biomechanical properties of neutrophils and endothelial cells during adhesion. Blood 97, 660–668.

Yagil C, Hubner N, Monti J, Schulz H, Sapojnikov M, Luft FC, Ganten D, Yagil Y (2005). Identification of hypertension-related genes through an integrated genomic-transcriptomic approach. Circ Res 96, 617–625.

Yamazaki D, Kurisu S, Takenawa T (2005). Regulation of cancer cell motility through actin reorganization. Cancer Sci 96, 379–386.

Zhang Q, Calafat J, Janssen H, Greenberg S (1999). ARF6 is required for growth factor- and rac-mediated membrane ruffling in macrophages at a stage distal to rac membrane targeting. Mol Cell Biol 19, 8158–8168.

Millán et al. BMC Biology 2010, 8:11
http://www.biomedcentral.com/1741-7007/8/11

BMC Biology

RESEARCH ARTICLE Open Access

Adherens junctions connect stress fibres between adjacent endothelial cells

Jaime Millán[1,2*], Robert J Cain[3], Natalia Reglero-Real[2], Carolina Bigarella[1], Beatriz Marcos-Ramiro[2], Laura Fernández-Martín[2], Isabel Correas[2], Anne J Ridley[1,3]

Abstract

Background: Endothelial cell-cell junctions maintain endothelial integrity and regulate vascular morphogenesis and homeostasis. Cell-cell junctions are usually depicted with a linear morphology along the boundaries between adjacent cells and in contact with cortical F-actin. However, in the endothelium, cell-cell junctions are highly dynamic and morphologically heterogeneous.

Results: We report that endothelial cell-cell junctions can attach to the ends of stress fibres instead of to cortical F-actin, forming structures that we name discontinuous adherens junctions (AJ). Discontinuous AJ are highly dynamic and are increased in response to tumour necrosis factor (TNF)-α, correlating with the appearance of stress fibres. We show that vascular endothelial (VE)-cadherin/β-catenin/α-catenin complexes in discontinuous AJ are linked to stress fibres. Moreover, discontinuous AJ connect stress fibres from adjacent cells independently of focal adhesions, of which there are very few in confluent endothelial cells, even in TNF-α-stimulated cells. RNAi-mediated knockdown of VE-cadherin, but not zonula occludens-1, reduces the linkage of stress fibres to cell-cell junctions, increases focal adhesions, and dramatically alters the distribution of these actin cables in confluent endothelial cells.

Conclusions: Our results indicate that stress fibres from neighbouring cells are physically connected through discontinuous AJ, and that stress fibres can be stabilized by AJ-associated multi-protein complexes distinct from focal adhesions.

Background

Endothelial cell-cell junctions maintain endothelial integrity and regulate vascular morphogenesis. A major role of the vascular endothelium is to control the movement of small solutes and leukocytes in and out of the bloodstream. Endothelial junctions consist of several different multi-protein complexes, whose relative abundance and roles in regulating permeability and leukocyte diapedesis depend on the endothelial cell type. Endothelial adherens junctions (AJ) and tight junctions (TJ) are the main regulators of paracellular permeability in the endothelium. Some junctional proteins unique to endothelial cells, including PECAM-1, ICAM-2 and S-endo I, also contribute to endothelial barrier function [1]. In endothelial AJ, the transmembrane vascular endothelial (VE)-cadherin binds the cytoplasmic proteins β-catenin and p120-catenin. β-catenin also binds α-catenin, which could link the AJ complex to actin filaments [2]. However, the established model of a direct link between cortical actin filaments (F-actin) and α-catenin in AJ in epithelial cells has been questioned by data demonstrating that the binding of α-catenin to β-catenin or F-actin is mutually exclusive, and suggesting that α-catenin stabilizes AJ by regulating actin polymerization instead of by linking F-actin to AJ [3,4].

Endothelial cell-cell junctions are regulated by a variety of extracellular stimuli, which often act by inducing reorganization of the actin cytoskeleton. For example, Rho guanosine triphosphate (GTPases) and their targets, the rho serine/threonine kinases (ROCKs), stimulate actomyosin-based contractility, generating stress fibres and focal adhesion (FA) and thereby contribute to the rapid increase in endothelial permeability in response to thrombin and histamine [5-8]. Stress fibres generated in response to these stimuli also reorganize junctional

* Correspondence: jmillan@cbm.uam.es
[1]University College London, Ludwig Institute for Cancer Research and Department of Biochemistry and Molecular Biology, London WC1E 6BT, UK

complexes [9-11]. Pro-inflammatory stimuli such as tumour necrosis factor (TNF)-α also induce long-term changes to endothelial cell-cell junctions, actin stress fibre reorganization and an increase in permeability [12,13].

Cell-cell junctions are usually depicted with a linear morphology along the boundaries between adjacent cells and in contact with cortical F-actin. Here we describe the distinct properties of endothelial cell-cell junctions that localize at the ends of stress fibres that we name discontinuous AJ. These structures are distinct from focal adhesions, which are found at the ends of stress fibres in subconfluent endothelial cells. In response to TNF-α, association of stress fibres with discontinuous AJ, but not focal adhesions, is increased, suggesting that AJ may play a role stabilizing stress fibres in confluent endothelial cells.

Results

Composition and dynamics of discontinuous AJ

Analysis of cell-cell junction distribution in human umbilical vein endothelial cells (HUVECs) revealed that, as well as localizing linearly along cell-cell borders similar to junctions in epithelial cells (Figure 1A, arrowhead), in some areas junctional proteins were distributed in multiple short linear structures that were almost orthogonal to cell-cell borders (Figure 1A, arrows) [14]. AJ components such as VE-cadherin, α-catenin, β-catenin or plakoglobin, TJ components such as zonula occludens-1 (ZO-1) and other junctional proteins, such as JAM-A or CD99 (not shown), appeared in these short linear structures that were often clustered in regions along cell-cell borders (Figure 1A). In some cases, these structures branched off linear junctional regions (Figure 1A, arrows). We call these structures discontinuous junctions, because the linear distribution along cell-cell borders is broken in these areas. In order to analyse the dynamics of discontinuous junctions, cells transiently expressing the AJ component p120-catenin tagged either with green fluorescent protein (p120-GFP) or red fluorescent protein (p120-dsRed) were mixed and analysed by time-lapse fluorescence microscopy (Figure 1B, Additional File 1). Endothelial AJ were highly dynamic and reorganized continually. Discontinuous junction linear structures orthogonal to the cell-cell border appeared and disappeared rapidly, often within a few minutes (Figure 1B. arrows, Additional File 1). Discontinuous junctions were generally formed from both adjacent cells, with an extension from one cell overlaying the structure within the neighbouring cell (Figure 1B, arrows, Additional File 1). Their appearance usually coincided with retraction of one cell border with respect to the other, leaving a finger-like protrusion and their disappearance occurred when one cell border extended back over the protrusion area. These results indicate that dynamic behaviour of endothelial cell-cell borders is responsible for the formation of discontinuous AJ structures.

Discontinuous AJ are associated with stress fibres at cell-cell borders

Cell-cell junctions are regulated by cortical F-actin [5]. In discontinuous AJ, VE-cadherin was found to align with the ends of stress fibres, some of which traversed the cell body form one side to the other. Stress fibres in one cell were often connected to stress fibres of adjacent cells through discontinuous AJ (Figure 2A, arrows) and discontinuous AJ structures clustered in regions where stress fibres coalesced to form stellate arrangements (Figure 2A, arrowheads). Analysis of adjacent cells where one cell expressed actin-Cherry and the other did not confirmed that discontinuous AJ can connect stress fibres between neighbouring cells (Figure 2B, arrowheads), suggesting that AJ complexes anchor stress fibres at endothelial cell-cell borders.

Electron microscopy analysis of endothelial cell-cell borders confirmed the connection of F-actin bundles (Figure 3A, arrows), distinct from subcortical F-actin, from neighbouring cells through electron-dense junctional structures (Fig. 3A, arrowheads). The shape of the intercellular junctional perimeter in relation to such cables was suggestive of tension exerted by these fibres on the connected junctions (Figure 3A, inset). In contrast, linear junctional regions showed no associated actin cables (Figure 3B).

Discontinuous AJ are associated with the end of stress fibres independently of focal adhesions (FA)

In most cultured cells, stress fibres are linked to FA, where integrins cluster [15]. Pro-inflammatory stimuli such as TNF-α or IL-1β induce actin stress fibres, cell elongation and contractility in endothelial cells [12] (Figure 4A). We therefore hypothesized that pro-inflammatory stimuli would alter the relative levels of discontinuous AJ. Endothelial cells were grown at confluency for 3 days and stimulated with TNF-α for 20 h. TNF-α induced cell elongation and an increase in stress fibres that were aligned parallel with the elongated axis of the cells, as previously described [13]. These stress fibres often appeared attached to discontinuous AJ, which were also increased in response to TNF-α (Figures 4, 5 and 6A). In these regions, stress fibres were frequently aligned in neighbouring cells (Figure 4B and 5A, boxed area). The TNF-α mediated induction of stress fibres (Figure 4A) was accompanied by an overall increase of F-actin detected by quantitation of phalloidin staining (Figure 6B). However, these stress fibres were rarely attached to FA as identified by localization of paxillin, a FA protein [16] (Figure 4A) and TNF-α

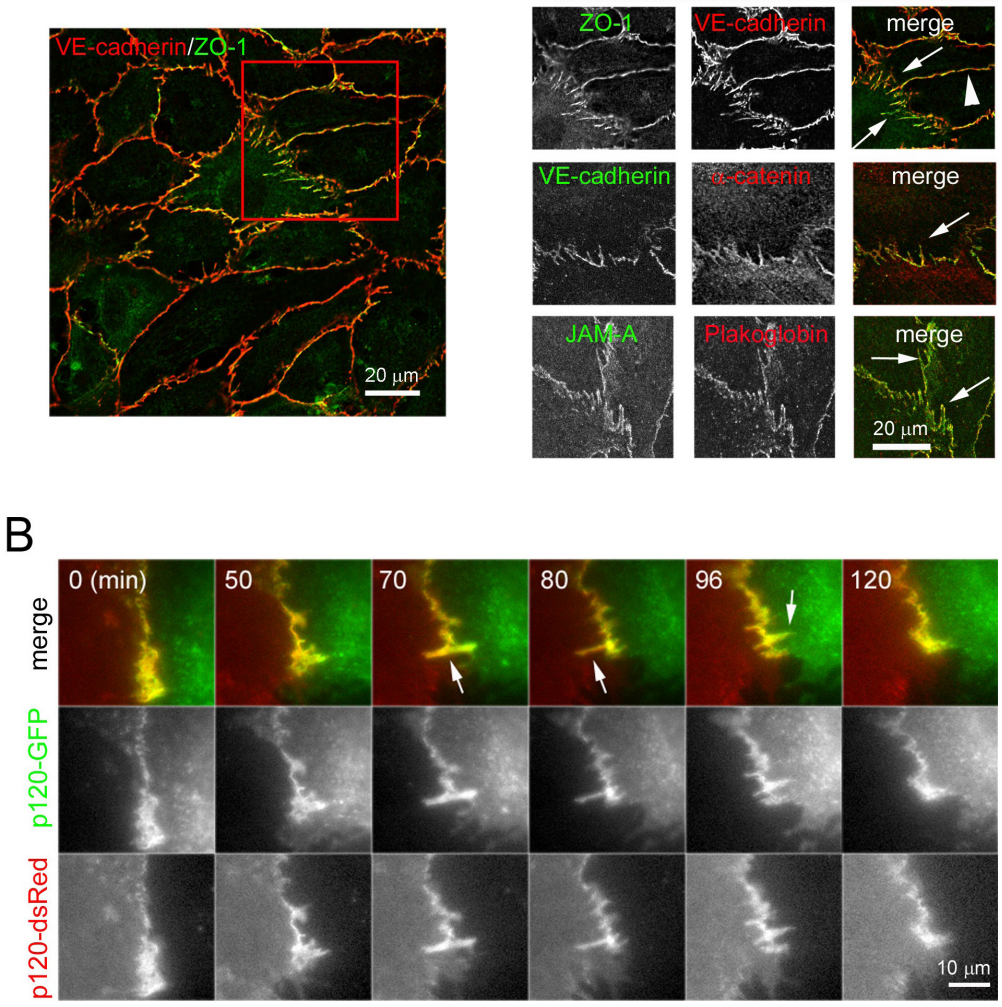

Figure 1 Composition of discontinuous adherens junction (AJ). (A) Human umbilical vein endothelial cells (HUVECs) were grown at confluency for 72 h in EGM-2 growth medium, fixed, permeabilized and stained with antibodies to the indicated junctional proteins. Top right panels show single staining of the merged image on the left. Arrows indicate discontinuous cell-cell junctions; arrowhead, linear cell-cell junctions. (B) HUVECs were nucleofected with plasmids coding for p120-catenin-green fluorescent protein (p120-GFP) or p120-catenin-red fluorescent protein (p120-dsRed), cells from the two transfections were mixed and plated at confluence for 24 h in growth medium. Cell images were acquired by fluorescence time-lapse microscopy, 1 frame/min. Representative images are shown. Arrows show discontinuous AJ.

did not induce a significant increase in the number of FA (Figure 6C). In contrast, stress fibres in sub-confluent cells were found attached to FA, which were far more abundant in sub-confluent compared to confluent cells (Figure 4A and 6C), even though the F-actin content and stress fibre levels of confluent and subconfluent HUVECs was comparable (Figures 4A and 6B), and even higher in response to TNF-α at confluence. This is in clear contrast to previously described responses to acute inflammatory stimuli, such as thrombin, which induce the formation of FAs concomitant with an increase in stress fibres (data not shown and [7,17-19]). Interestingly, TNF-α did not stimulate any detectable change in F-actin in subconfluent cells (Figure 6B). Finally, discontinuous AJ attached to stress fibres were not found associated with FA, since they did not co-localize with the FA components phospho(pY118)-paxillin (Figure 4B), talin or phospho(Y397)-focal adhesion kinase (FAK) (Figure 5), indicating that FA and discontinuous AJ are separate structures that anchor stress fibres in different areas of the endothelial monolayer [16].

In order to analyse in more detail the difference in stress fibre attachment sites between cells with and without cell-cell adhesions, we compared cells at the edge of scratch wounds with cells far from the scratch. Cells situated at the border of the wound had numerous stress fibres linked to FAs, whereas cells situated in the

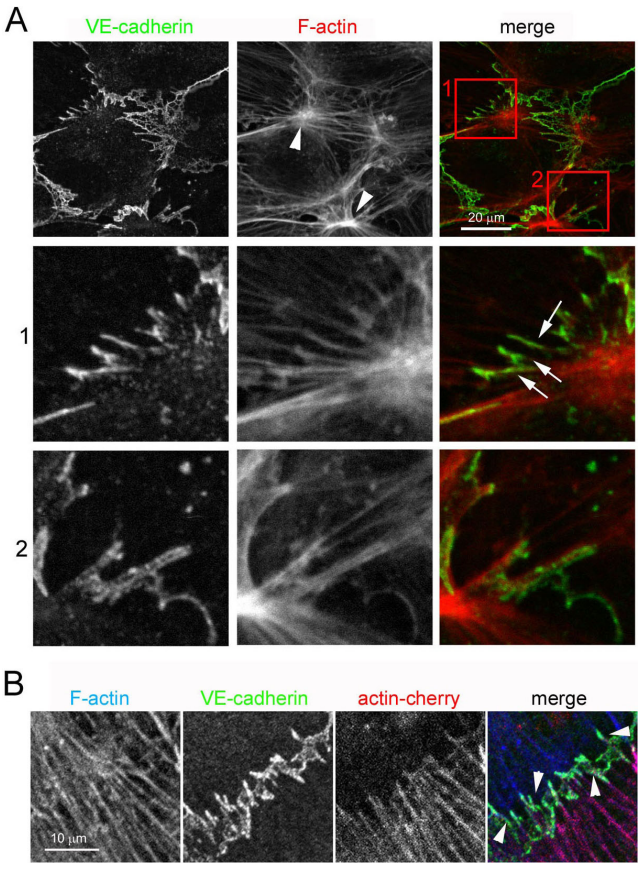

Figure 2 Discontinuous adherens junction (AJ) anchor stress fibres at cell borders. (A) Confluent human umbilical vein endothelial cells (HUVECs) in EGM-2 growth medium were stained for actin filaments (F-actin; TRITC-phalloidin) and vascular endothelial (VE)-cadherin. Bottom panels are enlargements of red boxed areas from top panel that are enriched in discontinuous AJ. (B) HUVECs were nucleofected with a plasmid encoding actin-cherry and plated at confluence for 24 h to 48 h in growth medium. Cells were fixed and stained for VE-cadherin or F-actin. Arrowheads indicate discontinuous AJ.

confluent region of the same monolayer had far fewer FA although stress fibre levels and F-actin were comparable (Figure 7; quantitation in Figure 8). Moreover, some stress fibres in cells at the scratch wound edge appeared connected to FA at one side and discontinuous junctions at the other (Figure 7, arrowheads) Altogether, these data suggest that discontinuous AJ can anchor the ends of stress fibres independently of FA in confluent endothelial cells.

Stress fibre tension mediates formation of discontinuous junctions

Our data indicate that discontinuous AJ form due to dynamic movements of cell-cell borders of adjacent endothelial cells and that they are linked to stress fibres. To investigate whether stress fibres directly affect the formation of discontinuous AJ, cells were treated with the ROCK inhibitor Y-27632, which significantly reduced stress fibres in TNF-α-stimulated HUVECs (Figure 9). Y-27632 reduced the number of discontinuous AJ, although the overall level of junctional VE-cadherin did not appear to be affected and instead the majority of AJ proteins had a linear distribution along cell-cell borders. This indicates that discontinuous AJ are formed as a consequence of stress fibre-induced tension acting on cell-cell junctions. Strikingly, ROCK inhibition did not prevent the permeability increase caused by TNF-α, indicating that this cytokine induces long-term changes in endothelial junctional composition that regulate permeability, independent of stress fibre assembly (data not shown and [13]).

AJs are necessary for stress fibre attachment to cell-cell junctions

In order to determine the contributions of cell-cell junctional components to stress fibre attachment to the junctions, VE-cadherin and ZO-1, components of AJ and TJ, respectively, were knocked down with short interfering RNAs (Figure 10A). VE-cadherin depletion did not completely inhibit the association of β-catenin with cell-cell borders, probably reflecting an association

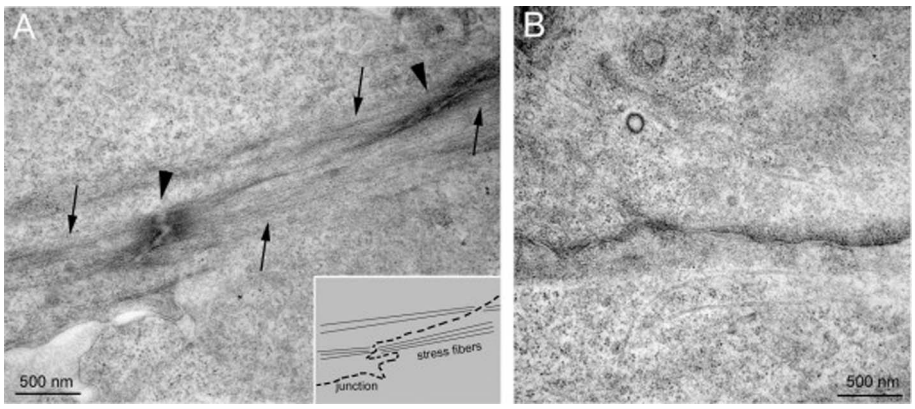

Figure 3 Electron microscopy analysis of endothelial cell-cell borders. Confluent human umbilical vein endothelial cells (HUVECs) either (B) unstimulated or (A) tumour necrosis factor-α-stimulated for 18 h were fixed and processed for electron microscopy. Arrows denote actin filament bundles, whilst arrowheads indicate position of electron-dense junctional structures. Inset: cartoon of panel A illustrating placement of stress fibres with respect to junctional contacts, confirming a connection between junctions and actin filaments, which is not observed at linear junctions (B).

of β-catenin with other cadherins or other junctional components such as PECAM-1 [20,21]. However, this remaining β-catenin no longer showed any localization to discontinuous structures in TNF-α-stimulated cells (Figure 10B and 10D). VE-cadherin depletion did not alter the overall F-actin content (Figure 10D) but altered the distribution of F-actin filaments: there was a decrease in parallel bundles of stress fibres attached to the junctions and, instead, stress fibres were often oriented in multiple directions and many terminated in FAs (Figure 10C). Cortical F-actin increased and cells no longer had an elongated shape (Figure 10B). In contrast, knockdown of ZO-1 did not significantly affect the distribution of AJ and actin stress fibres or cell elongation, suggesting that TJ are not so important for the maintenance of these structures.

Discussion

We show here that confluent HUVECs contain significantly less FA than subconfluent cells, even after stimulation with TNF-α which induces a large increase in stress fibres and overall F-actin content in confluent cells. Stress fibre formation is due to actomyosin contractility which requires them to be attached somewhere at both ends. Here we demonstrate that stress fibres are attached to VE-cadherin-mediated junctional complexes, although it is likely that some other junctional proteins are also linked to endothelial stress fibres, such as junctional adhesion molecule (JAM)-A or ZO-2-associated tight junctions. VE-cadherin engagement in confluent endothelial cells has been shown to reduce FA by modulating cell tension and spreading via RhoA [22]. In accordance with this, VE-cadherin reduction by small interfering RNA (siRNA) significantly increased FA in confluent cells, although it did not alter the F-actin content. These results explain previous observations on the distribution of tyrosine phosphorylated proteins in endothelial cells which, in subconfluent cells, localized predominantly in a FA-like pattern whereas in confluent cells they were mostly at intercellular borders [23]. The dynamic inter-conversion between linear and discontinuous AJ suggests that there could be a rapid tension-regulated switch of AJ proteins, which may be linked either to F-actin structures that protect the endothelial barrier, such as cortical F-actin [24], or to stress fibres. This link might be regulated, for example, by tension-induced unfolding of a linker protein in AJ, as has been postulated for p130Cas in FA [25].

Interestingly, cadherin complexes have been reported to associate with F-actin similar to stress fibres in transformed epithelial cells and endothelial cells undergoing remodelling (for example in response to wound healing or acute pro-inflammatory stimuli) [9-11,26]. In epithelial cells, E-cadherin has also been shown not to associate with F-actin via α-catenin. It has been proposed that there is no direct association between AJ and the cortical F-actin [4], although it remains possible that another AJ protein can connect AJ to cortical F-actin. Here, based on the specific distribution of discontinuous AJ, together with an analysis of the dynamics of the AJ component p120-catenin and F-actin and the effect of VE-cadherin depletion on stress fibres, we propose that endothelial discontinuous AJ formed by complexes of VE-cadherin, α-catenin, β-catenin and p120-catenin, can be physically linked to actin stress fibres. It is possible that a tension-regulated AJ protein links AJ to stress fibres only under tension but not in resting conditions where linear endothelial AJ are more similar to epithelial

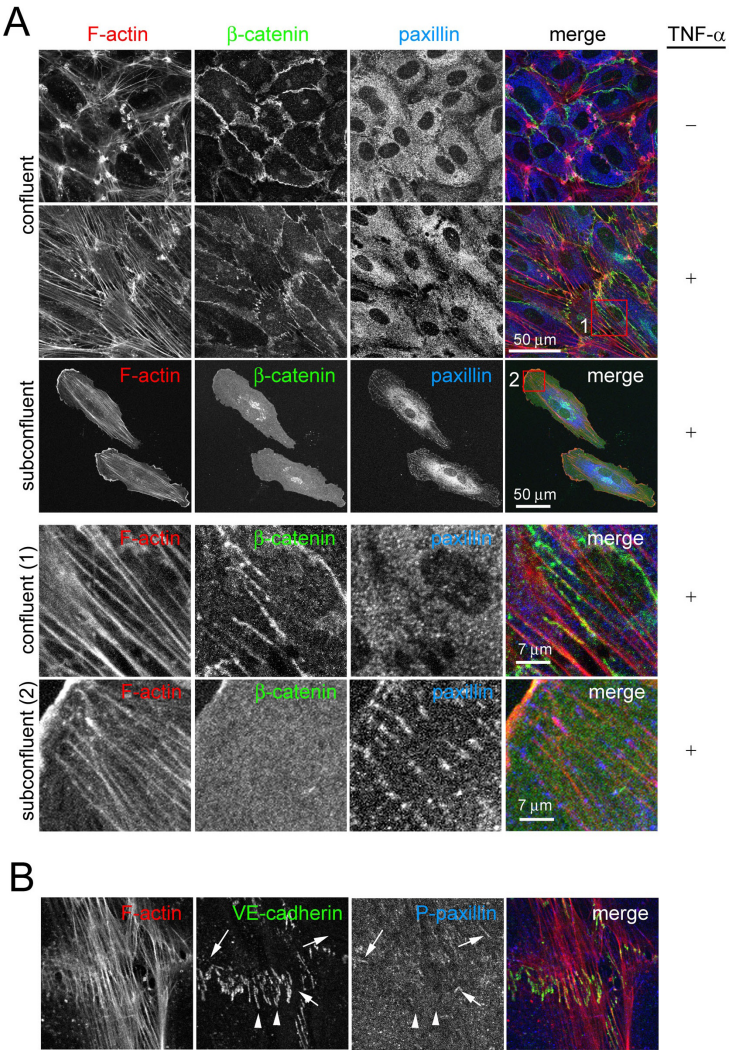

Figure 4 Effect of tumour necrosis factor (TNF)-α and confluence on discontinuous adherens junction (AJ), stress fibres and focal adhesions. (A) Effect of TNF-α on actin filament, β-catenin and paxillin distribution. Confluent human umbilical vein endothelial cells (HUVECs) were starved for 4 h and then, as indicated, stimulated with 10 ng/ml TNF-α for 20 h. In parallel, subconfluent HUVECs were also starved and stimulated with TNF-α. Cells were fixed and distribution of F-actin, β-catenin and paxillin was analyzed by immunofluorescence. Bottom panels show the red boxed areas indicated in merged images at higher magnification. (B) Distribution of F-actin, VE-cadherin and phospho-Y(118)-paxillin in TNF-α-stimulated confluent HUVECs. Arrowheads indicate discontinuous AJ, whereas arrows indicate focal adhesions detected by phospho-paxillin staining.

AJ and co-localize with cortical F-actin [26]. In agreement with this, stimuli that enhance endothelial barrier properties, such as cyclic adenosine monophosphate, increase the cortical F-actin belt but decrease stress fibres [27]. Taken together, our results and those of others indicate that, both in endothelial and epithelial cells, the association of F-actins such as stress fibres with AJ is regulated and not constitutive. This regulated association would, for example, facilitate cell-cell junction remodelling during wound healing or in response to inflammatory stimuli.

Another role of endothelial stress fibres during inflammation is likely to be the regulation of leucocyte transmigration. Adhesion receptors involved in leucocyte adhesion, such as ICAM-1 or VCAM-1 and transmigration, align with stress fibres in response to engagement [28,29]. ICAM-1 engagement increases RhoA activity and stress fibres [28] as well as regulating phosphorylation of VE-cadherin [30,31]. ICAM-1 and VCAM-1 crosslinking alter the integrity of VE-cadherin cell contacts [31,32]. In the light of these previous results, our data suggest that stress fibres are connectors from

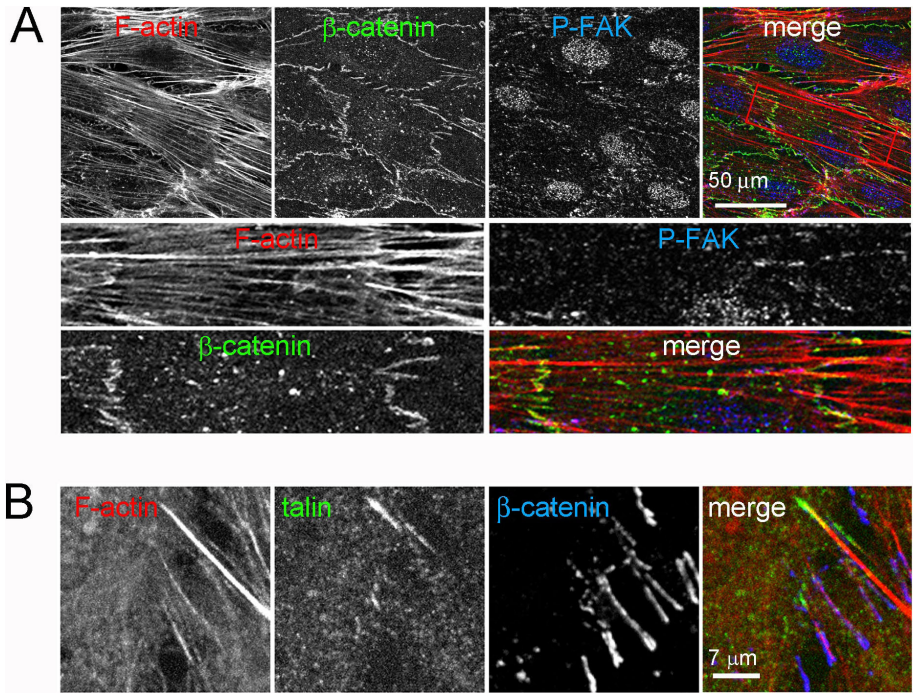

Figure 5 Discontinuous adherens junctions are distinct from focal adhesions. Confluent human umbilical vein endothelial cells were stimulated with 10 ng/ml tumour necrosis factor-α as in Figure 4. Cells were fixed and stained with TRITC-phalloidin, in order to detect actin filaments, with antibodies to β-catenin, phosphorylated FAK (p(Y397)FAK) (A) or TRITC-phalloidin and antibodies to detect talin and β-catenin (B). Bottom panels in (A) show the red-boxed area from the top panels (merge) at higher magnification.

apically localized receptors to cell-cell junctions, which may contribute to leukocyte transmigration during inflammation. Stress fibres thus not only regulate endothelial permeability to small solutes, but may also help to withstand the mechanical stress generated by leukocyte transmigration under shear stress. We propose that the linkage of stress fibres between neighbouring cells via discontinuous AJ contributes to increase stress resistance and to regulate the whole endothelial monolayer response to inflammation.

Conclusions

The current model for cell-cell junctional organization is largely inspired by studies in epithelium. In epithelial cells AJ and TJ are separately organized and associated with cortical actin, although recently it has been proposed that AJ are not directly linked to cortical actin [4]. The endothelium requires more dynamic and heterogeneous cell junctions in order to coordinate fast and local permeability increases to small molecules and cells from the bloodstream. Here we have shown that the ends of actin stress fibres, key actors in leukocyte transmigration and paracellular permeability regulation, are associated with cell-cell junctions. Cell-cell junctions can even connect stress fibres from neighbouring cells. Finally, we provide clear evidence that AJ are supramolecular protein complexes distinct to FAs able to stabilize stress fibres in confluent endothelial cells. Our results clearly show a distinct organization of endothelial F-actin at confluence which is likely to be relevant during permeability changes and leukocyte transendothelial migration and for endothelial inflammatory migration and angiogenesis.

Methods

Antibodies

Mouse monoclonal anti-VE-cadherin blocking antibody was obtained from BD Pharmingen (CA, USA; Cat. 555661). Anti-VE-cadherin (Cat. 610252), anti-α-catenin, anti p120-catenin, anti-FAK, anti-phospho-Y397-FAK and anti-paxillin (610051) mouse monoclonal antibodies were obtained from BD Transduction Laboratories (NJ, USA). Anti-β-catenin (C-2206) rabbit polyclonal and anti-talin (T-3287) mouse monoclonal antibodies were obtained from Sigma (Melbourne, Australia). Anti-α-catenin rabbit polyclonal antibody was obtained from Santa Cruz (CA, USA). Anti-γ-catenin mouse monoclonal antibody, anti-ZO-1 and anti-JAM-A rabbit polyclonal antibodies were obtained from Zymed (CA, USA). Anti-pY118-paxillin phospho-specific antibody (44-722) was obtained from Biosource (Nivelles, Belgium).

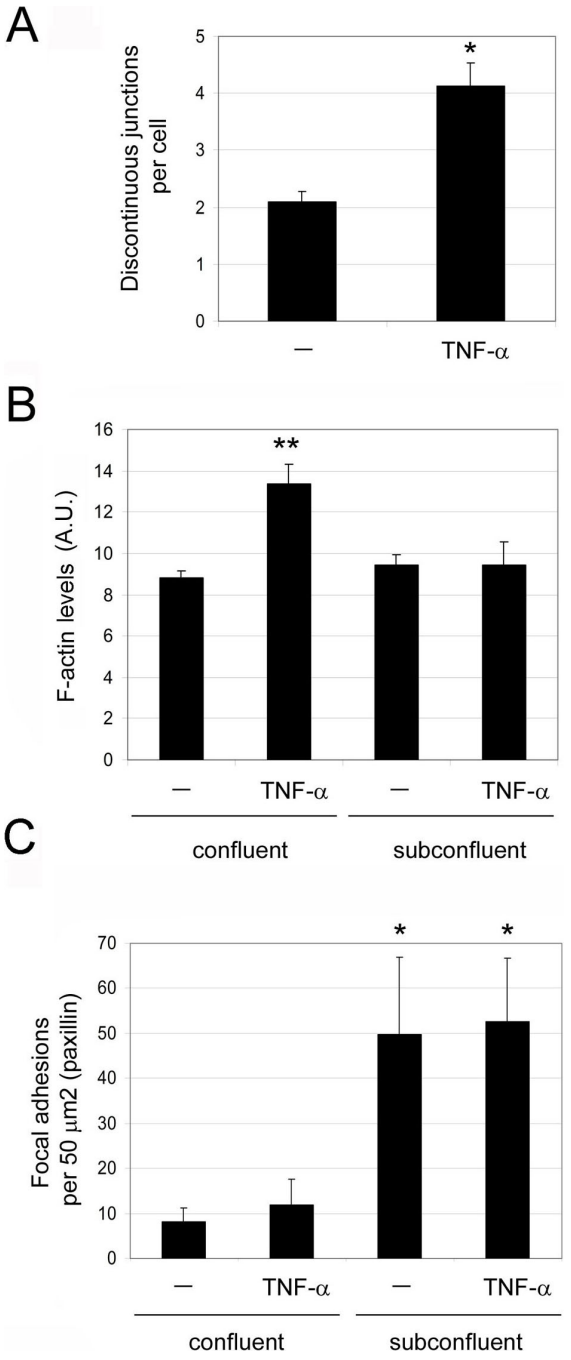

Figure 6 Quantitation of the effect of tumour necrosis factor (TNF)-α on discontinuous adherens factor, stress fibres and focal adhesions (FAs) in confluent and subconfluent human umbilical vein endothelial cells (HUVECs). (A) Quantitation of discontinuous junctions per cell with or without TNF-α stimulation. (B) Quantitation of actin filament staining from confocal images between confluent and subconfluent HUVECs with and without TNF-α stimulation as in Figure 4. (C) Quantitation of FA-like paxillin clusters in confluent and subconfluent HUVECs with and without TNF-α stimulation. Error bars indicate standard error of mean; $n \geq 3$ experiments. *, $P < 0.008$; **, $P < 0.001$, compared to confluent unstimulated cells. AU, arbitrary units.

Cell culture and transfection

HUVECs were obtained from Lonza (Wokingham, UK). They were cultured in Nunclon flasks pre-coated with 10 μg/ml human fibronectin in endothelial basal medium (EBM-2; (Lonza, MD, USA) supplemented with 2% fetal bovine serum (FBS), endothelial cell growth supplement EGM-2 (Lonza) (growth medium) in an atmosphere of 5% CO_2/95% air. When experiments were performed in starving conditions, confluent HUVECs were starved in EBM-2 medium supplemented with 1% fetal calf serum (starvation medium) prior to stimulation with 10 ng ml^{-1} TNFα. No major differences in FA content were detected in cells stimulated in growth medium or starving medium.

HUVECs were transiently transfected with 1-5 μg plasmid DNA/10^6 cells with a Nucleofector kit (VPB-1002) (Amaxa Biosystems, Cologne, Germany) according to the manufacturer's instructions, and used for experiments 24 h to 72 h after transfection. For experiments with cells expressing different fluorescently-tagged proteins in the same monolayer, 3×10^6 cells were transfected with each plasmid, pooled together, plated on two glass-bottom 35-mm dishes (MatTek Corporation, MA, USA) or two glass coverslips previously coated with fibronectin for 15 h and analysed 24 to 48 h after transfection. Since nucleofection can induce significant cell death, once transfected cells were plated, untransfected cells were sometimes added in order to provide sufficient cells to form of a confluent monolayer.

For siRNA transfection, a protocol derived from a modification of our previous method [29] was used for delivery of siRNA with high efficiency into primary endothelial cells. HUVECs were plated at sub-confluence (10^5 cells on each well of a six-well dish) in EBM-2 medium with no antibiotics. The following day cells were transfected by mixing 4 μl of oligofectamine with siRNA to a final concentration of 100 nM. Twenty-four hours after transfection cells were trypsinized and plated at confluence onto different dishes in order to perform parallel assays such as immunofluorescence and western blotting. Assays were performed 72 h after transfection.

Plasmids and siRNAs

In order to construct the p120-DsRed plasmid, p-EGFP-120^{ctn}- (generous gift from Keith Burridge) and dsRed vector from Clontech (CA, USA) were sequentially digested with AgeI and NotI enzymes and, then, the p120 vector without the GFP and the DsRed were ligated using the Ligase enzyme (New England Biolabs, Massachusetts, USA). β-Actin-GFP was a generous gift from Dr Beat Imhof. β-actin-Cherry was a generous gift from Ke Hu and Dr Ann Wheeler. The following siRNA oligonucleotides were obtained from the predesigned siGenome collection of Dharmacon (IL, USA). D-003641-01 (VE-cadherin), D-007746-01 (ZO-1). D-001210-01

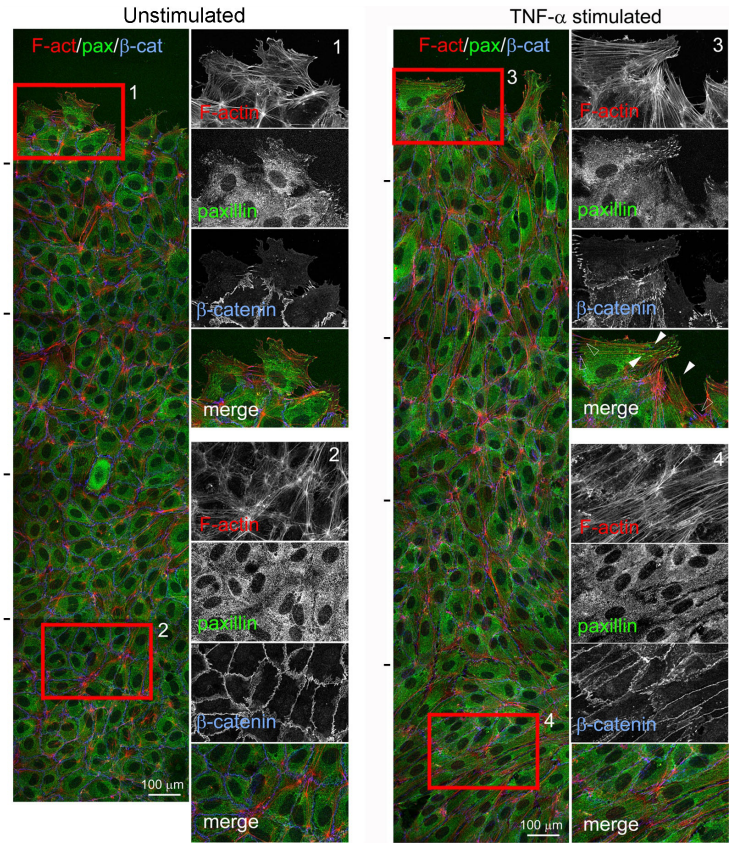

Figure 7 Effect of tumour necrosis factor (TNF)-α and confluence on discontinuous adherens junctions, stress fibres and focal adhesions. Confluent unstimulated human umbilical vein endothelial cells (HUVECs) (A), or HUVECs stimulated with 10 ng/ml TNF-α for 20 h (B) in growth medium, were scratched with a plastic tip and after 5 h cells were fixed and stained for actin filament, paxillin and β-catenin. All images are projections of *z*-stacks of confocal images. Left images show a general view of five confocal fields sequentially acquired and superimposed from the scratch edge (top) into the confluent monolayer (bottom). Black lines on left indicate the edges of each confocal field. Right panels show the boxed areas at higher magnification, either at the scratch edge (1 and 3) or within the confluent monolayer (2 and 4). Arrowheads show stress fibre tips associated to paxillin clusters, empty arrowheads points to the tips of the same stress fibres associated to discontinuous junctions on the other side.

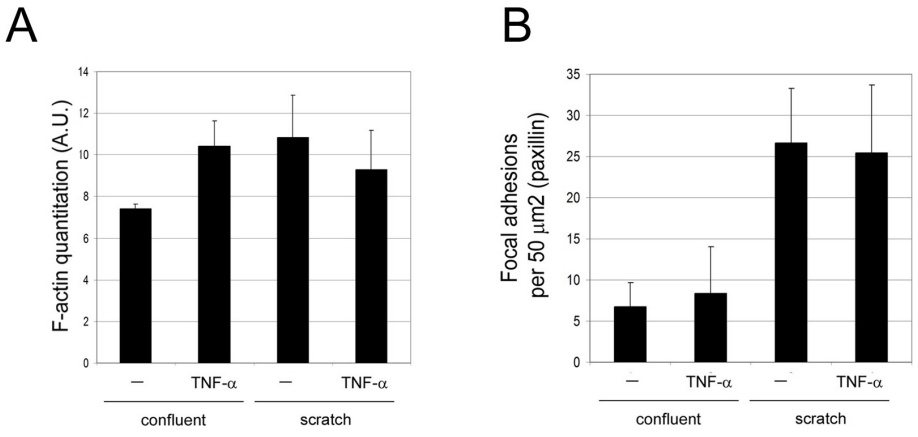

Figure 8 Quantitation of the effect of tumour necrosis factor (TNF)-α and confluence on stress fibres and focal adhesions (FAs) during the scratch asssay. Quantitation of actin filament levels (A) and FA-like paxillin clusters (B) from confocal images of cells at the scratch edge (scratch) and cells in confluent areas (confluent) with and without TNF-α. AU, arbitrary units.

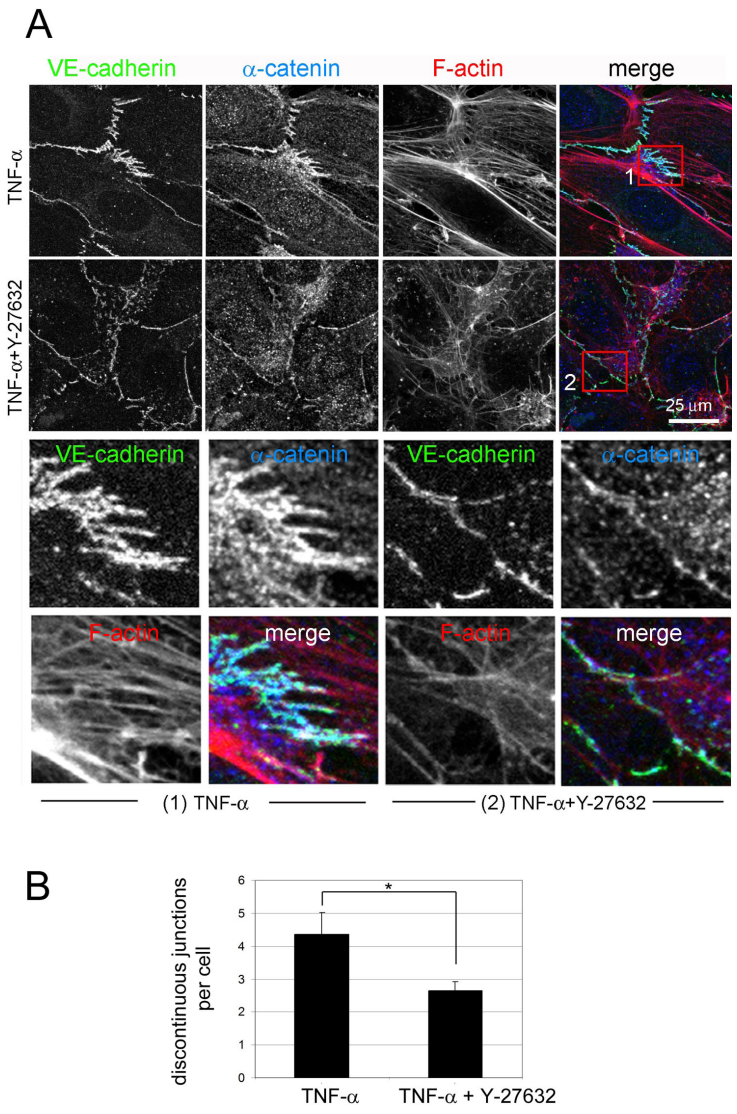

Figure 9 ROCK inhibition induces loss of discontinuous adherens junction. Human umbilical vein endothelial cells were plated at confluence for 48 h and stimulated, as indicated, with 10 ng/ml tumour necrosis factor (TNF)-α in growth medium or TNF-α with 5 μM Y-27632. Cells were then fixed and stained for vascular endothelial (VE)-cadherin, α-catenin and actin filament. Bottom panels show the boxed areas indicated in the merge images at higher magnification: (1) TNF-α, (2) TNF-α + Y-27632. (B) Quantitation of discontinuous junctions in TNF-α-stimulated cells with or without 5 μM Y-27632, +/- standard error of mean of three different experiments. *, $P < 0.016$.

(control (1)) or D-001810-01 (control (2)) non-targeting siRNA were used as controls in different experiments.

Confocal and time-lapse microscopy

For confocal microscopy, cells were fixed with 4% paraformaldehyde for 20 min, or at -20°C in 100% methanol for 5 min, for the detection of Talin. They were then blocked with tris-buffered saline (25 mM Tris pH 7.4, 150 mM NaCl) for 10 min, permeabilized for 5 min with phosphate buffered saline (PBS) containing 0.2% Triton X-100 at 4°C, blocked with PBS containing 1% bovine serum albumin and incubated at 37°C with primary then fluorophore-conjugated secondary antibodies or 1 μg/ml TRITC/FITC-labelled phalloidin. Specimens were mounted in DAKO fluorescent mounting medium (DAKO Corporation, CA, USA).

Confocal laser scanning microscopy was carried out with an LSM 510 (Zeiss, Welwyn Garden City, UK) mounted over an Axioplan microscope (Zeiss) using a ×40 1.3 NA oil immersion objective. In order to obtain Z stacks, three to six optical sections were taken over 4 μm. Intensity profiles were generated using the Zeiss LSM software.

Time-lapse microscopy was performed with a Nikon TE2000-E Eclipse Inverted microscope, in an

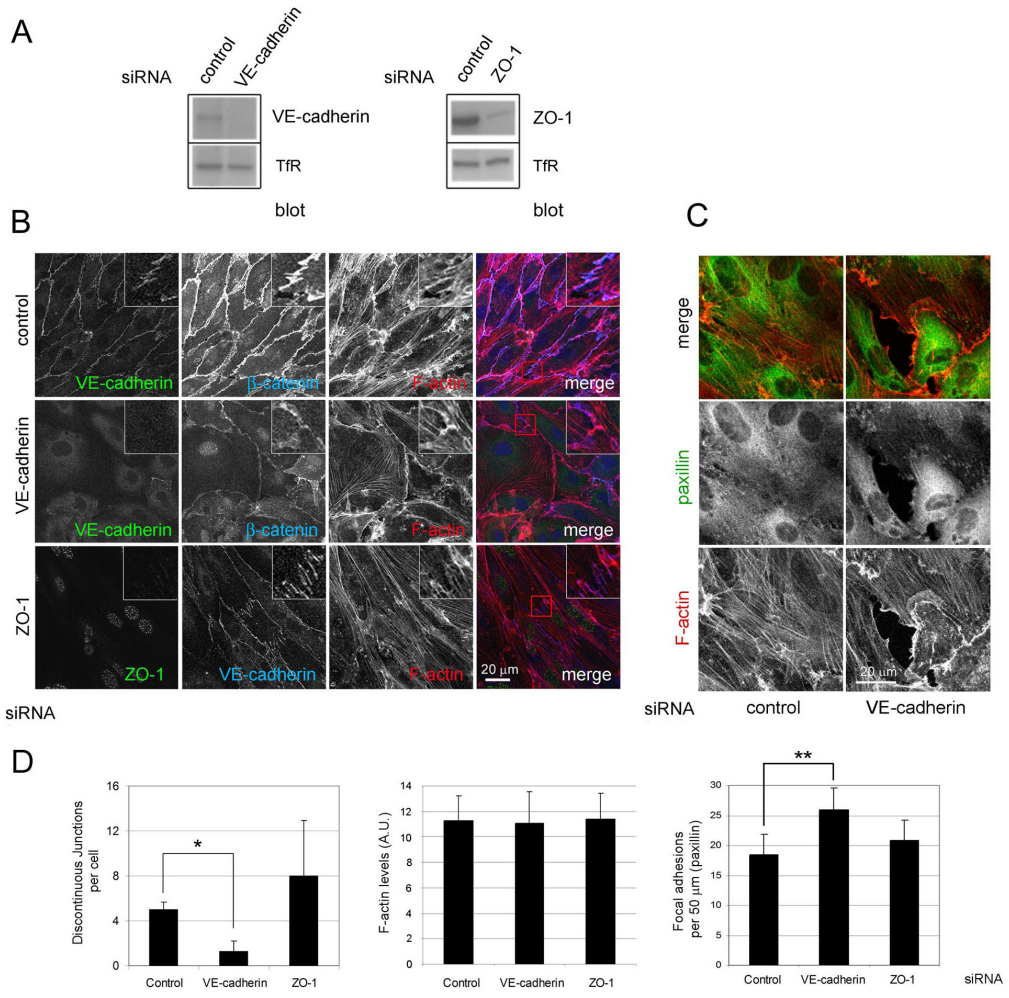

Figure 10 Vascular endothelial (VE)-cadherin and zonula occludens (ZO)-1 in junctional actin organization. Human umbilical vein endothelial cells (HUVECs) were transfected with small interfering RNA (siRNA) oligonucleotides targeting VE-cadherin, ZO-1 or a non-specific oligonucleotide control. After 24 h cells were trypsinized and plated at confluence and analysed 48 h later (72 h after transfection). Twenty hours before the analysis cells were stimulated with tumour necrosis factor (TNF)-α in growth medium. (A) Cells were lysed and the effect of each siRNA on the levels of VE-cadherin, ZO-1 and transferrin receptor (TfR) were analysed by western blotting. (B, C) siRNA-transfected HUVECs were stimulated with TNF-α, fixed and stained for the indicated junctional proteins and actin filament (F-actin) (B) or F-actin and paxillin (C). (D) Quantitation of discontinuous junctions, F-actin content and focal adhesions in siRNA-treated cells upon TNF-α stimulation. * $P < 0.045$; ** $P < 0.065$.

environmental chamber at 37°C. 20 mM HEPES (pH 7.4) was added to the cells 2 h before the experiment. Images were taken with a cooled CCD camera Hamamatsu Orca-ER C4742-95. Camera and shutter (Lambda Instruments, VA, USA) were controlled by Andor Q software. Movies were processed with Metamorph software.

Electron microscopy

TNF-α-stimulated or unstimulated HUVECs were fixed for electron microscopy using 2% glutaraldehyde in 60 mM PIPES, 25 mM HEPES, pH 7.3, 3 mM $MgCl_2$, 10 mM EGTA and 1% Triton TX-100, treated with 1% osmium tetroxide and dehydrated through a graded series of ethanol. The samples were then embedded in TAAB resin by conventional procedures, and 70 nm sections were cut using a Leica Ultracut E ultra microtome (Leica, Vienna, Austria). Sections were mounted onto 200 mesh copper grids and stained with lead citrate, before viewed on a H7600N transmission electron microscope (Leica). Digital images were captured using an AMT camera (Deben, Suffolk, UK).

Quantification of F-actin, FAs and discontinuous junctions

Confocal images from 8 to 30 cells per experiment from at least three different experiments were contrasted and analysed using LSM 510 software (Zeiss) in order to distinguish morphologically discontinuous junctions or

FA-like paxillin staining at the basal planes. For F-actin quantification, images from cells stained for TRITC-labelled phalloidin were exported in formats compatible with ImageJ software. ImageJ was used to obtain the mean fluorescent intensities from different cellular regions of confluent cells, subconfluent cells or cells at the border of a wound induced in a confluent monolayer with a plastic tip 5 h before. Data were processed and statistical significance determined using Student's *t*-test (Microsoft Excel).

Additional file 1: Movie 1. Human umbilical vein endothelial cells were nucleofected with plasmids encoding p120-catenin-green fluorescent protein and p120-catenin-red fluorescent protein (p120-dsRed) and plated at confluence for 24 h in growth medium. Cell images were acquired by fluorescence time-lapse microscopy, 1 frame/min. (See Figure 1.)
Click here for file
[http://www.biomedcentral.com/content/supplementary/1741-7007-8-11-S1.MOV]

Abbreviations

AJ: adherens junctions; cAMP: cyclic adenosine monophosphate; DsRED: red fluoroescent protein; FA: focal adhesion; F-actin: actin filament; GFP: green fluorescent protein; HUVEC: human umbilical vein endothelial cells; PBS: phosphate buffered saline; ROCK: rho kinase; siRNA: small interfering RNA; TJ: tight junctions; TNF: tumour necrosis factor; VE: vascular endothelial; ZO1: zonula occludens-1; FAK: focal adhesion kinase.

Acknowledgements

This work was supported by the Ludwig Institute for Cancer Research, Association for International Cancer Research (AICR) and the European Commission contract LSHG-CT-2003-502935 (MAIN). JM was supported by a Marie Curie fellowship (No. HPMF-CT-2000-01061) and a British Heart Foundation intermediate fellowship (No. FS/04/006), a grant from the Spanish Ministerio de Ciencia e Innovación (SAF2008-01936) and a Ramón y Cajal contract from the Spanish Government. NR is supported by a JAE predoctoral fellowship from CSIC (Spain). BM was supported by a FPI fellowship (SAF-2008-01936). We thank Alice Warley and Ken Brady (Centre for Ultrastructural Imaging, King's College London, UK) for technical assistance in the preparation of electron microscopy samples. We are grateful to Nicolas Reymond, Philippe Riou, Francisco Vega and other members of the Ridley laboratory, as well as to Juan Francisco Aranda and Miguel Alonso, for helpful discussions and technical support.

Author details

[1]University College London, Ludwig Institute for Cancer Research and Department of Biochemistry and Molecular Biology, London WC1E 6BT, UK. [2]Centro de Biología Molecular Severo Ochoa, CSIC-Universidad Autónoma de Madrid, Cantoblanco, 28049 Madrid, Spain. [3]Randall Division of Cell and Molecular Biophysics, King's College London, New Hunt's House, Guy's Campus, London SE1 1UL, UK.

Authors' contributions

JM designed experiments and performed experiments and wrote the manuscript. RC performed the electron microscopy experiments. NR did some of the immuno localizations of cell-cell junctional proteins. BM did some immunolocalizations and subsequent quantitations, LF maintained cell cultures, transfected plasmids and siRNAs and prepared cells on coverslips. IC provided cells, antibodies specific for junctional proteins and corrected the manuscript. CB started the project and made the p120-catenin-dsRed cDNA construct. AR supervised the project, designed experiments and wrote the manuscript.

Received: 4 April 2009
Accepted: 2 February 2010 Published: 2 February 2010

References

1. Bazzoni G, Dejana E: **Endothelial cell-to-cell junctions: molecular organization and role in vascular homeostasis.** *Physiol Rev* 2004, **84**:869-901.
2. Vincent PA, Xiao K, Buckley KM, Kowalczyk AP: **VE-cadherin: adhesion at arm's length.** *Am J Physiol Cell Physiol* 2004, **286**:C987-987.
3. Drees F, Pokutta S, Yamada S, Nelson WJ, Weis WI: **Alpha-catenin is a molecular switch that binds E-cadherin-beta-catenin and regulates actin-filament assembly.** *Cell* 2005, **123**:903-915.
4. Yamada S, Pokutta S, Drees F, Weis WI, Nelson WJ: **Deconstructing the cadherin-catenin-actin complex.** *Cell* 2005, **123**:889-901.
5. Wojciak-Stothard B, Ridley AJ: **Rho GTPases and the regulation of endothelial permeability.** *Vascul Pharmacol* 2002, **39**:187-199.
6. Braga VM: **Cell-cell adhesion and signalling.** *Curr Opin Cell Biol* 2002, **14**:546-556.
7. Gavard J, Gutkind JS: **Protein kinase C-related kinase and ROCK are required for thrombin-induced endothelial cell permeability downstream from Galpha12/13 and Galpha11/q.** *J Biol Chem* 2008, **283**:29888-29896.
8. Carbajal JM, Schaeffer RC Jr: **RhoA inactivation enhances endothelial barrier function.** *Am J Physiol* 1999, **277**:C955-955.
9. Lim MJ, Chiang ET, Hechtman HB, Shepro D: **Inflammation-induced subcellular redistribution of VE-cadherin, actin, and gamma-catenin in cultured human lung microvessel endothelial cells.** *Microvasc Res* 2001, **62**:366-382.
10. Konstantoulaki M, Kouklis P, Malik AB: **Protein kinase C modifications of VE-cadherin, p120, and beta-catenin contribute to endothelial barrier dysregulation induced by thrombin.** *Am J Physiol Lung Cell Mol Physiol* 2003, **285**:L434-434.
11. Hurst VI, Goldberg PL, Minnear FL, Heimark RL, Vincent PA: **Rearrangement of adherens junctions by transforming growth factor-beta1: role of contraction.** *Am J Physiol* 1999, **276**:L582-582.
12. Partridge CA, Horvath CJ, Del Vecchio PJ, Phillips PG, Malik AB: **Influence of extracellular matrix in tumor necrosis factor-induced increase in endothelial permeability.** *Am J Physiol* 1992, **263**:L627-633.
13. McKenzie JA, Ridley AJ: **Roles of Rho/ROCK and MLCK in TNF-alpha-induced changes in endothelial morphology and permeability.** *J Cell Physiol* 2007, **213**:221-8.
14. Noria S, Cowan DB, Gotlieb AI, Langille BL: **Transient and steady-state effects of shear stress on endothelial cell adherens junctions.** *Circ Res* 1999, **85**:504-514.
15. Schoenwaelder SM, Burridge K: **Bidirectional signaling between the cytoskeleton and integrins.** *Curr Opin Cell Biol* 1999, **11**:274-286.
16. Brown MC, Turner CE: **Paxillin: adapting to change.** *Physiol Rev* 2004, **84**:1315-1339.
17. Choudhury GG, Marra F, Abboud HE: **Thrombin stimulates association of src homology domain containing adaptor protein Nck with pp125FAK.** *Am J Physiol* 1996, **270**:F295-295.
18. Carbajal JM, Gratrix ML, Yu CH, Schaeffer RC Jr: **ROCK mediates thrombin's endothelial barrier dysfunction.** *Am J Physiol Cell Physiol* 2000, **279**: C195-204.
19. Han J, Liu G, Profirovic J, Niu J, Voyno-Yasenetskaya T: **Zyxin is involved in thrombin signaling via interaction with PAR-1 receptor.** *Faseb J* 2009, **23**:4193-206.
20. Navarro P, Ruco L, Dejana E: **Differential localization of VE- and N-cadherins in human endothelial cells: VE-cadherin competes with N-cadherin for junctional localization.** *J Cell Biol* 1998, **140**:1475-1484.
21. Ilan N, Madri JA: **PECAM-1: old friend, new partners.** *Curr Opin Cell Biol* 2003, **15**:515-524.
22. Nelson CM, Pirone DM, Tan JL, Chen CS: **Vascular endothelial-cadherin regulates cytoskeletal tension, cell spreading, and focal adhesions by stimulating RhoA.** *Mol Biol Cell* 2004, **15**:2943-2953.
23. Lampugnani MG, Corada M, Andriopoulou P, Esser S, Risau W, Dejana E: **Cell confluence regulates tyrosine phosphorylation of adherens junction components in endothelial cells.** *J Cell Sci* 1997, **110(Pt 17)**:2065-2077.
24. Fukuhara S, Sakurai A, Sano H, Yamagishi A, Somekawa S, Takakura N, Saito Y, Kangawa K, Mochizuki N: **Cyclic AMP potentiates vascular endothelial cadherin-mediated cell-cell contact to enhance endothelial**

barrier function through an Epac-Rap1 signaling pathway. *Mol Cell Biol* 2005, **25**:136-146.
25. Sawada Y, Tamada M, Dubin-Thaler BJ, Cherniavskaya O, Sakai R, Tanaka S, Sheetz MP: **Force sensing by mechanical extension of the Src family kinase substrate p130Cas.** *Cell* 2006, **127**:1015-1026.
26. Kametani Y, Takeichi M: **Basal-to-apical cadherin flow at cell junctions.** *Nat Cell Biol* 2006, **9**:92-98.
27. Baumer Y, Drenckhahn D, Waschke J: **cAMP induced Rac 1-mediated cytoskeletal reorganization in microvascular endothelium.** *Histochem Cell Biol* 2008, **129**:765-778.
28. Thompson PW, Randi AM, Ridley AJ: **Intercellular adhesion molecule (ICAM)-1, but not ICAM-2, activates RhoA and stimulates c-fos and rhoA transcription in endothelial cells.** *J Immunol* 2002, **169**:1007-1013.
29. Millan J, Hewlett L, Glyn M, Toomre D, Clark P, Ridley AJ: **Lymphocyte transcellular migration occurs through recruitment of endothelial ICAM-1 to caveola- and F-actin-rich domains.** *Nat Cell Biol* 2006, **8**:113-123.
30. Allingham MJ, van Buul JD, Burridge K: **ICAM-1-mediated, Src- and Pyk2-dependent vascular endothelial cadherin tyrosine phosphorylation is required for leukocyte transendothelial migration.** *J Immunol* 2007, **179**:4053-4064.
31. Turowski P, Martinelli R, Crawford R, Wateridge D, Papageorgiou AP, Lampugnani MG, Gamp AC, Vestweber D, Adamson P, Dejana E, *et al*: **Phosphorylation of vascular endothelial cadherin controls lymphocyte emigration.** *J Cell Sci* 2008, **121**:29-37.
32. van Wetering S, Berk van den N, van Buul JD, Mul FP, Lommerse I, Mous R, ten Klooster JP, Zwaginga JJ, Hordijk PL: **VCAM-1-mediated Rac signaling controls endothelial cell-cell contacts and leukocyte transmigration.** *Am J Physiol Cell Physiol* 2003, **285**:C343-343.

doi:10.1186/1741-7007-8-11
Cite this article as: Millán *et al.*: Adherens junctions connect stress fibres between adjacent endothelial cells. *BMC Biology* 2010 **8**:11.